

# Supramolecular Chemistry based on Multicomponent Self-Assembly with Pentaphosphaferrocenes, Silver Salts and Organic Nitriles



Dissertation zur Erlangung des  
Doktorgrades der Naturwissenschaften

**DR. RER. NAT.**

am Institut für Anorganische Chemie  
der Fakultät für Chemie und Pharmazie  
der Universität Regensburg

vorgelegt von

**Kevin Grill**

aus Landshut

im Jahr 2023

Diese Arbeit wurde angeleitet von Prof. Dr. Manfred Scheer.

Das Promotionsgesuch wurde eingereicht am: 26.07.2023

Tag der mündlichen Prüfung: 12.10.2023

Vorsitzender: Prof. Dr. Alkwin Slenczka

Prüfungsausschuss: Prof. Dr. Manfred Scheer

Prof. Dr. Nikolaus Korber

Prof. Dr. Frank-Michael Matysik



Universität Regensburg

**Eidesstattliche Erklärung**

Ich erkläre hiermit an Eides statt, dass ich die vorliegende Arbeit mit dem Titel „Supramolecular Chemistry based on Multicomponent Self-Assembly with Pentaphosphaferrocenes, Silver Salts and Organic Nitriles“ ohne unzulässige Hilfe Dritter und ohne Benutzung anderer als der angegebenen Hilfsmittel angefertigt habe; die aus anderen Quellen direkt oder indirekt übernommenen Daten und Konzepte sind unter Angabe des Literaturzitats gekennzeichnet.

---

Kevin Grill

This thesis was elaborated within the period from January 2020 until July 2023 in the Institute of Inorganic Chemistry at the University of Regensburg, under the supervision of Prof. Dr. Manfred Scheer.

Results of this work have already been published.

**List of Publications:**

E. Peresypkina, K. Grill, B. Hiltl, A. V. Virovets, W. Kremer, J. Hilgert, W. Tremel, M. Scheer, *Angew. Chem. Int. Ed.* **2021**, *60*, 12132-12142.

K. Grill, S. B. Dinauer, E. Peresypkina, A. V. Virovets, M. Scheer, *Chem. Eur. J.* **2023**, *29*, e202203963.

*To my family*

## Preface

The thesis starts with a general introduction about the research topic of supramolecular chemistry and specifies on spherical assemblies and coordination polymers (Chapter 1), followed by the research objectives (Chapter 2).

The following *Chapters 3-6* can be considered as self-contained and suitable for future publications. To ensure uniform design of this work, all chapters are subdivided into 'Introduction', 'Results and Discussion', 'Conclusion', 'Experimental Part', 'Crystallographic Details and Structure Refinement', 'Author Contributions' and 'References'. Additionally, if some of the presented results have already been partly discussed in other theses, it is stated at the end of the respective chapters in the paragraph 'Author Contributions'.

Furthermore, all chapters have the same text settings, and the numeration of compounds, figures, schemes and tables begins anew for reasons of future publishing. The depicted molecular structures may differ in their style.

A comprehensive conclusion of this work is presented at the end of this thesis (*Chapter 7*).

A list of abbreviations, a list of all numbered compounds, my curriculum vitae and the acknowledgements can be found in chapter 8.

## Table of Contents

<b>1.</b>	<b>Introduction .....</b>	<b>1</b>
1.1	Supramolecular Chemistry.....	1
1.2	Coordination Polymers .....	3
1.3	Discrete Supramolecules.....	5
1.4	Organometallic Building Blocks.....	9
1.5	Supramolecular Aggregates based on P <sub>n</sub> -ligand complexes.....	10
1.6	References .....	14
<b>2.</b>	<b>Research Objectives.....</b>	<b>21</b>
3.	Scaffold-constructing role of triflate: Polymeric Complexes and Discrete Supramolecules based on Pentaphosphaferrocene and Silver.....	22
3.1	Introduction .....	23
3.2	Results and Discussion .....	25
3.3	Conclusion.....	38
3.4	Experimental Part .....	39
3.5	Crystallographic Details and Structure Refinement .....	63
3.6	Author Contributions .....	70
3.7	References .....	70
<b>4.</b>	<b>Three-component Self-Assembly Changes its Course: A Leap from Simple Polymers to 3D Networks of Spherical Host-Guest Assemblies.....</b>	<b>74</b>
4.1	Introduction .....	75
4.2	Results and Discussion .....	76
4.3	Conclusion.....	90
4.4	Experimental Part .....	91
4.5	Crystallographic Details and Structure Refinement .....	121
4.6	Author Contributions .....	133
4.7	References .....	133

<b>5.</b>	<b>Across the Dimensions: A Three-Component Self-Assembly of Pentaphosphaferrocene-based Coordination Polymers.....</b>	<b>137</b>
5.1	Introduction.....	138
5.2	Results and Discussion.....	140
5.3	Conclusion.....	149
5.4	Experimental Part.....	150
5.5	Crystallographic Details and Structure Refinement.....	173
5.6	Author Contribution.....	180
5.7	References.....	180
<b>6.</b>	<b>Organic nitriles matter: A way to modify and connect discrete supramolecules based on bulky pentaphosphaferrocenes and Ag(I) .....</b>	<b>183</b>
6.1	Introduction.....	184
6.2	Results and Discussion.....	185
6.3	Conclusion.....	197
6.4	Exerimental Part.....	198
6.5	Crystallographic Details and Structure Refinement.....	220
6.6	Author Contributions.....	229
6.7	References.....	229
<b>7.</b>	<b>Conclusion.....</b>	<b>231</b>
<b>8.</b>	<b>Appendices.....</b>	<b>245</b>
8.1	Alphabetic List of Abbreviations.....	245
8.2	List of Numbered Compounds.....	247
8.3	Curriculum Vitae.....	249
8.4	Acknowledgments.....	251







# 1. Introduction

## 1.1 Supramolecular Chemistry

In 1894 by recognizing that enzymes and substrates interact similar to a “lock and key”, Fisher laid down the fundamental principles of molecular recognition and host-guest systems,<sup>[1]</sup> creating an extremely fertile soil for scientists all over the world who made supramolecular chemistry one of the most important interdisciplinary fields of research in the following century. However, it was not until J. Cram, Jean-Marie Lehn, and Charles J. Pedersen were awarded the Nobel Prize in Chemistry in 1987<sup>[2]</sup> for their development and use of molecules with structure-specific interactions of high selectivity that supramolecular chemistry became a well-respected chemical discipline.<sup>[2]</sup> Today, it is also referred to as the “chemistry beyond the molecule” that aims for the development of highly complex chemical aggregates of subunits held together by intermolecular, non-covalent forces.<sup>[3]</sup>

Modern supramolecular chemistry encompasses not only host-guest chemistry, which deals with “*the study of larger ‘host’ molecules that are capable of enclosing smaller ‘guest’ molecules via non-covalent interactions*”,<sup>[4]</sup> but also with the so called self-assembly, which is related to “*the spontaneous and reversible association of two or more components to form a larger, non-covalently bound aggregate*”.<sup>[4]</sup> The difference between these two closely related areas lies in the relative size and shape of the building blocks, meaning that the formation of a complex, in which a significantly larger assembly (host) wraps itself around the second smaller assembly (guest), is a narrower specific subject of host-guest chemistry. Accordingly, Fischer’s early insight stays consistent with today’s definition of host-guest systems.<sup>[5]</sup>

Nature itself is full of self-assembled supramolecular systems, like the famous double helical structure of the DNA. It is only through a closer look at these aggregates the overall potential of self-assembly processes becomes apparent. It only requires the design and synthesis of relatively simple building blocks and their subsequent spontaneous aggregation to create the building block of life.<sup>[5,6]</sup> To enable this spontaneous aggregation is possible, nature makes selective use of weak noncovalent interactions such as hydrogen bonds between the base pairs and  $\pi$ -systems to give the DNA stability and functionality. In addition to these, many other interactions such as  $\pi$ - $\pi$ , van der Waals, Coulombs, donor-acceptor are found in nature that are necessary to create these highly complex architectures. Supramolecular chemists exploit these “weak interactions” to create scaffolds that can match the complexity of natural system.<sup>[5,7]</sup>

In terms of the interactions driving self-assembly, supramolecular chemistry can be divided into three main categories: i) architectures that are based on H-bond interactions; ii) systems that are

using other noncovalent interactions like cation-anion, ion-dipole,  $\pi$ - $\pi$  stacking, cation- $\pi$ , van der Waals, as well as polar and non-polar interactions; and iii) arrangements that avail of metal-ligand bonds for the self-assembly, the so-called '*metallo-supramolecular chemistry*' or coordination-driven self-assembly.<sup>[7]</sup> While the first categories encounter increasing problems to direct weak interactions due to the growing complexity of supramolecules, the more predictable nature of the metal-ligand coordination sphere of coordination-driven self-assembly can provide a more accurate synthesis pathway.<sup>[5,7,8]</sup> This advantage is based on the fact that a particular geometry and binding motifs are encoded by corresponding molecular orbitals on the used metal/ligand.<sup>[9]</sup> Back in the 1990s, the group of Fujita<sup>[10,11]</sup> and Stang<sup>[12]</sup> utilised this concept and obtained a variety of metallamacrocycles and metallocages through their seminal synthesis strategies. Firstly, it requires donor building blocks, which are generally organic ligands with two or more donor atoms and fixed angles. These binding sites of the Lewis bases are based on functional groups containing nitrogen, oxygen, or other donor elements, such as sulphur or phosphorus; the latter two are far less frequently used (Figure 1.1). As potential ligands, fused conjugated aromatic and benzene ring substitutions are popular, as are ethynyl groups, and are especially useful to extend structures without changing their basic topology.<sup>[10,13,14]</sup> In addition, there are Lewis acidic metal cations in metal-containing subunits that are crucial for this approach due to their available coordination sites which are prearranged at fixed angle to each other to bind incoming donors.<sup>[7,14]</sup>

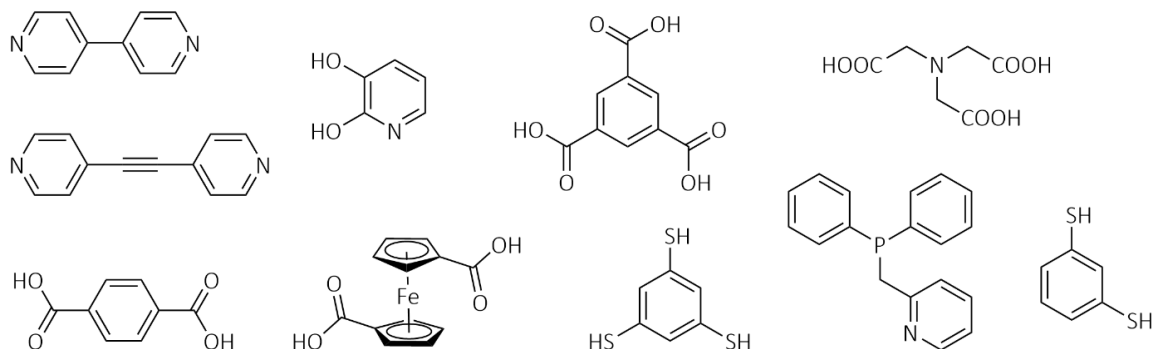


**Figure 1.1.** Selected examples of organic ligands as Lewis bases in coordination-driven self-assembly.

In order to predict the outcome of coordination-driven self-assembly more accurately, it is necessary to decide whether to use convergent or divergent building blocks. To be more precise, convergent components focus their binding sites on a central point, while divergent components encourage them to spread in multiple directions. By combining convergent and divergent binding sites in different ways, one obtains either discrete assemblies or polymeric networks, respectively. Discrete arrangements arise either when convergent ligands are used with inherently divergent metal ions, such as in the use of e.g., 2,2'-bipyridine ligands with divergent metals, or when divergent ligands are joined with e.g., convergent metal ion in which part of the coordination sphere is already occupied by chelating ligands such as ethylene diamine. If the two buildings blocks

are divergent, polymeric structures are usually formed due to the minimal directional specification.<sup>[4]</sup>

## 1.2 Coordination Polymers

In the last decades, coordination compounds with infinite structures have become particularly important, especially compounds with backbones built up by metal ions as nodes and ligands as linkers. The so-called “coordination polymers” (CP) appeared in the early 1960s and was first coined by J. C. Bailer in 1964, who worked with compounds with polymeric structure consisting of metals and ligands. Since then, the synthesis and characterization of infinite 1D, 2D and 3D networks has become a topic of high interest. As it was quickly recognised, inorganic materials are more resistant to thermal and oxidative conditions than their organic counterparts, research into coordination polymers was initially only application-oriented.<sup>[14,15]</sup>

One of the earliest representatives of CP's is the synthetic pigment commonly known as Prussian Blue, which has been known since the 1700s. But it was not until 1977, that with support of X-ray diffraction analysis a mixed-valent Fe(II)/Fe(III) framework with CN linkages in between was revealed (Figure 1.2a).<sup>[16]</sup> In 1897 Hoffman discovered that the addition of benzene to a Ni(CN)<sub>2</sub> solution of ammonia leads to a coordination framework. Powell's X-ray studies showed that although the Ni(CN)<sub>2</sub>(NH<sub>3</sub>)·C<sub>6</sub>H<sub>6</sub> had similar properties like Prussian blue, its structure was not a 3D polymeric framework, but consisted from parallel 2D sheets confining benzene-containing channels of ammine-capped nickel cations bridged by cyanide ligands.<sup>[17]</sup> These outstanding representatives promoted the discovery of other polymeric structures with different bridging ligands, guests and capping

moieties, cementing the field of coordination polymers as a distinct area of research.<sup>[18]</sup> A major breakthrough in this field was achieved when cyanide ligands were replaced by other organic ligands that quickly led to a variety of new metal-organic materials.<sup>[14]</sup> Using tetranitrile ligands (Figure 1.2b), the Robson's group achieved a decisive turnaround in the field of coordination

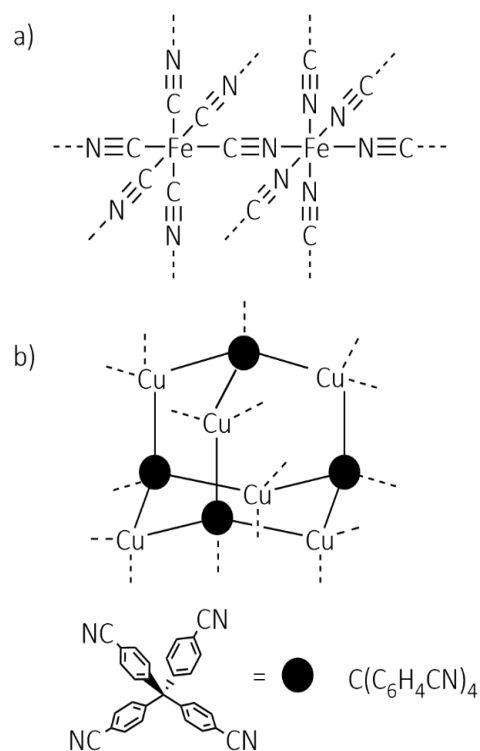


**Figure 1.2:** a) section of Prussian Blue  $\text{Fe}_4[\text{Fe}(\text{CN})_6]_3$ ; b)  $[\text{Cu}\{\text{C}(\text{C}_6\text{H}_4\text{CN})_4\}]_n^+$  Fragment of Robson's structure with

polymers in 1989 and, thus, also introduced the most iconic ditopic linear spacer to this day, the 4,4'-bipyridine ligands.<sup>[19]</sup>

After many outstanding results with this ditopic ligand, research interests gradually moved towards polytopic donor ligands.<sup>[20]</sup> In the late 1990s, the groups of Kitagawa<sup>[21]</sup> and Yaghi<sup>[22]</sup> attracted attention with their respective pyridyl- and carboxylate-based permanently microporous metal-organic materials, introducing the term metal-organic framework (MOF). The MOFs obtained by the two groups are featured by the reversible adsorption of gas. The term MOF is now widely used not only for simple metal-ligand CPs, but also for all extended assemblies consisting of mono- or multinuclear metal nodes as well as for microcrystalline materials with permanent porosity based on polynuclear clusters. Modern MOF syntheses are primarily application-driven and thus tailored MOFs are used e.g. in energy storage,<sup>[23]</sup> chemical purification,<sup>[24]</sup> sensing,<sup>[25]</sup> catalysis,<sup>[26]</sup> and other fields.<sup>[27]</sup> These syntheses aim to generate stable materials with extreme permanent porosity and therefore a large surface area. This is achieved through careful selection of Lewis basic donors and Lewis acidic acceptors as well as reaction conditions that lead to the thermodynamically favoured scaffolds.<sup>[14]</sup>

An excellent example of the design of coordination polymers or MOFs has been shown by Yaghi's group. The use of  $\text{Zn}(\text{NO}_3)_2 \cdot 4\text{H}_2\text{O}$  in a reaction with different rigid aromatic carboxylate ligands yielded to a well-controllable series of MOFs based on a network of a MOF-5 type (octahedral Zn-O-C clusters linked by organic ligands).<sup>[28]</sup> Tetrahedral oxo-centered nodes  $\text{Zn}_4\text{O}$  (Figure 1.3 b) are formed which are connected by the Lewis basic carboxylates and thus form a porous network (Figure 1.3a).

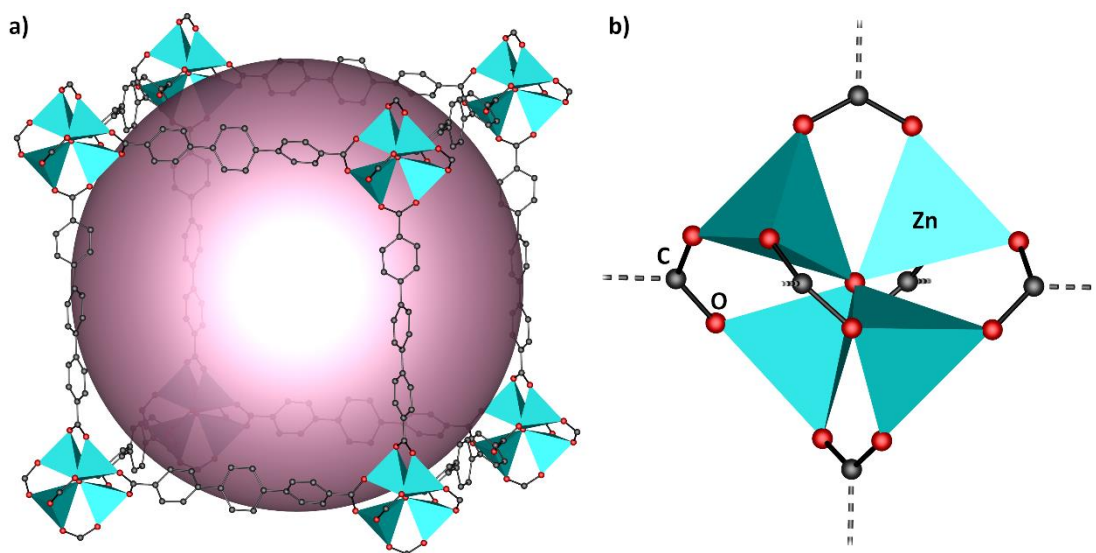


**Figure 1.3:** MOF of the group of Yaghi with a fixed-diameter pores of 28.8 Å (IRMOF-16). a) One pore of IRMOF-16, built up by eight  $\text{Zn}_4\text{O}$  nodes and twelve [1,1':4',1''-Terphenyl]-4,4''dicarboxylic acid ligands; b) Node of  $\text{Zn}_4\text{O}$  with connecting carboxylic ligands. The large violet sphere represents the largest van der Waals sphere that would fit in the cavities. <sup>[28]</sup> H atoms and minor parts of disorder are omitted for clarity.

### 1.3 Discrete Supramolecules

Host-guest chemistry also benefits from the use of directed metal-ligand bonding approach, as it can be used to control the shape and size of supramolecules as well as the inner cavity. This gives rise to a variety of metallasupramolecular arrangements with a wide range of applications, such as the stabilization of reactive intermediates in the inner void<sup>[29]</sup> or ability to act as a reaction vessel for specific organic reactions.<sup>[30]</sup>

Viewed from a more conceptual perspective, discrete supramolecular aggregates are obtained only from the combination of divergent and convergent building blocks.<sup>[4]</sup> Depending on the chosen type of building blocks, the results can be classified into i) clusters with a compact core which are surrounded by ligands and ii) supramolecules based on metal cations or polynuclear metal complexes (nodes) linked by organic ligands.<sup>[31]</sup> The former includes compounds of p-block and d-block metals. The p-block metal clusters, also called metalloids clusters, consist of compact cores held together by direct p-metal...p-metal bonding. The resulting shape of the metal core does differ from the bulk metal, and consists of one or more concentric polyhedral shells, sometimes with a central metal atom. Interestingly, this type of arrangements also creates so-called “naked metal atoms” on the surface of the cores; these atoms coordinate neither terminal nor bridging ligands.<sup>[31]</sup> Unprecedented metalloids are reported by the Schnöckel group with their aluminium clusters.<sup>[32]</sup> In 2004 the synthesis and characterisation of an  $[Al_{50}Cp^*_{12}]$  cluster was demonstrated and led to a metal core which is made of a  $\{Al_8\}$  fragment surrounded by further 42 aluminium atoms (Figure 1.4b). Twelve of these atoms are coordinated to the inserted Cp\* ligands, leaving 30 metal atoms “naked”. Another striking example of the metalloid type is the largest gallium cluster  $[Ga_{84}[N(SiMe_3)_2]_{20}]^{1-}$  obtained by Schnepf und Schnöckel in 2001. It consists of a  $Ga_2$  unit in the centre of the cluster core, surrounded by 64 “naked” metal atoms and 20  $N(SiMe_3)_2$  ligand bearing Ga atoms.<sup>[33]</sup>

Giant clusters with transition metal core (d-block metal core) have been studied since late 1960s. However, it was not until 1980 that the supposed first giant cluster with compact metal core could be characterized by Martinengo and Ciani due to the advancement in structure determination techniques.<sup>[34]</sup> The central core of such clusters is stabilized by the coordination of carbonyls, phosphines, thiolates, and alkynyls, which directly coordinate to “shell” metal atoms of the cluster.<sup>[35]</sup> Thus, giant transition metal clusters can be subdivided into core, shell, and ligand environment; the resulting functionality of the cluster depends on all three components.<sup>[36]</sup> The largest examples of transitional metal clusters are built up by coinage metals. Here, the group of Zheng with a  $[Ag_{374}(SPh-tBu)_{84}]$  cluster achieved a diameter of 4.4 nm (Figure 1.4a),<sup>[37]</sup> followed by

[Ag<sub>490</sub>S<sub>114</sub>(SC<sub>5</sub>H<sub>11</sub>)<sub>114</sub>] of the group of Fenske with a larger number of metal atoms in the cluster but a smaller cluster diameter of 3.8 nm.<sup>[38]</sup> In addition, the cluster of Dass with its Au<sub>279</sub> metal core is the heaviest transition metal cluster so far.<sup>[39]</sup>

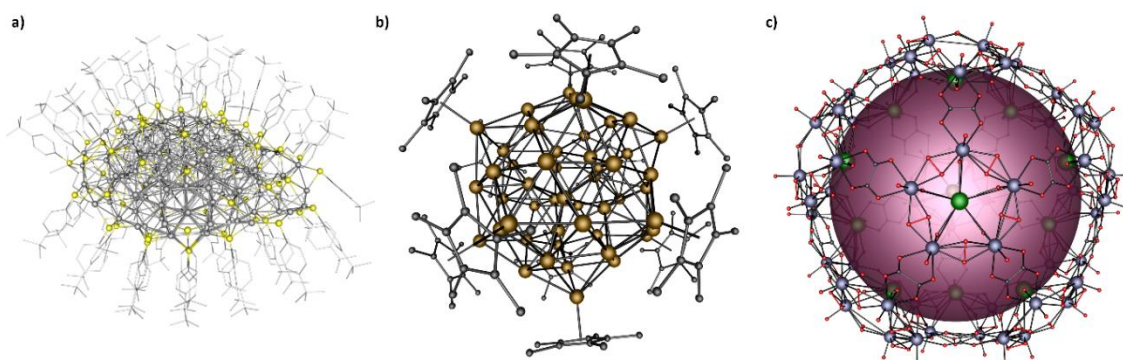


**Figure 1.4:** a) largest transitional metal cluster by Zheng [Ag<sub>374</sub>(SPh-*t*Bu)<sub>84</sub>] (Ag: grey, S: yellow, C: black);<sup>[37]</sup> b) Metalloid cluster by Schnöckel [Al<sub>50</sub>Cp\*<sub>12</sub>] (Al: brown);<sup>[32]</sup> c) Burns' actinide cluster with potassium atoms (green), uranium atoms (purple) and bridging oxalate ligands (O: red).<sup>[40–42]</sup> The large violet sphere represents the largest van der Waals spheres that would fit in the cavities. H atoms and minor parts of disorder are omitted for clarity.

In addition to the clusters presented above, there are also clusters with a metal-anionic core. These numerous giant clusters consist of a compact central core of metal cations surrounded by anionic terminal or bridging ligands such as oxides, hydroxides, chalcogenides, pnictogenides but also acetates, nitrates, and sulphates. The cationic or anionic feature is also expressed in the nomenclature of these clusters, which is why these compounds are called “metalates”. One of the most studied classes in this category are the polyoxometalates (POMs), which consist of metal oxide or hydroxide cores. Compared to the previously described clusters, the cores here can comprise d-/p-/f-block metals as well as actinoids.<sup>[31]</sup> In this category, besides the clusters with compact core, there are cores referred to as nanorods,<sup>[43]</sup> wheel-shaped,<sup>[44]</sup> peanut-like,<sup>[45]</sup> cube<sup>[46]</sup>- or dumbbell-shaped<sup>[47]</sup> clusters and many more.<sup>[31]</sup> The largest representative of POMs is obtained in Zhang's group, which consists of 52 titanium atoms arranged in an elongated nanorod and reaches an impressive outer dimension of 4.7 nm.<sup>[43]</sup> With the potassium salt of  $[\{(UO_2)(O_2)\}_{60}(C_2O_4)_{30}]^{60-}$  (Figure 1.4c) Burns' group discovered an amazing actinide cluster.<sup>[40–42]</sup> This anion consists of 60 uranium atoms linked by bridging peroxy- and oxalate-ligands to give spheres with fullerene topology (see below).

In addition to the clusters with a compacted core that have been described above, there are also spacer-based supramolecules. In this case the size and shape of the arrangement is not as much determined by compact metal-containing core as rather by the mutual arrangement of the metal centres, which are connected *via* various organic ligands (spacers). As this field of research is chemically very diversified, it can be difficult to assign certain assemblies to a precise subcategory. One such subcategory is giant oligomeric molecules and ions. Here oligomeric supramolecules,



mono- or polynuclear metal nodes are linked *via* spacers to form an oligomeric assemblies of various hybrid inorganic-organic compounds.<sup>[31]</sup> The size and shape of these oligomers depend on the components used. One approach toward this kind of arrangements is to use already large building blocks in order to obtain even larger assemblies afterwards. With this strategy, prefabricated POMs can become, for example, POM-based cages and polymers of cages or MOFs. This opens up a promising new pathway of functionalities in guest encapsulation, energy conversion, catalysis and many more.<sup>[31,48]</sup> Outstanding examples of supramolecules of this type are provided by Ding and Zheng with their giant polynuclear mixed-metal  $\text{Eu}^{3+}/\text{Co}^{2+}/\text{POM}$  complex based on eight  $\text{Eu}_2\text{W}_2$ -substituted building blocks which are linked by twelve citrate anions and seven  $\text{Co}^{2+}$  cations.<sup>[49]</sup>

Another, but much more deeply investigated subcategory of spacer-based supramolecules are giant hollow molecules or ions, so-called metal-organic polyhedra (MOP).<sup>[31]</sup> They have a wide range of applications and, with the right choice of building blocks, can reach an impressive size of 8 nm in diameter,<sup>[50,51]</sup> which can compete with biological macromolecules such as haemoglobin (~5 nm) and ovalbumin (~7 nm).<sup>[31,52]</sup> In contrast, the largest POM, the 'hedgehog' with a  $\{\text{Mo}_{368}\}$  metal core from the Müller group, reaches 6.3 nm.<sup>[53]</sup> In addition, to the unprecedented size of some MOPs, the cavities created in some supramolecules can be used for the encapsulation of guest molecules. In this way, Nitzschke's group was able to encapsulate testosterone or even strychnine in the cavity of their  $[\text{Ni}_3\text{Zn}_6(\text{C}_{68}\text{H}_{44}\text{N}_{12})_3(\text{C}_{42}\text{H}_{36}\text{N}_{12})_2]^{12+}$ .<sup>[54]</sup> Fujita's group used this approach to capture and stabilise the dinuclear ruthenium complex  $[(\eta^5\text{-indenyl})\text{Ru}(\text{CO})_2]_2$  in their  $[\{\text{Pd}(\text{en})\}_6(\text{C}_{18}\text{H}_{12}\text{N}_6)_4]^{12+}$ .<sup>[55]</sup>

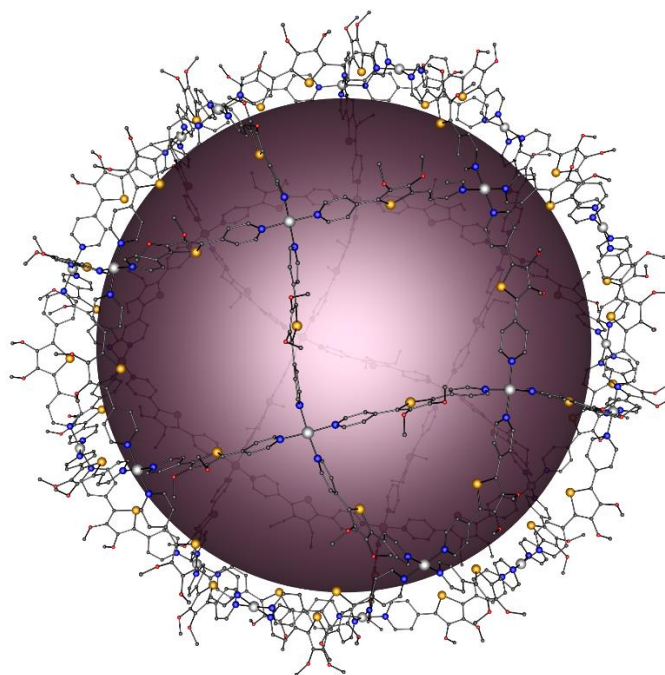


**Figure 1.5:** Largest MOP by the group of Fujita with diameter size of 8nm. (Se: orange, C: black, N: blue, Pd: grey, O: oxygen). The large violet sphere represents the largest van der Waals sphere that would fit in the cavities.<sup>[51]</sup> H atoms and minor parts of disorder are omitted for clarity.

For the sake of completeness, the covalently connected analogues to spherical molecules, the so-called fullerenes, should also be mentioned at this point. Alongside with graphite and diamond, they are the third allotropic modification of carbon, and the discovery was awarded with the Nobel prize for H. Kroto,<sup>[56]</sup> R. Curl<sup>[57]</sup> and R. Smalley<sup>[58]</sup> in 1996.<sup>[59]</sup> Fullerenes achieve a unique stability when they consist of 12 five-membered rings and an even number of six-membered rings (Euler's theorem), while the five membered rings must not touch each other (IPR: isolated pentagon rule).<sup>[60]</sup> Due to the intensive research on fullerenes, they have a wide range of applications nowadays including catalysis, sensing, capacitors, solar cells and fuel cells.<sup>[61]</sup> By far, the most famous representative of this class is the Buckminster fullerene  $I_h$ -C<sub>60</sub> (12 five- and 20 six-membered rings), which is also the smallest possible fullerene according to the rules above.<sup>[62]</sup> As in the giant molecules already mentioned, fullerenes are also capable to include other guest molecules or atoms. Researchers have already succeeded in encapsulating metal,<sup>[63]</sup> main group atoms (N<sup>[64,65]</sup> or P<sup>[66]</sup>), noble gas atoms<sup>[65,67]</sup> or even small molecules such as H<sub>2</sub>,<sup>[68]</sup> CO,<sup>[69]</sup> N<sub>2</sub><sup>[70]</sup> or H<sub>2</sub>O.<sup>[71]</sup> Most recently, a type of monometallic endohedral azafullerene (MEAF) has been synthesized by Yang and Popov. The discovery of La@C<sub>81</sub>N provides a new way to tune the electronic properties of metallic endohedral fullerenes through skeletal modifications of the carbon cage.<sup>[72]</sup>

## 1.4 Organometallic Building Blocks

All the examples of coordination-driven assemblies mentioned so far are mainly based on the strategy of Lewis acid acceptors (metal ions or clusters) and Lewis base donors (organic ligands). Already in the late 20<sup>th</sup> century, the groups of Stang,<sup>[12]</sup> Fujita<sup>[10]</sup> and Verkade<sup>[73]</sup> used chelating ligands to block two coordination sites of the metal atom, for example ethylenediamine or 1,3-bis(diphenylphosphino)propane. The obtained organometallic complex continues to act as an acceptor and coordinates the organic ligand 4,4'-bipyridine in these cases to build up macrocycles (Figure 1.6a). This approach can be further developed by introducing organic  $\pi$ -systems (arenes or cyclopentadienyls) to block three coordination sites on a metal ion, forcing the remaining coordination sites to convergent alignment. The blocking ligands act more as spectator ligands and are relatively inert to substitution reactions. In addition, they can be used to finetune the solubility and redox properties of the complexes.<sup>[74]</sup> The remaining three coordination sites opposite to the  $\pi$ -ligand can still be used for coordination of various N-, O-, S- or P-donor ligands. A macrocycle similar to Stang's (Figure 1.6a) has been obtained with blocking  $\pi$ -ligands by Tatsumi.<sup>[75]</sup> Here, an Ir complex with a blocking Cp\* ligand is used. A Cl atom and two pyrazine ligands bind to the free coordination sites of each Ir atom, which links four ligand complexes together to form a macrocycle (Figure 1.6b). Rauchfuss' group was able to demonstrate host-guest capability with the complex  $[\{\text{CpCo}(\text{CN})_3\}_4\{\text{Cp}^*\text{Rh}\}_4]$ .<sup>[76]</sup> In addition,  $\text{K}^+$ ,  $\text{Cs}^+$  and  $\text{Rb}^+$  ions, respectively, can be encapsulated in this cube out of a mixture of different organometallic building blocks, thus demonstrating the versatility of such building blocks.

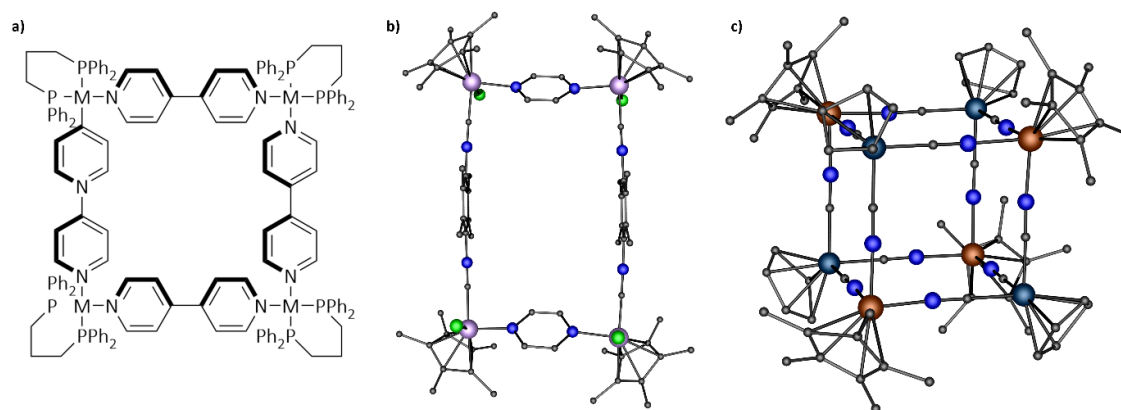


**Figure 1.6.** a) Tetranuclear macrocyclic  $\text{M} = \text{Pt}(\text{II})/\text{Pd}(\text{II})$  complex of Stang,<sup>[12]</sup> b) Cationic  $[\{\text{Cp}^*\text{IrCl}\}_4]$ -based macrocycle with different organic ligands,<sup>[75]</sup> c) Host-guest complex  $[\{\text{CpCo}(\text{CN})_3\}_4\{\text{Cp}^*\text{Rh}\}_4]$ .<sup>[76]</sup>

Compared to the organometallic aggregates described so far, which mainly consist of Lewis acid metal acceptor and organic or organometallic Lewis-base donor with N or O donor groups, our group focuses on supramolecular aggregates based on polyphosphorus ligands ( $\text{P}_n$ ). These  $\text{P}_n$  ligand complexes are composed of substituent-free P atoms that are solely bound to other P or metal

atoms, a central metal atom, and a blocking  $\pi$ -ligand. The lone pairs at the  $P_n$  ligand consequently make the organometallic building blocks to Lewis base donors (Figure 1.7). Cyclo- $P_n$  complexes have been known since 1978 after the pioneering work Sacconi, who characterized the first metal complex with an  $\eta^3$ - $P_3$  ligand of Co or Ni.<sup>[77]</sup> Since then, a wide variety of neutral  $P_n$  ligand complexes have been discovered<sup>[78–80]</sup> such as dinuclear complexes,<sup>[81]</sup> complexes with other metal<sup>[82]</sup> or Cp ligands,<sup>[83]</sup> or even  $E_n$  ligand complexes with the heavier homologues of group 15 elements ( $E = \text{As}, \text{Sb}, \text{Bi}$ ).<sup>[84]</sup> The complexes in Figure 1.7 are accessible from thermolysis or photolysis of white phosphorous ( $P_4$ ) with the respective carbonyl complex.<sup>[78–80]</sup>

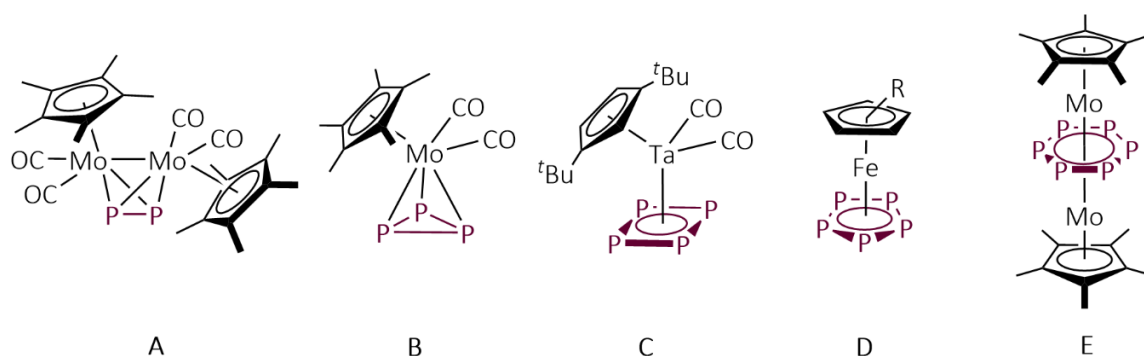


**Figure 1.7.** Selected examples of  $P_n$  ligand complexes ( $n = 2-6$ ). ( $\text{Cp}^R = \text{Me}_5$  (\*),  $\text{Me}_4\text{Et}$  (x),  $\text{Bn}_5$  (Bn),  $t\text{Bu}_2$  (’),  $t\text{Bu}_3$  (’’’))

## 1.5 Supramolecular Aggregates based on $P_n$ -ligand complexes

Since the  $P_n$  ligand complexes can act as Lewis bases due to one available free lone pair per P atom, supramolecular assemblies can also be created upon the addition of suitable metal salts. With regard to the early results with coinage metal salts and *cyclo*- $P_3$  ligand complexes by Peruzzini and Stoppioni,<sup>[85]</sup> our group was able to construct first coordination polymers based on  $[\{\text{CpMo}(\text{CO})_2\}_2\{\mu, \eta^{2:2}\text{-P}_2\}]$  (**A**) and  $\text{AgNO}_3$  or  $\text{CuBr}$ .<sup>[86]</sup> This work has been the foundation for numerous dimeric and 1D polymeric arrangements based on the  $P_2$ -ligand complex  $[\{\text{CpM}(\text{CO})_2\}_2\{\mu, \eta^{2:2}\text{-P}_2\}]$  (type **A**: Mo, Cr, W) and metal halide salts or weakly coordinating anions (WCAs).<sup>[87,88,89]</sup> Incorporation of the third component in form of an organic N donor ligand interestingly leads to further aggregation to 1D, 2D and 3D organometallic based coordination polymers (Figure 1.8a).<sup>[90,91]</sup> The self-assembly with  $P_n$  ligand complexes of type **B** and **E** is much less studied comparing to the other examples presented in Figure 1.7. For instance, reactions between  $[\text{CpM}(\text{CO})_2(\eta^3\text{-P}_3)]$  (**B**,  $M = \text{Cr}, \text{Mo}$ ) and  $\text{CuTEF}$  ( $\text{TEF} = \text{Al}(\text{OC}(\text{CF}_3)_3)_4$ ) lead to monomeric or dimeric coordination products, while 1D coordination polymers can be obtained with the heavier homologue  $\text{AgTEF}$  or  $\text{AgOTf}$  ( $\text{OTf} = \text{SO}_3\text{CF}_3$ ) and  $[\text{Cp}^R\text{Mo}(\text{CO})_2(\eta^3\text{-P}_3)]$  (**B**,  $\text{Cp}^R = \text{Cp}, \text{Cp}^*$ ) (Figure 1.8b).<sup>[89,92]</sup> Type **E** triple-decker complexes offer only planar coordination possibilities due to the

lack of  $P_n$  end-deck, which limits the dimensionality of the resulting supramolecular architecture from the outset. Nevertheless, some results could be achieved with the triple-decker complex  $[(CpMo)_2(\eta^6-P_6)]$ .<sup>[93]</sup> By reacting this complex with the copper(I) halides  $CuX$  ( $X = Br, I$ ), 2D coordination polymers could be obtained (Figure 1.8c).<sup>[94,95]</sup>

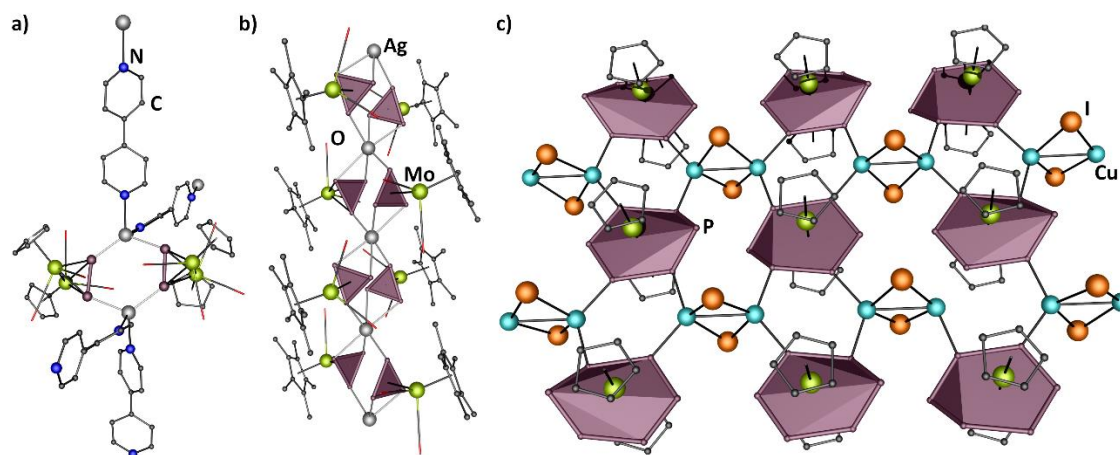


**Figure 1.8.** Selected examples of coordination polymers based on type **A**, **B** and **E**  $P_n$  ligand complexes. a) Section of 3D polymer based on  $[(CpMo(CO)_2)_2\{\mu,\eta^{2:2}-P_2\}]$ , AgTEF and bipyridyl linker.<sup>[90]</sup> b) Cationic 1D polymer chain of  $[Cp^*Mo(CO)_2(\eta^3-P_3)]$  and AgTEF.<sup>[92]</sup> c) 2D polymer based on  $[(CpMo)_2(\eta^6-P_6)]$  and  $CuI$ .<sup>[94]</sup> H atoms, TEF counterions and minor parts of disorder are omitted for clarity.

Cyclo- $P_4$  ligand complexes (type **C**) have been studied rather more closely so far than  $P_n$  ligand complexes of type **B** and **E**. Compared to type **B**, the enlarged end-deck of type **C** offers more coordination possibilities and thus a greater variation of coordination compounds. This was first demonstrated with the reaction of  $[(Cp^R Ta(CO)_2(\eta^4-P_4))]$  ( $Cp^R = Cp''$  (1,3- $C_5H_3tBu_2$ ),  $Cp'''$  (1,2,4- $C_5H_2tBu_3$ ), with  $CuX$  ( $X = Cl, Br, I$ ).<sup>[96,97]</sup> In addition to 2D polymers, spherical 0D supramolecules based on  $[(Cp'' Ta(CO)_2(\eta^4-P_4))]$  and Cu halides can also be obtained. An excellent example is the sphere  $[(Cp'' Ta(CO)_2(\eta^4-P_4))_6\{CuBr\}_8]$ , which is built up by typical six-membered rings of  $\{P_4Cu_2\}$ . This leads to an octahedral arrangement of the cyclo- $P_4$  units, whereby the copper atoms form a  $Cu_8$  cube (Figure 1.9a).<sup>[96]</sup>

Progress has also been made in the field of cyclo- $P_4$  ligand complexes by the change to heavy analogues of the coinage metals. Explicitly,  $AgSbF_6$  was used, as Ag halide salts are not accessible to their poor solubility in common solvents. With the Lewis base  $[(Cp'' Ta(CO)_2(\eta^4-P_4))]$  and the coinage metal salt with the weakly coordinating anion (WCA)  $AgSbF_6$ , a 1D polymer could be obtained. By adding to this system two more components, an organic ligand  $NC(CH_2)_7CN$  and a potential guest molecule ( $P_4Se_3$ ), a 2D polymer of linked cylindrical supramolecular nodes is obtained, with the guest molecule enclosed in the nodes (Figure 1.9b)).<sup>[95,98]</sup>

Of all the types shown above, the cyclo- $P_5$  ligand complex is the best-studied building block so far. By providing an additional P atom in the cyclo- $P_n$  end deck ligand complex, an even more

significant variation of coordination opportunities is compared to cyclo-P<sub>4</sub> ligand complexes (type C). In the case of complex ligands of type D, the number of coordination sites can only be restricted by the steric demand of the Cp<sup>R</sup> ligand of the Lewis base. The first steps in the self-assembly of supramolecular assemblies were made in this field with [Cp\*Fe(η<sup>5</sup>-P<sub>5</sub>)] (Cp\* = C<sub>5</sub>Me<sub>5</sub>) and Cu halide salts, which led not only to numerous multi-dimensional polymers but also to discrete spherical supramolecules.<sup>[95,99,100]</sup> The resulting chain polymers showed large gaps between the chains, caused by the embedding of diverse molecules such as solvents or even more unstable difficult guests like P<sub>4</sub> or As<sub>4</sub>. The incorporation of the last two showed a stabilisation effect on the otherwise unstable E<sub>4</sub> molecules, as the resulting polymer remains stable for several weeks even under the influence of air and light.<sup>[100]</sup>

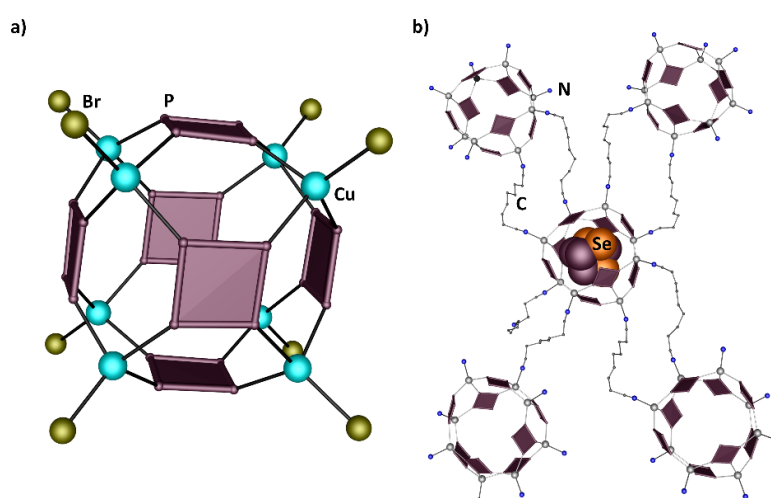


**Figure 1.9.** a)  $[(\text{Cp}^{\text{r}}\text{Ta}(\text{CO})_2(\eta^4\text{-P}_4))_6\{\text{CuBr}\}_8]$  supramolecule.<sup>[96]</sup> b) section of the 2D polymer of  $\{\text{P}_4\text{Se}_3\}@[\{(\text{Cp}^{\text{r}}\text{Ta}(\text{CO})_2(\eta^4\text{-P}_4))\text{Ag}\}\text{Ag}_8]^{8+}$ .<sup>[98]</sup> H atoms,  $\text{SbF}_6^-$  counterions, Cp<sup>r</sup> ligands, Ta atoms and minor parts of disorder are omitted for clarity.

In addition to these already impressive polymers, numerous pioneering spherical supramolecular aggregates have been obtained. Since most of these aggregates have a large cavity, it was logical to investigate the host-guest properties of these assemblies in more detail. Thus, in addition to one [Cp\*Fe(η<sup>5</sup>-P<sub>5</sub>)] (Figure 1.10b),<sup>[101]</sup> two [Cp\*Fe(η<sup>5</sup>-P<sub>5</sub>)] molecules could also be encapsulated in this assemblies.<sup>[102]</sup> The first host-sphere, with its 90 inorganic atoms, also bears a structural similarity to a C<sub>60</sub> Buckminsterfullerene.<sup>[101]</sup> Here, the cyclo-P<sub>5</sub> rings of the [Cp\*Fe(η<sup>5</sup>-P<sub>5</sub>)] are surrounded by six-membered rings of {P<sub>4</sub>Cu<sub>2</sub>}, leaving this framework without edge-linked pentagons and hence obeying the isolated-pentagon rule (IPR). In addition, other guest molecules such as C<sub>60</sub>,<sup>[103]</sup> Cp<sub>2</sub>Co<sup>[104]</sup> and other ones<sup>[105]</sup> could also be encapsulated into a pentaphosphaferrocene [Cp\*Fe(η<sup>5</sup>-P<sub>5</sub>)]-Cu halide based supramolecule. A noteworthy result here is also the encapsulation of the triple decker complex  $[(\text{CpCr})_2(\mu, \eta^{5:5}\text{-As}_5)]$ , because it does not form a usual supramolecular sphere, but rather a bowl (Figure 1.10c). Due to the opening of the host

molecule by the protruding guest, for the first time not only  $\pi$ -interactions between the guest and its own host molecule can take place, but also  $\pi$ - $\pi$ -interactions between the guest and the next host molecule, resulting in a 1D supramolecular assembly.<sup>[106]</sup>

Impressive results with copper halide salts were also repeated with pentaphosphaferrocene [ $\text{Cp}^{\text{R}}\text{Fe}(\eta^5\text{-P}_5)$ ] (type **D**) with sterically more demanding Cp ligands ( $\text{Cp}^{\text{R}} = \text{Cp}^{\text{Bn}} (\text{C}_5\text{Bn}_5)$ ,<sup>[107]</sup>  $\text{Cp}^{\text{BIG}} (\text{C}_5(4\text{-}n\text{BuC}_6\text{H}_4)_5)$ <sup>[108]</sup>). In both cases, the cavity is too small to contain larger molecules than solvent molecules. As described previously, sterically demanding  $\text{Cp}^{\text{R}}$  ligands can affect the coordination capabilities of a pentaphosphaferrocene. However, these  $\text{Cp}^{\text{R}}$  ligands also have a major influence on the solubility of the respective [ $\text{Cp}^{\text{R}}\text{Fe}(\eta^5\text{-P}_5)$ ] as well as on the solubility of the resulting aggregates, which can on the one hand enable characterisation in solution, and on the other hand, greatly complicate crystallisation.<sup>[95]</sup>

The next step in this field of research with type **D** building blocks was the use of weakly coordinating anions (WCAs). This made it possible not only to avoid coordinating solvents, which are usually needed to dissolve copper halide salts and in previous discussed structures usually blocked coordination sites on the copper atoms, but also the use of other Lewis bases besides pentaphosphaferrocenes. Initial successes were achieved with the coordinating CuOTf (OTf =  $\text{SO}_3\text{CF}_3$ ). In combination with [ $\text{Cp}^{\text{R}}\text{Fe}(\eta^5\text{-P}_5)$ ], a 2D polymer with [ $\text{Cp}^*\text{Fe}(\eta^5\text{-P}_5)$ ] and a supramolecular sphere based on [ $\text{Cp}^{\text{Bn}}\text{Fe}(\eta^5\text{-P}_5)$ ] were obtained (Figure 1.10a).<sup>[109]</sup> The most metal-deficient supramolecule based on cyclo- $\text{P}_n$  ligand complexes was formed with CuTEF (TEF =  $\text{Al}\{\text{OC}(\text{CF}_3)_3\}_4$ ) and [ $\text{Cp}^{\text{R}}\text{Fe}(\eta^5\text{-P}_5)$ ].<sup>[110]</sup> This cationic supersphere  $(\text{CH}_2\text{Cl}_2)@\{[\text{Cp}^{\text{R}}\text{Fe}(\eta^5: \eta^1, \eta^1\text{-P}_5)]\text{Cu}_8\}^{3+}$  consisting of eight metal atoms and 1,3-dicoordinated  $\text{P}_5$  ligands and stabilizing  $[\text{TEF}]^-$  anions, possesses twelve vacant positions which are potentially available for heterometal postmodifications.

Coordination polymers also could be obtained by using Cu salts with very large anions such as  $\text{TEF}^-$  and  $\text{FAI}^-$  ( $\text{FAI}\{\text{OC}_6\text{F}_{10}(\text{C}_6\text{F}_5)\}_3^-$ ).<sup>[87,89,111]</sup> For both  $\text{CuX}$  ( $X = \text{Cl}, \text{Br}$ ) and  $\text{CuWCA}$  ( $\text{WCA} = \text{BF}_4, \text{PF}_6$ ) a series of [ $\text{Cp}^*\text{Fe}(\eta^5\text{-P}_5)$ ]-based 1D and 2D polymers could be obtained by adding an organic ligand (4,4'-bipyridine, 1,2-di(4-pyridyl)ethylene, bis-(diphenylphosphinomethyl)phenylphosphine), respectively, as a third component.<sup>[112]</sup>

Besides numerous polymers and discrete supramolecules based on copper salts and [ $\text{Cp}^{\text{R}}\text{Fe}(\eta^5\text{-P}_5)$ ], only few has been done so far, the heavier coinage metal salts. Despite the linear or triangular coordination environment of gold, which significantly limits supramolecular chemistry with these salts, some coordination polymers could be obtained with different Au salts ( $[(\text{tht})\text{AuCl}]$ ,  $[(\text{tht})_2\text{Au}]\text{SbF}_6$ ) and [ $\text{Cp}^{\text{R}}\text{Fe}(\eta^5\text{-P}_5)$ ] ( $\text{Cp}^{\text{R}} = \text{Cp}^*$ ,  $\text{Cp}^x (\text{C}_5\text{Me}_4\text{Et})$ ,  $\text{Cp}^{\text{Bn}}$ ).<sup>[113]</sup>

In the past, only little research has been done with Ag salts in combination with cyclo- $\text{P}_5$  ligand complexes. The polymeric chains obtained show the manifold potential of  $\text{Ag}(\text{WCA})$  salts in

combination with pentaphosphaferrocenes.<sup>[114]</sup> The more flexible coordination environment of Ag could make a decisive difference in supramolecular chemistry, leading to an even larger variety of polymers and supramolecules compared to copper. Due to the insolubility of Ag halides in common solvents, this chemistry is inevitably limited to Ag(WCA) salts. Moreover, this would have advantage of dispensing with coordinating solvents and thus keeping coordination sites on the Ag atom open, which could increase both the coordination possibilities and the dimensionality of the possible resulting frameworks. At the same time, these free coordination sites open the possibility of using specifically coordinating organic ligands as connectors (linkers) in order to obtain even larger and more branched scaffolds. Since in previous work with Ag salts only a giant WCA (TEF) in combination with  $[\text{Cp}^*\text{Fe}(\eta^5\text{-P}_5)]$  was used, both the influence of smaller WCAs as with Cu and the influence of different sterically demanding pentaphosphaferrocenes on the possible formation of polymers and discrete supramolecular assemblies would be interesting to investigate.

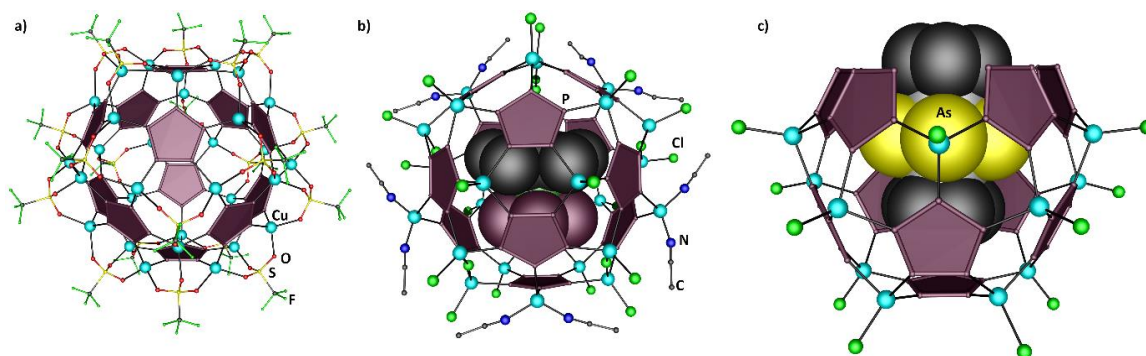


**Figure 1.10.** Selected examples with cyclo- $\text{P}_5$  ligand complexes of  $[\text{Cp}^R\text{Fe}(\eta^5\text{-P}_5)]$  and Cu salts. a)  $[(\text{Cp}^{\text{Bn}}\text{Fe}(\eta^5\text{-P}_5))_{12}\{\text{CuOTf}\}_{19.6}]$  sphere (OTf =  $\text{SO}_3\text{CF}_3$ );<sup>[109]</sup> b) Anionic supramolecule with  $[\text{Cp}^*\text{Fe}(\eta^5\text{-P}_5)]$  guest molecule encapsulated in  $[\text{Cu}(\text{MeCN})_4]^+[\{\text{Cp}^*\text{Fe}(\eta^5\text{-P}_5)\}_{12}\text{Cu}_{24}\text{Cl}_{25}(\text{MeCN})_8}]^-$ ;<sup>[101]</sup> c)  $[\text{Cp}^*\text{Fe}(\eta^5\text{-P}_5)]$ -based nano bowl  $[(\text{Cp}^*\text{Fe}(\eta^5\text{-P}_5))_{11}(\text{CuCl})_{15}]$  with  $[(\text{CpCr})_2(\mu, \eta^{5:5}\text{-As}_5)]$  guest.<sup>[106]</sup>

## 1.6 References

- [1] E. Fischer, *Ber. Dtsch. Chem. Ges.* **1894**, 27, 2985.
- [2] "The Nobel Prize in Chemistry 1987", can be found under <https://www.nobelprize.org/prizes/chemistry/1987/summary/>, **Nobel Prize Outreach AB 2023. Mon. 2023.**
- [3] a) J.-M. Lehn, *Proc. Natl. Acad. Sci. U.S.A.* **2002**, 99, 4763; b) J.-M. Lehn, *Angew. Chem. Int. Ed.* **1988**, 27, 89.
- [4] J. W. Steed, D. R. Turner, K. Wallace, *Core Concepts in Supramolecular Chemistry and Nanochemistry. From Supramolecules to Nanotechnology*, John Wiley & Sons, Chichester, **2007.**



- [5] J. W. Steed, D. R. Turner, K. J. Wallace, *Core concepts in supramolecular chemistry and nanochemistry*, Wiley, Hoboken, NJ, **2007**.
- [6] C. R. Calladine, *Understanding DNA. The Molecule and How It Works*, Elsevier Science & Technology, Saint Louis, **2004**.
- [7] R. Chakrabarty, P. S. Mukherjee, P. J. Stang, *Chem. Rev.* **2011**, *111*, 6810.
- [8] J. W. Steed, J. L. Atwood, *Supramolecular chemistry*, Wiley, Hoboken, NJ, Chichester, West Sussex, **2022**.
- [9] A. Y. Robin, K. M. Fromm, *Coord. Chem. Rev.* **2006**, *250*, 2127.
- [10] M. Fujita, J. Yazaki, K. Ogura, *J. Am. Chem. Soc.* **1990**, *112*, 5645.
- [11] M. Fujita, J. Yazaki, K. Ogura, *Chem. Lett.* **1991**, *20*, 1031.
- [12] P. J. Stang, D. H. Cao, *J. Am. Chem. Soc.* **1994**, *116*, 4981.
- [13] a) F. A. Cotton, C. Lin, C. A. Murillo, *Inorg. Chem.* **2001**, *40*, 478; b) F. A. Cotton, L. M. Daniels, C. Lin, C. A. Murillo, S.-Y. Yu, *Dalton Trans.* **2001**, 502; c) L. Yang, X. Cui, Z. Zhang, Q. Yang, Z. Bao, Q. Ren, H. Xing, *Angew. Chem. Int. Ed.* **2018**, *57*, 13145; d) E. Sharmin, F. Zafar in *Metal-Organic Frameworks* (Eds.: F. Zafar, E. Sharmin), IntechOpen, **2016**; e) Y. Suenaga, H. Konaka, T. Sugimoto, T. Kuroda-Sowa, M. Maekawa, M. Munakata, *Inorg. Chem. Commun.* **2003**, *6*, 389; f) M. C. Gimeno, P. G. Jones, A. Laguna, M. Laguna, R. Terroba, *Inorg. Chem.* **1994**, *33*, 3932; g) L. G. AbdulHalim, M. S. Bootharaju, Q. Tang, S. Del Gobbo, R. G. AbdulHalim, M. Eddaoudi, D. Jiang, O. M. Bakr, *J. Am. Chem. Soc.* **2015**, *137*, 11970; h) J. A. Hopkins, D. Lionetti, V. W. Day, J. D. Blakemore, *J. Organomet. Chem.* **2020**, *921*, 121294; i) Z. Ji, C. Trickett, X. Pei, O. M. Yaghi, *J. Am. Chem. Soc.* **2018**, *140*, 13618.
- [14] T. R. Cook, Y.-R. Zheng, P. J. Stang, *Chem. Rev.* **2013**, *113*, 734.
- [15] a) S. Kitagawa, R. Kitaura, S. Noro, *Angew. Chem. Int. Ed.* **2004**, *43*, 2334; b) U. Hofmann, *Angew. Chem.* **1963**, *75*, 1208.
- [16] H. J. Buser, D. Schwarzenbach, W. Petter, A. Ludi, *Inorg. Chem.* **1977**, *16*, 2704.
- [17] J. H. Rayner, H. M. Powell, *J. Chem. Soc.* **1952**, *0*, 319.
- [18] D. Farrusseng (Ed.) *Metal-organic frameworks. Applications from catalysis to gas storage*, Wiley-VCH, Weinheim, **2011**.
- [19] B. F. Hoskins, R. Robson, *J. Am. Chem. Soc.* **1989**, *111*, 5962.
- [20] M. Fujita, Y. J. Kwon, S. Washizu, K. Ogura, *J. Am. Chem. Soc.* **1994**, *116*, 1151.
- [21] M. Kondo, T. Yoshitomi, H. Matsuzaka, S. Kitagawa, K. Seki, *Angew. Chem. Int. Ed.* **1997**, *36*, 1725.
- [22] H. Li, M. Eddaoudi, T. L. Groy, O. M. Yaghi, *J. Am. Chem. Soc.* **1998**, *120*, 8571.
- [23] M. P. Suh, H. J. Park, T. K. Prasad, D.-W. Lim, *Chem. Rev.* **2012**, *112*, 782.

- [24] J.-R. Li, J. Sculley, H.-C. Zhou, *Chem. Rev.* **2012**, *112*, 869.
- [25] L. E. Kreno, K. Leong, O. K. Farha, M. Allendorf, R. P. van Duyne, J. T. Hupp, *Chem. Rev.* **2012**, *112*, 1105.
- [26] A. Corma, H. García, F. X. Llabrés i Xamena, *Chem. Rev.* **2010**, *110*, 4606.
- [27] a) C. Wang, T. Zhang, W. Lin, *Chem. Rev.* **2012**, *112*, 1084; b) P. Horcajada, R. Gref, T. Baati, P. K. Allan, G. Maurin, P. Couvreur, G. Férey, R. E. Morris, C. Serre, *Chem. Rev.* **2012**, *112*, 1232.
- [28] M. Eddaoudi, J. Kim, N. Rosi, D. Vodak, J. Wachter, M. O'Keeffe, O. M. Yaghi, *Science* **2002**, *295*, 469.
- [29] a) P. Mal, B. Breiner, K. Rissanen, J. R. Nitschke, *Science* **2009**, *324*, 1697; b) S. Sato, J. Iida, K. Suzuki, M. Kawano, T. Ozeki, M. Fujita, *Science* **2006**, *313*, 1273.
- [30] a) D. Zhang, T. K. Ronson, J. R. Nitschke, *Acc. Chem. Res.* **2018**, *51*, 2423; b) I. A. Bhat, A. Devaraj, P. Howlader, K.-W. Chi, P. S. Mukherjee, *Chem. Commun.* **2018**, *54*, 4814; c) C. M. Hong, R. G. Bergman, K. N. Raymond, F. D. Toste, *Acc. Chem. Res.* **2018**, *51*, 2447.
- [31] A. V. Virovets, E. Peresyphkina, M. Scheer, *Chem. Rev.* **2021**, *121*, 14485.
- [32] J. Vollet, J. R. Hartig, H. Schnöckel, *Angew. Chem. Int. Ed.* **2004**, *43*, 3186.
- [33] a) A. Schnepf, H. Schnöckel, *Angew. Chem. Int. Ed.* **2001**, *40*, 711; b) A. Schnepf, B. Jee, H. Schnöckel, E. Weckert, A. Meents, D. Lübbert, E. Herrling, B. Pilawa, *Inorg. Chem.* **2003**, *42*, 7731.
- [34] S. Martinengo, G. Ciani, A. Sironi, *J. Am. Chem. Soc.* **1980**, *102*, 7564.
- [35] a) L. L.-M. Zhang, T. C. W. Mak, *Angew. Chem. Int. Ed.* **2017**, *56*, 16228; b) Z. Lei, X.-K. Wan, S.-F. Yuan, Z.-J. Guan, Q.-M. Wang, *Acc. Chem. Res.* **2018**, *51*, 2465.
- [36] T. Higaki, Q. Li, M. Zhou, S. Zhao, Y. Li, S. Li, R. Jin, *Acc. Chem. Res.* **2018**, *51*, 2764.
- [37] H. Yang, Y. Wang, X. Chen, X. Zhao, L. Gu, H. Huang, J. Yan, C. Xu, G. Li, J. Wu et al., *Nat. Commun.* **2016**, *7*, 12809.
- [38] C. E. Anson, A. Eichhöfer, I. Issac, D. Fenske, O. Fuhr, P. Sevilano, C. Persau, D. Stalke, J. Zhang, *Angew. Chem. Int. Ed.* **2008**, *47*, 1326.
- [39] N. A. Sakthivel, S. Theivendran, V. Ganeshraj, A. G. Oliver, A. Dass, *J. Am. Chem. Soc.* **2017**, *139*, 15450.
- [40] J. Ling, C. M. Wallace, J. E. S. Szymanski, P. C. Burns, *Angew. Chem. Int. Ed.* **2010**, *49*, 7271.
- [41] J. Qiu, P. C. Burns, *Chem. Rev.* **2013**, *113*, 1097.
- [42] P. C. Burns, M. Nyman, *Dalton Trans.* **2018**, *47*, 5916.
- [43] W.-H. Fang, L. Zhang, J. Zhang, *J. Am. Chem. Soc.* **2016**, *138*, 7480.
- [44] M. Manoli, R. Inglis, M. J. Manos, V. Nastopoulos, W. Wernsdorfer, E. K. Brechin, A. J. Tasiopoulos, *Angew. Chem. Int. Ed.* **2011**, *50*, 4441.

- [45] N.-F. Li, Q.-F. Lin, X.-M. Luo, J.-P. Cao, Y. Xu, *Inorg. Chem.* **2019**, *58*, 10883.
- [46] X.-J. Kong, L.-S. Long, R.-B. Huang, L.-S. Zheng, T. D. Harris, Z. Zheng, *Chem. Commun.*, **2009**, 4354.
- [47] Y. Zhou, X.-Y. Zheng, J. Cai, Z.-F. Hong, Z.-H. Yan, X.-J. Kong, Y.-P. Ren, L.-S. Long, L.-S. Zheng, *Inorg. Chem.* **2017**, *56*, 2037.
- [48] S. Li, Y. Zhou, N. Ma, J. Zhang, Z. Zheng, C. Streb, X. Chen, *Angew. Chem. Int. Ed.* **2020**, *59*, 8537.
- [49] Q. Han, Z. Li, X. Liang, Y. Ding, S.-T. Zheng, *Inorg. Chem.* **2019**, *58*, 12534.
- [50] D. Fujita, Y. Ueda, S. Sato, H. Yokoyama, N. Mizuno, T. Kumasaka, M. Fujita, *Chem* **2016**, *1*, 91.
- [51] D. Fujita, Y. Ueda, S. Sato, N. Mizuno, T. Kumasaka, M. Fujita, *Nature* **2016**, *540*, 563.
- [52] H. P. Erickson, *Biol. Proced. Online* **2009**, *11*, 32.
- [53] A. Müller, E. Beckmann, H. Bögge, M. Schmidtman, A. Dress, *Angew. Chem. Int. Ed.* **2002**, *41*, 1162.
- [54] F. J. Rizzuto, J. P. Carpenter, J. R. Nitschke, *J. Am. Chem. Soc.* **2019**, *141*, 9087.
- [55] S. Horiuchi, T. Murase, M. Fujita, *J. Am. Chem. Soc.* **2011**, *133*, 12445.
- [56] H. Kroto, *Angew. Chem. Int. Ed.* **1997**, *36*, 1578.
- [57] R. F. Curl, *Angew. Chem. Int. Ed.* **1997**, *36*, 1566.
- [58] R. E. Smalley, *Angew. Chem. Int. Ed.* **1997**, *36*, 1594.
- [59] H. W. Kroto, J. R. Heath, S. C. O'Brien, R. F. Curl, R. E. Smalley, *Nature* **1985**, *318*, 162.
- [60] H. Li, H. Zhang, *Ars Math. Contemp.* **2018**, *15*, 487.
- [61] A. V. Baskar, M. R. Benzigar, S. N. Talapaneni, G. Singh, A. S. Karakoti, J. Yi, A. H. Al-Muhtaseb, K. Ariga, P. M. Ajayan, A. Vinu, *Adv. Funct. Mater.* **2022**, *32*, 2106924.
- [62] a) J. B. Howard, J. T. McKinnon, Y. Makarovskiy, A. L. Lafleur, M. E. Johnson, *Nature* **1991**, *352*, 139; b) W. Krätschmer, L. D. Lamb, K. Fostiropoulos, D. R. Huffman, *Nature* **1990**, *347*, 354.
- [63] a) C. R. Wang, T. Kai, T. Tomiyama, T. Yoshida, Y. Kobayashi, E. Nishibori, M. Takata, M. Sakata, H. Shinohara, *Nature* **2000**, *408*, 426; b) H. Shinohara, H. Yamaguchi, N. Hayashi, H. Sato, M. Ohkohchi, Y. Ando, Y. Saito, *J. Phys. Chem.* **1993**, *97*, 4259; c) J. R. Heath, S. C. O'Brien, Q. Zhang, Y. Liu, R. F. Curl, F. K. Tittel, R. E. Smalley, *J. Am. Chem. Soc.* **1985**, *107*, 7779.
- [64] a) M. T. Almeida, T. Pawlik, A. Weidinger, M. Höhne, R. Alcalá, J. Spaeth, *Phys. Rev. Lett.* **1996**, *77*, 1075; b) M. Maejima, H. Shiromaru, K. Kikuchi, T. Kodama, T. Wakabayashi, *Carbon Trends* **2022**, *9*, 100212.
- [65] Y. Morinaka, S. Sato, A. Wakamiya, H. Nikawa, N. Mizorogi, F. Tanabe, M. Murata, K. Komatsu, K. Furukawa, T. Kato et al., *Nat. Commun.* **2013**, *4*, 1554.
- [66] C. Knapp, N. Weiden, H. Kass, K.-P. Dinse, B. Pietzak, M. Waiblinger, A. Weidinger, *Mol. Phys.* **1998**, *95*, 999.

- [67] a) M. Saunders, H. A. Jiménez-Vázquez, R. J. Cross, R. J. Poreda, *Science* **1993**, *259*, 1428; b) A. Khong, H. A. Jiménez-Vázquez, M. Saunders, R. J. Cross, J. Laskin, T. Peres, C. Lifshitz, R. Strongin, A. B. Smith, *J. Am. Chem. Soc.* **1998**, *120*, 6380.
- [68] K. Komatsu, M. Murata, Y. Murata, *Science* **2005**, *307*, 238.
- [69] T. Peres, B. Cao, W. Cui, A. Khong, R. Cross, M. Saunders, C. Lifshitz, *Int. J. Mass Spectrom.* **2001**, *210-211*, 241.
- [70] T. Suetsuna, N. Dragoë, W. Harneit, A. Weidinger, H. Shimotani, S. Ito, H. Takagi, K. Kitazawa, *Chem. Eur. J.* **2002**, *8*, 5079.
- [71] K. Kurotobi, Y. Murata, *Science* **2011**, *333*, 613.
- [72] W. Xiang, X. Jiang, Y.-R. Yao, J. Xin, H. Jin, R. Guan, Q. Zhang, M. Chen, S.-Y. Xie, A. A. Popov et al., *J. Am. Chem. Soc.* **2022**, *144*, 21587.
- [73] P. Stricklen, J. Verkade, *J. Am. Chem. Soc.* **1983**, *105*, 2494.
- [74] K. Severin, *Chem. Commun.* **2006**, 3859.
- [75] H. Suzuki, Y. Yamamoto, N. Tajima, K. Tatsumi, *Chem. Commun.* **2000**, 1801.
- [76] M. Ramesh, T. B. Rauchfuss, *J. Organomet. Chem.* **2004**, *689*, 1425.
- [77] M. Di Vaira, C. A. Ghilardi, S. Midollini, L. Sacconi, *J. Am. Chem. Soc.* **1978**, *100*, 2550.
- [78] O. J. Scherer, H. Sitzmann, G. Wolmershäuser, *Angew. Chem. Int. Ed.* **1985**, *24*, 351.
- [79] O. J. Scherer, R. Winter, G. Wolmershuser, *Z. Anorg. Allg. Chem.* **1993**, *619*, 827.
- [80] O. J. Scherer, T. Brück, *Angew. Chem.* **1987**, *99*, 59.
- [81] O. J. Scherer, J. Schwalb, G. Wolmershäuser, W. Kaim, R. Gross, *Angew. Chem. Int. Ed.* **1986**, *25*, 363.
- [82] O. J. Scherer, T. Brück, G. Wolmershäuser, *Chem. Ber.* **1988**, *121*, 935.
- [83] O. J. Scherer, H. Sitzmann, G. Wolmershäuser, *J. Organomet. Chem.* **1984**, *268*, C9-C12.
- [84] a) O. J. Scherer, C. Blath, G. Wolmershäuser, *J. Organomet. Chem.* **1990**, *387*, C21-C24; b) J. R. Harper, A. L. Rheingold, *J. Organomet. Chem.* **1990**, *390*, c36-c38; c) W. Clegg, N. A. Compton, R. Errington, N. C. Norman, *Polyhedron* **1988**, *7*, 2239.
- [85] a) M. Di Vaira, M. P. Ehses, M. Peruzzini, P. Stoppioni, *Polyhedron* **1999**, *18*, 2331; b) M. Di Vaira, P. Stoppioni, M. Peruzzini, *Dalton Trans.* **1990**, 109.
- [86] J. Bai, E. Leiner, M. Scheer, *Angew. Chem. Int. Ed.* **2002**, *41*, 783.
- [87] M. Elsayed Moussa, M. Piesch, M. Fleischmann, A. Schreiner, M. Seidl, M. Scheer, *Dalton Trans.* **2018**, *47*, 16031.
- [88] a) M. Elsayed Moussa, P. A. Shelyganov, B. Wegley, M. Seidl, M. Scheer, *Eur. J. Inorg. Chem.* **2019**, *2019*, 4241; b) M. Elsayed Moussa, S. Welsch, L. J. Gregoriades, G. Balázs, M. Seidl, M. Scheer, *Eur. J. Inorg. Chem.* **2018**, *2018*, 1683; c) M. Elsayed Moussa, M. Fleischmann, E. V.

- Peresyphkina, L. Dütsch, M. Seidl, G. Balázs, M. Scheer, *Eur. J. Inorg. Chem.* **2017**, 2017, 3222; d) M. Scheer, L. J. Gregoriades, M. Zabel, J. Bai, I. Krossing, G. Brunklaus, H. Eckert, *Chem. Eur. J.* **2008**, 14, 282; e) M. Scheer, L. J. Gregoriades, M. Zabel, M. Sierka, L. Zhang, H. Eckert, *Eur. J. Inorg. Chem.* **2007**, 2007, 2775; f) M. Scheer, L. Gregoriades, J. Bai, M. Sierka, G. Brunklaus, H. Eckert, *Chem. Eur. J.* **2005**, 11, 2163.
- [89] M. Fleischmann, S. Welsch, E. V. Peresyphkina, A. V. Virovets, M. Scheer, *Chem. Eur. J.* **2015**, 21, 14332.
- [90] M. Elsayed Moussa, E. Peresyphkina, A. V. Virovets, D. Venus, G. Balázs, M. Scheer, *CrystEngComm* **2018**, 20, 7417.
- [91] a) M. E. Moussa, M. Seidl, G. Balázs, M. Zabel, A. V. Virovets, B. Attenberger, A. Schreiner, M. Scheer, *Chem. Eur. J.* **2017**, 23, 16199; b) M. Elsayed Moussa, B. Attenberger, M. Seidl, A. Schreiner, M. Scheer, *Eur. J. Inorg. Chem.* **2017**, 2017, 5616; c) M. Elsayed Moussa, B. Attenberger, E. V. Peresyphkina, M. Fleischmann, G. Balázs, M. Scheer, *Chem. Commun.* **2016**, 52, 10004; d) B. Attenberger, E. V. Peresyphkina, M. Scheer, *Inorg. Chem.* **2015**, 54, 7021; e) B. Attenberger, S. Welsch, M. Zabel, E. Peresyphkina, M. Scheer, *Angew. Chem. Int. Ed.* **2011**, 50, 11516.
- [92] L. J. Gregoriades, B. K. Wegley, M. Sierka, E. Brunner, C. Gröger, E. V. Peresyphkina, A. V. Virovets, M. Zabel, M. Scheer, *Chem.: Asian J.* **2009**, 4, 1578.
- [93] M. Fleischmann, F. Dielmann, L. J. Gregoriades, E. V. Peresyphkina, A. V. Virovets, S. Huber, A. Y. Timoshkin, G. Balázs, M. Scheer, *Angew. Chem. Int. Ed.* **2015**, 54, 13110.
- [94] C. Heindl, E. V. Peresyphkina, D. Lüdeker, G. Brunklaus, A. V. Virovets, M. Scheer, *Chem. Eur. J.* **2016**, 22, 2599.
- [95] E. Peresyphkina, A. Virovets, M. Scheer, *Coord. Chem. Rev.* **2021**, 446, 213995.
- [96] F. Dielmann, E. V. Peresyphkina, B. Krämer, F. Hastreiter, B. P. Johnson, M. Zabel, C. Heindl, M. Scheer, *Angew. Chem. Int. Ed.* **2016**, 55, 14833.
- [97] B. P. Johnson, F. Dielmann, G. Balázs, M. Sierka, M. Scheer, *Angew. Chem. Int. Ed.* **2006**, 45, 2473.
- [98] E. Peresyphkina, M. Bielmeier, A. Virovets, M. Scheer, *Chem. Sci.* **2020**, 11, 9067.
- [99] a) F. Dielmann, A. Schindler, S. Scheuermayer, J. Bai, R. Merkle, M. Zabel, A. V. Virovets, E. V. Peresyphkina, G. Brunklaus, H. Eckert et al., *Chem. Eur. J.* **2012**, 18, 1168; b) E. Peresyphkina, H. Brake, A. Virovets, M. Scheer, *CCDC 2038694: Experimental Crystal Structure Determination*, Cambridge Crystallographic Data Centre, **2020**; c) E. Peresyphkina, A. Kunz, C. Heindl, A. V. Virovets, M. Scheer, *CCDC 2038299: Experimental Crystal Structure Determination*, Cambridge

- Crystallographic Data Centre, **2020**; d) J. Bai, A. V. Virovets, M. Scheer, *Angew. Chem. Int. Ed.* **2002**, *41*, 1737.
- [100] C. Schwarzmaier, A. Schindler, C. Heindl, S. Scheuermayer, E. V. Peresytkina, A. V. Virovets, M. Neumeier, R. Gschwind, M. Scheer, *Angew. Chem. Int. Ed.* **2013**, *52*, 10896.
- [101] J. Bai, A. V. Virovets, M. Scheer, *Science* **2003**, *300*, 781.
- [102] S. Welsch, C. Gröger, M. Sierka, M. Scheer, *Angew. Chem. Int. Ed.* **2011**, *50*, 1435.
- [103] M. Scheer, A. Schindler, R. Merkle, B. P. Johnson, M. Linseis, R. Winter, C. E. Anson, A. V. Virovets, *J. Am. Chem. Soc.* **2007**, *129*, 13386.
- [104] E. Peresytkina, C. Heindl, A. Virovets, H. Brake, E. Mädl, M. Scheer, *Chem. Eur. J.* **2018**, *24*, 2503.
- [105] a) A. Schindler, C. Heindl, G. Balázs, C. Gröger, A. V. Virovets, E. V. Peresytkina, M. Scheer, *Chem. Eur. J.* **2012**, *18*, 829; b) E. V. Peresytkina, C. Heindl, A. Schindler, M. Bodensteiner, A. V. Virovets, M. Scheer, *Z. Kristallogr. Cryst. Mater.* **2014**, *229*, 735.
- [106] H. Brake, E. Peresytkina, C. Heindl, A. V. Virovets, W. Kremer, M. Scheer, *Chem. Sci.* **2019**, *10*, 2940.
- [107] a) F. Dielmann, M. Fleischmann, C. Heindl, E. V. Peresytkina, A. V. Virovets, R. M. Gschwind, M. Scheer, *Chem. Eur. J.* **2015**, *21*, 6208; b) F. Dielmann, C. Heindl, F. Hastreiter, E. V. Peresytkina, A. V. Virovets, R. M. Gschwind, M. Scheer, *Angew. Chem. Int. Ed.* **2014**, *53*, 13605.
- [108] S. Heindl, E. Peresytkina, J. Sutter, M. Scheer, *Angew. Chem. Int. Ed.* **2015**, *54*, 13431.
- [109] C. Heindl, E. Peresytkina, A. V. Virovets, I. S. Bushmarinov, M. G. Medvedev, B. Krämer, B. Dittrich, M. Scheer, *Angew. Chem. Int. Ed.* **2017**, *56*, 13237.
- [110] J. Schiller, E. Peresytkina, A. V. Virovets, M. Scheer, *Angew. Chem. Int. Ed.* **2020**, *59*, 13647.
- [111] C. Heindl, S. Heindl, D. Lüdeker, G. Brunklaus, W. Kremer, M. Scheer, *Inorg. Chim. Acta* **2014**, *422*, 218.
- [112] a) M. E. Moussa, S. Welsch, M. Lochner, E. V. Peresytkina, A. V. Virovets, M. Scheer, *Eur. J. Inorg. Chem.* **2018**, *2018*, 2689; b) M. Elsayed Moussa, B. Attenberger, E. V. Peresytkina, M. Scheer, *Dalton Trans.* **2018**, *47*, 1014.
- [113] H. Brake, E. Peresytkina, A. V. Virovets, W. Kremer, C. Klimas, C. Schwarzmaier, M. Scheer, *Inorg. Chem.* **2021**, *60*, 6027.
- [114] M. Scheer, L. J. Gregoriades, A. V. Virovets, W. Kunz, R. Neueder, I. Krossing, *Angew. Chem. Int. Ed.* **2006**, *45*, 5689.

## 2. Research Objectives

As demonstrated in the introduction,  $P_n$  ligand complexes as Lewis bases are versatile building blocks in combination with Lewis acidic metal salts in supramolecular chemistry. Especially with  $[\text{Cp}^R\text{Fe}(\eta^5\text{-P}_5)]$  in combination with copper salts, a wide variation of different polymeric assemblies and discrete nano-sized spherical aggregates could be obtained in the past. Emerging challenges such as solubilities of building blocks or assemblies, selectivity of self-assembly reactions, etc. were faced with different combinations of copper salts  $\text{CuX}$  ( $X = \text{Cl}, \text{Br}, \text{I}, \text{SO}_3\text{CF}_3$ ) and various sterically demanding Cp ligands of  $[\text{Cp}^R\text{Fe}(\eta^5\text{-P}_5)]$ ; the latter having a major influence on the solubility of the assemblies. First results with  $[\text{Cp}^*\text{Fe}(\eta^5\text{-P}_5)]$  and  $\text{Ag}(\text{WCA})$  demonstrated the better accessibility of Ag atoms in supramolecular arrangements due to their more flexible coordination environment compared to copper. Due to the insolubility of silver halides salts in common organic solvents, the use of  $\text{Ag}(\text{WCA})$  salts in combination with  $[\text{Cp}^R\text{Fe}(\eta^5\text{-P}_5)]$  represent, the most promising approach for generating silver-based supramolecules by self-assembly aggregation. Hence, an objective of this thesis is:

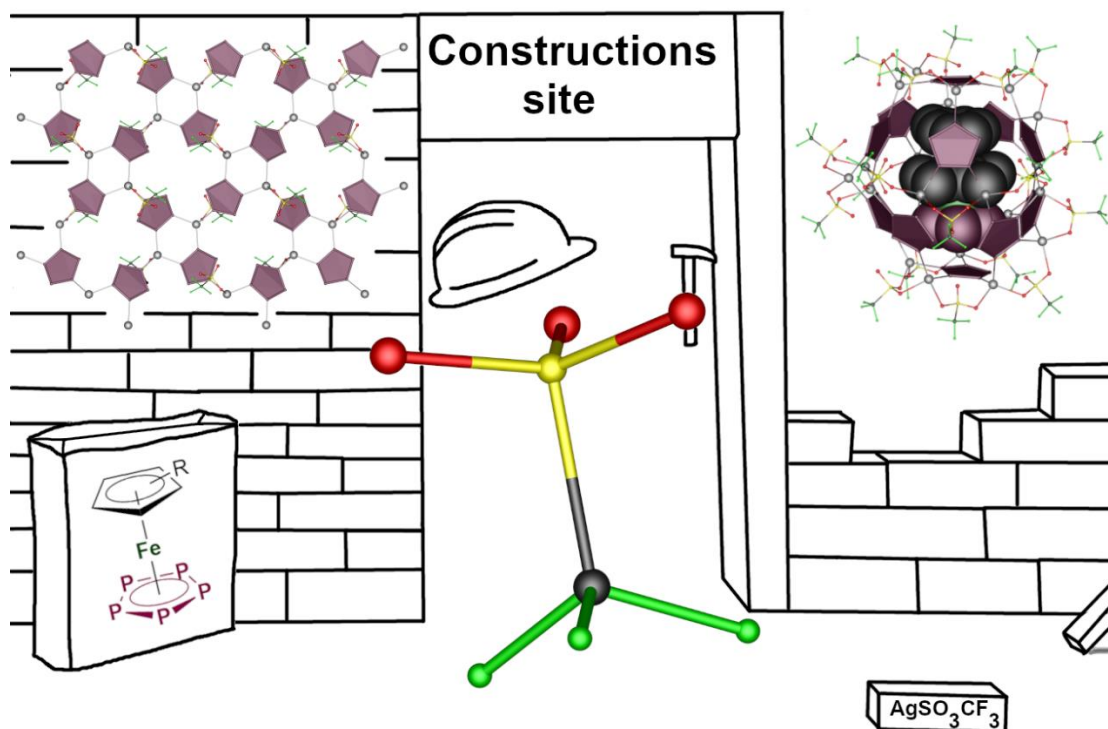
- Effective transfer of the previous  $\text{Cu}(\text{SO}_3\text{CF}_3)$  systems to  $\text{Ag}(\text{SO}_3\text{CF}_3)$  with subsequent investigation of the coordination behaviour to different sterically demanding Cp ligands of  $[\text{Cp}^R\text{Fe}(\eta^5\text{-P}_5)]$  ( $\text{Cp}^R = \text{Cp}^*, \text{Cp}^x, \text{Cp}^{\prime\prime}, \text{Cp}^{\text{Bn}}$ ).

Using  $\text{Cu}(\text{WCA})$  ( $\text{BF}_4^-$ ,  $\text{PF}_6^-$ ) salts,  $[\text{Cp}^*\text{Fe}(\eta^5\text{-P}_5)]$  and pyridine based rigid organic ligands as third component, polymers could already be obtained using self-assembly approaches. The possible absence of coordinating solvents in  $\text{Ag}(\text{WCA})$  salts compared to  $\text{Cu}(\text{WCA})$  leaves possible coordination sites at the Ag atom open, allowing an enhanced versatility of the self-assembly process. The free lone pair at the N in pyridine based-ligands has limited coordination possibilities due to the steric demand of the aromatic residue. The introduction of sterically less demanding N-based functional groups is therefore the logical step to obtain the most versatile self-assembly system in supramolecular chemistry. Hence, further objectives of this thesis are:

- Establishing flexible aliphatic dinitrile ligands  $\text{NC}(\text{CH}_2)_x\text{CN}$  ( $x = 1\text{-}10$ ) as third component to a  $[\text{Cp}^R\text{Fe}(\eta^5\text{-P}_5)]$  ( $\text{Cp}^R: \text{Cp}^*, \text{Cp}^{\text{Bn}}$ ) and  $\text{AgSbF}_6$  based three-component self-assembly system,
- Investigation of the influence of rigid aromatic dinitrile ligands on a three-component self-assembly system based on  $[\text{Cp}^R\text{Fe}(\eta^5\text{-P}_5)]$  ( $\text{Cp}^R: \text{Cp}^*, \text{Cp}^{\prime\prime}, \text{Cp}^{\text{Bn}}$ ),  $\text{AgSbF}_6$  and *o/m/p*- $(\text{NC})_2\text{C}_6\text{H}_4$ ,
- Investigation of the coordination behaviour of  $[\text{Cp}^{\text{Bn}}\text{Fe}(\eta^5\text{-P}_5)]$  with  $\text{AgSbF}_6$  and *p*- $(\text{NC})(\text{C}_6\text{H}_4)\text{Cl}$  ligands, as well as the use of coordinating solvents in the self-assembly system of this building blocks.

### 3. Scaffold-constructing role of triflate: Polymeric Complexes and Discrete Supramolecules based on Pentaphosphaferrocene and Silver

Kevin Grill, Eugenia Peresykina, Barbara Hiltl, Claudia Heintl, Alexander V. Virovets, Werner Kremer, Jan Hilgert, Wolfgang Tremel and Manfred Scheer



**Abstract:** After having successfully employed the self-assembly system of pentaphosphaferrocenes  $[\text{Cp}^R\text{Fe}(\eta^5\text{-P}_5)]$  ( $\text{Cp}^* = \eta^5\text{-C}_5\text{Me}_5$  (**A**),  $\text{Cp}^{\text{Bn}} = \eta^5\text{-C}_5(\text{CH}_2\text{C}_6\text{H}_5)_5$  (**D**) and  $\text{Cu}(\text{SO}_3\text{CF}_3)$ , showing the decisive scaffold constructing role of  $\text{SO}_3\text{CF}_3^-$  this concept is now extended to  $\text{Ag}(\text{SO}_3\text{CF}_3)$ . Furthermore, various sterically demanding pentaphosphaferrocenes were used to gain important insight into their influence on the self-assembly. For this, we performed one-pot reactions with  $[\text{Cp}^R\text{Fe}(\eta^5\text{-P}_5)]$  ( $\text{Cp}^*$  (**A**),  $\text{Cp}^x = \eta^5\text{-C}_5\text{Me}_4\text{Et}$  (**B**),  $\text{Cp}'' = \eta^5\text{-C}_5\text{H}_3(\text{tBu})_2$  (**C**),  $\text{Cp}^{\text{Bn}}$  (**D**)) and  $\text{Ag}(\text{SO}_3\text{CF}_3)$  as a part of systematic study to obtain a series of unprecedented polymers and discrete, host-guest capable spherical supramolecules with isomeric Ag cores. All compounds were characterized by NMR spectroscopy, mass spectrometry, elemental analysis, and single-crystal X-ray diffraction.



### 3.1 Introduction

Over the last few decades, diverse methods to create discrete spherical aggregates targeting different purposes have emerged from the fast-growing field of supramolecular chemistry. Regarding discrete atomic precise clusters as a link between metal atoms and nanoparticles,<sup>[1]</sup> especially for Ag and Cu many different types are known, the metal core itself being protected from aggregation by thiolates, phosphines or alkynyls.<sup>[2]</sup> For instance, the Ag<sub>374</sub> core with its 4.4 nm molecular size by the group of Zheng is by far the largest structurally characterized metal nanocluster.<sup>[3]</sup> Another class of discrete spheres aims at characteristics and applications, which go along with properties of hollow spheres being able to act as hosts for smaller molecules. With an adequate inner void these host molecules can be suitable as reaction vessels,<sup>[4]</sup> molecular container stabilizing labile compounds<sup>[5]</sup> or accelerators for catalytic reactions<sup>[6]</sup>. These self-assembled supramolecular aggregates often show highly symmetric polyhedral scaffolds, built up by various metal cations (Co,<sup>[7,8]</sup> Pd,<sup>[9]</sup> Pt,<sup>[10]</sup> Cu,<sup>[8,11,12]</sup> Ag,<sup>[11,13,14]</sup> Zn,<sup>[15]</sup> Cd<sup>[8,16]</sup>) as vertices and mainly polytopic organic linkers as edges or faces.

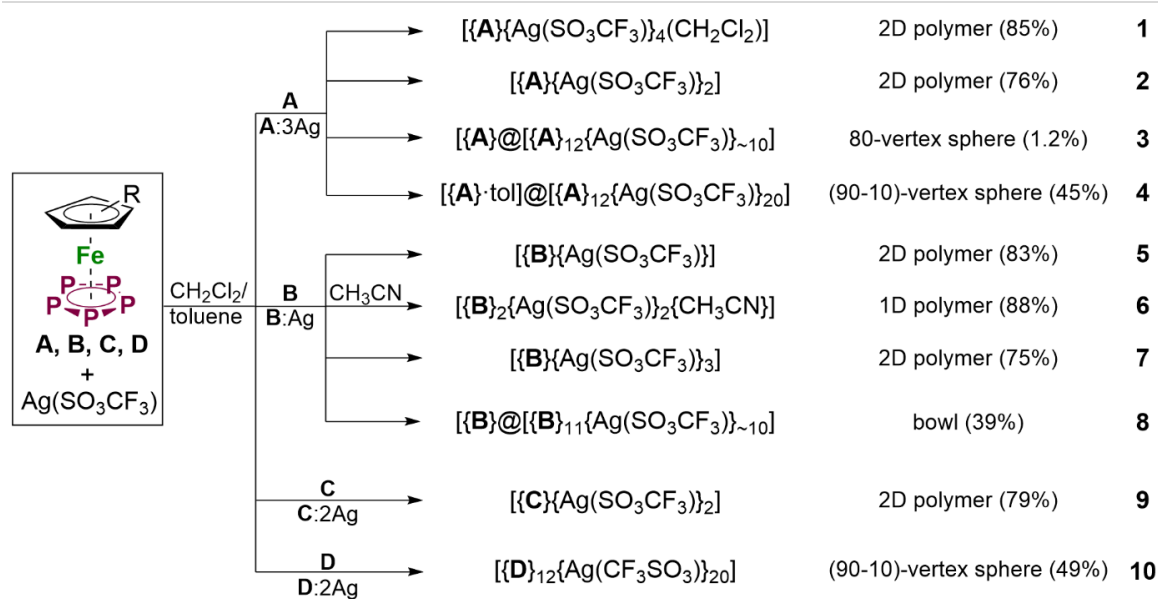
Notably, while there is a huge number of Pd-, Pt- and Cu- containing spherical supramolecular cages, examples involving Ag<sup>+</sup> are still very rare in contrast to the abundance of Ag-containing spherical clusters without an accessible inner void. A combination of both classes for self-assembled supramolecular spheres was reported by the group of Sun featuring as Ag<sub>180</sub> buckyball-like cage as a metal core protected by *i*PrS<sup>-</sup> and SO<sub>3</sub>CH<sub>3</sub><sup>-</sup>.<sup>[14]</sup> Thereby, in contrast to many cluster compounds, it exhibits an icosahedral symmetry as well as an inner cavity like other cage compounds, which in this case is occupied by solvent molecules.

Previously, we succeeded in synthesizing huge nano-scaled hollow self-assembled aggregates,<sup>[17,18,19,20]</sup> partly exhibiting fullerene-topology,<sup>[21–23]</sup> by using a combination of five-fold symmetric organometallic pentaphosphaferrocenes and Cu salts (halides, triflate, teflonate) as building blocks.<sup>[19,21,24,25]</sup> Possessing inner cavity, these aggregates can act as versatile hosts for small guest molecules and even stabilize labile molecules like P<sub>4</sub> and As<sub>4</sub>.<sup>[26]</sup> Although pentaphosphaferrocene-based supramolecules are not limited to Cu halides, they form expanded range of compounds compared to those based on other metal salts. However, by using triflate anions with their coordination ability and spatial requirements,<sup>[25]</sup> besides a 2D coordination polymer  $[\{\mathbf{A}\}\{\text{Cu}(\text{SO}_3\text{CF}_3)\}]_n$  with terminal triflate anions, the supramolecule (CH<sub>2</sub>Cl<sub>2</sub>)<sub>1.4</sub>@ $[\{\mathbf{D}\}]_{12}\{\text{Cu}(\text{CF}_3\text{SO}_3)\}_{19.6}$  was obtained which possessed two enantiomeric forms with *D*<sub>2</sub> and *D*<sub>5</sub> point symmetry. The supramolecule revealed the truly scaffold-constructing role of triflate anions and showed their potential for constructing new supramolecular cores. In this case the

spherical scaffold gets expanded by the insertion of bridging triflate ligands in between the tetrahedrally coordinated copper cations.

This fact inspired us to use the scaffold-constructing behaviour of triflate anion in the self-assembly system containing another coinage metal. Gold, as a two-coordinate cation, has linear or planar coordination geometry around the metal centre and in this case would spatially restrict the system from the beginning.<sup>[27]</sup> Silver, however, has larger coordination numbers than gold and being able to adopt various coordination environments compared to copper. This makes  $\text{Ag}(\text{SO}_3\text{CF}_3)$  the best candidate for further investigation taking into account the fact that its ability to form supramolecular scaffolds with polyphosphorus ligands have already been demonstrated.<sup>[28,29]</sup>

In the following, we report on a systematic study and the successful application of  $\text{AgSO}_3\text{CF}_3$  ( $\text{AgOTf}$ ) in the coordination chemistry of  $[\text{Cp}^R\text{Fe}(\eta^5\text{-P}_5)]$  (**A**:  $\text{Cp}^* = (\eta^5\text{-C}_5\text{Me}_5)$ , **B**:  $\text{Cp}^x = (\eta^5\text{-C}_5\text{Me}_4\text{Et})$ , **C**:  $\text{Cp}^R = \text{Cp}'' (\eta^5\text{-C}_5\text{H}_3\text{tBu}_2\text{-1,3})$ , **D**:  $\text{Cp}^{\text{Bn}} = (\eta^5\text{-C}_5(\text{CH}_2\text{C}_6\text{H}_5)_5)$ ), yielding in the self-assembly of both coordination polymers and spherical host-guest ready supramolecular complexes. In addition to the pentaphosphaferrocenes **A** and **D** already used in the self-assembly reactions with  $\text{CuOTf}$ , further members of the family with different steric bulk were introduced to compare with previous results of  $\text{Ag}(\text{I})$  coordination and to gain a better insight into the influence of steric demand of *cyclo*- $\text{P}_5$  complexes on self-assembly pathways. In addition to the characterization by X-ray crystallography, NMR spectroscopy and mass spectrometry, the remarkable stability of some herein described spherical aggregates in solution enabled DOSY NMR spectroscopy and the sample preparation for subsequent investigation by transmission electron microscopy (TEM).



R: **A**: Cp\* =  $\eta^5\text{-C}_5\text{Me}_5$ ; **B**: Cp<sup>x</sup> =  $\eta^5\text{-C}_5\text{Me}_4\text{Et}$ ; **C**: Cp'' =  $\eta^5\text{-C}_5(\text{tBu})_2$ ; **D**: Cp<sup>Bn</sup> =  $\eta^5\text{-C}_5(\text{CH}_2\text{C}_6\text{H}_5)_5$

**Scheme 3.1.** One-pot self-assembly reactions of **A**, **B**, **C** and **D** with  $\text{Ag}(\text{SO}_3\text{CF}_3)$ . Isolated crystalline yields are given in parenthesis.

## 3.2 Results and Discussion

### Coordination polymers based on $[\text{Cp}^*\text{Fe}(\eta^5\text{-P}_5)]$ (**A**), $[\text{Cp}^x\text{Fe}(\eta^5\text{-P}_5)]$ (**B**) or $[\text{Cp}''\text{Fe}(\eta^5\text{-P}_5)]$ (**C**)

For all reactions, a suspension of  $\text{AgOTf}$  in  $\text{CH}_2\text{Cl}_2$  was first stirred over 12h at room temperature, preheated to  $40^\circ\text{C}$  and sonicated for 2h. Afterwards a toluene solution of the corresponding  $\text{P}_5$  ligand complex (**A-C**) was carefully layered over the suspension in  $\text{CH}_2\text{Cl}_2$ . The one-pot reactions were controlled by using molar ratios and different concentrations in the respective layers (Scheme 3.1). In a reaction of **A** with  $\text{AgOTf}$  in a ratio **A**:3 and  $\text{AgOTf}$  concentration of 15 mmol/L, the 2D polymer  $[\{\mathbf{A}\}\{\text{Ag}(\text{SO}_3\text{CF}_3)\}_4(\text{CH}_2\text{Cl}_2)]$  (**1**: yellow plates, 85%) was isolated. A further increase of the  $\text{AgOTf}$  concentration to 44 mmol/L leads to the formation of the 2D polymer  $[\{\mathbf{A}\}\{\text{Ag}(\text{SO}_3\text{CF}_3)\}_2]$  (**2**: yellow plates, 76%). For complex **B**, with a **B**:3Ag ratio no crystalline product was observed despite numerous attempts. Using an equimolar ratio and a concentration of 7 mmol/L resulted in the 2D polymer  $[\{\mathbf{B}\}\{\text{Ag}(\text{SO}_3\text{CF}_3)\}]_n$  (**5**: brown prisms, 83%). To synthesize of the 1D polymer  $[\{\mathbf{B}\}_2\{\text{Ag}(\text{SO}_3\text{CF}_3)\}_2\{\text{CH}_3\text{CN}\}]_n$  (**6**: brown needles, 88%),  $\text{Ag}(\text{SO}_3\text{CF}_3)$  was first dissolved in a mixture of  $\text{CH}_2\text{Cl}_2$  and  $\text{CH}_3\text{CN}$  (9:1) to give 9 mmol/L solution that was then layered with a toluene solution of **B** to obtain an equimolar ratio of **B**:Ag. After complete diffusion the mother liquor was halved *via* evaporation in vacuum and afterwards layered with hexane, whereby **6** is crystallized after a week. Under more diluted conditions with a concentration of **B** of 5 mmol/L and a ratio of **B**:1 the 2D polymer  $[\{\mathbf{B}\}\{\text{Ag}(\text{SO}_3\text{CF}_3)\}_3]_n$  (**7**: yellow needles, 75%) in 1:1 ratio is accessible. No crystalline product was observed for complex **C** in an equimolar ratio despite many attempts were made. In the

reaction of **C** and AgOTf in a ratio of 1:2 and a AgOTf concentration of 0.09 mmol/L, a 2D polymer  $[\text{C}\{\text{Ag}(\text{SO}_3\text{CF}_3)\}_2]_n$  (**9**; yellow needles, 79%) was the only obtainable product.

According to single crystal X-ray structure analysis, the 2D polymeric structure of **1** is built up by chains of  $[\{\text{A}\}\{\text{Ag}(\text{SO}_3\text{CF}_3)\}_4(\text{CH}_2\text{Cl}_2)]_n$  (Figure 3.1a). These chains are formed by pentacoordinated  $\text{P}_5$  ligands, whereby only two out of five Ag atoms (in 1,3-positions of the  $\text{P}_5$  ligand) coordinate directly to the next  $\text{P}_5$  ligand and therefore joins them.

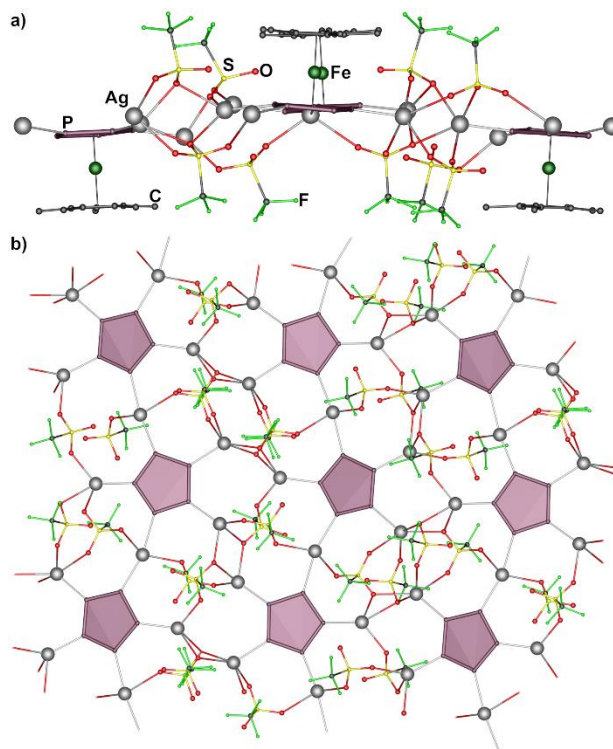


**Figure 3.1.** A section of the 2D polymer of **1**. a) 2D network in **1** with interconnecting OTf anions. b) 2D network. H atoms are omitted for clarity.

The chains formed are connected by coordinated silver triflate chains. In the overall 2D structure, every four neighbouring *cyclo*- $\text{P}_5$  fragments encompass four interchain silver cations connected to four triflate anions (Figure 3.1b). At that each interchain Ag atom links one *cyclo*- $\text{P}_5$  ligand and three OTf anions. In addition to tridentate and bidentate OTf anions that bind different Ag cations *via* their O donor atoms, there are also end-on coordinated OTf anions in which one O atom binds two different Ag atoms.

The 2D network of **2** consists of  $[\{\text{A}\}\{\text{Ag}(\text{SO}_3\text{CF}_3)\}_2]$  (Figure 3.2b) repeating units whereby the *cyclo*- $\text{P}_5$  ligands show a 1,2,4-coordination mode to the Ag atoms, which in turn possess a tetrahedral environment. The coordination of metal cations to the *cyclo*- $\text{P}_5$  ligands gives six-membered  $\{\text{Ag}_2\text{P}_4\}$  rings further connected by ligands; a structural motif typical for pentaphosphaferrocene coordination complexes.<sup>[30]</sup> The OTf anions act in equal parts as  $\mu_2$ - or  $\mu_3$ -bridging ligands *via* coordination of two oxygen atoms to Ag atoms. This creates four-membered

{Ag<sub>2</sub>O<sub>2</sub>}, six-membered {Ag<sub>2</sub>P<sub>4</sub>} and eight-membered {Ag<sub>2</sub>O<sub>4</sub>S<sub>2</sub>} rings which build up the 2D network pattern. Noteworthy, toluene molecules are intercalated between the 2D layers. The almost parallel arrangement (0.6°) and the short interplanar distances (3.58 - 3.62 Å) between the toluene molecules and the *cyclo*-P<sub>5</sub> ligands of one layer indicate π-π stacking interactions, whereas Cp\*...tol interactions to the neighbouring layer is much weaker due to the slipped geometry and interplanar distance of ~3.6 Å, which is rather long for organic aromatic systems (Figure 3.2a).

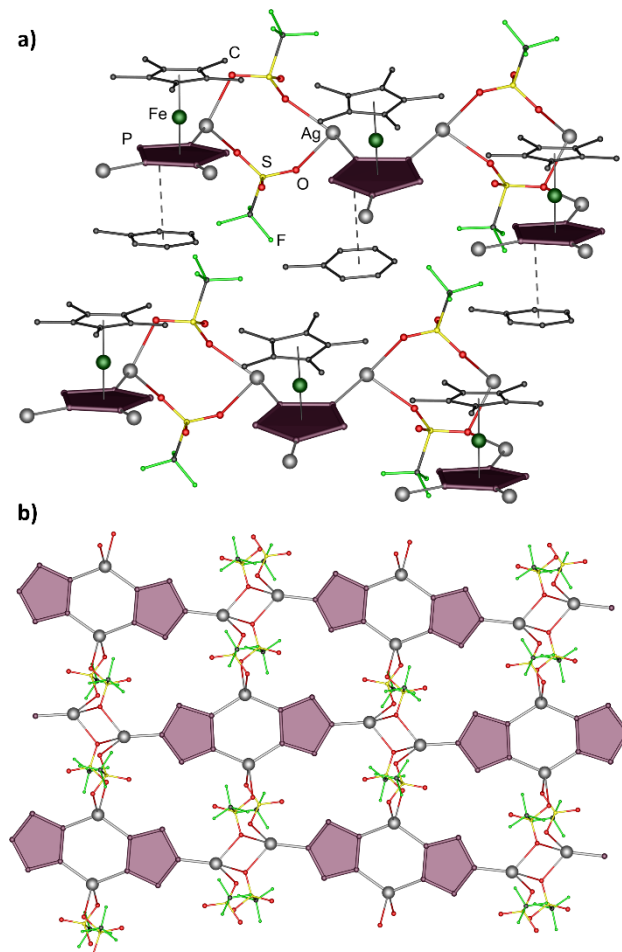


**Figure 3.2.** a) Illustration of the π-π interaction between intercalated toluene molecules and the *cyclo*-P<sub>5</sub> ligands of **2**. b) Section of the 2D network **2**. H atoms are partly omitted for clarity.

The structure of compound **5** consists of undulating 2D sheets of [{**B**}{Ag(SO<sub>3</sub>CF<sub>3</sub>)}]<sub>n</sub>. In each of them, all *cyclo*-P<sub>5</sub> ligands are coordinated to Ag atoms in a 1,2,4-mode (Figure 3.3), whereby the Ag cations are tetrahedrally coordinated to give small six-membered rings of {P<sub>4</sub>Ag<sub>2</sub>} and large 16-membered rings of {P<sub>12</sub>Ag<sub>4</sub>}. All triflate anions are terminal and stand out of the plane of the layer. This 2D structural motif was frequently observed in polymeric complexes formed by the building block **A** and Cu halides (Cl,<sup>[19]</sup> Br<sup>[31]</sup>, I<sup>[31]</sup>) as well as CuOTf,<sup>[25]</sup> where the similarity to Cu halides occurs due to terminal coordination of the triflate anion.

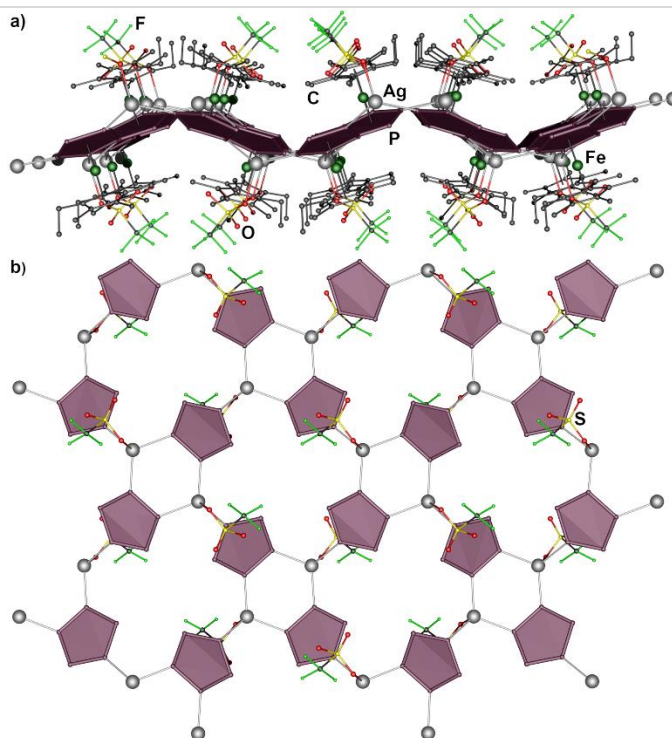


**Figure 3.3.** The neutral 2D network of **5**  $[\{\mathbf{B}\}\{\text{Ag}(\text{SO}_3\text{CF}_3)\}]_n$ : a) side view and b) simplified network structure. H atoms and  $\text{Cp}^\times$  ligands (in b) are omitted for clarity.

In the reaction of **B** with  $\text{AgOTf}$  and in the presence of the coordinating solvent  $\text{CH}_3\text{CN}$  a 1D polymeric compound **6** is formed. The polymeric chain  $[\{\mathbf{B}\}_2\{\text{Ag}(\text{SO}_3\text{CF}_3)\}_2\{\text{CH}_3\text{CN}\}]_n$  is built up by *cyclo*- $\text{P}_5$  ligands that are linked in either a 1,3- or a 1,2-mode to Ag cations (Figure 3.4). The latter also form two bonds (2.79–2.88 Å) *via* a  $\eta^{1:2}$ -coordination according to  $\pi$ -type interactions similar to those in  $[\{\mathbf{A}\}_2\text{Ag}_3(\text{NC}(\text{CH}_2)_4\text{CN})]_n(\text{SbF}_6)_{3n}$  (2.83–2.93 Å).<sup>[28]</sup> This leads to two different coordination modes of the Ag cations, for which in addition to the two  $\sigma$ -type coordinated P atoms of two **B** ligands and a terminal OTf anion, the coordination environment is completed either by an acetonitrile molecule, resulting in a tetrahedral coordination or by an additional interaction of a  $\pi$ -type forming a pseudo-tetrahedral coordination sphere. In this way, eight-membered rings  $\{\text{P}_6\text{Ag}_2\}$  between the slipped opposing *cyclo*- $\text{P}_5$  ligands (dot-to-plane distance for  $\text{P}_5 \cdots \text{P}_5$  3.43 Å) are formed. In this case the acetonitrile molecules block any possible increase of dimensionality. A similar structural motif was observed in polymeric complexes of building block **A** and Cu salts with non-coordinating anions, whereas the higher dimensionality is prevented not by ligands, but by large anions.

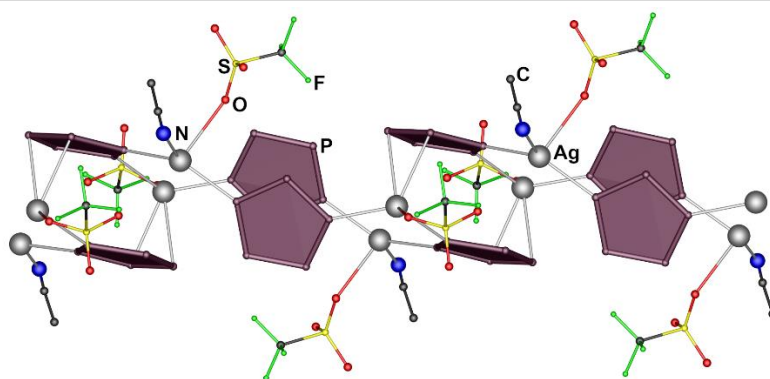


**Figure 3.4.** The section of a 1D chain in **6**. Cp<sup>x</sup> atoms are omitted for clarity.

In the 2D polymer  $[\{\mathbf{B}\}\{\text{Ag}(\text{SO}_3\text{CF}_3)\}_3]_n$  (**7**) all P atoms of the *cyclo*-P<sub>5</sub> ligands are coordinated to Ag atoms (Figure 3.5). Similar to **1**, all P atoms of *cyclo*-P<sub>5</sub> ligands are pentacoordinated and form a chain underlying motif with Ag atoms. In this case, however, instead of chains in which only two silver atoms out of five directly join two P<sub>5</sub> rings, the chains are based in fused six-membered {P<sub>4</sub>Ag<sub>2</sub>} rings sharing P-P edges. The silver atoms are tetrahedrally or pseudo-tetrahedrally coordinated. There are two types of OTf anions bound to the chain side: One acts as a tridentate ligand and connects the chains to a 2D polymer, the other is terminally bound to an Ag cation. Interestingly, compounds **1** and **7** represent the first two examples of a polymeric structure based on the pentacoordinated pentaphosphaferrocene units. Heretofore this coordination was considered to lead solely to discrete supramolecules.<sup>[32]</sup>

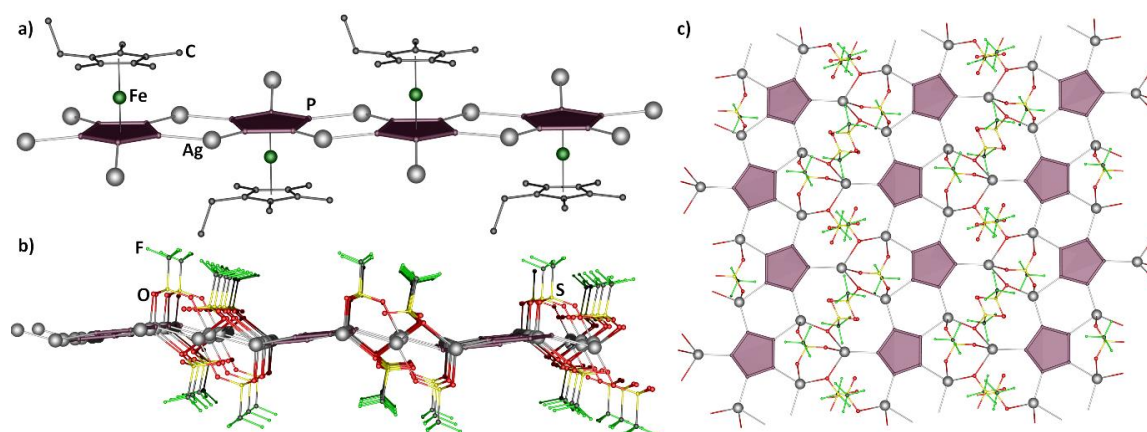


**Figure 3.5.** 2D network in **7**: a) a chain fragment with bridging OTf anions; b) side view and c) top view of the polymeric layer formed by di- and tridentate OTf anions. H atoms are omitted for clarity.

The change to complex **C** in a reaction with AgOTf leads to the 2D polymer of **9**, which structure is build up by chains of  $[\{\mathbf{C}\}\{\text{Ag}(\text{SO}_3\text{CF}_3)\}_2]_n$  (Figure 3.6a). All *cyclo*-P<sub>5</sub> ligands of **C** coordinate to Ag atoms in a 1,2,4-mode and additionally form a longer  $\pi$ -coordination contact (2.70 Å) with an opposing Ag atom similar to those in  $[\{\mathbf{A}\}_4\text{Ag}_4(\text{NC}(\text{CH}_2)_5\text{CN})]_n(\text{SbF}_6)_{4n}$  (2.80 Å, 3.09 Å).<sup>[28]</sup> The Ag atoms possess a pseudo tetrahedral coordination, and in combination with the *cyclo*-P<sub>5</sub> ligands form alternating six-membered rings of {P<sub>4</sub>Ag<sub>2</sub>} and eight-membered rings of {P<sub>6</sub>Ag<sub>2</sub>}. There are two

different types of OTf anions in the crystal structure; one links the formed rings to a chain, the other bridges to the neighbouring 1D strand and thus builds up the 2D polymer (Figure 3.6b).

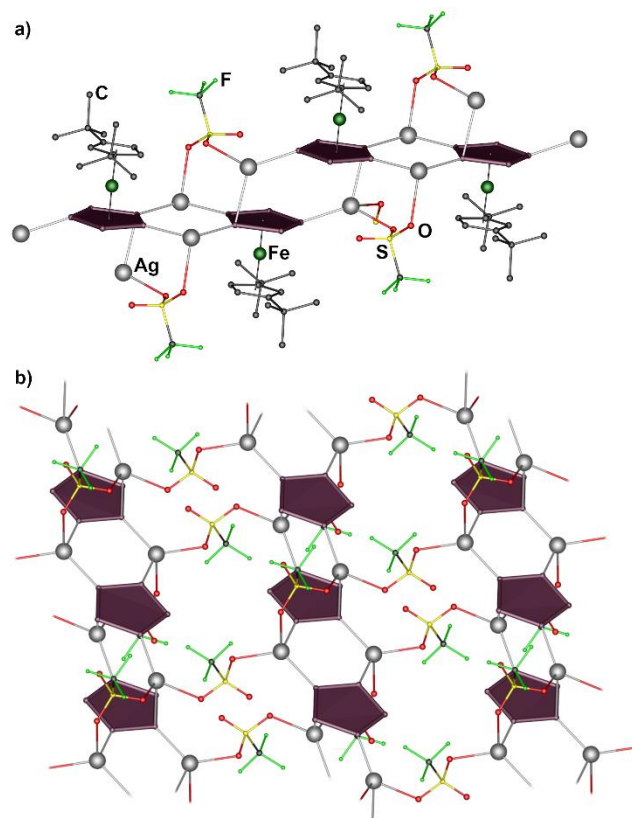


**Figure 3.6.** The 2D network of **9** a) a section of the chain motif  $[\{C\}\{Ag(SO_3CF_3)_2\}_2]_n$ ; b) 2D network formed by interconnecting  $SO_3CF_3^-$  anions. H atoms are omitted for clarity.

All isolated coordination polymers based on **A/B/C** and AgOTf possess two-dimensional structure when non-coordinating solvents are used in the reaction. By using a  $CH_3CN/CH_2Cl_2$  (1:9) mixture, the concentration of coordinating solvent  $CH_3CN$  is high enough to block some coordination sites at the Ag cations that consequently leads to reducing the dimensionality to 1D and results in polymeric strands. When using different  $P_5$  ligand complexes (**A-D**), the influence of the bulkiness of the Cp ligands could be traced: While with **C** only one type of 2D polymer was formed, with **A** or **B**, two 2D polymeric complexes for each building block are obtained. Along with the increasing steric demand of different Cp ligands, the solubility of the products can be enhanced. Remarkably, for complex **D** of the highest steric bulk no coordination polymers were achievable but discrete supramolecules.

#### Discrete host-guest able supramolecules based on $[Cp^*Fe(\eta^5-P_5)]$ (**A**), $[Cp^xFe(\eta^5-P_5)]$ (**B**) or $[Cp^{Bn}Fe(\eta^5-P_5)]$ (**D**)

While self-assembly with complexes **B** and **C** result in manifold coordination polymers, using different concentrations, discrete supramolecules can be obtained for complex **A** in addition to the



polymeric products **1** and **2**. Maintaining the ratio **A**:3Ag (see above) but reducing the concentration, a 4 mmol/L toluene solution of **A** was layered on a 12 mmol/L suspension of AgOTf in CH<sub>2</sub>Cl<sub>2</sub> which led to the formation of a discrete supramolecular complex  $\{\mathbf{A}\}@\{\{\mathbf{A}\}_{12}(\text{AgSO}_3\text{CF}_3)_x\}$  ( $x \approx 10$ , preliminary) (**3**: brown prisms or dodecahedra, 1.2%) and is sometimes accompanied by the occurrence of the coordination polymer of **2** (Scheme 3.1). By further dilution of the AgOTf/CH<sub>2</sub>Cl<sub>2</sub> suspension to 10 mmol/L, a 3.3 mmol/L toluene solution was layered over this suspension to obtain the discrete sphere  $\{\{\mathbf{A}\}(\text{C}_7\text{H}_8)\}@\{\{\mathbf{A}\}_{12}(\text{AgSO}_3\text{CF}_3)_{20}\}$  (**4**: green-brown rhombohedra, 45%). It should be mentioned that the idealised cores of **3** and **4** are isomeric. Interestingly, the formation of this supramolecule is occasionally accompanied by the idealized isomeric core of **3**. Further dilutions do not benefit the formation of any supramolecule. With a stirring reaction between **B** and a 0.03 mmol/L AgOTf solution in CH<sub>2</sub>Cl<sub>2</sub> for two days and a subsequent layering with hexane and storage at 0°C, a supramolecule with open architecture  $\{\mathbf{B}\}@\{\{\mathbf{B}\}_{11}(\text{AgSO}_3\text{CF}_3)_x\}$  ( $x \approx 10$ , preliminary) (**8**: dark green blocks, 39%) was obtained.

For the reaction between **D** and AgOTf, despite all previously used reaction conditions and concentrations used in the case of **A-C** were tested, only with a ratio of 1:2 in the layering of a 3.5 mmol/L toluene solution of **D** onto a 6.9 mmol/L AgOTf CH<sub>2</sub>Cl<sub>2</sub> suspension, crystals of the spherical supramolecule  $\{\{\mathbf{D}\}_{12}(\text{Ag}(\text{SO}_3\text{CF}_3))_{20}\}$  (**10**: red-brown crystals, 49%) were obtained as the only product to be achieved.

The structure of compounds **3** and **4** were elucidated by single crystal X-ray diffraction as discrete spherical host-guest assemblies crystallizing in monoclinic and triclinic crystal systems, respectively. In both cases their idealized cores are built up by 12 units of **C**, 20 Ag and 20 OTf entities. The  $\{\mathbf{A}\}@\{\{\mathbf{A}\}_{12}(\text{AgSO}_3\text{CF}_3)_{\sim 10}\}$  (preliminary) scaffold of compound **3** consists entirely of 12 five-membered (P<sub>5</sub>) and 30 six-membered rings {P<sub>4</sub>Ag<sub>2</sub>} obeying the isolated-pentagon rule and showing an icosahedral connectivity, making it a carbon-free I<sub>h</sub>-C<sub>80</sub> fullerene analogue, which also gives rise to the name '80-vertex sphere'. All Ag atoms possess a tetrahedral coordination environment, resulting from the end-on coordination of the OTf anions. Compared to **3**, the sphere  $\{\{\mathbf{A}\}(\text{C}_7\text{H}_8)\}@\{\{\mathbf{A}\}_{12}(\text{Ag}(\text{SO}_3\text{CF}_3))_{20}\}$  (preliminary) of **4** consists of 12 five-membered (P<sub>5</sub>) rings enclosed by twelve-membered rings of {P<sub>10</sub>Ag<sub>4</sub>}. The number of twelve-membered rings surrounding the P<sub>5</sub> ligands depends on the coordination of the P<sub>5</sub> ligands. Ten of the ligands of **A** coordinate to Ag atoms in a 1,2,4-mode and are thus encircled by three {P<sub>10</sub>Ag<sub>4</sub>} rings, while the remaining two ligands coordinate in a 1,2,3,4-fashion and are thus encompassed by four twelve-membered rings. The Ag<sup>+</sup> cations in **4** are all tetrahedrally coordinated by two P atoms of two different *cyclo*-P<sub>5</sub> ligands and two O atoms of different OTf anions, whereas the latter act as μ<sub>2</sub>-bridging ligands. This builds up a carbon-free icosidodecahedron analogue of **4**, with thirty positions

for Ag atoms. However, since there are only twenty OTf counterions in the idealised structure, this sphere can be described as a (90-10) vertex sphere for charge balance reasons. However, the experimentally obtained composition of their scaffolds differs from the idealized ones. In **3**, this difference arises from the partial occupancy of  $\{\text{AgSO}_3\text{CF}_3\}$  units and results in a composition of the scaffold  $[\{\mathbf{A}\}_{12}(\text{AgSO}_3\text{CF}_3)_x]$  ( $x \approx 10$ ). Each of ten positions, which is available, but not occupied by Ag atoms cause 12-membered rings  $\{\text{Ag}_3\text{P}_9\}$  in the scaffold of **3** and therefore changes the coordination mode of  $\text{P}_5$  ligand complex **A**, reducing the number of P atoms bound to silver cations. However, these  $\sim 10$  Ag cations are disordered over 20 available positions in a random way, leading to different indefinite isomeric scaffolds or different molecular forms. One of the possible scaffolds with 1,2-, 1,3- and 1,2,4-coordination modes of **A** is shown in Figure 3.7b. In Figure 3.7a, the idealized scaffold with  $x = 20$  is depicted with its incorporated guest **A**, and the twelve *cyclo*- $\text{P}_5$  ligands are situated at the vertices of an icosahedron. These structural characteristics underline the relation of **3** to previously reported 80-vertex spheres, based on Cu halides or weakly coordinating anions.<sup>[17,22,33]</sup> Similar to **3**, in  $[\{\mathbf{D}\}_{12}(\text{CuX})_{20-n}]$  cores ( $x = \text{Br}, \text{Cl}$ ), the CuX positions were also found to be partly vacant, ranging from  $n = 0 - 4.8$  per sphere. However, the minimum CuX content in a spherical 80-vertex core observed by X-ray structure analysis was found in a system with non-coordinating anion. The core in the case of  $[\{\mathbf{C}\}_{12}\{\text{Cu}(\text{CH}_3\text{CN})\}_8][\text{Al}(\text{OC}_4\text{F}_9)_4]_8$  contains only eight copper cations which is therefore the most porous 80-vertex host scaffold possible.<sup>[33]</sup> Compared to these results for Cu-containing supramolecules, the Ag-based analogue **3** with about 10 metal vacancies is among the most porous supramolecules in general, and in the case of Ag the most metal-deficient host scaffold so far. The inner cavity of **3** with diameter of 1.2 nm is occupied with one molecule of **A** (0.7 nm in length). The guest molecule is shifted from the centre of the cavity, because of  $\pi$ -stacking interactions indicated by short interplanar distances of the *cyclo*- $\text{P}_5$  ligands of the guest and the host molecule. Since the scaffold is severely disordered, involving even units of **A**, no exact distances between the host and the guest can be given.

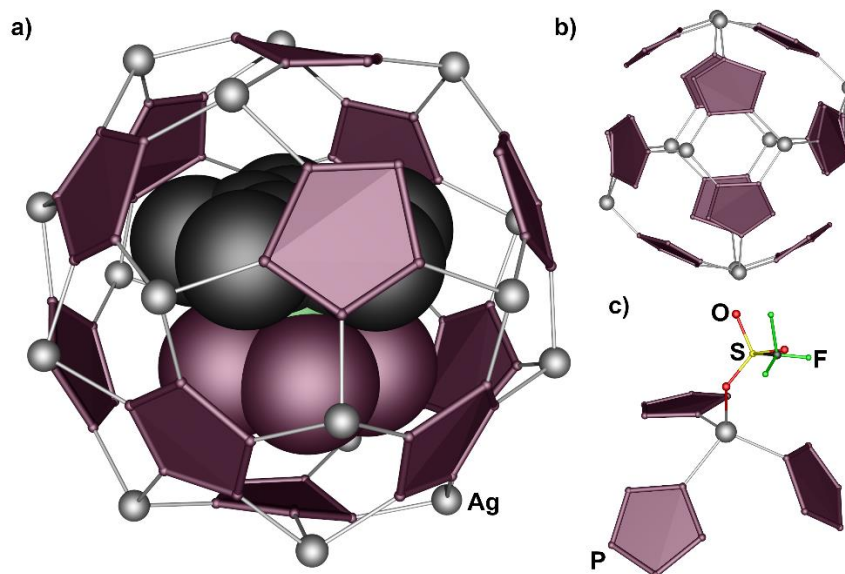


**Figure 3.7.** a) Idealized scaffold of **3** with guest molecule **A** shown in space-filling model, b) one possible isomeric scaffold (A<sub>12</sub>Ag<sub>10</sub>), d) end-on coordination mode of SO<sub>3</sub>CF<sub>3</sub><sup>-</sup>. Cp ligands and H atoms are omitted for clarity.

Compound **4** with a sum formula of  $[\{\mathbf{A}\}(\text{C}_7\text{H}_8)]_{12}[\{\mathbf{A}\}_{12}\{\text{Ag}(\text{SO}_3\text{CF}_3)\}_{20}]$  crystallizes in triclinic space group  $P\bar{1}$  with two crystallographically unique spherical supramolecules in the unit cell. Interestingly, one of them is ordered, whereas the other one shows disordering over at least three positions, with the major component amounting to about 85 - 86%, according to preliminary data. Gratifyingly, it generally represents the first example of a spherical supramolecule based on pentaphosphaferrocenes and coinage metal salts mostly showing ordering in the solid state. Most previously reported compounds were refined as idealized or average structures and described as solid solutions of different isomers or similar molecules with varying metal content.<sup>[14,17,22,34]</sup> For instance, in the scaffold of the recently presented isostructural Cu-containing compound  $[\{\mathbf{D}\}_{12}(\text{CuSO}_3\text{CF}_3)_{20-n}]$  ( $n = 0.4$ ) the Cu atoms are statistically distributed over 30 positions.<sup>[25]</sup> To specify the vacancies of Cu and SO<sub>3</sub>CF<sub>3</sub>, this compound was described as a mixture of spheres with different values of  $n$  and thus different metal-deficiency. For the idealized complete sphere  $[\{\mathbf{D}\}_{12}(\text{CuSO}_3\text{CF}_3)_{20}]$  with  $n = 0$  the molecular structure of possible isomers was theoretically reconstructed to give four isomers of  $D_2$  and  $D_5$  point symmetries, each existing in two enantiomeric forms. DFT calculations were performed to optimize their geometry and relative stability, which revealed that  $D_2$  isomer is slightly more stable, only by 2.5 kcal/mol, than the  $D_5$  isomer.

The arrangement of Ag atoms in (90-10)-vertex sphere of **4** possesses a similar structure of the inorganic scaffold as the  $D_2$  isomer of  $[\{\mathbf{D}\}_{12}(\text{CuSO}_3\text{CF}_3)_{20}]$  is theoretically reconstructed from an average structure, and many other spheres based on pentaphosphaferrocenes.<sup>[17,20,22,23]</sup> In contrast to the Cu-analogue, the inorganic scaffold of **4** is remarkably distorted compared to the almost spherical supramolecules of  $[\{\mathbf{D}\}_{12}(\text{CuSO}_3\text{CF}_3)_{19.6}]$ . In the Cu case the difference between non-valent

intramolecular P...P contacts with and without Cu-bridges is only 0.2 Å, due to the short average Cu-P bond lengths of 2.16 Å, leading to a uniform architecture. In contrast to this, due to the larger covalent radius of Ag and therefore longer Ag-P bonds ( $d_{\text{av}}(\text{Ag-P}) = 2.46 \text{ \AA}$  (**4**)), the distances between Ag-bridged *cyclo*-P<sub>5</sub> ligands are by ~0.6 Å longer than respective non-valent P...P contacts between two unbridged *cyclo*-P<sub>5</sub> ligands. This difference induces a distortion of the 14-membered rings and, consequently, the inorganic scaffold of **4** is ellipsoidally-, not spherically-shaped. The outer dimensions supramolecule **4** reach a size of up to 2.5 nm.<sup>[49]</sup>

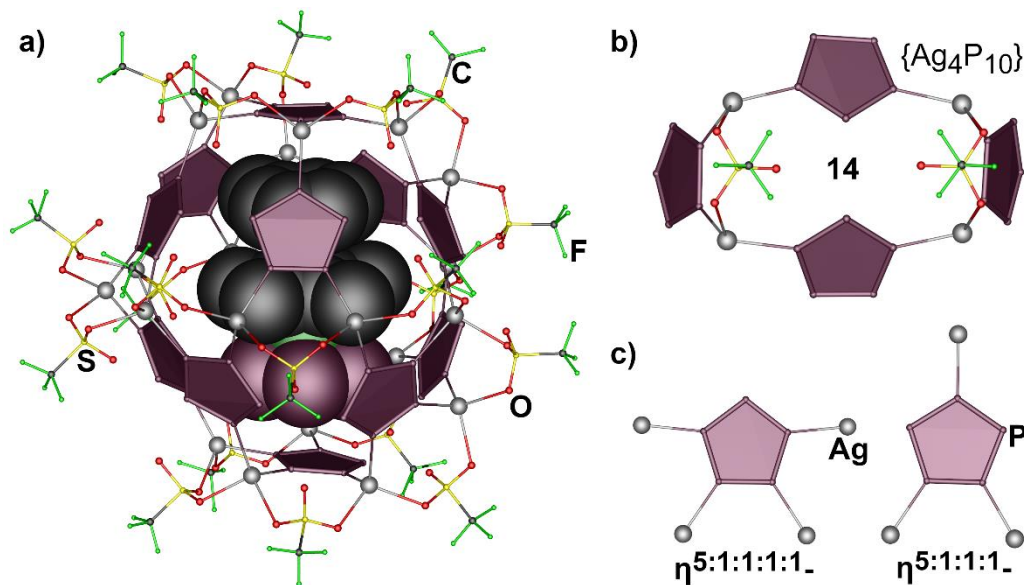


**Figure 3.8.** a) Supramolecule **4** with guest molecules shown in space-filling style. b) 14-membered ring of the inorganic scaffold of **4**, c) coordination motifs of *cyclo*-P<sub>5</sub> ligands of **1**. H atoms and Cp ligands are omitted for clarity.

The inner cavity of **4** has a diameter of 1.4 nm<sup>[50]</sup> and is therefore about 0.2 nm larger comparing to the cavity of **3**. Into the larger inner void fits besides a molecule of **A** an additional molecule of toluene (C<sub>7</sub>H<sub>8</sub>) between the Cp\* group of the guest and one of the *cyclo*-P<sub>5</sub> moieties of the host molecule (Figure 3.8a), stabilized by  $\pi$ - $\pi$  interactions to both sides of the inner surface of the host (dot-to-plane distances for P<sub>5</sub><sup>host</sup>...toluene 3.66 Å, for Cp\*<sup>guest</sup>...toluene 3.44 Å). This represents the first supramolecular assembly found to be incorporated by spherical supramolecules based on P<sub>n</sub> complexes. The supramolecular guest assembly is shifted from the centre of the cavity by  $\pi$ -stacking interactions which indicates short interplanar distances of the *cyclo*-P<sub>5</sub> ligand of the guest and the host molecule of 0.38 nm. In comparison to [{**D**]<sub>12</sub>(CuSO<sub>3</sub>CF<sub>3</sub>)<sub>20</sub>], the cavity is 0.04 nm larger and can enclose guest molecules, whereas in [{**D**]<sub>12</sub>(CuSO<sub>3</sub>CF<sub>3</sub>)<sub>20</sub>] only solvent molecules are found in the cavity.<sup>[25]</sup>

Besides numerous polymers with **B** (see above), the supramolecular assembly **8** {**B**}@[{**B**]<sub>11</sub>(AgSO<sub>3</sub>CF<sub>3</sub>)<sub>~10</sub>] with open architecture can also be obtained (Figure 3.9). The bowl-like supramolecule is composed of *cyclo*-P<sub>5</sub> ligands of **B** with different 1,2-/1,2,4- and 1,2,3,4-

coordination motifs to Ag atoms. Hence, 6-membered  $\{\text{Ag}_2\text{P}_4\}$  and 12-membered  $\{\text{Ag}_3\text{P}_9\}$  rings are formed. The bowl has a similar inorganic scaffold compared to  $\{\mathbf{A}\}@[\{\mathbf{A}\}_{12}(\text{AgSO}_3\text{CF}_3)_x]$  (**3**), but with a missing lid of  $\{\text{Ag}_4\text{P}_5\}$ . Interestingly, a molecule of **B** is encapsulated in the bowl as a guest. The inner diameter is up to 1.2 nm<sup>[50]</sup>, which represents the same size as that of the inorganic spherical scaffold of **3**. The guest is oriented in such way that it can establish  $\pi$ -contacts with a *cyclo*-P<sub>5</sub> ligand of the host. The ethyl group of **B** protrudes in one direction, which prevents the bowl from closing into a sphere. As it is a preliminary structure, no details about bond lengths or distances can be given yet. However, if one compares this structure with previous ones, a similarity to the structure  $[(\text{CpCr})_2(\mu, \eta^{5:5}\text{-As}_5)]@[\{\mathbf{A}\}_{11}\{\text{CuX}\}_{15-n}]$  ( $x = \text{Cl}$ ,  $n = 0.45$ ;  $x = \text{Br}$ ,  $n = 1.55$ ) obtained with Cu halides are observed.<sup>[35]</sup> In a reaction **A** and CuX with the template  $[(\text{CpCr})_2(\mu, \eta^{5:5}\text{-As}_5)]$  a bowl-like scaffold is formed, whereby the encapsulated template protrudes from the bowl, so that its host can no longer be encapsulated into a sphere. A crucial difference compared to the bowl-like supramolecule **8** is that due to the somewhat more sterically demanding Cp ligand **B** ( $\text{CpEtMe}_4$ ), no extra template is needed for such a structure compared to the structure with **A** ( $\text{CpMe}_5$ ). This makes **8** the first Ag-based bowl-like supramolecule with *cyclo*-P<sub>5</sub> ligand complexes. Surprisingly, a reaction of **A** with CuOTf leads to the 1D polymer  $[\{\mathbf{A}\}\{\text{Cu}(\text{CF}_3\text{SO}_3)\}]_n$ .<sup>[25]</sup> This underlines that both the *cyclo*-P<sub>5</sub> ligand complex **B** and AgOTf are necessary to build up this bowl-like aggregate **8**.

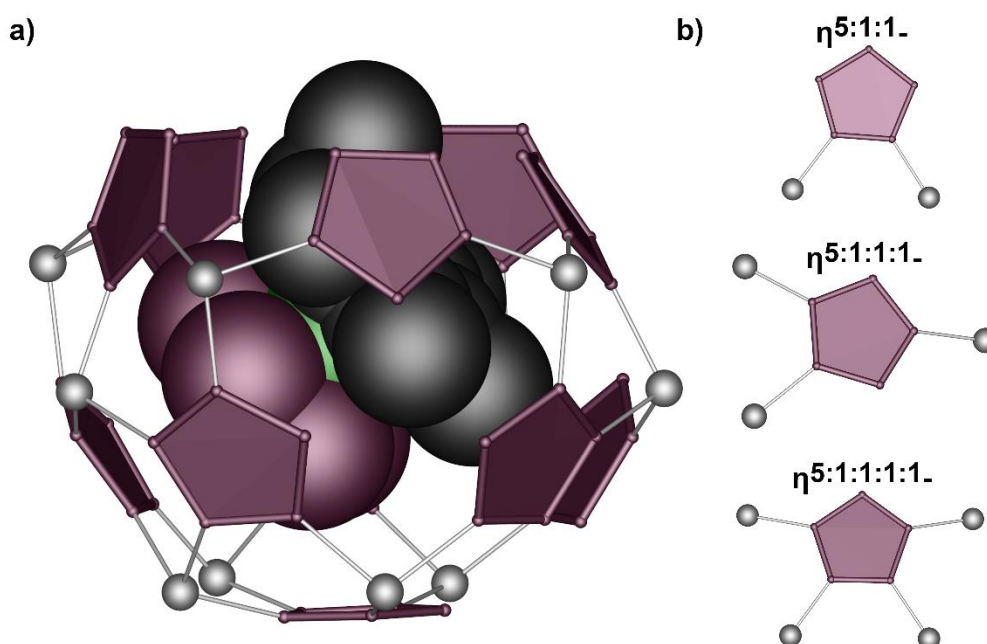


**Figure 3.9.** a) inorganic scaffold of **8** with guest **B** molecule encapsulated, b) different types of coordination motifs of **8**. Cp ligands, counterions and H atoms are omitted for clarity.

The Cp<sup>Bn</sup> derivative **10** reveals many characteristics underlining its structural similarity to the (90-10)-vertex<sup>[36]</sup> sphere **4** and  $[\{\mathbf{D}\}_{12}(\text{CuSO}_3\text{CF}_3)_{19.6}]$ , respectively.<sup>[25]</sup> Thus, the average structure exhibits an idealized icosidodecahedral symmetric shape, consisting of 12 *cyclo*-P<sub>5</sub> ligands, about

20  $\text{Ag}^+$  cations, disordered over 30 positions, and about 20 trigonal-coordinated OTf moieties (Figure 3.10). Hence, assumedly similar  $D_2$  and  $D_5$  isomers of **10** co-exist, like those reconstructed and optimized for the CuOTf-containing sphere and the  $D_2$  isomer reliably experimentally observed in the crystal structure of **4**. Like discussed for **4**, the actual scaffold of **4** is supposed to show an intrinsic ellipsoidal-shaped distortion, when compared to the Cu-based sphere. Due to the preliminary data and the average structure, this distortion could not be concretized, yet. The spherical framework of **10** provides an inner cavity with a diameter of about 13 Å, which is most likely occupied by  $\text{CH}_2\text{Cl}_2$  molecules. Compared to the diameter of **4**, the diameter for **10** represents the mean value of the minimal and the maximal diameter of **4**. As **D** is by 0.5 nm larger in size than **A**, the supramolecules in **10** reach outer diameters of 3.3 nm<sup>[49]</sup>.

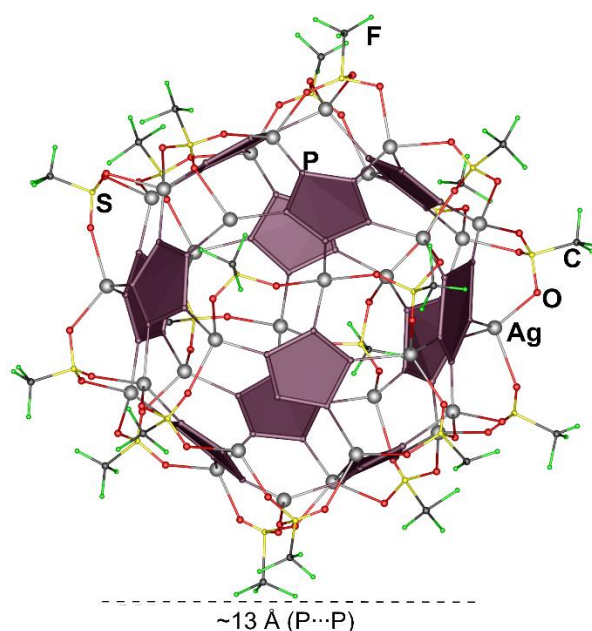


**Figure 3.10.** Average structure of the inorganic scaffold of **10**. Cp ligands and H atoms are omitted for clarity.

The benzyl ligands of **D** remarkably increase the solubility of the supramolecular compound.<sup>[17]</sup> Compared to **3** and **4**, compound **10** shows good solubility in  $\text{CH}_2\text{Cl}_2$ , toluene and thf, whereas upon solution in  $\text{CH}_3\text{CN}$  or pyridine instant fragmentation is observed. In the  $^1\text{H}$  NMR spectrum four broad signals corresponding to the methylene as well as to the aromatic protons for the  $\text{Cp}^{\text{Bn}}$  ligands are observed ( $\delta$  (ppm): 4.13, 6.27, 6.74, 6.93). These are slightly downfield shifted comparing to the literature which indicates a coordination of **D** also in solution. The broad signals in the  $^{31}\text{P}\{^1\text{H}\}$  NMR spectrum at  $\delta = -42$  ppm, 70 ppm and 128 ppm as well as a sharp singlet at  $\delta = 154$  ppm for free **D**, are observable at room temperature and do not change significantly upon cooling to 193 K. Similarly, in comparison to free **D**, up-field shifted broad signals, could also be observed in the  $^{31}\text{P}\{^1\text{H}\}$ -MAS NMR spectrum ( $\delta = -37.28$  ( $\omega_{1/2} = 4479$  Hz), 117.6 ( $\omega_{1/2} = 14375$  Hz)). These different broad signals are reminiscent of the obtained spectra for metal-deficient 80-vertex derivatives

[(**D**)<sub>12</sub>(CuX)<sub>20-n</sub>] (X = Cl, Br; n ≤ 4.6), though the signals of **9** are distributed over a wider range and are shifted to higher fields.<sup>[17]</sup> A comprehensive NMR study concerning these fullerene derivatives revealed that the broad signals can be attributed to different coordination modes of the *cyclo*-P<sub>5</sub> ligands resulting from different porosity.<sup>[17]</sup> In the case of the idealized sphere in **10** one can assume that the same isomers with D<sub>2</sub> and D<sub>5</sub> symmetries are possible present as for the similar Cu containing [(Cp<sup>Bn</sup>Fe(η<sup>5</sup>-P<sub>5</sub>))<sub>12</sub>(CuSO<sub>3</sub>CF<sub>3</sub>)<sub>20</sub>]. Therefore, three different coordination modes of the *cyclo*-P<sub>5</sub> ligand towards the Ag<sup>+</sup> cations are expected to be found in the mixture of these isomers in the crystalline phase, namely 1,2,4-, 1,2,3,4- (for D<sub>2</sub> isomer) and 1,2,3,4,5- modes (specific only for D<sub>5</sub> isomer in combination with 1,2,3,4-mode)). Hence, the broad signals in the <sup>31</sup>P{<sup>1</sup>H} NMR spectrum of **10** might be interpreted analogously to the CuX-based sphere as overlapping signals of differently coordinated *cyclo*-P<sub>5</sub> ligands. The sharp signal of free complex **D** at room temperature indicates that partial dissociation of the aggregates might have taken place in solution. However, diffusion ordered spectroscopy (DOSY) for **10** showed that the hydrodynamic radius of the species in solution correlates well with that derived from the preliminary X-ray structure analysis (DOSY: d = 3.4 nm, solid state: d = 3.3 nm) (see experimental part). Taking advantage of the relative stability of **10** in solution, confirmed by the DOSY experiments, this compound was also examined by transmission electron microscopy (TEM). For this purpose, crystals of **10** were dissolved in CH<sub>2</sub>Cl<sub>2</sub> and the resulting solution was dropped on a copper grid coated with amorphous carbon and measured in vacuo on a FEI Tecnai G2 Spirit Twin transmission electron microscope with an acceleration voltage of 120 kV. The average diameter of the particles is 2.7 nm (Figure 3.11), whereas the expected maximal outer diameter measured from the furthest opposite H...H is 3.3 nm. The difference can be explained by the fact that the lighter atoms H and C in the outer shell of the sphere are hardly visible due to the low contrast to the grid. The inner scaffold based on the heaviest atoms Ag, S, Fe, P gives 2.3 nm.<sup>[37]</sup>

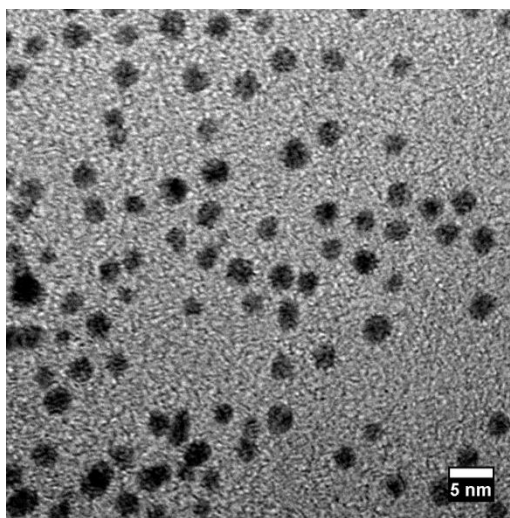


Figure 3.11. TEM record of a dispersed **10**.

### 3.3 Conclusion

In summary, the self-assembly system with  $[\text{Cp}^{\text{R}}\text{Fe}(\eta^5\text{-P}_5)]$  ( $\text{Cp}^* = \eta^5\text{-C}_5\text{Me}_5$  (**A**),  $\text{Cp}^{\text{x}} = \eta^5\text{-C}_5\text{Me}_4\text{Et}$  (**B**),  $\text{Cp}^{\text{r}} = \eta^5\text{-C}_5\text{H}_3(\text{tBu})_2$  (**C**),  $\text{Cp}^{\text{Bn}} = \eta^5\text{-C}_5(\text{CH}_2\text{C}_6\text{H}_5)_5$  (**D**)) and  $\text{Ag}(\text{SO}_3\text{CF}_3)$  ( $\text{AgOTf}$ ) sheds light onto influence and solubility of different sterically demanding pentaphosphaferrocens on the obtained coordination products and desired hollow supramolecules capable of guest encapsulation. Compared to the self-assembly involving  $\text{CuOTf}$ , the successful transfer to  $\text{AgOTf}$  demonstrates that the more flexible coordination sphere of  $\text{Ag}(\text{I})$  with pentaphosphaferrocenes of different solubilities and steric demand leads to a much broader variety of new coordination polymers and discrete spherical supramolecules, whereby coordinating anions may act as additional scaffold-constructing building blocks or serve as a terminal ligand, than with  $\text{CuOTf}$ . In the latter case structural similarities to  $\text{Cu}$  halide systems appear. In this systematic study, in addition to the influence of building blocks with different steric demand (**A-D**) and the scaffold-constructing features of  $\text{AgOTf}$ , the dependence of the results on different reaction conditions like concentration, solvent and molar ratio was also investigated. This has allowed isolating a wide variety of unprecedented 1D/2D coordination polymers for the building blocks **A/B/C** as well as impressive discrete supramolecules with novel host-guest properties for *cyclo*- $\text{P}_5$  ligand complexes with **A/B/D**. It has been shown that even small differences in bulkiness, e.g. between **A** and **B**, significantly influence the outcome. In addition to two 2D polymers (**1,2**) for the smallest *cyclo*- $\text{P}_5$  ligand complex **A** used, whereby in **1** the first pentacoordinated *cyclo*- $\text{P}_5$  ligands could be represented in polymers, spherical 80-vertex and (90-10)-vertex supramolecules were also obtained. With an inner diameter of up to 1.2 nm (**3**) and 1.4 nm (**4**), both supramolecules can enclose guest molecules **A** (**3**) and a supramolecular assembly of an **A** (guest) and a toluene molecule in a cavity of **4**. The outer diameter for **4** reached a phenomenal size of 2.5 nm, which represents the largest spherical arrangement based on five-fold symmetric building block **A** and  $\text{Ag}$  units, whereas the 80-vertex sphere of **3** represents the most porous *cyclo*- $\text{P}_5$  ligand-based host scaffold. Due to the partial occupancy of  $\{\text{AgSO}_3\text{CF}_3\}$  units different isomeric scaffolds ( $\text{D}_2$ ) or molecular forms of **4** result, which are severely disordered in the crystal packing due to their similar outer shape. Comparison of these results with those of the slightly larger **B** shows that minimal differences in steric demand have a large impact. In addition to another example of pentacoordinated *cyclo*- $\text{P}_5$  complexes in polymer **7** and another 2D polymer **5**, an unprecedented structure type for *cyclo*- $\text{P}_5$  ligand complexes with  $\text{Ag}(\text{I})$  salts was obtained as shown in the bowl-like supramolecule **8**. The inorganic scaffold is similar to the 80-vertex sphere **3** (**A**), but the enclosed **B** molecule protrudes from the bowl-like arrangement with its ethyl group, which means that no lid in form of another **B** molecule can be coordinated to close up the core of a supramolecule. The inner diameter of the bowl is up to 1.2 nm and thus has the same inner



diameter as **3**. To investigate how the two-component self-assembly system reacts to other coordinating molecules besides OTf<sup>-</sup> counterions, acetonitrile was used in a reaction and a 1D polymer **6** was obtained. This shows that although the solvent molecule and OTf<sup>-</sup> compete for coordination, neither coordinate preferentially and only the dimensionality gets further restricted.

A further increase of the sterical demand of the Cp<sup>R</sup> ligand (**C**), interestingly reduced the set of possible coordination compounds to a 2D polymer (**9**). With one of the most sterically demanding *cyclo*-P<sub>5</sub> ligand complex **D**, a further spherical (90-10)-vertex supramolecule **10** was obtained. Due to the disorder of the Ag cations over 30 positions, D<sub>2</sub> (as for **4**) and D<sub>5</sub> isomers might co-exist. The supramolecules of **10** reach an outer diameter of 3.3 nm, which was confirmed by transmission electron microscopy. Only solvent molecules fit in the inner void of **10**.

These results demonstrate that the OTf anion can be successfully used as scaffold-constructing unit for not only self-assembly of pentaphosphaferrocenes with Cu(I), but also with Ag(I). However, along with similarities many innovations became possible with the introduction of Ag(I) only. The use of *cyclo*-P<sub>5</sub> ligand complexes gives a unique insight into the influence of steric demand on the self-assembly of this system.

### 3.4 Experimental Part

#### General Remarks

All reactions were performed under an inert atmosphere of dry nitrogen with standard vacuum, Schlenk and glove-box techniques. Solvents were purified, dried, and degassed prior to use by standard procedures. [Cp<sup>\*</sup>Fe(η<sup>5</sup>-P<sub>5</sub>)]<sup>[38]</sup>, [Cp<sup>x</sup>Fe(η<sup>5</sup>-P<sub>5</sub>)]<sup>[39]</sup>, [Cp<sup>''</sup>Fe(η<sup>5</sup>-P<sub>5</sub>)]<sup>[40]</sup>, [Cp<sup>Bn</sup>Fe(η<sup>5</sup>-P<sub>5</sub>)]<sup>[41]</sup>, were synthesized following reported procedures. Commercially available AgSO<sub>3</sub>CF<sub>3</sub>, 99.95% was used without further purification.

Solution NMR spectra were recorded on a Bruker Avance 300 or 400 spectrometer. The <sup>31</sup>P{<sup>1</sup>H} MAS spectrum was measured on a Bruker Avance 300 spectrometer. The DOSY spectra were recorded on an Avance III HD 600 (600.25 MHz) spectrometer equipped with a z gradient (53.5 Gauss/cm), 5 mm TCI cryo probe and BVT 3000 unit at 298 K. The NMR data was processed with the Bruker program TopSpin® 3.2 and the diffusion coefficient was calculated with the Bruker software T1/T2 relaxation package. For the calibration of the <sup>1</sup>H chemical shifts and for the temperature- and viscosity-correction of the diffusion coefficients, TMS (tetramethylsilane) was added. The <sup>1</sup>H-diffusion measurement was performed with the convection suppressing DSTE (double stimulated echo) pulse sequence, developed by *Mueller* and *Jerschow*<sup>[42]</sup> in a pseudo 2D mode. 120 dummy scans and 16 scans were used with a relaxation delay of 2 s. Sinusoidal shapes were used for the gradient and a linear gradient ramp with 20 or 5 increments between 5 and 95%

of the maximum gradient strength was applied for the diffusion relevant gradients. For the homospoil gradients, -13.7, 20 and 17.13 G cm<sup>-1</sup> were applied. The length of the gradient pulse  $\delta$  was adjusted for every species in the sample to achieve appropriate signal attenuation curves, giving values for  $\delta$  of 2.0 ms for TMS and 3.4 or 3.6 ms for the supramolecules. A diffusion time  $\Delta$  of 45 ms was used.

The corresponding ESI-MS spectra were acquired on a ThermoQuest Finnigan MAT TSQ 7000 mass spectrometer. CHN Elemental analyses were performed on a Vario EL III apparatus, whereas the elements for **4**, **10** were determined by the Catalysis Research Center of the Technical University Munich and **3** was determined by "MikroLab – Mikroanalytisches Laboratorium Kolbe" by Photometry, Atomic Absorption Spectroscopy or Tritrimetry. The storage and handling under air lead to the aggregation of water to the crystalline samples **4** and **10**, due to the hygroscopic behavior of the SO<sub>3</sub>CF<sub>3</sub> groups. Furthermore, the determination of Ag and Fe in one sample showed to be defective. Thus, these values show a large deviance with respect to calculated ones.

The Transmission electron microscopy (TEM) measurements were carried out on a FEI Tecnai G2 Spirit Twin transmission electron microscope equipped with a field emission gun and processed with an acceleration voltage of 120 kV. The machine is fitted with a LaB6 cathode, and the pictures were recorded with a Gatan US1000 CCD-camera (2k × 2k). The analysis of the pictures was done with the graphic software Fiji.<sup>[43]</sup> For the preparation of the samples were the nanoparticles dispersed in dichloromethane and 20  $\mu$ L were dropped on copper grids coated with amorphous carbon.

Due to the insolubility of the products based on [Cp\*Fe( $\eta^5$ -P<sub>5</sub>)], [Cp\*Fe( $\eta^5$ -P<sub>5</sub>)] and [Cp''Fe( $\eta^5$ -P<sub>5</sub>)] in common solvents, the NMR measurements were performed with CD<sub>3</sub>CN under destruction of the structure. Due to the poor solubility of Ag(SO<sub>3</sub>CF<sub>3</sub>) in dichloromethane, the suspension was first stirred (RT, 12h) and then hung into a preheated (40 °C, 2h) ultrasonic bath before further usage.

### Synthesis of Synthesis of [{Cp\*Fe( $\eta^5$ -P<sub>5</sub>)}<sub>4</sub>{Ag(SO<sub>3</sub>CF<sub>3</sub>)<sub>4</sub>}(CH<sub>2</sub>Cl<sub>2</sub>)] (**1**)

In a Schlenk tube a solution of Ag(SO<sub>3</sub>CF<sub>3</sub>) (32 mg, 0.13 mmol) in CH<sub>2</sub>Cl<sub>2</sub> (8 mL) is carefully layered with a green solution of [Cp\*Fe( $\eta^5$ -P<sub>5</sub>)] (15 mg, 0.04 mmol) in toluene (8 mL). Thereby, the phase boundary turns yellow. During the diffusion process, the formation of small yellow plates of **1** below the phase boundary can be observed. After complete diffusion the mother liquor is decanted, the crystals are washed with hexane (3 x 10 mL) and dried *in vacuo*.

Analytical data of **1**

**Yield:** 49 mg (0.034 mmol, 85% referred to  $[\text{Cp}^*\text{Fe}(\eta^5\text{-P}_5)]$ )

$^1\text{H}$  NMR ( $\text{CD}_3\text{CN}$ ):  $\delta$  [ppm] = 1.49 (s,  $\text{Cp}^*\text{Fe}(\eta^5\text{-P}_5)$ ).

$^{31}\text{P}\{^1\text{H}\}$  NMR ( $\text{CD}_3\text{CN}$ ):  $\delta$  [ppm] = 123.08 (s,  $\text{Cp}^*\text{Fe}(\eta^5\text{-P}_5)$ ).

$^{19}\text{F}$  NMR ( $\text{CD}_3\text{CN}$ ):  $\delta$  [ppm] = -78.01 (s,  $\text{AgSO}_3\text{CF}_3$ )

**Positive ion ESI-MS** ( $\text{CH}_3\text{CN}$ ):  $m/z$  (%) = 147.9  $[\text{Ag}(\text{CH}_3\text{CN})]^+$ , 188.9  $[\text{Ag}(\text{CH}_3\text{CN})_2]^+$ , 229.9  $[\text{Ag}(\text{CH}_3\text{CN})_3]^+$ , 271.0  $[\text{Ag}(\text{CH}_3\text{CN})_4]^+$ , 452.8  $[(\text{Cp}^*\text{Fe}(\eta^5\text{-P}_5)\text{Ag})]^+$ , 493.8  $[(\text{Cp}^*\text{Fe}(\eta^5\text{-P}_5)\text{Ag}(\text{CH}_3\text{CN}))]^+$ , 534.8  $[(\text{Cp}^*\text{Fe}(\eta^5\text{-P}_5)\text{Ag}(\text{CH}_3\text{CN})_2)]^+$ , 710.6  $[(\text{Cp}^*\text{Fe}(\eta^5\text{-P}_5))\text{Ag}_2(\text{SO}_3\text{CF}_3)]^+$ , 798.7  $[(\text{Cp}^*\text{Fe}(\eta^5\text{-P}_5))_2\text{Ag}]^+$ , 966.53  $[(\text{Cp}^*\text{Fe}(\eta^5\text{-P}_5))\text{Ag}_3(\text{SO}_3\text{CF}_3)_2]^+$ , 1056.6  $[(\text{Cp}^*\text{Fe}(\eta^5\text{-P}_5))_2\text{Ag}_2(\text{SO}_3\text{CF}_3)]^+$ , 1312.4  $[(\text{Cp}^*\text{Fe}(\eta^5\text{-P}_5))_2\text{Ag}_3(\text{SO}_3\text{CF}_3)_2]^+$ , 1570.3  $[(\text{Cp}^*\text{Fe}(\eta^5\text{-P}_5))_2\text{Ag}_4(\text{SO}_3\text{CF}_3)_3]^+$ , 1658.3  $[(\text{Cp}^*\text{Fe}(\eta^5\text{-P}_5))_3\text{Ag}_3(\text{SO}_3\text{CF}_3)_2]^+$ , 1916.2  $[(\text{Cp}^*\text{Fe}(\eta^5\text{-P}_5))_3\text{Ag}_4(\text{SO}_3\text{CF}_3)_3]^+$

**Negative ion ESI-MS** ( $\text{CH}_3\text{CN}$ ):  $m/z$  (%) = 148.9  $[\text{SO}_3\text{CF}_3]^-$ , 404.8  $[\text{Ag}(\text{SO}_3\text{CF}_3)_2]^-$ .

**Elemental analysis:** Calculated (%) for  $[(\text{Cp}^*\text{Fe}(\eta^5\text{-P}_5))\{\text{Ag}(\text{SO}_3\text{CF}_3)\}_4(\text{CH}_2\text{Cl}_2)]$  (1458.64 g/mol): 12.35 C, 1.17 H, 8.79 S; found: 12.19 C, 1.69 H, 9.02 S.

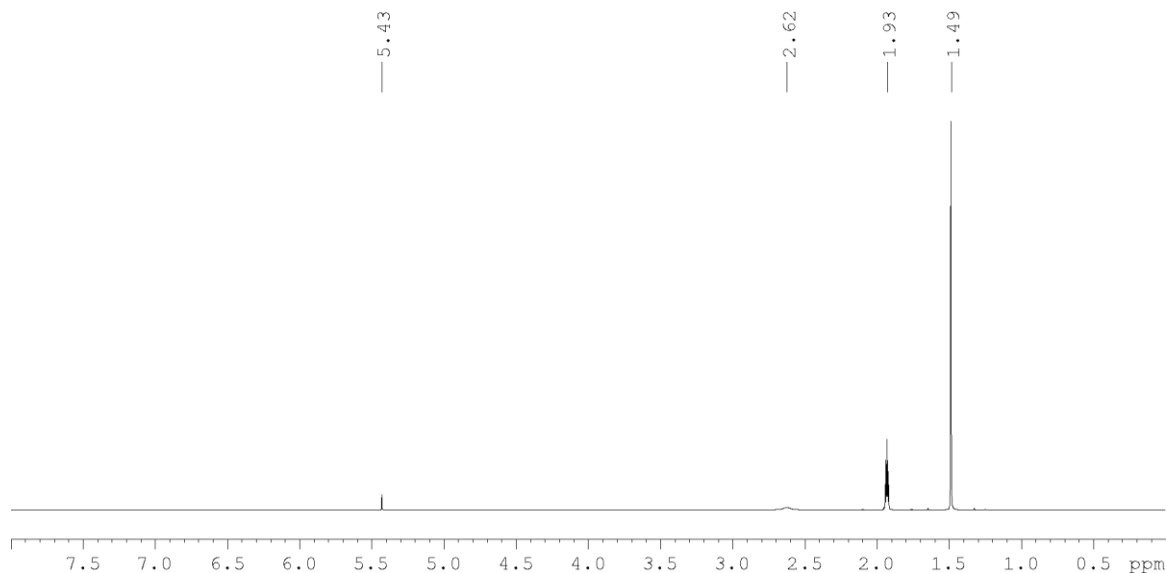


**Figure 3.12.**  $^1\text{H}$  NMR spectrum of **1**. (1.93  $\text{CH}_3\text{CN}$ , 2.62  $\text{H}_2\text{O}$ , 5.43  $\text{CH}_2\text{Cl}_2$ )

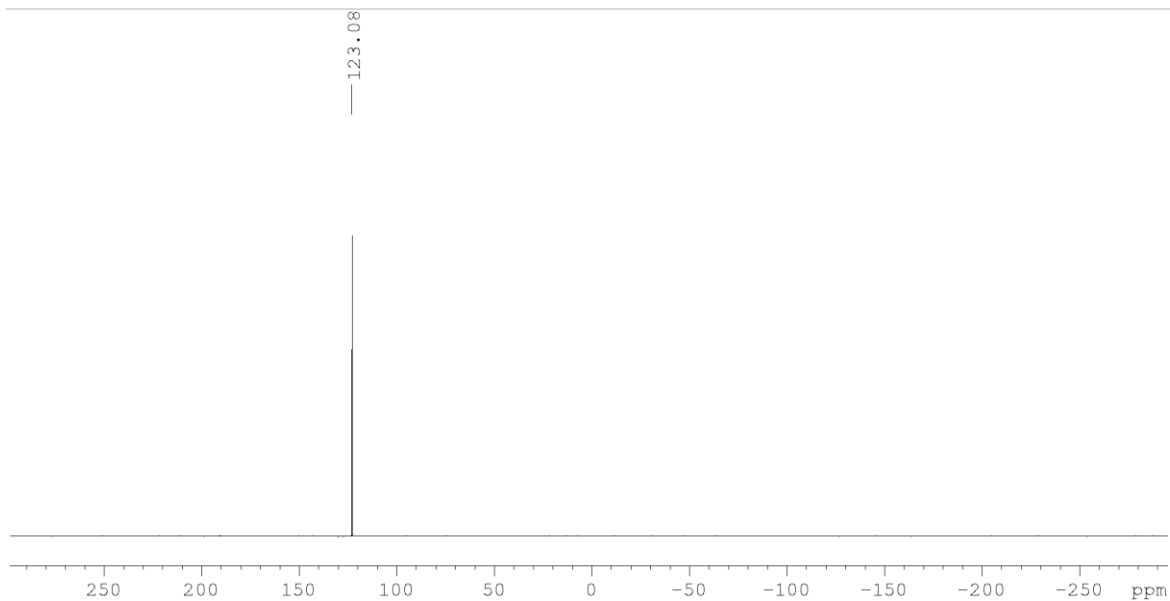


Figure 3.13.  $^{31}\text{P}\{^1\text{H}\}$  NMR spectrum of **1**.

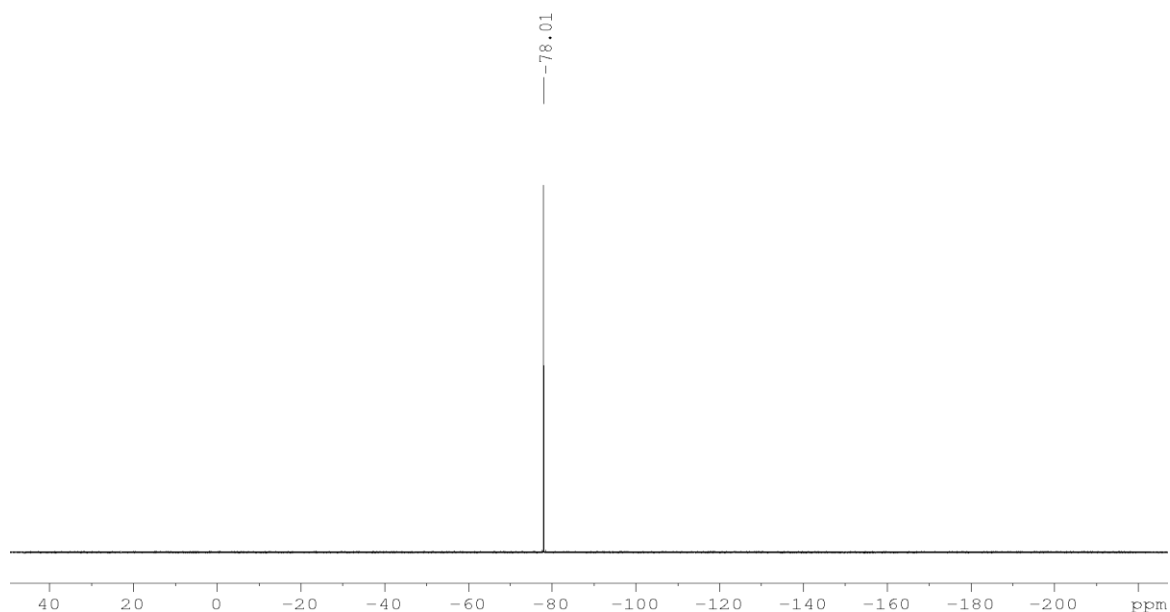


Figure 3.14.  $^{19}\text{F}$  NMR spectrum of **1**.

### Synthesis of $[(\text{Cp}^*\text{Fe}(\eta^5\text{-P}_5))\{\text{Ag}(\text{SO}_3\text{CF}_3)\}_2]$ (**2**)

In a Schlenk tube a solution of  $\text{Ag}(\text{SO}_3\text{CF}_3)$  (114 mg, 0.44 mmol) in  $\text{CH}_2\text{Cl}_2$  (10 mL) is carefully layered with a green solution of  $[\text{Cp}^*\text{Fe}(\eta^5\text{-P}_5)]$  (55 mg, 0.16 mmol) in toluene (11 mL). Thereby, the phase boundary turns yellow. During the diffusion process, the formation of small yellow plates of **2** below the phase boundary can be observed. After complete diffusion the mother liquor is decanted, the crystals are washed with hexane (3 x 10 mL) and dried *in vacuo*.

Analytical data of **2**

**Yield:** 125 mg (0.12 mmol, 76% referred to  $[\text{Cp}^*\text{Fe}(\eta^5\text{-P}_5)]$ ).

**$^1\text{H}$  NMR** ( $\text{CD}_3\text{CN}$ ):  $\delta$  [ppm] = 1.47 (s,  $[\text{Cp}^*\text{Fe}(\eta^5\text{-P}_5)]$ ).

**$^{31}\text{P}\{^1\text{H}\}$  NMR** ( $\text{CD}_3\text{CN}$ ):  $\delta$  [ppm] = 132.89 (s,  $[\text{Cp}^*\text{Fe}(\eta^5\text{-P}_5)]$ )

**$^{19}\text{F}$  NMR** ( $\text{CD}_3\text{CN}$ ):  $\delta$  [ppm] = -78.06 (s,  $\text{AgSO}_3\text{CF}_3$ ).

**Positive ion ESI-MS** ( $\text{CH}_3\text{CN}$ ):  $m/z$  (%) = 493.9  $[(\text{Cp}^*\text{Fe}(\eta^5\text{-P}_5))\text{Ag}(\text{CH}_3\text{CN})]^+$ , 798.9  $[(\text{Cp}^*\text{Fe}(\eta^5\text{-P}_5))_2\text{Ag}]^+$ .

**Negative ion ESI-MS** ( $\text{CH}_3\text{CN}$ ):  $m/z$  (%) = 148.7  $[\text{SO}_3\text{CF}_3]^-$ , 404.7  $[\text{Ag}(\text{SO}_3\text{CF}_3)_2]^-$ .

**Elemental analysis:** Calculated (%) for  $[(\text{Cp}^*\text{Fe}(\eta^5\text{-P}_5))\{\text{Ag}(\text{SO}_3\text{CF}_3)\}_2(\text{CH}_2\text{Cl}_2)_2]$  (1029.69 g/mol): 16.33 C, 1.86 H, 6.23 S; found: 15.81 C, 2.29 H, 6.76 S.

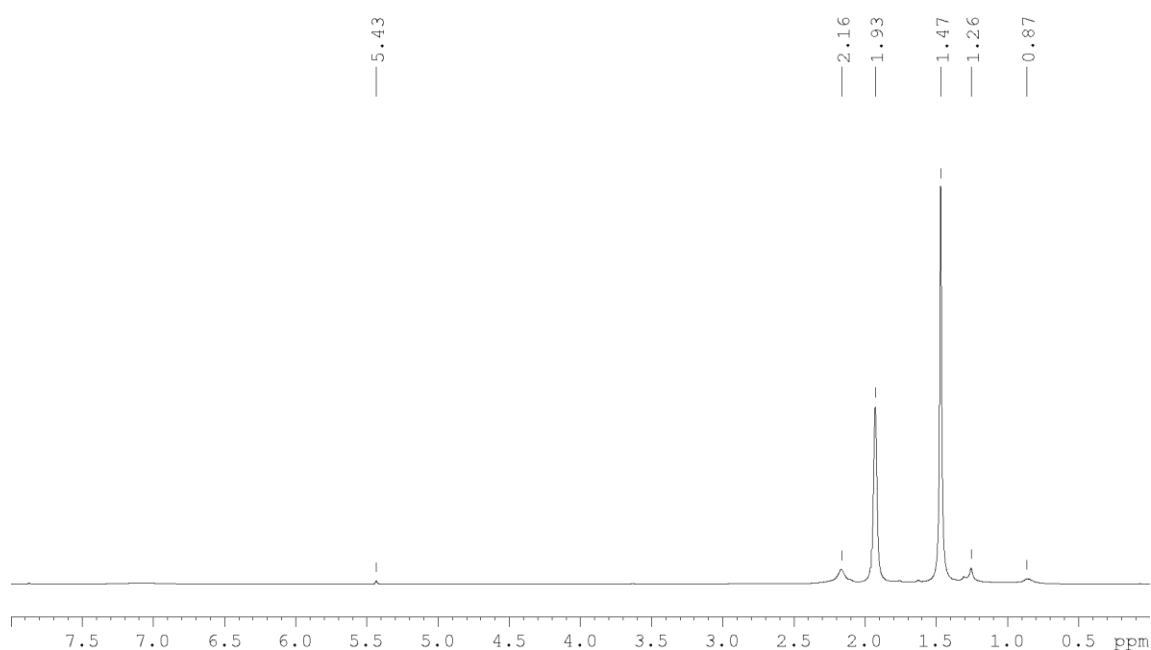


**Figure 3.15.**  $^1\text{H}$  NMR spectrum of **2**. (0.87 and 1.26 solvent residue, 1.93  $\text{CH}_3\text{CN}$ , 2.16  $\text{H}_2\text{O}$ , 5.43  $\text{CH}_2\text{Cl}_2$ ).

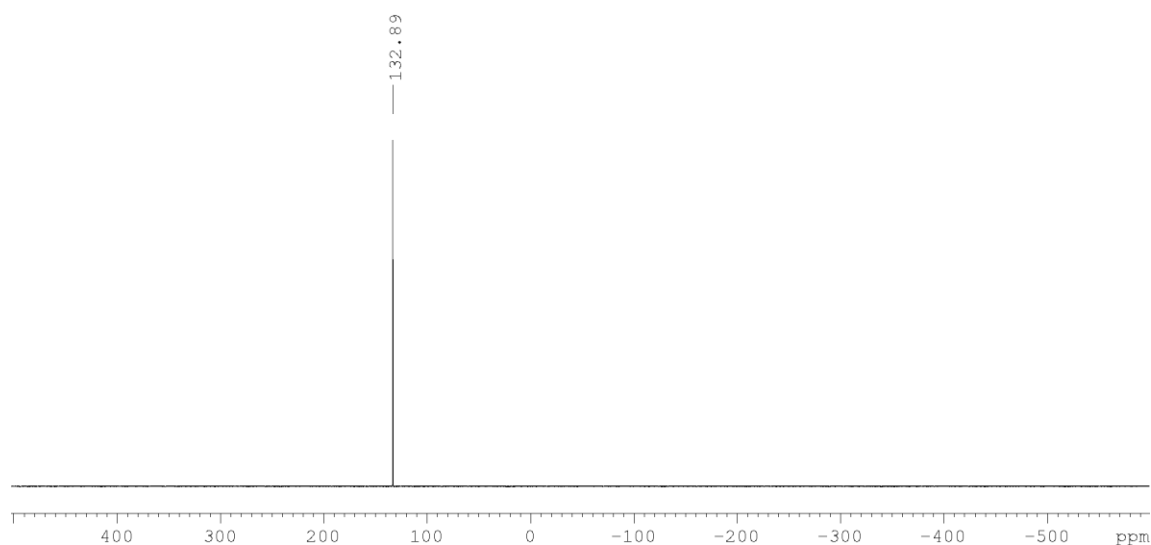


**Figure 3.16.**  $^{31}\text{P}\{^1\text{H}\}$  NMR spectrum of **2**.

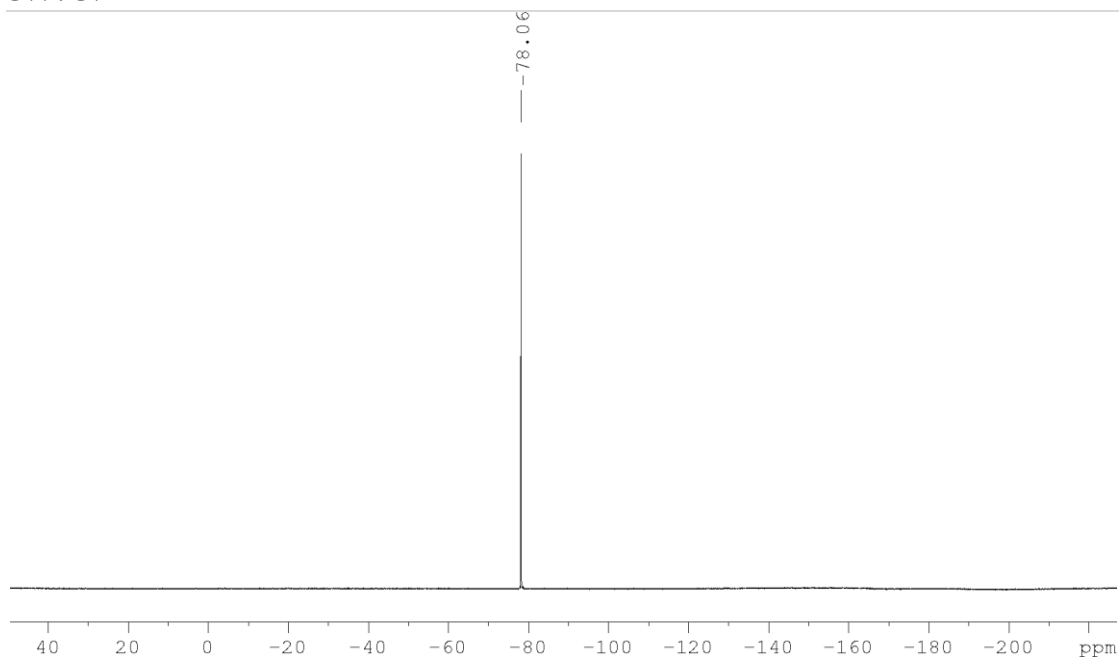


Figure 3.17. <sup>19</sup>F NMR spectrum of **2**.

### Synthesis [Cp\*Fe(η<sup>5</sup>-P<sub>5</sub>)]@{{Cp\*Fe(η<sup>5</sup>-P<sub>5</sub>)}<sub>12</sub>{Ag(SO<sub>3</sub>CF<sub>3</sub>)}<sub>x</sub> (x ≈ 10) (**3**)

In a thin Schlenk tube a solution of Ag(SO<sub>3</sub>CF<sub>3</sub>) (32 mg, 0.125 mmol) in CH<sub>2</sub>Cl<sub>2</sub> (10 mL) is carefully layered with a green solution of [Cp\*Fe(η<sup>5</sup>-P<sub>5</sub>)] (15 mg, 0.043 mmol) in toluene (10 mL). During the diffusion process, crystals of compound **1** are often observed below the former phase boundary. After three weeks first brown prisms of **3** can be observed above the phase boundary. After complete diffusion, the mother liquor is decanted, the crystals are washed with hexane (3 x 5 mL) and dried *in vacuo*. The crystals can be separated manually.

Analytical data of **3**:

**Yield:** 3.6 mg (0.51 μmol, 1.2 % referred to [Cp\*Fe(η<sup>5</sup>-P<sub>5</sub>)])

**<sup>1</sup>H NMR** (CD<sub>3</sub>CN): δ [ppm] = 1.49 (s, [Cp\*Fe(η<sup>5</sup>-P<sub>5</sub>)])

**<sup>31</sup>P{<sup>1</sup>H} NMR** (CD<sub>3</sub>CN): δ [ppm] = 130.76 (s, [Cp\*Fe(η<sup>5</sup>-P<sub>5</sub>)])

**<sup>19</sup>F NMR** (CD<sub>3</sub>CN): δ [ppm] = -78.04 (s, AgSO<sub>3</sub>CF<sub>3</sub>).

**Positive ion ESI-MS** (CH<sub>3</sub>CN): *m/z* (%) = 148.0 Ag(CH<sub>3</sub>CN)<sup>+</sup>, 189.0 Ag(CH<sub>3</sub>CN)<sub>2</sub><sup>+</sup>, 230.0 Ag(CH<sub>3</sub>CN)<sub>3</sub><sup>+</sup>, 453.1 {{Cp\*Fe(η<sup>5</sup>-P<sub>5</sub>)}Ag}<sup>+</sup>, 494.1 {{Cp\*Fe(η<sup>5</sup>-P<sub>5</sub>)}Ag(CH<sub>3</sub>CN)}<sup>+</sup>, 535.2 {{Cp\*Fe(η<sup>5</sup>-P<sub>5</sub>)}Ag(CH<sub>3</sub>CN)<sub>2</sub>}<sup>+</sup>, 799.2 {{Cp\*Fe(η<sup>5</sup>-P<sub>5</sub>)<sub>2</sub>Ag}<sup>+</sup>, 1057.3 {{Cp\*Fe(η<sup>5</sup>-P<sub>5</sub>)<sub>2</sub>Ag<sub>2</sub>(SO<sub>3</sub>CF<sub>3</sub>)}<sup>+</sup>, 1313.4 {{Cp\*Fe(η<sup>5</sup>-P<sub>5</sub>)<sub>2</sub>Ag<sub>3</sub>(SO<sub>3</sub>CF<sub>3</sub>)<sub>2</sub>}<sup>+</sup>, 1571.5 {{Cp\*Fe(η<sup>5</sup>-P<sub>5</sub>)<sub>2</sub>Ag<sub>4</sub>(SO<sub>3</sub>CF<sub>3</sub>)<sub>3</sub>}<sup>+</sup>, 1661.6 {{Cp\*Fe(η<sup>5</sup>-P<sub>5</sub>)<sub>3</sub>Ag<sub>3</sub>(SO<sub>3</sub>CF<sub>3</sub>)<sub>2</sub>}<sup>+</sup>, 1917.6 {{Cp\*Fe(η<sup>5</sup>-P<sub>5</sub>)<sub>3</sub>Ag<sub>4</sub>(SO<sub>3</sub>CF<sub>3</sub>)<sub>3</sub>}<sup>+</sup>,

**Negative ion ESI-MS** (CH<sub>3</sub>CN): *m/z* (%) = 148.9 [SO<sub>3</sub>CF<sub>3</sub>]<sup>-</sup>.

**Elemental analysis:** Calculated (%) for  $[\{\text{Cp}^*\text{Fe}(\eta^5\text{-P}_5)\}_{13}(\text{AgCF}_3\text{SO}_3)_{10.15}]$  (7105.08 g/mol): C 23.69, H 2.77, S 4.58, Ag 15.41, Fe 10.22, P 28.34, F 8.14; found: C 23.44, H 2.94, S 4.39, Ag 14.92, Fe 10.00, P 27.71, F 7.77.

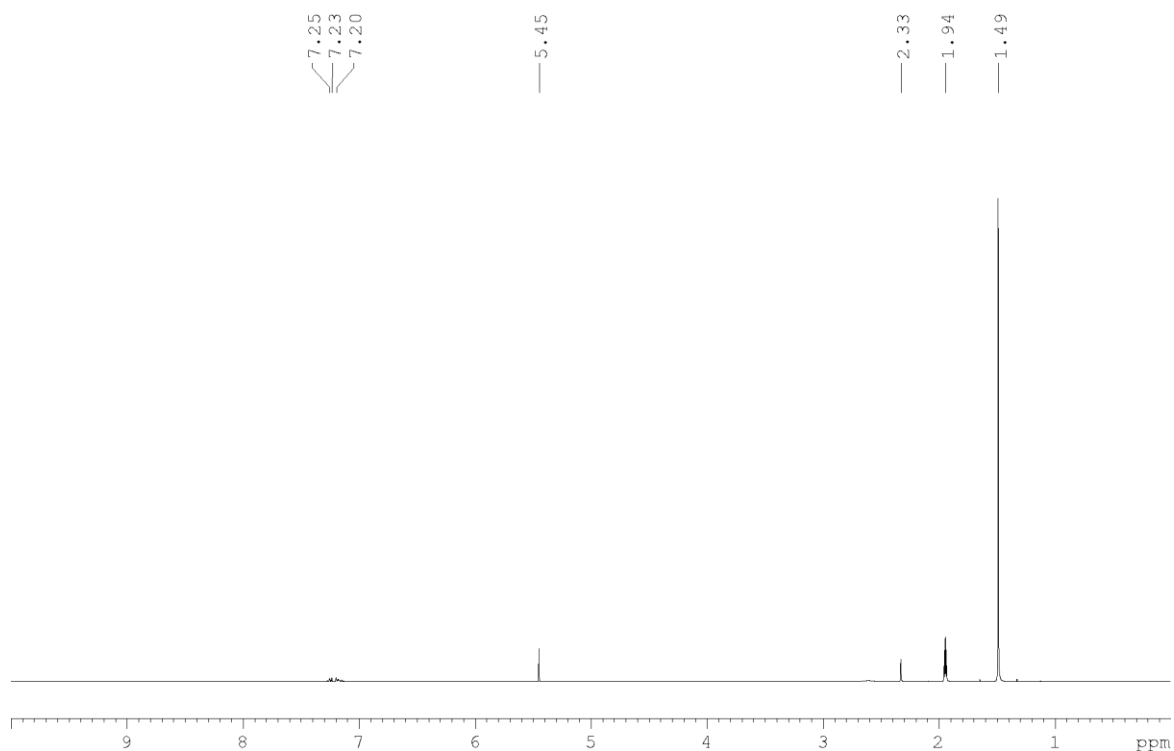


**Figure 3.18.**  $^1\text{H}$  NMR spectrum of **3**. (1.94  $\text{CH}_3\text{CN}$ , 5.45  $\text{CH}_2\text{Cl}_2$ , 7.20-7.25 toluene).

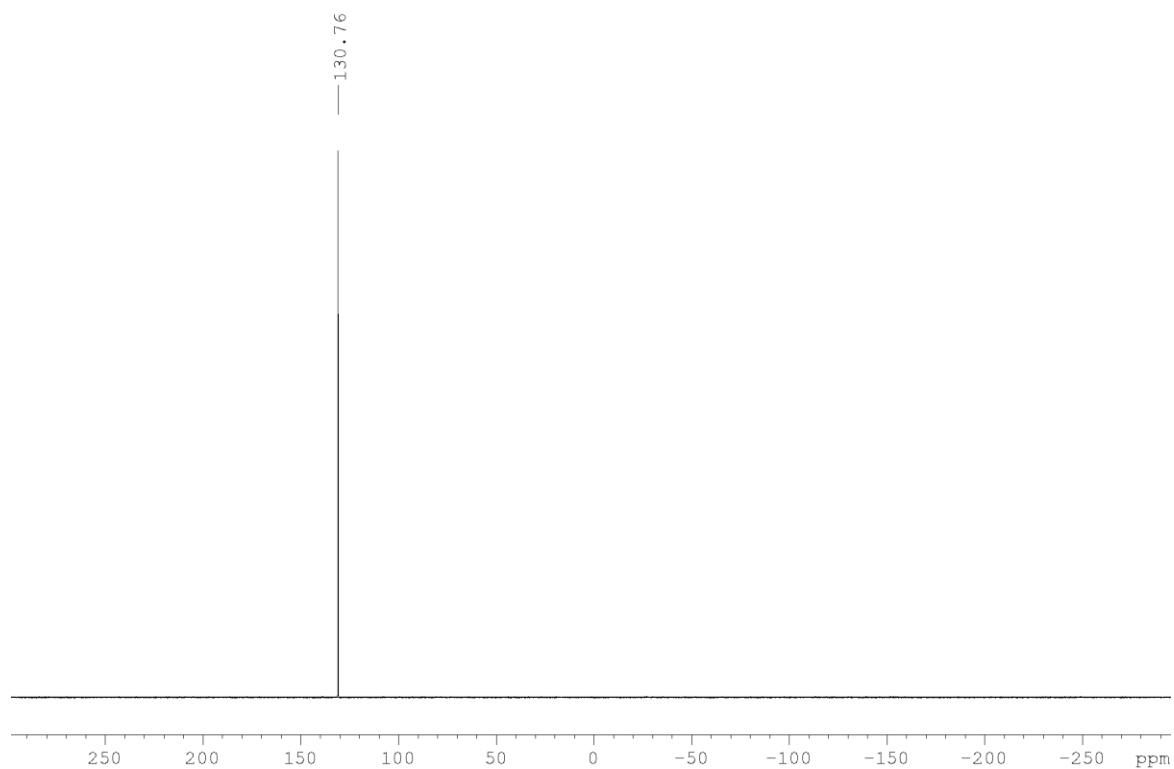


**Figure 3.19.**  $^{31}\text{P}\{^1\text{H}\}$  NMR spectrum of **3**.

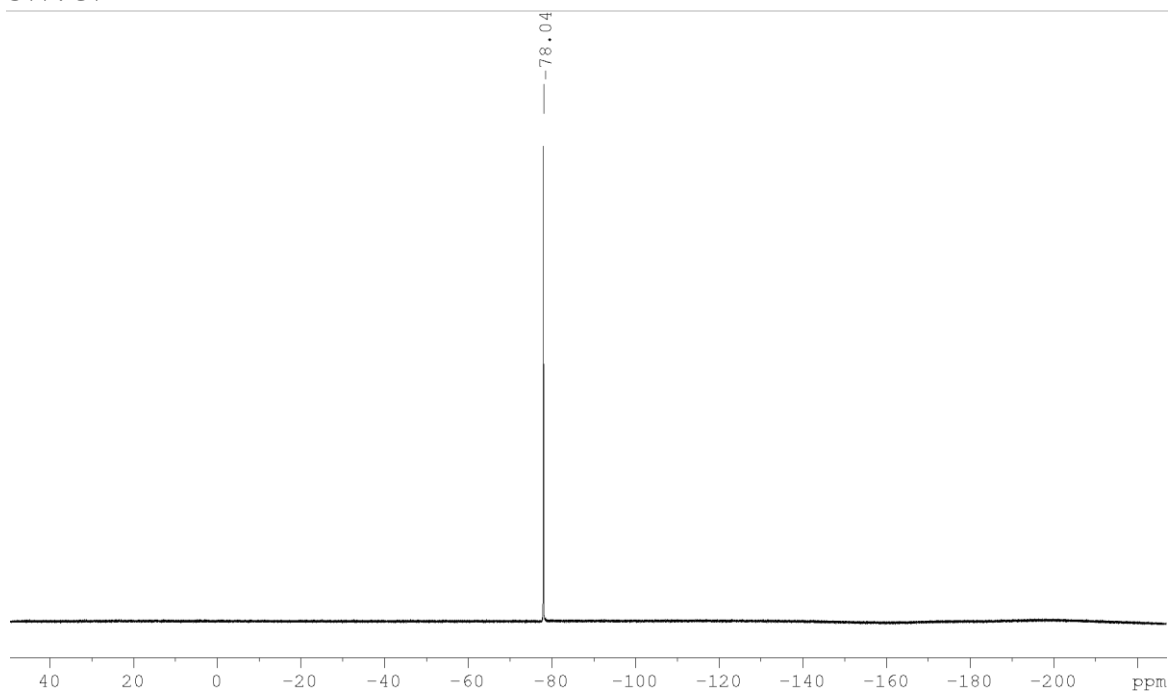


Figure 3.20.  $^{19}\text{F}$  NMR spectrum of **3**.

#### Synthesis of $[\{\text{Cp}^*\text{Fe}(\eta^5\text{-P}_5)\}\text{-tol}]@[\{\{\text{Cp}^*\text{Fe}(\eta^5\text{-P}_5)\}_{12}\{\text{Ag}(\text{SO}_3\text{CF}_3)\}_{20}\}]$ (**4**)

In a thin Schlenk tube a solution of  $\text{Ag}(\text{SO}_3\text{CF}_3)$  (32 mg, 0.125 mmol) in  $\text{CH}_2\text{Cl}_2$  (12 mL) is carefully layered with a green solution of  $[\text{Cp}^*\text{Fe}(\eta^5\text{-P}_5)]$  (15 mg, 0.043 mmol) in toluene (12 mL). Thereby the phase boundary turns yellow. During the diffusion process, the formation of greenish brown rhombohedra of **4** can be observed, which are sometimes accompanied of the isomeric compound **3**. After complete diffusion, the mother liquor is decanted, the crystals are washed with hexane (3 x 5 mL) and dried *in vacuo*.

Analytical data of **4**:

**Yield:** 18 mg (1.8  $\mu\text{mol}$ , 45% referred to  $[\text{Cp}^*\text{Fe}(\eta^5\text{-P}_5)]$ )

$^1\text{H}$  NMR ( $\text{CD}_3\text{CN}$ ):  $\delta$  [ppm] = 1.46 (s,  $[\text{Cp}^*\text{Fe}(\eta^5\text{-P}_5)]$ ).

$^{31}\text{P}\{^1\text{H}\}$  NMR ( $\text{CD}_3\text{CN}$ ):  $\delta$  [ppm] = 134.25 (s,  $[\text{Cp}^*\text{Fe}(\eta^5\text{-P}_5)]$ ).

$^{19}\text{F}\{^1\text{H}\}$  NMR ( $\text{CD}_3\text{CN}$ ):  $\delta$  [ppm] = -77.8 (s, br,  $(\text{SO}_3\text{CF}_3)^-$ ).

**Positive ion ESI-MS** ( $\text{CH}_3\text{CN}$ ):  $m/z$  (%) = 452.8  $[\{\text{Cp}^*\text{Fe}(\eta^5\text{-P}_5)\}\text{Ag}]^+$ , 493.8  $[\{\text{Cp}^*\text{Fe}(\eta^5\text{-P}_5)\}\text{Ag}(\text{CH}_3\text{CN})]^+$ ,  
 798.8  $[\{\text{Cp}^*\text{Fe}(\eta^5\text{-P}_5)\}_2\text{Ag}]^+$ , 1056.6  $[\{\text{Cp}^*\text{Fe}(\eta^5\text{-P}_5)\}_2\text{Ag}_2(\text{SO}_3\text{CF}_3)]^+$ , 1312.7  
 $[\{\text{Cp}^*\text{Fe}(\eta^5\text{-P}_5)\}_2\text{Ag}_3(\text{SO}_3\text{CF}_3)_2]^+$ , 1570.5  $[\{\text{Cp}^*\text{Fe}(\eta^5\text{-P}_5)\}_2\text{Ag}_4(\text{SO}_3\text{CF}_3)_3]^+$ , 1660.7  
 $[\{\text{Cp}^*\text{Fe}(\eta^5\text{-P}_5)\}_3\text{Ag}_3(\text{SO}_3\text{CF}_3)_2]^+$ , 1826.6  $[\{\text{Cp}^*\text{Fe}(\eta^5\text{-P}_5)\}_2\text{Ag}_5(\text{SO}_3\text{CF}_3)_4]^+$ , 1916.6  
 $[\{\text{Cp}^*\text{Fe}(\eta^5\text{-P}_5)\}_3\text{Ag}_4(\text{SO}_3\text{CF}_3)_3]^+$ , 2084.3  $[\{\text{Cp}^*\text{Fe}(\eta^5\text{-P}_5)\}_2\text{Ag}_6(\text{SO}_3\text{CF}_3)_5]^+$ , 2172.2  $[\{\text{Cp}^*\text{Fe}(\eta^5\text{-P}_5)\}_3$



$\text{Ag}_5(\text{SO}_3\text{CF}_3)_4]^+$ , 2172.6  $[\{\text{Cp}^*\text{Fe}(\eta^5\text{-P}_5)\}_3\text{Ag}_5(\text{SO}_3\text{CF}_3)_4]^+$ , 2430.2  $[\{\text{Cp}^*\text{Fe}(\eta^5\text{-P}_5)\}_3\text{Ag}_6(\text{SO}_3\text{CF}_3)_5]^+$ ,  
2686.1  $[\{\text{Cp}^*\text{Fe}(\eta^5\text{-P}_5)\}_3\text{Ag}_7(\text{SO}_3\text{CF}_3)_6]^+$ , 2946.0  $[\{\text{Cp}^*\text{Fe}(\eta^5\text{-P}_5)\}_3\text{Ag}_8(\text{SO}_3\text{CF}_3)_7]^+$ ,

**Negative ion ESI-MS** ( $\text{CH}_3\text{CN}$ ):  $m/z$  (%) = 148.8  $[\text{SO}_3\text{CF}_3]^-$ , 406.7  $[\text{Ag}(\text{SO}_3\text{CF}_3)_2]^-$ .

**Elemental analysis:** Calculated (%) for  $[\{\text{Cp}^*\text{Fe}(\eta^5\text{-P}_5)\}_{13}(\text{AgCF}_3\text{SO}_3)_{20}(\text{C}_7\text{H}_7)(\text{H}_2\text{O})_{20}]$  (10088.54 g/mol): C 18.69, H 2.43, S 6.36, Ag 21.38, Fe 7.20, O 12.69, P 18.03; found: C 17.9, H 2.15, S 7.01, Ag 21.4, Fe 6.47, O 12.08, P 18.03. In the laboratory carrying out the full elemental analysis, it was not possible to treat the sample in the absence of oxygen and moisture, which is why a considerable increase in weight was observed.

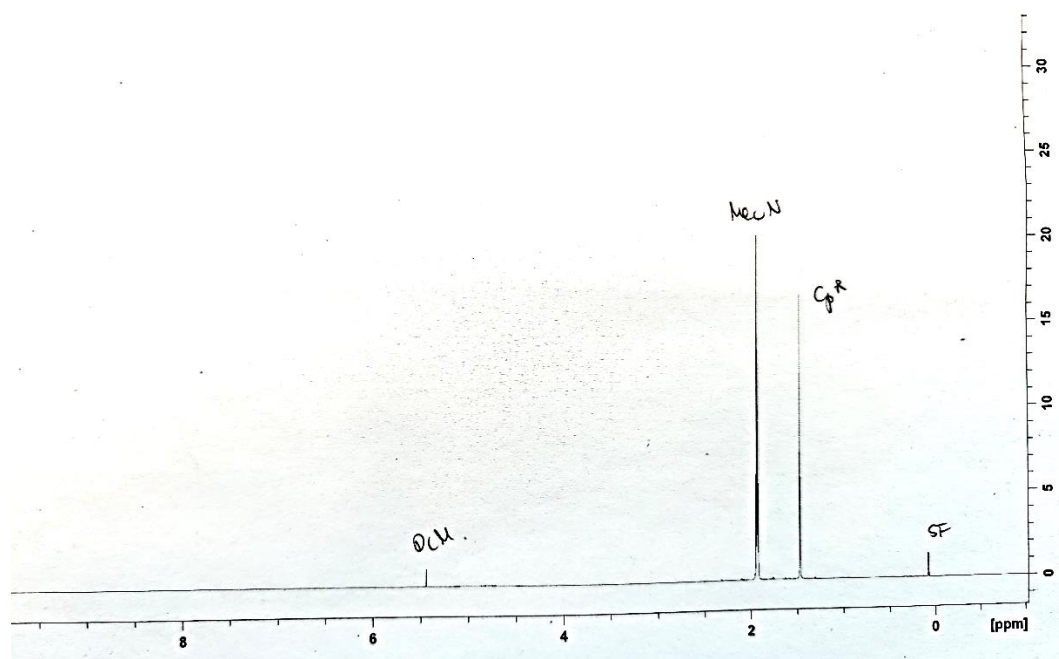


**Figure 3.21.**  $^1\text{H}$  NMR spectrum of **4**. (1.9  $\text{CH}_3\text{CN}$ , 5.4  $\text{CH}_2\text{Cl}_2$ ).

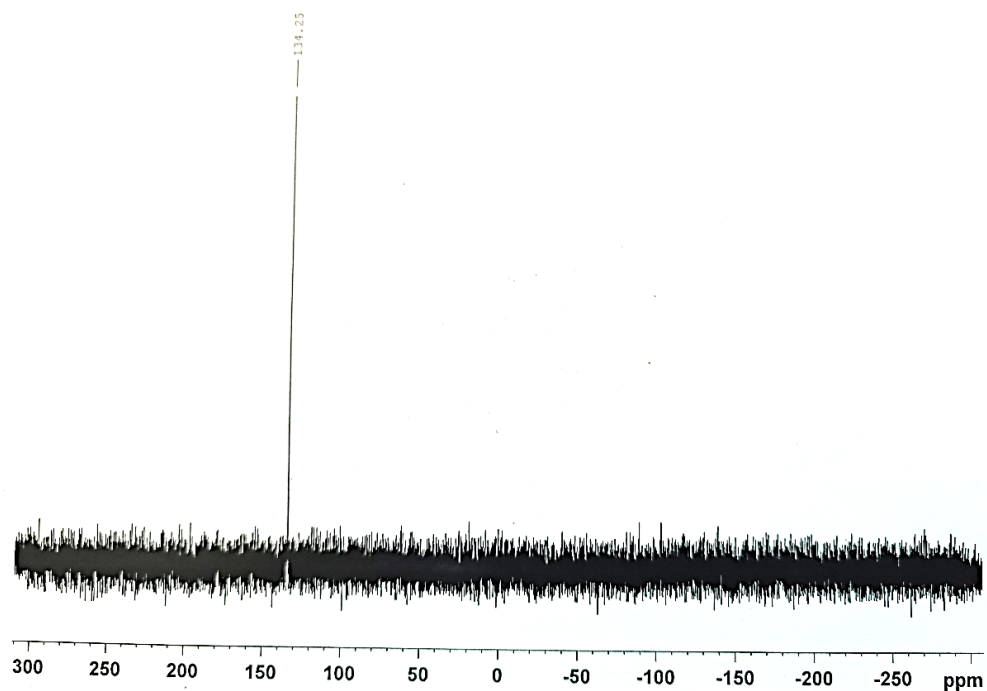


Figure 3.22.  $^{31}\text{P}\{^1\text{H}\}$  NMR spectrum of 4.

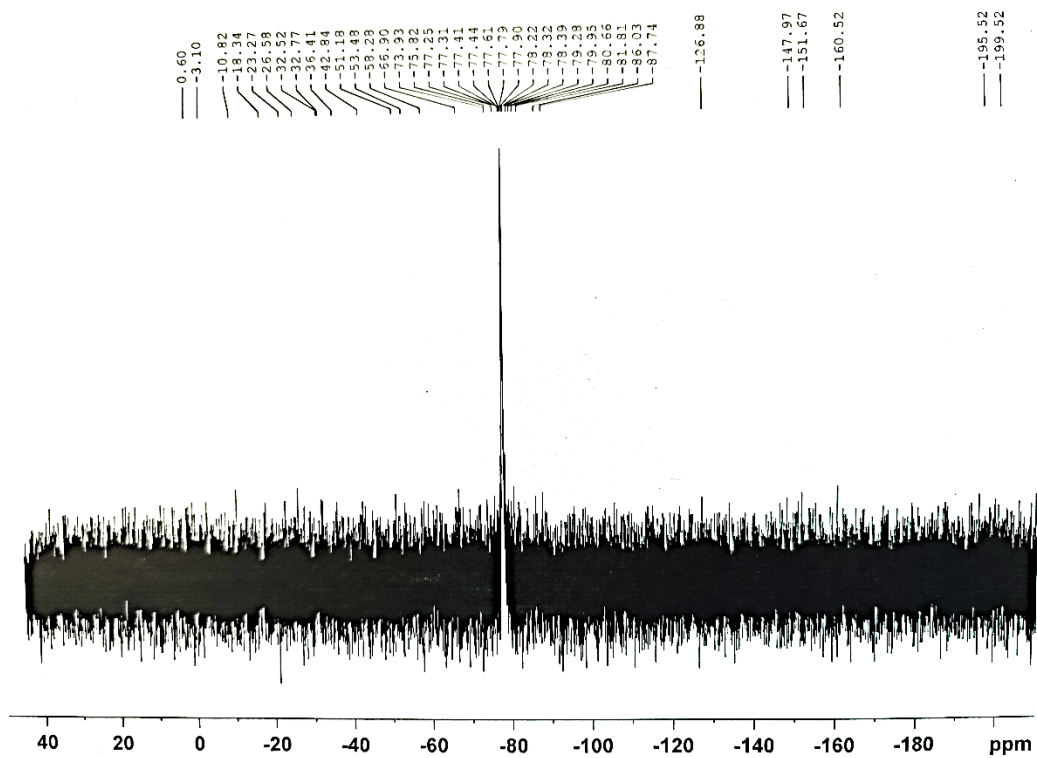


Figure 3.23.  $^{19}\text{F}$  NMR spectrum of 4.

### Synthesis of $[(\text{Cp}^*\text{Fe}(\eta^5\text{-P}_5))\{\text{Ag}(\text{SO}_3\text{CF}_3)\}]$ (**5**)

In a thin Schlenk tube a suspension of  $\text{Ag}(\text{SO}_3\text{CF}_3)$  (14 mg, 0.04 mmol) in  $\text{CH}_2\text{Cl}_2$  (6 mL) is carefully layered with a green solution of  $[\text{Cp}^*\text{Fe}(\eta^5\text{-P}_5)]$  (11 mg, 0.04 mmol) in toluene (6 mL). Thereby, the phase boundary turns yellow. After complete diffusion and a meanwhile appearing color change to brown, brown blocks of **5** are observed on the glass wall. The mother liquor is decanted, the crystals are washed with hexane (2 x 5 mL) and dried *in vacuo*.

Analytical data of **5**

**Yield:** 23 mg (0.033 mmol, 83 % referred to  $[\text{Cp}^*\text{Fe}(\eta^5\text{-P}_5)]$ )

**$^1\text{H}$  NMR** ( $\text{CD}_3\text{CN}$ ):  $\delta$  [ppm] = 0.78 (t,  $\text{CpMe}_4\text{CH}_2\text{CH}_3\text{Fe}(\eta^5\text{-P}_5)$ ), 1.48 (d,  $\text{CpMe}_4\text{CH}_2\text{CH}_3\text{Fe}(\eta^5\text{-P}_5)$ ), 1.98 (q,  $\text{CpMe}_4\text{CH}_2\text{CH}_3\text{Fe}(\eta^5\text{-P}_5)$ ).

**$^{31}\text{P}\{^1\text{H}\}$  NMR** ( $\text{CD}_3\text{CN}$ ):  $\delta$  [ppm] = 136.58 (s,  $\text{Cp}^*\text{Fe}(\eta^5\text{-P}_5)$ ).

**$^{19}\text{F}$  NMR** ( $\text{CD}_3\text{CN}$ ):  $\delta$  [ppm] = -78.04 (s,  $\text{AgSO}_3\text{CF}_3$ ).

**Positive ion ESI-MS** ( $\text{CH}_3\text{CN}$ ):  $m/z$  (%) = 147.9  $[\text{Ag}(\text{CH}_3\text{CN})]^+$ , 188.9  $[\text{Ag}(\text{CH}_3\text{CN})_2]^+$ , 229.9  $[\text{Ag}(\text{CH}_3\text{CN})_3]^+$ , 466.8  $[\text{Cp}^*\text{Fe}(\eta^5\text{-P}_5)\text{Ag}]^+$ , 507.8  $[\text{Cp}^*\text{Fe}(\eta^5\text{-P}_5)\text{Ag}(\text{CH}_3\text{CN})]^+$ , 548.8  $[\text{Cp}^*\text{Fe}(\eta^5\text{-P}_5)\text{Ag}(\text{CH}_3\text{CN})_2]^+$ , 826.7  $[(\text{Cp}^*\text{Fe}(\eta^5\text{-P}_5))_2\text{Ag}]^+$ , 1084.6  $[(\text{Cp}^*\text{Fe}(\eta^5\text{-P}_5))_2\text{Ag}_2(\text{SO}_3\text{CF}_3)]^+$ , 1340.4  $[(\text{Cp}^*\text{Fe}(\eta^5\text{-P}_5))_2\text{Ag}_3(\text{SO}_3\text{CF}_3)_2]^+$ , 1700.4  $[(\text{Cp}^*\text{Fe}(\eta^5\text{-P}_5))_3\text{Ag}_3(\text{SO}_3\text{CF}_3)_2]^+$ , 1958.2  $[(\text{Cp}^*\text{Fe}(\eta^5\text{-P}_5))_3\text{Ag}_4(\text{SO}_3\text{CF}_3)_3]^+$ .

**Negative ion ESI-MS** ( $\text{CH}_3\text{CN}$ ):  $m/z$  (%) = 148.9  $[\text{SO}_3\text{CF}_3]^-$ , 404.8  $[\text{Ag}(\text{SO}_3\text{CF}_3)_2]^-$ .

**Elemental analysis:** Calculated (%) for  $[(\text{Cp}^*\text{Fe}(\eta^5\text{-P}_5))\{\text{Ag}(\text{SO}_3\text{CF}_3)\}(\text{CH}_2\text{Cl}_2)]$  (701.84 g/mol) = 22.25 C, 2.73 H, 4.57 S; found: 22.53 C, 3.11 H, 4.67 S.

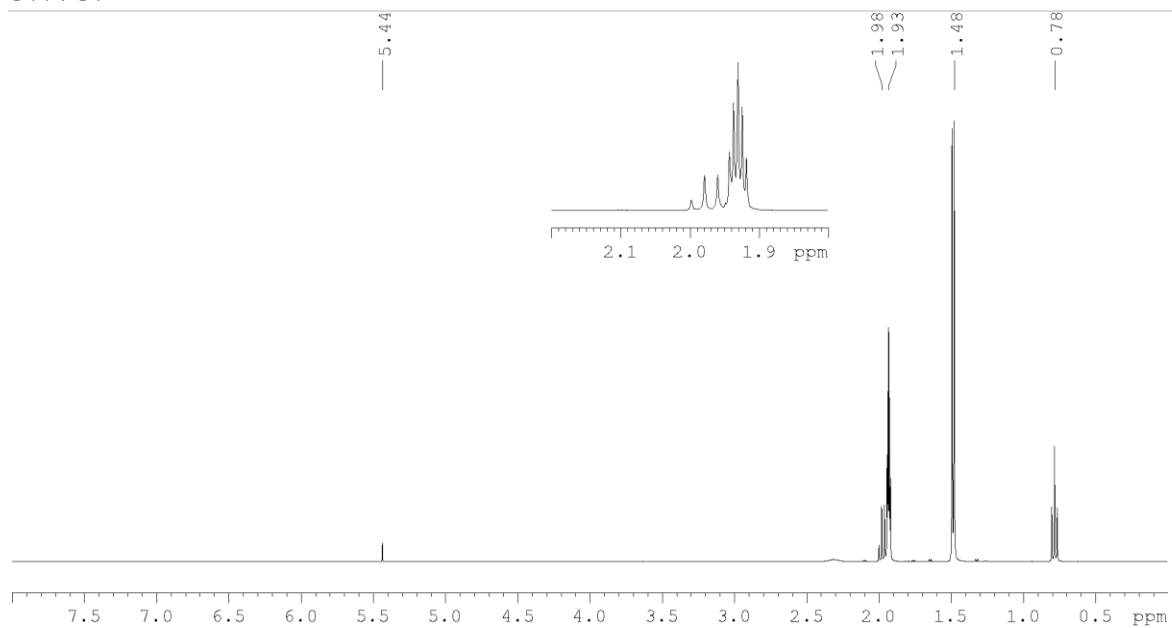


Figure 3.24.  $^1\text{H}$  NMR spectrum of **5**. (1.93  $\text{CH}_3\text{CN}$ , 5.44  $\text{CH}_2\text{Cl}_2$ ).

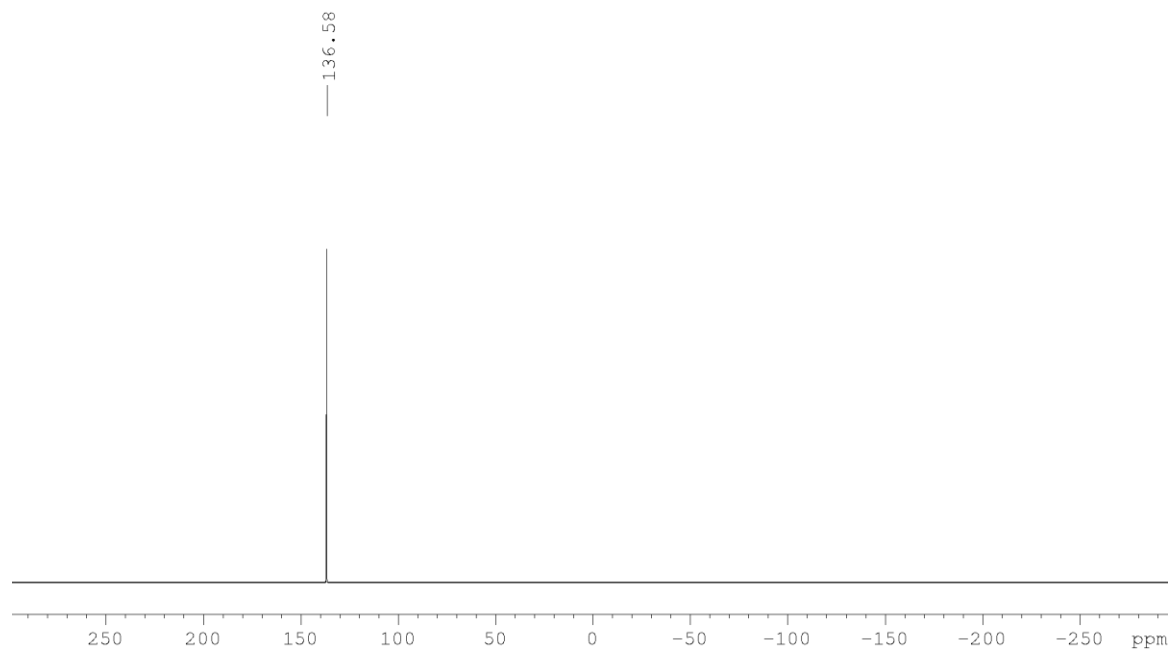


Figure 3.25.  $^{31}\text{P}\{^1\text{H}\}$  NMR spectrum of **5**.

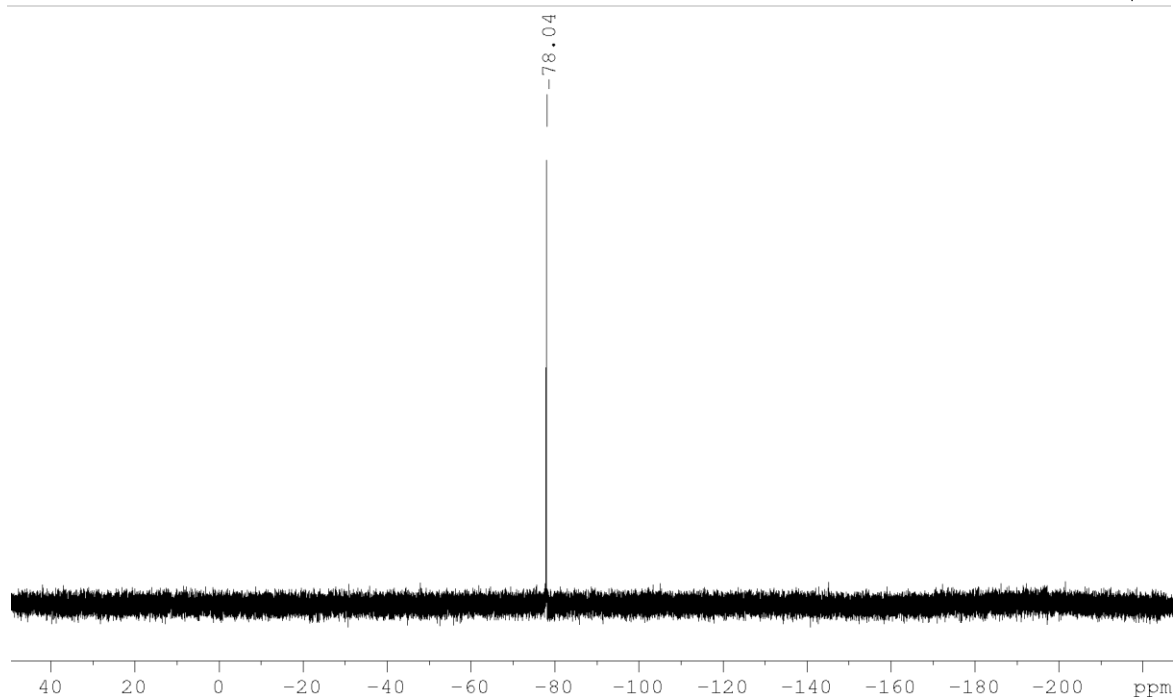


Figure 3.26.  $^{19}\text{F}$  NMR spectrum of **5**.

#### Synthesis of $[\{\text{Cp}^x\text{Fe}(\eta^5\text{-P}_5)\}_2\{\text{Ag}(\text{SO}_3\text{CF}_3)\}_2\{\text{CH}_3\text{CN}\}]$ (**6**)

In a thin Schlenk tube a solution of  $\text{Ag}(\text{SO}_3\text{CF}_3)$  (14 mg, 0.04 mmol) in  $\text{CH}_2\text{Cl}_2$  (5 mL) and  $\text{CH}_3\text{CN}$  (0.5 mL) is carefully layered with a green solution of  $[\text{Cp}^x\text{Fe}(\eta^5\text{-P}_5)]$  (11 mg, 0.04 mmol) in toluene (5 mL). Thereby, the phase boundary turns yellow. After full diffusion and a meanwhile appearing color change to brown, the amount of the solution is halved to 5 mL *via* evaporation on vacuum and afterwards layered with hexane (5 mL). After a week brown needles of **6** are observed at the phase boundary. After complete diffusion the mother liquor is decanted, the crystals are washed with hexane (2 x 5 mL) and dried *in vacuo*.

Analytical data of **6**

**Yield:** 44 mg (0.035 mmol, 88 % referred to  $[\text{Cp}^x\text{Fe}(\eta^5\text{-P}_5)]$ )

$^1\text{H}$  NMR ( $\text{CD}_3\text{CN}$ ):  $\delta$  [ppm] = 0.78 (t,  $\text{CpMe}_4\text{CH}_2\text{CH}_3\text{Fe}(\eta^5\text{-P}_5)$ ), 1.47 (d,  $\text{CpMe}_4\text{CH}_2\text{CH}_3\text{Fe}(\eta^5\text{-P}_5)$ ), 1.95 (s,  $\text{Cp}^x\text{Fe}(\eta^5\text{-P}_5)$ ), 1.98 (q,  $\text{CpMe}_4\text{CH}_2\text{CH}_3\text{Fe}(\eta^5\text{-P}_5)$ ).

$^{31}\text{P}\{^1\text{H}\}$  NMR ( $\text{CD}_3\text{CN}$ ):  $\delta$  [ppm] = 137.29 (s,  $\text{Cp}^x\text{Fe}(\eta^5\text{-P}_5)$ ), 137.38 (s,  $\text{Cp}^x\text{Fe}(\eta^5\text{-P}_5)$ )

The two singulets refer to different indefinable coordination fragments between  $[\text{Cp}^x\text{Fe}(\eta^5\text{-P}_5)]$  and Ag atoms.

$^{19}\text{F}$  NMR ( $\text{CD}_3\text{CN}$ ):  $\delta$  [ppm] = -78.04 (s,  $\text{AgSO}_3\text{CF}_3$ ).

**Positive ion ESI-MS** ( $\text{CH}_3\text{CN}$ ):  $m/z$  (%) = 147.9  $[\text{Ag}(\text{CH}_3\text{CN})]^+$ , 188.9  $[\text{Ag}(\text{CH}_3\text{CN})_2]^+$ , 466.8  $[\text{Cp}^x\text{Fe}(\eta^5\text{-P}_5)\text{Ag}]^+$ , 507.8  $[\text{Cp}^x\text{Fe}(\eta^5\text{-P}_5)\text{Ag}(\text{CH}_3\text{CN})]^+$ , 548.8  $[\text{Cp}^x\text{Fe}(\eta^5\text{-P}_5)\text{Ag}(\text{CH}_3\text{CN})_2]^+$ , 826.7

$[(Cp^xFe(\eta^5-P_5))_2Ag]^+$ , 1084.6  $[(Cp^xFe(\eta^5-P_5))_2Ag_2(SO_3CF_3)]^+$ , 1340.4  $[(Cp^xFe(\eta^5-P_5))_2Ag_3(SO_3CF_3)_2]^+$ , 1700.4  $[(Cp^xFe(\eta^5-P_5))_3Ag_3(SO_3CF_3)_2]^+$ , 1958.2  $[(Cp^xFe(\eta^5-P_5))_3Ag_4(SO_3CF_3)_3]^+$ .

**Negative ion ESI-MS** (CH<sub>3</sub>CN):  $m/z$  (%) = 148.9 [SO<sub>3</sub>CF<sub>3</sub>]<sup>-</sup>.

**Elemental analysis:** Calculated (%) for  $\{(Cp^xFe(\eta^5-P_5))_2\{Ag(SO_3CF_3)\}_2\{CH_3CN\}$  (1274.88 g/mol): 24.50 C, 2.93 H, 1.10 N, 5.03 S; found: 24.55 C, 3.05 H, 0.71 N, 4.99 S.

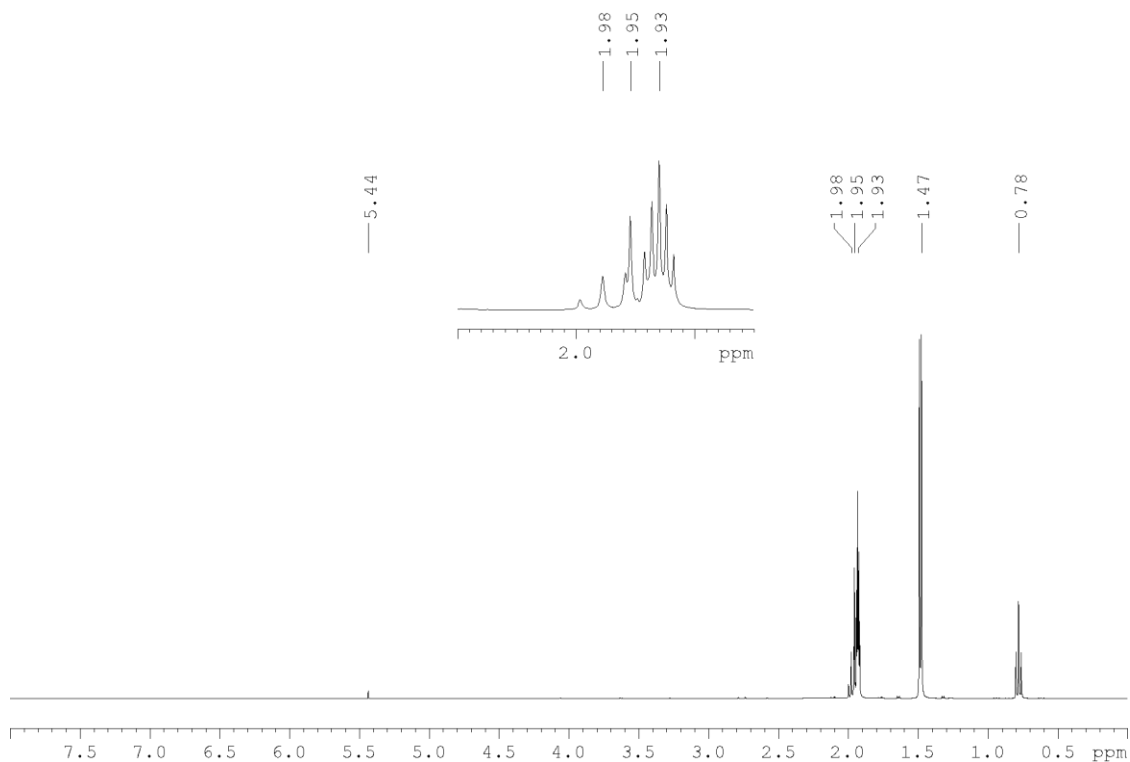


**Figure 3.27.** <sup>1</sup>H NMR spectrum of **6**. (1.93 CH<sub>3</sub>CN, 5.44 CH<sub>2</sub>Cl<sub>2</sub>)

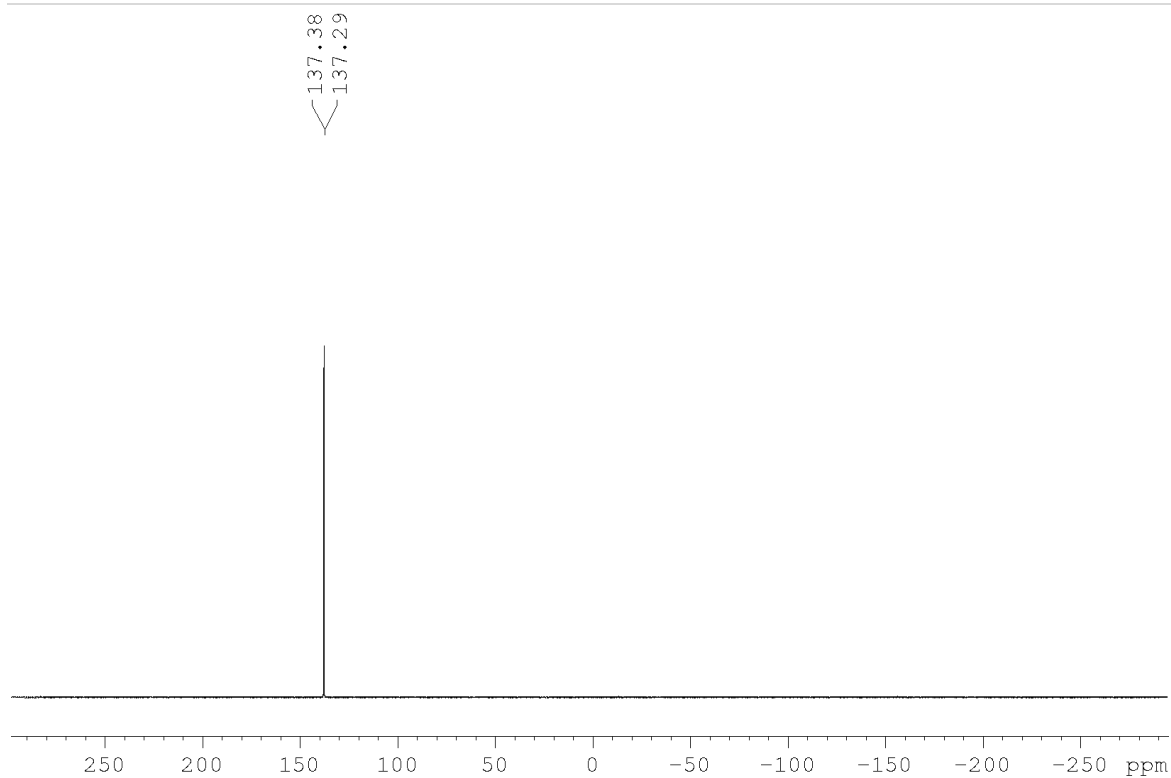


Figure 3.28.  $^{31}\text{P}\{^1\text{H}\}$  NMR spectrum of **6**.

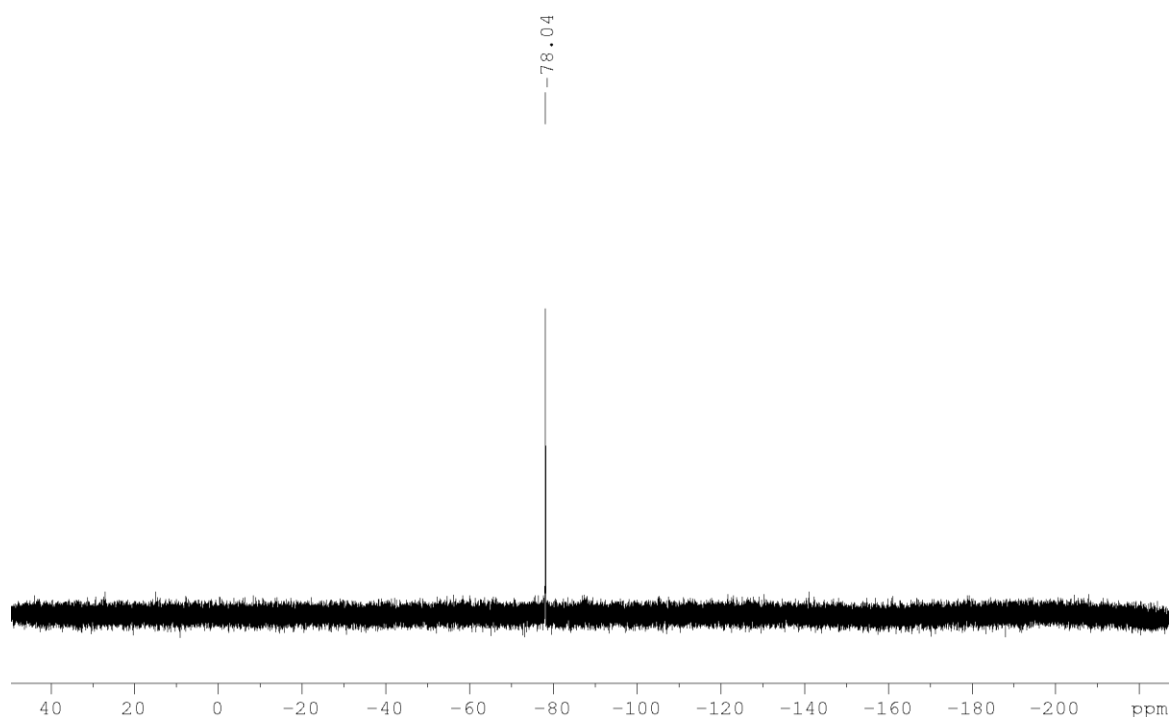


Figure 3.29.  $^{19}\text{F}$  NMR spectrum of **6**.

### Synthesis of $[\{\text{Cp}^*\text{Fe}(\eta^5\text{-P}_5)\}\{\text{Ag}(\text{SO}_3\text{CF}_3)\}_3]$ (**7**)

In a thin Schlenk tube a suspension of  $\text{Ag}(\text{SO}_3\text{CF}_3)$  (14 mg, 0.04 mmol) in  $\text{CH}_2\text{Cl}_2$  (8 mL) is carefully layered with a green solution of  $[\text{Cp}^*\text{Fe}(\eta^5\text{-P}_5)]$  (11 mg, 0.04 mmol) in toluene (8 mL). Thereby, the

phase boundary turns yellow. After two weeks brown needles of yellowish needles of **7** are observed at the phase boundary. After complete diffusion the mother liquor is decanted, the crystals are washed with hexane (3 x 5 mL) and dried *in vacuo*.

Analytical data of **7**

**Yield:** 36 mg (0.03 mmol, 75% referred to  $[(\text{Cp}^*\text{Fe}(\eta^5\text{-P}_5))]$ )

**$^1\text{H}$  NMR** ( $\text{CD}_3\text{CN}$ ):  $\delta$  [ppm] = 0.79 (t,  $\text{CpMe}_4\text{CH}_2\text{CH}_3\text{Fe}(\eta^5\text{-P}_5)$ ), 1.49 (d,  $\text{CpMe}_4\text{CH}_2\text{CH}_3\text{Fe}(\eta^5\text{-P}_5)$ ), 1.98 (q,  $\text{CpMe}_4\text{CH}_2\text{CH}_3\text{Fe}(\eta^5\text{-P}_5)$ ).

**$^{31}\text{P}\{^1\text{H}\}$  NMR** ( $\text{CD}_3\text{CN}$ ):  $\delta$  [ppm] = 126.48 (s,  $\text{Cp}^*\text{Fe}(\eta^5\text{-P}_5)$ ), 126.62 (s,  $(\text{Cp}^*\text{Fe}(\eta^5\text{-P}_5))$ ), 126.77 (s,  $(\text{Cp}^*\text{Fe}(\eta^5\text{-P}_5))$ ).

**$^{19}\text{F}$  NMR** ( $\text{CD}_3\text{CN}$ ):  $\delta$  [ppm] = -78.00 (s,  $\text{AgSO}_3\text{CF}_3$ ).

**Positive ion ESI-MS** ( $\text{CH}_3\text{CN}$ ):  $m/z$  (%) = 147.9  $[\text{Ag}(\text{CH}_3\text{CN})]^+$ , 188.9  $[\text{Ag}(\text{CH}_3\text{CN})_2]^+$ , 229.9  $[\text{Ag}(\text{CH}_3\text{CN})_3]^+$ , 271.0  $[\text{Ag}(\text{CH}_3\text{CN})_4]^+$ , 466.8  $[\text{Cp}^*\text{Fe}(\eta^5\text{-P}_5)\text{Ag}]^+$ , 507.8  $[\text{Cp}^*\text{Fe}(\eta^5\text{-P}_5)\text{Ag}(\text{CH}_3\text{CN})]^+$ , 548.8  $[\text{Cp}^*\text{Fe}(\eta^5\text{-P}_5)\text{Ag}(\text{CH}_3\text{CN})_2]^+$ , 724.6  $[(\text{Cp}^*\text{Fe}(\eta^5\text{-P}_5))\text{Ag}_2(\text{SO}_3\text{CF}_3)]^+$ , 826.7  $[(\text{Cp}^*\text{Fe}(\eta^5\text{-P}_5))_2\text{Ag}]^+$ , 1084.6  $[(\text{Cp}^*\text{Fe}(\eta^5\text{-P}_5))_2\text{Ag}_2(\text{SO}_3\text{CF}_3)]^+$ , 1340.4  $[(\text{Cp}^*\text{Fe}(\eta^5\text{-P}_5))_2\text{Ag}_3(\text{SO}_3\text{CF}_3)_2]^+$ , 1598.3  $[(\text{Cp}^*\text{Fe}(\eta^5\text{-P}_5))_2\text{Ag}_4(\text{SO}_3\text{CF}_3)_3]^+$ , 1700.4  $[(\text{Cp}^*\text{Fe}(\eta^5\text{-P}_5))_3\text{Ag}_3(\text{SO}_3\text{CF}_3)_2]^+$ , 1958.2  $[(\text{Cp}^*\text{Fe}(\eta^5\text{-P}_5))_3\text{Ag}_4(\text{SO}_3\text{CF}_3)_3]^+$ .

**Negative ion ESI-MS** ( $\text{CH}_3\text{CN}$ ):  $m/z$  (%) = 148.9  $[\text{SO}_3\text{CF}_3]^-$ , 404.8  $[\text{Ag}(\text{SO}_3\text{CF}_3)_2]^-$ .

**Elemental analysis:** Calculated (%) for  $[(\text{Cp}^*\text{Fe}(\eta^5\text{-P}_5))\{\text{Ag}(\text{SO}_3\text{CF}_3)\}_3(\text{CH}_2\text{Cl}_2)]$  (1215.73 g/mol): 14.82 C, 1.58 H, 8.51 S; found: 14.66 C, 1.9 H, 8.24 S.



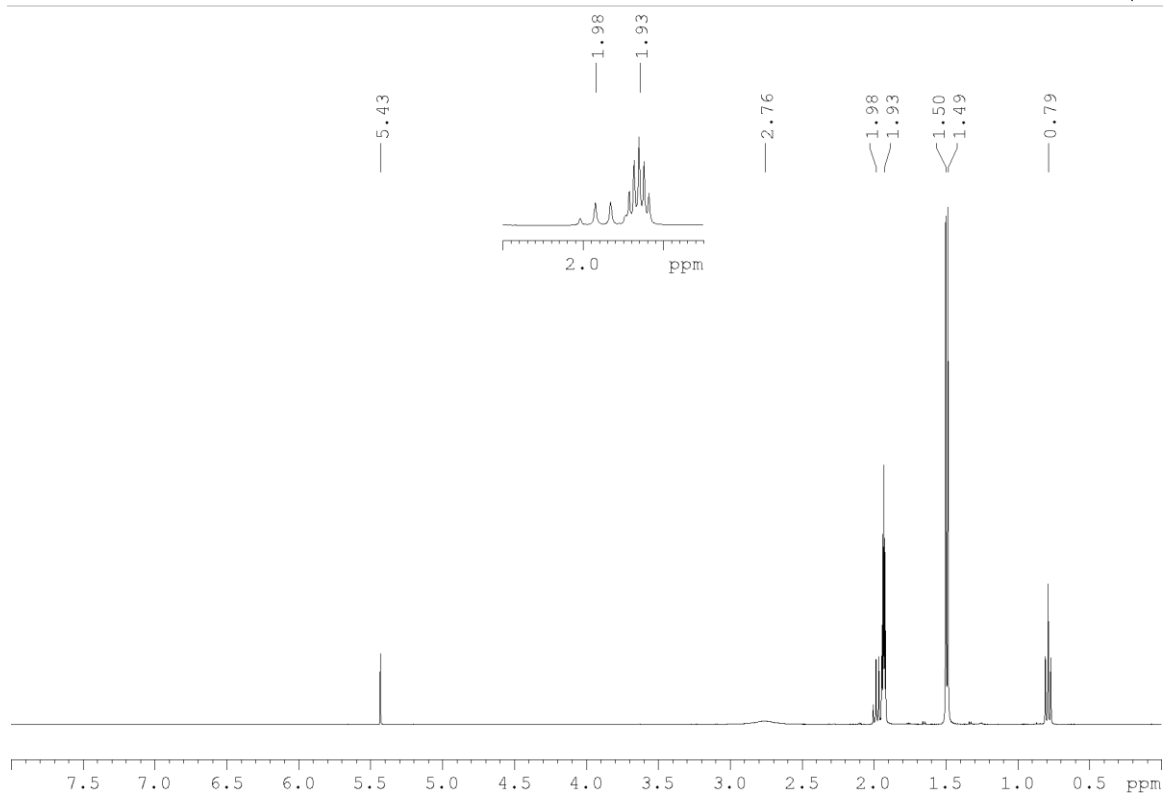


Figure 3.30.  $^1\text{H}$  NMR of spectrum 7. (1.93  $\text{CH}_3\text{CN}$ , 2.76  $\text{H}_2\text{O}$ , 5.43  $\text{CH}_2\text{Cl}_2$ )

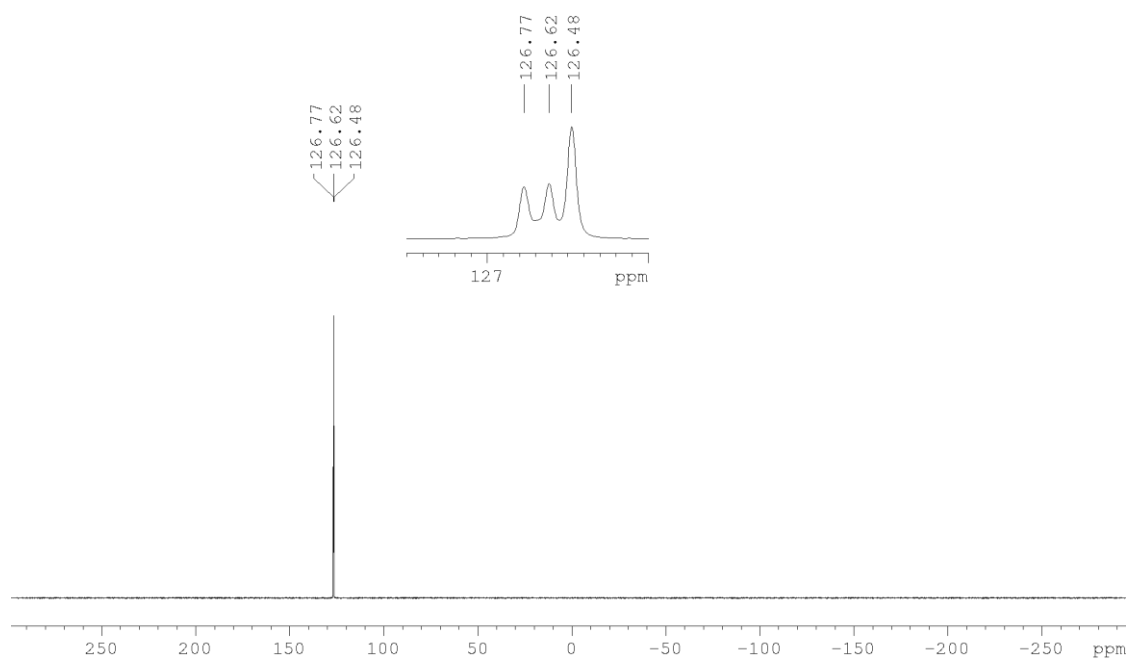


Figure 3.31.  $^{31}\text{P}\{^1\text{H}\}$  NMR spectrum of 7.

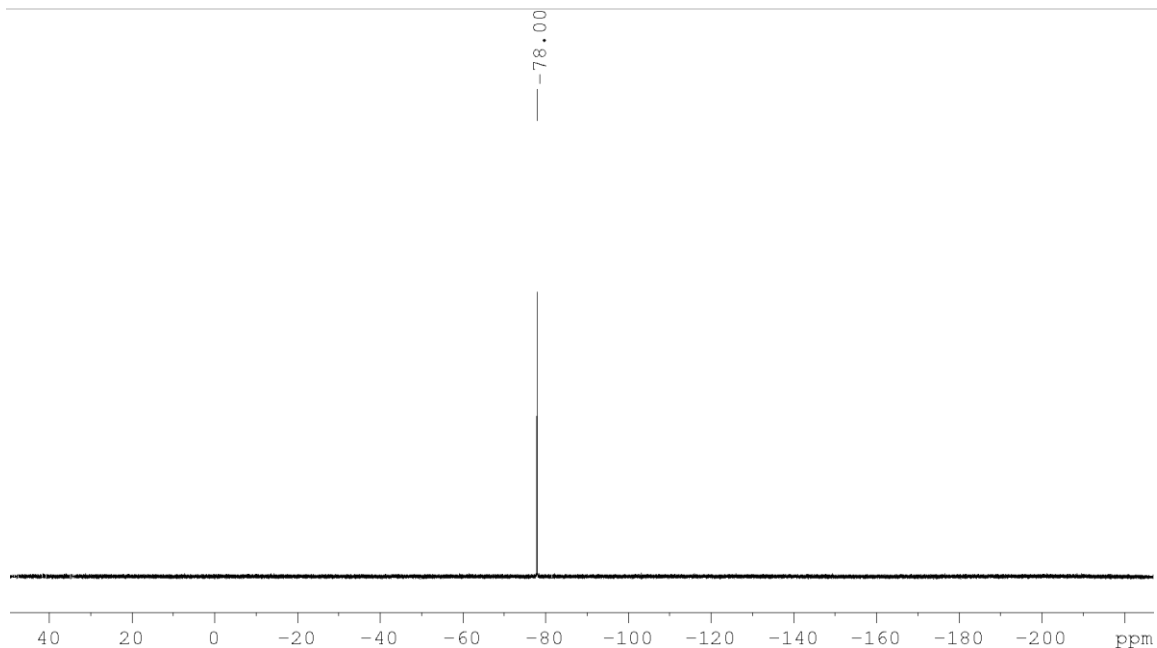


Figure 3.32.  $^{19}\text{F}$  NMR spectrum of **7**.

### Synthesis of $\{\text{Cp}^x\text{Fe}(\eta^5\text{-P}_5)\}@\{[\text{Cp}^x\text{Fe}(\eta^5\text{-P}_5)]_{11}(\text{AgSO}_3\text{CF}_3)_{\sim 10}\}$ (**8**)

In a Schlenk  $\text{Ag}(\text{SO}_3\text{CF}_3)$  (11 mg, 0.04 mmol) and  $[\text{Cp}^x\text{Fe}(\eta^5\text{-P}_5)]$  (14 mg, 0.04 mmol) are suspended in  $\text{CH}_2\text{Cl}_2$  (15 mL) and stirred for two days. Meanwhile, a color change from green to olive green can be observed. After everything is dissolved, hexane was layered onto the solution and the layering was cooled to  $0^\circ\text{C}$ . After three weeks dark-green blocks of **8** can be observed on the bottom of the Schlenk. The mother liquor is decanted after complete diffusion, the crystals are washed with hexane (3 x 5 mL) and dried *in vacuo*.

Analytical data of **8**

**Yield:** 107 mg (0.016 mmol, 39% referred to  $[\text{Cp}^x\text{Fe}(\eta^5\text{-P}_5)]$ )

**$^1\text{H}$  NMR** ( $\text{CD}_3\text{CN}$ ):  $\delta$  [ppm] = 0.77 (t,  $\text{CpMe}_4\text{CH}_2\text{CH}_3\text{Fe}(\eta^5\text{-P}_5)$ ), 1.48 (d,  $\text{CpMe}_4\text{CH}_2\text{CH}_3\text{Fe}(\eta^5\text{-P}_5)$ ), 1.97 (q,  $\text{CpMe}_4\text{CH}_2\text{CH}_3\text{Fe}(\eta^5\text{-P}_5)$ ).

**$^{31}\text{P}\{^1\text{H}\}$  NMR** ( $\text{CD}_3\text{CN}$ ):  $\delta$  [ppm] = 138.96 (s,  $\text{Cp}^x\text{Fe}(\eta^5\text{-P}_5)$ ), 139.15 (s,  $\text{Cp}^x\text{Fe}(\eta^5\text{-P}_5)$ )

The two singulets refer to different indefinable coordination fragments between  $[\text{Cp}^x\text{Fe}(\eta^5\text{-P}_5)]$  and Ag atoms.

**$^{19}\text{F}$  NMR** ( $\text{CD}_3\text{CN}$ ):  $\delta$  [ppm] = -78.08 (s,  $\text{AgSO}_3\text{CF}_3$ ).

**Positive ion ESI-MS** ( $\text{CH}_3\text{CN}$ ):  $m/z$  (%) = 466.8  $[\text{Cp}^x\text{Fe}(\eta^5\text{-P}_5)\text{Ag}]^+$ , 507.8  $[\text{Cp}^x\text{Fe}(\eta^5\text{-P}_5)\text{Ag}(\text{CH}_3\text{CN})]^+$ , 548.9  $[\text{Cp}^x\text{Fe}(\eta^5\text{-P}_5)\text{Ag}(\text{CH}_3\text{CN})_2]^+$ , 826.7  $[(\text{Cp}^x\text{Fe}(\eta^5\text{-P}_5))_2\text{Ag}]^+$ , 970.7  $[(\text{Cp}^x\text{Fe}(\eta^5\text{-P}_5))_2\text{Ag}(\text{CH}_3\text{CN})_6]^+$ , 1084.6  $[(\text{Cp}^x\text{Fe}(\eta^5\text{-P}_5))_2\text{Ag}_2(\text{SO}_3\text{CF}_3)]^+$ , 1567.6  $[(\text{Cp}^x\text{Fe}(\eta^5\text{-P}_5))_3\text{Ag}_2(\text{SO}_3\text{CF}_3)(\text{CH}_3\text{CN})_3]^+$ , 1958.3  $[(\text{Cp}^x\text{Fe}(\eta^5\text{-P}_5))_3\text{Ag}_4(\text{SO}_3\text{CF}_3)_3]^+$ .

Negative ion ESI-MS ( $\text{CH}_3\text{CN}$ ):  $m/z$  (%) = 148.9 [ $\text{SO}_3\text{CF}_3$ ]<sup>-</sup>.

Elemental analysis: Calculated (%) for  $\{\text{Cp}^x\text{Fe}(\eta^5\text{-P}_5)\}@\{[\text{Cp}^x\text{Fe}(\eta^5\text{-P}_5)]_{11}(\text{AgSO}_3\text{CF}_3)_{10}\}$  (6889.06 g/mol): C 24.76, H 2.98, S 4.65; found: C 25.01, H 3.26, S 4.60.

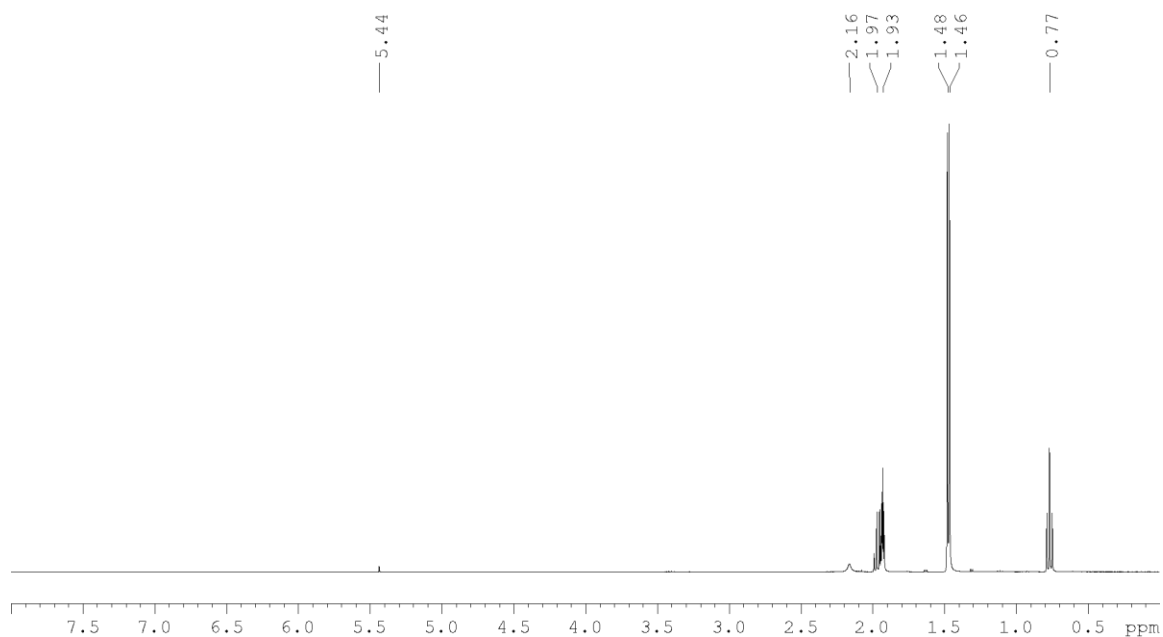


Figure 3.33.  $^1\text{H}$  NMR spectrum of **8**. (1.93  $\text{CH}_3\text{CN}$ , 2.16  $\text{H}_2\text{O}$ , 5.44  $\text{CH}_2\text{Cl}_2$ )

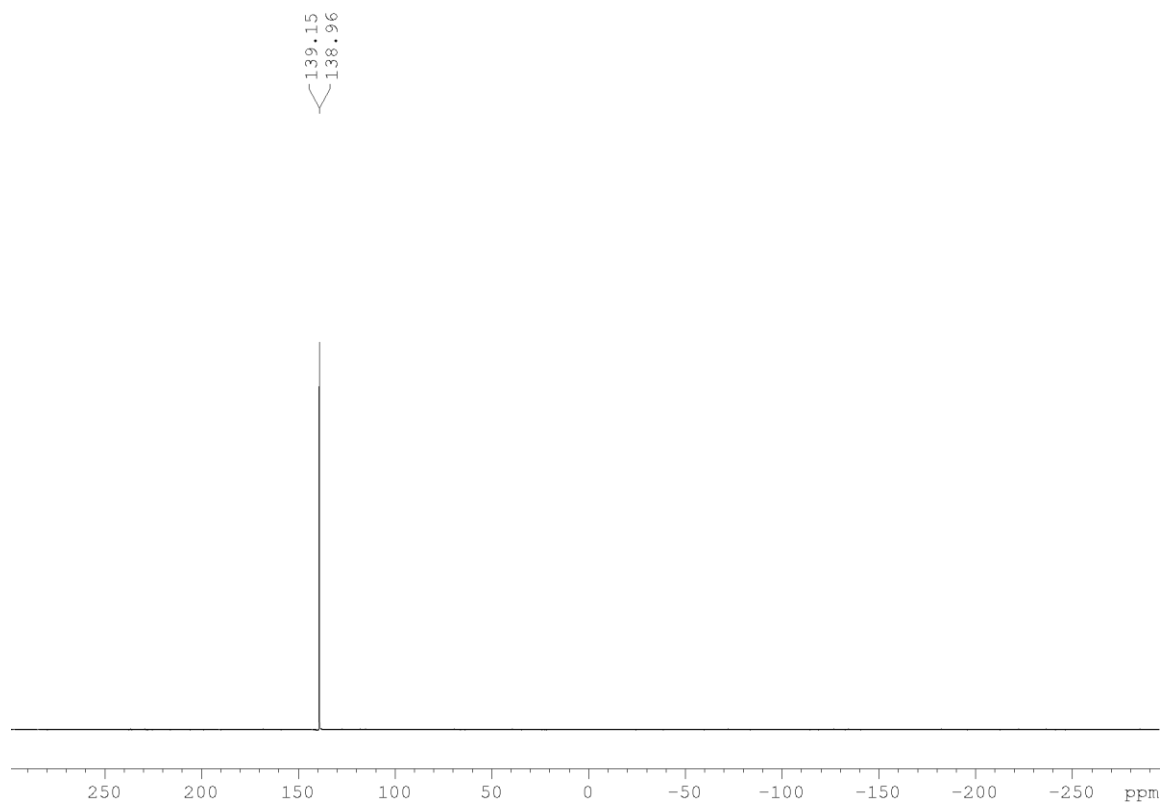


Figure 3.34.  $^{31}\text{P}\{^1\text{H}\}$  NMR spectrum of **8**.

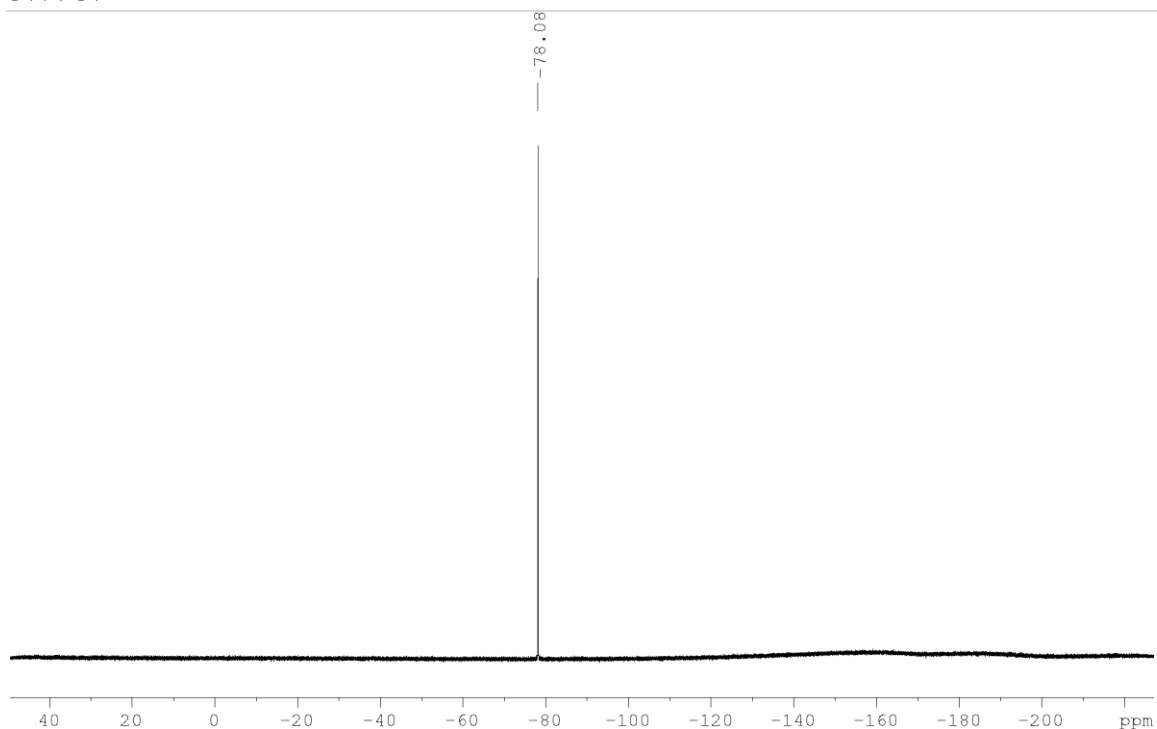


Figure 3.35.  $^{19}\text{F}$  NMR spectrum of **8**.

### Synthesis of $[(\text{Cp}''\text{Fe}(\eta^5\text{-P}_5))\{\text{Ag}(\text{SO}_3\text{CF}_3)\}_2]$ (**9**)

In a thin Schlenk tube a suspension of  $\text{Ag}(\text{SO}_3\text{CF}_3)$  (22 mg, 0.08 mmol) in  $\text{CH}_2\text{Cl}_2$  (9 mL) is carefully layered with a green solution of  $[\text{Cp}''\text{Fe}(\eta^5\text{-P}_5)]$  (15.5 mg, 0.04 mmol) in toluene (9 mL). After a week yellowish needle of **9** are observed at the phase boundary. After complete diffusion the mother liquor is decanted, the crystals are washed with hexane (3 x 5 mL) and dried *in vacuo*.

Analytical data of **9**

**Yield:** 31 mg (0.031 mmol, 79% referred to  $[\text{Cp}''\text{Fe}(\eta^5\text{-P}_5)]$ )

**$^1\text{H}$  NMR** ( $\text{CD}_3\text{CN}$ ):  $\delta$  [ppm] = 1.19 (s,  $\text{Cp}(\text{C}(\text{CH}_3)_3)_2\text{Fe}(\eta^5\text{-P}_5)$ ), 4.28 (s,  $\text{Cp}''\text{Fe}(\eta^5\text{-P}_5)$ ), 4.37 (s,  $\text{Cp}''\text{Fe}(\eta^5\text{-P}_5)$ ).

**$^{31}\text{P}\{^1\text{H}\}$  NMR** ( $\text{CD}_3\text{CN}$ ):  $\delta$  [ppm] = 143.75 (s,  $[\text{Cp}''\text{Fe}(\eta^5\text{-P}_5)]$ ), 143.86 (s,  $[\text{Cp}''\text{Fe}(\eta^5\text{-P}_5)]$ ), 143.95 (s,  $[\text{Cp}''\text{Fe}(\eta^5\text{-P}_5)]$ ).

The three singulets refer to different indefinable coordination fragments between  $[\text{Cp}''\text{Fe}(\eta^5\text{-P}_5)]$  and Ag atoms. (see Figure 37)

**$^{19}\text{F}$  NMR** ( $\text{CD}_3\text{CN}$ ):  $\delta$  [ppm] = -77.99 (s,  $\text{AgSO}_3\text{CF}_3$ ).

**Positive ion ESI-MS** ( $\text{CH}_3\text{CN}$ ):  $m/z$  (%) = 147.9  $[\text{Ag}(\text{CH}_3\text{CN})]^+$ , 188.9  $[\text{Ag}(\text{CH}_3\text{CN})_2]^+$ , 229.9  $[\text{Ag}(\text{CH}_3\text{CN})_3]^+$ , 271.0  $[\text{Ag}(\text{CH}_3\text{CN})_4]^+$ , 494.8 9  $[\text{Cp}''\text{Fe}(\eta^5\text{-P}_5)\text{Ag}]^+$ , 535.9  $[(\text{Cp}''\text{Fe}(\eta^5\text{-P}_5)\text{Ag}(\text{CH}_3\text{CN}))]^+$ , 576.9  $[(\text{Cp}''\text{Fe}(\eta^5\text{-P}_5)\text{Ag}(\text{CH}_3\text{CN})_2)]^+$ , 882.84  $[(\text{Cp}''\text{Fe}(\eta^5\text{-P}_5))_2\text{Ag}]^+$ , 1140.6  $[(\text{Cp}''\text{Fe}(\eta^5\text{-P}_5))_2\text{Ag}]^+$ .

$\text{P}_5)_2\text{Ag}_2(\text{SO}_3\text{CF}_3)]^+$ , 1396.5  $[(\text{Cp}''\text{Fe}(\eta^5\text{-P}_5))_2\text{Ag}_3(\text{SO}_3\text{CF}_3)_2]^+$ , 1784.5  $[(\text{Cp}''\text{Fe}(\eta^5\text{-P}_5))_3\text{Ag}_3(\text{SO}_3\text{CF}_3)_2]^+$ ,  
2042.3  $[(\text{Cp}''\text{Fe}(\eta^5\text{-P}_5))_3\text{Ag}_4(\text{SO}_3\text{CF}_3)_3]^+$ .

**Negative ion ESI-MS** ( $\text{CH}_3\text{CN}$ ):  $m/z$  (%) = 148.9  $[\text{SO}_3\text{CF}_3]^-$ .

**Elemental analysis:** Calculated (%) for  $[(\text{Cp}''\text{Fe}(\eta^5\text{-P}_5))(\text{AgSO}_3\text{CF}_3)_2(\text{CH}_2\text{Cl}_2)]$  (986.84 g/mol): C 19.47,  
H 2.35, S 6.50; found: C 19.04, H 2.99, S 6.56.

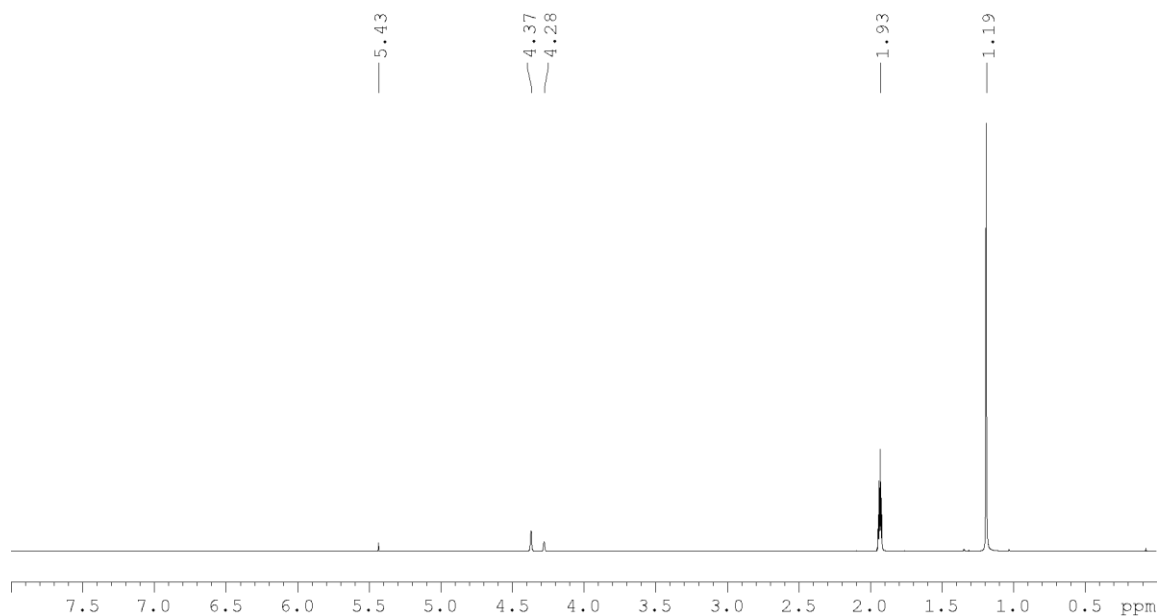


**Figure 3.36.**  $^1\text{H}$  NMR spectrum of **9**. (1.93  $\text{CH}_3\text{CN}$ , 5.43  $\text{CH}_2\text{Cl}_2$ )

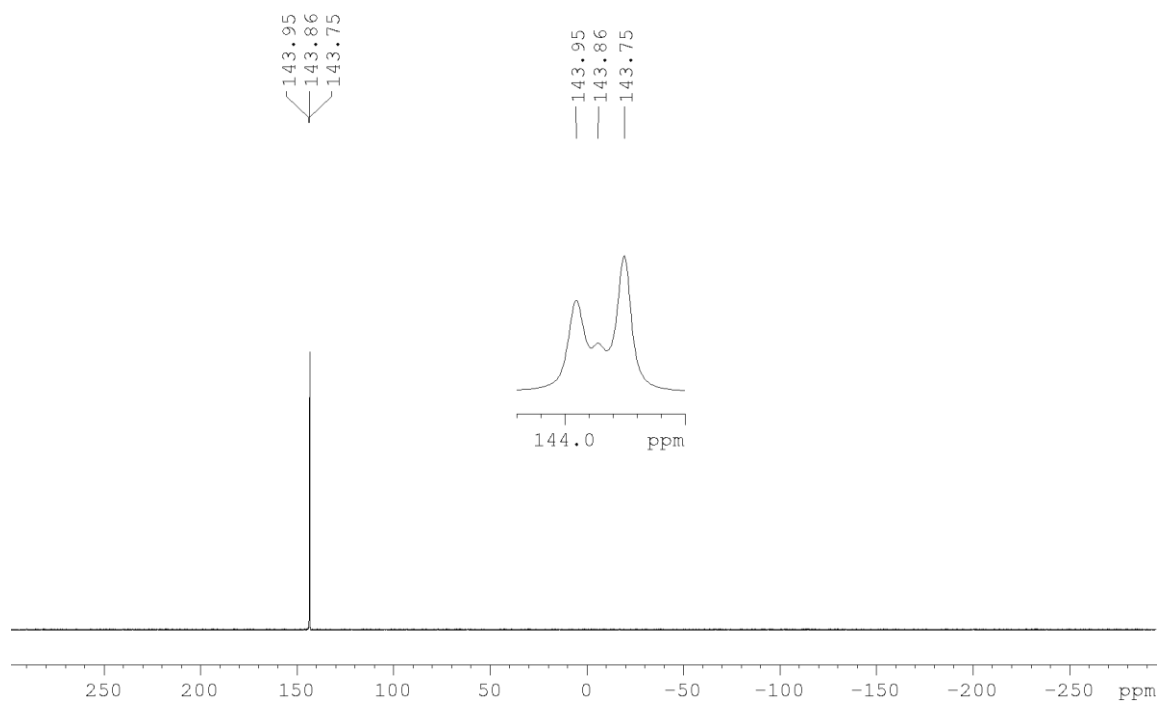


**Figure 3.37.**  $^{31}\text{P}\{^1\text{H}\}$  NMR spectrum of **9**.

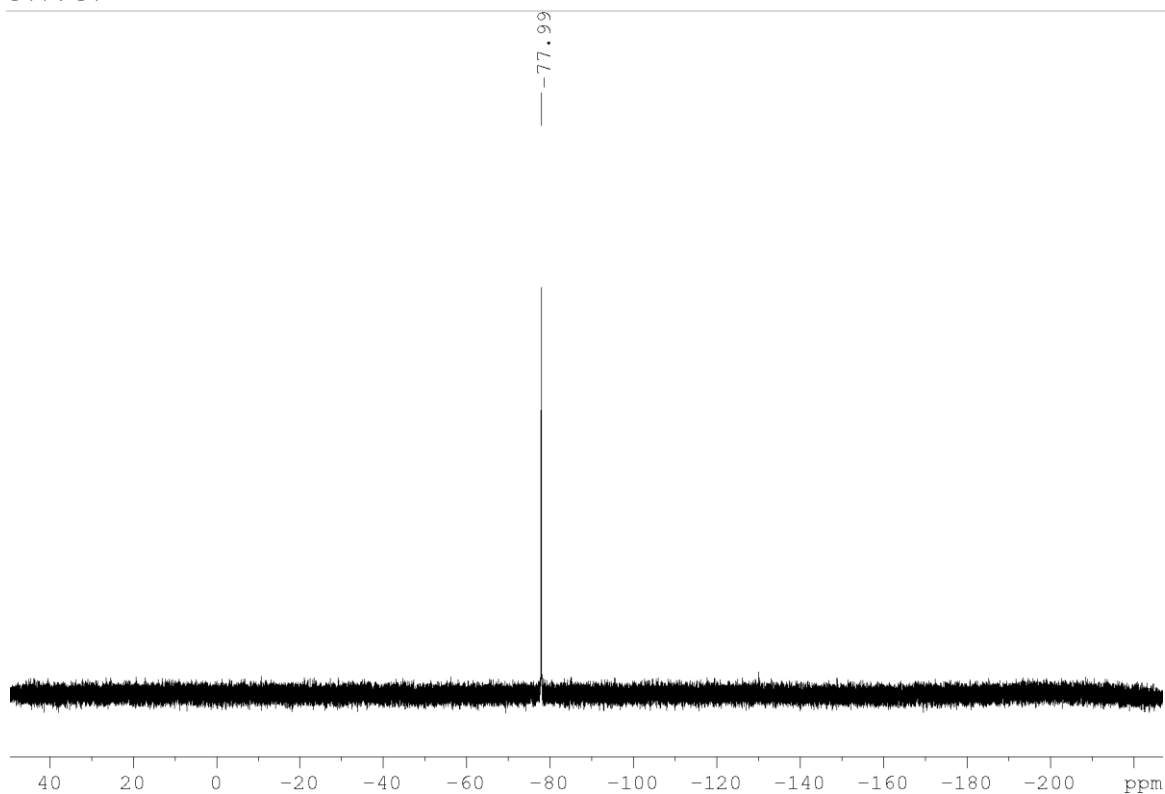


Figure 3.38.  $^{19}\text{F}$  NMR spectrum of **9**.

### Synthesis of $[\{\text{Cp}^{\text{Bn}}\text{Fe}(\eta^5\text{-P}_5)\}_{12}\{\text{Ag}(\text{CF}_3\text{SO}_3)\}_{20}]$ (**10**)

A suspension of  $\text{AgCF}_3\text{SO}_3$  (14 mg, 0,055 mmol) in  $\text{CH}_2\text{Cl}_2$  (8 mL) is carefully layered with a green solution of  $[\text{Cp}^{\text{Bn}}\text{Fe}(\eta^5\text{-P}_5)]$  (20 mg, 0.028 mmol) in toluene (8 mL). After complete diffusion, the brownish solution is layered with hexane. A few hours later, the growth of deep red-brown crystals of **9** can be observed at the phase boundary. After complete diffusion, the mother liquor is decanted, the crystals are washed with hexane (3 x 5 mL) and dried *in vacuo*.

Analytical data of **10**:

**Yield:** 17 mg (1.1  $\mu\text{mol}$ , 49% referred to  $[\text{Cp}^{\text{Bn}}\text{Fe}(\eta^5\text{-P}_5)]$ )

**$^1\text{H}$  NMR** ( $\text{CD}_2\text{Cl}_2$ , 293K)  $\delta$  [ppm] = 4.13 (m,  $[\text{Cp}^{\text{Bn}}\text{Fe}(\eta^5\text{-P}_5)]$ ), 6.27 (m,  $[\text{Cp}^{\text{Bn}}\text{Fe}(\eta^5\text{-P}_5)]$ ), 6.74 (m,  $[\text{Cp}^{\text{Bn}}\text{Fe}(\eta^5\text{-P}_5)]$ ), 6.93 (m,  $[\text{Cp}^{\text{Bn}}\text{Fe}(\eta^5\text{-P}_5)]$ ).

**$^{31}\text{P}\{^1\text{H}\}$  NMR** ( $\text{CD}_2\text{Cl}_2$ , 293 K):  $\delta$  [ppm] = -41.67 (s(br),  $[\text{Cp}^{\text{Bn}}\text{Fe}(\eta^5\text{-P}_5)]$ ), 69.51 (s(br),  $[\text{Cp}^{\text{Bn}}\text{Fe}(\eta^5\text{-P}_5)]$ ), 127.89 (s(br),  $[\text{Cp}^{\text{Bn}}\text{Fe}(\eta^5\text{-P}_5)]$ ), 154.89 (s,  $[\text{Cp}^{\text{Bn}}\text{Fe}(\eta^5\text{-P}_5)]$ ),

**$^{31}\text{P}\{^1\text{H}\}$  MAS NMR:**  $\delta$  [ppm] = 117.66 (m(br),  $\omega = 14375$  Hz,  $[\text{Cp}^{\text{Bn}}\text{Fe}(\eta^5\text{-P}_5)]$ ), -37.28 (m(br),  $\omega = -4479$  Hz,  $[\text{Cp}^{\text{Bn}}\text{Fe}(\eta^5\text{-P}_5)]$ )

**DOSY:** dissolved starting materials:  $M = 3357$  g/mol,  $d = 3.4$  nm, dissolved crystal:  $M = 2613$  g/mol,  $d = 3.0$  nm; calculated for  $[\{\text{Cp}^{\text{Bn}}\text{Fe}(\eta^5\text{-P}_5)\}_{12}(\text{AgSO}_3\text{CF}_3)_{20}]$ :  $M = 13856$  g/mol, 3.3 nm.

**Positive ion ESI-MS** ( $\text{CH}_2\text{Cl}_2/\text{CH}_3\text{CN}$ ):  $m/z$  (%) = 531.2  $[\text{Cp}^{\text{Bn}}\text{O}]^+$ , 833.1  $[\{\text{Cp}^{\text{Bn}}\text{Fe}(\eta^5\text{-P}_5)\}\text{Ag}]^+$ , 874.1  $[\{\text{Cp}^{\text{Bn}}\text{Fe}(\eta^5\text{-P}_5)\}\text{Ag}(\text{CH}_3\text{CN})]^+$ , 1091.0  $[\{\text{Cp}^{\text{Bn}}\text{Fe}(\eta^5\text{-P}_5)\}\text{Ag}_2\text{SO}_3\text{CF}_3]^+$ , 1561.3  $[\{\text{Cp}^{\text{Bn}}\text{Fe}(\eta^5\text{-P}_5)\}_2\text{Ag}]^+$ , 1817.5  $[\{\text{Cp}^{\text{Bn}}\text{Fe}(\eta^5\text{-P}_5)\}_2\text{Ag}_2\text{SO}_3\text{CF}_3]^+$ , 2075.6  $[\{\text{Cp}^{\text{Bn}}\text{Fe}(\eta^5\text{-P}_5)\}_2\text{Ag}_3(\text{SO}_3\text{CF}_3)_2]^+$ , 2331.0  $[\{\text{Cp}^{\text{Bn}}\text{Fe}(\eta^5\text{-P}_5)\}_2\text{Ag}_4(\text{SO}_3\text{CF}_3)_3]^+$ .

**Negative ion ESI-MS** ( $\text{CH}_2\text{Cl}_2/\text{CH}_3\text{CN}$ ):  $m/z$  (%) = 148.6  $[\text{SO}_3\text{CF}_3]^-$ , 406.7  $[\text{Ag}(\text{SO}_3\text{CF}_3)_2]^-$ , 502.7  $[\text{Fe}(\text{SO}_3\text{CF}_3)_3]^-$

**Elemental analysis:** Calculated (%) for  $[\{\text{Cp}^{\text{Bn}}\text{Fe}(\eta^5\text{-P}_5)\}_{12}(\text{AgSO}_3\text{CF}_3)_{20}(\text{H}_2\text{O})_{40}(\text{CH}_2\text{Cl}_2)_5]$  (15001.3 g/mol): C 40.43, H 3.43, S 4.28, Ag 14.38, Fe 4.47, O 10.67, P 12.39; found: C 40.33, H 2.97, S 4.75, Ag 18.20, Fe 4.19, O 10.66, P 12.39. In the laboratory carrying out the full elemental analysis, it was not possible to treat the sample in the absence of oxygen and moisture, which is why a considerable increase in weight was observed.

**TEM measurements:** measured diameter of selected aggregates /nm: 2.07, 2.10, 2.27, 2.33, 2.45, 2.54, 2.68, 2.74, 2.74, 2.74, 2.77, 2.77, 2.83, 2.89, 3.00, 3.06, 3.06, 3.18, 3.24, 2.33. Mean value: 2.7(3) nm; Expected diameter:  $\approx$  3.30 nm.

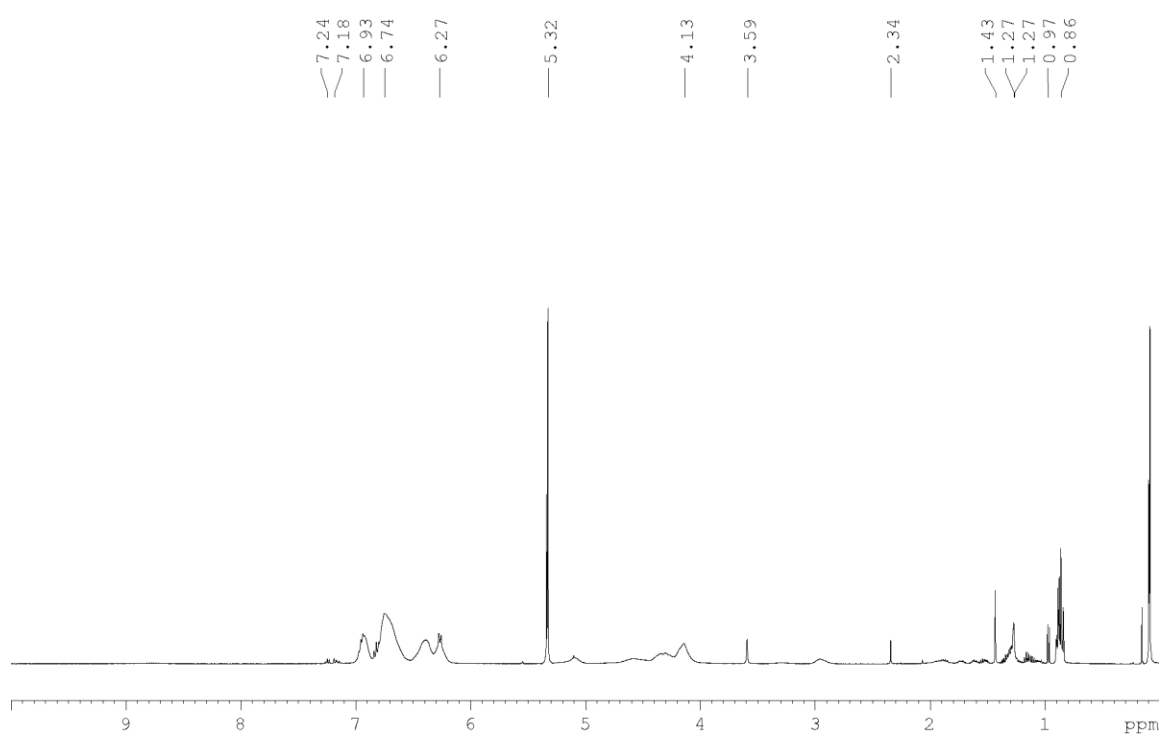


**Figure 3.39.**  $^1\text{H}$  NMR spectrum of **10**. (0.09 grease, 0.86 hexane, 0.97 grease 1.27 hexane, 1.44 solvent residues, 2.34 toluene, 5.32  $\text{CH}_2\text{Cl}_2$ , 7.18 toluene, 7.24 toluene)

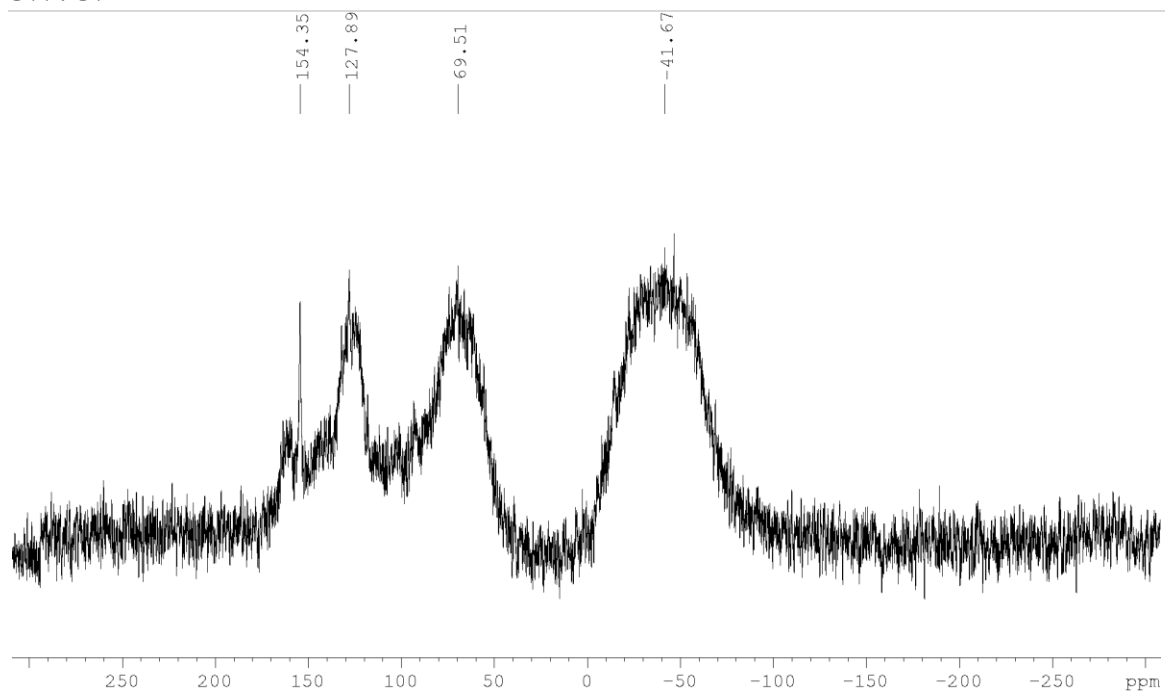


Figure 3.40.  $^{31}\text{P}\{^1\text{H}\}$  NMR spectrum of 10.

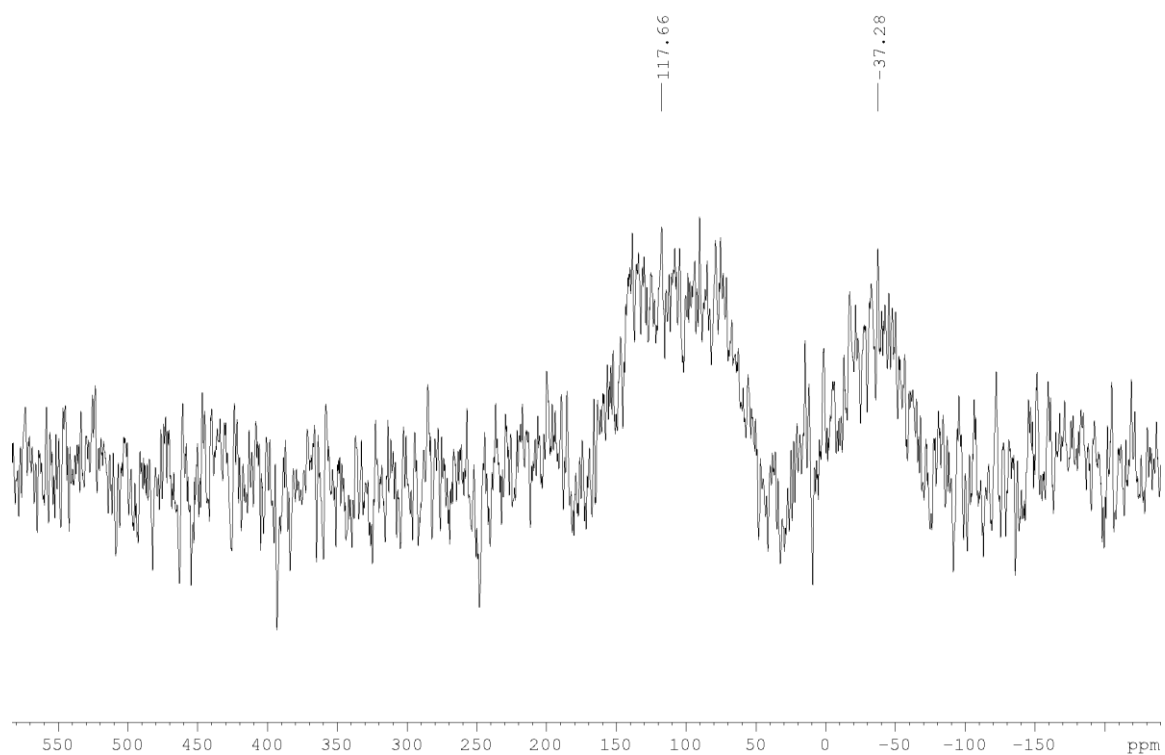


Figure 3.41.  $^{31}\text{P}\{^1\text{H}\}$  MAS NMR spectrum of 10.



### 3.5 Crystallographic Details and Structure Refinement

#### Experimental

Crystals of **1-10** were taken from a Schlenk flask under a stream of argon and immediately covered with perfluorinated Fomblin® mineral oil to prevent decomposition and a loss of solvent. The quickly chosen single crystals covered by a protective film of the oil were immediately placed into a stream of cold nitrogen ( $T = 90 - 123 \text{ K}$ ) with the pre-centered goniometer head with CryoMount® and mounted on the goniometer of a diffractometer.

Crystals of **1**, **4**, **9** and **10** were carefully selected, mounted on a magnetic holder with CryoMount®, checked for quality and stored into a Dewar vessel in liquid nitrogen using standard cryocrystallography tools. After a few weeks, they were transported to the DESY PETRA III synchrotron (Hamburg, Germany). Using standard cryovial technique, it was placed into a Dewar vessel filled with liquid nitrogen among other crystals. A robotic mounting/demounting using UNIPUCK standard was used for further manipulations in the P11 beamline hutch.<sup>[44]</sup>

The data for **3**, **4** and **10** were collected on an Agilent Technologies diffractometer equipped with a Titan<sup>S2</sup> CCD detector and a SuperNova CuK $\alpha$  microfocus source  $\omega$  scans. Unfortunately, undesirable icing of the single crystals was observed during all experiments for supramolecules **3**, **4** and **10** performed in-house due to time-consuming measurement strategies caused by low symmetry and high exposure times. For this reason, alternative datasets were collected at 80 K at the DESY PETRA III synchrotron (beamlines P11 or P24). In addition, data for **1** and **9** were also collected at P11 beamline.

X-ray diffraction experiment for **2**, **4** and **5** were measured at 16-20(2) K or at 100 K at beamline P24<sup>[45]</sup> at DESY PETRA III synchrotron equipped with Huber 3-cycle diffractometer and Pilatus3 CdTe 1M detector and an open-flow He LT system. Data collection was performed by 360°  $\phi$ -rotation with 0.1° per readout at a wavelength  $\lambda = 0.56 \text{ \AA}$  (22.14 keV) or 0.50 (24.8 keV).

The diffraction data for **6** at 123 K were collected on a Rigaku XtaLAB Synergy R diffractometer equipped with a HyPix-Arc 150 detector and a CuK $\alpha$  rotating-anode X-ray source using 0.5°  $\omega$  scans.

Data reduction for **1** was performed with XDS program.<sup>[46]</sup> Data reduction for crystal structures **2-10** was performed with CrysAlisPro software.<sup>[47]</sup> Analytical absorption correction for **6** measured in-house, was applied based on crystal faces; whereas for synchrotron diffraction experiments for a number of single crystals (**2-10**), an empirical absorption correction based on averaging of the equivalent reflections was used.

#### Structure refinement

The structures were solved by direct methods with *SHELXT*<sup>[48]</sup> and were refined by full-matrix least-squares method against  $F^2$  in anisotropic approximation using multiprocessor variable

memory versions of *SHELXL* (2014-2018). All non-hydrogen atoms were refined in anisotropic approximation, while the hydrogen atoms were refined riding on pivot atoms.

In **3**, **4**, **9** and **10**, the inorganic scaffold is severely disordered over more than two close positions. The occupation factors for disordered heavy atoms were refined with fixed isotropic  $U_{iso}$  similar to the average  $U_{iso}$  (usually 0.03 - 0.05 Å<sup>-2</sup>) for the fully occupied heavy atoms in the corresponding structure.

The refinement of supramolecular structures are still in progress due to thousands of refined parameters and large time per refinement cycle (e.g. up to 20 min/cycle in case of **4**).

Crystallographic data and further details for **1** - **10** of the diffraction experiments are given in *Tables 1-5*.

**Table 3.1.** Experimental details for **1** and **2**.

Crystal data	1	2
Chemical formula	$[(C_{10}H_{15}FeP_5)Ag_4(O_3SCF_3)_4] \cdot CH_2Cl_2$	$[(C_{10}H_{15}FeP_5)Ag_2(O_3SCF_3)_2] \cdot C_7H_8$
Structural formula	$C_{14}H_{15}Ag_4F_{12}FeO_{12}P_5S_4 \cdot CH_2Cl_2$	$C_{12}H_{15}Ag_2F_6FeO_6P_5S_2 \cdot C_7H_8$
$M_r$	1458.60	951.97
Crystal system, space group	Orthorhombic, Pbca	monoclinic, P21/c
Temperature (K)	80	100
$a, b, c$ (Å)	21.4611(2), 16.21441(9), 43.2848(3)	11.06511(14), 18.36613(15), 15.35742(13)
$\alpha, \beta, \gamma$ (°)	90, 90, 90	97.7058 (9)
$V$ (Å <sup>3</sup> )	15062.21 (19)	3092.80 (5)
$Z$	16	4
$F(000)$	11168	1864
$D_x$ (Mg m <sup>-3</sup> )	2.573	2.044
Radiation type	Synchrotron, $\lambda = 0.68880$ Å	Synchrotron, $\lambda = 0.56002$ Å
$\mu$ (mm <sup>-1</sup> )	2.89	1.13
Crystal shape and colour	Brown-green plate	Green plate
Crystal size (mm)	0.05 × 0.03 × 0.01	0.20 × 0.20 × 0.08
Data collection		
Diffractionmeter	Synchrotron, P11 beamline at DESY Petra III, DECTRIS PILATUS 6M	Synchrotron, P24 beamline at DESY, Huber diffractometer, Pilatus3 CdTe 1M
Absorption correction	Multi-scan	Multi-scan
$T_{min}, T_{max}$	0.472, 1.000	0.404, 1.000
No. of measured, independent and observed [ $I > 2\sigma(I)$ ] reflections	95043, 13952, 10862	43690, 8169, 7385
$R_{int}$	0.094	0.054
$(\sin \theta/\lambda)_{max}$ (Å <sup>-1</sup> )	0.610	0.739
Range of $h, k, l$	$h = -23 \rightarrow 25, k = -19 \rightarrow 19, l = -52 \rightarrow 52$	$h = -15 \rightarrow 15, k = -26 \rightarrow 26, l = -21 \rightarrow 21$
Refinement		
$R[F^2 > 2\sigma(F^2)], wR(F^2), S$	0.069, 0.202, 1.03	0.035, 0.102, 1.06
No. of reflections	13952	8175
No. of parameters	1008	376
No. of restraints	0	0
H-atom treatment	H-atom parameters constrained	H-atom parameters constrained
$\Delta_{max}, \Delta_{min}$ (e Å <sup>-3</sup> )	3.30, -1.71	1.27, -1.68

Computer programs for **1**: local software, *CrysAlis PRO* 1.171.41.21a (Rigaku OD, 2019), SHELXT2015/3 (Sheldrick, 2015), SHELXL2014/7 (Sheldrick, 2014); for **2**: *CrysAlis PRO* 1.171.42.43a (Rigaku OD, 2022), SHELXL2018/5 (Sheldrick, 2018), SHELXL2018/3 (Sheldrick, 2018).

**Table 3.2.** Experimental details for **3** and **4**.

Crystal data	<b>3*</b>	<b>4*</b>
Chemical formula	C <sub>157</sub> H <sub>203</sub> Ag <sub>20</sub> F <sub>60</sub> Fe <sub>13</sub> O <sub>60</sub> P <sub>65</sub> S <sub>20</sub> (*)	C <sub>75</sub> H <sub>140</sub> Ag <sub>10</sub> F <sub>20</sub> Fe <sub>12</sub> O <sub>66</sub> P <sub>60</sub> S <sub>10</sub>
<i>M<sub>r</sub></i>	9728.23 (*)	6405.56
Crystal system, space group	triclinic, <i>P</i> $\bar{1}$	monoclinic, <i>P</i> 2 <sub>1</sub> / <i>n</i>
Temperature (K)	89.9(4)	90
<i>a</i> , <i>b</i> , <i>c</i> (Å)	26.6210(3), 37.4009(4) 46.1126(4)	24.2545(3), 24.7264(4), 24.3865(4)
$\alpha$ , $\beta$ , $\gamma$ (°)	84.3257(8), 82.8394(8) 86.8296(9)	93.649 (1)
<i>V</i> (Å <sup>3</sup> )	45287.7(8)	14595.6 (4)
<i>Z</i>	4	2
<i>F</i> (000)	21043 (*)	6280 (*)
<i>D<sub>x</sub></i> (Mg m <sup>-3</sup> )	1.573 (*)	1.458 (*)
Radiation type	synchrotron	synchrotron
Crystal shape and colour	brown prism	dark brown prism
Crystal size (mm)	0.3 × 0.15 × 0.1	0.4 × 0.3 × 0.3

\*preliminary data. Computer programs: local software, *CrysAlis PRO* 1.171.41.21a (Rigaku OD, 2019).

**Table 3.3.** Experimental details for **5** and **6**.

Crystal data	5	6
Structural formula	$[(C_{11}H_{17}FeP_5)Ag(O_3SCF_3)]$	$[(C_{11}H_{17}FeP_5)_2(AgO_3SCF_3)_2(CH_3CN)]$
Sum formula	$C_{12}H_{17}AgF_3FeO_3P_5S$	$C_{26}H_{37}Ag_2F_6Fe_2NO_6P_{10}S_2$
$M_r$	616.89	1274.82
Crystal system, space group	Orthorhombic, <i>Pbcn</i>	Monoclinic, <i>P2<sub>1</sub>/c</i>
Temperature (K)	20	123
$a, b, c$ (Å)	12.97732(16), 25.0729(3), 13.08101(13)	12.6413(2), 27.2860(3), 26.1257(7)
$\alpha, \beta, \gamma$ (°)	90, 90, 90	103.321(3)
$V$ (Å <sup>3</sup> )	4256.29(8)	8769.1(3)
$Z$	8	8
$F(000)$	2432	5040
$D_x$ (Mg m <sup>-3</sup> )	1.925	1.931
Radiation type	Synchrotron, $\lambda = 0.56002$ Å	Cu $K\alpha$
$\mu$ (mm <sup>-1</sup> )	1.10	17.20
Crystal shape and colour	Green rounded plate	Red needle
Crystal size (mm)	0.1 × 0.1 × 0.1	0.48 × 0.05 × 0.04
Data collection		
Diffractometer	P24 beamline, PETRA III, DESY, Huber diffractometer, Pilatus3 CdTe 1M	XtaLAB Synergy R, DW system, HyPix-Arc 150
Absorption correction	Multi-scan	Gaussian
$T_{min}, T_{max}$	0.611, 1.000	0.079, 1.000
No. of measured, independent and observed [ $I > 2\sigma(I)$ ] reflections	58763, 6311, 6022	90178, 17693, 13830
$R_{int}$	0.047	0.031
$(\sin \theta/\lambda)_{max}$ (Å <sup>-1</sup> )	0.734	0.625
Range of $h, k, l$	$h = -18 \rightarrow 18, k = -35 \rightarrow 35, l = -18 \rightarrow 18$	$h = -15 \rightarrow 13, k = -34 \rightarrow 33, l = -32 \rightarrow 32$
Refinement		
$R[F^2 > 2\sigma(F^2)], wR(F^2), S$	0.037, 0.107, 1.11	0.042, 0.130, 1.07
No. of reflections	6311	17693
No. of parameters	398	1196
No. of restraints	0	0
H-atom treatment	H-atom parameters constrained	H-atom parameters constrained
$\Delta\rho_{max}, \Delta\rho_{min}$ (e Å <sup>-3</sup> )	1.77, -1.34	1.36, -1.32

Computer programs: *CrysAlis PRO* 1.171.41.93a (Rigaku OD, 2020), *SHELXT2018/5* (Sheldrick, 2018), *SHELXL2018/3* (Sheldrick, 2018).

**Table 3.4.** Experimental details for **7** and **8**.

Crystal data	<b>7</b>	<b>8*</b>
Structural formula	$[(C_{10}H_{15}FeP_5)_2Ag_3(O_3SCF_3)_3] \cdot CH_2Cl_2$	$\{Cp^*Fe(\eta^5-P_5)\} @ \{[Cp^*Fe(\eta^5-P_5)]_{11}(AgSO_3CF_3)_{-10}\}^*$
Sum formula	$C_{14}H_{17}Ag_3F_9FeO_9P_5S_3 \cdot CH_2Cl_2$	$C_{1284.97}O_{189.10}F_{142.78}P_{673.23}Cl_{19.55}Fe_{146.11}Ag_{120.3}S_{86.59}N_{3.53}$
$M_r$	1215.69	>81371.02
Crystal system, space group	Monoclinic, $P2_1/m$	Monoclinic, $Cc$
Temperature (K)	16	100
$a, b, c$ (Å)	11.1290(2), 12.8304(2), 11.9185(4)	76.9048(4), 36.97930(12), 33.75535(15)
$\beta$ (°)	101.923(3)	120.8094(6)
$V$ (Å <sup>3</sup> )	1665.13(7)	82448.9(6)
$Z$	2	12
$F(000)$	1172	> 51788
$D_x$ (Mg m <sup>-3</sup> )	2.425	> 2.145
Radiation type	Synchrotron, $\lambda = 0.500$ Å	Synchrotron, $\lambda = 0.56002$ Å
$\mu$ (mm <sup>-1</sup> )	1.04	> 0.95
Crystal shape and colour	Yellow square prism	brown square truncated plate
Crystal size (mm)	0.20 × 0.05 × 0.05	0.40 × 0.25 × 0.08
Data collection		
Diffractometer	P24 beamline, Huber P24 beamline, Huber	P24 beamline, Huber
	diffractometer, PILATUS CdTe 1M	diffractometer, PILATUS CdTe 1M
Absorption correction	Multi-scan	multi-scan
$T_{min}, T_{max}$	0.214, 1.000	0.699, 1.000
No. of measured, independent and observed [ $I > 2s(I)$ ] reflections	28421, 5226, 4637	600432, 200286, 167607
$R_{int}$	0.069	0.0269
Range of $h, k, l$	$h = -15 \rightarrow 15, k = -18 \rightarrow 18, l = -16 \rightarrow 16$	$h = -107 \rightarrow 107, k = -53 \rightarrow 53, l = -46 \rightarrow 47$
Refinement		
$R[F^2 > 2s(F^2)], wR(F^2), S$	0.035, 0.105, 1.07	0.113, 0.339, 1.503
No. of reflections	5226	200286
No. of parameters	283	5114
No. of restraints	0	2
H-atom treatment	H-atom parameters constrained	H-atom parameters not defined
$\Delta\rho_{max}, \Delta\rho_{min}$ (e Å <sup>-3</sup> )	2.08, -1.22	4.80, -2.38

\*preliminary data. Computer programs for **7**: local software at P11 beamline, PETRA III, DESY, XDS (Kabsch, 2010), *SHELXT2018/5* (Sheldrick, 2018), *SHELXL2018/3* (Sheldrick, 2018); for **8**: *CrysAlis PRO* 1.171.41.83a (Rigaku OD, 2020), *SHELXT2018/5* (Sheldrick, 2018), *SHELXL2018/3* (Sheldrick, 2018).

**Table 3.5.** Experimental details for **9** and **10**.

Crystal data	9	10*
Chemical formula	[(C <sub>13</sub> H <sub>21</sub> FeP <sub>5</sub> )Ag <sub>2</sub> (O <sub>3</sub> SCF <sub>3</sub> ) <sub>2</sub> ]	C <sub>500</sub> H <sub>420</sub> Ag <sub>20</sub> F <sub>60</sub> Fe <sub>12</sub> O <sub>60</sub> P <sub>60</sub> S <sub>20</sub> (*)
<i>M<sub>r</sub></i>	901.88	13856.01 (*)
Crystal system, space group	Triclinic, <i>P1</i>	monoclinic, <i>C2/c</i>
Temperature (K)	100	90
<i>a</i> , <i>b</i> , <i>c</i> (Å)	10.077(2), 10.750(2), 14.208(1)	46.5470(4), 32.1063(4), 91.7761(12)
$\alpha$ , $\beta$ , $\gamma$ (°)	80.826(2), 72.968(2), 67.757(6)	90, 97.7119(10), 90
<i>V</i> (Å <sup>3</sup> )	1360.1(6)	135914(3)
<i>Z</i>	2	8
<i>F</i> (000)	880	> 57610 (*)
<i>D<sub>x</sub></i> (Mg m <sup>-3</sup> )	2.202	> 1.8
Radiation type	Synchrotron, $\lambda = 0.6199$ Å	Synchrotron, $\lambda = 0.6199$ Å
$\mu$ (mm <sup>-1</sup> )	1.70	> 1
Crystal shape	Green elongated plate	red prism
Crystal size (mm)	0.10 × 0.03 × 0.01	0.45 × 0.24 × 0.20
Data collection		
Diffractometer	P11 beamline, PETRA III, DESY, Eiger2 X 16M	P11 beamline, PETRA III, DESY
Absorption correction	Empirical, based on equivalents	Synchrotron
<i>T<sub>min</sub></i> , <i>T<sub>max</sub></i>	0.941, 0.987	
No. of measured, independent and observed [ <i>I</i> > 2σ( <i>I</i> )] reflections	18158, 4934, 4771	
<i>R<sub>int</sub></i>	0.019	
(sin $\theta/\lambda$ ) <sub>max</sub> (Å <sup>-1</sup> )	0.622	
Range of <i>h</i> , <i>k</i> , <i>l</i>	<i>h</i> = -11→12, <i>k</i> = -13→13, <i>l</i> = -17→17	
Refinement		
<i>R</i> [ <i>F</i> <sup>2</sup> > 2σ( <i>F</i> <sup>2</sup> )], <i>wR</i> ( <i>F</i> <sup>2</sup> ), <i>S</i>	0.022, 0.059, 1.05	
No. of reflections	4934	
No. of parameters	340	
No. of restraints	0	
H-atom treatment	H-atom parameters constrained	
$\Delta$ <sub>max</sub> , $\Delta$ <sub>min</sub> (e Å <sup>-3</sup> )	2.21, -0.97	

\*preliminary data. Computer programs: local software, *CrysAlis PRO* 1.171.41.21a (Rigaku OD, 2019), *SHELXT2015/3* (Sheldrick, 2015), *SHELXL2014/7* (Sheldrick, 2014).

### 3.6 Author Contributions

- ❖ The synthesis and characterization of compound **1,5-9** was performed by K. Grill.
- ❖ The synthesis and characterization of compound **2** was performed by Dr. C. Heintl.
- ❖ The synthesis and characterization of compound **2,4,10** is also part of the PhD thesis of Dr. C. Heintl (University of Regensburg, 2015).
- ❖ The synthesis of **3** was done by K. Grill and Dr. B. Hiltl. The characterization was done by Dr. B. Hiltl. The compound is also part of Dr. B. Hiltl's PhD thesis. The full elemental analysis was done by K. Grill.
- ❖ The synthesis and characterization for **4** was done by Dr. B. Hiltl and Dr. C. Heintl. The compound is also part of Dr. B. Hiltl's PhD thesis (University of Regensburg 2018).
- ❖ The synthesis and parts of the chemical characterization methods of **10** are also part of the master thesis of B. Hiltl (University of Regensburg 2014).
- ❖ The manuscript (introduction, results and discussion, experimental part, conclusion, references) was written by K. Grill. The description of **3, 4** and **10** was written by K. Grill and Dr. B. Hiltl.
- ❖ The section "crystallographic details and structure refinement" was written by Dr. E. Peresykina
- ❖ All synchrotron measurements were performed by Dr. E. Peresykina and A. V. Virovets, including sample preparation.
- ❖ Compound **6** was measured by K. Grill.
- ❖ The data reduction and all calculations were performed by Dr. E. Peresykina and A. V. Virovets.
- ❖ DOSY measurements were performed by Dr. F. Hastreiter.
- ❖ MAS NMR investigation of **10** was performed by Prof. W. Kremer.
- ❖ TEM measurements were performed by Dr. J. Hilgert.

### 3.7 References

- [1] I. Chakraborty, T. Pradeep, *Chem. Rev.* **2017**, *117*, 8208.
- [2] a) C. E. Anson, A. Eichhöfer, I. Issac, D. Fenske, O. Fuhr, P. Sevilano, C. Persau, D. Stalke, J. Zhang, *Angew. Chem. Int. Ed.* **2008**, *47*, 1326; b) B. Li, R.-W. Huang, J.-H. Qin, S.-Q. Zang, G.-G. Gao, H.-W. Hou, T. C. W. Mak, *Chem. Eur. J.* **2014**, *20*, 12416; c) F. Gruber, M. Jansen, *Angew. Chem. Int. Ed.* **2010**, *49*, 4924; d) L.-M. Zhang, T. C. W. Mak, *J. Am. Chem. Soc.* **2016**, *138*, 2909; e) S. C. K. Hau, M. C.-L. Yeung, V. W.-W. Yam, T. C. W. Mak, *J. Am. Chem. Soc.* **2016**, *138*, 13732.



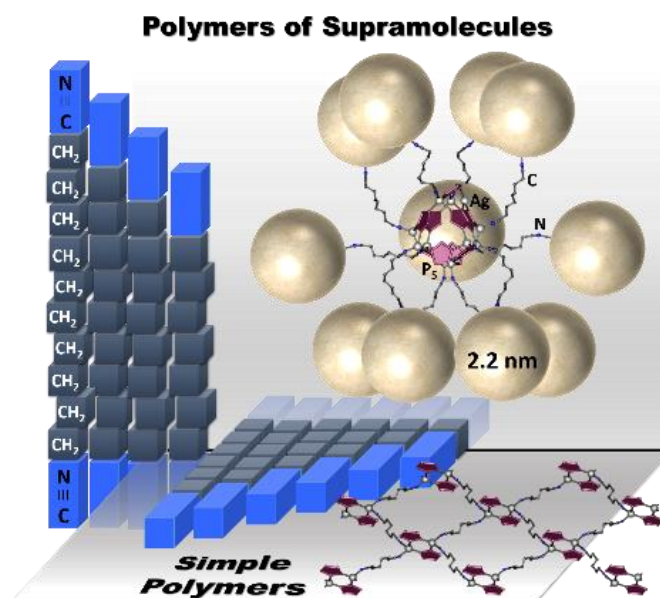
- [3] H. Yang, Y. Wang, X. Chen, X. Zhao, L. Gu, H. Huang, J. Yan, C. Xu, G. Li, J. Wu et al., *Nat. Commun.* **2016**, *7*, 12809.
- [4] a) K. Takaoka, M. Kawano, T. Ozeki, M. Fujita, *Chem. Commun.* **2006**, 1625; b) Y. Inokuma, N. Kojima, T. Arai, M. Fujita, *J. Am. Chem. Soc.* **2011**, *133*, 19691.
- [5] a) S. Sato, J. Iida, K. Suzuki, M. Kawano, T. Ozeki, M. Fujita, *Science* **2006**, *313*, 1273; b) P. Mal, B. Breiner, K. Rissanen, J. R. Nitschke, *Science* **2009**, *324*, 1697.
- [6] C. J. Hastings, M. D. Pluth, R. G. Bergman, K. N. Raymond, *J. Am. Chem. Soc.* **2010**, *132*, 6938.
- [7] a) S. Matsuzaki, T. Arai, K. Ikemoto, Y. Inokuma, M. Fujita, *J. Am. Chem. Soc.* **2014**, *136*, 17899; b) Y.-N. Liu, J.-L. Hou, Z. Wang, R. K. Gupta, Z. Jagličić, M. Jagodič, W.-G. Wang, C.-H. Tung, Di Sun, *Inorg. Chem.* **2020**, *59*, 5683; c) C. G. P. Taylor, A. J. Metherell, S. P. Argent, F. M. Ashour, N. H. Williams, M. D. Ward, *Chem. Eur. J.* **2020**, *26*, 3065.
- [8] N. K. Al-Rasbi, I. S. Tidmarsh, S. P. Argent, H. Adams, L. P. Harding, M. D. Ward, *J. Am. Chem. Soc.* **2008**, *130*, 11641.
- [9] a) D. Fujita, Y. Ueda, S. Sato, H. Yokoyama, N. Mizuno, T. Kumasaka, M. Fujita, *Chem* **2016**, *1*, 91; b) D. Fujita, Y. Ueda, S. Sato, N. Mizuno, T. Kumasaka, M. Fujita, *Nature* **2016**, *540*, 563; c) J. Ferrando-Soria, A. Fernandez, D. Asthana, S. Nawaz, I. J. Vitorica-Yrezabal, G. F. S. Whitehead, C. A. Muryn, F. Tuna, G. A. Timco, N. D. Burton et al., *Nat. Commun.* **2019**, *10*, 3720; d) Y. Fang, T. Murase, S. Sato, M. Fujita, *J. Am. Chem. Soc.* **2013**, *135*, 613; e) K. Harris, D. Fujita, M. Fujita, *Chem. Commun.* **2013**, *49*, 6703; f) I. A. Bhat, D. Samanta, P. S. Mukherjee, *J. Am. Chem. Soc.* **2015**, *137*, 9497; g) Y. Tamura, H. Takezawa, M. Fujita, *J. Am. Chem. Soc.* **2020**, *142*, 5504.
- [10] a) S. Mukherjee, P. S. Mukherjee, *Chem. Commun.* **2014**, *50*, 2239; b) C. Cesari, B. Berti, T. Funaioli, C. Femoni, M. C. Iapalucci, D. Pontiroli, G. Magnani, M. Riccò, M. Bortoluzzi, F. M. Vivaldi et al., *Inorganic chemistry* **2022**, *61*, 12534; c) E. Cattabriga, I. Ciabatti, C. Femoni, T. Funaioli, M. C. Iapalucci, S. Zacchini, *Inorganic chemistry* **2016**, *55*, 6068.
- [11] O. Oms, T. Jarrosson, L. H. Tong, A. Vaccaro, G. Bernardinelli, A. F. Williams, *Chem. Eur. J.* **2009**, *15*, 5012.
- [12] M. S. Islas, J. J. Martínez Medina, L. L. López Tévez, T. Rojo, L. Lezama, M. Griera Merino, L. Calleros, M. A. Cortes, M. Rodriguez Puyol, G. A. Echeverría et al., *Inorg. Chem.* **2014**, *53*, 5724.
- [13] a) N. Giri, S. L. James, *Chem. Commun.* **2011**, *47*, 1458; b) S. Bestgen, O. Fuhr, B. Breitung, V. S. Kiran Chakravadhanula, G. Guthausen, F. Hennrich, W. Yu, M. M. Kappes, P. W. Roesky, D. Fenske, *Chem. Sci.* **2017**, *8*, 2235.

- [14] Z. Wang, H.-F. Su, Y.-Z. Tan, S. Schein, S.-C. Lin, W. Liu, S.-A. Wang, W.-G. Wang, C.-H. Tung, Di Sun et al., *Proc. Natl. Acad. Sci. U.S.A.* **2017**, *114*, 12132.
- [15] a) X.-Z. Song, S.-Y. Song, C. Qin, S.-Q. Su, S.-N. Zhao, M. Zhu, Z.-M. Hao, H.-J. Zhang, *Cryst. Growth Des.* **2012**, *12*, 253; b) C. R. Göb, A. Ehnbohm, L. Sturm, Y. Tobe, I. M. Oppel, *Chem. Eur. J.* **2020**, *26*, 3609.
- [16] S. P. Argent, A. Greenaway, M. C. Del Gimenez-Lopez, W. Lewis, H. Nowell, A. N. Khlobystov, A. J. Blake, N. R. Champness, M. Schröder, *J. Am. Chem. Soc.* **2012**, *134*, 55.
- [17] F. Dielmann, M. Fleischmann, C. Heindl, E. V. Peresyphkina, A. V. Virovets, R. M. Gschwind, M. Scheer, *Chem. Eur. J.* **2015**, *21*, 6208.
- [18] a) C. Heindl, E. V. Peresyphkina, A. V. Virovets, W. Kremer, M. Scheer, *J. Am. Chem. Soc.* **2015**, *137*, 10938; b) M. Scheer, A. Schindler, J. Bai, B. P. Johnson, R. Merkle, R. Winter, A. V. Virovets, E. V. Peresyphkina, V. A. Blatov, M. Sierka et al., *Chem. Eur. J.* **2010**, *16*, 2092.
- [19] S. Welsch, C. Gröger, M. Sierka, M. Scheer, *Angew. Chem. Int. Ed.* **2011**, *50*, 1435.
- [20] E. Peresyphkina, C. Heindl, A. Virovets, H. Brake, E. Mädl, M. Scheer, *Chem. Eur. J.* **2018**, *24*, 2503.
- [21] J. Bai, A. V. Virovets, M. Scheer, *Science* **2003**, *300*, 781.
- [22] S. Heindl, E. Peresyphkina, J. Sutter, M. Scheer, *Angew. Chem. Int. Ed.* **2015**, *54*, 13431.
- [23] M. Scheer, A. Schindler, C. Gröger, A. V. Virovets, E. V. Peresyphkina, *Angew. Chem. Int. Ed.* **2009**, *48*, 5046.
- [24] a) M. Elsayed Moussa, M. Piesch, M. Fleischmann, A. Schreiner, M. Seidl, M. Scheer, *Dalton Trans.* **2018**, *47*, 16031; b) F. Dielmann, A. Schindler, S. Scheuermayer, J. Bai, R. Merkle, M. Zabel, A. V. Virovets, E. V. Peresyphkina, G. Brunklaus, H. Eckert et al., *Chem. Eur. J.* **2012**, *18*, 1168.
- [25] C. Heindl, E. Peresyphkina, A. V. Virovets, I. S. Bushmarinov, M. G. Medvedev, B. Krämer, B. Dittrich, M. Scheer, *Angew. Chem. Int. Ed.* **2017**, *56*, 13237.
- [26] a) C. Schwarzmaier, A. Schindler, C. Heindl, S. Scheuermayer, E. V. Peresyphkina, A. V. Virovets, M. Neumeier, R. Gschwind, M. Scheer, *Angew. Chem. Int. Ed.* **2013**, *52*, 10896; b) A. Schindler, C. Heindl, G. Balázs, C. Gröger, A. V. Virovets, E. V. Peresyphkina, M. Scheer, *Chem. Eur. J.* **2012**, *18*, 829.
- [27] H. Brake, E. Peresyphkina, A. V. Virovets, W. Kremer, C. Klimas, C. Schwarzmaier, M. Scheer, *Inorg. Chem.* **2021**, *60*, 6027.
- [28] E. Peresyphkina, K. Grill, B. Hiltl, A. V. Virovets, W. Kremer, J. Hilgert, W. Tremel, M. Scheer, *Angew. Chem. Int. Ed.* **2021**, *60*, 12132-12142.

- [29] a) E. Peresyphkina, M. Bielmeier, A. Virovets, M. Scheer, *Chem. Sci.* **2020**, *11*, 9067; b) K. Grill, S. B. Dinauer, E. Peresyphkina, A. V. Virovets, M. Scheer, *Chem. Eur. J.* **2023**, *29*, e202203963.
- [30] E. Peresyphkina, A. Virovets, M. Scheer, *Coord. Chem. Rev* **2021**, *446*, 213995.
- [31] J. Bai, A. V. Virovets, M. Scheer, *Angew. Chem. Int. Ed.* **2002**, *41*, 1737.
- [32] E. Peresyphkina, A. Virovets, M. Scheer, *Coord. Chem. Rev* **2021**, *446*, 213995.
- [33] J. Schiller, E. Peresyphkina, A. V. Virovets, M. Scheer, *Angew. Chem. Int. Ed.* **2020**, *59*, 13647.
- [34] F. Dielmann, C. Heindl, F. Hastreiter, E. V. Peresyphkina, A. V. Virovets, R. M. Gschwind, M. Scheer, *Angew. Chem. Int. Ed.* **2014**, *53*, 13605.
- [35] H. Brake, E. Peresyphkina, C. Heindl, A. V. Virovets, W. Kremer, M. Scheer, *Chem. Sci.* **2019**, *10*, 2940.
- [36] 90 vertex sphere but keeping in mind 10 vacant positions.
- [37] Maximal distance of two opposing S atoms plus twice the van der Waals radius of S (180 pm from A. Bondi, *J. Phys. Chem.* 1964, *68*, 3, 441–451).
- [38] M. Detzel, G. Friedrich, O. J. Scherer and G. Wolmershäuser, *Angew. Chem. Int. Ed.* **1995**, *34*, 1321.
- [39] O. J. Scherer, T. Brück, G. Wolmershäuser, *Chem. Ber.* **1988**, *121*, 935.
- [40] O. J. Scherer, H. Sitzmann, G. Wolmershäuser, *J. Organomet. Chem.* **1984**, *268*, C9-C12.
- [41] F. Dielmann, R. Merkle, S. Heini, M. Scheer, *Z. Naturforsch.* **2009**, *64*, 3.
- [42] a) A. Jerschow, N. Müller, *J. Magn. Reson.* 1997, *125*, 372–375. b) C. S. Johnson, *Prog. Nucl. Magn. Reson. Spectrosc.* 1999, *34*, 203–256; c) W. S. Price, *Concepts Magn. Reson.* 1998, *10*, 197–237; d) E. O. Stejskal, J. E. Tanner, *J. Chem. Phys.* **1965**, *42*, 288–292.
- [43] a) C. T. Rueden, J. Schindelin, M. C. Hiner, et al. *BMC Bioinform.* **2017**, *18*, 529; b) C. A. Schneider, W. S. Rasband, K. W. Eliceiri, *Nat. methods* **2012**, *9*, 7, 671–675; c) J. Schindelin, I. Arganda-Carreras, E. Frise, et al. *Nat. methods* **2012**, *9*, 7, 676–682.
- [44] A. Burkhardt, T. Pakendorf, B. Reime, et al, *Eur. Phys. J. Plus* **2016**, *131*, 56–64.
- [45] [https://photon-science.desy.de/facilities/petra\\_iii/beamlines/p24\\_chemical\\_crystallography/eh2/index\\_eng.html](https://photon-science.desy.de/facilities/petra_iii/beamlines/p24_chemical_crystallography/eh2/index_eng.html)
- [46] W. Kabsch, *Acta Cryst. sect. D* 2010, *D66*, 125.
- [47] CrysAlisPro, different versions (Rigaku OD).
- [48] G. M. Sheldrick, *Acta Cryst. sect. C* 2015, *C71*, 3.
- [49] The outer diameter was calculated from the sum of the maximum distance of two H atoms of 1 and two times the van-der-Waals radius of H.
- [50] The inner diameter was calculated from difference of the distance of centroids of two opposite cyclo-P5 ligands and two times the van-der-Waals radius of P.

## 4. Three-component Self-Assembly Changes its Course: A Leap from Simple Polymers to 3D Networks of Spherical Host-Guest Assemblies

E. Peresykina, K. Grill, B. Hiltl, A. V. Virovets, W. Kremer, J. Hilgert, W. Tremel, M. Scheer, *Angew. Chem. Int. Ed.* **2021**, *60*, 12132-12142. Reproduced by permission of Wiley-VCH GmbH, which can be viewed [online](#).



### Abstract:

One-pot self-assembly reactions of the polyphosphorus complex [Cp\*Fe( $\eta^5$ -P<sub>5</sub>)] (**A**), a coinage metal salt AgSbF<sub>6</sub> and flexible aliphatic dinitriles NC(CH<sub>2</sub>)<sub>x</sub>CN ( $x = 1 - 10$ ) yield 1D, 2D and 3D coordination polymers. The seven-membered backbone of the dinitrile was experimentally found as the borderline for the self-assembly system furnishing products of different kinds. At  $x < 7$ , various rather simple polymers are exclusively formed possessing either 0D or 1D Ag/**A** structural motifs connected by dinitrile spacers, while at  $x \geq 7$ , the self-assembly switches to unprecedented extraordinary 3D networks of nano-sized host-guest assemblies (SbF<sub>6</sub>)@[**A**]<sub>9</sub>Ag<sub>11</sub>]<sup>11+</sup> ( $x = 7$ ) or **A**@([**A**]<sub>12</sub>Ag<sub>12</sub>]<sup>12+</sup> ( $x = 8 - 10$ ) linked by dinitriles. The polycationic nodes represent the first superspheres based on **A** and silver and are host-guest able. All products are characterized by NMR spectroscopy, MS spectrometry and single-crystal X-ray diffraction. The assemblies [**A**]<sub>12</sub>Ag<sub>12</sub>]<sup>12+</sup> were visualized by transmission electron microscopy.

## 4.1 Introduction

In supramolecular chemistry the understanding of self-assembly processes is a challenge, and controlling such processes for practical purposes is an even more ingenious and skilful task. Such is the design of matrices for guest encapsulation and storage applicable in chemo sensing, drug delivery and controlled absorption.<sup>[1]</sup> The manifold approaches in this research area investigated over the past years are conceptually based on either guest-oriented or host-oriented strategies. The first concept implies the fitting of the local environment to the guest molecules and therefore utilizes supramolecular host cages<sup>[2]</sup> and capsules<sup>[3]</sup> which are structurally tailored for the size and shape<sup>[4]</sup> of the guest or expediently functionalized<sup>[5]</sup> to facilitate host-guest interactions.<sup>[6]</sup> The second concept suggests furnishing extended space for guest molecules within the pores of the host and therefore uses microporous polymeric matrices<sup>[7]</sup>, or mesoporous materials.<sup>[8]</sup> To rationalize the design of infinite networks with the desired structure and function from pre-organized or self-assembled building blocks and linking units even new fields of research have emerged.<sup>[9]</sup> A combination of these approaches could have the best of both worlds, and the materials combining advantageous properties of finite capsules and of bulk porous materials could close this conceptual gap.

First approaches in this direction were demonstrated by the Atwood group.<sup>[10]</sup> Using self-assembly of pyrogallol[4]arenes (L) as polydentate ligands with  $M^{II}$  salts ( $M^{II} = \text{Cu, Ni, Mg}$ ), the series of crystalline 1D and 2D supramolecular coordination polymers (CPs) were obtained, in which large metal-organic polyhedra  $[M_{24}L_6]$  (MOP) represented the nodes, while the terminal groups of the same ligands L additionally join MOPs as linkers to give supramolecular CPs.<sup>[10]</sup> This elegant one-pot two-component self-assembly approach is however restricted to the ligands capable of such dual function. A straightforward one-pot reaction of a metal salt, a MOP-building ligand and a spacer would be a desirable simplification on the synthetic route. However, to the best of our knowledge, no supramolecular CPs obtained in this way are reported. In many cases the polyhedral metal complexes have to be isolated first. Apparently, coordination polymers with nodes consisting of single metal cations or small compact metal complexes are formed instead or together with the desired supramolecular product. The pre-formed supramolecular nodes<sup>[11]</sup> are required to be activated for further direct polymerization,<sup>[11b,c]</sup> or spacer ligands have to be introduced in the second step.<sup>[11d,12]</sup> Besides inconvenient two-stage synthesis, their further polymerization often leads to amorphous products, which property significantly complicates characterization of the product. Additionally, metal-organic polyhedra incorporated in supramolecular CPs could be enhanced if the MOPs possessed a functionality as for instance the targeted encapsulation of a guest, still a rare phenomenon in this area of supramolecular chemistry.<sup>[10f]</sup> We have been

successfully examining the host-guest properties of various spherical aggregates based on the polyphosphorus complexes  $[\text{Cp}^{\text{R}}\text{Fe}(\eta^5\text{-P}_5)]$  ( $\text{Cp}^{\text{R}} = \text{Cp}^{\text{*}}(\mathbf{A})$ ,  $\text{Cp}^{\text{Bn}} = (\text{Cp}(\text{CH}_2\text{Ph})_5)$ ) and  $\text{CuX}$  or  $\text{CuX}_2$  ( $\text{X} = \text{Cl}, \text{Br}, \text{I}$  or triflate).<sup>[13]</sup> Their nano-sized inorganic scaffolds can contain eight to 24 *cyclo*- $\text{P}_5$  units and dozens of copper atoms or  $\{\text{Cu}_n\text{X}_m\}$  fragments.<sup>[14]</sup> To use these supramolecular aggregates as hosting nodes joined in a polymeric structure it is necessary to provide coordination sites at the metal cations for the additional linkers, which should be longer than the van der Waals contact of the supramolecules. Moreover, the desired polymer of supramolecules should be accessible via a one-pot self-assembly. For this purpose we have chosen the silver salt with the non-coordinating anion  $\text{SbF}_6^-$ , which in the reaction with polyphosphorus ligand **A** would be able to form fullerene-like host-guest able supramolecules bearing free coordination sites at the silver centers. To link these in-situ generated supramolecules, the flexible aliphatic dinitriles  $\text{NC}(\text{CH}_2)_x\text{CN}$  (**DNx**,  $x = 1 - 10$ ) were selected as their coordination chemistry with silver salts has already been investigated.<sup>[15]</sup>

Herein we report on a controllable three-component self-assembly system, leading either to CPs or to supramolecular CPs containing host-guest able nodes. During this study a phenomenon of the dramatic change of the self-assembly course from CP to supramolecular CP was discovered: For **DNx** with  $x = 1 - 6$ , the self-assembly leads to simple CPs, while starting from  $x > 7$ , the self-assembly suddenly leaps towards the formation of supramolecular CPs, only sporadically accompanied by CPs as minor products. The resulting supramolecular CPs are obtained in one-pot reactions in high yields and the supramolecular nodes are convenient for further implementation in host-guest chemistry.

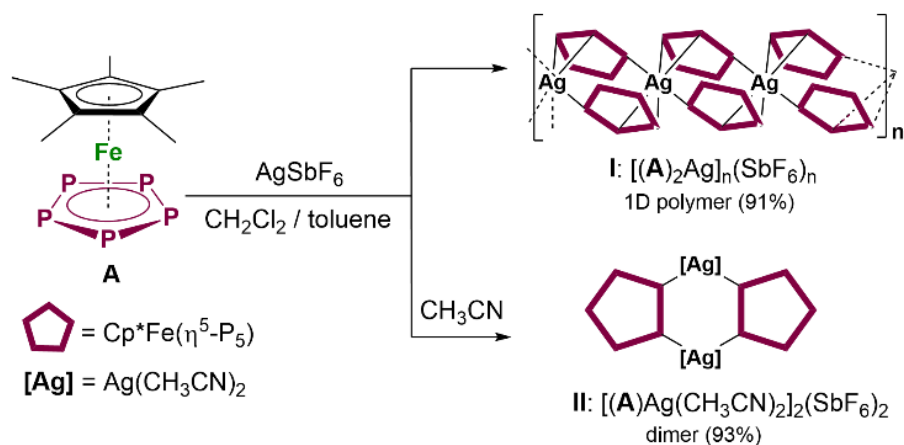
## 4.2 Results and Discussion

### Two-Component Self-Assembly

To prove that free coordination sites at silver cations can be generated, the two-component self-assembly of **A** and  $\text{AgSbF}_6$  in both coordinating and non-coordinating solvents was investigated beforehand (Scheme 4.1). A solution of  $\text{AgSbF}_6$  in  $\text{CH}_2\text{Cl}_2$  was first layered with a mixture of  $\text{CH}_2\text{Cl}_2$  and toluene (2:1) to prevent the formation of powder and then with a solution of **A** in toluene. After one day, dark brown crystals of the 1D polymer  $[(\mathbf{A})_2\text{Ag}]_n(\text{SbF}_6)_n$  (**I**) had formed. By changing the solvent of the Ag-containing layer to a mixture of  $\text{CH}_2\text{Cl}_2$  and  $\text{CH}_3\text{CN}$  (2:1) and layering the fully diffused reaction solution with *n*-pentane, green plates of a dimeric  $[(\mathbf{A})\text{Ag}(\text{CH}_3\text{CN})_2]_2(\text{SbF}_6)_2$  complex (**II**) was obtained. The compounds **I** and **II** with 1:1 and 1:2 stoichiometric ratios of **A**: $\text{AgSbF}_6$ , respectively, could be isolated in excellent crystalline yields.

According to the X-ray structure analysis, the *cyclo*- $\text{P}_5$  ligands in the 1D polymer **I** coordinate in a 1,2,3-mode to Ag atoms, which are pseudo-tetrahedrally coordinated by six P atoms of four *cyclo*-

$P_5$  ligands of the units **A** (Figure 4.1a). The analogous cationic parts of **I** and of the earlier described 1D polymer  $[(A)_2Ag]_n[Al\{OC(CF_3)_3\}_4]_n$ <sup>[16]</sup> together with the related mass and NMR spectroscopic features also suggest a monomer-oligomer equilibrium in solution.<sup>[17]</sup>



**Scheme 4.1.** Reactions of **A** with  $\text{AgSbF}_6$  in different solvents. Isolated crystalline yields are given in parentheses.

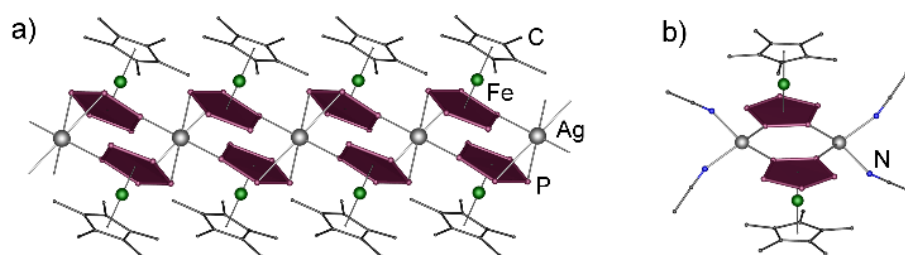
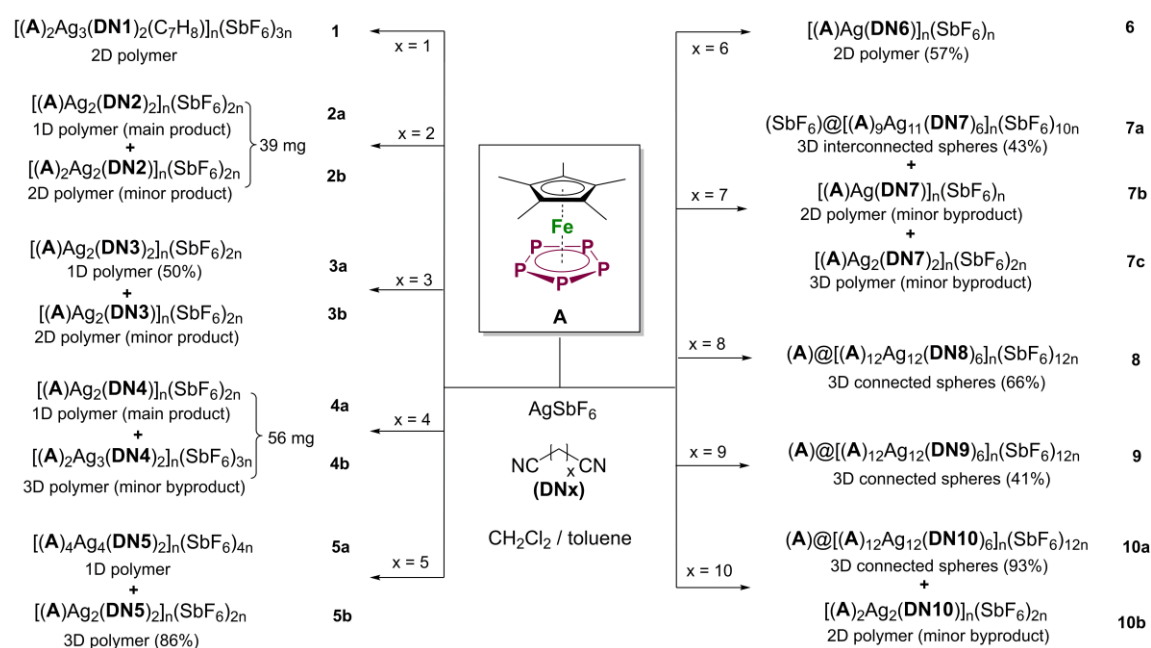


**Figure 4.1.** Structure of the cationic a) 1D polymer **I** and b) dimer **II**. H atoms are omitted for clarity.

### Three-Component Self-Assembly

For three-component self-assembly reactions, a solution of  $\text{AgSbF}_6$  in  $\text{CH}_2\text{Cl}_2$  was layered with a mixture of  $\text{CH}_2\text{Cl}_2$  and toluene and then with a toluene solution of **A** and the flexible **DN $x$**  ( $x = 1 - 10$ ). The selectivity of the reaction was controlled by using a reduced concentration of 2 mmol/L in the respective layers and an equimolar ratio of  $\text{Ag}:\mathbf{A}$ . The corresponding dinitrile was added in a 10-fold excess with respect to **A**. Increasing the concentration of the Ag salt and **A** or decreasing the excess of dinitrile both yielded a 1D polymeric byproduct **I**. Combining the **DN $x$**  and complex **A** in the toluene layer turned out to be decisive, because flexible aliphatic dinitriles readily react with  $\text{Ag}^+$  to give insoluble polymeric products.<sup>[15f]</sup> However, these products turned out to be unavoidable in the case of shorter **DN $x$**  ( $x < 4$ ) even when using this precaution (see SI). Using the shortest dinitrile, dicyanomethane  $\text{NC}(\text{CH}_2)\text{CN}$ , a 2D polymer  $[(A)_2\text{Ag}_3(\text{DN1})_2(\text{C}_7\text{H}_8)]_n(\text{SbF}_6)_{3n}$  (**1**) is isolated selectively irrespective of the used stoichiometric ratios of  $\mathbf{A}:\text{AgSbF}_6$  which only influences the amount of the colorless by-product  $[\text{Ag}(\text{DN1})](\text{SbF}_6)$ , which can be separated manually (Scheme 4.2). For the dinitrile **DN2**, two polymeric products are formed as a mixture of 1D

$[(A)Ag_2(DN2)_2]_n(SbF_6)_{2n}$  (**2a**: plates) and 2D  $[(A)_2Ag_2(DN2)]_n(SbF_6)_{2n}$  (**2b**: needles) polymers accompanied by small amounts of the **A**-free product  $[Ag(DN2)](SbF_6)$ . Using **DN3** gives 1D  $[(A)Ag_2(DN3)_2]_n(SbF_6)_{2n}$  (**3a**: plates) and a smaller amount of a 2D polymer  $[(A)Ag_2(DN3)]_n(SbF_6)_{2n}$  (**3b**: prisms). The main product **3a** can be isolated selectively, while only few crystals of **3b** occur. Going further to **DN4**, a 2D polymer  $[(A)Ag_2(DN4)]_n(SbF_6)_{2n}$  (**4a**) is accompanied by a few crystals of the first 3D polymer in the system **A**/AgSbF<sub>6</sub>/DN<sub>x</sub>  $[(A)_2Ag_3(DN4)_2]_n(SbF_6)_{3n}$  (**4b**) and by a small unavoidable impurity of  $[Ag(DN4)](SbF_6)$ . With **DN5**, a 1D  $[(A)_4Ag_4(DN5)_2]_n(SbF_6)_{4n}$  (**5a**) and a 3D  $[(A)Ag_2(DN5)_2]_n(SbF_6)_{2n}$  (**5b**) polymer are obtained at 1:2 (mixture **5a** and **5b**) and at 1:1 (**5b**) stoichiometric ratios of **A**:AgSbF<sub>6</sub>. Extending the linking unit to  $x = 6$ , a 2D polymer  $[(A)Ag(DN6)]_n(SbF_6)_n$  (**6**) is formed selectively, irrespective of the used stoichiometric ratios of **A**:AgSbF<sub>6</sub>. No phase transformation between major and minor products was observed when keeping under mother liquor solution (or freshly prepared solvent mixture of the same composition) for at least six months.



**Scheme 4.2.** One-pot self-assembly reactions of **A**, AgSbF<sub>6</sub> and flexible dinitriles DN<sub>x</sub>. Isolated crystalline yields are given in parentheses.

Going further to **DN7**, the system becomes versatile enough to form the unique representative of an unprecedented class of 3D supramolecular coordination polymers  $[(SbF_6)@[(A)_9Ag_{11}(DN7)_6]]_n(SbF_6)_{10n}$  (**7a**) in which unique spherical aggregates, metal-*organometallic* polyhedra, act as nodes. This major product is accompanied by the 2D  $[(A)Ag(DN7)]_n(SbF_6)_n$  (**7b**) and 3D  $[(A)Ag_2(DN7)_2]_n(SbF_6)_{2n}$  (**7c**) CPs as minor by-products. Though the stoichiometric ratios in **7a** to **7c** differ, they could not be isolated selectively, not even by using different stoichiometric ratios or different concentrations of the starting materials. For longer



dinitriles with  $x = 8$  and  $9$ , the formation of simple CPs was not observed. Instead, unprecedented 3D supramolecular CPs, the polymeric networks of supramolecular spherical aggregates  $[(A)@{(A)_{12}Ag_{12}(DNx)_6}]_n(SbF_6)_{12n}$  ( $x = 8$  (**8**),  $9$  (**9**) and  $10$  (**10a**)) were obtained in moderate to excellent crystalline yields (Scheme 4.2). Note that, in the case of **DN10**, the formation of the 1D CP I could not be impeded completely, along with the occasional formation of a few crystals of a 2D CP  $[(A)_2Ag_2(DN10)]_n(SbF_6)_{2n}$  (**10b**) as the second minor by-product. All crystalline compounds are differently tinted green-brown; the 2D polymeric compounds are often dichroic green-to-brown.

#### Simple polymers based on DN $x$ with $x = 1 - 7$ and **10b**.

According to the X-ray diffraction, the simple polymers based on **A**,  $AgSbF_6$  and flexible dinitriles possess 1D to 3D dimensionalities, with the variety arising from only two types of  $Ag/cyclo-P_5$  subunits, finite (Figure 4.2a,b) and 1D chains (Figure 4.3-4.5), whereas 1D polymeric structural motifs can be additionally augmented by **DN $x$**  (Figure 4.6). The types of the 0D nodes and 1D subunits are summarized in Table 1. The 0D motifs are only found for the **DN5-7** in case of a medium-length aliphatic chain, while 1D motifs occur for any **DN $x$**  linker lengths. The overall dimensionality of the resulting structures seems to be governed by the ratio of the building blocks in the product rather than by the linker length as no clear tendency shows except that, with longer linkers, 3D structures (**DN4-DN7**) gradually outnumber the 1D polymeric motifs (**DN2-DN5**). However, 2D motifs dominate for all dinitriles with the exception of **DN5**, and isotopic motifs occur quite at random (see below). The structures with the same ratio of **A:Ag:DN $x$**  can demonstrate both similar and different connectivity depending on the various coordination modes of the pentaphosphaferrocene **A**.

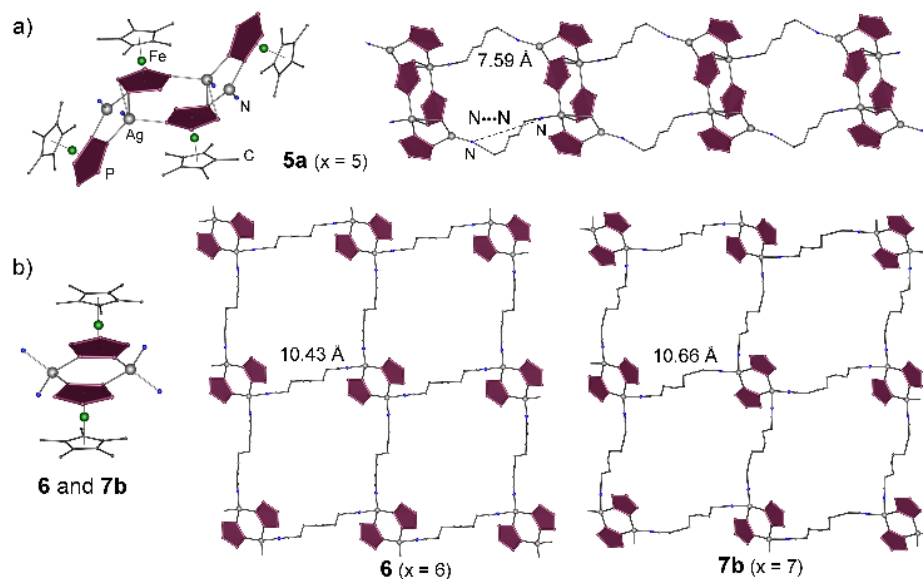


**Figure 4.2** Structure of the cationic networks based on finite Ag-P fragments: a) tetrameric node of the 1D polymer in **5a** and b) dimeric node in the isotopic 2D networks **6** and **7b** including the intramolecular N...N contacts in dinitrile linkers. {Cp\*Fe} fragments and H atoms are not shown for clarity

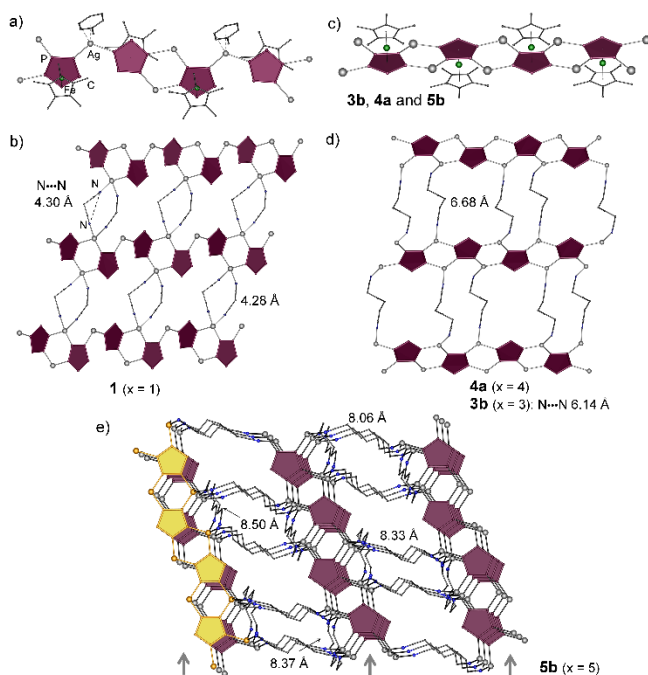


**Figure 4.3.** Structure of the cationic networks based on 1D Ag-P fragments: a-b)  $[(A)_2Ag_3(C_7H_8)]_n^{3n+}$  in **1**; c) 1D strand  $[(A)Ag_2]_n^{2n+}$  in the isotopic 2D layers of d) **3b** and **4a** as well as e) in a 3D network of **5b** including the intramolecular N...N contacts in linkers. {Cp\*Fe} fragments and H atoms are not shown.

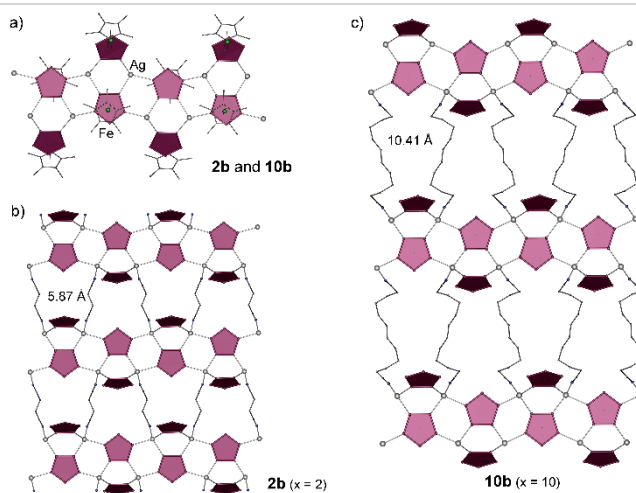


**Figure 4.4.** Structure of a) a 1D cationic motif  $[(A)Ag]_n^{n+}$ , b) a 2D polymer of isotypic **2b** and c) **10b** including the intramolecular N...N contacts in dinitrile linkers. {Cp\*Fe} and H atoms are omitted.

The 2D network in **1** consists of parallel 1D strands  $[(A)_2Ag_3]_n^{3n+}$  with *cyclo*-P<sub>5</sub> ligands of the units **A** coordinating Ag atoms in alternating 1,2,3- and 1,2,4-coordination modes (Table 4.1, Figure 4.3a). The strands are bridged by two angular dinitriles coordinating the same Ag atoms of the strand (Figure 4.3b). Interestingly, a toluene molecule is additionally coordinated to a two-coordinate silver atom with Ag-C distances of 2.44(1)-2.62(1) Å. This feature makes **1** unique as all other compounds in the family possess no such interactions despite the fact that toluene is also used as a solvent and is often present in the crystal structures of these compounds as a solvate molecule. For the dinitrile **DN2**, the 1D polymer (**2a**) furnishes a chain of the *cyclo*-P<sub>5</sub> ligands coordinating Ag atoms in a 1,2,3,4-mode. The Ag ions are in turn tetrahedrally coordinated by pairs of dinitriles chelating neighbouring Ag atoms of the same chain (Table S29, Figure 4.6a). Also a 2D motif (**2b**) is possible for this linker, which is based on the 1D polymeric bands  $[(A)Ag]_n$  of *cyclo*-P<sub>5</sub> ligands in a 1,2,3,4-mode similar to the chains in **2a**, but, instead of two augmenting linkers, the neighboring Ag atoms are decorated additionally by a molecule **A** in a 1,2-coordination mode. The dinitriles connect the bands in a 2D network with identical trapezoidal meshes (Figure 4.4a, b).

For the dinitrile **DN3**, the major product is a 1D polymer (**3a**) whose structure is similar to that in **2a** (Figure 4.6a), as the dinitrile ligands are only long enough to chelate Ag atoms coordinated to the positions 1 and 2 of the unit **A** within the strand giving rise to this augmented motif, which disappears for longer dinitriles. A 2D polymer (**3b**), a minor product in this reaction, is based on  $[(A)Ag_2]_n^{2n+}$  strands, in which *cyclo*-P<sub>5</sub> ligands of **A** coordinate in a 1,2,3,4-mode to Ag atoms being in a triangular environment.

**Table 4.1.** Coordination modes and motifs in simple polymers

Polymer <sup>[a]</sup>	Node <sup>[b]</sup>	A:Ag:DNx	<i>cyclo</i> -P <sub>5</sub> coordination	CN(Ag) <sup>[c]</sup>
------------------------	---------------------	----------	---	-----------------------

<b>1</b> (2D)	$[(A)_2Ag_3]_n^{3n+}$	2 : 3 : 2	1,2,3; 1,2,4	2P+2N, 2P+2C
<b>2a</b> (1D)	$[(A)Ag_2(DN2)_2]_n^{n+}$	1 : 2 : 2	1,2,3,4	2P+2N
<b>2b</b> (2D)	$[(A)Ag]_n^{n+}$	2 : 2 : 1	1,2,3,4; 1,2	3P+1N
<b>3a</b> (1D)	$[(A)Ag_2(DN3)_2]_n^{n+}$	1 : 2 : 2	1,2,3,4	2P+2N
<b>3b</b> (2D)	$[(A)Ag_2]_n^{2n+}$	1 : 2 : 1	1,2,3,4	2P+1N
<b>4a</b> (2D)	$[(A)Ag_2]_n^{2n+}$	1 : 2 : 1	1,2,3,4	2P+1N
<b>4b</b> (3D)	$[(A)_2Ag_3]_n^{3n+}$	2 : 3 : 2	1,2,4	2P+1N, 2P+2N
<b>5a</b> (1D)	$[(A)_4Ag_4]^{4+}$	2 : 2 : 1	1,2	2P+1N, 3P+1N
<b>5b</b> (3D)	$[(A)Ag_2]_n^{2n+}$	1 : 2 : 2	1,2,3,4	2P+2N
<b>6</b> (2D)	$[(A)_2Ag_2]^{2+}$	1 : 1 : 1	1,2	2P+2N
<b>7b</b> (2D)	$[(A)_2Ag_2]^{2+}$	1 : 1 : 1	1,2	2P+2N
<b>7c</b> (3D)	$[(A)Ag_2(DN7)_{0.5}]_n^{2n+}$	1 : 2 : 2	1,2,3,4	3P+1N
<b>10b</b> (2D)	$[(A)Ag]_n^{n+}$	2 : 2 : 1	1,2,3,4; 1,2	3P+1N

[a] dimensionality is given in parentheses. [b] n always corresponds to 1D motifs; [c] coordination environment.

For the linker **DN4**, a 2D polymer (**4a**) repeating the motif of **3b** is formed (Figure 4.3d) accompanied by a few crystals of a 3D polymer (**4b**). The latter shows a unique structure within its family being built up by puckered chains  $[(A)_2Ag_3]_n^{3n+}$  with tetrameric repeating units (Figure 4.5). In each repeating unit, two opposed *cyclo*-P<sub>5</sub> ligands coordinate to Ag atoms in a 1,2,4-mode. The other two *cyclo*-P<sub>5</sub> ligands coordinate Ag atoms in a 1,2-mode and additionally form two longer  $\pi$ -contacts (2.83-2.93 Å). The Ag atoms possess either a trigonal or a distorted pseudo-tetrahedral coordination, the latter also including two  $\pi$ -contacts (Figure 4.5a). The dinitrile ligands connect parallel chains in a 3D polymeric structure (Figure 4.5c).

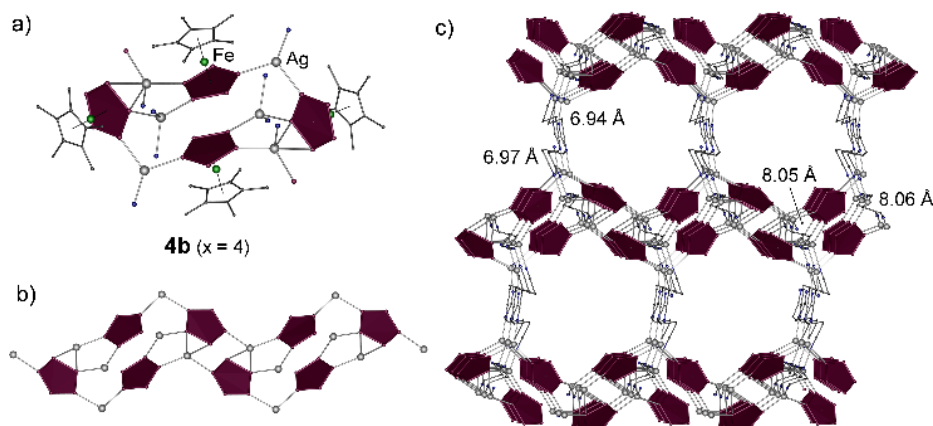


**Figure 4.5.** a) Repeating tetrameric unit; b) a 1D polymeric motif  $[(A)_2Ag_3]_n^{3n+}$  connected in c) a 3D network in **4b**. {Cp\*Fe} and H atoms are omitted.

The ladder-like 1D polymer in **5a** is built up by tetrameric units  $[(\mathbf{A})_4\text{Ag}_4]^{4+}$  (Figure 4.2a). The Ag atoms show either a trigonal or a distorted pseudo-tetrahedral coordination. Two *cyclo*-P<sub>5</sub> ligands coordinate to Ag atoms in a 1,2-mode. The other two *cyclo*-P<sub>5</sub> ligands coordinate Ag atoms in a 1,3-mode and additionally form two longer  $\pi$ -contacts (2.80, 3.09 Å) with the opposing Ag atom similar to those in **4b** and  $[(\mathbf{A})_2\text{Ag}]_n[\text{Al}\{\text{OC}(\text{CF}_3)_3\}_4]_n$  (2.80–2.81 Å).<sup>[16]</sup>

Another 3D network in the series is **5b** representing parallel 1D strands  $[(\mathbf{A})\text{Ag}_2]_n^{2n+}$ , the same as in **4a**, connected by dinitriles (Figure 4.3c, e). The strands are built up by 1,2,3,4-coordinated *cyclo*-P<sub>5</sub> ligands and Ag atoms, but, in contrast to **4a**, in a tetrahedral environment. The linkers connect each 1D strand to four other ones resulting in a 3D structure.

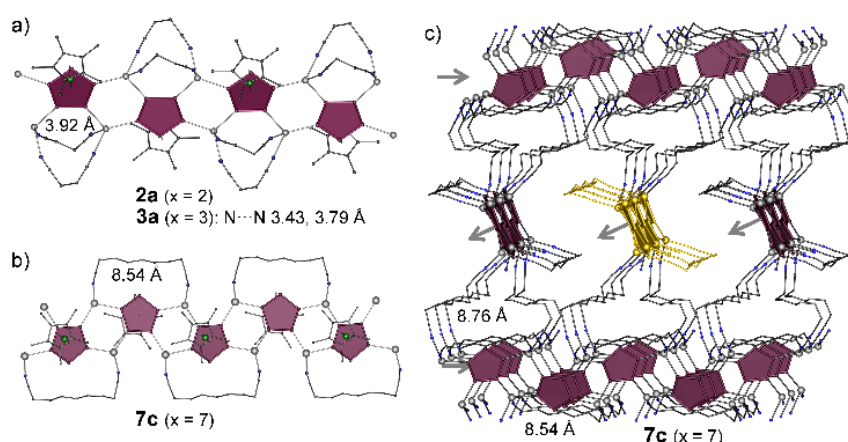


**Figure 4.6.** Structure of the cationic networks based on 1D Ag-P fragments augmented by dinitriles: a chain  $[(\mathbf{A})\text{Ag}_2(\text{DNx})_2]_n^{n+}$  in isotopic a) **2a** and **3a**; b) a strand  $[(\mathbf{A})\text{Ag}_2(\text{DN7})_{0.5}]_n^{2n+}$ ; c) 3D network of **7c** including the intramolecular N...N contacts in linkers. {Cp\*Fe} and H atoms are not shown.

For the dinitrile **DN6**, the resulting 2D polymer **6** is built up by dimeric nodes  $[(\mathbf{A})_2\text{Ag}_2]^{2+}$  (cf. dimer II), which are connected *via* the flexible linkers to give a square net (Figure 4.2b). Each *cyclo*-P<sub>5</sub> ligand coordinates in a 1,2-mode to tetrahedrally coordinated Ag atoms. A similar 2D framework is also formed in **7b**, a byproduct of the self-assembly of **A**, AgSbF<sub>6</sub> and **DN7**. In contrast to **6**, the dimeric nodes in **7b** are not parallel, but alternately turned about (Figure 4.2b). The 3D polymer **7c** is the other minor byproduct of the reaction with **DN7**. The 1D strands  $[(\mathbf{A})\text{Ag}_2]_n^{2n+}$  are similar to those in **4a** and **5b**, but form alternating stacks. Moreover, the dinitrile ligands are sufficiently long to chelate Ag atoms coordinated to the positions 1 and 4 of the unit **A** belonging to the same strand thus forming another augmented motif than that for the shorter dinitriles **DN2** and **DN3**. Thereby, only half of the linkers connect the strands in a 3D network of **7c** (Figure 4.6b, c).

The self-assembly with **DNx** (x = 8, 9) furnished no simple CPs (see below). In the minor byproduct **10b** of the self-assembly involving the **DN10**, a 2D polymeric framework of interconnected 1D strands  $[(\mathbf{A})\text{Ag}]_n^{n+}$  unexpectedly repeats the structural motif previously observed for the **2b** structure, based on one of the shortest linkers, **DN2** (Figure 4.4).

### 3D Supramolecular Coordination Polymers

The discontinuous switch in the one-pot self-assembly of **A**, AgSbF<sub>6</sub> and flexible **DNx** starts at  $x \geq 7$ . The main product **7a** of the self-assembly between **A**, AgSbF<sub>6</sub> and **DN7** is the first representative of a novel class of 3D supramolecular CPs based on polyphosphorus ligands, being also the first example of a supersphere based on **A** and Ag (Figure 4.7). Here, unprecedented 56-vertex polycationic assemblies [(**A**)<sub>9</sub>Ag<sub>11</sub>]<sup>11+</sup> act as nodes. These nodes of C<sub>s</sub> point symmetry possess the shape of a tricapped trigonal prism outlined by the centers of the P<sub>5</sub> rings. Nine *cyclo*-P<sub>5</sub> ligands show four different coordination modes (Figure 4.7c). The Ag atoms are tetrahedrally or pseudo-tetrahedrally coordinated (Table 4.2). The Ag-N bond lengths for the end-on coordination mode of the dinitriles amount to 2.19 - 2.34 Å, whereas the Ag-N bonds for the less common η<sup>2</sup>-coordination are significantly elongated (2.95 and 3.20 Å), but still in agreement with literature data.<sup>[18]</sup>

**Table 4.2.** Selected structural characteristics of **7a-10a**.

Compound	Node	Ag-P <sup>[a]</sup>	∅ <sub>[b]</sub> <sup>out</sup>	∅ <sub>[b]</sub> <sup>in</sup>	<b>DNx</b> <sub>[b]</sub>	linear <b>DNx</b> <sup>[c]</sup>
<b>7a</b>	[( <b>A</b> ) <sub>9</sub> Ag <sub>11</sub> ] <sup>11+</sup>	2.40-2.61(σ) 2.72-2.88(π)	2.21	0.56	8.95-10.82	11.94
<b>8</b>	[( <b>A</b> ) <sub>12</sub> Ag <sub>12</sub> ] <sup>12+</sup>	2.44-2.60	2.44	0.80	9.99-10.58	13.38
<b>9</b>	[( <b>A</b> ) <sub>12</sub> Ag <sub>12</sub> ] <sup>12+</sup>	2.42-2.63	2.43	0.74	10.44-10.87	14.50
<b>10a</b>	[( <b>A</b> ) <sub>12</sub> Ag <sub>12</sub> ] <sup>12+</sup>	2.48-2.55	2.40	0.83	10.75-11.99	15.90

[a] range of bond distances (in Å); [b] outer and inner diameter of the node, nm; a range of the effective lengths [b] and [c] calculated length in the linear conformation of DNx linkers.<sup>[19]</sup>

The outer diameter of the spherical cationic assembly amounts to 2.21 nm,<sup>[20]</sup> which, to date, makes it the smallest spherical assembly based on the five-fold symmetric building block **A** along with the 80-vertex scaffold [(**A**)<sub>12</sub>(CuX)<sub>20</sub>] (X = Cl, Br) of 2.29 nm.<sup>[14]</sup> Each supramolecular node acts also as a molecular container for an SbF<sub>6</sub><sup>-</sup> counter-anion. The anion is ordered in a void of 0.56 × 0.60 nm with F atoms pointing in-between *cyclo*-P<sub>5</sub> ligands to avoid short intermolecular contacts. As a result, numerous F...P van der Waals contacts are formed in a range of 3.21 - 3.36 Å. The encapsulation of SbF<sub>6</sub><sup>-</sup> shows that the nodes are capable of host-guest chemistry. The single crystal X-ray structure analysis of **8-10a** also revealed the 3D supramolecular CPs of unique spherical polycationic nodes connected by dinitriles (Figures 4.8, 4.9). However, in comparison to **7a**, the nodes show a completely different structure: The larger 72-vertex node [(**A**)@(**A**)<sub>12</sub>Ag<sub>12</sub>]<sup>12+</sup> consists of 12 units of **A**, which are arranged in an icosahedron of 12 Ag atoms systematically capping 12 of the 20 available trigonal faces. The remaining eight faces give rise to 12-membered {Ag<sub>3</sub>P<sub>9</sub>} rings in the inorganic scaffold (Figure 4.8b, c). Every *cyclo*-P<sub>5</sub> ligand coordinates to Ag atoms in a 1,2,4-mode, presenting the first spherical aggregate exclusively composed of three-coordinated units of

**A.** The Ag atoms are tetrahedrally coordinated by three units of **A** and one dinitrile linker bridging two neighboring spheres (Figure 4.8a).

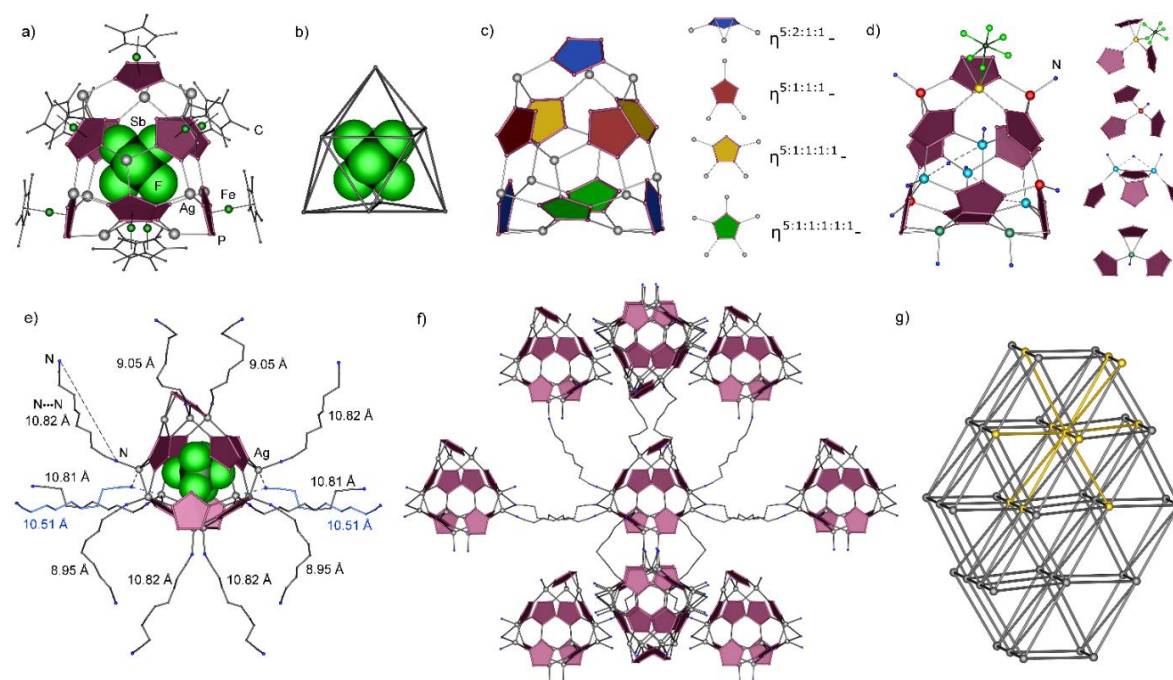


**Figure 4.7.** Polymer **7a** with supramolecular assemblies as nodes. a) The  $(\text{SbF}_6)@[(\text{A})_9\text{Ag}_{11}]^{10+}$  node; b) tricapped trigonal prism formed by the centers of the  $\text{P}_5$  rings. Different coordination modes of c) the *cyclo*- $\text{P}_5$  ligands and d) the Ag atoms highlighted by color; e) the node with outgoing linkers; f) section of the 3D cationic network, also shown in yellow in g) simplified 10-connected overall network.

An icosahedral arrangement of 12 *cyclo*- $\text{P}_5$  units was also observed for the spherical supramolecules based on the *cyclo*- $\text{P}_5$  complexes and Cu halides  $[(\text{Cp}^R\text{Fe}(\eta^5\text{-P}_5))_{12}\{\text{CuX}\}_{20-n}]$  ( $\text{Cp}^R = \text{Cp}^*(\mathbf{A}), \text{Cp}^{\text{Bn}}(\mathbf{B})$ ;  $\text{X} = \text{Cl}, \text{Br}$ ;  $n = 0 - 4.8$ ).<sup>[13c,e,14b]</sup> Unlike Ag-based cationic nodes, the Cu-containing nodes are neutral, and all trigonal faces of an icosahedron are statistically capped with  $(20-n)$  CuX units (Figure 4.8c). However, in **8-10a**, owing to the coordination of dinitrile linkers, the 12 silver and exactly eight vacant positions in the cationic nodes are ordered. In addition, Ag-based cationic scaffolds are more flexible due to the more deformable coordination sphere of Ag as compared to Cu.<sup>[21]</sup> The Ag-P bond lengths vary in a wide range (Table 2). For this reason, the cationic nodes are geometrically distorted causing crystallographic disorder (see Supporting Information for detail).

The IR spectra of crystals of **7a-10a** confirm the coordination of dinitriles to the Ag atoms, as the observed stretching mode of the nitrile group at  $\tilde{\nu} = 2270 \text{ cm}^{-1}$  (**7a**)  $\tilde{\nu} = 2264 \text{ cm}^{-1}$  (**8**),  $2269 \text{ cm}^{-1}$  (**9**),  $2268 \text{ cm}^{-1}$  (**10a**) is slightly blue-shifted compared to that of the free dinitriles at  $\tilde{\nu} = 2247 \text{ cm}^{-1}$ .

Each spherical node in **8-10a** of  $2.07 \times 2.44 \text{ nm}$  encapsulates a molecule of **A** in the inner cavity of  $0.79 \times 0.97 \text{ nm}$  (Figure 4.8a, c). Interestingly, similar Cu-based supramolecules  $[(\mathbf{A})_{12}\text{Cu}_{20-n}]$  are slightly smaller ( $2.31 \text{ nm}$ ) due to shorter M-P bonds (Cu-P:  $2.24\text{-}2.31 \text{ \AA}$ ) and cannot incorporate a non-spherical molecule of **A** in their spherical cavity of  $\varnothing 0.81 \text{ nm}$ .<sup>[14b]</sup> Therefore, the encapsulation must be realized directly during the formation of this sphere. The guest molecule **A** in the cavity of

the nodes is disordered over six positions so that the *cyclo*-P<sub>5</sub> unit in every orientation of the guest is opposite to the one of the six *cyclo*-P<sub>5</sub> rings of the node scaffold. The flexibility of the Ag coordination environment<sup>[21]</sup> allows the scaffold to adjust to the shape of the guest molecule: It is slightly elongated in the direction of the axis of the guest molecule **A** to 2.44 nm and narrowed to 2.07 nm in other directions (cf. SI for details).<sup>[20]</sup> Such adjustability of the core is also favored by the lower denticity of the pentaphosphaferrocene units, showing that the encapsulation of the guest occurs simultaneously during the formation process of the sphere and the linkage to other units.

Depending on the orientation of the guest **A**, different host-guest interactions occur. In two of the six orientations, the P<sub>5</sub> ring of the guest is parallel to two of the P<sub>5</sub> rings of the host (**8**: 0.1(2)° and **9**: 0.3(2)°). The corresponding interplanar *cyclo*-P<sub>5</sub>(guest)⋯*cyclo*-P<sub>5</sub>(host) distances of 3.79(1) (**8**) and 3.80(1) Å (**9**) point to rather weak π-π interactions (cf. SI). In other orientations of the guest molecule **A**, the *cyclo*-P<sub>5</sub> planes are inclined by 3.2(5)-8.5(1)° (**8**) and 3.3(2)-9.5(1)° (**9**), suggesting only van der Waals host-guest interactions. In all positions of the guest in **10a**, one can suggest only slightly inclined orientations of the P<sub>5</sub> rings of the guest and the host (1.8(5)-4.6(5)°) with interplanar distances of 3.68(2)-3.82(1) Å.

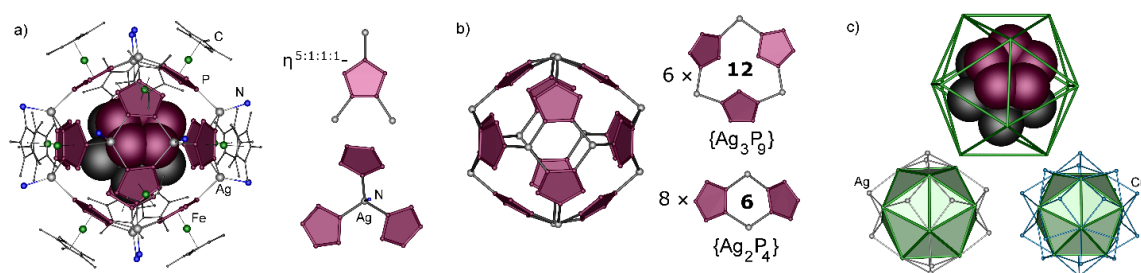


**Figure 4.8.** Supramolecular assemblies as nodes in the 3D networks **8** - **10** (a) [(**A**)@(**A**)<sub>12</sub>Ag<sub>12</sub>]<sup>12+</sup> as nodes with the coordination mode of the *cyclo*-P<sub>5</sub> ligands and the Ag atoms; (b) Inorganic core based on 6- and 12-membered rings; (c) Icosahedron formed by centers of the P<sub>5</sub> rings and its variations with Ag and Cu caps.<sup>[14b]</sup>

Remarkably, the supramolecular CPs do not show decomposition being stored in a glovebox, and can be kept under mother liquor solution for six months or longer. Only if exposed to the air, or upon changes of mother liquor solution composition, a degradation of **7-10** takes place to give **I** and presumably corresponding colourless **A**-free compound of silver and dinitrile.

### Solid State NMR Study for the Supramolecular CP **8**

To additionally investigate host-guest interactions in the solid state, a <sup>31</sup>P MAS NMR measurement was exemplified for one of the two isotopic compounds, namely **8** (Figure 4.9d), with a broad signal at 125 ppm with an integral intensity of 60 being observed (half width  $\tilde{\omega} \sim 5800$ Hz), which can most likely be attributed to the P atoms of the core.

The width of the signal agrees with the deformable coordination sphere of Ag. Two respective sharp signals at 150 ppm and 169 ppm with integral intensities of  $\sim 2.5$  can be attributed to the



different orientations of the guest molecules **A** in the host scaffold. The signal at 150 ppm being close to the signal of the free complex **A** (149 ppm) can be assigned to the guest molecule **A** participating in weak van der Waals interactions with the host. The signal at 169 ppm, downfield shifted to the signal of the free complex **A**, resembles the chemical shift in the  $^{31}\text{P}$  MAS NMR spectrum of the molecule **A** encapsulated in a 90-vertex supramolecule  $[(\mathbf{A})_{12}(\text{CuCl})_{25}(\text{CH}_3\text{CN})_{10}]$  ( $X = \text{Cl}, \text{Br}$ ) (160 ppm) featuring weak  $\pi$ - $\pi$  interactions between *cyclo*- $\text{P}_5$  ligands of the host and the guest.<sup>[22]</sup> The corresponding geometry of the  $\text{P}_5 \cdots \text{P}_5$  interactions with interplanar distances of 3.86-4.03 Å and angles  $< 0.9^\circ$  is in good agreement with the one observed in **8**.<sup>[22]</sup> The same should be valid for **9** due to its close crystallographic similarity with **8**.

### The 3D Supramolecular CP Network Topologies in **7a-10a**

The 10-connected network of  $[(\mathbf{A})_9\text{Ag}_{11}]^{11+}$  assemblies in **7a** can be topologically classified<sup>[23]</sup> as **bcu-x-10-Fmmm**.<sup>[9c]</sup> Each supramolecular node is linked to ten others *via* 12 dinitrile ligands: single connections with eight neighbors and double connections with two neighbors (Figure 4.7e, f). Two additional  $\eta^2$ -coordinated dinitrile linkers per node facilitate these double connections.

The polymeric networks formed by  $[(\mathbf{A})_{12}\text{Ag}_{12}]^{12+}$  assemblies are isotypic for **8** and **9**, but differ for **10a**. Each sphere in **8** or **9** is connected *via* 12 dinitrile ligands to eight neighboring spheres: six of them are 1- and two are 3-connected (Figure 4.9a-c). The triple connections form parallel layers, which are spanned and joint together by the single connections to give the 8-connected nets assigned<sup>[23]</sup> to the **bcu**<sup>[9c]</sup> topology (body-centred cubic, Figure 4.9c). In contrast, each sphere in **10a** is connected to six others *via* 12 of the longest linkers, each pair of nodes being 2-connected. The respective topology of the underlying net is primitive cubic (**pcu**, Figure 4.9g).<sup>[9c,23]</sup>

In the crystal, the dinitrile linkers are folded by 9-20% (**7a**), 21-25% (**8**), 25-29% (**9**) and 28-33% (**10a**) which is illustrated by shortened intramolecular  $\text{N} \cdots \text{N}$  distances compared to the corresponding linear conformation of the **DNx** molecules (Figure 4.9a, e; Table 4.2). This fact demonstrates the increasing folding of the higher homologs of the **DNx**.

To understand the nature of the crystallographic disorder in these highly disordered structures, X-ray diffraction studies at 100 and 10K were performed for **9**, as well as at 90 and 30K for **10a**. The guest molecules, the scaffold, linkers and  $\text{SbF}_6^-$  anions stay positionally disordered even at temperatures as low as 10K, pointing out the static nature of the disorder. The cooling to 10-30K leads to the additional non-uniform shortening of the dinitrile units only by 0.06-0.09 Å (see published SI, Table S28).

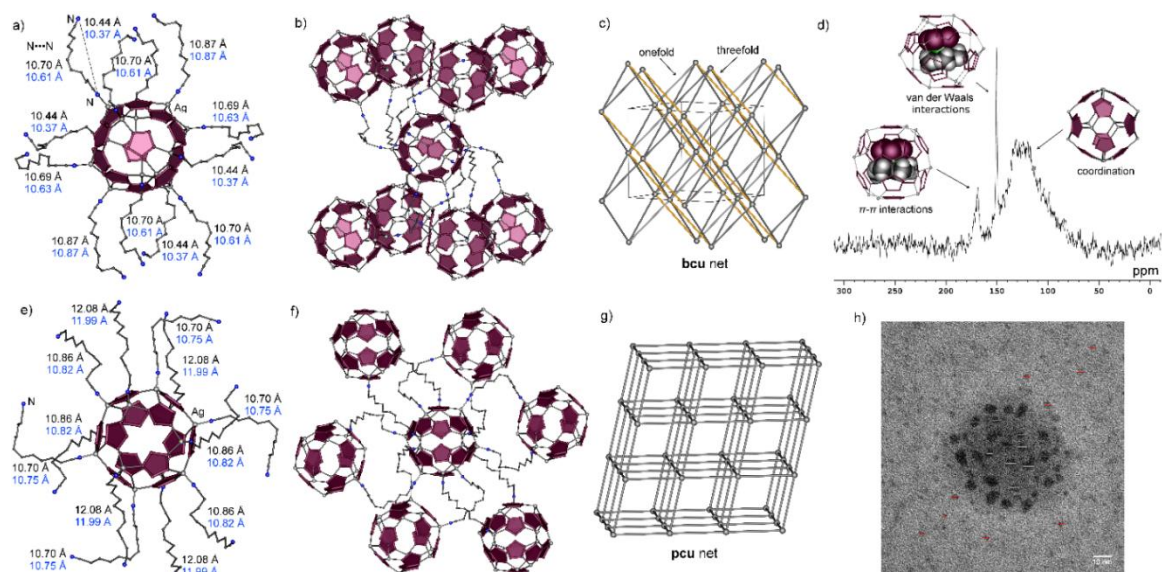


**Figure 4.9.** 3D Networks of supramolecular assemblies in **8-10a**. Node with 12 bridging linkers in (a) **9** and (e) **10a**; the lengths N...N at 100K (black) and 10K or 30 K (blue); A section of the 3D cationic network in (b) **8** and (f) **10a**; (c) 8-connected underlying net in **8** and **9** and (g) 6-connected underlying net in **10a**; (d)  $^{31}\text{P}$  MAS NMR spectrum of **8** and h) TEM record of **8** dispersed in  $\text{CH}_2\text{Cl}_2$ .

**Transmission electron microscopy (TEM) studies** for compound **8** were conducted (Figure 4.9h). As the solid **8** is not soluble, but only dispersible in polar solvents such as  $\text{CH}_2\text{Cl}_2$  after ultrasonication, it is not expected to give an isotropic distribution of the individual spherical nodes. **8** contains 12-fold positively charged organometallic cores and  $\text{SbF}_6^-$  counterions, held together by weak electrostatic interactions due to their low charge densities. Unlike neutral metal or metal oxide nanoparticles (e.g. Ag or  $\text{Fe}_3\text{O}_4$ ), the cores of **8** are not protected by capping ligands and, hence, the building units of **8** are prone to aggregation, and therefore the TEM images show smaller and larger aggregates. The smallest aggregates have mean diameters between 3.1 (red bars) and 4.5 (white bars) nm, each of them larger than the maximal dimension of 2.44 nm for the individual spherical node. Larger aggregates were observed by scanning probe microscopy (SPM). As the small aggregates, are formed by evaporation of the dispersion medium during TEM sample preparation, are not well defined, “irregular spheres” appear in the projected view of a TEM image. EDX analysis of the particles gives an Ag:Fe ratio of approx. 1:1 as expected from the experimentally found metal ratio.

### The Effect of the Linker Length

The length variation of the  $\text{DN}_x$  linker ( $x = 1-10$ ) does not significantly influence the connectivity of the resulting CPs but, at  $x = 7$ , discontinuously switches the three-component self-assembly of **A**, the coinage metal salt of a weakly coordinating anion  $\text{AgSbF}_6$  and aliphatic dinitrile, from simple CPs at  $x < 1-6$  to the unprecedented 3D supramolecular CPs **7a**, **8**, **9** and **10a** at  $x \geq 7$ . Remarkably, the tendency to form supramolecular CPs is so strong that it requires no change to the self-

assembly system such as the delivery of a special template molecule,<sup>[21b]</sup> since the templating ion ( $\text{SbF}_6^-$  in **7a**) or a molecule (**A** in **8-10a**) are always present in the system and therefore cannot be the driving force behind such an unusual behavior in self-assembly.

Although the simple CPs still occur with **DN7** and **DN10** as minor products, the main pathway of the self-assembly is dominated by the formation of supramolecular CPs, the novel class of organometallic compounds. After the borderline  $x = 7$ , the simple CPs **7b**, **7c** and **10b** suddenly become minor products despite their structural similarities to **6**, **4a** (and **5b**), and **2b**, respectively, being major products in the respective reactions. This fact can be explained by the conformation of the flexible linkers and their effective lengths (specified by the intramolecular distances  $\text{N}\cdots\text{N}$ ). In the 3D polymers **5b** and **6c** based on similar infinite strands  $[(\text{A})\text{Ag}_2]^{2+}$ , the crosslinking dinitriles possess comparable effective  $\text{N}\cdots\text{N}$  lengths of 8.06 - 8.50 Å for **5b** and 8.76 Å for **7c**, though their aliphatic backbone differs by two  $\text{CH}_2$  groups. In the similar 2D networks **5** and **6b**, the actual lengths of the linkers with the respective **DN6** and **DN7** are even closer-spaced, namely 10.43 Å (**6**) and 10.66 Å (**7b**). The formation of simple CPs at  $x \geq 7$  might be hindered as the folding of the aliphatic chains is unfavorable for  $x$  smaller than 11-17.<sup>[24]</sup> However, one can see from Table 2 that the effective linker length for  $x = 7-10$  grows slower than the calculated length of the linear **DNx** molecules (see SI for more detail).

For the 3D supramolecular CP **7a** (Figure 4.7e), eight of the 12 **DNx** linkers are longer or comparable in length (10.81 - 10.82 Å) than any of the lower homologs **DNx** in a linear conformation (9.39 Å ( $x = 5$ ) and 10.88 Å ( $x = 6$ )). Similar linker lengths are observed for 3D networks connected with the **DNx**,  $x = 8, 9$  and 10, which are not effectively longer than in **7a**. Such linker lengths ( $> 10.4-10.5$  Å as compared with the effective linker length 10.44 Å in the last simple CP **6**) might be necessary for accommodating ten  $\text{SbF}_6^-$  anions that compensate the charge of a polycationic node in the outer sphere, which is not the case for the CPs with simple mono- to tetracationic nodes. Moreover, the longer length ensures reasonable van der Waals contacts between the spheres. Interestingly, for the 3D supramolecular CPs ( $x \geq 7$ ), a tendency to a lower connectivity of the network with the elongation of the flexible dinitrile linker becomes evident: a 10-connected network in **7a**, 8 in **8** and **9**, and a 6-connected network in **10a**.

As **DN8** and **DN9** do not afford simple polymers, only linker lengths in the supramolecular CP **10a** and the CP **10b** can be compared (Table 2). On average, the linkers in CP **10b** (11.41 Å) are longer than in the supramolecular CP **10a** (av. 11.19 Å), the latter showing a wider range of 10.75-11.99 Å **DN10** length variation (Table 2). However, **DN10** linkers are significantly folded (cf. 15.9 Å in linear conformation, Table S28).

Obviously, some architectures are realized due to more specific tendencies. In this way, the augmented motifs in **2a**, **3a** and suddenly again in **7c** occur when linker length and conformation become complimentary to the Ag...Ag distance between coordinated Ag atoms first at 1,2-positions at the *cyclo*-P<sub>5</sub> ligands of **A** (5.0 – 5.3 Å for **DN2** and **DN3**) or at the 1,4-positions (8.1 – 8.2 Å for **DN7**). The most striking similarity of the networks is in **2b** and **10b** despite the difference of eight CH<sub>2</sub>-groups in the linker lengths, demonstrating almost twice the expansion of the resulting 2D layers. This exemplifies that the simple expansion of the 2D network is irrelevant to the **DNx** folding and is stabilized by it. However, the CP **10b** is obtained in much lower yields than **2b**, overruled by the preferred formation of the supramolecular CP **10a**.

### Characterization of 1-10 in solution

While the compounds **I** and **II** are moderately soluble in CH<sub>2</sub>Cl<sub>2</sub>, the polymers **1-10b** are insoluble in hexane, toluene, CH<sub>2</sub>Cl<sub>2</sub>, thf and Et<sub>2</sub>O. Yet, all compounds readily dissolve in CH<sub>3</sub>CN or pyridine at the cost of the degradation of the coordination network as well as of the supramolecular architecture and nodes. Therefore, in the <sup>1</sup>H, <sup>13</sup>C, <sup>31</sup>P and <sup>31</sup>P{<sup>1</sup>H} NMR spectra of the polymers treated by CD<sub>2</sub>Cl<sub>2</sub>/pyridine, only signals attributed to the free complex **A** and the dinitriles are detectable.

The peaks in the positive- and negative-ion mode of the ESI MS spectra correspond to various oligomeric fragments. The largest three-component fragments in the positive-ion mode for **I** or **1** can be assigned at  $m/z = 798.9$  or  $798.9$  to a monocation  $[(\mathbf{A})_2\text{Ag}]^+$ . The peak at  $m/z = 2869.1$  corresponds to  $[(\mathbf{A})_5\text{Ag}_4(\text{SbF}_6)_3]^+$  for **II**, at  $m/z = 2176$  to  $[(\mathbf{A})_3\text{Ag}_4(\text{SbF}_6)_3]^+$  for **2**, at  $m/z = 2519.8$  to  $[(\mathbf{A})_3\text{Ag}_5(\text{SbF}_6)_4]^+$  for **3a**, and at  $m/z = 2178.2$  to  $[(\mathbf{A})_4\text{Ag}_3(\text{SbF}_6)_2]^+$  for **4**. The largest three-component fragments at  $m/z = 2077.0$  and  $m/z = 2426.0$  were identified as  $[(\mathbf{A})_3\text{Ag}_3(\text{SbF}_6)_2(\text{DN5})_2]^+$  and  $[(\mathbf{A})_3\text{Ag}_3(\text{SbF}_6)_4(\text{DN5})]^-$  (**5a**),  $m/z = 2418.2$  and  $m/z = 2772.0$  to  $[(\mathbf{A})_3\text{Ag}_4(\text{SbF}_6)_3(\text{DN5})_2]^+$  and  $[(\mathbf{A})_4\text{Ag}_3(\text{SbF}_6)_4(\text{DN5})]^-$  (**5b**),  $m/z = 1622.4$  to  $[(\mathbf{A})_2\text{Ag}_3(\text{SbF}_6)_2(\text{DN6})]^+$  (**6**). In the ESI MS spectra of **7a**, **8 - 10**, oligomeric fragments can be detected and assigned at  $m/z = 1636.6$  as  $[(\mathbf{A})_2\text{Ag}_3(\text{SbF}_6)_2(\text{DN7})]^+$  (**7a**),  $m/z = 3729$  for  $[(\mathbf{A})_9\text{Ag}_2(\text{DN8})(\text{SbF}_6)]^+$  (**8**) and  $m/z = 2521.98$  or  $2522.0$  for  $[(\mathbf{A})_4\text{Ag}_4(\text{SbF}_6)_3]^+$  for **9** or for **10a**.

## 4.3 Conclusion

For the first time, 3D supramolecular CP networks built up by nano-sized organometallic Ag-based spherical aggregates, ready for host-guest interactions, were systematically obtained using the control of linker lengths. Utilizing the weakly coordinating anion SbF<sub>6</sub><sup>-</sup> along with the five-fold symmetric building block pentaphosphaferrocene [Cp\*Fe(η<sup>5</sup>-P<sub>5</sub>)] (**A**) and Ag<sup>+</sup>, the predesigned free

coordination sites on the Ag ion make the coordination by N-donor linkers possible. A detailed and systematic study on the three-component self-assembly of these building blocks and flexible linkers  $\text{NC}(\text{CH}_2)_x\text{CN}$  (**DNx**,  $x = 1 - 10$ ) showed that the variability of the conformations and thus the adjustable lengths of the linkers lead to the formation of diverse 1D to 3D coordination polymers. As a result, with **DNx** ( $x = 1 - 6$ ), rather simple CPs are observed. With  $x = 7$ , the flexibility of the system brings it to a qualitatively novel level of aggregation and allows the formation of the first representative of an unprecedented spherical host scaffold, the 56-vertex polycationic host-guest assembly  $(\text{SbF}_6^-)@[(\text{A})_9\text{Ag}_{11}]^{11+}$ , connected in a 3D supramolecular coordination polymer **7a**. When even longer linkers (**DN8-10**) are used, the self-assembly system again switches to larger nano-sized supramolecular 72-vertex nodes of supramolecular CPs  $(\text{A})@[(\text{A})_{12}\text{Ag}_{12}]^{12+}$  serving as containers for the host molecules of **A**. Thus, two isotopic and one unique 3D supramolecular CPs  $[(\text{A})@[(\text{A})_{12}\text{Ag}_{12}(\text{DNx})_6]]_n(\text{SbF}_6)_{12n}$  ( $x = 8$  (**8**), 9 (**9**) and 10 (**10a**)) were selectively isolated and structurally characterized. Moreover, for the first time, despite the insolubility of the supramolecular networks, by using TEM techniques, the visualization of giant spherical subunits was possible.

The ability of the three-component system to self-assemble in spherical polyphosphorus supramolecules over simple polymers in the absence of additional stimuli reveals immense perspectives arising from the combination of the assemblies readily offering host-guest chemistry with the advantages of 3D networks and their use in diverse applications. Based on our previous experience, targeted guest encapsulation seems also feasible, which offers the next step in this research and opens wide perspectives in tailoring the structure and property of the supramolecular nodes.

## 4.4 Experimental Part

### General Remarks

All reactions were performed under an inert atmosphere of dry nitrogen with standard vacuum, Schlenk and glove-box techniques. Solvents were purified, dried and degassed prior to use by standard procedures.  $[\text{Cp}^*\text{Fe}(\eta^5\text{-P}_5)]^{[25]}$  and  $\text{NC}(\text{CH}_2)_x\text{CN}$  ( $x = 1, 2, 3, 9$ )<sup>[26]</sup> were synthesized following reported procedures. Commercially available chemicals ( $\text{AgSbF}_6$ ,  $\text{NC}(\text{CH}_2)_x\text{CN}$  ( $x = 1, 4-10$ )) were used without further purification. Solution NMR spectra were recorded on a Bruker Avance 300 or 400 spectrometer. The  $^{31}\text{P}\{^1\text{H}\}$  MAS spectrum was measured on a Bruker Avance 300. The corresponding ESI-MS spectra were acquired on a ThermoQuest Finnigan MAT TSQ 7000 mass spectrometer. CHN Elemental analyses were performed on a Vario EL III apparatus.

**Synthesis of  $[\{\text{Cp}^*\text{Fe}(\eta^{5:2:1}\text{-P}_5)\}_2\text{Ag}]_n[\text{SbF}_6]_n$  (I)**

In a Schlenk tube a solution of  $\text{AgSbF}_6$  (28 mg, 0.08 mmol) in  $\text{CH}_2\text{Cl}_2$  (8 mL) is carefully layered with a green solution of  $[\text{Cp}^*\text{Fe}(\eta^5\text{-P}_5)]$  (14 mg, 0.04 mmol) in toluene (8 mL). Thereby, the phase boundary turns turbid. After a few days, the formation of dark brown laths of I at the phase boundary can be observed. After complete diffusion, the mother liquor is decanted, the crystals are washed with hexane ( $3 \times 10$  mL) and dried *in vacuo*.

Analytical data of I:

**Yield:** 19 mg (0.018 mmol, 91% referred to  $[\text{Cp}^*\text{Fe}(\eta^5\text{-P}_5)]$ )

**$^1\text{H}$  NMR** ( $\text{CD}_2\text{Cl}_2$ ):  $\delta$  [ppm] = 1.39 (s,  $[\text{Cp}^*\text{Fe}(\eta^5\text{-P}_5)]$ ).

**$^{31}\text{P}\{^1\text{H}\}$  NMR** ( $\text{CD}_2\text{Cl}_2$ ):  $\delta$  [ppm] = 152 (s,  $[\text{Cp}^*\text{Fe}(\eta^5\text{-P}_5)]$ ).

**Positive ion ESI-MS** ( $\text{CH}_2\text{Cl}_2/\text{CH}_3\text{CN}$ ):  $m/z$  (%) = 798.9 (100)  $[\{\text{Cp}^*\text{Fe}(\eta^5\text{-P}_5)\}_2\text{Ag}]^+$ , 345.9 (22)  $[\text{Cp}^*\text{Fe}(\eta^5\text{-P}_5)]^+$ .

**Negative ion ESI-MS** ( $\text{CH}_2\text{Cl}_2/\text{CH}_3\text{CN}$ ):  $m/z$  (%) = 762.7 (26)  $[(\text{SbF}_6)_3\text{Fe}]^-$ , 546.7 (47)  $[(\text{SbF}_6)_2\text{FeF}]^-$ , 234.7 (100)  $[\text{SbF}_6]^-$ .

**Elemental analysis:** Calculated (%) for  $[\{\text{Cp}^*\text{Fe}(\eta^5\text{-P}_5)\}_2\{\text{AgSbF}_6\}(\text{CH}_2\text{Cl}_2)_4]$  (1375.23 g/mol): C 20.96, H 2.79; found: C 20.43, H 2.71.

**Further details on I:**

Like the  $[\text{Al}\{\text{OC}(\text{CF}_3)_3\}_4]^-$ -containing compound, I is moderately soluble in  $\text{CH}_2\text{Cl}_2$ . In the  $^1\text{H}$  NMR spectrum of I the signal corresponding to the  $\text{Cp}^*$  ligand is visible, whereas the  $^{31}\text{P}\{^1\text{H}\}$  NMR spectrum shows a singlet at 152 ppm. After performing theoretical studies and low temperature NMR spectroscopy in the case of  $[\text{Ag}\{\text{Cp}^*\text{Fe}(\eta^{5:2:1}\text{-P}_5)\}_2]_n[\text{Al}\{\text{OC}(\text{CF}_3)_3\}_4]_n$ , this singlet was assigned to the monocation  $[\{\text{Cp}^*\text{Fe}(\eta^5\text{-P}_5)\}_2\text{Ag}]^+$ . This fragment is also observed in the ESI MS spectrum for compound I as the largest fragment at  $m/z = 798.9$ .

**Synthesis of  $[\{\text{Cp}^*\text{Fe}(\eta^{5:1:1}\text{-P}_5)\}\{\text{Ag}(\text{CH}_3\text{CN})_2\}]_2[\text{SbF}_6]_2$  (II)**

In a Schlenk tube a solution of  $\text{AgSbF}_6$  (54 mg, 0.15 mmol) in a solvent mixture of  $\text{CH}_3\text{CN}/\text{CH}_2\text{Cl}_2$  (4 mL, 1:1) is carefully layered with a green solution of  $[\text{Cp}^*\text{Fe}(\eta^5\text{-P}_5)]$  (28 mg, 0.08 mmol) in toluene (5 mL). Thereby, the phase boundary turns turbid. After a few days, the formation of green plates of II at the phase boundary can be observed. After complete diffusion, the colorless mother liquor is decanted, the crystals are washed with hexane ( $3 \times 10$  mL) and dried *in vacuo*.

Analytical data of II:

**Yield:** 57 mg (0.0372 mmol, 93% referred to  $[\text{Cp}^*\text{Fe}(\eta^5\text{-P}_5)]$ )

**<sup>1</sup>H NMR** (CD<sub>3</sub>CN):  $\delta$  [ppm] = 1.45 (s, 15H, [Cp\*Fe( $\eta^5$ -P<sub>5</sub>)]), 1.96 (s, 6H, CH<sub>3</sub>CN).

**<sup>31</sup>P{<sup>1</sup>H} NMR** (CD<sub>3</sub>CN):  $\delta$  [ppm] = 140.80 (s, [Cp\*Fe( $\eta^5$ -P<sub>5</sub>)]).

**<sup>19</sup>F NMR** (CD<sub>3</sub>CN):  $\delta$  [ppm] = -122.71 (octet, Sb<sup>123</sup>F<sub>6</sub>), -122.70 (sextet, Sb<sup>121</sup>F<sub>6</sub>).

**Positive ion ESI-MS** (CH<sub>3</sub>CN):  $m/z$  (%) = 2869.1 [{Cp\*Fe( $\eta^5$ -P<sub>5</sub>)<sub>5</sub>Ag<sub>4</sub>(SbF<sub>6</sub>)<sub>3</sub>]<sup>+</sup>, 2525.1  
 [{Cp\*Fe( $\eta^5$ -P<sub>5</sub>)<sub>4</sub>Ag<sub>4</sub>(SbF<sub>6</sub>)<sub>3</sub>]<sup>+</sup>, 2217.6      [{Cp\*Fe( $\eta^5$ -P<sub>5</sub>)<sub>4</sub>Ag<sub>3</sub>(SbF<sub>6</sub>)<sub>2</sub>(CH<sub>3</sub>CN)]<sup>+</sup>, 2178.9  
 [{Cp\*Fe( $\eta^5$ -P<sub>5</sub>)<sub>4</sub>Ag<sub>3</sub>(SbF<sub>6</sub>)<sub>2</sub>]<sup>+</sup>, 1873.9      [{Cp\*Fe( $\eta^5$ -P<sub>5</sub>)<sub>3</sub>Ag<sub>3</sub>(SbF<sub>6</sub>)<sub>2</sub>(CH<sub>3</sub>CN)]<sup>+</sup>, 1834.8  
 [{Cp\*Fe( $\eta^5$ -P<sub>5</sub>)<sub>3</sub>Ag<sub>3</sub>(SbF<sub>6</sub>)<sub>2</sub>]<sup>+</sup>, 1568.7      [{Cp\*Fe( $\eta^5$ -P<sub>5</sub>)<sub>3</sub>Ag<sub>2</sub>(SbF<sub>6</sub>)(CH<sub>3</sub>CN)]<sup>+</sup>, 1527.4  
 [{Cp\*Fe( $\eta^5$ -P<sub>5</sub>)<sub>3</sub>Ag<sub>2</sub>(SbF<sub>6</sub>)(CH<sub>3</sub>CN)]<sup>+</sup>, 1488.8      [{Cp\*Fe( $\eta^5$ -P<sub>5</sub>)<sub>3</sub>Ag<sub>2</sub>(SbF<sub>6</sub>)]<sup>+</sup>, 1219.5  
 [{Cp\*Fe( $\eta^5$ -P<sub>5</sub>)<sub>2</sub>Ag<sub>2</sub>(SbF<sub>6</sub>)(CH<sub>3</sub>CN)]<sup>+</sup>, 1183.7      [{Cp\*Fe( $\eta^5$ -P<sub>5</sub>)<sub>2</sub>Ag<sub>2</sub>(SbF<sub>6</sub>)(CH<sub>3</sub>CN)]<sup>+</sup>, 1142.9  
 [{Cp\*Fe( $\eta^5$ -P<sub>5</sub>)<sub>2</sub>Ag<sub>2</sub>(SbF<sub>6</sub>)]<sup>+</sup>, 798.8      [{Cp\*Fe( $\eta^5$ -P<sub>5</sub>)<sub>2</sub>Ag]<sup>+</sup>, 493.7 (100)      [{Cp\*Fe( $\eta^5$ -P<sub>5</sub>)Ag(CH<sub>3</sub>CN)]<sup>+</sup>,  
 453.8      [{Cp\*Fe( $\eta^5$ -P<sub>5</sub>)Ag]<sup>+</sup>.

**Negative ion ESI-MS** (CH<sub>3</sub>CN):  $m/z$  (%) = 234.7 (100) [SbF<sub>6</sub>]<sup>-</sup>.

**Elemental analysis:** Calculated (%) for [{Cp\*Fe( $\eta^5$ -P<sub>5</sub>)}{Ag(CH<sub>3</sub>CN)<sub>2</sub>}(SbF<sub>6</sub>)<sub>2</sub>] (1543.32 g/mol):  
 C 21.79, H 2.74, N 3.63; found: C 21.87, H 2.82, N 3.73.

### Synthesis of [(Cp\*Fe( $\eta^5$ -P<sub>5</sub>))<sub>2</sub>Ag<sub>3</sub>(NC(CH<sub>2</sub>)CN)<sub>2</sub>(C<sub>7</sub>H<sub>8</sub>)<sub>n</sub>](SbF<sub>6</sub>)<sub>3n</sub> (**1**)

In a Schlenk tube a solution of AgSbF<sub>6</sub> (28 mg, 0.08 mmol) in CH<sub>2</sub>Cl<sub>2</sub> (25 mL) is carefully layered first with a solvent mixture of CH<sub>2</sub>Cl<sub>2</sub>/toluene (8 mL, 2:1) and then with a green solution of [Cp\*Fe( $\eta^5$ -P<sub>5</sub>)] (14 mg, 0.04 mmol) and NC(CH<sub>2</sub>)CN (1 mL, 0.4 M in CH<sub>2</sub>Cl<sub>2</sub>) in toluene (25 mL). After one day, the formation of greenish rods of **1** at the phase boundary was observed. In the same time, colorless crystals of **III** can be observed side by side to **1**. After complete diffusion, the light green mother liquor was decanted, the crystals are washed with CH<sub>2</sub>Cl<sub>2</sub> (3 x 5 mL) and pentane (2 x 5 mL) and dried *in vacuo*.

Analytical data of **1**:

**Yield:** 42 mg (mixture of **1** and **III**).

**<sup>1</sup>H NMR** (CD<sub>2</sub>Cl<sub>2</sub>):  $\delta$  [ppm] = 1.37 (s, 15 H, [Cp\*Fe( $\eta^5$ -P<sub>5</sub>)]), 3.63 (s, 2 H, NC(CH<sub>2</sub>)CN).

**<sup>31</sup>P{<sup>1</sup>H} NMR** (CD<sub>2</sub>Cl<sub>2</sub>):  $\delta$  [ppm] = 154.97 (s, [Cp\*Fe( $\eta^5$ -P<sub>5</sub>)]).

**<sup>19</sup>F NMR** (CD<sub>2</sub>Cl<sub>2</sub>):  $\delta$  [ppm] = -139.29 (SbF<sub>6</sub>)

**Positive ion ESI-MS** (CH<sub>3</sub>CN):  $m/z$  (%) = 798.7 [{Cp\*Fe( $\eta^5$ -P<sub>5</sub>)<sub>2</sub>Ag]<sup>+</sup>,

**Negative ion ESI-MS** (CH<sub>3</sub>CN):  $m/z$  (%) = 234.9 (100) [SbF<sub>6</sub>]<sup>-</sup>.

**Elemental analysis:** Calculated (%) for [{Cp\*Fe( $\eta^5$ -P<sub>5</sub>)<sub>2</sub>}(AgSbF<sub>6</sub>)<sub>3</sub>(NC(CH<sub>2</sub>)CN)<sub>2</sub>(C<sub>7</sub>H<sub>8</sub>)] (1946.99 g/mol): C 20.36, H 2.17, N 2.88; found: C 20.42, H 1.82, N 2.95.

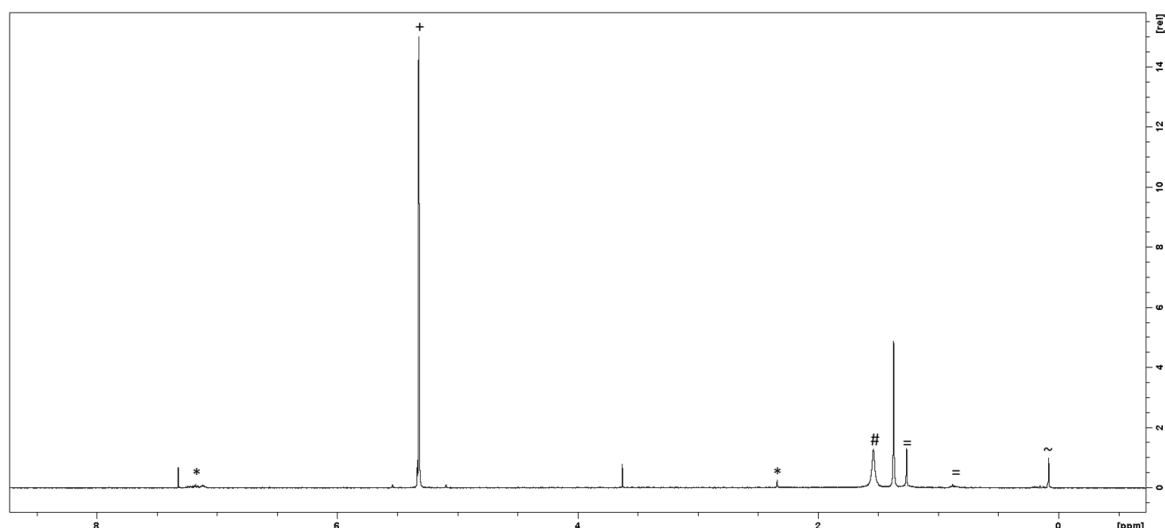


Figure 4.10.  $^1\text{H}$  NMR spectrum of **1** (\* is toluene, + is dichloromethane, # is water, = is pentane and ~ is grease)

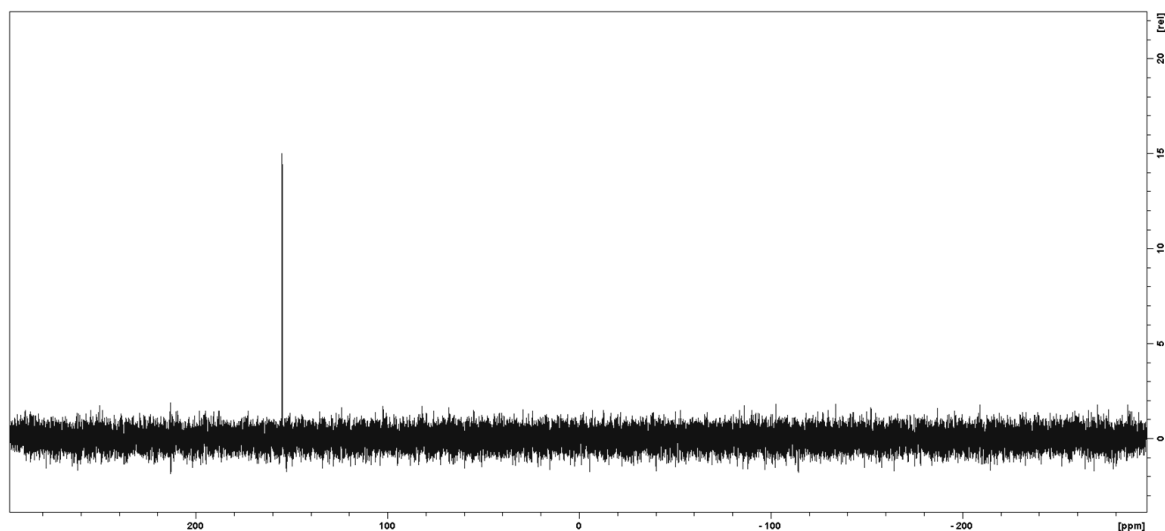


Figure 4.11.  $^{31}\text{P}$  NMR spectrum of **1**.

### Synthesis of $[\{\text{Cp}^*\text{Fe}(\eta^5\text{-P}_5)\}\{\text{Ag}(\text{NC}(\text{CH}_2)_2\text{CN})\}_2]_n(\text{SbF}_6)_{2n}$ (**2a**) and $[\{\text{Cp}^*\text{Fe}(\eta^5\text{-P}_5)\}_2\text{Ag}_2\{\text{NC}(\text{CH}_2)_2\text{CN}\}]_n(\text{SbF}_6)_{2n}$ (**2b**)

In a Schlenk tube a solution of  $\text{AgSbF}_6$  (28 mg, 0.08 mmol) in  $\text{CH}_2\text{Cl}_2$  (25 mL) is carefully layered first with a solvent mixture of  $\text{CH}_2\text{Cl}_2$ /toluene (8 mL, 2:1) and then with a green solution of  $[\text{Cp}^*\text{Fe}(\eta^5\text{-P}_5)]$  (14 mg, 0.04 mmol) and  $\text{NC}(\text{CH}_2)_2\text{CN}$  (1 mL, 0.4 M in  $\text{CH}_2\text{Cl}_2$ ) in toluene (25 mL). After one day, the formation of green plates **2a**, greenish needles **2b** and white crystals at the phase boundary was observed. After complete diffusion, the light green mother liquor was decanted, the crystals are washed with  $\text{CH}_2\text{Cl}_2$  (3 x 8 mL) and pentane (2 x 5 mL) and dried *in vacuo*. The products cannot be separated neither chemically nor by hand due to the size and shape of the crystals.

Analytical data of **2**:



**Yield:** 39 mg (mixture of **2a** and **2b**)

**<sup>1</sup>H NMR** (pyridine-d<sub>5</sub>): δ [ppm] = 1.27 (s, [Cp\*Fe(η<sup>5</sup>-P<sub>5</sub>)], 3.03 (s, NC(CH<sub>2</sub>)<sub>2</sub>CN)),

**<sup>31</sup>P{<sup>1</sup>H} NMR** (pyridine-d<sub>5</sub>): δ [ppm] = 152.29 ([Cp\*FeP<sub>5</sub>])

**<sup>19</sup>F NMR** (pyridine-d<sub>5</sub>): [ppm] = -126.0 (m, SbF<sub>6</sub>)

**Positive ion ESI-MS:** (CH<sub>3</sub>CN): *m/z* (%) = 2176 [{Cp\*Fe(η<sup>5</sup>-P<sub>5</sub>)<sub>3</sub>Ag<sub>4</sub>(SbF<sub>6</sub>)<sub>3</sub>}<sup>+</sup>, 1832.3 [{Cp\*Fe(η<sup>5</sup>-P<sub>5</sub>)<sub>3</sub>Ag<sub>3</sub>(SbF<sub>6</sub>)<sub>2</sub>}<sup>+</sup>, 1527.37 [{Cp\*Fe(η<sup>5</sup>-P<sub>5</sub>)<sub>2</sub>Ag<sub>3</sub>(SbF<sub>6</sub>)<sub>2</sub>(CH<sub>3</sub>CN)}<sup>+</sup>, 1566.2 [{Cp\*Fe(η<sup>5</sup>-P<sub>5</sub>)<sub>2</sub>Ag<sub>3</sub>(SbF<sub>6</sub>)<sub>2</sub>(NC(CH<sub>2</sub>)<sub>2</sub>CN)}<sup>+</sup>, 1486.34 [{Cp\*Fe(η<sup>5</sup>-P<sub>5</sub>)<sub>2</sub>Ag<sub>3</sub>(SbF<sub>6</sub>)<sub>2</sub>}<sup>+</sup>, 1181.1 [{Cp\*Fe(η<sup>5</sup>-P<sub>5</sub>)<sub>2</sub>Ag<sub>3</sub>(SbF<sub>6</sub>)<sub>2</sub>(CH<sub>3</sub>CN)}<sup>+</sup>, 1142.5 [{Cp\*Fe(η<sup>5</sup>-P<sub>5</sub>)<sub>2</sub>Ag<sub>2</sub>(SbF<sub>6</sub>)<sub>2</sub>}<sup>+</sup>, 867.67 [{Cp\*Fe(η<sup>5</sup>-P<sub>5</sub>)<sub>2</sub>Ag<sub>2</sub>(SbF<sub>6</sub>)<sub>2</sub>(NC(CH<sub>2</sub>)<sub>2</sub>CN)}<sup>+</sup>, 837.65 [{Cp\*Fe(η<sup>5</sup>-P<sub>5</sub>)<sub>2</sub>Ag<sub>2</sub>(SbF<sub>6</sub>)<sub>2</sub>(CH<sub>3</sub>CN)}<sup>+</sup>, 798.7 [{Cp\*Fe(η<sup>5</sup>-P<sub>5</sub>)<sub>2</sub>Ag}]+, 493.9 (100) [{Cp\*Fe(η<sup>5</sup>-P<sub>5</sub>)<sub>2</sub>Ag}]+, 452.8 [{Cp\*Fe(η<sup>5</sup>-P<sub>5</sub>)<sub>2</sub>Ag}]+.

**Negative ion ESI-MS:** (CH<sub>3</sub>CN): *m/z* (%) = 234.9 (100) [SbF<sub>6</sub>]<sup>-</sup>.

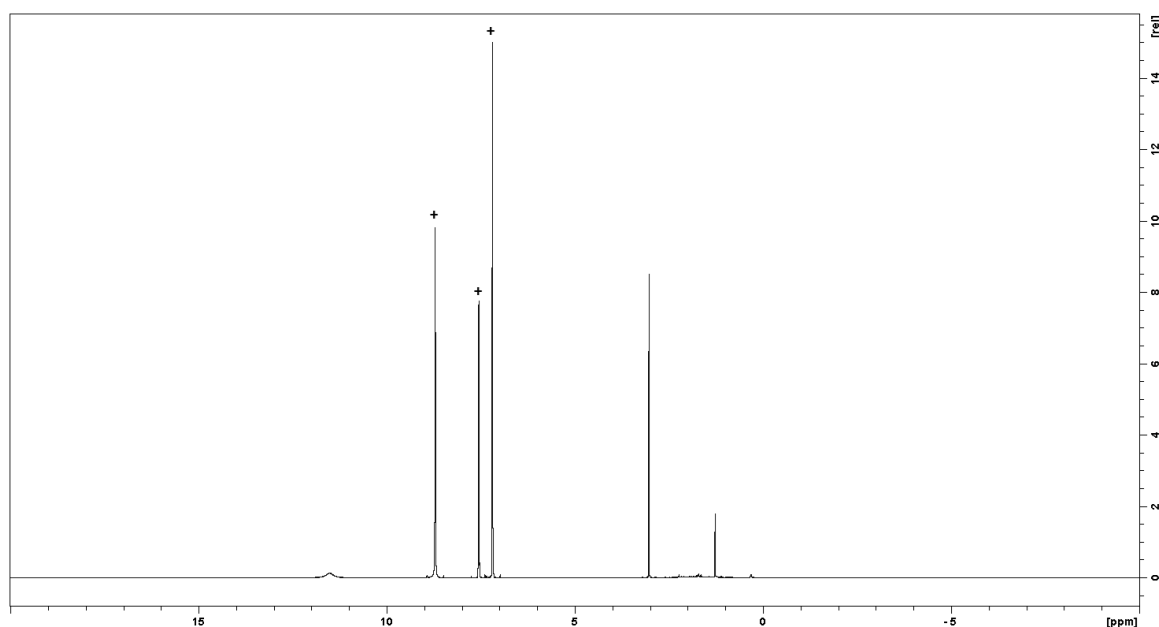


**Figure 4.12.** <sup>1</sup>H NMR spectrum of **2** (+ pyridine).

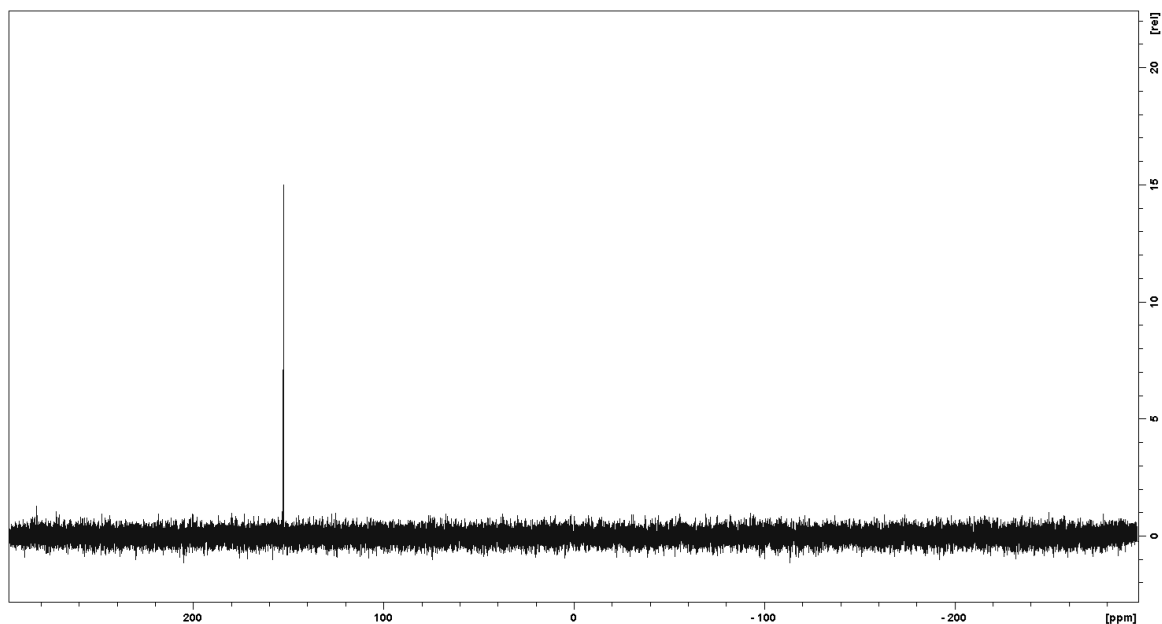


Figure 4.13.  $^{31}\text{P}$  NMR spectrum of **2**.

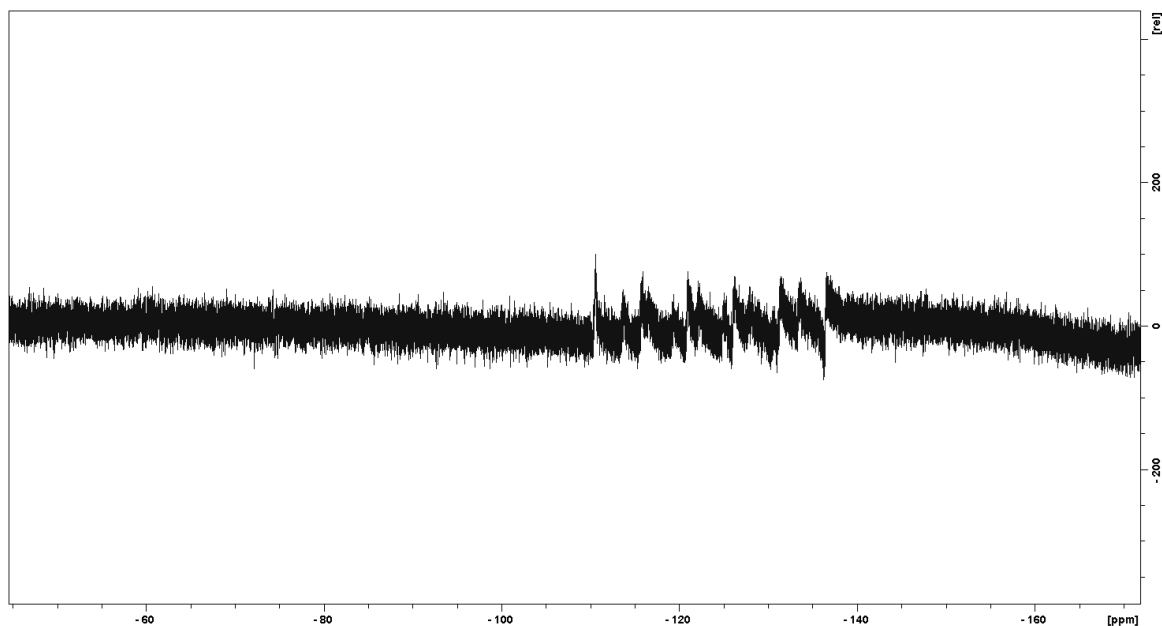


Figure 4.14.  $^{19}\text{F}$  NMR spectrum of **2**.

Synthesis of  $[(\text{Cp}^*\text{Fe}(\eta^5\text{-P}_5))\{\text{Ag}(\text{NC}(\text{CH}_2)_3\text{CN})\}_2]_n[\text{SbF}_6]_{2n}$  (**3a**) and  $[(\text{Cp}^*\text{Fe}(\eta^5\text{-P}_5))\{\text{Ag}_2(\text{NC}(\text{CH}_2)_3\text{CN})\}]_n[\text{SbF}_6]_{2n}$  (**3b**)

In a Schlenk tube a solution of  $\text{AgSbF}_6$  (28 mg, 0.08 mmol) in  $\text{CH}_2\text{Cl}_2$  (25 mL) is carefully layered first with a solvent mixture of  $\text{CH}_2\text{Cl}_2$ /toluene (10 mL, 2:1) and then with a green solution of  $[\text{Cp}^*\text{Fe}(\eta^5\text{-P}_5)]$  (14 mg, 0.04 mmol) and  $\text{NC}(\text{CH}_2)_3\text{CN}$  (1 mL, 0.4 M in  $\text{CH}_2\text{Cl}_2$ ) in toluene (25 mL). After one night, the phase boundary turns yellow and after one day the formation of green plates **3a** and prisms of **3b** at the phase boundary was observed. After complete diffusion, the light green mother

liquor is decanted, the crystals are washed with CH<sub>2</sub>Cl<sub>2</sub> (3 × 8 mL) and with pentane (2 × 5 mL) and dried *in vacuo*.

Analytical data of **3a**:

**Yield:** 28 mg (0.020 mmol, 49.7% based on [Cp\*Fe(η<sup>5</sup>-P<sub>5</sub>)])

**<sup>1</sup>H NMR** (pyridine-d<sub>5</sub>): δ [ppm] = 1.27 (s, [Cp(CH<sub>3</sub>)<sub>5</sub>Fe(η<sup>5</sup>-P<sub>5</sub>)]), 1.85 (s, NC(CH<sub>2</sub>)<sub>3</sub>CN), 2.57 (s, (NC(CH<sub>2</sub>)<sub>3</sub>CN)).

**<sup>31</sup>P{<sup>1</sup>H} NMR** (pyridine-d<sub>5</sub>): δ [ppm] = 152.31 ([Cp\*FeP<sub>5</sub>])

**<sup>19</sup>F NMR** (pyridine-d<sub>5</sub>): no signal was detected.

**Positive ion ESI-MS** (CH<sub>3</sub>CN): *m/z* (%) = 2519.8 [Cp\*Fe(η<sup>5</sup>-P<sub>5</sub>)<sub>3</sub>Ag<sub>5</sub>(SbF<sub>6</sub>)<sub>4</sub>]<sup>+</sup>, 2176 [Cp\*Fe(η<sup>5</sup>-P<sub>5</sub>)<sub>3</sub>Ag<sub>4</sub>(SbF<sub>6</sub>)<sub>3</sub>]<sup>+</sup>, 1924.19 [Cp\*Fe(η<sup>5</sup>-P<sub>5</sub>)<sub>2</sub>Ag<sub>4</sub>(SbF<sub>6</sub>)<sub>3</sub>(NC(CH<sub>2</sub>)<sub>3</sub>CN)]<sup>+</sup>, 1832.3 [Cp\*Fe(η<sup>5</sup>-P<sub>5</sub>)<sub>3</sub>Ag<sub>3</sub>(SbF<sub>6</sub>)<sub>2</sub>]<sup>+</sup>, 1527.37 [Cp\*Fe(η<sup>5</sup>-P<sub>5</sub>)<sub>2</sub>Ag<sub>3</sub>(SbF<sub>6</sub>)<sub>2</sub>(CH<sub>3</sub>CN)]<sup>+</sup>, 1234.47 [Cp\*Fe(η<sup>5</sup>-P<sub>5</sub>)Ag<sub>3</sub>(SbF<sub>6</sub>)<sub>2</sub>(NC(CH<sub>2</sub>)<sub>3</sub>CN)]<sup>+</sup>, 1181.15 [Cp\*Fe(η<sup>5</sup>-P<sub>5</sub>)Ag<sub>3</sub>(SbF<sub>6</sub>)<sub>2</sub>(CH<sub>3</sub>CN)]<sup>+</sup>, 1142.5 [Cp\*Fe(η<sup>5</sup>-P<sub>5</sub>)<sub>2</sub>Ag<sub>2</sub>(SbF<sub>6</sub>)]<sup>+</sup>, 890.67 [Cp\*Fe(η<sup>5</sup>-P<sub>5</sub>)Ag<sub>2</sub>(SbF<sub>6</sub>)(NC(CH<sub>2</sub>)<sub>3</sub>CN)]<sup>+</sup>, 837.65 [Cp\*Fe(η<sup>5</sup>-P<sub>5</sub>)Ag<sub>2</sub>(SbF<sub>6</sub>)(CH<sub>3</sub>CN)]<sup>+</sup>, 798.7 [Cp\*Fe(η<sup>5</sup>-P<sub>5</sub>)<sub>2</sub>Ag]<sup>+</sup>, 493.9 (100) [Cp\*Fe(η<sup>5</sup>-P<sub>5</sub>)Ag(CH<sub>3</sub>CN)]<sup>+</sup>, 452.8 [Cp\*Fe(η<sup>5</sup>-P<sub>5</sub>)Ag]<sup>+</sup>.

**Negative ion ESI-MS** (CH<sub>3</sub>CN): *m/z* (%) = 578.7 Ag(SbF<sub>6</sub>)<sup>-</sup>, 234.9 (100) [SbF<sub>6</sub>]<sup>-</sup>.

**Elemental analysis:** Calculated (%) for [Cp\*Fe(η<sup>5</sup>-P<sub>5</sub>)]<sub>2</sub>[Ag(NC(CH<sub>2</sub>)<sub>3</sub>CN)]<sub>2</sub><sub>n</sub>[SbF<sub>6</sub>]<sub>2n</sub>(CH<sub>2</sub>Cl<sub>2</sub>)<sub>2</sub> (1391.26 g/mol): C 18.99 %, H 2.25 %, N 4.03 %; found: C 19.12 %, H 2.03 %, N 4.03 %.

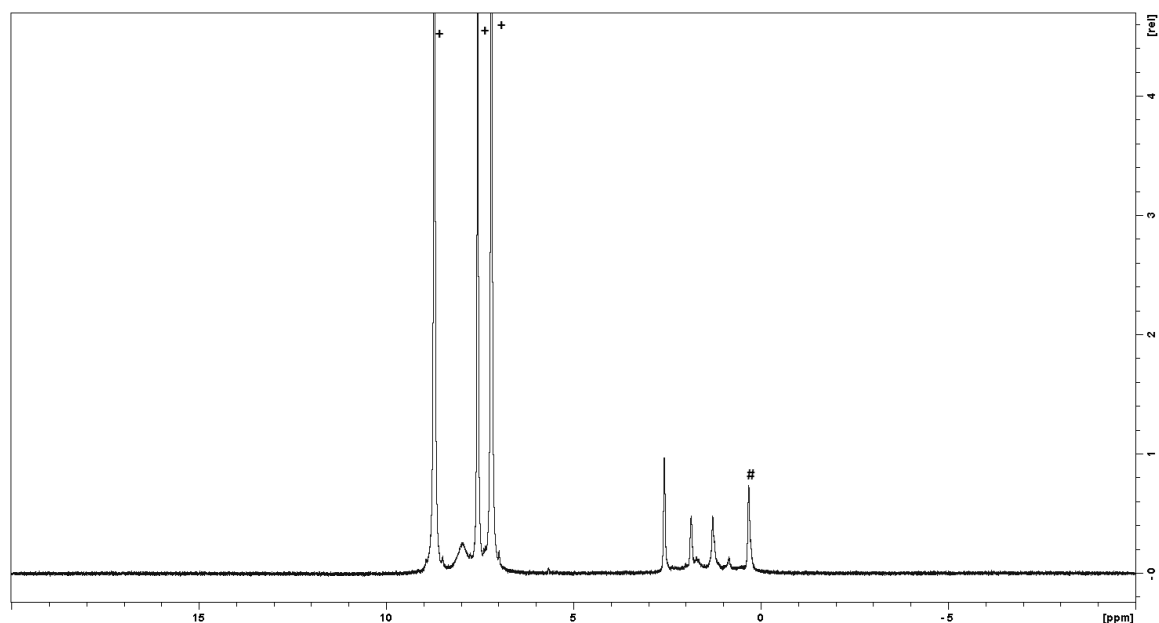


**Figure 4.15.** <sup>1</sup>H NMR spectrum of **3** (+ pyridine, # grease).

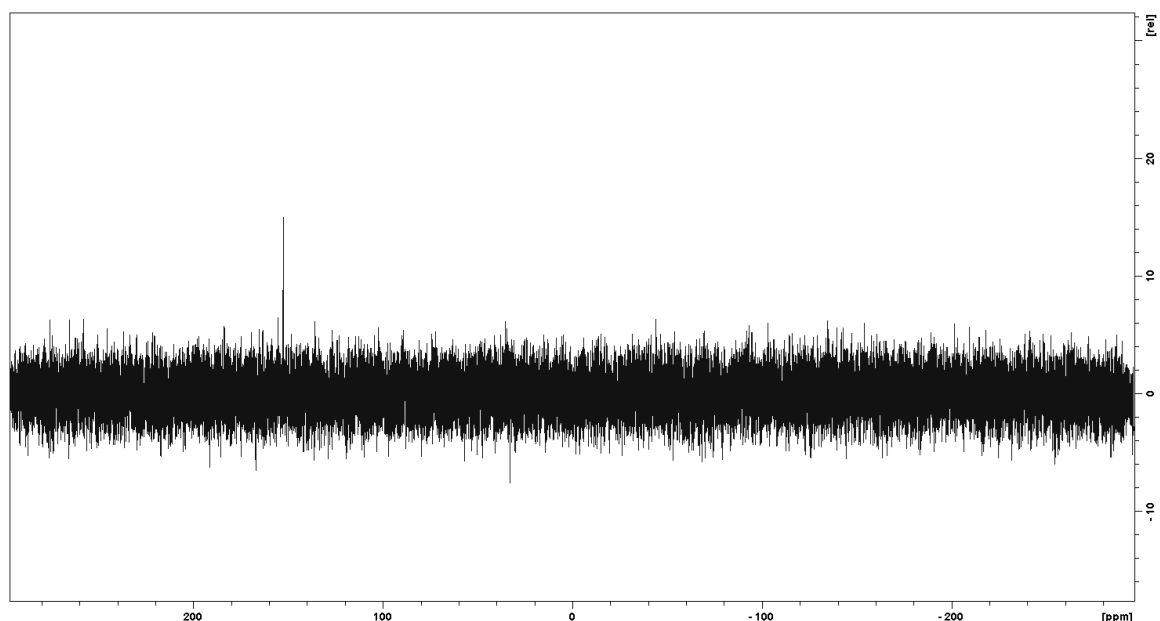


Figure 4.16.  $^{31}\text{P}$  NMR spectrum of **3**.

### Synthesis of $[\{\text{Cp}^*\text{Fe}(\eta^5\text{-P}_5)\}_4\{\text{Ag}_4(\text{NC}(\text{CH}_2)_4\text{CN})_2\}]_n[\text{SbF}_6]_{4n}$ (**4a**) and $[\{\text{Cp}^*\text{Fe}(\eta^5\text{-P}_5)\}_2\{\text{Ag}_3(\text{NC}(\text{CH}_2)_4\text{CN})_2\}]_n[\text{SbF}_6]_{3n}$ (**4b**)

In a Schlenk tube a solution of  $\text{AgSbF}_6$  (28 mg, 0.08 mmol) in  $\text{CH}_2\text{Cl}_2$  (25 mL) is carefully layered first with a solvent mixture of  $\text{CH}_2\text{Cl}_2$ /toluene (10 mL, 2:1) and then with a green solution of  $[\text{Cp}^*\text{Fe}(\eta^5\text{-P}_5)]$  (14 mg, 0.04 mmol) and  $\text{NC}(\text{CH}_2)_4\text{CN}$  (1 mL, 0.4 M in  $\text{CH}_2\text{Cl}_2$ ) in toluene (25 mL). After a few hours, the phase boundary turns yellow. After one day the formation of **4a** in form of green needles, **4b** in form of few brown blocks and  $[\text{Ag}(\text{NC}(\text{CH}_2)_4\text{CN})_2][\text{SbF}_6]$  in form of white solid can be observed. After complete diffusion, the light green mother liquor is decanted, the crystals are washed with  $\text{CH}_2\text{Cl}_2$  ( $3 \times 8$  mL) and with pentane ( $2 \times 5$  mL) and dried *in vacuo*. The products can be separated neither chemically nor by hand due to the size and shape of the crystals.

Analytical data of **4**:

**Yield:** 56 mg (mixture of **4a**, **4b** and  $[\text{Ag}(\text{NC}(\text{CH}_2)_4\text{CN})_2][\text{SbF}_6]$ ).

$^1\text{H}$  NMR (pyridine/ $\text{CD}_2\text{Cl}_2$ ):  $\delta$  [ppm] = 1.43 (s,  $[\text{Cp}(\text{CH}_3)_5\text{Fe}(\eta^5\text{-P}_5)]$ ), 1.81 (m, 4H,  $\text{NC}(\text{CH}_2)_4\text{CN}$ ), 2.41 (m,  $\text{NC}(\text{CH}_2)_4\text{CN}$ ).

$^{31}\text{P}\{^1\text{H}\}$  NMR ( $\text{CD}_2\text{Cl}_2$ ):  $\delta$  [ppm] = 152.0 (s,  $[\text{Cp}^*\text{Fe}(\eta^5\text{-P}_5)]$ ).

$^{19}\text{F}$  NMR ( $\text{CD}_2\text{Cl}_2$ ): no signal was detected.

**Positive ion ESI-MS** ( $\text{CH}_3\text{CN}$ ):  $m/z$  (%) = 2178.2  $[\{\text{Cp}^*\text{Fe}(\eta^5\text{-P}_5)\}_4\text{Ag}_3(\text{SbF}_6)_2]^+$ , 1938.21  $[\{\text{Cp}^*\text{Fe}(\eta^5\text{-P}_5)\}_2\text{Ag}_4(\text{SbF}_6)_3(\text{NC}(\text{CH}_2)_4\text{CN})]^+$ , 1832.3  $[\{\text{Cp}^*\text{Fe}(\eta^5\text{-P}_5)\}_3\text{Ag}_3(\text{SbF}_6)_2]^+$ , 1594.41  $[\{\text{Cp}^*\text{Fe}(\eta^5\text{-P}_5)\}_2\text{Ag}_3(\text{SbF}_6)_2(\text{NC}(\text{CH}_2)_4\text{CN})]^+$ , 1142.5  $[\{\text{Cp}^*\text{Fe}(\eta^5\text{-P}_5)\}_2\text{Ag}_2(\text{SbF}_6)]^+$ , 798.7  $[\{\text{Cp}^*\text{Fe}(\eta^5\text{-P}_5)\}_2\text{Ag}]^+$ , 493.9 (100)  $[\{\text{Cp}^*\text{Fe}(\eta^5\text{-P}_5)\}\text{Ag}(\text{CH}_3\text{CN})]^+$ , 452.8  $[\{\text{Cp}^*\text{Fe}(\eta^5\text{-P}_5)\}\text{Ag}]^+$ .

Negative ion ESI-MS ( $\text{CH}_3\text{CN}$  (1:1)):  $m/z$  (%) = 234.9 (100)  $[\text{SbF}_6]^-$ .

Elemental analysis: Calculated (%) for  $[\text{Ag}(\text{NC}(\text{CH}_2)_4\text{CN})_2][\text{SbF}_6]$  (559.90 g/mol): C 25.74 %, H 2.88 %, N 10.01 %; found: C 25.54 %, H 2.62 %, N 9.81 %.

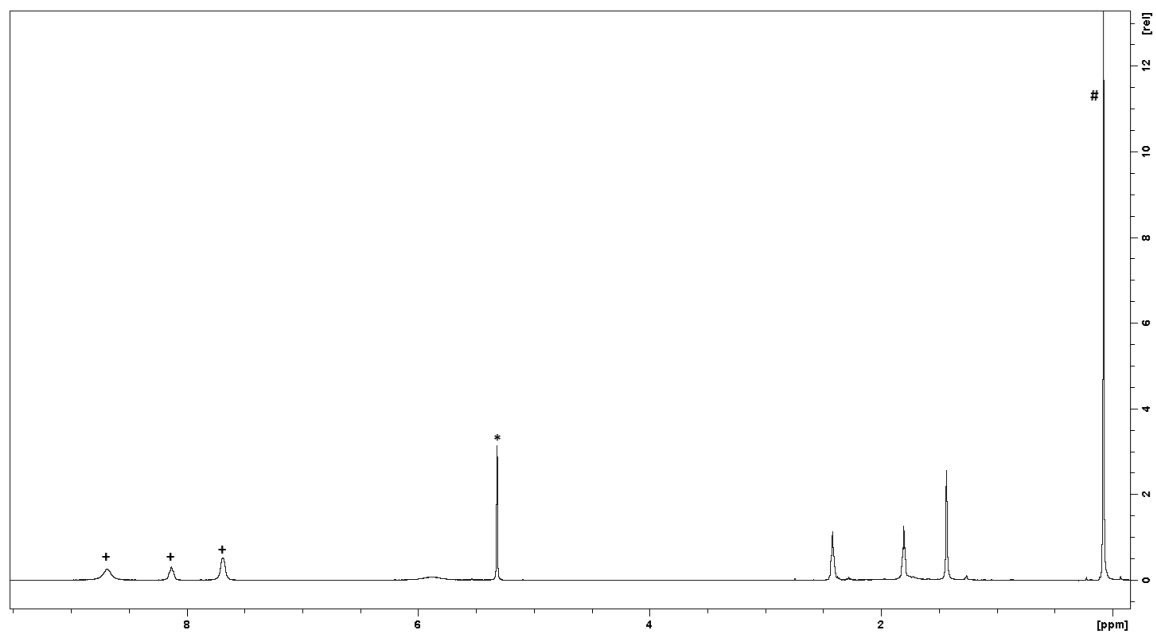


Figure 4.17.  $^1\text{H}$  NMR spectrum of **4**. (+ pyridine, \* dichloromethane, # grease)

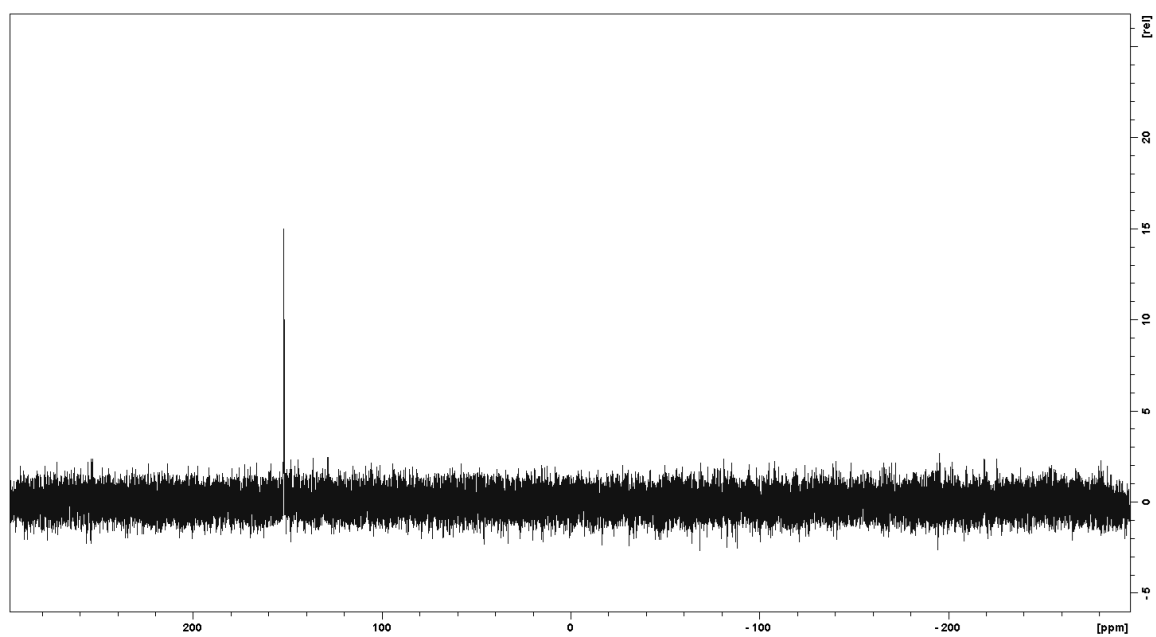


Figure 4.18.  $^{31}\text{P}$  NMR spectrum of **4**

**Synthesis of  $\{[Cp^*Fe(\eta^5-P_5)]_4[Ag_4(NC(CH_2)_5CN)_2]\}_n[SbF_6]_{4n}$  (5a) and  $\{[Cp^*Fe(\eta^5-P_5)]_3[Ag_3(NC(CH_2)_5CN)_2]\}_n[SbF_6]_n$  (5b)**

In a Schlenk tube a solution of  $AgSbF_6$  (18 mg, 0.05 mmol) in  $CH_2Cl_2$  (25 mL) is carefully layered first with a solvent mixture of  $CH_2Cl_2$ /toluene (10 mL, 2:1) and then with a green solution of  $[Cp^*Fe(\eta^5-P_5)]$  (18 mg, 0.05 mmol) and  $NC(CH_2)_5CN$  (1 mL, 0.4 M in  $CH_2Cl_2$ ) in toluene (25 mL). After a few hours, the phase boundary turns yellow and after one day, the formation of green rods of **5a** and red rods of **5b** at the phase boundary was observed. After complete diffusion, the light green mother liquor is decanted, the crystals are washed with  $CH_2Cl_2$  (3 × 10 mL) and dried *in vacuo*.

Analytical data of inseparable mixture of **5a** and **5b**:

**Yield:** 47 mg (mixture of **5a** and **5b**)

**$^1H$  NMR** (pyridine/ $CD_2Cl_2$ ):  $\delta$  [ppm] = 1.45 (s, 30H,  $[Cp(CH_3)_5Fe(\eta^5-P_5)]$ ), 1.60 (m, 2H, C-4,  $NC(CH_2)_5CN$ ), 1.69 (m, 4H, C-3/C-5,  $NC(CH_2)_5CN$ ), 2.38 (t, 4H, C-2/C-6,  $NC(CH_2)_5CN$ ), 7.45 (m,  $\beta$ -H, pyridine), 7.85 (m,  $\gamma$ -H, pyridine), 8.57 (m,  $\alpha$ -H, pyridine).

**$^{13}C$  NMR** (pyridine/ $CD_2Cl_2$ ):  $\delta$  [ppm] = 10.69 ( $[Cp(CH_3)_5Fe(\eta^5-P_5)]$ ), 93.04 ( $[C_5(CH_3)_5Fe(\eta^5-P_5)]$ ), 124.7 ( $\beta$ -C, pyridine), 137.81 ( $\gamma$ -C, pyridine), 149.31 ( $\alpha$ -C, pyridine).

**$^{31}P\{^1H\}$  NMR** (pyridine/ $CD_2Cl_2$ ):  $\delta$  [ppm] = 143.46 (s,  $[Cp^*Fe(\eta^5-P_5)]$ ).

**$^{19}F$  NMR** (pyridine/ $CD_2Cl_2$ ): no signal was detected.

**Positive ion ESI-MS** ( $CH_2Cl_2/CH_3CN$  (1:1)):  $m/z$  (%) = 2522  $\{[Cp^*Fe(\eta^5-P_5)]_4Ag_4(SbF_6)_3\}^+$ , 2178.2  $\{[Cp^*Fe(\eta^5-P_5)]_4Ag_3(SbF_6)_2\}^+$ , 2176  $\{[Cp^*Fe(\eta^5-P_5)]_3Ag_4(SbF_6)_3\}^+$ , 2077  $\{[Cp^*Fe(\eta^5-P_5)]_3Ag_3(SbF_6)_2(NC(CH_2)_5CN)_2\}^+$ , 1955  $\{[Cp^*Fe(\eta^5-P_5)]_3Ag_3(SbF_6)_2(NC(CH_2)_5CN)\}^+$ , 1832.3  $\{[Cp^*Fe(\eta^5-P_5)]_3Ag_3(SbF_6)_2\}^+$ , 1608.4  $\{[Cp^*Fe(\eta^5-P_5)]_2Ag_3(SbF_6)_2(NC(CH_2)_5CN)\}^+$ , 1387  $\{[Cp^*Fe(\eta^5-P_5)]_2Ag_2(SbF_6)(NC(CH_2)_5CN)_2\}^+$ , 1265  $\{[Cp^*Fe(\eta^5-P_5)]_2Ag_2(SbF_6)(NC(CH_2)_5CN)\}^+$ , 1142.5  $\{[Cp^*Fe(\eta^5-P_5)]_2Ag_2(SbF_6)\}^+$ , 918.7  $\{[Cp^*Fe(\eta^5-P_5)]Ag_2(SbF_6)(NC(CH_2)_5CN)\}^+$ , 798.7  $\{[Cp^*Fe(\eta^5-P_5)]_2Ag\}^+$ , 493.9 (100)  $\{[Cp^*Fe(\eta^5-P_5)]Ag(CH_3CN)\}^+$ , 452.8  $\{[Cp^*Fe(\eta^5-P_5)]Ag\}^+$ .

**Negative ion ESI-MS** ( $CH_2Cl_2/CH_3CN$  (1:1)):  $m/z$  (%) = 2647.9  $\{[Cp^*Fe(\eta^5-P_5)]_4Ag_3(SbF_6)_4\}^-$ , 2426  $\{[Cp^*Fe(\eta^5-P_5)]_3Ag_3(SbF_6)_4(NC(CH_2)_5CN)\}^-$ , 2301.9  $\{[Cp^*Fe(\eta^5-P_5)]_3Ag_3(SbF_6)_4\}^-$ , 2078.1  $\{[Cp^*Fe(\eta^5-P_5)]_3Ag_2(SbF_6)_3(NC(CH_2)_5CN)\}^-$ , 1958.1  $\{[Cp^*Fe(\eta^5-P_5)]_3Ag_2(SbF_6)_3\}^-$ , 1739.2  $\{[Cp^*Fe(\eta^5-P_5)]_2Ag_2(SbF_6)_3(NC(CH_2)_5CN)\}^-$ , 1612.2  $\{[Cp^*Fe(\eta^5-P_5)]_2Ag_2(SbF_6)_3\}^-$ , 234.9 (100)  $[SbF_6]^-$ .

**IR:**  $\tilde{\nu}/cm^{-1}$  = 2964 (vw), 2274 (vw), 1478 (w), 1425 (w), 1378 (w), 1020 (w), 655 (s).

**Synthesis of  $\{[Cp^*Fe(\eta^5-P_5)]_3[Ag_3(NC(CH_2)_5CN)_2]\}_n[SbF_6]_n$  (5b)**

In a Schlenk tube a solution of  $AgSbF_6$  (35 mg, 0.1 mmol) in  $CH_2Cl_2$  (25 mL) is carefully layered first with a solvent mixture of  $CH_2Cl_2$ /toluene (10 mL, 2:1) and then with a green solution of

[Cp\*Fe( $\eta^5$ -P<sub>5</sub>)] (18 mg, 0.05 mmol) and NC(CH<sub>2</sub>)<sub>5</sub>CN (1 mL, 0.4 M in CH<sub>2</sub>Cl<sub>2</sub>) in toluene (25 mL). After a few hours, the phase boundary turns yellow and after one day, the formation of red rods of **5b** at the phase boundary can be observed. After complete diffusion, the light green mother liquor is decanted, the crystals are washed with CH<sub>2</sub>Cl<sub>2</sub> (3 x 10 mL) and dried *in vacuo*.

Analytical data of **5b**:

**Yield:** 57 mg (0.045 mmol), 86% based on [Cp\*Fe( $\eta^5$ -P<sub>5</sub>)].

**<sup>1</sup>H NMR** (pyridine/CD<sub>2</sub>Cl<sub>2</sub>):  $\delta$  [ppm] = 1.46 (15H, [Cp\*Fe( $\eta^5$ -P<sub>5</sub>)]), 1.62 (4H, C-3, NC(CH<sub>2</sub>)<sub>5</sub>CN), 1.72 (8H, C-2/C-4, NC(CH<sub>2</sub>)<sub>5</sub>CN), 2.41 (8H, C-1/C-5, NC(CH<sub>2</sub>)<sub>5</sub>CN), 7.54 (m,  $\beta$ -H, pyridine), 7.83 (m,  $\gamma$ -H, pyridine), 8.72 (m,  $\alpha$ -H, pyridine).

**<sup>13</sup>C NMR** (pyridine/CD<sub>2</sub>Cl<sub>2</sub>):  $\delta$  [ppm] = 10.65 [Cp\*Fe( $\eta^5$ -P<sub>5</sub>)], 24.71 (NC(CH<sub>2</sub>)<sub>5</sub>CN), 27.75 (NC(CH<sub>2</sub>)<sub>5</sub>CN), no other signals were detected.

**<sup>31</sup>P{<sup>1</sup>H} NMR** (pyridine/CD<sub>2</sub>Cl<sub>2</sub>):  $\delta$  [ppm] = 139.78 ([Cp\*Fe( $\eta^5$ -P<sub>5</sub>)]).

**<sup>19</sup>F NMR** (pyridine/CD<sub>2</sub>Cl<sub>2</sub>): no signal was detected.

**Positive ion ESI-MS** (CH<sub>2</sub>Cl<sub>2</sub>/CH<sub>3</sub>CN (1:1)):  $m/z$  (%) = 2418.2 [Cp\*Fe( $\eta^5$ -P<sub>5</sub>)<sub>3</sub>Ag<sub>4</sub>(SbF<sub>6</sub>)<sub>3</sub>(NC(CH<sub>2</sub>)<sub>5</sub>CN)<sub>2</sub>]<sup>+</sup>, 2074.3 [Cp\*Fe( $\eta^5$ -P<sub>5</sub>)<sub>3</sub>Ag<sub>3</sub>(SbF<sub>6</sub>)<sub>2</sub>(NC(CH<sub>2</sub>)<sub>5</sub>CN)<sub>2</sub>]<sup>+</sup>, 1955 [Cp\*Fe( $\eta^5$ -P<sub>5</sub>)<sub>3</sub>Ag<sub>3</sub>(SbF<sub>6</sub>)<sub>2</sub>(NC(CH<sub>2</sub>)<sub>5</sub>CN)]<sup>+</sup>, 1832.3 [Cp\*Fe( $\eta^5$ -P<sub>5</sub>)<sub>3</sub>Ag<sub>3</sub>(SbF<sub>6</sub>)<sub>2</sub>]<sup>+</sup>, 1731 [Cp\*Fe( $\eta^5$ -P<sub>5</sub>)<sub>2</sub>Ag<sub>3</sub>(SbF<sub>6</sub>)<sub>2</sub>(NC(CH<sub>2</sub>)<sub>5</sub>CN)<sub>2</sub>]<sup>+</sup>, 1608.4 [Cp\*Fe( $\eta^5$ -P<sub>5</sub>)<sub>2</sub>Ag<sub>3</sub>(SbF<sub>6</sub>)<sub>2</sub>(NC(CH<sub>2</sub>)<sub>5</sub>CN)]<sup>+</sup>, 1384.6 [Cp\*Fe( $\eta^5$ -P<sub>5</sub>)<sub>2</sub>Ag<sub>2</sub>(SbF<sub>6</sub>)(NC(CH<sub>2</sub>)<sub>5</sub>CN)<sub>2</sub>]<sup>+</sup>, 1265 [Cp\*Fe( $\eta^5$ -P<sub>5</sub>)<sub>2</sub>Ag<sub>2</sub>(SbF<sub>6</sub>)(NC(CH<sub>2</sub>)<sub>5</sub>CN)]<sup>+</sup>, 1142.5 [Cp\*Fe( $\eta^5$ -P<sub>5</sub>)<sub>2</sub>Ag<sub>2</sub>(SbF<sub>6</sub>)]<sup>+</sup>, 918.7 [Cp\*Fe( $\eta^5$ -P<sub>5</sub>)Ag<sub>2</sub>(SbF<sub>6</sub>)(NC(CH<sub>2</sub>)<sub>5</sub>CN)]<sup>+</sup>, 798.7 [Cp\*Fe( $\eta^5$ -P<sub>5</sub>)<sub>2</sub>Ag]<sup>+</sup>, 493.9 (100) [Cp\*Fe( $\eta^5$ -P<sub>5</sub>)Ag(CH<sub>3</sub>CN)]<sup>+</sup>, 452.8 [(Cp\*Fe( $\eta^5$ -P<sub>5</sub>))Ag]<sup>+</sup>.

**Negative ion ESI-MS** (CH<sub>2</sub>Cl<sub>2</sub>/CH<sub>3</sub>CN (1:1)):  $m/z$  (%) = 2772 [Cp\*Fe( $\eta^5$ -P<sub>5</sub>)<sub>4</sub>Ag<sub>3</sub>(SbF<sub>6</sub>)<sub>4</sub>(NC(CH<sub>2</sub>)<sub>5</sub>CN)]<sup>-</sup>, 2647.9 [Cp\*Fe( $\eta^5$ -P<sub>5</sub>)<sub>4</sub>Ag<sub>3</sub>(SbF<sub>6</sub>)<sub>4</sub>]<sup>-</sup>, 2544.0 [Cp\*Fe( $\eta^5$ -P<sub>5</sub>)<sub>3</sub>Ag<sub>3</sub>(SbF<sub>6</sub>)<sub>4</sub>(NC(CH<sub>2</sub>)<sub>5</sub>CN)<sub>2</sub>]<sup>-</sup>, 2426 [Cp\*Fe( $\eta^5$ -P<sub>5</sub>)<sub>3</sub>Ag<sub>3</sub>(SbF<sub>6</sub>)<sub>4</sub>(NC(CH<sub>2</sub>)<sub>5</sub>CN)]<sup>-</sup>, 2299.9 [Cp\*Fe( $\eta^5$ -P<sub>5</sub>)<sub>3</sub>Ag<sub>3</sub>(SbF<sub>6</sub>)<sub>4</sub>]<sup>-</sup>, 2078.1 [Cp\*Fe( $\eta^5$ -P<sub>5</sub>)<sub>3</sub>Ag<sub>2</sub>(SbF<sub>6</sub>)<sub>3</sub>(NC(CH<sub>2</sub>)<sub>5</sub>CN)]<sup>-</sup>, 1958.1 [Cp\*Fe( $\eta^5$ -P<sub>5</sub>)<sub>3</sub>Ag<sub>2</sub>(SbF<sub>6</sub>)<sub>3</sub>]<sup>-</sup>, 1612.2 [Cp\*Fe( $\eta^5$ -P<sub>5</sub>)<sub>2</sub>Ag<sub>2</sub>(SbF<sub>6</sub>)<sub>3</sub>]<sup>-</sup>, 234.9 (100) [SbF<sub>6</sub>]<sup>-</sup>.

**Elemental analysis:** Calculated (%) for [Cp\*Fe( $\eta^5$ -P<sub>5</sub>)](AgSbF<sub>6</sub>)<sub>2</sub>(NC(CH<sub>2</sub>)<sub>5</sub>CN)<sub>2</sub> (1277.51 g/mol): C 22.56, H 2.76, N 4.39; found: C 21.75, H 2.85, N 4.07.

**IR:**  $\tilde{\nu}$ /cm<sup>-1</sup> = 2930 (vw), 2266 (w), 1615 (vw), 1462 (w), 1418 (w), 1375 (w), 1016 (w), 651 (s).

### Synthesis of [Cp\*Fe( $\eta^5$ -P<sub>5</sub>)]<sub>n</sub>[Ag(NC(CH<sub>2</sub>)<sub>6</sub>CN)]<sub>n</sub>[SbF<sub>6</sub>]<sub>n</sub> (**6**)

In a Schlenk tube a solution of AgSbF<sub>6</sub> (14 mg, 0.04 mmol) in CH<sub>2</sub>Cl<sub>2</sub> (15 mL) is carefully layered with a green solution of [Cp\*Fe( $\eta^5$ -P<sub>5</sub>)] (14 mg, 0.04 mmol) and NC(CH<sub>2</sub>)<sub>6</sub>CN (1 mL, 0.4 mmol, 0.4 M in CH<sub>2</sub>Cl<sub>2</sub>) in toluene (15 mL). Thereby, the phase boundary turns yellow. After a few days, the

formation of green-brown prismatic crystals of **6** at the phase boundary was observed. After complete diffusion, the light green mother liquor is decanted, the crystals are washed with hexane ( $3 \times 10$  mL) and dried *in vacuo*.

Analytical data of **6**:

**Yield:** 19 mg (0.023 mmol, 57% based on  $[\text{Cp}^*\text{Fe}(\eta^5\text{-P}_5)]$ ).

**$^1\text{H}$  NMR** ( $\text{CD}_2\text{Cl}_2/\text{pyridine}$ ):  $\delta$  [ppm] = 1.43 (s, 15H,  $[\text{Cp}(\text{CH}_3)_5\text{Fe}(\eta^5\text{-P}_5)]$ ), 1.47 (m, 4H,  $\text{NC}(\text{CH}_2)_6\text{CN}$ ), 1.66 (m, 4H,  $\text{NC}(\text{CH}_2)_6\text{CN}$ ), 2.36 (t, 4H,  $\text{NC}(\text{CH}_2)_6\text{CN}$ ).

**$^{13}\text{C}$  NMR** ( $\text{CD}_2\text{Cl}_2/\text{pyridine}$ ):  $\delta$  [ppm] = 10.66 ( $[\text{Cp}(\text{CH}_3)_5\text{Fe}(\eta^5\text{-P}_5)]$ ), 16.98 (C-2,  $\text{NC}(\text{CH}_2)_6\text{CN}$ ), 25.13 (C-3,  $\text{NC}(\text{CH}_2)_6\text{CN}$ ), 27.86 (C-4,  $\text{NC}(\text{CH}_2)_6\text{CN}$ ), 149.75 ( $\text{NC}(\text{CH}_2)_6\text{CN}$ ).

**$^{31}\text{P}\{^1\text{H}\}$  NMR** ( $\text{CD}_2\text{Cl}_2/\text{pyridine}$ ):  $\delta$  [ppm] = 141.20 (s,  $[\text{Cp}^*\text{Fe}(\eta^5\text{-P}_5)]$ ).

**$^{19}\text{F}$  NMR** ( $\text{CD}_2\text{Cl}_2/\text{pyridine}$ ): no signal was detected.

**Positive ion ESI-MS** ( $\text{CH}_2\text{Cl}_2/\text{CH}_3\text{CN}$  (1:1)):  $m/z$  (%) = 2522.0  $[\{\text{Cp}^*\text{Fe}(\eta^5\text{-P}_5)\}_4\text{Ag}_4(\text{SbF}_6)_3]^+$ , 2178.2  $[\{\text{Cp}^*\text{Fe}(\eta^5\text{-P}_5)\}_4\text{Ag}_3(\text{SbF}_6)_2]^+$ , 2176  $[\{\text{Cp}^*\text{Fe}(\eta^5\text{-P}_5)\}_3\text{Ag}_4(\text{SbF}_6)_3]^+$ , 1832.3  $[\{\text{Cp}^*\text{Fe}(\eta^5\text{-P}_5)\}_3\text{Ag}_3(\text{SbF}_6)_2]^+$ , 1622.4  $[\{\text{Cp}^*\text{Fe}(\eta^5\text{-P}_5)\}_2\text{Ag}_3(\text{SbF}_6)_2(\text{NC}(\text{CH}_2)_6\text{CN})]^+$ , 1412.6  $[\{\text{Cp}^*\text{Fe}(\eta^5\text{-P}_5)\}_2\text{Ag}_2(\text{SbF}_6)(\text{NC}(\text{CH}_2)_6\text{CN})_2]^+$ , 1278.6  $[\{\text{Cp}^*\text{Fe}(\eta^5\text{-P}_5)\}_2\text{Ag}_2(\text{SbF}_6)(\text{NC}(\text{CH}_2)_6\text{CN})]^+$ , 1142.5  $[\{\text{Cp}^*\text{Fe}(\eta^5\text{-P}_5)\}_2\text{Ag}_2(\text{SbF}_6)]^+$ , 932.7  $[\{\text{Cp}^*\text{Fe}(\eta^5\text{-P}_5)\}_2\text{Ag}_2(\text{SbF}_6)(\text{NC}(\text{CH}_2)_6\text{CN})]^+$ , 798.7  $[\{\text{Cp}^*\text{Fe}(\eta^5\text{-P}_5)\}_2\text{Ag}]^+$ , 493.9 (100)  $[\{\text{Cp}^*\text{Fe}(\eta^5\text{-P}_5)\}_2\text{Ag}(\text{CH}_3\text{CN})]^+$ , 452.8  $[\{\text{Cp}^*\text{Fe}(\eta^5\text{-P}_5)\}_2\text{Ag}]^+$ .

**Negative ion ESI-MS** ( $\text{CH}_2\text{Cl}_2/\text{CH}_3\text{CN}$  (1:1)):  $m/z$  (%) = 2647.9  $[\{\text{Cp}^*\text{Fe}(\eta^5\text{-P}_5)\}_4\text{Ag}_3(\text{SbF}_6)_4]^-$ , 1613.0  $[\{\text{Cp}^*\text{Fe}(\eta^5\text{-P}_5)\}_2\text{Ag}_2(\text{SbF}_6)_3]^-$ , 234.9 (100)  $[\text{SbF}_6]^-$ .

**Elemental analysis:** Calculated (%) for  $[\{\text{Cp}^*\text{Fe}(\eta^5\text{-P}_5)\}_2\text{Ag}(\text{SbF}_6)(\text{NC}(\text{CH}_2)_6\text{CN})]$  (825.75 g/mol): C 26.18, H 3.30, N 3.39; found: C 25.50, H 3.22, N 3.27.

**IR:**  $\tilde{\nu}/\text{cm}^{-1}$  = 2929 (vw), 2273 (vw), 1476 (w), 1379 (w), 1020 (w), 656 (s).

**Synthesis of  $[\{\text{SbF}_6\}@\{\{\text{Cp}^*\text{Fe}(\eta^5\text{-P}_5)\}_9\{\text{Ag}_{11}(\text{NC}(\text{CH}_2)_7\text{CN})_6\}}]_n[\text{SbF}_6]_{10n}$  (**7a**) with by-products  $[\{\text{Cp}^*\text{Fe}(\eta^5\text{-P}_5)\}_2\{\text{Ag}(\text{NC}(\text{CH}_2)_7\text{CN})\}]_n[\text{SbF}_6]_n$  (**7b**) and  $[\{\text{Cp}^*\text{Fe}(\eta^5\text{-P}_5)\}_2\{\text{Ag}_2(\text{NC}(\text{CH}_2)_7\text{CN})\}]_n[\text{SbF}_6]_{2n}$  (**7c**)**

In a Schlenk tube a solution of  $\text{AgSbF}_6$  (14 mg, 0.04 mmol) in  $\text{CH}_2\text{Cl}_2$  (25 mL) is carefully layered first with a solvent mixture of  $\text{CH}_2\text{Cl}_2/\text{toluene}$  (10 mL, 2:1) and then with a green solution of  $[\text{Cp}^*\text{Fe}(\eta^5\text{-P}_5)]$  (14 mg, 0.04 mmol) and  $\text{NC}(\text{CH}_2)_7\text{CN}$  (1 mL, 0.04 mmol, 0.4 M in  $\text{CH}_2\text{Cl}_2$ ) in toluene (25 mL). After a few hours, the phase boundary turns yellow and after one day, the formation of brown plates of **7a** at the phase boundary was observed. Furthermore a few green polyhedra of **7b** and green plates of **7c** appear at the phase boundary. After complete diffusion, the light yellow mother liquor is decanted, the crystals are washed with  $\text{CH}_2\text{Cl}_2$  ( $3 \times 10$  mL) and dried *in vacuo*. **7a** was isolated by manually separating the crystals from those of **7b** and **7c**.



Analytical data of **7a**:

**Yield:** 15 mg (0.0019 mmol, 43% based on [Cp\*Fe( $\eta^5$ -P<sub>5</sub>)]).

**<sup>1</sup>H NMR** (pyridine/CD<sub>2</sub>Cl<sub>2</sub>):  $\delta$  [ppm] = 1.38 (2H, C-4, NC(CH<sub>2</sub>)<sub>7</sub>CN), 1.46 (4H, C-3/C-5, NC(CH<sub>2</sub>)<sub>7</sub>CN), 1.65 (4H, C-2/C-6, NC(CH<sub>2</sub>)<sub>7</sub>CN), 2.34 (t, 4H, C-1/C-7, NC(CH<sub>2</sub>)<sub>7</sub>CN), 7.56 (m,  $\beta$ -H, pyridine), 7.97 (m,  $\gamma$ -H, pyridine), 8.67 (m,  $\alpha$ -H, pyridine), no signal was found for the Cp\* residue.

**<sup>13</sup>C NMR** (pyridine/CD<sub>2</sub>Cl<sub>2</sub>):  $\delta$  [ppm] = 16.99 (C-1/C-7, NC(CH<sub>2</sub>)<sub>7</sub>CN), 25.26 (C-2/C-6, NC(CH<sub>2</sub>)<sub>7</sub>CN), 27.96 (C-4, NC(CH<sub>2</sub>)<sub>7</sub>CN), 28.34 (C-3/C-5, NC(CH<sub>2</sub>)<sub>7</sub>CN), 119.78 (NC(CH<sub>2</sub>)<sub>7</sub>CN), 125.09 ( $\beta$ -C, pyridine), 139.23 ( $\gamma$ -C, pyridine), 147.50 ( $\alpha$ -C, pyridine), no signal was found for the Cp\* residue.

**<sup>31</sup>P{<sup>1</sup>H} NMR** (pyridine/CD<sub>2</sub>Cl<sub>2</sub>):  $\delta$  [ppm] = 151.53 ([Cp\*Fe( $\eta^5$ -P<sub>5</sub>)]).

**<sup>31</sup>P MAS NMR:**  $\delta$  [ppm] = 134.27 (m(br),  $\omega_{1/2}$  = 3483 Hz, [Cp\*Fe( $\eta^5$ -P<sub>5</sub>)]).

**<sup>19</sup>F NMR** (pyridine/CD<sub>2</sub>Cl<sub>2</sub>): no signal was detected.

**Positive ion ESI-MS** (CH<sub>3</sub>CN):  $m/z$  (%) = 2522.06 [{Cp\*Fe( $\eta^5$ -P<sub>5</sub>)<sub>5</sub>Ag<sub>3</sub>(SbF<sub>6</sub>)<sub>2</sub>]<sup>+</sup>, 2178.28  
[Cp\*Fe( $\eta^5$ -P<sub>5</sub>)<sub>4</sub>Ag<sub>3</sub>(SbF<sub>6</sub>)<sub>2</sub>]<sup>+</sup>, 1832.44 [Cp\*Fe( $\eta^5$ -P<sub>5</sub>)<sub>3</sub>Ag<sub>3</sub>(SbF<sub>6</sub>)<sub>2</sub>]<sup>+</sup>, 1636.64  
[Cp\*Fe( $\eta^5$ -P<sub>5</sub>)<sub>2</sub>Ag<sub>3</sub>(SbF<sub>6</sub>)<sub>2</sub>(NC(CH<sub>2</sub>)<sub>7</sub>CN)]<sup>+</sup>, 1292.75 [Cp\*Fe( $\eta^5$ -P<sub>5</sub>)<sub>2</sub>Ag<sub>2</sub>(SbF<sub>6</sub>)(NC(CH<sub>2</sub>)<sub>7</sub>CN)]<sup>+</sup>, 1178.94  
[Cp\*Fe( $\eta^5$ -P<sub>5</sub>)<sub>2</sub>Ag<sub>2</sub>(SbF<sub>6</sub>)(CH<sub>3</sub>CN)]<sup>+</sup>, 1142.58 [Cp\*Fe( $\eta^5$ -P<sub>5</sub>)<sub>2</sub>Ag<sub>2</sub>(SbF<sub>6</sub>)]<sup>+</sup>, 946.74  
[Cp\*Fe( $\eta^5$ -P<sub>5</sub>)Ag<sub>2</sub>(SbF<sub>6</sub>)(NC(CH<sub>2</sub>)<sub>7</sub>CN)]<sup>+</sup>, 798.77 [Cp\*Fe( $\eta^5$ -P<sub>5</sub>)<sub>2</sub>Ag]<sup>+</sup>, 603.03  
[Cp\*Fe( $\eta^5$ -P<sub>5</sub>)Ag(NC(CH<sub>2</sub>)<sub>7</sub>CN)]<sup>+</sup>, 493.97 (100) [Cp\*Fe( $\eta^5$ -P<sub>5</sub>)Ag(CH<sub>3</sub>CN)]<sup>+</sup>, 452.94  
[Cp\*Fe( $\eta^5$ -P<sub>5</sub>)Ag]<sup>+</sup>.

**Negative ion ESI-MS** (CH<sub>3</sub>CN):  $m/z$  (%) = 234.9 (100) [SbF<sub>6</sub>]<sup>-</sup>.

**Elemental analysis:** Calculated (%) for [[SbF<sub>6</sub>]<sub>10</sub>@[Cp\*Fe( $\eta^5$ -P<sub>5</sub>)<sub>9</sub>Ag<sub>11</sub>(NC(CH<sub>2</sub>)<sub>7</sub>CN)<sub>6</sub>]][SbF<sub>6</sub>]<sub>10</sub>  
(7794.56 g/mol): C 22.19, H 2.83, N 2.16; found: C 22.47, H 3.17, N 2.30.

**IR:**  $\tilde{\nu}/\text{cm}^{-1}$  = 3626 (vw), 2942 (vw), 2358 (vw), 2270 (vw), 1476 (vw), 1423 (vw), 1378 (vw), 655 (vs).

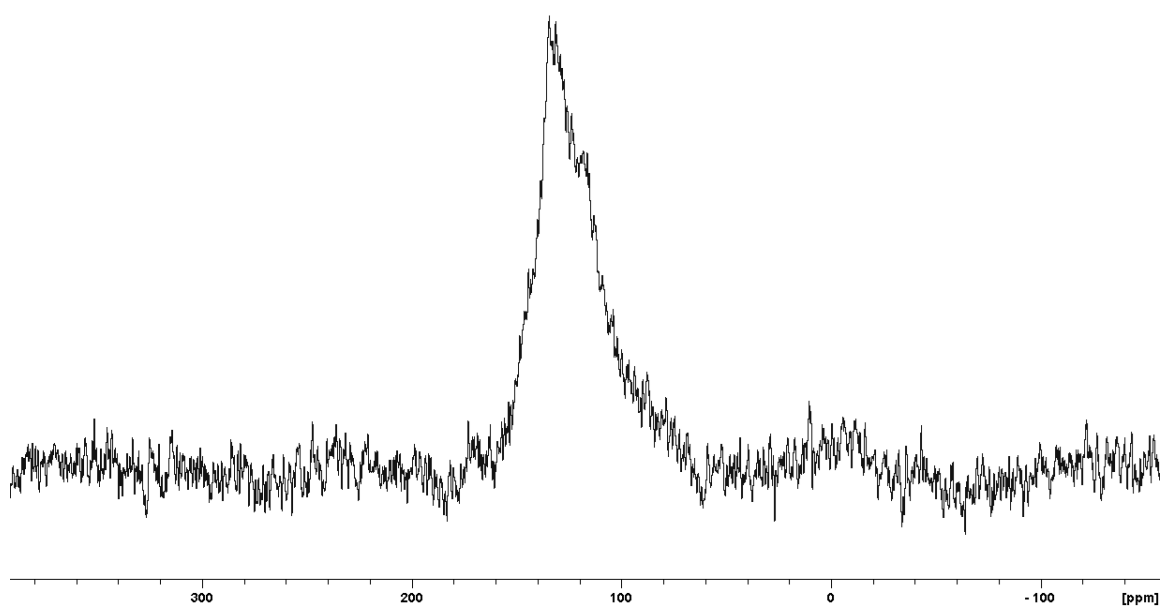


Figure 4.19.  $^{31}\text{P}\{^1\text{H}\}$  MAS NMR spectrum of **7a**.

#### Further spectroscopic details on **II**, **1-7**:

Compound **II** is hardly soluble in  $\text{CH}_2\text{Cl}_2$ , but readily dissolves in  $\text{CH}_3\text{CN}$ . In the  $^1\text{H}$  NMR spectrum of **II** in  $\text{CD}_3\text{CN}$  signals corresponding to the  $\text{Cp}^*$  residue and the  $\text{CH}_3\text{CN}$  ligands are visible, whereas in the  $^{31}\text{P}\{^1\text{H}\}$  NMR spectrum one singlet at 140.8 ppm can be attributed to the P atoms of **A**. As just one singlet is visible, dynamic behaviour of the Ag-P coordinative bonds is most likely to occur in solution similar to the cases of **I** and  $[\text{Ag}\{\text{Cp}^*\text{Fe}(\eta^{5:2:1}\text{-P}_5)\}_2]_n [\text{Al}\{\text{OC}(\text{CF}_3)_3\}_4]_n$ .<sup>[16]</sup> In the ESI MS spectrum the largest detected signal at  $m/z = 2869.1$  can be attributed to  $[\{\text{Cp}^*\text{Fe}(\eta^5\text{-P}_5)\}_5\text{Ag}_4(\text{SbF}_6)_3]^+$  as an aggregate of several dimeric units in the gas phase.

As all herein discussed polymeric compounds based on **A**,  $\text{AgSbF}_6$  and flexible dinitriles, have a decreasing solubility with expanding the ligand length in common solvents as  $\text{CH}_2\text{Cl}_2$  or toluene, but undergo partial fragmentation upon dissolving them in  $\text{CH}_3\text{CN}$  or pyridine. To enable characterization in solution by NMR and MS spectroscopy, all polymers were first fragmented by adding pyridine or  $\text{CH}_3\text{CN}$ .

In the  $^1\text{H}$  NMR spectra of **1** in  $\text{CD}_2\text{Cl}_2$  the expected signals for **A** and the linker could be observed in the expected stoichiometric ratio of 1 : 1, whereas in the  $^{31}\text{P}\{^1\text{H}\}$  spectrum a signal at 154.97 ppm can be assigned to the P atoms of free **A**.

The polymers of **2a** and **2b** come along as an inseparable mixture wherefore a statement about the ratios cannot be done. The mixture is insoluble in  $\text{CH}_2\text{Cl}_2$ , hexane or toluene, therefore, the NMR spectra of **2** were measured in pyridine- $d_5$ . That means only fragments of the polymers can be observed. The expected signals for **A** and  $\text{NC}(\text{CH}_2)_2\text{CN}$  (**2**) can be observed in the  $^1\text{H}$  NMR spectra. In the  $^{19}\text{F}$  NMR spectra the multiplett at -126.0 ppm can be assigned to the F atoms of the  $\text{SbF}_6^-$

anion. The singlet at 154.97 ppm in the  $^{31}\text{P}$  NMR spectra can be attributed to the free complex **A** (153 ppm).

Due to the lack of crystals of **3b**, all spectroscopic characterization was made of **3a**. The polymer **3a** is insoluble in  $\text{CH}_2\text{Cl}_2$ , hexane or toluene. It is dissolved in pyridine- $d_5$  and therefore only fragments of the polymer can be detected. For **3a** the  $^{31}\text{P}$  NMR spectra shows free complex **A**. The signals in the  $^1\text{H}$  NMR can be assigned to **A** (1.27 ppm) and  $\text{NC}(\text{CH}_2)_3\text{CN}$  (1.85 ppm, 2.57 ppm).

**4** is a mixture of inseparable **4a** and **4b**. The  $^1\text{H}$  NMR spectra shows the typical signal for **A** at 1.43 ppm and signals at 1.81 ppm and 2.41 ppm which can be assigned to  $(\text{NC}(\text{CH}_2)_4\text{CN})$ . The  $^{31}\text{P}$  NMR spectra shows the signal of free complex **A**.

In the respective  $^1\text{H}$  NMR spectra of **5a** and **5b** in  $\text{CD}_2\text{Cl}_2/\text{pyridine}$  the expected ratios of **A** :  $\text{NC}(\text{CH}_2)_5\text{CN}$  are observed with the integral intensities of 2 : 1 (**5a**) and 1 : 2 (**5b**), whereas signals for the ligand **A** are observed in the  $^{31}\text{P}\{^1\text{H}\}$  NMR spectra at 143.3 ppm (**5a**) and 139.8 ppm (**5b**). These signals are still upfield shifted compared to the signal of the free complex **A** (153 ppm),<sup>[27]</sup> which can be explained by incomplete fragmentation of the network.

For **6** in the  $^1\text{H}$  NMR and  $^{13}\text{C}$  NMR spectra of the partial fragmented compound the expected signals for ligand **1** and the linker could be observed in the expected stoichiometric ratio of 1 : 1.

The polymer of linked spheres **7a** is insoluble in solvents as hexane, toluene,  $\text{CH}_2\text{Cl}_2$ , thf and  $\text{Et}_2\text{O}$ . Only in  $\text{CH}_3\text{CN}$  or pyridine, it dissolves readily to give a deep red solution, though accompanied by fragmentation of the coordination network and supramolecular nodes. For this reason, in the  $^1\text{H}$  NMR and in the  $^{13}\text{C}$  NMR spectrum in  $\text{CD}_2\text{Cl}_2/\text{pyridine}$ , only signals corresponding to free **A** and the dinitrile linker molecule are visible, whereas in the  $^{31}\text{P}\{^1\text{H}\}$  spectrum a signal at 151.53 ppm can be assigned to the P atoms of free **A**.

### Synthesis of $[[\text{Cp}^*\text{Fe}(\eta^5\text{-P}_5)]@[[\text{Cp}^*\text{Fe}(\eta^{5:1:1}\text{-P}_5)]_{12}\{\text{Ag}_{12}(\text{NC}(\text{CH}_2)_8\text{CN})_6\}]_n[\text{SbF}_6]_{12n}$ (**8**)

In a Schlenk tube a solution of  $\text{AgSbF}_6$  (17 mg, 0.05 mmol) in  $\text{CH}_2\text{Cl}_2$  (25 mL) is carefully layered first with a solvent mixture of  $\text{CH}_2\text{Cl}_2/\text{toluene}$  (10 mL, 2:1) and then with a green solution of  $[\text{Cp}^*\text{Fe}(\eta^5\text{-P}_5)]$  (17 mg, 0.05 mmol) and  $\text{NC}(\text{CH}_2)_8\text{CN}$  (1 mL, 0.4 mmol, 0.4 M in  $\text{CH}_2\text{Cl}_2$ ) in toluene (25 mL). After a few hours, the phase boundary turns yellow and after one day, the formation of dark brown-green plates of **8** at the phase boundary can be observed. Furthermore a few crystals of  $[[\text{Cp}^*\text{Fe}(\eta^{5:2:1}\text{-P}_5)]_2\text{Ag}]_n[\text{SbF}_6]_n$  (**I**) appear at the phase boundary. After complete diffusion, the light-yellow mother liquor is decanted, the crystals are washed with  $\text{CH}_2\text{Cl}_2$  ( $3 \times 10$  mL) to remove  $[[\text{Cp}^*\text{Fe}(\eta^{5:2:1}\text{-P}_5)]_2\text{Ag}]_n[\text{SbF}_6]_n$  and dried *in vacuo*.

Analytical data of **8**:

**Yield:** 24 mg (0.0025 mmol, 66% referred to [Cp\*Fe( $\eta^5$ -P<sub>5</sub>)])

**<sup>1</sup>H NMR** (pyridine/CD<sub>2</sub>Cl<sub>2</sub>):  $\delta$  [ppm] = 1.34 (m, 24 H, C-4, (NC(CH<sub>2</sub>)<sub>8</sub>CN)), 1.43 (s, 195 H, [Cp\*Fe( $\eta^5$ -P<sub>5</sub>)]), 1.64 (m, 24 H, C-3, (NC(CH<sub>2</sub>)<sub>8</sub>CN)), 1.81 (m, 24 H, C-2, (NC(CH<sub>2</sub>)<sub>8</sub>CN)), 2.33 (t, 24 H, C-1, (NC(CH<sub>2</sub>)<sub>8</sub>CN)), 7.38 (m,  $\beta$ -H, pyridine), 7.79 (m,  $\gamma$ -H, pyridine), 8.58 (m,  $\alpha$ -H, pyridine).

**<sup>13</sup>C{<sup>1</sup>H} NMR** (pyridine/CD<sub>2</sub>Cl<sub>2</sub>):  $\delta$  [ppm] = 10.64 [Cp(CH<sub>3</sub>)<sub>5</sub>Fe( $\eta^5$ -P<sub>5</sub>)], 17.00 (C-1, NC(CH<sub>2</sub>)<sub>8</sub>CN), 25.33 (C-2, NC(CH<sub>2</sub>)<sub>8</sub>CN), 28.46 (C-3, NC(CH<sub>2</sub>)<sub>8</sub>CN), 28.5 (C-4, NC(CH<sub>2</sub>)<sub>8</sub>CN), 124.3 ( $\beta$ -C, pyridine), 137.01 ( $\gamma$ -C, pyridine), 149.45 ( $\alpha$ -C, pyridine), 149.50 (NC(CH<sub>2</sub>)<sub>8</sub>CN).

**<sup>31</sup>P{<sup>1</sup>H} NMR** (pyridine/CD<sub>2</sub>Cl<sub>2</sub>):  $\delta$  [ppm] = 144.14 (s, 60P, [Cp\*Fe( $\eta^5$ -P<sub>5</sub>)]), 144.81 (s, 5P, [Cp\*Fe( $\eta^5$ -P<sub>5</sub>)]).

**<sup>31</sup>P MAS NMR** :  $\delta$  [ppm] = 125.1 (m(br),  $\omega_{1/2}$  = 5000 Hz, 55 P [Cp\*Fe( $\eta^5$ -P<sub>5</sub>)] host), 150.23 (s, 5 P [Cp\*Fe( $\eta^5$ -P<sub>5</sub>)] guest), 168.63 (s(br),  $\omega_{1/2}$  = 360 Hz, 5 P [Cp\*Fe( $\eta^5$ -P<sub>5</sub>)] guest).

**<sup>19</sup>F NMR** (pyridine/CD<sub>2</sub>Cl<sub>2</sub>): no signal was detected.

**Positive ion ESI-MS** (CH<sub>3</sub>CN):  $m/z$  (%) = 3729 [{Cp\*Fe( $\eta^5$ -P<sub>5</sub>)}<sub>9</sub>Ag<sub>2</sub>(SbF<sub>6</sub>)(NC(CH<sub>2</sub>)<sub>8</sub>CN)]<sup>+</sup>, 3564 [{Cp\*Fe( $\eta^5$ -P<sub>5</sub>)}<sub>9</sub>Ag<sub>2</sub>(SbF<sub>6</sub>)]<sup>+</sup>, 3383 [{Cp\*Fe( $\eta^5$ -P<sub>5</sub>)}<sub>8</sub>Ag<sub>2</sub>(SbF<sub>6</sub>)(NC(CH<sub>2</sub>)<sub>8</sub>CN)]<sup>+</sup>, 3220 [{Cp\*Fe( $\eta^5$ -P<sub>5</sub>)}<sub>8</sub>Ag<sub>2</sub>(SbF<sub>6</sub>)]<sup>+</sup>, 3037 [{Cp\*Fe( $\eta^5$ -P<sub>5</sub>)}<sub>7</sub>Ag<sub>2</sub>(SbF<sub>6</sub>)(NC(CH<sub>2</sub>)<sub>8</sub>CN)]<sup>+</sup>, 2867.37 [{Cp\*Fe( $\eta^5$ -P<sub>5</sub>)}<sub>7</sub>Ag<sub>2</sub>(SbF<sub>6</sub>)]<sup>+</sup>, 2690 [{Cp\*Fe( $\eta^5$ -P<sub>5</sub>)}<sub>6</sub>Ag<sub>2</sub>(SbF<sub>6</sub>)(NC(CH<sub>2</sub>)<sub>8</sub>CN)]<sup>+</sup>, 2520 [{Cp\*Fe( $\eta^5$ -P<sub>5</sub>)}<sub>6</sub>Ag<sub>2</sub>(SbF<sub>6</sub>)]<sup>+</sup>, 2340 [{Cp\*Fe( $\eta^5$ -P<sub>5</sub>)}<sub>5</sub>Ag<sub>2</sub>(SbF<sub>6</sub>)(NC(CH<sub>2</sub>)<sub>8</sub>CN)]<sup>+</sup>, 2177.80 [{Cp\*Fe( $\eta^5$ -P<sub>5</sub>)}<sub>5</sub>Ag<sub>2</sub>(SbF<sub>6</sub>)]<sup>+</sup>, 1998.08 [{Cp\*Fe( $\eta^5$ -P<sub>5</sub>)}<sub>4</sub>Ag<sub>2</sub>(SbF<sub>6</sub>)(NC(CH<sub>2</sub>)<sub>8</sub>CN)]<sup>+</sup>, 1834.07 [{Cp\*Fe( $\eta^5$ -P<sub>5</sub>)}<sub>4</sub>Ag<sub>2</sub>(SbF<sub>6</sub>)]<sup>+</sup>, 1650.22 [{Cp\*Fe( $\eta^5$ -P<sub>5</sub>)}<sub>3</sub>Ag<sub>2</sub>(SbF<sub>6</sub>)(NC(CH<sub>2</sub>)<sub>8</sub>CN)]<sup>+</sup>, 1488.25 [{Cp\*Fe( $\eta^5$ -P<sub>5</sub>)}<sub>3</sub>Ag<sub>2</sub>(SbF<sub>6</sub>)]<sup>+</sup>, 1306.51 [{Cp\*Fe( $\eta^5$ -P<sub>5</sub>)}<sub>2</sub>Ag<sub>2</sub>(SbF<sub>6</sub>)(NC(CH<sub>2</sub>)<sub>8</sub>CN)]<sup>+</sup>, 1142.43 [{Cp\*Fe( $\eta^5$ -P<sub>5</sub>)}<sub>2</sub>Ag<sub>2</sub>(SbF<sub>6</sub>)]<sup>+</sup>, 1124.74 [{Cp\*Fe( $\eta^5$ -P<sub>5</sub>)}Ag<sub>2</sub>(SbF<sub>6</sub>)(NC(CH<sub>2</sub>)<sub>8</sub>CN)]<sub>2</sub><sup>+</sup>, 960.64 [{Cp\*Fe( $\eta^5$ -P<sub>5</sub>)}Ag<sub>2</sub>(SbF<sub>6</sub>)(NC(CH<sub>2</sub>)<sub>8</sub>CN)]<sup>+</sup>, 798.58 [{Cp\*Fe( $\eta^5$ -P<sub>5</sub>)}<sub>2</sub>Ag]<sup>+</sup>, 616.84 [Ag<sub>2</sub>(CH<sub>3</sub>CN)<sub>4</sub>(SbF<sub>6</sub>)]<sup>+</sup>, 581 [Ag<sub>2</sub>(CD<sub>3</sub>CN)<sub>3</sub>(SbF<sub>6</sub>)]<sup>+</sup>, 537.05 [Ag<sub>2</sub>(CD<sub>3</sub>CN)<sub>2</sub>(SbF<sub>6</sub>)]<sup>+</sup>, 493.73 (100) [{Cp\*Fe( $\eta^5$ -P<sub>5</sub>)}Ag(CH<sub>3</sub>CN)]<sup>+</sup>, 452.76 [{Cp\*Fe( $\eta^5$ -P<sub>5</sub>)}Ag]<sup>+</sup>, 435.10 [Ag(NC(CH<sub>2</sub>)<sub>8</sub>CN)]<sub>2</sub><sup>+</sup>, 270.98 [Ag(NC(CH<sub>2</sub>)<sub>8</sub>CN)]<sup>+</sup> or [Ag(CH<sub>3</sub>CN)]<sub>4</sub><sup>+</sup>.

**Negative ion ESI-MS** (CH<sub>2</sub>Cl<sub>2</sub>/CH<sub>3</sub>CN):  $m/z$  (%) = 234.84 (100) [SbF<sub>6</sub>]<sup>-</sup>.

**Elemental analysis:** Calculated (%) for [Cp\*Fe( $\eta^5$ -P<sub>5</sub>)]<sub>12</sub>(AgSbF<sub>6</sub>)<sub>12</sub>(NC(CH<sub>2</sub>)<sub>8</sub>CN)<sub>6</sub> (9606.11 g/mol): C 23.76, H 3.05, N 1.75; found: C 23.24, H 3.16, N 1.42.

**IR:**  $\tilde{\nu}$ /cm<sup>-1</sup> = 2934 (vw), 2266 (vw), 1476 (w), 1424 (w), 1377 (w), 1074 (vw), 1020 (w), 655 (s).

**TEM measurements:** measured diameter of selected aggregates /nm, marked in white: 4.03, 4.27, 4.76, 4.70, 3.42, 4.40, 5.32, 5.31, 4.17, 4.58. Mean value: 4.5(5) nm; marked in red: 2.84, 2.81, 2.81, 3.05, 3.79, 2.87, 3.42, 2.57, 3.42, 2.57, 3.42, 3.60. Mean value: 3.1(4). Expected diameter (Cp\*...Cp\*):  $\approx$  2.30 nm.

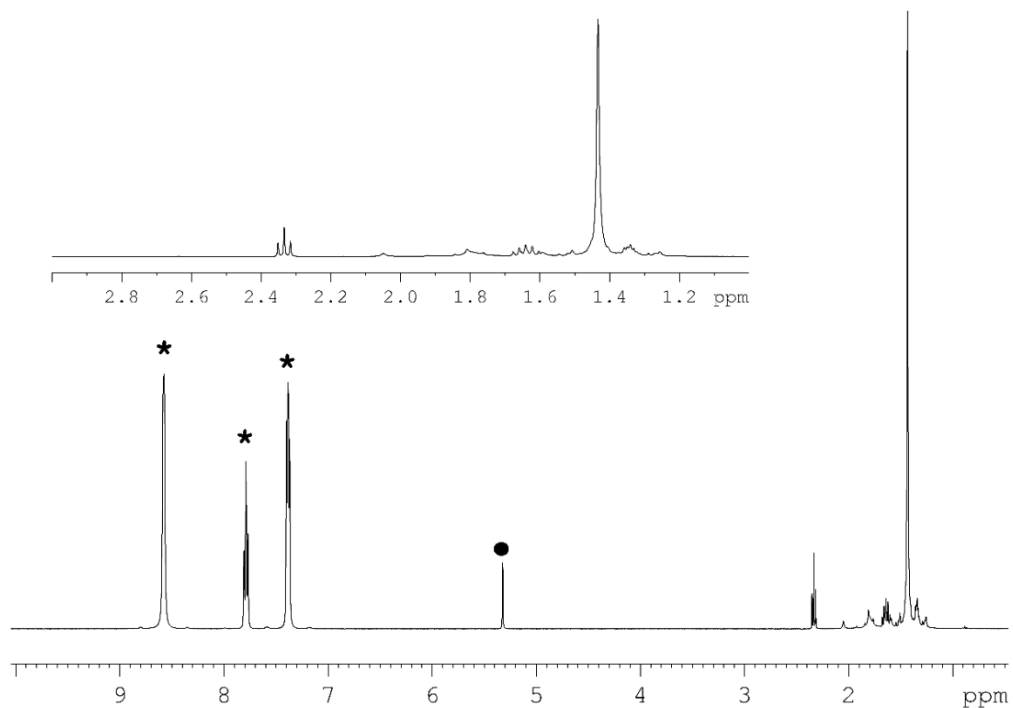


**Figure 4.20.**  $^1\text{H}$  NMR spectrum (pyridine/ $\text{CD}_2\text{Cl}_2$ ) of **8**. Marked signals are assigned to solvents ( $\star$  = pyridine,  $\bullet$  =  $\text{CD}_2\text{Cl}_2$ ).

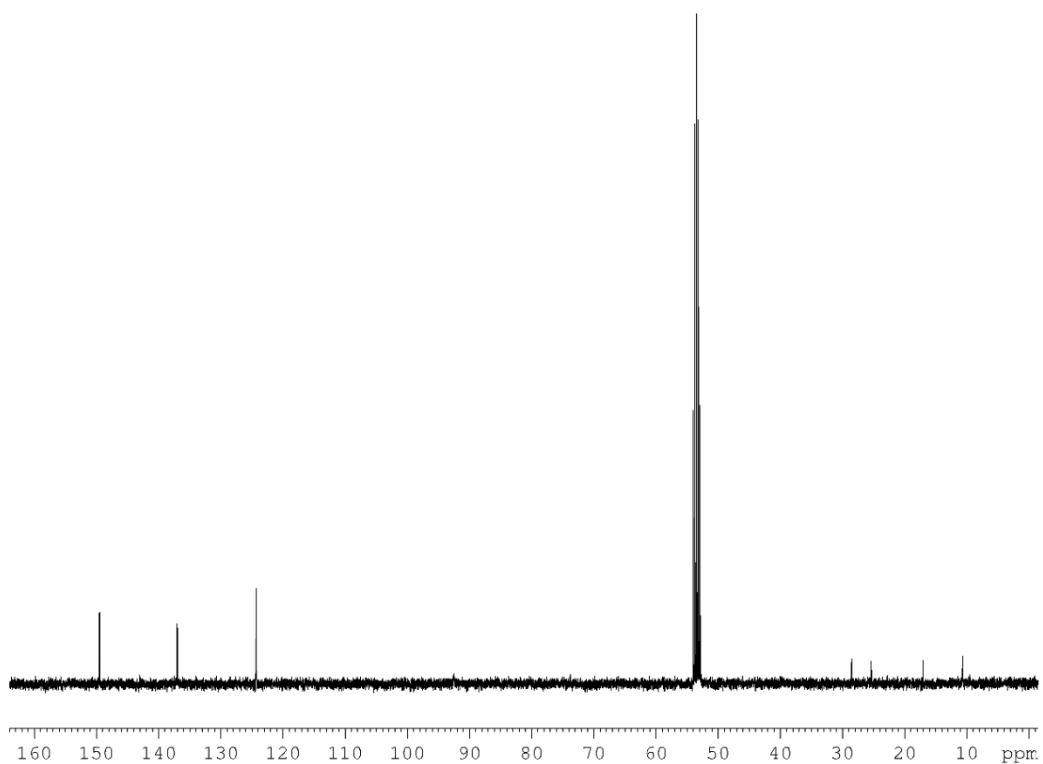


**Figure 4.21.**  $^{13}\text{C}\{^1\text{H}\}$  NMR spectrum ( $\text{CD}_2\text{Cl}_2$ /pyridine) of **8**.

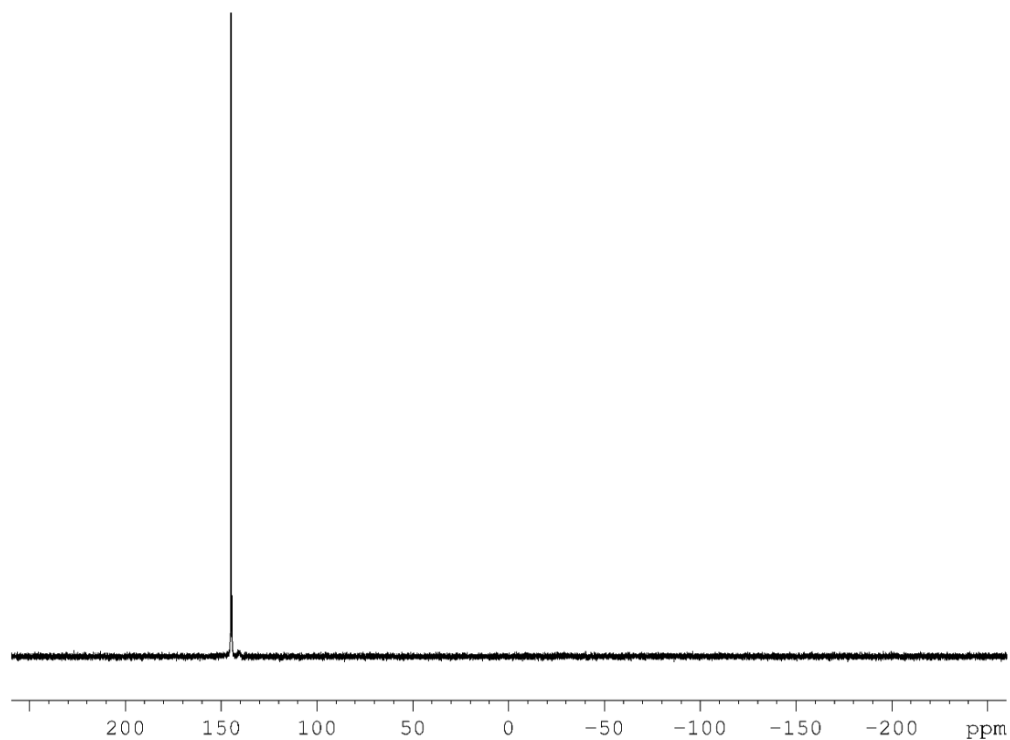


Figure 4.22.  $^{31}\text{P}\{^1\text{H}\}$  NMR spectrum ( $\text{CD}_2\text{Cl}_2/\text{pyridine}$ ) of **8**.

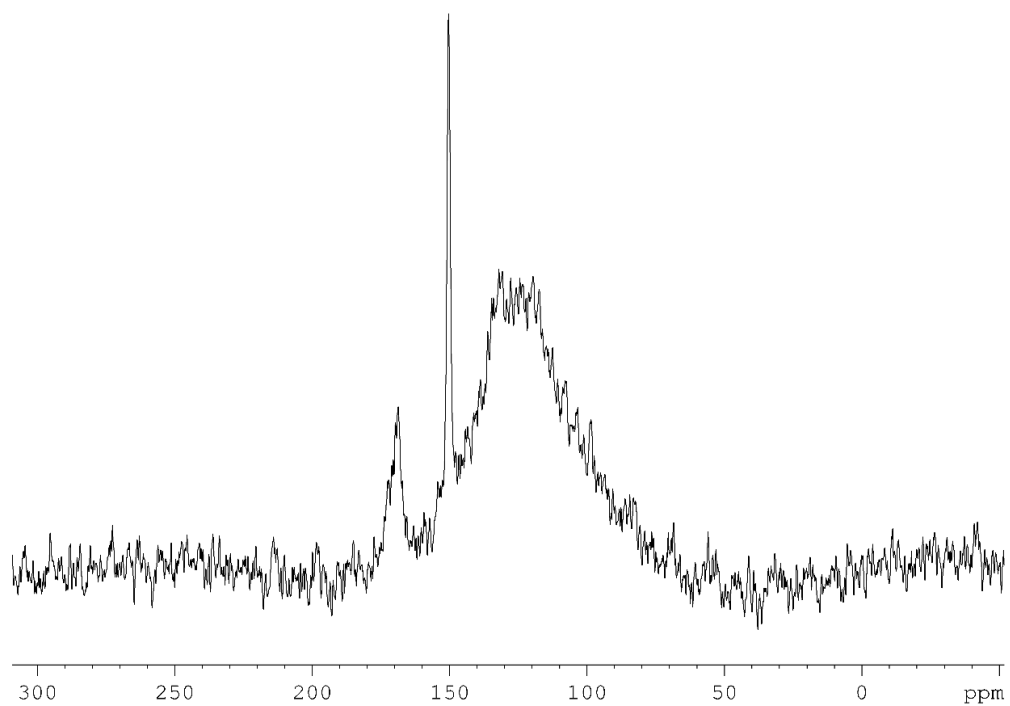
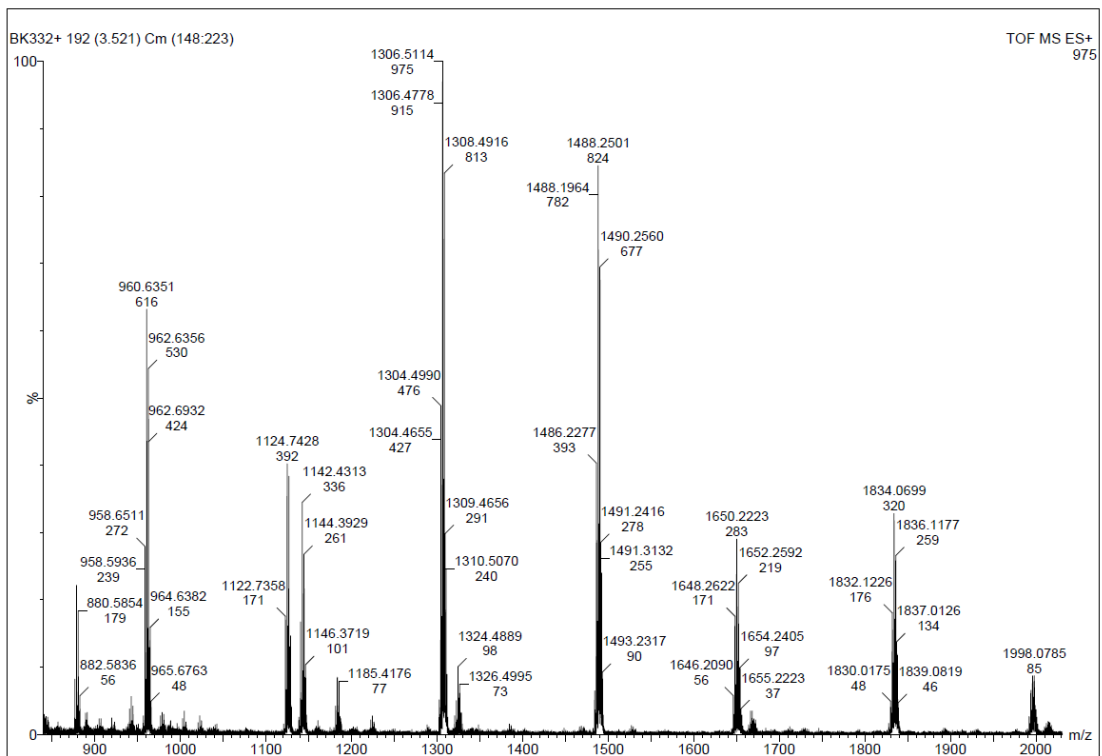
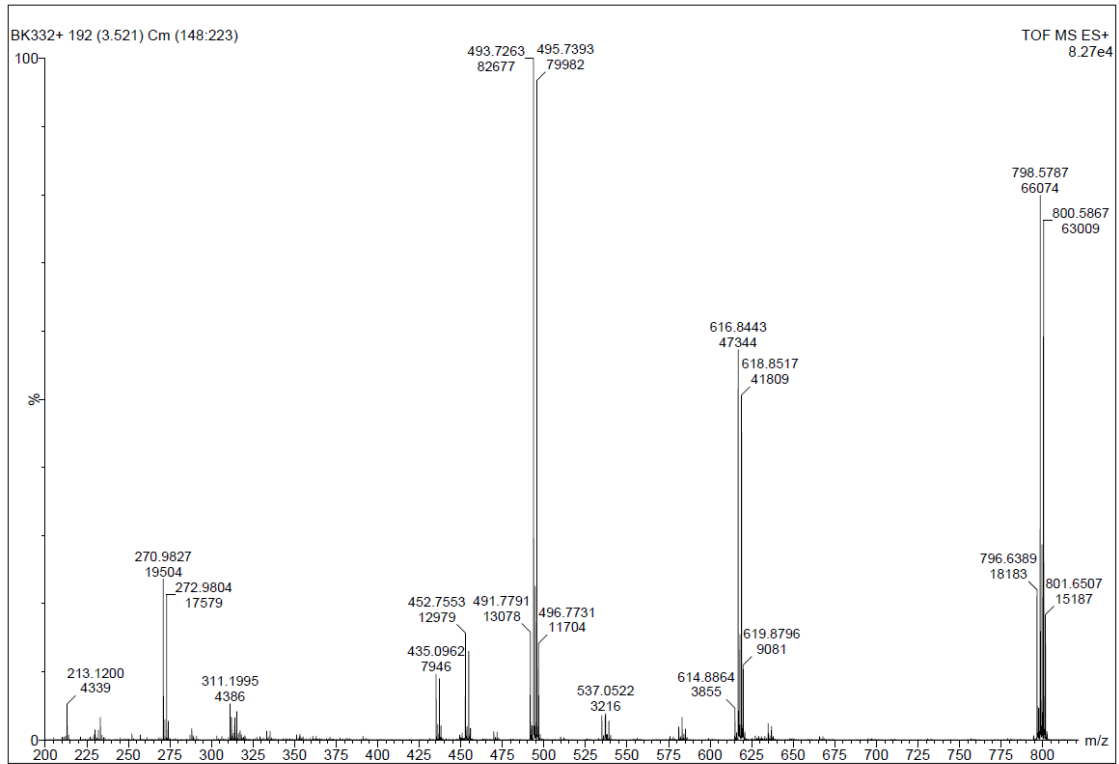


Figure 4.23.  $^{31}\text{P}\{^1\text{H}\}$  MAS NMR spectrum ( $\text{CD}_2\text{Cl}_2/\text{pyridine}$ ) of **8**.







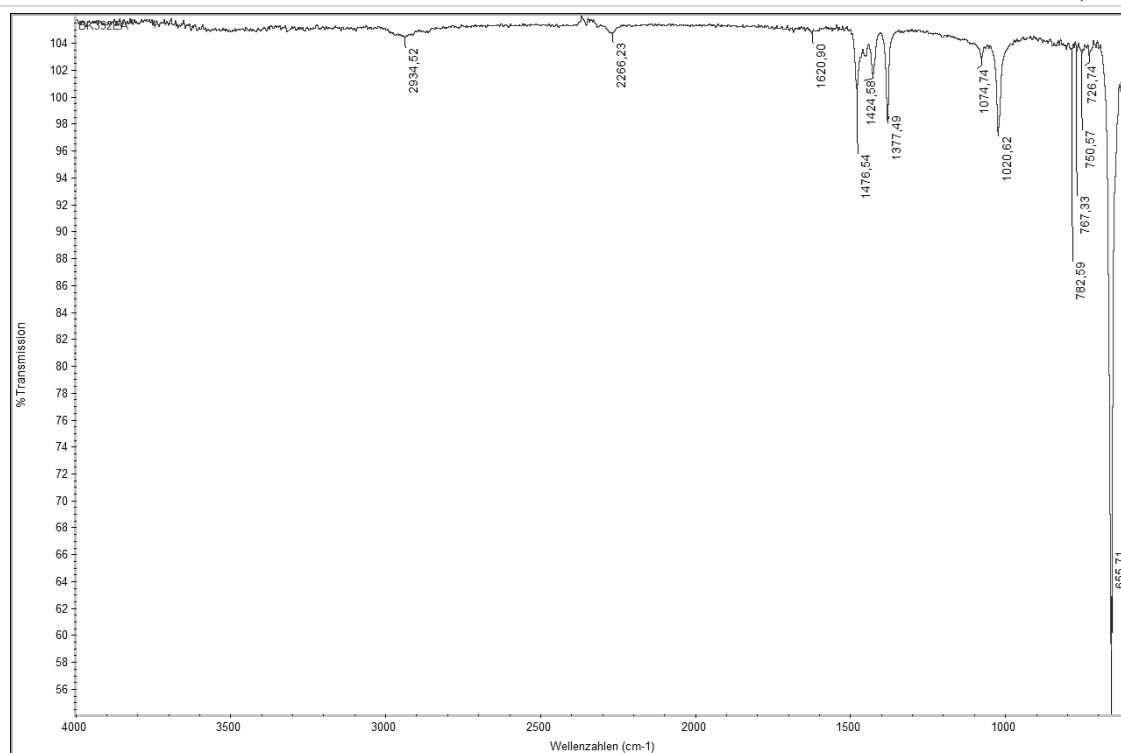


Figure 4.26. IR spectrum of **8**.

### Synthesis of $[[\text{Cp}^*\text{Fe}(\eta^5\text{-P}_5)]@[\{\text{Cp}^*\text{Fe}(\eta^{5:1:1}\text{-P}_5)\}_{12}\{\text{Ag}_{12}(\text{NC}(\text{CH}_2)_9\text{CN})_6\}]]_n[\text{SbF}_6]_{12n}$ (**9**)

In a Schlenk tube a solution of  $\text{AgSbF}_6$  (17 mg, 0.05 mmol) in  $\text{CH}_2\text{Cl}_2$  (25 mL) is carefully layered first with a solvent mixture of  $\text{CH}_2\text{Cl}_2$ /toluene (10 mL, 2:1) and then with a green solution of  $[\text{Cp}^*\text{Fe}(\eta^5\text{-P}_5)]$  (17 mg, 0.05 mmol) and  $\text{NC}(\text{CH}_2)_9\text{CN}$  (1 mL, 0.4 mmol, 0.4 M in  $\text{CH}_2\text{Cl}_2$ ) in toluene (25 mL). After a few hours, the phase boundary turns yellow and after one day, the formation of dark brown-green plates of **9** at the phase boundary can be observed. Furthermore a few crystals of  $[\{\text{Cp}^*\text{Fe}(\eta^{5:2:1}\text{-P}_5)\}_2\text{Ag}]_n[\text{SbF}_6]_n$  (**I**) appear at the phase boundary. After complete diffusion, the light-yellow mother liquor is decanted, the crystals are washed with  $\text{CH}_2\text{Cl}_2$  ( $3 \times 10$  mL) to remove  $[\{\text{Cp}^*\text{Fe}(\eta^{5:2:1}\text{-P}_5)\}_2\text{Ag}]_n[\text{SbF}_6]_n$  and dried *in vacuo*.

Analytical data of **9**:

**Yield:** 15 mg (0.0015 mmol, 41% referred to  $[\text{Cp}^*\text{Fe}(\eta^5\text{-P}_5)]$ )

**$^1\text{H}$  NMR** ( $\text{CD}_2\text{Cl}_2$ /pyridine):  $\delta$  [ppm] = 1.33 (m, C-4/C-5/C-6/C-7/C-8,  $\text{NC}(\text{CH}_2)_9\text{CN}$ ), 1.45 (s,  $[\text{Cp}(\text{CH}_3)_5\text{Fe}(\eta^5\text{-P}_5)]$ ), 1.64 (m, C-3/C-9,  $\text{NC}(\text{CH}_2)_9\text{CN}$ ), 2.34 (m, 24H, C-2/C-10,  $\text{NC}(\text{CH}_2)_9\text{CN}$ ).

**$^{13}\text{C}\{^1\text{H}\}$  NMR** ( $\text{CD}_2\text{Cl}_2$ /pyridine):  $\delta$  [ppm] = 10.76 ( $[\text{Cp}(\text{CH}_3)_5\text{Fe}(\eta^5\text{-P}_5)]$ ), 17.02 (C-2/C-10,  $\text{NC}(\text{CH}_2)_9\text{CN}$ ), 25.35 (C-3/C-9,  $\text{NC}(\text{CH}_2)_9\text{CN}$ ), 28.58 (C-4/C-5/C-7/C-8,  $\text{NC}(\text{CH}_2)_9\text{CN}$ ), 28.96 (C-6,  $\text{NC}(\text{CH}_2)_9\text{CN}$ ), 93.17 ( $[\text{C}_5(\text{CH}_3)_5\text{Fe}(\eta^5\text{-P}_5)]$ ), 125.59 ( $\beta$ -C, pyridine), 137.4 ( $\text{NC}(\text{CH}_2)_9\text{CN}$ ), 139.34 ( $\gamma$ -C, pyridine), 148.49 ( $\alpha$ -C, pyridine).

**$^{31}\text{P}\{^1\text{H}\}$  NMR** ( $\text{CD}_2\text{Cl}_2$ /pyridine):  $\delta$  [ppm] = 142.98 (s,  $[\text{Cp}^*\text{Fe}(\eta^5\text{-P}_5)]$ ).

**Positive ion ESI-MS** ( $\text{CH}_2\text{Cl}_2/\text{CH}_3\text{CN}$ ):  $m/z$  (%) = 2521.98  $[\{\text{Cp}^*\text{Fe}(\eta^5\text{-P}_5)\}_4\text{Ag}_4(\text{SbF}_6)_3]^+$ , 2354.21  $[\{\text{Cp}^*\text{Fe}(\eta^5\text{-P}_5)\}_3\text{Ag}_4(\text{SbF}_6)_3(\text{NC}(\text{CH}_2)_9\text{CN})]^+$ , 2178.18  $[\{\text{Cp}^*\text{Fe}(\eta^5\text{-P}_5)\}_3\text{Ag}_4(\text{SbF}_6)_3]^+$ , 1832.26  $[\{\text{Cp}^*\text{Fe}(\eta^5\text{-P}_5)\}_3\text{Ag}_3(\text{SbF}_6)_2]^+$ , 1664.49  $[\{\text{Cp}^*\text{Fe}(\eta^5\text{-P}_5)\}_3\text{Ag}_2(\text{SbF}_6)(\text{NC}(\text{CH}_2)_9\text{CN})]^+$ , 1142.54  $[\{\text{Cp}^*\text{Fe}(\eta^5\text{-P}_5)\}_2\text{Ag}(\text{NC}(\text{CH}_2)_9\text{CN})(\text{CH}_3\text{CN})_4]^+$ , 974.77  $[\{\text{Cp}^*\text{Fe}(\eta^5\text{-P}_5)\}_2\text{Ag}_2(\text{SbF}_6)(\text{NC}(\text{CH}_2)_9\text{CN})]^+$ , 953.14  $[\{\text{Cp}^*\text{Fe}(\eta^5\text{-P}_5)\}_2\text{Ag}_2(\text{SbF}_6)(\text{CH}_3\text{CN})_4]^+$ , 798.75 (100)  $[\{\text{Cp}^*\text{Fe}(\eta^5\text{-P}_5)\}_2\text{Ag}_2(\text{SbF}_6)]^+$ , 630.97  $[\{\text{Cp}^*\text{Fe}(\eta^5\text{-P}_5)\}_2\text{Ag}(\text{NC}(\text{CH}_2)_9\text{CN})]^+$ , 493.85  $[\{\text{Cp}^*\text{Fe}(\eta^5\text{-P}_5)\}_2\text{Ag}(\text{CH}_3\text{CN})]^+$ , 452.8  $[\{\text{Cp}^*\text{Fe}(\eta^5\text{-P}_5)\}_2\text{Ag}]^+$ , 285.05  $[\text{Ag}(\text{NC}(\text{CH}_2)_9\text{CN})]^+$ , 188.96  $[\text{Ag}(\text{CH}_3\text{CN})_2]^+$ , 147.93  $[\text{Ag}(\text{CH}_3\text{CN})]^+$ , 106.90  $[\text{Ag}]^+$ .

**Negative ion ESI-MS** ( $\text{CH}_2\text{Cl}_2/\text{CH}_3\text{CN}$ ):  $m/z$  (%) = 2648  $[\{\text{Cp}^*\text{Fe}(\eta^5\text{-P}_5)\}_4\text{Ag}_3(\text{SbF}_6)_4]^-$ , 1958.14  $[\{\{\text{Cp}^*\text{Fe}(\eta^5\text{-P}_5)\}_3\text{Ag}_2(\text{SbF}_6)_3\}^-]$ , 234.89 (100)  $[\text{SbF}_6]^-$ .

**Elemental analysis:** Calculated (%) for  $[\text{Cp}^*\text{Fe}(\eta^5\text{-P}_5)]@[\{\text{Cp}^*\text{Fe}(\eta^5\text{-P}_5)\}_{12}(\text{AgSbF}_6)_{12}(\text{NC}(\text{CH}_2)_9\text{CN})_6]$  (9690.29 g/mol): C 24.29, H 3.15, N 1.73; found: C 24.54, H 3.24, N 1.66.

**IR:**  $\tilde{\nu}/\text{cm}^{-1}$  = 2928 (vw), 2269 (vw), 1476 (vw), 1427 (vw), 1377 (w), 1020 (w), 656 (vs).

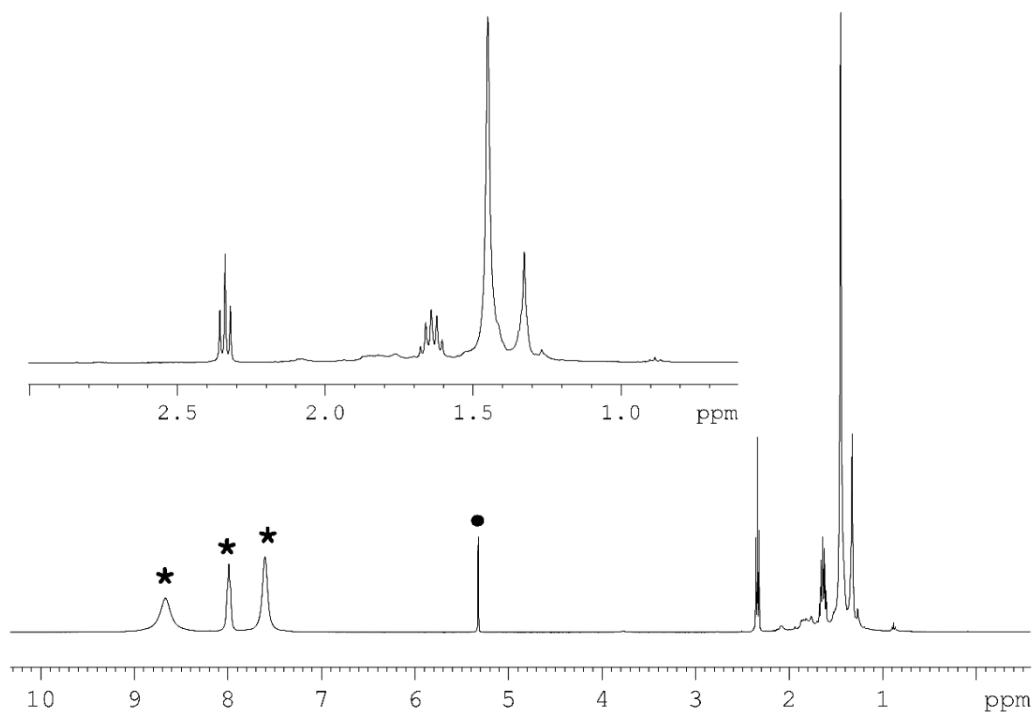


**Figure 4.27.**  $^1\text{H}$  NMR spectrum (pyridine/ $\text{CD}_2\text{Cl}_2$ ) of **9**. Marked signals are assigned to solvents (★ = pyridine, ● =  $\text{CD}_2\text{Cl}_2$ ).

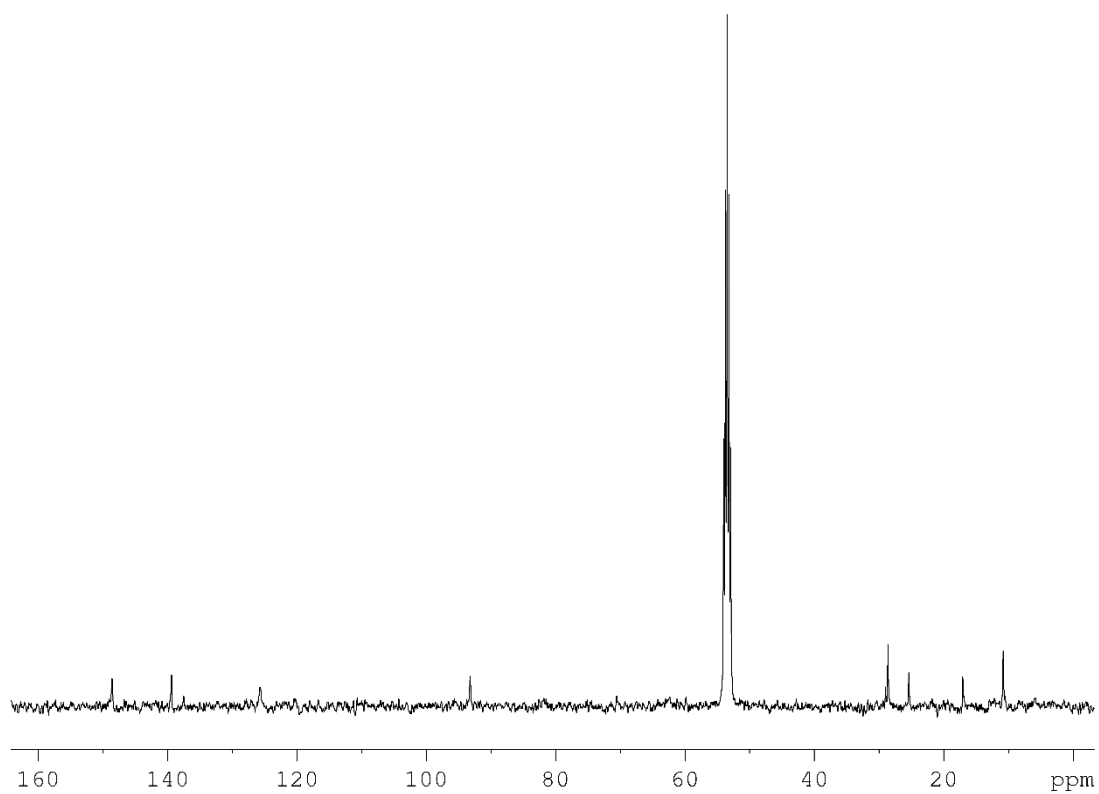


**Figure 4.28.**  $^{13}\text{C}\{^1\text{H}\}$  NMR spectrum ( $\text{CD}_2\text{Cl}_2$ /pyridine) of **9**.

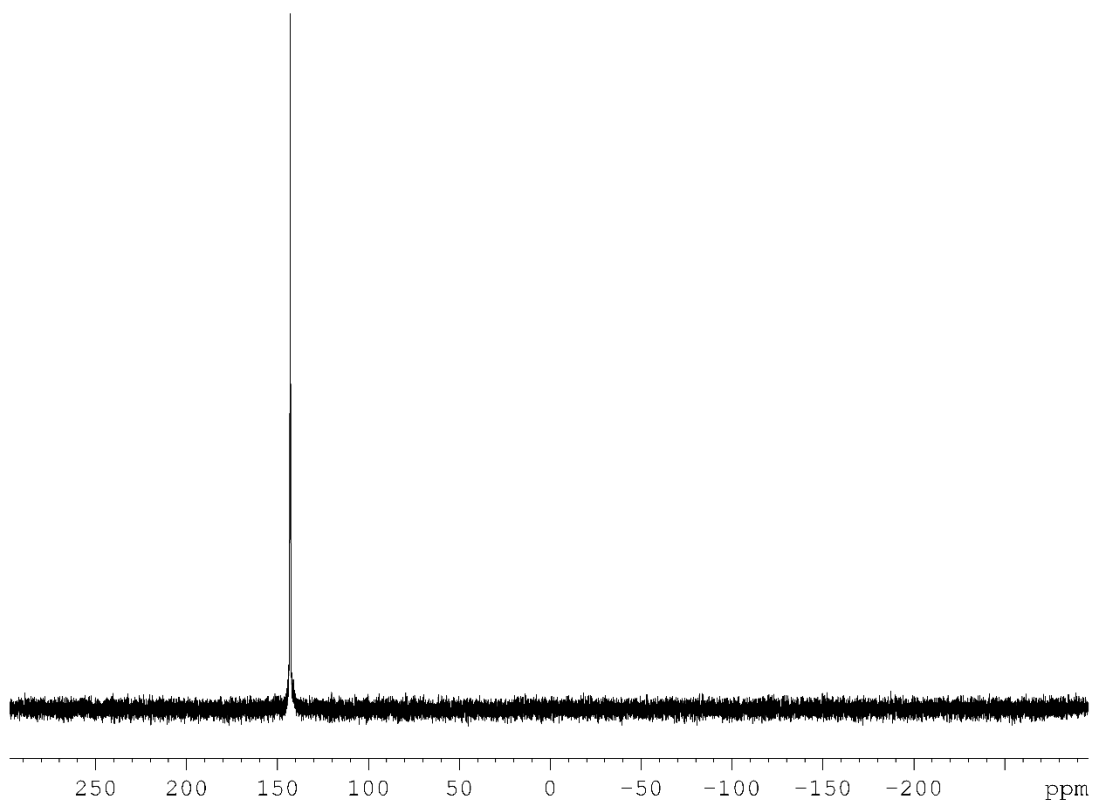


Figure 4.29.  $^{31}\text{P}\{^1\text{H}\}$  NMR spectrum ( $\text{CD}_2\text{Cl}_2/\text{pyridine}$ ) of **9**.

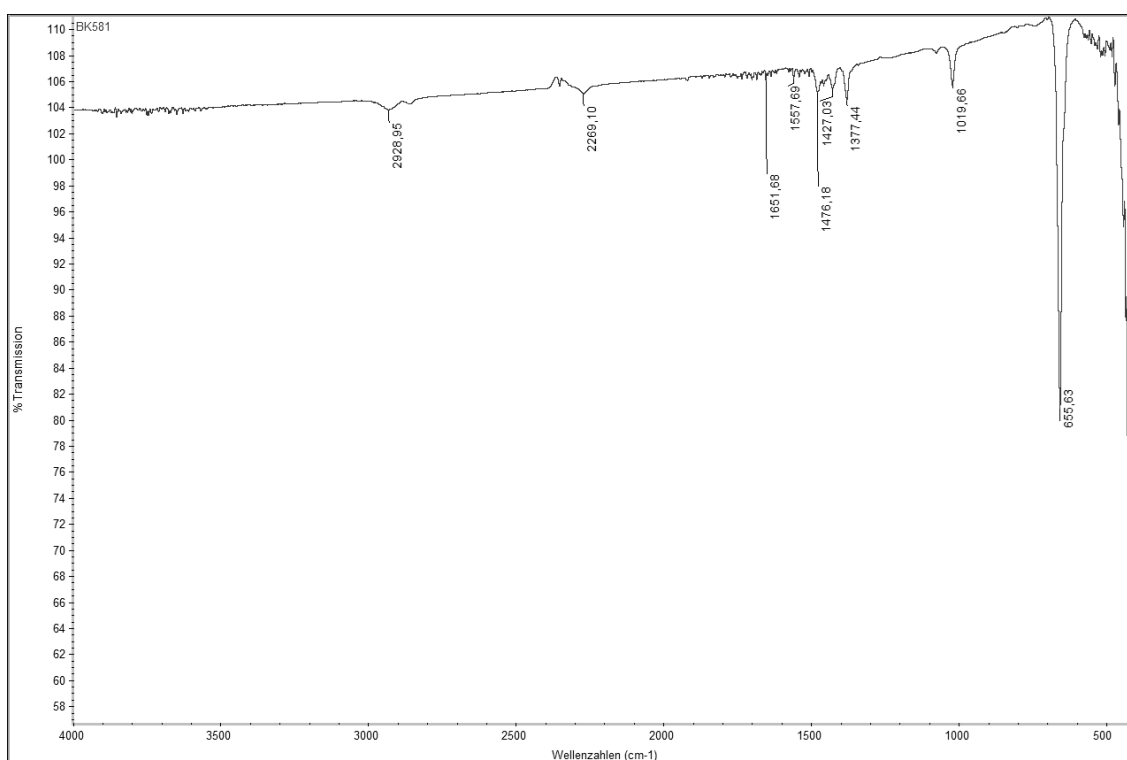
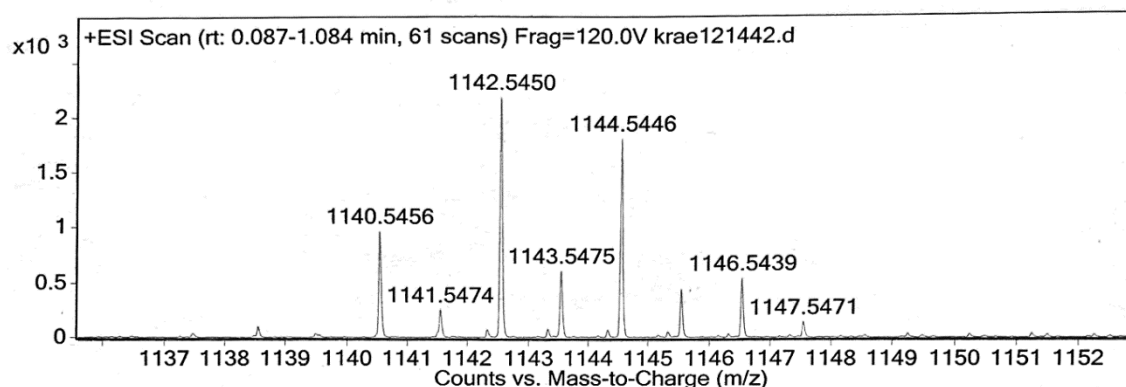
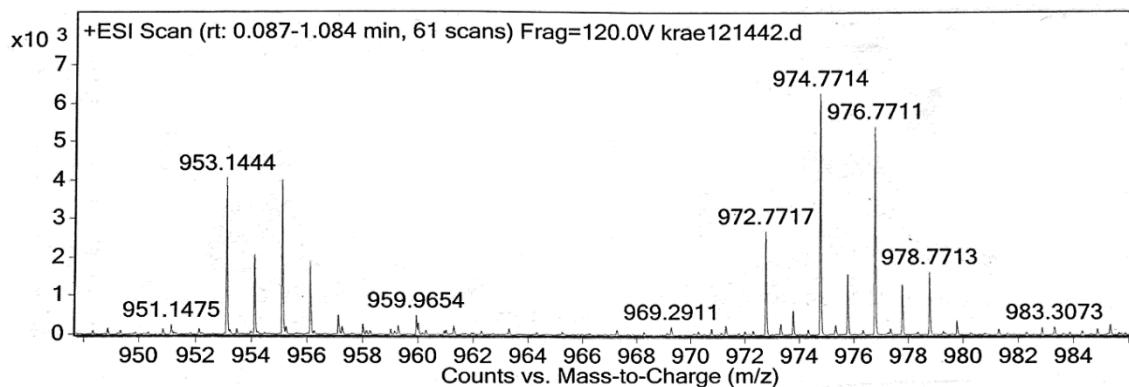
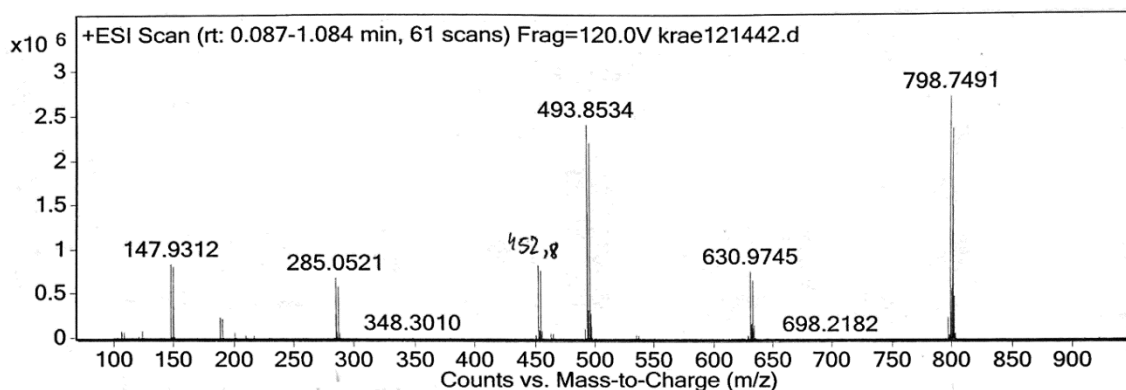
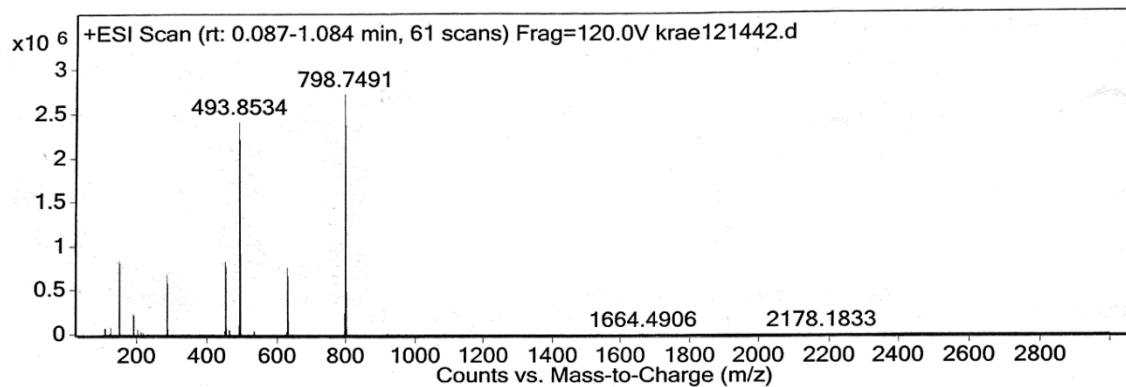


Figure 4.30. IR spectrum of **9**.



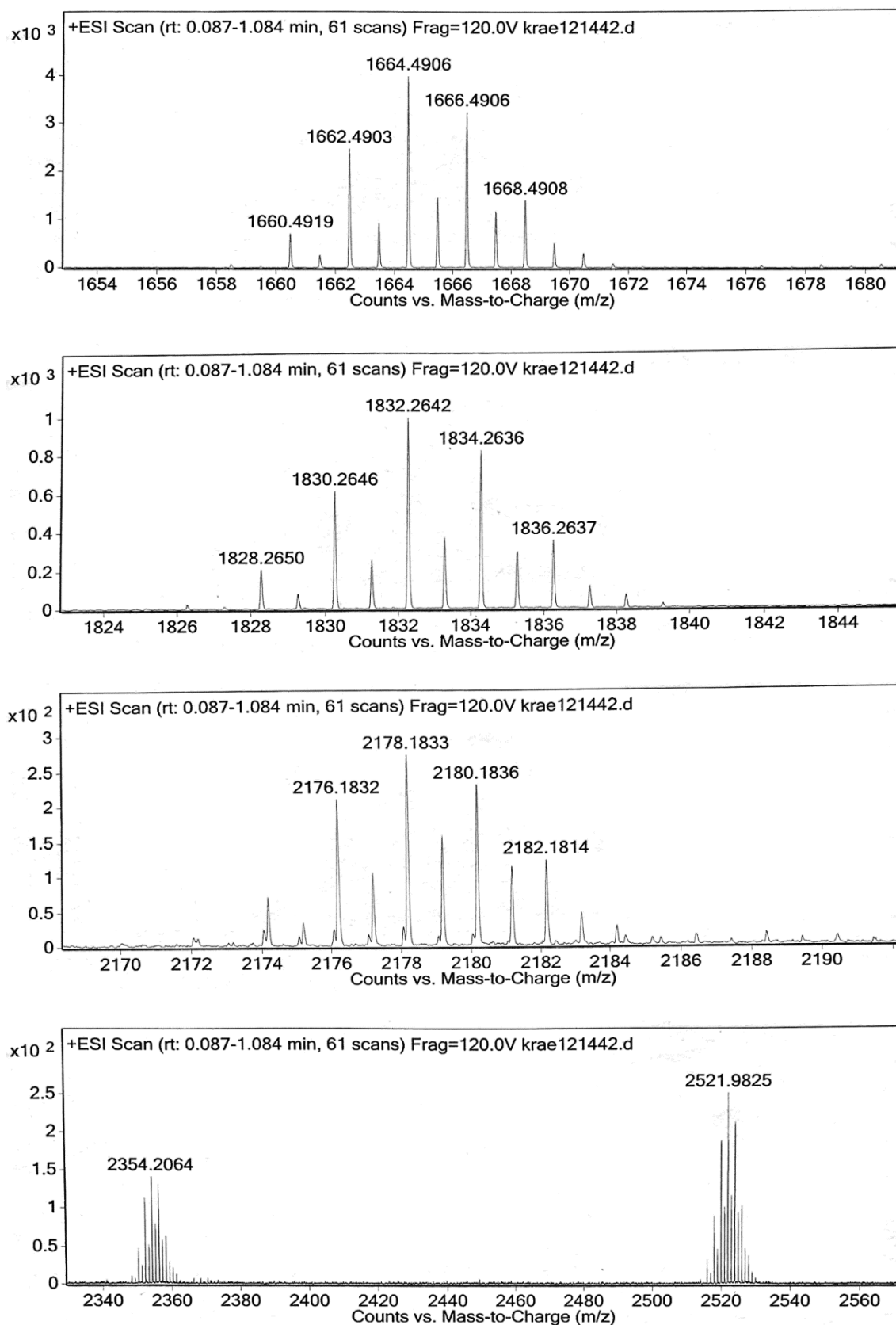


Figure 4.31. Positive ion ESI-MS spectra ( $\text{CH}_2\text{Cl}_2/\text{CH}_3\text{CN}$ ) of 9.

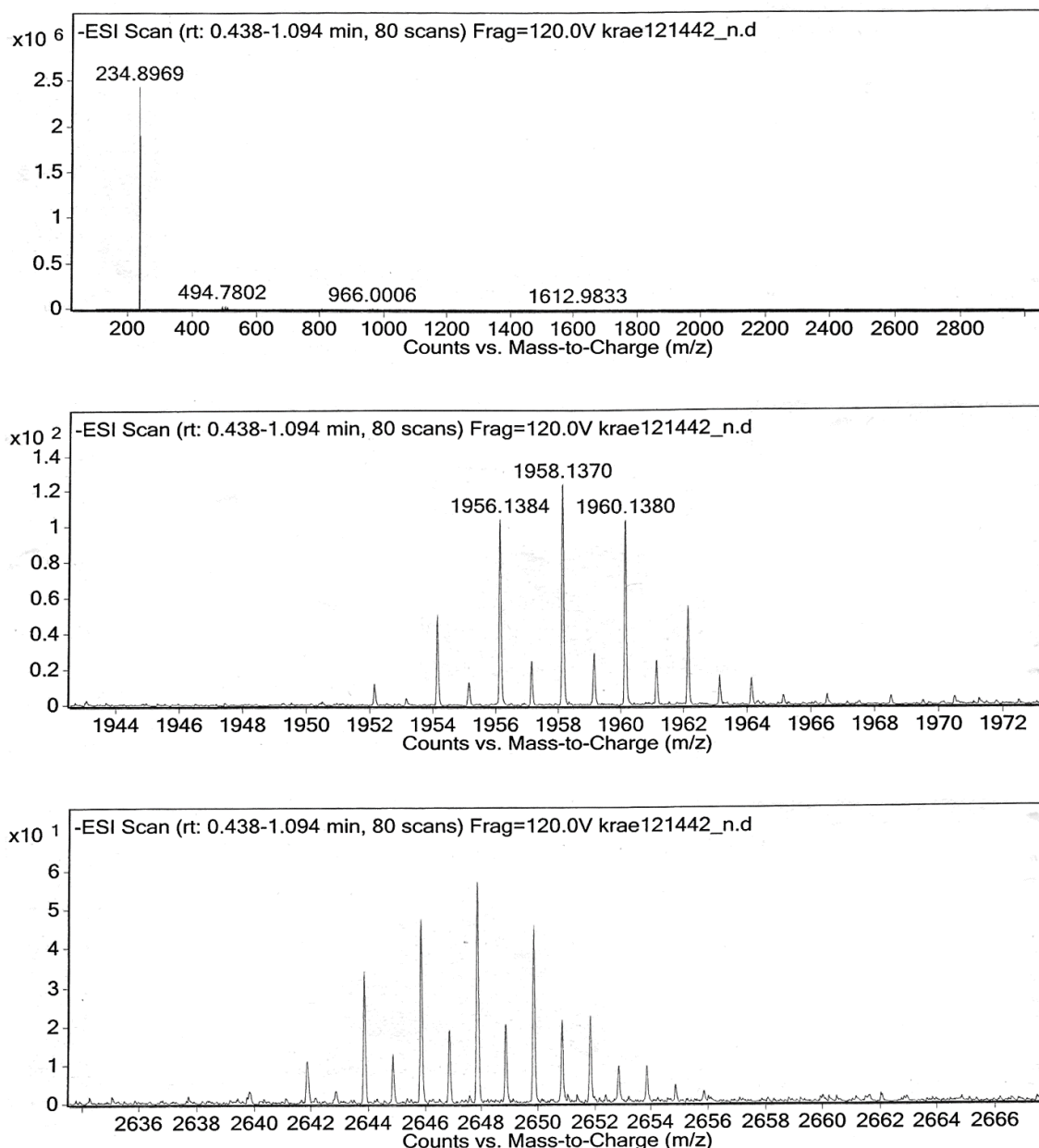


Figure 4.32. Negative ion ESI-MS spectra ( $\text{CH}_2\text{Cl}_2/\text{CH}_3\text{CN}$ ) of **9**.

Synthesis of  $[[\text{Cp}^*\text{Fe}(\eta^5\text{-P}_5)]@{\{[\text{Cp}^*\text{Fe}(\eta^{5:1:1:1}\text{-P}_5)]_{12}[\text{Ag}_{12}(\text{NC}(\text{CH}_2)_{10}\text{CN})_6]\}_n}[\text{SbF}_6]_{12n}]$  (**10a**) and  $[[\text{Cp}^*\text{Fe}(\eta^5\text{-P}_5)]_2\{\text{Ag}_2(\text{NC}(\text{CH}_2)_{10}\text{CN})\}_n][\text{SbF}_6]_{2n}$  (**10b**)

In a Schlenk tube a solution of  $\text{AgSbF}_6$  (34 mg, 0.1 mmol) in  $\text{CH}_2\text{Cl}_2$  (25 mL) is carefully layered first with a solvent mixture of  $\text{CH}_2\text{Cl}_2$ /toluene (10 mL, 2:1) and then with a green solution of  $[\text{Cp}^*\text{Fe}(\eta^5\text{-P}_5)]$  (34 mg, 0.1 mmol) and  $\text{NC}(\text{CH}_2)_{10}\text{CN}$  (2 mL, 0.8 mmol, 0.4 M in  $\text{CH}_2\text{Cl}_2$ ) in toluene (25 mL). After a few hours, the phase boundary turns yellow and after one day, the formation of brown-green plates of **10a** at the phase boundary can be observed. Furthermore a few crystals of  $[[\text{Cp}^*\text{Fe}(\eta^{5:2:1}\text{-P}_5)]_2\text{Ag}]_n[\text{SbF}_6]_n$  appear at the phase boundary. Occasionally the formation of **10b**

was observed. After complete diffusion, the light yellow mother liquor is decanted, the crystals are washed with  $\text{CH}_2\text{Cl}_2$  ( $3 \times 10$  mL) to remove  $\{[\text{Cp}^*\text{Fe}(\eta^{5:2:1}\text{-P}_5)]_2\text{Ag}\}_n[\text{SbF}_6]_n$  and dried *in vacuo*.

Analytical data of **10a**:

**Yield:** 71 mg (0.0073 mmol, 93 % referred to  $[\text{Cp}^*\text{Fe}(\eta^5\text{-P}_5)]$ )

**$^1\text{H}$  NMR** ( $\text{CD}_2\text{Cl}_2/\text{pyridine}$ ):  $\delta$  [ppm] = 1.31 (s, 48H, C-5/C-6/C-7/C-8,  $\text{NC}(\text{CH}_2)_{10}\text{CN}$ ), 1.41 (s, 24H, C-4/C-9,  $\text{NC}(\text{CH}_2)_{10}\text{CN}$ ), 1.44 (s, 195H,  $[\text{Cp}^*\text{Fe}(\eta^5\text{-P}_5)]$ ), 1.64 (m, 24H, C-3/C-10,  $\text{NC}(\text{CH}_2)_{10}\text{CN}$ ), 2.33 (t, 24H, C-2/C-11,  $\text{NC}(\text{CH}_2)_{10}\text{CN}$ ), 7.37 (m,  $\beta$ -H, pyridine), 7.77 (m,  $\gamma$ -H, pyridine), 8.59 (m,  $\alpha$ -H, pyridine).

**$^{13}\text{C}$  NMR** ( $\text{CD}_2\text{Cl}_2/\text{pyridine}$ ):  $\delta$  [ppm] = 10.63 ( $\text{Cp}(\text{CH}_3)_5\text{Fe}(\eta^5\text{-P}_5)$ ), 17.01 (C-2/C-11,  $\text{NC}(\text{CH}_2)_8\text{CN}$ ), 25.34 (C-3/C-10,  $\text{NC}(\text{CH}_2)_8\text{CN}$ ), 28.6 (C-4/C-9,  $\text{NC}(\text{CH}_2)_8\text{CN}$ ), 28.67 (C-5/C-8,  $\text{NC}(\text{CH}_2)_8\text{CN}$ ), 29.14 (C-6/C-7,  $\text{NC}(\text{CH}_2)_8\text{CN}$ ), 124.19 ( $\beta$ -C, pyridine), 136.85 ( $\gamma$ -C, pyridine), 146.45 ( $\alpha$ -C, pyridine). No signal for ( $\text{NC}(\text{CH}_2)_8\text{CN}$ ) was found.

**$^{31}\text{P}\{^1\text{H}\}$  NMR** ( $\text{CD}_2\text{Cl}_2/\text{pyridine}$ ):  $\delta$  [ppm] = 145.15 (s (br),  $[\text{Cp}^*\text{Fe}(\eta^5\text{-P}_5)]$ ), 145.57 (s (vbr),  $[\text{Cp}^*\text{Fe}(\eta^5\text{-P}_5)]$ ).

**$^{19}\text{F}$  NMR** ( $\text{CD}_2\text{Cl}_2/\text{pyridine}$ ): no signal was detected.

**Positive ion ESI-MS** ( $\text{CH}_2\text{Cl}_2/\text{CH}_3\text{CN}$  (1:1)):  $m/z$  (%) = 2522.0  $[\{[\text{Cp}^*\text{Fe}(\eta^5\text{-P}_5)]_4\text{Ag}_4(\text{SbF}_6)_3\}]^+$ , 2178.2  $[\{[\text{Cp}^*\text{Fe}(\eta^5\text{-P}_5)]_4\text{Ag}_3(\text{SbF}_6)_2\}]^+$ , 1832.3  $[\{[\text{Cp}^*\text{Fe}(\eta^5\text{-P}_5)]_3\text{Ag}_3(\text{SbF}_6)_2\}]^+$ , 1678.5  $[\{[\text{Cp}^*\text{Fe}(\eta^5\text{-P}_5)]_2\text{Ag}_3(\text{SbF}_6)_2(\text{NC}(\text{CH}_2)_{10}\text{CN})\}]^+$ , 798.7  $[\{[\text{Cp}^*\text{Fe}(\eta^5\text{-P}_5)]_2\text{Ag}\}]^+$ , 645.0  $[\{[\text{Cp}^*\text{Fe}(\eta^5\text{-P}_5)]\text{Ag}(\text{NC}(\text{CH}_2)_{10}\text{CN})\}]^+$ , 493.9 (100)  $[\{[\text{Cp}^*\text{Fe}(\eta^5\text{-P}_5)]\text{Ag}(\text{CH}_3\text{CN})\}]^+$ , 452.8  $[\{[\text{Cp}^*\text{Fe}(\eta^5\text{-P}_5)]\text{Ag}\}]^+$ .

**Negative ion ESI-MS** ( $\text{CH}_2\text{Cl}_2/\text{CH}_3\text{CN}$  (1:1)):  $m/z$  (%) = 2647.9  $[\{[\text{Cp}^*\text{Fe}(\eta^5\text{-P}_5)]_4\text{Ag}_3(\text{SbF}_6)_4\}]^-$ , 1958.1  $[\{[\text{Cp}^*\text{Fe}(\eta^5\text{-P}_5)]_3\text{Ag}_2(\text{SbF}_6)_3\}]^-$ , 234.9 (100)  $[\text{SbF}_6]^-$ .

**Elemental analysis:** Calculated (%) for  $[\text{Cp}^*\text{Fe}(\eta^5\text{-P}_5)]_{12}[\text{AgSbF}_6]_{12}(\text{NC}(\text{CH}_2)_{10}\text{CN})_6(\text{C}_7\text{H}_8)$  (9866.57 g/mol): C 25.44, H 3.30, N 1.70; found: C 25.66, H 3.29, N 1.67.

**IR:**  $\tilde{\nu}/\text{cm}^{-1}$  = 2930 (vw), 2268 (vw), 1476 (w), 1425 (w), 1378 (w), 1075 (vw), 1020 (w), 656 (s).



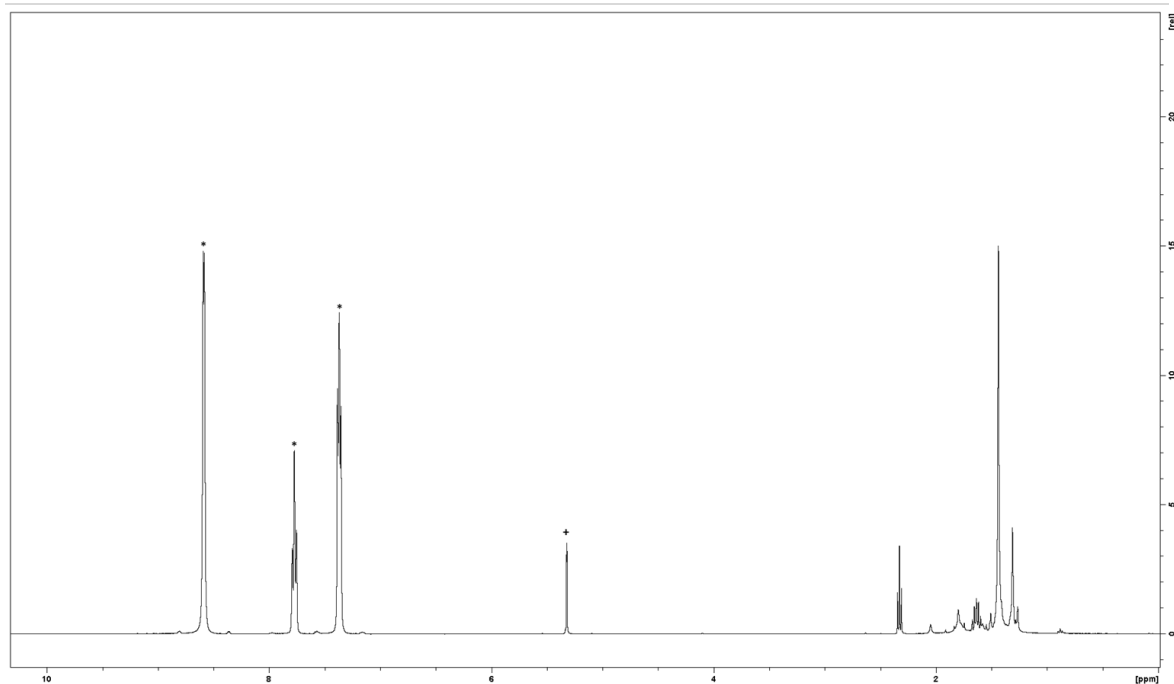


Figure 4.33.  $^1\text{H}$  NMR spectrum (pyridine/ $\text{CD}_2\text{Cl}_2$ ) of **10a**. Marked signals are assigned to solvents (★ = pyridine, + =  $\text{CD}_2\text{Cl}_2$ )

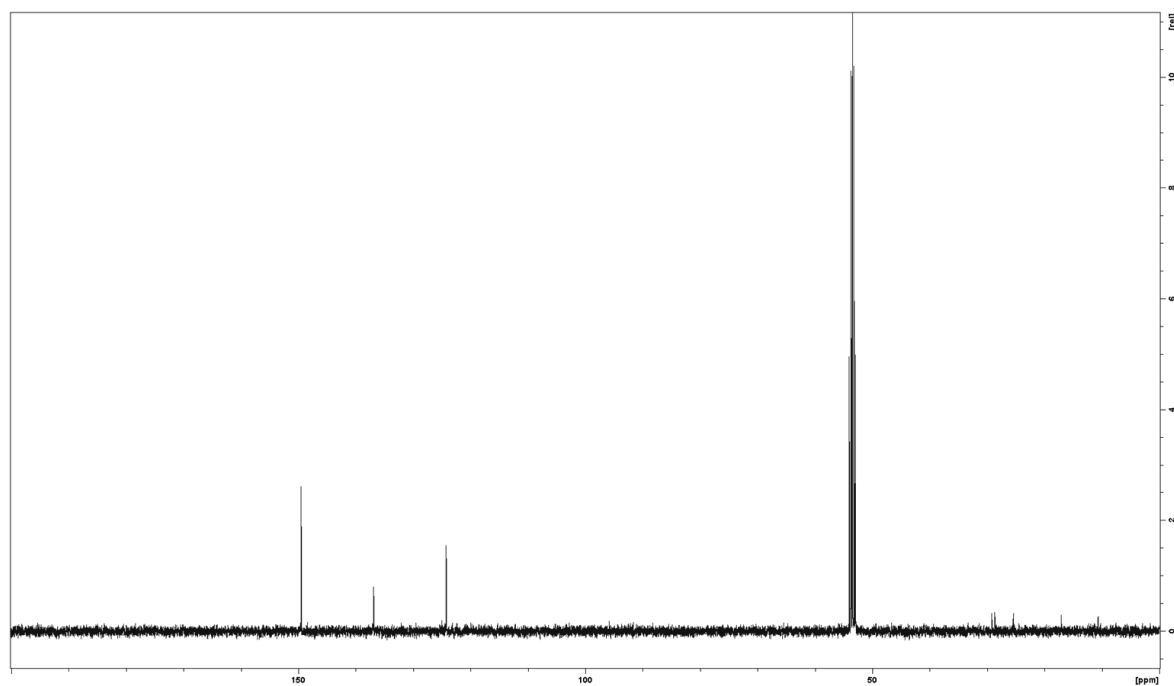


Figure 4.34.  $^{13}\text{C}\{^1\text{H}\}$  NMR spectrum ( $\text{CD}_2\text{Cl}_2$ /pyridine) of **10a**.

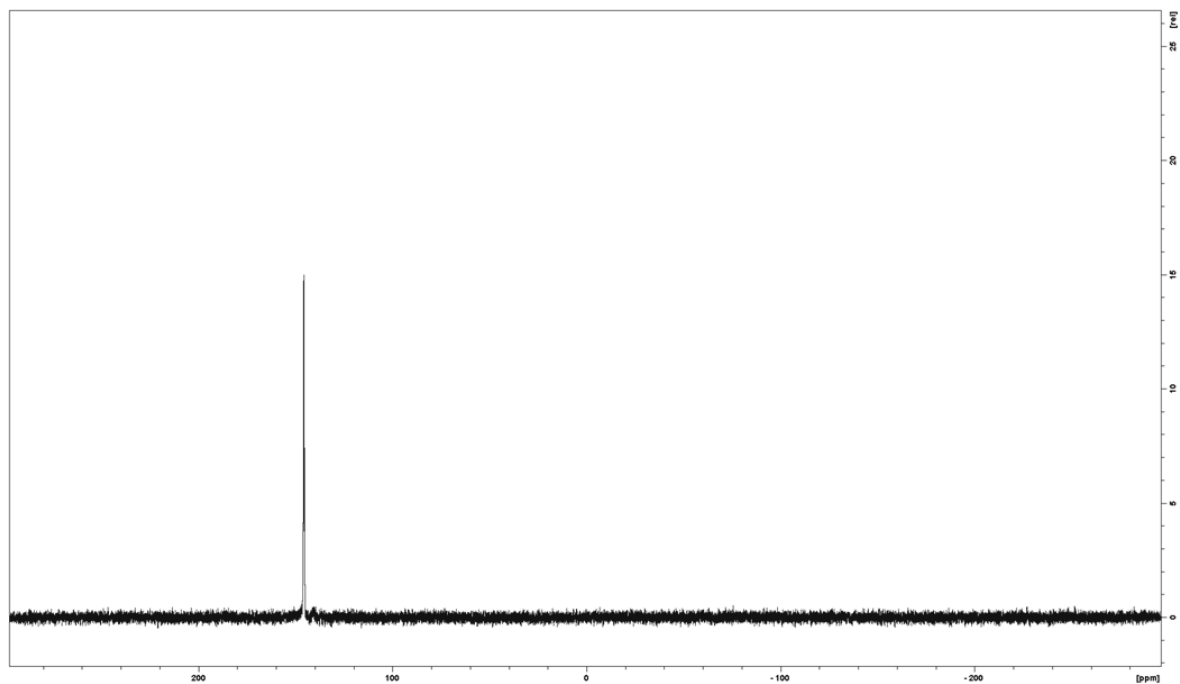


Figure 4.35.  $^{31}\text{P}$  NMR spectrum ( $\text{CD}_2\text{Cl}_2/\text{pyridine}$ ) of **10a**.

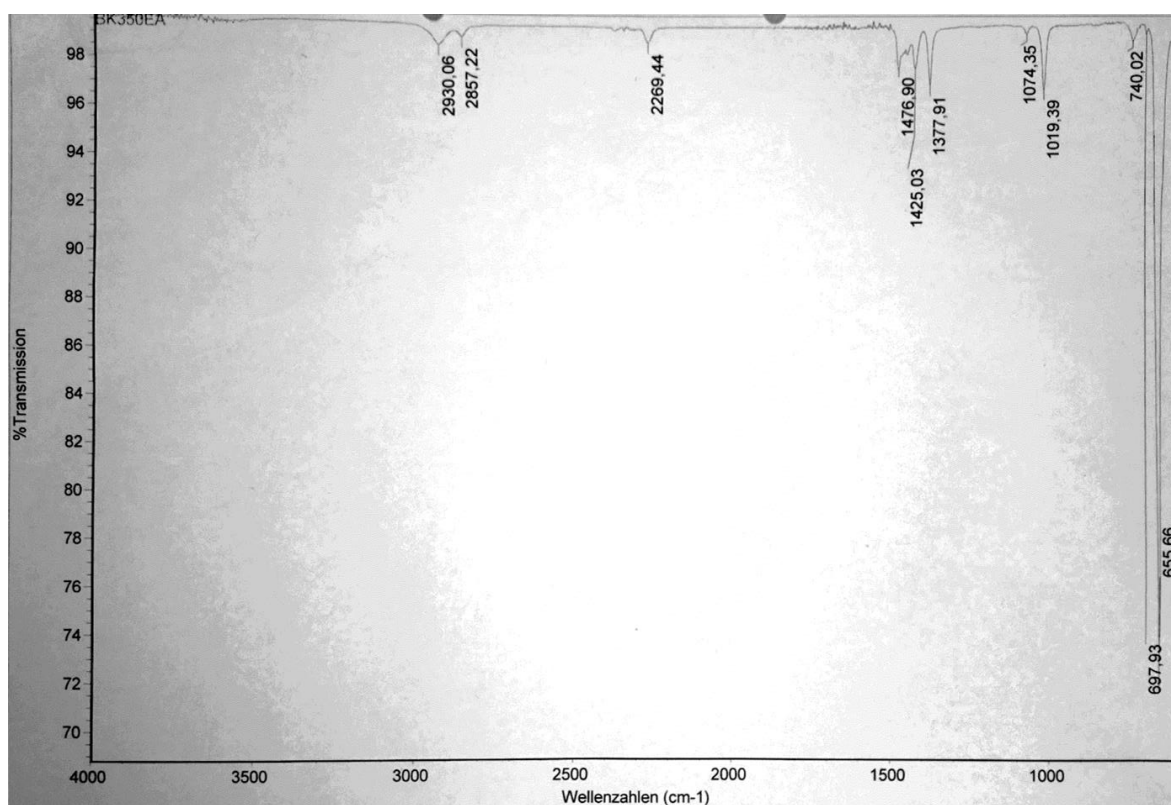


Figure 4.36. IR spectrum of **10a**.

## 4.5 Crystallographic Details and Structure Refinement

Crystals of **I**, **II**, **1-4**, **5a-7b**, **8-9** and **10b** were taken from a Schlenk flask under a stream of argon and immediately covered with perfluorinated Fomblin® mineral oil to prevent decomposition and a loss of solvent. The quickly chosen single crystals covered by a drop of the oil were directly placed into a stream of cold nitrogen with the pre-centered goniometer head with CryoMount® and attached to the goniometer of a diffractometer. The single crystals of **7c** and **10a** were carefully selected, mounted on a magnetic holder, checked for quality and placed into a Dewar vessel in liquid nitrogen using standard cryocrystallography tools. After a few weeks it was taken to the DESY PETRA III synchrotron. Using standard procedures, it was placed into a vessel filled with liquid nitrogen among other crystals. A robotic mounting/demounting was used for further manipulations in the P11 beamline hutch for **7a**.<sup>[28]</sup>

The diffraction data for **1-3b**, **5a-7b**, **10a** (90K) and **10b** were collected on a Rigaku diffractometer equipped with a Titan<sup>S2</sup> CCD detector and a SuperNova CuK $\alpha$  microfocus source using either 1° (**2a** (plates), **2b** (needles), **3b**, **5a**, **5b**, **6**, **7b**) or 0.5° (**1**, **7c**, **8**, **9** and **10a** (90K))  $\omega$  scans depending mostly on the unit cell constants. The diffraction data for **III** were collected on a Rigaku XtaLAB Synergy R diffractometer equipped with a HyPix-Arc 150 detector and a CuK $\alpha$  rotating-anode X-ray source using 0.5°  $\omega$  scans at 100 K. X-ray diffraction experiments for **I**, and **7c** were measured at 80 K at the DESY PETRA III synchrotron (beamline P11) using robotic mounting.<sup>[4]</sup> Data collection for **7c** was performed by 360°  $\phi$ -rotation with 0.2° scan width and exposure 0.12 s per frame at wavelength  $\lambda = 0.6199 \text{ \AA}$  (20 keV). The data for **II** and **3a**, were collected on an Agilent Technologies diffractometer equipped with an Atlas<sup>S2</sup> CCD detector and a SuperNova CuK $\alpha$  microfocus source using 1°  $\omega$  scans at 123 or 150 K, respectively. The data for **4** were measured on an Agilent Technologies diffractometer equipped with Eos CCD detector and a SuperNova MoK $\alpha$  microfocus source using 0.5°  $\omega$  scans at 120 K. The data for **3a** were collected on an Agilent Technologies diffractometer equipped with Atlas CCD detector and a SuperNova CuK $\alpha$  microfocus source using 0.5°  $\omega$  scans at 150 K because it was observed that at lower temperatures a phase transition takes place accompanied by cracking of the crystal. The phase transition according to our data takes place in a range of  $T = 120\text{-}125 \text{ K}$ .

To collect diffraction data at helium temperature to suppress severe disorder, the crystals of **9** were carefully selected, mounted on a magnetic holder, checked for quality and placed into a Dewar vessel with liquid nitrogen using standard cryocrystallography tools. After a few weeks it was taken to the DESY PETRA III synchrotron. Using standard procedures it was placed into a special Dewar vessel filled with liquid nitrogen among other crystals. A robotic mounting/demounting was used for further manipulations in the P11 beamline hutch.<sup>[4]</sup> X-ray diffraction experiment for **9** was

measured using one-circle diffractometer and DECTRIS PILATUS 6M pixel array detector at 10(2) K using open-flow helium cryo system Cryocool-LHe (CRYO Industries of America, Inc.). The data were acquired by 360°  $\phi$ -rotation with 0.3° scan width and exposure 0.3 s per frame at wavelength  $\lambda = 0.6701 \text{ \AA}$  (18.5 keV). Unfortunately, radiolysis persisted using the same crystal of **8** for the measurements at 100K and at 10K.

X-ray diffraction experiment for **10a (30 K)** was measured at 30 K at DESY PETRA III synchrotron (beamline P24)<sup>[29]</sup> equipped with Huber 3-cycle diffractometer and MAR165 CCD detector and an open-flow He LT system. Data collection for was performed by 360°  $\phi$ -rotation with 0.25° scan width and exposure 3 s per frame at a wavelength  $\lambda = 0.56076 \text{ \AA}$  (22.11 keV).

Data reduction for all crystal structures, except for **I**, was performed with CrysAlisPro software.<sup>[30]</sup> Analytical absorption correction for **5a-7b**, **8**, **9** and **10 (90 K)** was applied based on crystal faces. For **I**, **7c** and **10a (30 K)** empirical absorption correction based on equivalent reflections.

The structures were solved by direct methods with *SHELXT* and were refined by full-matrix least-squares method against  $F^2$  in anisotropic approximation using multiprocessor variable memory versions of *SHELXL (2014-2015)*.<sup>[31]</sup> The model received for **7c** from a preliminary X-ray experiment at an in-house diffractometer was used to refine the structure. All non-hydrogen atoms were refined anisotropically, while the hydrogen atoms were refined riding on pivot atoms.

The crystal of **III** was found to be a two-component twin with twin components rotated around [0 0 -1] direction by 90 deg. Twin batches were refined as 0.58/0.41.

In **5b**, **7a**, and **7b** the  $\text{SbF}_6^-$  counter-anions are disordered over two or more close positions. The occupation factors for disordered positions of Sb atoms were refined with fixed isotropic  $U_{\text{iso}}$  similar to the average  $U_{\text{iso}}$  (usually 0.025-0.035  $\text{\AA}^{-2}$ ) for the fully occupied heavy atoms in the corresponding structure. For **7a** and **7b**, the disorder is so severe, that for minor disordered positions of the  $\text{SbF}_6^-$  anions, not all fluorine atoms were located from the difference Fourier map. For the same reason, the fluorine atoms in very close positions were refined using restraint a.d.p. parameters. In case of small occupancy, F atoms were refined isotropically.

The flexible linker molecules also showed a strong tendency for disorder. In **5b**, **7a**, **7b** the dinitrile molecules were disordered typically over two close positions with different occupancies. Their molecular site occupancy factors (equal s.o.f.'s for all atoms of a molecule) were refined using the FVAR instruction of SHELX with isotropic displacement parameters fixed at  $U_{\text{iso}} = 0.05 \text{ \AA}^{-2}$ . The resulting occupancies were fixed and the C and N atoms with occupancies of more than 0.5 were refined in anisotropic approximation. Some minor positions of the linker molecules were refined

with restraint geometry. The restraints were removed at the final stage of the refinement when possible. The disorder of the solvent molecules  $\text{CH}_2\text{Cl}_2$  was treated in a similar way.

For the refinement of the structure **9**, the model obtained from **9a** was used. For the refinement of the structure **10a (90 K)**, the model obtained from **10a (30K)** was used. No significant change in structural detail was noticed for **9** and **9a**. For **10a**, the disordering is the linkers, silver atoms, counteranions and solvent content is slightly different. The structure refinement for the supramolecular compounds **7c-10a** is complicated by disorder of the silver atoms and in some cases also pentaphosphaferrocene building blocks in the inorganic cores of the supramolecular nodes, by severe disorder of the guest molecules of pentaphosphaferrocene, dinitrile linkers, counter-anions  $\text{SbF}_6^-$  and solvent molecules  $\text{CH}_2\text{Cl}_2$ . In **8** and **9a**, three of six unique pentaphosphaferrocene units are disordered over two positions. The  $\text{SbF}_6^-$  counter-anions are disordered over two to five close positions. The occupation factors for disordered positions of heavy atoms were refined with fixed isotropic  $U_{\text{iso}}$  similar to the average  $U_{\text{iso}}$  (usually 0.025-0.035  $\text{\AA}^{-2}$ ) for the fully occupied heavy atoms in the corresponding structure. The flexible linker molecules also showed a strong tendency for disorder. The dinitrile molecules were disordered typically over two or four close positions (one or two unique ones) with the same or different occupancies depending on the presence or absence of symmetry constraints. Their molecular site occupancy factors (equal s.o.f.'s for all atoms of a molecule) were refined using the FVAR instruction of SHELX with isotropic displacement parameters fixed at  $U_{\text{iso}} = 0.060 \text{ \AA}^{-2}$  for compound **8** and **9** (for  $T = 100 \text{ K}$ ) and to  $U_{\text{iso}} = 0.045$  for compound **9** (for  $T = 10 \text{ K}$ ). The resulting occupancies were fixed, and the C and N atoms with occupancies of more than 0.5 were refined in anisotropic approximation. Some minor positions of the linker molecules were refined with restraint geometry. Most of the restraints were removed at the final stage of the refinement when possible. The guest molecule is disordered in the cavity of the supramolecular node over six positions. Three of them are unique; others are related to them by an inversion. The relative occupancy factors were refined according to the aforementioned procedure. Some of the P and C atoms of these different positions are overlapped, their occupancies factor were calculated as a sum of the occupancies of the corresponding positions. Due to the overlap hydrogen atoms were not refined in their calculated positions as the riding model does not allow such a refinement. Hydrogen atoms were refined in calculated positions using riding on pivot atom model unless stated otherwise. The disorder of the solvent  $\text{CH}_2\text{Cl}_2$  molecules was treated in a similar way.

The fact of similar disorder for the isotopic structures **8** and **9** at 100 and 10 K, as well as for **10a**, confirms the fact that the disorder of the structural fragments (linkers, scaffold, counter anions and guest pentaphosphaferrocenes) has static nature and cannot be 'frozen out'.

The refinement of the guest molecule disordered over six close positions was made as a rigid body refinement. The geometry of the molecule Cp\*FeP<sub>5</sub> was transferred from CSD<sup>[32]</sup> the crystal structure of 3,4-diphenylquinolininium hexafluoro-antimony deposited under RefCode JABWAN.<sup>[23a,33]</sup> Analogously, the refinement of the disordered counter-anions SbF<sub>6</sub><sup>-</sup> was performed using idealized octahedral geometry.

The topologies of the underlying nets and packings for structures of **8**, **9** and **10a** were calculated with TOPOSPro.<sup>[33]</sup> All ORTEP drawings for **8** and **9a** were made in Olex2.<sup>[34]</sup> Other figures are made in POV-Ray.<sup>[35]</sup>

CIF files with comprehensive information on the details of the diffraction experiments and full tables of bond lengths and angles for **I - 10b** are deposited in Cambridge Crystallographic Data Centre under the deposition codes CCDC-1886598 (**I**), CCDC-1886599 (**II**), CCDC-2050950 (**III**), CCDC-2047567 (**1**), CCDC-2047569 (**2a**), CCDC-2047568 (**2b**), CCDC-2047570 (**3a**), CCDC-2047572 (**3b**), CCDC-2047571 (**4a**), CCDC-2047573 (**4b**), CCDC-1886600 (**5a**), CCDC-1886601 (**5b**), CCDC-1886602 (**6**), CCDC-1886603 (**7a**), CCDC-1886604 (**7b**), and CCDC-1886605 (**7c**), CCDC-1960938 (**8**), CCDC-1960940 (**9**), CCDC-2047575 (**10a (30K)**), CCDC-2067328 (**10a (90K)**) and CCDC-2047574 (**10b**).

**Table 4.3.** Experimental details for compounds I, II and III.

Crystal data	I	II	III
CCDC Code	CCDC-1886598	CCDC-1886599	CCDC-2050950
Chemical formula	(C <sub>20</sub> H <sub>30</sub> AgFe <sub>2</sub> P <sub>10</sub> )·(SbF <sub>6</sub> )	C <sub>28</sub> H <sub>42</sub> Ag <sub>2</sub> Fe <sub>2</sub> N <sub>4</sub> P <sub>10</sub> ·2(SbF <sub>6</sub> )	C <sub>6</sub> H <sub>4</sub> AgN <sub>4</sub> SbF <sub>6</sub>
<i>M<sub>r</sub></i>	1035.46	1543.29	475.75
Crystal system, space group	Monoclinic, <i>C2/c</i>	Triclinic, <i>P1</i>	Triclinic, <i>P1</i>
Temperature (K)	80	123	100
<i>a</i> , <i>b</i> , <i>c</i> (Å)	26.73026(13), 11.20485(4), 10.94534(6)	8.3225(2), 14.1342(4)	12.2260(3), 5.8312(3), 17.9564(9)
$\alpha$ , $\beta$ , $\gamma$ (°)	90, 90.0027(4), 90	100.321(2), 109.233(2)	106.292(2), 90, 97.130(5), 90
<i>V</i> (Å <sup>3</sup> )	3278.22(3)	1243.48(6)	601.22 (5)
<i>Z</i>	4	1	2
<i>F</i> (000)	2016	744	440
<i>D<sub>x</sub></i> (Mg m <sup>-3</sup> )	2.098	2.061	2.628
Radiation type	Synchrotron, $\lambda = 0.6199$ Å	CuK $\alpha$	CuK $\alpha$
$\mu$ (mm <sup>-1</sup> )	1.93	23.01	31.58
Crystal color and shape	Dark brown lath	Clear green plate	Clear colorless prism
Crystal size (mm)	0.15 × 0.10 × 0.05	0.23 × 0.11 × 0.06	0.09 × 0.09 × 0.04
<b>Data collection</b>			
Diffractometer	Synchrotron, beamline P11 at DESY Petra III, DECTRIS PILATUS M6	Xcalibur, Atlas <sup>S2</sup> , ultra	Gemini XtaLAB Synergy R, DW system, HyPix-Arc 150
Absorption correction	Multi-scan	Analytical	Gaussian
<i>T<sub>min</sub></i> , <i>T<sub>max</sub></i>	0.312, 1.000	0.068, 0.367	0.195, 0.520
No. of measured independent and observed [ <i>I</i> > 2 $\sigma$ ( <i>I</i> )] reflections	33178, 6355, 6272	17665, 4370, 3894	2253, 1091, 1072
<i>R<sub>int</sub></i>	0.045	0.038	0.074
( <i>sin</i> $\theta$ / $\lambda$ ) <sub>max</sub> (Å <sup>-1</sup> )	0.839	0.596	0.618
Range of <i>h</i> , <i>k</i> , <i>l</i>	<i>h</i> = -39 → 39, <i>k</i> = -16 → 16, <i>l</i> = -15 → 13	<i>h</i> = -9 → 9, <i>k</i> = -14 → 14, <i>l</i> = -16 → 16	<i>h</i> = -6 → 7, <i>k</i> = -7 → 6, <i>l</i> = -21 → 21
<b>Refinement</b>			
<i>R</i> [ <i>F</i> <sup>2</sup> > 2 $\sigma$ ( <i>F</i> <sup>2</sup> )], <i>wR</i> ( <i>F</i> <sup>2</sup> ), <i>S</i>	0.036, 0.097, 1.06	0.021, 0.050, 0.96	0.044, 0.121, 1.09
No. of reflections	6355	4370	1091
No. of parameters	190	278	84
No. of restraints	0	0	0
H-atom treatment	H-atom parameters constrained	H-atom parameters constrained	H-atom parameters constrained
$\Delta$ <sub>max</sub> , $\Delta$ <sub>min</sub> (e Å <sup>-3</sup> )	2.32, -4.85	0.48, -0.71	1.12, -1.39

Computer programs for I: XDS, (Kabsch, 2010), CrysAlis PRO 1.171.39.37b (Rigaku OD, 2017), SHELXT2014/7 (Sheldrick, 2014), SHELXL2014/7 (Sheldrick, 2014); for II: CrysAlis PRO 1.171.38.41 (Rigaku OD, 2015), SHELXT2014 (Sheldrick, 2014), SHELXL2014/7 (Sheldrick, 2014); for III: CrysAlis PRO 1.171.41.83a (Rigaku OD, 2020), SHELXT 2014/5 (Sheldrick, 2014), SHELXL2018/3 (Sheldrick, 2018).

**Table 4.4.** Experimental details for compounds **1**, **2a** and **2b**.

Crystal data	<b>1</b>	<b>2a</b>	<b>2b</b>
CCDC Codes	CCDC-2047567	CCDC-2047569	CCDC-2047568
Chemical formula	C <sub>33</sub> H <sub>42</sub> Ag <sub>3</sub> Fe <sub>2</sub> N <sub>4</sub> P <sub>10</sub> ·3(F <sub>6</sub> Sb)·2(C <sub>7</sub> H <sub>8</sub> )	(C <sub>18</sub> H <sub>23</sub> N <sub>4</sub> FeP <sub>5</sub> Ag <sub>2</sub> )(F <sub>6</sub> Sb) <sub>2</sub> ·CH <sub>2</sub> Cl <sub>2</sub>	C <sub>20</sub> H <sub>30</sub> Ag <sub>2</sub> Fe <sub>2</sub> N <sub>2</sub> P <sub>10</sub> ·2(SbF <sub>6</sub> )·C
<i>M<sub>r</sub></i>	2131.23	1278.27	1544.10
Crystal system, space group	Triclinic, <i>P1</i>	Triclinic, <i>P1</i>	Triclinic, <i>P1</i>
Temperature (K)	90	90	90
<i>a</i> , <i>b</i> , <i>c</i> (Å)	12.49204(16), 13.29045(15), 21.8762(2)	12.1881(3), 13.3092(4)	12.2977(4), 12.8858(3), 13.6522(3), 14.1606(3)
$\alpha$ , $\beta$ , $\gamma$ (°)	95.2254(8), 97.7408(10), 107.1419(11)	95.452(3), 109.089(3)	91.639(2), 90.9298(19), 90.3439(18), 108.923(2)
<i>V</i> (Å <sup>3</sup> )	3406.07 (7)	1872.86 (10)	2356.04 (10)
<i>Z</i>	2	2	2
<i>F</i> (000)	2052	1212	1480
<i>D<sub>x</sub></i> (Mg m <sup>-3</sup> )	2.078	2.267	2.177
Radiation type	Cu <i>K</i> α	Cu <i>K</i> α	Cu <i>K</i> α
$\mu$ (mm <sup>-1</sup> )	22.36	26.68	25.24
Crystal color and shape	Green-brown prism	Brown-to-green prism	Green rod
Crystal size (mm)	0.16 × 0.10 × 0.10	0.10 × 0.06 × 0.04	0.18 × 0.03 × 0.02
<b>Data collection</b>			
Diffractometer	SuperNova, Titan <sup>S2</sup>	SuperNova, Titan <sup>S2</sup>	SuperNova, Titan <sup>S2</sup>
Absorption correction	Gaussian	Gaussian	Gaussian
<i>T<sub>min</sub></i> , <i>T<sub>max</sub></i>	0.187, 0.373	0.141, 0.487	0.212, 0.761
No. of measured independent and observed reflections [ <i>I</i> > 2σ( <i>I</i> )]	23555, 13194, 11276	14440, 7347, 6089	15978, 9134, 7335
<i>R<sub>int</sub></i>	0.024	0.031	0.029
(sin θ/λ) <sub>max</sub> (Å <sup>-1</sup> )	0.624	0.623	0.624
Range of <i>h</i> , <i>k</i> , <i>l</i>	<i>h</i> = -13→15, <i>k</i> = -16→15, <i>l</i> = -27→25	<i>h</i> = -10→15, <i>k</i> = -15→15, <i>l</i> = 16→15	<i>h</i> = -13→15, <i>k</i> = -16→17, <i>l</i> = -17→11
<b>Refinement</b>			
<i>R</i> [ <i>F</i> <sup>2</sup> > 2σ( <i>F</i> <sup>2</sup> )], <i>wR</i> ( <i>F</i> <sup>2</sup> ), <i>S</i>	0.037, 0.100, 1.06	0.024, 0.055, 0.96	0.025, 0.054, 0.91
No. of reflections	13194	7347	9134
No. of parameters	1229	438	540
No. of restraints	7	0	0
H-atom treatment	H-atom parameters constrained	H-atom parameters constrained	H-atom parameters constrained
$\Delta$ <sub>max</sub> , $\Delta$ <sub>min</sub> (e Å <sup>-3</sup> )	1.73, -2.74	0.61, -0.73	1.30, -0.82

Computer programs for **1** and **2b**: CrysAlis PRO 1.171.40.66a (Rigaku OD, 2019), SHELXS2015/3 (Sheldrick, 2015), SHELXL2014/7 (Sheldrick, 2014). Computer programs for **2a**: CrysAlis PRO 1.171.40.66a (Rigaku OD, 2019), SHELXT2018/5 (Sheldrick, 2018), SHELXL2018/3 (Sheldrick, 2018).



**Table 4.5.** Experimental details for compounds **3a**, **3b** and **4a**.

Crystal data	<b>3a</b>	<b>3b</b>	<b>4a</b>
CCDC Code	CCDC-2047570	CCDC-2047572	CCDC-2047571
Chemical formula	C <sub>20</sub> H <sub>27</sub> Ag <sub>2</sub> FeN <sub>4</sub> P <sub>5</sub> ·(SbF <sub>6</sub> ) <sub>2</sub> ·CH <sub>2</sub> Cl <sub>2</sub>	C <sub>18.10</sub> H <sub>25.40</sub> Ag <sub>2</sub> Cl <sub>2</sub> F <sub>12</sub> FeN <sub>2</sub> P <sub>5</sub> S <sub>2</sub>	C <sub>16</sub> H <sub>23</sub> Ag <sub>2</sub> FeN <sub>2</sub> P <sub>5</sub> ·F <sub>6</sub> Sb·CH <sub>2</sub> Cl <sub>2</sub>
<i>M<sub>r</sub></i>	1306.32	1239.84	1226.23
Crystal system, space group	Orthorhombic, <i>Pnma</i>	triclinic, <i>P1</i>	Monoclinic, <i>C2/c</i>
Temperature (K)	150	90	120
<i>a</i> , <i>b</i> , <i>c</i> (Å)	25.3430(5), 13.2234(3), 11.7419(2)	11.4756 (7), 13.2231 (7), 13.5703 (5)	29.0898(11), 13.2096(2), 23.0319(9)
$\alpha$ , $\beta$ , $\gamma$ (°)	90, 90, 90	97.558 (4), 107.230 (4), 103.624 (5)	90, 127.777(6), 90
<i>V</i> (Å <sup>3</sup> )	3934.96 (14)	1865.96 (17)	6995.3(6)
<i>Z</i>	4	2	8
<i>F</i> (000)	2488	1174	4640
<i>D<sub>x</sub></i> (Mg m <sup>-3</sup> )	2.205	2.207	2.329
Radiation type	Cu K $\alpha$	Cu K $\alpha$	Cu K $\alpha$
$\mu$ (mm <sup>-1</sup> )	25.40	26.72	3.49
Crystal color and shape	Green rod	Green-brown prism	Green prism
Crystal size (mm)	0.40 × 0.05 × 0.03	0.17 × 0.09 × 0.08	0.26 × 0.08 × 0.05
Data collection			
Diffractometer	SuperNova, Atlas	SuperNova, Titan <sup>S2</sup>	SuperNova, Eos
Absorption correction	Gaussian	Gaussian	Gaussian
<i>T<sub>min</sub></i> , <i>T<sub>max</sub></i>	0.060, 0.745	0.223, 0.516	0.629, 1.000
No. of measured, independent and observed [ <i>i</i> > 2 $\sigma$ ( <i>I</i> )] reflections	10505, 4189, 3428	13153, 7287, 5591	24316, 7927, 6898
<i>R<sub>int</sub></i>	0.026	0.048	0.021
( <i>sin</i> $\theta$ / $\lambda$ ) <sub>max</sub> (Å <sup>-1</sup> )	0.629	0.624	0.649
Range of <i>h</i> , <i>k</i> , <i>l</i>	<i>h</i> = -31→28, <i>k</i> = -15→12, <i>l</i> = -14→12	<i>h</i> = -14→13, <i>k</i> = -16→16, <i>l</i> = -14→16	<i>h</i> = -27→37, <i>k</i> = -17→17, <i>l</i> = -29→28
Refinement			
<i>R</i> [ <i>F</i> <sup>2</sup> > 2 $\sigma$ ( <i>F</i> <sup>2</sup> )], <i>wR</i> ( <i>F</i> <sup>2</sup> ), <i>S</i>	0.026, 0.069, 0.95	0.047, 0.121, 0.96	0.042, 0.118, 1.08
No. of reflections	4189	7287	7927
No. of parameters	256	555	459
No. of restraints	0	204	15
H-atom treatment	H-atom parameters constrained	H-atom parameters constrained	H-atom parameters constrained
$\Delta$ <sub>max</sub> , $\Delta$ <sub>min</sub> (e Å <sup>-3</sup> )	0.69, -0.85	1.55, -1.29	2.84, -3.06

Computer programs: SHELXS2018/5 (Sheldrick, 2018), SHELXT2018/3 (Sheldrick, 2018); for **3a** and **4a**: CrysAlis PRO 1.171.39.45g (Rigaku OD, 2018), for **3b**: CrysAlis PRO 1.171.40.66a (Rigaku OD, 2019).

**Table 4.6.** Experimental details for compounds **4b**, **5a** and **5b**.

Crystal data	<b>4b</b>	<b>5a</b>	<b>5b</b>
CCDC Code	CCDC-2047573	CCDC-1886600	CCDC-1886601
Chemical formula	C <sub>32</sub> H <sub>46</sub> Ag <sub>3</sub> Fe <sub>2</sub> N <sub>4</sub> P <sub>10</sub> ·3(SbF <sub>6</sub> )·0.5(CH <sub>2</sub> Cl <sub>2</sub> )·1.25(C <sub>7</sub> H <sub>8</sub> )	C <sub>27.50</sub> H <sub>41</sub> Ag <sub>2</sub> ClF <sub>12</sub> Fe <sub>2</sub> N <sub>2</sub> P <sub>10</sub> Sb <sub>2</sub>	C <sub>25.50</sub> H <sub>38</sub> Ag <sub>2</sub> Cl <sub>3</sub> F <sub>12</sub> FeN <sub>4</sub> P <sub>5</sub> Sb <sub>2</sub>
<i>M<sub>r</sub></i>	2096.61	1543.71	1404.89
Crystal system, space group	Monoclinic, <i>P</i> 2 <sub>1</sub>	triclinic, <i>P</i> 1	triclinic, <i>P</i> 1
Temperature (K)	90	123	123
<i>a</i> , <i>b</i> , <i>c</i> (Å)	13.85056(17), 31.6811(3), 15.16461(16)	12.3068(5), 15.5935(8), 88.491(4)	14.2078(7), 11.9353(3), 26.2100(6)
$\alpha$ , $\beta$ , $\gamma$ (°)	90, 99.0769 (12), 90	67.494 (5), 72.042(4)	82.699 (2), 84.780(2), 76.923(2)
<i>V</i> (Å <sup>3</sup> )	6570.92 (13)	2383.1(2)	4562.4(2)
<i>Z</i>	4	2	4
<i>F</i> (000)	4030	1486	2700
<i>D<sub>x</sub></i> (Mg m <sup>-3</sup> )	2.119	2.151	2.045
Radiation type	Cu K $\alpha$	Cu K $\alpha$	Cu K $\alpha$
$\mu$ (mm <sup>-1</sup> )	23.53	24.401	22.489
Crystal shape and color	Brown plate	red rod	green rod
Crystal size (mm)	0.09 × 0.09 × 0.04	0.248 × 0.065 × 0.020	0.697 × 0.153 × 0.060
Data collection			
Diffractometer	SuperNova, Titan <sup>S2</sup>	SuperNova, Titan <sup>S2</sup>	SuperNova, Titan <sup>S2</sup>
Absorption correction	Gaussian	Gaussian	Gaussian
<i>T<sub>min</sub></i> , <i>T<sub>max</sub></i>	0.200, 0.516	0.128, 0.652	0.029, 0.371
No. of measured, independent and observed [ <i>I</i> > 2 $\sigma$ ( <i>I</i> )] reflections	49253, 25706, 23215	17537, 9354, 7209	33255, 17920, 12304,
<i>R<sub>int</sub></i>	0.047	0.0393	0.0587
( <i>sin</i> $\theta$ / $\lambda$ ) <sub>max</sub> (Å <sup>-1</sup> )	0.626	0.625	0.624
Range of <i>h</i> , <i>k</i> , <i>l</i>	<i>h</i> = -17→16, <i>k</i> = -39→39, <i>l</i> = -18→16	<i>h</i> = -15 → 12, <i>k</i> = -16 → 17, <i>l</i> = -19 → 18	<i>h</i> = -13 → 14, <i>k</i> = -18 → 18, <i>l</i> = -23 → 32
Refinement			
<i>R</i> [ <i>F</i> <sup>2</sup> > 2 $\sigma$ ( <i>F</i> <sup>2</sup> )], <i>wR</i> ( <i>F</i> <sup>2</sup> ), <i>S</i>	0.054, 0.146, 1.07	0.0375, 0.0937, 0.938	0.0592, 0.1678, 0.942
No. of reflections	25706	9354	17920
No. of parameters	1606	545	1071
No. of restraints	47	0	0
H-atom treatment	H-atom parameters constrained	H-atom parameters constrained	H-atom parameters constrained
$\Delta$ <sub>max</sub> , $\Delta$ <sub>min</sub> (e Å <sup>-3</sup> )	1.49, -2.19	1.675, -1.267	2.818, -1.751
Absolute structure	Refined as an inversion twin.	-	-
Absolute structure parameter	0.209 (7)	-	-

Computer programs for **4b**: CrysAlis PRO 1.171.40.66a (Rigaku OD, 2019), SHELXT2018/5 (Sheldrick, 2018), SHELXL2018/3 (Sheldrick, 2018); for **5a** and **5b**: CrysAlisPro 1.171.38.41 (Rigaku OD, 2015), SHELXT-2014/7 (Sheldrick, 2014), SHELXL-2014/7 (Sheldrick, 2014).

**Table 4.7.** Experimental details for compounds **6** and **7a**.

Crystal data	<b>6</b>	<b>7a</b>
CCDC Code	CCDC-1886602	CCDC-1886603
Chemical formula	C <sub>36</sub> H <sub>54</sub> Ag <sub>2</sub> F <sub>12</sub> Fe <sub>2</sub> N <sub>4</sub> P <sub>10</sub> Sb <sub>2</sub>	C <sub>159.70</sub> H <sub>238.40</sub> Ag <sub>11</sub> Cl <sub>3.40</sub> F <sub>66</sub> Fe <sub>9</sub> N <sub>12</sub> P <sub>45</sub> Sb <sub>11</sub>
<i>M<sub>r</sub></i>	1651.47	8123.06
Crystal system, space group	triclinic, <i>P</i> 1	orthorhombic, <i>Pnna</i>
Temperature (K)	90	90
<i>a</i> , <i>b</i> , <i>c</i> (Å)	8.0920(5), 13.5264(8), 14.1133(9)	34.3655(3), 31.1270(3), 24.70440(19)
<i>α</i> , <i>β</i> , <i>γ</i> (°)	70.068(5), 75.001(5), 79.357(5)	90, 90, 90
<i>V</i> (Å <sup>3</sup> )	1394.83(15)	26426.2(4)
<i>Z</i>	1	4
<i>F</i> (000)	804	15678
<i>D<sub>x</sub></i> (Mg m <sup>-3</sup> )	1.966	2.042
Radiation type	Cu <i>Kα</i>	Cu <i>Kα</i>
<i>μ</i> (mm <sup>-1</sup> )	20.451	22.63
Crystal shape	prism	plate
Color	green-brown	brown
Crystal size (mm)	0.16 × 0.09 × 0.06	0.195 × 0.167 × 0.084
<b>Data collection</b>		
Diffractometer	SuperNova, Titan <sup>S2</sup>	SuperNova, Titan <sup>S2</sup>
Absorption correction	Gaussian	Gaussian
<i>T<sub>min</sub></i> , <i>T<sub>max</sub></i>	0.177, 0.407	0.144, 0.354
No. of measured, independent and observed [ <i>I</i> > 2σ( <i>I</i> )] reflections	10398, 5493, 4633	73587, 26212, 20911
<i>R<sub>int</sub></i>	0.046	0.0415
(sin θ/λ) <sub>max</sub> (Å <sup>-1</sup> )	0.623	0.623
Range of <i>h</i> , <i>k</i> , <i>l</i>	<i>h</i> = -10 → 8, <i>k</i> = -16 → 16, <i>l</i> = -17 → 17	<i>h</i> = -30 → 42, <i>k</i> = -32 → 38, <i>l</i> = -26 → 30
<b>Refinement</b>		
<i>R</i> [ <i>F</i> <sup>2</sup> > 2σ( <i>F</i> <sup>2</sup> )], <i>wR</i> ( <i>F</i> <sup>2</sup> ), <i>S</i>	0.0410, 0.1065, 0.981	0.0619, 0.1684, 1.017
No. of reflections	5493	26212
No. of parameters	307	1751
No. of restraints	0	34
H-atom treatment	H-atom parameters constrained	H-atom parameters constrained
Δ <sub>max</sub> , Δ <sub>min</sub> (e Å <sup>-3</sup> )	1.051, -1.419	0.0619, 0.1684, 1.017

Computer programs for **6**: CrysAlisPro 1.171.38.41 (Rigaku OD, 2015), SHELXT (Sheldrick, 2014), SHELXL-2014/7 (Sheldrick, 2014); Computer programs for **7a**: CrysAlisPro 1.171.38.42b (Rigaku OD, 2015), SHELXS-2014/7 (Sheldrick, 2014), SHELXL-2014/7 (Sheldrick, 2014)

**Table 4.8.** Experimental details for compounds **7b** and **7c**.

Crystal data	<b>7b</b>	<b>7c</b>
CCDC Code	CCDC-1886604	CCDC-1886605
Chemical formula	C <sub>19</sub> H <sub>29</sub> AgF <sub>6</sub> FeN <sub>2</sub> P <sub>5</sub> Sb	C <sub>28</sub> H <sub>43</sub> Ag <sub>2</sub> FeN <sub>4</sub> P <sub>5</sub> ·2(SbF <sub>6</sub> )·0.25(CH <sub>2</sub> Cl <sub>2</sub> )
<i>M<sub>r</sub></i>	839.76	1354.83
Crystal system, space group	monoclinic, <i>P</i> 2 <sub>1</sub> / <i>n</i>	tetragonal, <i>P</i> 4 <sub>3</sub> 2 <sub>1</sub> 2
Temperature (K)	123	80
<i>a</i> , <i>b</i> , <i>c</i> (Å)	8.2734(4), 25.6048(13), 14.3471(7)	12.61455(16), 12.61455(16), 56.871(4)
$\beta$ (°)	105.856(5)	90
<i>V</i> (Å <sup>3</sup> )	2923.6(3)	9049.7 (6)
<i>Z</i>	4	8
<i>F</i> (000)	1640	5236
<i>D<sub>x</sub></i> (Mg m <sup>-3</sup> )	1.908	1.989
Radiation type	Cu <i>K</i> $\alpha$	synchrotron, $\lambda$ = 0.6199 Å
$\mu$ (mm <sup>-1</sup> )	19.57	1.81
Crystal shape	polyhedron	plate
Color	green	green
Crystal size (mm)	0.38 × 0.18 × 0.10	0.10 × 0.10 × 0.08
Data collection		
Diffractometer	SuperNova, Titan <sup>S2</sup>	Synchrotron, beamline P11, DESY Petra III, DECTRIS PILATUS 6M
Absorption correction	Gaussian	Multi-scan
<i>T<sub>min</sub></i> , <i>T<sub>max</sub></i>	0.038, 0.354	0.011, 1.000
No. of measured, independent and observed [ <i>I</i> > 2 $\sigma$ ( <i>I</i> )] reflections	9261, 5218, 4752	41206, 9945, 6353
<i>R<sub>int</sub></i>	0.067	0.061
( <i>sin</i> $\theta$ / $\lambda$ ) <sub>max</sub> (Å <sup>-1</sup> )	0.599	0.641
Range of <i>h</i> , <i>k</i> , <i>l</i>	<i>h</i> = -8 → 9, <i>k</i> = -22 → 30, <i>l</i> = -15 → 17	<i>h</i> = -15 → 15, <i>k</i> = -16 → 16, <i>l</i> = -58 → 72
Refinement		
<i>R</i> [ <i>F</i> <sup>2</sup> > 2 $\sigma$ ( <i>F</i> <sup>2</sup> )], <i>wR</i> ( <i>F</i> <sup>2</sup> ), <i>S</i>	0.079, 0.229, 1.09	0.058, 0.160, 0.94
No. of reflections	5218	9945
No. of parameters	342	510
No. of restraints	0	8
H-atom treatment	H-atom parameters constrained	H-atom parameters constrained
$\Delta$ <sub>max</sub> , $\Delta$ <sub>min</sub> (e Å <sup>-3</sup> )	1.83, -2.56	0.75, -0.80
Absolute structure parameter	-	-0.04 (3)

Computer programs for **7b**: CrysAlis PRO 1.171.38.41 (Rigaku OD, 2015), SHELXS2014/7 (Sheldrick, 2014), SHELXL2014/7 (Sheldrick, 2014; Computer programs for **7c**: CrysAlis PRO 1.171.39.37b (Rigaku OD, 2017), SHELXT2014/7 (Sheldrick, 2014), SHELXL2014/7 (Sheldrick, 2014).

**Table 4.9.** Experimental details for compounds **8** and **9** at different temperatures.

Crystal data	<b>8</b>	<b>9</b>	<b>9a</b>
CCDC Codes	CCDC-1960938	CCDC-1960939	CCDC-1960940
Chemical formula	C <sub>190</sub> H <sub>291</sub> Ag <sub>12</sub> Fe <sub>13</sub> N <sub>12</sub> P <sub>65</sub> · 12(SbF <sub>6</sub> )·(CH <sub>2</sub> Cl <sub>2</sub> ) <sub>6.2</sub>	C <sub>196</sub> H <sub>303</sub> Ag <sub>12</sub> Fe <sub>13</sub> N <sub>12</sub> P <sub>65</sub> · 12(SbF <sub>6</sub> )·(CH <sub>2</sub> Cl <sub>2</sub> ) <sub>6.5</sub>	C <sub>196</sub> H <sub>303</sub> Ag <sub>12</sub> Fe <sub>13</sub> N <sub>12</sub> P <sub>65</sub> · 12(SbF <sub>6</sub> )·(CH <sub>2</sub> Cl <sub>2</sub> ) <sub>6.5</sub>
<i>M<sub>r</sub></i>	10132.41	10220.81	10220.81
Crystal system, space group	orthorhombic, <i>Pccn</i>	orthorhombic, <i>Pccn</i>	orthorhombic, <i>Pccn</i>
Temperature (K)	100.0(2)	100.0(2)	10(2)
<i>a</i> , <i>b</i> , <i>c</i> (Å)	30.9896(3), 34.8444(3), 32.1679(3)	35.1511(2), 31.49534(16), 32.1736(2)	31.49535(16), 35.1511(2), 32.1736(2)
<i>V</i> (Å <sup>3</sup> )	34735.3(5)	35619.2(4)	35619.3(3)
<i>Z</i>	4	4	4
<i>F</i> (000)	19650	19850	19850
<i>D<sub>x</sub></i> (Mg m <sup>-3</sup> )	1.938	1.906	1.925
Radiation type	Cu <i>K</i> α	Cu <i>K</i> α	synchrotron (λ = 0.6702)
μ (mm <sup>-1</sup> )	20.28	20.65	2.17
Crystal shape	plate	prism	prism
Color	green-brown	green-brown	green-brown
Crystal size (mm)	0.29 × 0.23 × 0.09	0.42 × 0.34 × 0.23	0.10 × 0.10 × 0.10
<b>Data collection</b>			
Diffractometer	SuperNova, Titan <sup>S2</sup>	SuperNova, Titan <sup>S2</sup>	P11 beamline, Petra III, DECTIS Pilatus 6M
Absorption correction	Gaussian	Gaussian	empirical
<i>T<sub>min</sub></i> , <i>T<sub>max</sub></i>	0.036, 0.317	0.022, 0.152	0.405, 1.000
No. of measured, independent and observed [ <i>I</i> > 2σ( <i>I</i> )] reflections	120028, 34782, 26172	175339, 35882, 29146	224468, 43660, 36175
<i>R<sub>int</sub></i>	0.0564	0.077	0.0393
(sin θ/λ) <sub>max</sub> (Å <sup>-1</sup> )	0.624	0.623	0.667
Range of <i>h</i> , <i>k</i> , <i>l</i>	<i>h</i> = -38 → 25, <i>k</i> = -43 → 41, <i>l</i> = -30 → 39	<i>h</i> = -39 → 43, <i>k</i> = -38 → 39, <i>l</i> = -38 → 39	<i>h</i> = -43 → 46, <i>k</i> = -41 → 41, <i>l</i> = -42 → 42
<b>Refinement</b>			
<i>R</i> [ <i>F</i> <sup>2</sup> > 2σ( <i>F</i> <sup>2</sup> )], <i>wR</i> ( <i>F</i> <sup>2</sup> ), <i>S</i>	0.060, 0.167, 0.98	0.0720, 0.1999, 1.021	0.0540, 0.1610, 1.013
No. of reflections	34782	35882	43660
No. of parameters	2334	2436	2476
No. of restraints	21	154	188
H-atom treatment	H atom parameters constrained	H-atom parameters constrained	H atom parameters constrained
Δ <sub>max</sub> , Δ <sub>min</sub> (e Å <sup>-3</sup> )	1.93, -2.68	3.33, -2.15	1.57, -1.39

Computer programs: CrysAlis PRO 1.171.38.42b (Rigaku OD, 2015), SHELXS2014/7 (Sheldrick, 2014), SHELXL2018/3 (Sheldrick, 2018).

**Table 4.10.** Experimental details for compounds **10a** at different temperatures and **10b**.

Crystal data	10a (30 K)	10a (90 K)	10b
CCDC Code	CCDC-2047575	CCDC-2067328	CCDC-2047574
Chemical formula	C <sub>212.80</sub> H <sub>329.70</sub> Ag <sub>12</sub> Cl <sub>5.50</sub> F <sub>72</sub> F <sub>6</sub> e <sub>13</sub> N <sub>12</sub> P <sub>65</sub> Sb <sub>12</sub>	C <sub>202</sub> H <sub>315</sub> Ag <sub>12</sub> Fe <sub>12</sub> N <sub>12</sub> P <sub>65</sub> ·12(SbF <sub>6</sub> )·C <sub>7</sub> H <sub>8</sub> ·2.07(CH <sub>2</sub> Cl <sub>2</sub> )	C <sub>32</sub> H <sub>50</sub> Ag <sub>2</sub> Fe <sub>2</sub> N <sub>2</sub> P <sub>10</sub> ·2(SbF <sub>6</sub> )·C
<i>M<sub>r</sub></i>	10113.68	10042.11	1656.30
Crystal system, space group	Monoclinic, <i>P</i> 2 <sub>1</sub> / <i>n</i>	Monoclinic, <i>P</i> 2 <sub>1</sub> / <i>n</i>	Monoclinic, <i>P</i> 2 <sub>1</sub> / <i>m</i>
Temperature (K)	30	90	123
<i>a</i> , <i>b</i> , <i>c</i> (Å)	22.37406(12), 34.14239(13), 23.9793(2)	22.4242(3), 23.8955(4)	34.1771(4), 11.7403(2), 12.5880(2), 19.0497 (4)
$\alpha$ , $\beta$ , $\gamma$ (°)	90, 93.3646(6), 90	90, 93.4230(12), 90	105.899 (2)
<i>V</i> (Å <sup>3</sup> )	18286.28 (19)	18280.7 (4)	2707.60 (9)
<i>Z</i>	2	2	2
<i>F</i> (000)	9842	9770	1608
<i>D<sub>x</sub></i> (Mg m <sup>-3</sup> )	1.837	1.824	2.032
Radiation type	Synchrotron, $\lambda$ = 0.56076 Å	Cu <i>K</i> $\alpha$	Cu <i>K</i> $\alpha$
$\mu$ (mm <sup>-1</sup> )	1.25	19.56	21.64
Crystal shape	Plate	Plate	Block
Color	Brown	Brown	Green
Crystal size (mm)	0.2 × 0.2 × 0.1	0.28 × 0.15 × 0.05	0.20 × 0.17 × 0.08
Data collection			
Diffractometer	P24 beamline, Huber diffractometer, MAR165 CCD	SuperNova, Titan <sup>S2</sup>	SuperNova, Titan <sup>S2</sup>
Absorption correction	Multi-scan	Gaussian	Gaussian
<i>T<sub>min</sub></i> , <i>T<sub>max</sub></i>	0.681, 1.000	0.419, 1.000	0.088, 0.345
No. of measured, independent and observed [ <i>I</i> > 2 $\sigma$ ( <i>I</i> )] reflections	178485, 40172, 27437	67821, 35467, 19016	10544, 5533, 4662
<i>R<sub>int</sub></i>	0.024	0.048	0.039
( <i>sin</i> $\theta$ / $\lambda$ ) <sub>max</sub> (Å <sup>-1</sup> )	0.641	0.625	0.623
Range of <i>h</i> , <i>k</i> , <i>l</i>	<i>h</i> = -28→28, <i>k</i> = -43→43, <i>l</i> = -30→30	<i>h</i> = -26→26, <i>k</i> = -41→36, <i>l</i> = - 29→20	<i>h</i> = -14→11, <i>k</i> = -15→11, <i>l</i> = -23→19
Refinement			
Refinement on	<i>F</i> <sup>2</sup>	<i>F</i> <sup>2</sup>	<i>F</i> <sup>2</sup>
<i>R</i> [ <i>F</i> <sup>2</sup> > 2 $\sigma$ ( <i>F</i> <sup>2</sup> )], <i>wR</i> ( <i>F</i> <sup>2</sup> ), <i>S</i>	0.086, 0.294, 1.11	0.088, 0.267, 0.93	0.040, 0.104, 0.99
No. of reflections	40172	35467	5533
No. of parameters	1771	1644	328
No. of restraints	89	104	0
H-atom treatment	H-atom constrained	H-atom constrained	H-atom constrained
$\Delta$ <sub>max</sub> , $\Delta$ <sub>min</sub> (e Å <sup>-3</sup> )	5.38, -2.17	5.27, -1.85	0.90, -1.79

Computer programs for **10a** and **10b**: CrysAlis PRO 1.171.38.42b (Rigaku OD, 2015), SHELXS2013 (Sheldrick, 2013), SHELXL2013 (Sheldrick, 2013).

## 4.6 Author Contributions

- ❖ The synthesis and characterization of compound **I, II and 5a+b, 8, 9, 10a+b** was performed by Dr. B. Hiltl.
- ❖ The synthesis and characterization of compound **III, 1-4** was performed by K. Grill.
- ❖ The synthesis and characterization of compound **6, 7a-c** was performed by K. Grill and Dr. B. Hiltl and was also part of the Bachelor thesis of K. Grill (University of Regensburg, **2017**).
- ❖ The compound **I, II, 5a+b, 6, 7a-c, 8, 9, 10a+b** was also part of Dr. B. Hiltl's PhD-Thesis (University of Regensburg **2018**).
- ❖ The publication was written by Dr. E. Peresytkina and K. Grill.
- ❖ The experimental part was written by Dr. E. Peresytkina and K. Grill.
- ❖ The section "crystallographic details and structure refinement" was written by Dr. E. Peresytkina
- ❖ All in-house X-ray structure analyses structures were performed by Dr. E. Peresytkina and A. V. Virovets. All Synchrotron measurements including sample preparation, data reduction and all calculations were performed by Dr. E. Peresytkina and A. V. Virovets.
- ❖ MAS NMR investigation was performed by Prof. W. Kremer.
- ❖ TEM measurements were performed by Dr. J. Hilgert.

## 4.7 References

- [1] T.R. Cook, Y.-R. Zheng, P.J. Stang, *Chem. Rev.* **2013**, *113*, 734-777.
- [2] a) M. Mastalerz, *Acc. Chem. Res.* **2018**, *51*, 2411-2422; b) M. De Rosa, P. La Manna, C. Talotta, A. Soriente, C. Gaeta, P. Neri, *Frontiers in Chemistry* **2018**, *6*, 84; c) Q. Shi, M.P. Mower, D.G. Blackmond, J. Rebek, Jr., *Proc. Natl. Acad. Sci. USA* **2016**, *113*, 9199-9203; d) P. Ballester, M. Fujita, J. Rebek, Jr., *Chem. Soc. Rev.* **2015**, *44*, 392-393; e) A. Granzhan, C. Schouwey, T. Riis-Johannessen, R. Scopelliti, K. Severin, *J. Am. Chem. Soc.* **2011**, *133*, 7106-7115; f) W. Meng, A.B. League, T.K. Ronson, J.K. Clegg, W.C. Isley, D. Semrouni, L. Gagliardi, C.J. Cramer, J.R. Nitschke, *J. Am. Chem. Soc.* **2014**, *136*, 3972-3980.
- [3] Y. Inokuma, M. Kawano, M. Fujita, *Nat. Chem.* **2011**, *3*, 349-358.
- [4] a) M. Otte, *ACS Catal.* **2016**, *6*, 6491-6510; b) F. J. Rizzuto, L. K. S. von Krbeke, J. R. Nitschke, *Nature Rev. Chem.* **2019**, *3*, 204-222; c) A. Granzhan, T. Riis-Johannessen, R. Scopelliti, K. Severin, *Angew. Chem. Int. Ed.* **2010**, *49*, 5515-5518; d) G. Liu, M. Zeller, K. Su, J. Pang, Z. Ju, D. Yuan, M. Hong, *Chem. Eur. J.* **2016**, *22*, 17345-17350.

- [5] a) S.J. Barrow, S. Kaser, M.J. Rowland, J. del Barrio, O.A. Scherman, *Chem. Rev.* **2015**, *115*, 12320-12406; b) C. J. Hastings, M.D. Pluth, R.G. Bergman, K.N. Raymond, *J. Am. Chem. Soc.* **2010**, *132*, 6938-6940.
- [6] K. Rissanen, *Chem. Soc. Rev.* **2017**, *46*, 2638-2648.
- [7] a) E.T.C. Vogt, G.T. Whiting, A.D. Chowdhury, B.M. Weckhuysen in *Advances in Catalysis, Vol. 58* (Ed.: F. C. Jentoft), Elsevier, Amsterdam, **2015**, pp 143-314; b) N. Jiang, R. Shang, S.G.J. Heijman, L.C. Rietveld, *Water Res.* **2018**, *144*, 145-161; c) L. Bacakova, M. Vandrovцова, I. Kopova, I. Jirka, *Biomat. Sci.* **2018**, *6*, 974-989; d) I. Stassen, N. Burtch, A. Talin, P. Falcaro, M. Allendorf, R. Ameloot, *Chem. Soc. Rev.* **2017**, *46*, 3185-3241; e) L. Wang, M. Zheng, Z. Xie, *J. Mater. Chem. B* **2018**, *6*, 707-717; f) L. Zhu, X.-Q. Liu, H.-L. Jiang, L.-B. Sun, *Chem. Rev.* **2017**, *117*, 8129-8176; g) X. Yang, Q. Xu, *Cryst. Growth Des.* **2017**, *17*, 1450-1455.
- [8] A.E. Seitz, F. Hippauf, W. Kremer, S. Kaskel, M. Scheer, *Nat. Commun.* **2018**, *9*, 361.
- [9] a) K.E. Cordova, O.M. Yaghi, *Mater. Chem. Front.* **2017**, *1*, 1304-1309; b) C.S. Diercks, Y. Liu, K.E. Cordova, O.M. Yaghi, *Nature Materials* **2018**, *17*, 301-307; c) M. O'Keeffe, M.A. Peskov, S.J. Ramsden, O.M. Yaghi, *Accts. Chem. Res.* **2008**, *41*, 1782-1789.
- [10] a) C. Zhang, F. Wang, R. S. Patil, C. L. Barnes, T. Li, J. L. Atwood, *Chem. Eur. J.* **2018**, *24*, 14335-14340; b) R. M. McKinlay, G. W. V. Cave, J. L. Atwood, *PNAS*, **2005**, *102*, 5944-5948; c) C. Zhang, R. S. Patil, C. Liu, C. L. Barnes, J. L. Atwood, *J. Am. Chem. Soc.* **2017**, *139*, 2920-2923; d) A. V. Mossine, C. M. Mayhan, D. A. Fowler, S. J. Teat, C. A. Deakyne, J. L. Atwood, *Chem. Sci.* **2014**, *5*, 2297-2303; e) L. Shao, B. Hua, X. Hu, D. Stalla, S.P. Kelley, J. L. Atwood, *J. Am. Chem. Soc.* **2020**, *142*, 7270-7275; f) D. A. Fowler, A. V. Mossine, C. M. Beavers, S. J. Teat, S. J. Dalgarno, J. L. Atwood, *J. Am. Chem. Soc.* **2011**, *133*, 11069-11071.
- [11] a) E.-S. M. El-Sayed, D. Yuan, *Chem. Lett.* **2020**, *49*, 28-53; b) X.-Y. Xie, F. Wu, X. Liu, W.-Q. Tao, Y. Jiang, X.-Q. Liu, L.-B. Sun, *Chem. Commun.*, **2019**, *55*, 6177-6180; c) G. Lal, M. Derakhshandeh, F. Akhtar, D. M. Spasyuk, J.-B. Lin, M. Trifkovic, G. K. H. Shimizu, *J. Am. Chem. Soc.*, **2019**, *141*, 1045-1053; d) A. Carné-Sánchez, G. A. Craig, P. Larpent, T. Hirose, M. Higuchi, S. Kitagawa, K. Matsuda, K. Urayama, S. Furukawa, *Nat. Commun.*, **2018**, *9*, 2506.
- [12] a) H. Jung, D. Moon, Chun, H. *Bull. Korean Chem. Soc.* **2011**, *32*, 2489-2492; b) M. L. Schneider, O. M. Linder-Patton, W. M. Bloch, *Chem. Commun.*, **2020**, *56*, 12969-12972.
- [13] a) E. Peresypkina, C. Heindl, A. Virovets, H. Brake, E. Mädl, M. Scheer, *Chem. Eur. J.* **2018**, *24*, 2503-2508; b) J. Bai, A.V. Virovets, M. Scheer, *Science* **2003**, *300*, 781-783; c) F. Dielmann, M. Fleischmann, C. Heindl, E.V. Peresypkina, A.V. Virovets, R.M. Gschwind, M. Scheer, *Chem. Eur. J.* **2015**, *21*, 6208-6214; d) C. Schwarzmaier, A. Schindler, C. Heindl, S. Scheuermayer, E.V. Peresypkina, A.V. Virovets, M. Neumeier, R. Gschwind, M. Scheer, *Angew. Chem. Int. Ed.*

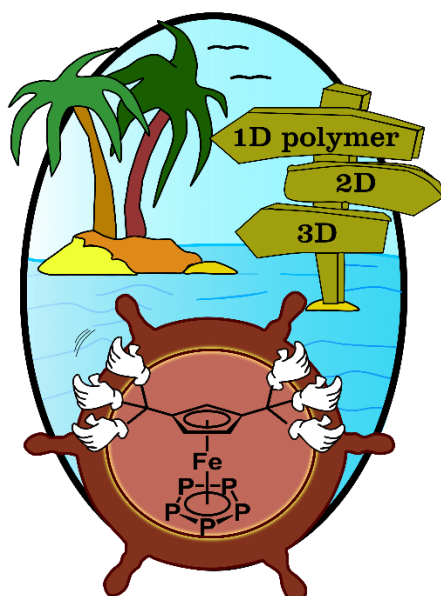


- 2013**, 52, 10896-10899; e) A. Schindler, C. Heindl, G. Balazs, C. Groeger, A.V. Virovets, E.V. Peresyphkina, M. Scheer, *Chem. Eur. J.* **2012**, 18, 829-835; f) M. Scheer, A. Schindler, R. Merkle, B.P. Johnson, M. Linseis, R. Winter, C.E. Anson, A.V. Virovets, *J. Am. Chem. Soc.* **2007**, 129, 13386-13387; g) C. Heindl, E. Peresyphkina, A. V. Virovets, I. S. Bushmarinov, M. G. Medvedev, B. Kraemer, B. Dittrich, M. Scheer, *Angew. Chem., Int. Ed.* **2017**, 56, 13237-13243.
- [14] a) E. Peresyphkina, C. Heindl, A.V. Virovets, M. Scheer, Inorganic superspheres in *Clusters – Contemporary Insight in Structure and Bonding*, Vol. 174, (Ed.: Dehnen S.) Springer, Cham, **2016**, pp 321-373; b) M. Scheer, A. Schindler, C. Gröger, A.V. Virovets, E.V. Peresyphkina, *Angew. Chem. Int. Ed.* **2009**, 48, 5046-5049; c) C. Heindl, E.V. Peresyphkina, A.V. Virovets, W. Kremer, M. Scheer, *J. Am. Chem. Soc.* **2015**, 137, 10938-10941.
- [15] a) M. Elsayed Moussa, S. Evariste, B. Krämer, R. Reau, M. Scheer, C. Lescop, *Angew. Chem. Int. Ed.* **2018**, 57, 795-799; b) M. Elsayed Moussa, B. Attenberger, E. V. Peresyphkina, M. Fleischmann, G. Balázs, M. Scheer, *Chem. Commun.* **2016**, 52, 10004 – 10007; (c) Lennartson, P. Southon, N. F. Sciortino, C. J. Kepert, C. Frandsen, S. Morup, S. Piligkos, C. J. McKenzie, *Chem. Eur. J.* **2015**, 21, 16066-16072; (d) K. Chainok, W. Saphu, P. Khemthong, D. J. Harding, *Z. Anorg. Allg. Chem.* **2013**, 639, 2134-2137; (e) A. Westcott, N. Whitford, M. J. Hardie, *Inorg. Chem.* **2004**, 43, 3663-3672; (f) L. i, G. Ciani, D. M. Proserpio, S. Rizzato, *CrystEngComm* **2002**, 4, 413-425.
- [16] M. Scheer, L. J. Gregoriades, A. V. Virovets, W. Kunz, R. Neueder, I. Krossing, *Angew. Chem. Int. Ed.* **2006**, 45, 5689-5693.
- [17] For further detail of the analytical data, see Supporting Information.
- [18] T. Sakano, M. Okano, K. Osakada, *J. Inorg. Organomet. Polym. Mater.* **2009**, 19, 35-45.
- [19] The length of the linker in linear conformation was calculated with CHEM3D Ultra by Perkin Elmer Informatics Inc., **2019** Version 19.1.08.
- [20] The outer diameter of the supramolecular node was calculated as the distance of two outermost H atoms plus twice the van der Waals radius of H (0.11 nm according to R. S. Rowland, R. Taylor, *J. Phys. Chem.* **1996**, 100, 7384-7391). The void dimensions were calculated as the minimum × maximum distances between two opposing P atoms minus twice the van der Waals radius of P (0.180 nm).
- [21] a) M.A. Carvajal, J.J. Novoa, S. Alvarez, *J. Am. Chem. Soc.* **2004**, 126, 1465-1477; b) E. Peresyphkina, M. Bielmeier, A. V. Virovets, M. Scheer, *Chem. Sci.*, **2020**, 11, 9067-9071.
- [22] M. Scheer, A. Schindler, J. Bai, B.P. Johnson, R. Merkle, R. Winter, A.V. Virovets, E.V. Peresyphkina, V.A. Blatov, M. Sierka, H. Eckert *Chem. Eur. J.* **2010**, 16, 2092-2107.

- [23] a) V. A. Blatov, A. P. Shevchenko, D. M. Proserpio, *Cryst. Growth Des.* **2014**, *14*, 3576-3586;  
b) V. A. Blatov, M. O'Keeffe, D. M. Proserpio, *CrystEngComm.* **2010**, *12*, 44-48.
- [24] a) N. Byrd, R. J. Bartlett, J. A. Montgomery, Jr., *J. Phys. Chem. A* **2014**, *118*, 1706-1712; b) N. O. B. Lüttschwager, T. N. Wassermann, R. A. Mata, M. A. Suhm, *Angew. Chem. Int. Ed.* **2013**, *52*, 463-466.
- [25] M. Detzel, G. Friedrich, O.J. Scherer, G. Wolmershäuser, *Angew. Chem. Int. Ed.*, **1995**, *34*, 1321.
- [26] A. Ashnagar, N. Gharib Naseri, S. Alboghobesh, *Biosciences, Biotechnology Research Asia*, **2007**, *4*, 65-70.
- [27] O.J. Scherer, T. Brück, *Angew. Chem.* **1987**, *99*, 59.
- [28] A. Burkhardt, T. Pakendorf, B. Reime, *Eur. Phys. J. Plus* **2016**, *131*, 56-64.
- [29] [https://photon-science.desy.de/facilities/petra\\_iii/beamlines/p24\\_chemical\\_crystallography/eh2/index\\_eng.html](https://photon-science.desy.de/facilities/petra_iii/beamlines/p24_chemical_crystallography/eh2/index_eng.html)
- [30] CrysAlisPro, different versions (Rigaku OD).
- [31] G.M. Sheldrick, *Acta Cryst. C* **2015**, *C71*, 3.
- [32] C.R. Groom, I.J. Bruno, M.P. Lightfoot, C.S. Ward, *Acta Cryst. B* **2016**, *72*, 171-179.
- [33] M. O'Keeffe, M. A. Peskov, S. J. Ramsden, O. M. Yaghi, *Acc. Chem. Res.* **2008**, *41*, 1782-1789, <http://rcsr.net>.
- [34] O. V. Dolomanov, L. J. Bourhis, R. J. Gildea, J. A. K. Howard, H. Puschmann, *J. Appl. Cryst.* **2009**, *42*, 339-341.
- [35] POV-Ray. <https://www.povray.org>

## 5. Across the Dimensions: A Three-Component Self-Assembly of Pentaphosphaferrocene-based Coordination Polymers

Kevin Grill, Sabrina B. Dinauer, Eugenia Peresyphkina, Alexander V. Virovets, and Manfred Scheer, *Chem. Eur. J.* **2023**, 29, e202203963. Reproduced by permission of Wiley-VCH GmbH, which can be viewed [online](#).



**Abstract:** Pentaphosphaferrocenes [ $\text{Cp}^R\text{Fe}(\eta^5\text{-P}_5)$ ] ( $\text{Cp}^* = \eta^5\text{-C}_5\text{Me}_5$ ) (**A**),  $\text{Cp}'' = \eta^5\text{-C}_5\text{H}_3\text{tBu}_{2-1,3}$  (**B**)) are excellent building blocks for polymeric assemblies in supramolecular chemistry in combination with coinage metal salts of weakly coordinating anions such as  $\text{AgSbF}_6$ . Adding rigid aromatic dinitriles ortho/meta/para- $(\text{NC})_2\text{C}_6\text{H}_4$  in a one-pot reaction between [ $\text{Cp}^R\text{Fe}(\eta^5\text{-P}_5)$ ] and  $\text{AgSbF}_6$  leads to various coordination polymers (CPs) by a three-component self-assembly. The sterical demand of the differently substituted cyclopentadiene ligands as well as the rigid constitution of the isomeric dinitriles  $(\text{NC})_2\text{C}_6\text{H}_4$  play a key role in the formation of the isolated CPs. All CPs were characterized by NMR spectroscopy, mass spectrometry, elemental analysis, and single-crystal X-ray diffraction.

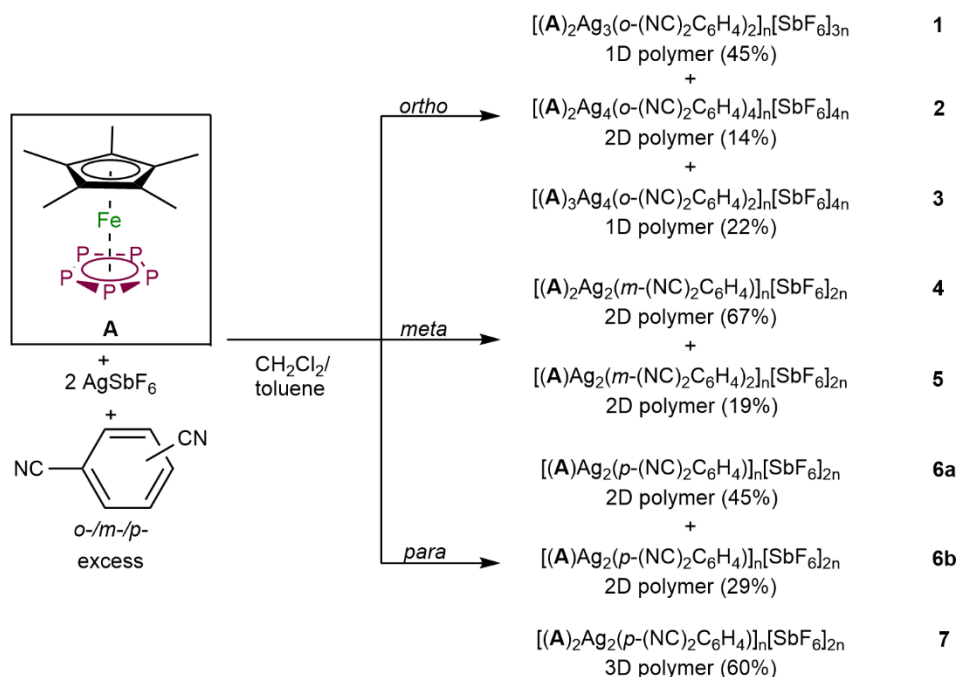
## 5.1 Introduction

Based on the interdisciplinary impact of chemistry, physics and biology on supramolecular chemistry, this area presents one of the most fascinating and rapidly growing topics in current chemistry. Due to both versatility and variability, supramolecular chemistry spans a broad field of research and applications e.g. in drug delivery, catalysis, molecular storage, etc.<sup>[1]</sup> Supramolecular chemistry relies on the concept of molecular self-assembly<sup>[2]</sup> and focuses mostly rather weak interactions such as hydrogen bonding, van der Waals or  $\pi$ - $\pi$  interactions.<sup>[3]</sup> Some supramolecular assemblies are large enough to create cavities for smaller guest molecules.<sup>[4]</sup> Additionally, metallosupramolecular chemistry uses metal ions as fundamental building blocks beside organic ligands.<sup>[5]</sup> Hence, well-defined reaction conditions as well as a sophisticated molecular design of the used building blocks are required.<sup>[6]</sup>

First studies in this challenging field of metallosupramolecular chemistry were highlighted by Fujita and Ogura in 1990 with the self-assembly of Pd(II)-based macrocyclic<sup>[7]</sup> and polymeric structures. Beside the first tetranuclear square complex  $[(\text{en})\text{Pd}(4,4'\text{-bpy})]_4(\text{NO}_3)_8$ , which attracted considerable interest,<sup>[8]</sup> the authors were also able to obtain a 2D coordination network consisting of Cd(II) and 4,4'-bipyridine.<sup>[9]</sup> Imparting this system, more flexibility by using benzene-based ligands with flexible pyridine arms resulted in the formation of infinite networks of ladders and bricks.<sup>[10]</sup> These infinite polycatenane frameworks consist of 60-membered rings (ladder) or 90-membered rings (brick) and show the influence of the organic ligands on the resulting connectivity of the supramolecular assembly. Therefore, the choice of the organic ligand has, on the one hand, a decisive impact on the freedom of the self-assembly system and, on the other hand, the system can be controlled *via* modifications of the ligand.<sup>[11]</sup>

Moreover, the metal center and therefore the associated metal salt has a considerable impact on the system as well. Among coinage metals, gold being a two-coordinate cation has a linear or planar coordination geometry around the metal center,<sup>[12]</sup> scarcely providing sufficient coordination sites. Copper(I) cations supply from three to four coordination sites, however, copper salts either contain copper complex cations with coordinated solvent molecules or dissolve in organic media only upon complexation with solvents as for instance acetonitrile, which would compete with the targeted organic ligand for coordination and uncontrollable block coordination sites at the metal center. To grant free coordination sites at the metal centers, one is restricted to using non-blocking counterions or solvents. However, the silver salt of the non-coordinating anion  $\text{SbF}_6^-$  lacks the aforesaid disadvantages and is known, together with polyphosphorus ligands, to build supramolecular assemblies bearing free coordination sites at the silver centers that can be immediately coordinated by N-donor ligands in a one-step self-assembly reaction.<sup>[13]</sup>

As we have already shown, the polyphosphorus complexes used in two-component self-assembly reactions with  $[\text{Cp}^{\text{R}}\text{Fe}(\eta^5\text{-P}_5)]$  ( $\text{Cp}^{\text{R}} = \text{Cp}^*$  (**A**),  $\text{Cp}^{\text{Bn}} = \text{Cp}(\text{CH}_2\text{Ph})_5$ ) and  $\text{CuX}$  ( $\text{X} = \text{Cl}, \text{Br}, \text{I}$  or triflate) or  $\text{CuX}_2$  ( $\text{X} = \text{Cl}, \text{Br}$ ) form various spherical aggregates with host-guest properties.<sup>[14]</sup> Their reactivity relies on the



**Scheme 5.1.** One-pot self-assembly reactions of **A**,  $\text{AgSbF}_6$ , and aromatic isomers of *o-/m-/p*-( $\text{NC}$ )<sub>2</sub>C<sub>6</sub>H<sub>4</sub>. Isolated crystalline yields are given in parentheses.

substituent-free P atoms that are solely bound to other P or metal atoms which influence the steric and electronic properties on the coordinating P atoms and therefore enable a unique coordination chemistry.

Combining polyphosphorus complexes with  $\text{AgSbF}_6$  and organic ligands lead to a three-component self-assembly system possessing flexibility, variability, and versatility, therefore showing a high potential for the formation of both supramolecular assemblies and multi-dimensional coordination polymers.

Following this idea, with the aim to obtain such supramolecular aggregates, we have recently reported a controllable one-pot three-component self-assembly system consisting of **A**,  $\text{AgSbF}_6$  and flexible aliphatic dinitriles of the type  $\text{NC}(\text{CH}_2)_x\text{CN}$  ( $x = 1\text{-}10$ ).<sup>[15]</sup> Surprisingly, we observed that the length and flexibility of an aliphatic chain of the organic ligand influence the outcome of the self-assembly system. By increasing the length of the aliphatic dinitrile and therefore giving the system more and more adjusting capabilities, the system builds different 1D-3D coordination polymers with short linkers ( $x \leq 6$ ), and astonishingly changes its course in the case of longer linkers ( $x \geq 7$ ) where it leads to nanosized organometallic host-guest spherical assemblies connected in various 3D supramolecular coordination networks.

This fact raises the question as to what will happen if the three-component self-assembly system is restricted to some extent. On the one hand, more sterically demanding polyphosphorus complexes can be used, which should strongly influence the coordination sphere of a metal cation due to the increasing steric hinderance. Additionally, the solubility of the polyphosphorus complex will change, which would also influence the respective reaction conditions.<sup>[16]</sup> On the other hand, choosing more rigid organic linkers with fixed bite angles and a known arrangement of the donor groups could lead to a more controllable outcome.

With these considerations in mind, we decided to use the isomers of the rigid aromatic dinitrile *ortho/meta/para*-(NC)<sub>2</sub>C<sub>6</sub>H<sub>4</sub> as organic linker, due to the electronic effects of the aromatic part and the fixed angles, and, besides **A**, another polyphosphorus complex with a slightly higher sterical demand [Cp<sup>''</sup>Fe(η<sup>5</sup>-P<sub>5</sub>)] (Cp<sup>''</sup> = η<sup>5</sup>-C<sub>5</sub>H<sub>3</sub>tBu<sub>2-1,3</sub> (**B**)) to study the influence of sterical hinderance of two *t*Bu groups onto the self-assembly outcome. Herein we report a systematic study of the three-component self-assembly system of **A** or **B** polyphosphorus building blocks, AgSbF<sub>6</sub> and rigid aromatic dinitriles *ortho/meta/para*-(NC)<sub>2</sub>C<sub>6</sub>H<sub>4</sub> showing that the resulting coordination polymers of different dimensionalities and connectivity are accessible depending on the position of the nitrile functionalities in the dinitrile ligands and the sterical influence of the cyclopentadienyl ligand of the substituted pentaphosphaferrocene. The influence of these factors on the products of the self-assembly is analysed.

## 5.2 Results and Discussion

### Three-Component Self-Assembly using [Cp<sup>\*</sup>Fe(η<sup>5</sup>-P<sub>5</sub>)] (**A**)

For all reactions, a solution of AgSbF<sub>6</sub> in CH<sub>2</sub>Cl<sub>2</sub> was first layered with a mixture of CH<sub>2</sub>Cl<sub>2</sub> and toluene (2:1) and then with a toluene solution of **A** and the isomeric rigid aromatic dinitrile *o/m/p*-(NC)<sub>2</sub>C<sub>6</sub>H<sub>4</sub>. The one-pot reactions were controlled *via* using different concentrations in the respective layers and a ratio of **A**:2Ag (Scheme 5.1). The corresponding dinitrile was added in a 10-fold excess with respect to **A** to prohibit restrictions by the amount of organic ligand in the form of a stock solution or as pure compound. In all reactions, brown laths of the known 1D polymer [(**A**)<sub>2</sub>Ag]<sub>n</sub>[SbF<sub>6</sub>]<sub>n</sub> co-crystallize as byproduct<sup>[15]</sup> as well as unavoidable colorless crystals of a compound containing AgSbF<sub>6</sub> and the respective dinitrile linker. The latter was not of interest due to missing **A** and was not further investigated (see SI for detail). Noteworthy, a direct synthesis with stoichiometric ratios to the desired products failed despite many attempts resulting in the mentioned byproducts.

In the reaction of *o*-(NC)<sub>2</sub>C<sub>6</sub>H<sub>4</sub>, **A** and AgSbF<sub>6</sub> with a concentration of 2 mmol L<sup>-1</sup> in the respective layers, a mixture consisting of a 1D polymer [(**A**)<sub>2</sub>Ag<sub>3</sub>(*o*-(NC)<sub>2</sub>C<sub>6</sub>H<sub>4</sub>)<sub>2</sub>]<sub>n</sub>[SbF<sub>6</sub>]<sub>3n</sub> (**1**: brown blocks), a 2D

polymer  $[\{\mathbf{A}\}_2\text{Ag}_4(o\text{-(NC)}_2\text{C}_6\text{H}_4)_4]_n[\text{SbF}_6]_{4n}$  (**2**: yellow plates) and another 1D polymer  $[\{\mathbf{A}\}_3\text{Ag}_4(o\text{-(NC)}_2\text{C}_6\text{H}_4)_2]_n[\text{SbF}_6]_{4n}$  (**3**: brown laths) were obtained. All products **1-3** and the co-crystallizing byproducts could be separated manually under the microscope. Changes of the stoichiometric ratio or concentration showed no direct influence on the selectivity of the desired products, but drastically changed the amount of the colorless compound containing only  $\text{AgSbF}_6$  and the linker. The same reaction conditions in the case of  $m\text{-(NC)}_2\text{C}_6\text{H}_4$  lead to a mixture of two polymeric products, 2D  $[\{\mathbf{A}\}_2\text{Ag}_2(m\text{-(NC)}_2\text{C}_6\text{H}_4)]_n[\text{SbF}_6]_{2n}$  (**4**: yellow plates) and  $[\{\mathbf{A}\}\text{Ag}_2(m\text{-(NC)}_2\text{C}_6\text{H}_4)_2]_n[\text{SbF}_6]_{2n}$  (**5**: brown laths). Nevertheless, these diluted conditions used in the case of  $o/m\text{-(NC)}_2\text{C}_6\text{H}_4$  could not be successfully applied to the  $p\text{-(NC)}_2\text{C}_6\text{H}_4$  isomer, as no product crystallized in this case. Therefore, the concentration of the respective layers was increased to  $4 \text{ mmol L}^{-1}$  and a fivefold excess of the corresponding aromatic dinitrile with respect to **A** was used to provide enough organic ligand material and, at the same time, to limit the number of possible byproducts. In this way, two 2D polymeric products were obtained. In the solid state, the two solvatomorphic phases of a compound  $[\{\mathbf{A}\}\text{Ag}_2(p\text{-(NC)}_2\text{C}_6\text{H}_4)]_n[\text{SbF}_6]_{2n}$  (**6a**: brown blocks and **6b**: yellow needles) were found. Keeping an equimolar ratio of **A**:Ag but increasing the amount of organic linker  $p\text{-(NC)}_2\text{C}_6\text{H}_4$  to a 10-fold excess with respect to **A** leads to a 3D polymer  $[\{\mathbf{A}\}_2\text{Ag}_2(p\text{-(NC)}_2\text{C}_6\text{H}_4)]_n[\text{SbF}_6]_{2n}$  (**7**: brown prisms) (Scheme 5.1). Remarkably, when keeping the crystals in mother liquor for at least eight months, the ratio between major and minor products was not observed to change, which makes the possibility of their mutual transformation unlikely.

According to single crystal X-ray structure analysis, the polymers based on **A**,  $\text{AgSbF}_6$ , and the rigid aromatic dinitriles span all dimensionalities from 1D to 3D. All polymers consist of infinite  $\text{Ag}/\text{cyclo-P}_5$  1D subunits (Figures 5.1-5.7) decorated by the organic ligands, with the ratio and coordination mode of the  $\text{cyclo-P}_5$  ring to the Ag cations varying, which gives rise to different 1D subunits. In addition, the chemical environment of the isomeric dinitriles seems to predetermine the dimensionality of the formed products to a certain extent. For the *ortho* isomer, 1D and 2D polymers are found, all other isomers lead to the formation of 2D or 3D polymers. This is probably due to the small distance between the nitrile functionalities in  $o\text{-(NC)}_2\text{C}_6\text{H}_4$ . Therefore, owing to the smallest bite angle ( $\sim 60^\circ$ ), the *ortho* linker seems to be able to bridge the silver ions in the 1,2-positions of the  $\text{cyclo-P}_5$  ligands, which leads to 1D chain polymers (Figures 5.1, 5.3), but can also interconnect 1D subunits to give a 2D polymer (Figure 5.2). With an increasing distance between the nitriles of the linker, 2D (*meta/para*) and 3D polymers (*para*) are more likely to be formed. In the last two cases, the isomeric aromatic rigid linkers act only as a crosslinking spacer to give rise to more extended infinite networks.

The 1D polymer in **1** is built up by  $[\{\mathbf{A}\}_2\text{Ag}_3]_n^{3n+}$  units, with the *cyclo*-P<sub>5</sub> ligands of **A** coordinating to the Ag atoms in alternating 1,2,3- and 1,2,3,4-coordination modes (Figure 5.1), with Ag ions being tetrahedrally or trigonally coordinated, building the six-membered rings of {P<sub>4</sub>Ag<sub>2</sub>} of the 1D chain. The organic ligand coordinates always to a tetrahedrally and a trigonally coordinated Ag atom on the side of the chain. All tetrahedrally coordinated Ag atoms are linked to two organic ligands and two *cyclo*-P<sub>5</sub> ligands while the Ag atoms in the trigonal environment coordinate to one organic ligand and two *cyclo*-P<sub>5</sub> ligands. The Cp\* ligands of **A** alternate in opposite directions with respect to the P<sub>5</sub> rings.

The 2D polymer **2** consists of parallel 1D strands  $[\{\mathbf{A}\}_2\text{Ag}_4]_n^{4n+}$ . All *cyclo*-P<sub>5</sub> ligands are coordinated in a 1,2,3,4-mode to Ag atoms (Figure 5.2). Additionally, two dinitriles are coordinated to each Ag cation completing its tetrahedral environment, while one coordinates to the next silver ion in the same strand and the other binds the silver ion of the next strand. Interestingly, some of the non-bridging dinitriles of each strand face the dinitrile of the next strand, with an interplanar distance of 3.52(1) Å indicating weak  $\pi$ - $\pi$  interactions due to significantly slipped relative positions of the aromatic systems. Most of the aromatic rings do not participate in stacking as they are isolated by counter anions or solvent molecules of the crystallization.

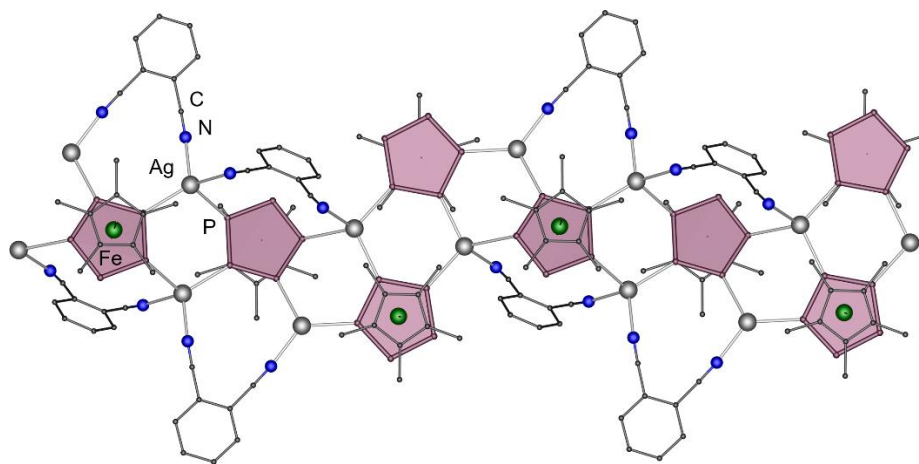


**Figure 5.1.** The cationic 1D polymer in **1**. H atoms are omitted for clarity.



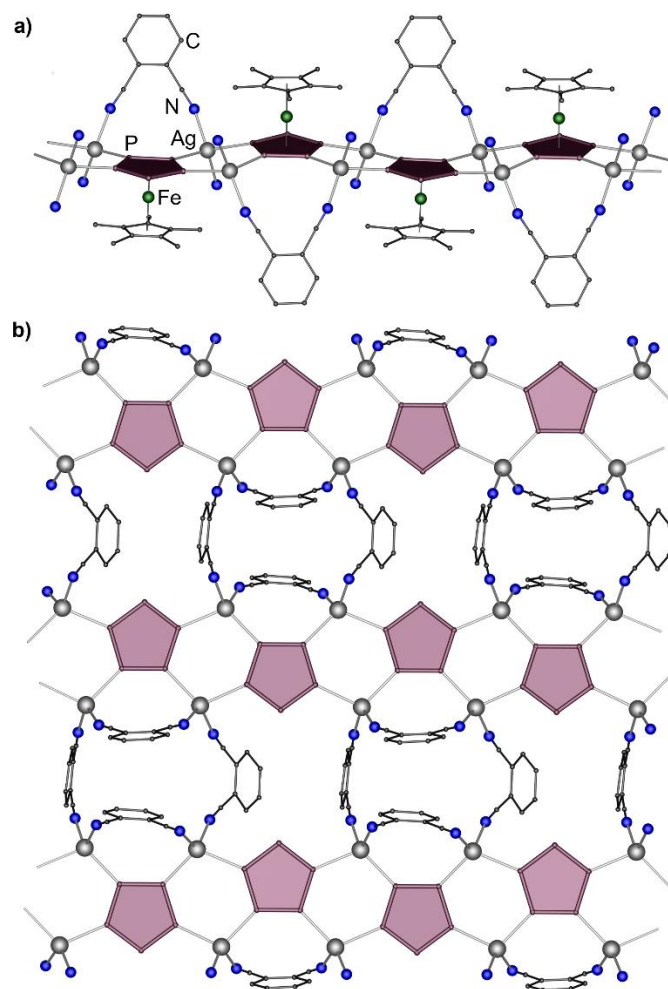


**Figure 5.2.** The 2D cationic network of **2** a) a section of the cationic motif  $[(\mathbf{A})_2\text{Ag}_4]^{4n+}$ ; b) 2D cationic network with interconnecting  $o\text{-(NC)}_2\text{C}_6\text{H}_4$  ligands. H atoms are omitted for clarity.

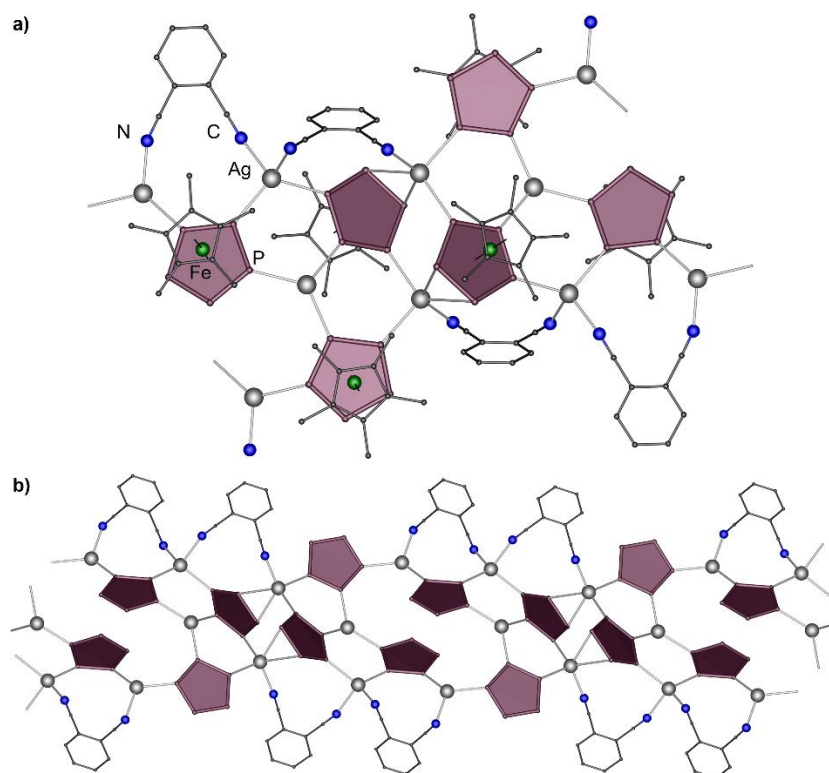


**Figure 5.3.** Structure of a) the repeating unit and b) a section of the 1D polymer  $[\{\mathbf{A}\}_3\text{Ag}_4(o\text{-}(\text{NC})_2\text{C}_6\text{H}_4)_2]_n^{4n+}$  (**3**). H atoms are omitted for clarity.

Compared to **1**, the 1D polymer **3** is built up by  $[\{\mathbf{A}\}_3\text{Ag}_4]_n^{4n+}$  units, with the *cyclo*-P<sub>5</sub> ligands being coordinated in a 1,2,3- or in a 1,2,3,4-coordination mode to the silver cations (Figure 5.3). Interestingly, the *cyclo*-P<sub>5</sub> ligand coordinates in an  $\eta^{1:2}$ -coordination mode to one of the Ag cations thus forming a pseudo-tetrahedral environment. Therefore, the strands of five six-membered rings and one large 16-membered ring  $\{\text{P}_{12}\text{Ag}_4\}$  which separate the adjacent six-membered rings within the strand are built. This distinguishes the structural motif of **3** from that of **1**, which exclusively consists of six-membered rings.

In the reaction of **A**,  $\text{AgSbF}_6$  and *m*-(NC)<sub>2</sub>C<sub>6</sub>H<sub>4</sub>, two 2D polymers can be obtained. **4** consists of strands of  $[\{\mathbf{A}\}_2\text{Ag}_2]_n^{2n+}$ , with the *cyclo*-P<sub>5</sub> ligands coordinating in a 1,2,4-coordination mode to Ag atoms (Figure 5.4a). Additionally, all Ag atoms are coordinated by a dinitrile ligand which completes a tetrahedral environment of the Ag atoms. The dinitriles interconnect two adjacent strands and therefore build the 2D polymeric layer (Figure 5.4b). The nearest *cyclo*-P<sub>5</sub> ligands in the strand establish a tubular structure with a narrow diameter of 3.41(3) Å, which prevents the encapsulation of solvent molecules or counter ions (Figure 5.4c).

The other product of the same reaction but of different stoichiometry gives a new 2D architecture  $[\{\mathbf{A}\}\text{Ag}_2(p\text{-}(\text{NC})_2\text{C}_6\text{H}_4)_2]_n^{2n+}$  (**5**), which is also based on similar 1D strands of  $[\{\mathbf{A}\}_2\text{Ag}_4]_n^{4n+}$  as in **2** and has a similar coordination environment of Ag(I) cations (Figure 5.5). However, due to the larger bite angle of the ligand, the coordination of the neighbouring Ag ions via bridging dinitrile

is prohibited. Instead, in **5**, double dinitrile bridges are formed between a pair of silver atoms belonging to the different chains.

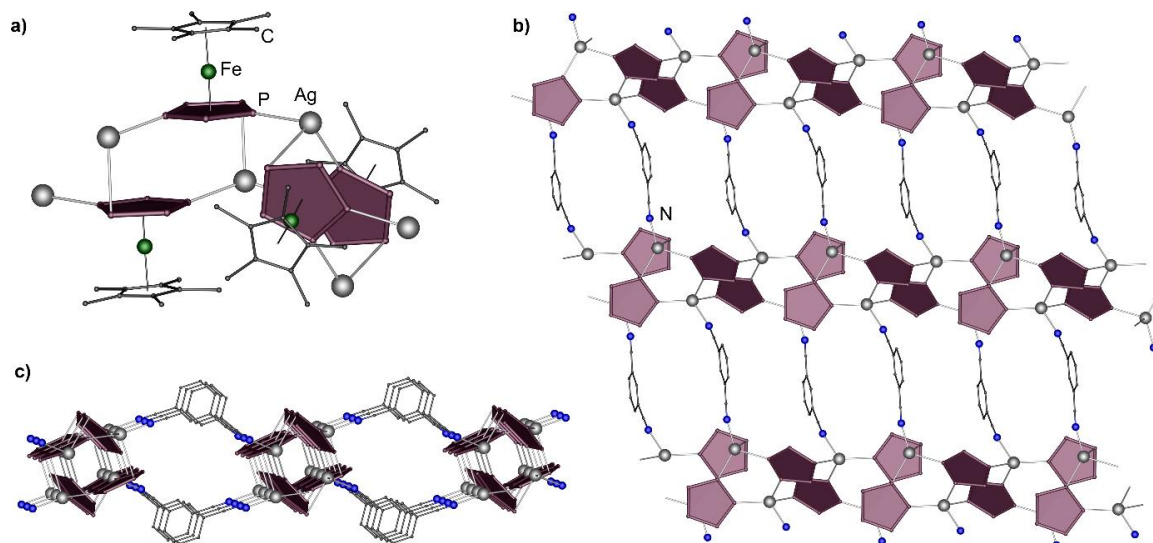


**Figure 5.4.** The 2D cationic network of **4**. a) tetrameric fragment; b) the strands of **4** are interconnected via bridging *m*-(NC)<sub>2</sub>C<sub>6</sub>H<sub>4</sub> ligands, c) tube-like, built up by opposed *cyclo*-P<sub>5</sub> ligands. H atoms are omitted for clarity.

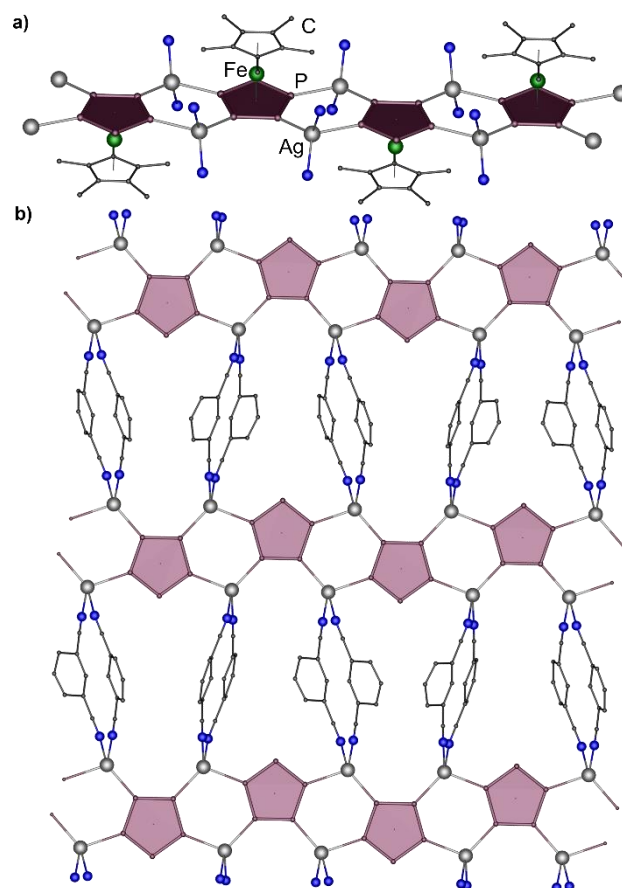


**Figure 5.5.** a) The 1D cationic chain and b) the interconnection through the organic ligand *m*-(NC)<sub>2</sub>C<sub>6</sub>H<sub>4</sub> to form the 2D polymer **5**.

Two 2D polymers of **6a** and **6b** are identical in connectivity and consist of parallel 1D strands  $[\{\mathbf{A}\}\text{Ag}_2]_n^{2n+}$  units with *cyclo*-P<sub>5</sub> ligands coordinating to Ag atoms in a 1,2,3,4-coordination mode, with six-membered rings of {P<sub>4</sub>Ag<sub>2</sub>} being formed (Figure 5.6). All Ag atoms coordinate to a *p*-(NC)<sub>2</sub>C<sub>6</sub>H<sub>4</sub> ligand which leads to trigonally coordinated Ag atoms. The linkers join the 1D strands to a 2D network. Two solvatomorphic modifications are formed in the same crystallization and differ mainly in the solvent portion which, for **6a**, consists of CH<sub>2</sub>Cl<sub>2</sub> solely and, for **6b**, of toluene and CH<sub>2</sub>Cl<sub>2</sub>. This fact and the relative flexibility of the Ag coordination sphere led to a somewhat different geometrical conformation of the resulting layer (cf. Figure 5.6b,c). Interestingly, the  $\pi$ - $\pi$  interactions between the *p*-(NC)<sub>2</sub>C<sub>6</sub>H<sub>4</sub> ligands in the smaller meshes of the layers occur in both modifications featuring interplanar distances of 3.22(3) Å for the major position of the disordered ligands (0.55/0.45) and 3.47(2) Å for the minor one (for **6a**), and 3.356(8) Å for **6b**, in which the rigid dinitrile ligands are ordered. The reason for this disorder can arise from the fact that in **6b** the SbF<sub>6</sub><sup>-</sup> anion occupies each of the neighboring larger meshes, whereas in **6a** two CH<sub>2</sub>Cl<sub>2</sub> molecules are disordered in each mesh, that also causes correlated disordering of the ligands. Further difference between the solvatomorphs can be found in the space formed by slightly corrugated layers, which is in the case of **6a** occupied by disordered SbF<sub>6</sub><sup>-</sup> anions and additional CH<sub>2</sub>Cl<sub>2</sub> solvent molecules. In **6b**, SbF<sub>6</sub><sup>-</sup> anions weakly link and toluene and CH<sub>2</sub>Cl<sub>2</sub> molecules interlay the 2D sheets. There are no significant Cp\*...Cp\* interactions found.

Slight adjustments of the reaction conditions led to a 3D polymer **7** with 1D tubular strands of  $[\{\mathbf{A}\}_2\text{Ag}_2]_n^{2n+}$ , which are connected *via* the aromatic linkers (Figure 5.7). The *cyclo*-P<sub>5</sub> ligands coordinate Ag atoms either in a 1,2,4- or in a 1,3-coordination mode. The coordination environment of the Ag cations is completed tetrahedrally or trigonally by *p*-(NC)<sub>2</sub>C<sub>6</sub>H<sub>4</sub> linkers which interconnect the tubular strands to the 3D network. Thus, the linkers are connected to two either tri- or tetra-coordinated Ag cations of the neighbouring 1D strands.

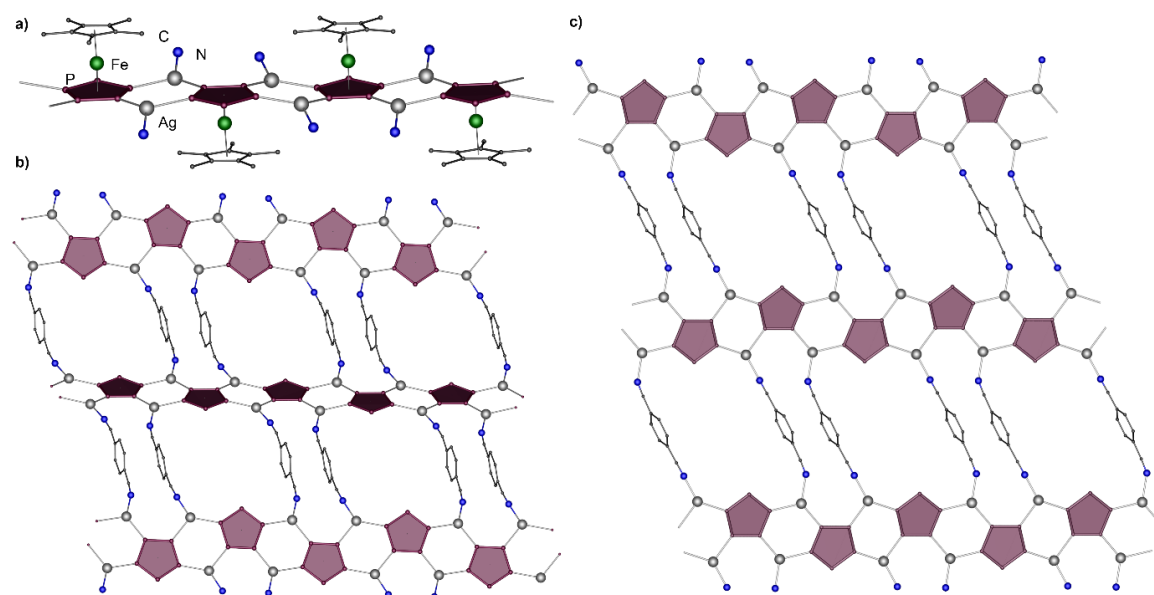


**Figure 5.6.** A section of the cationic 2D polymers **6a** and **6b**: a) a 1D cationic motif of  $[\{A\}Ag_2]_n^{2n+}$ , 1D strands are interconnected by  $p\text{-(NC)}_2\text{C}_6\text{H}_4$  ligands, b) in **6a** and c) **6b**. H atoms are omitted for clarity.

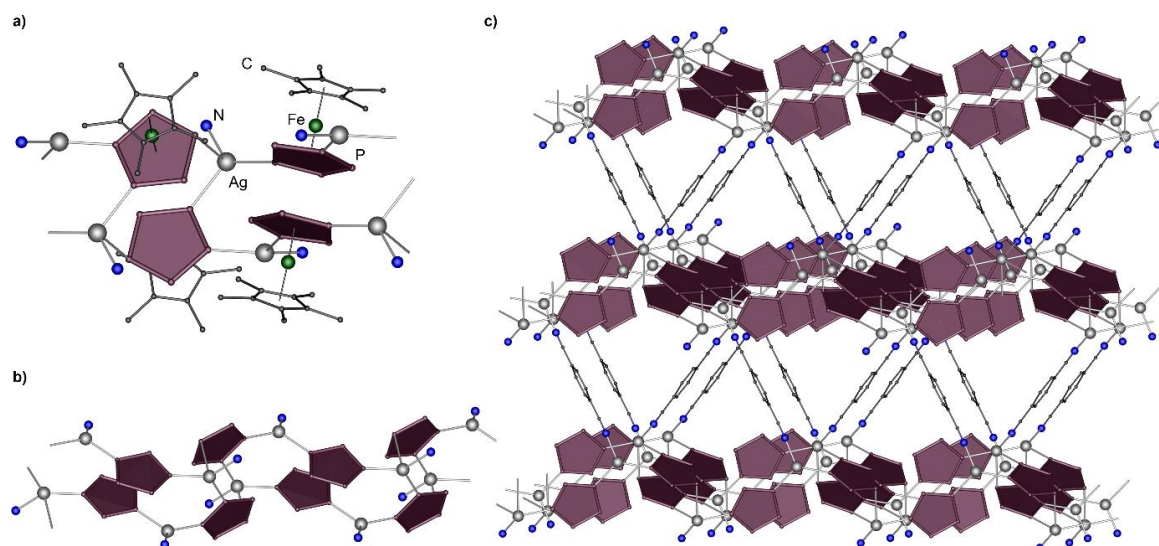
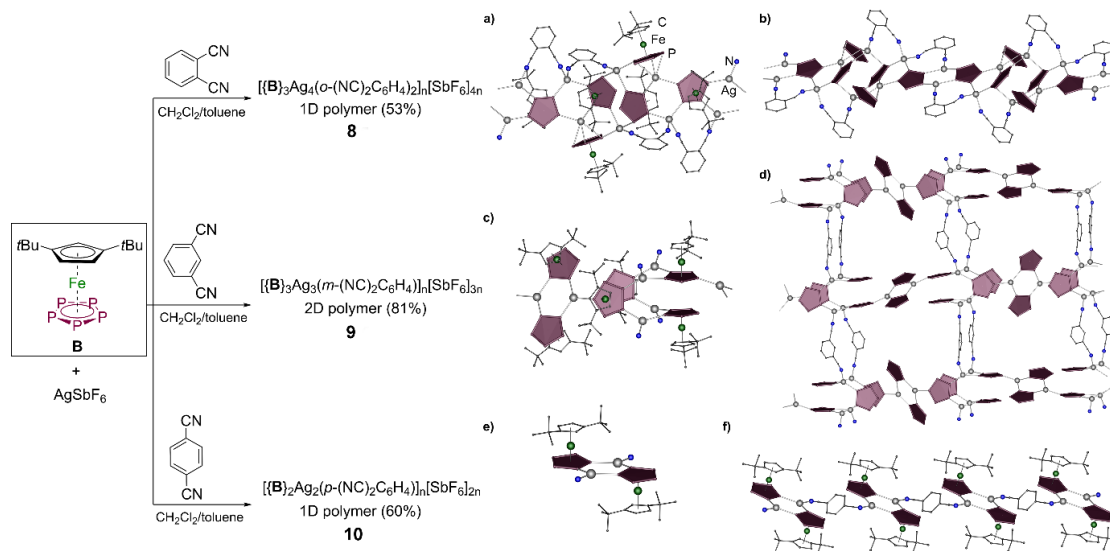


**Figure 5.7.** a) Repeating tetrameric unit of a strand in **7**, b) 1D polymeric motif of  $[\{A\}_2Ag_2]_n^{2n+}$ , c) 3D network in **7**. H atoms are omitted for clarity.

### Three-Component Self-Assembly with $[Cp^*\text{Fe}(\eta^5\text{-P}_5)]$ (**B**)

The manifold results of the three-component self-assembly with **A**,  $\text{AgSbF}_6$  and  $o/m/p\text{-(NC)}_2\text{C}_6\text{H}_4$  raised the question as to whether the steric bulk of the larger **B** would decidedly influence the self-assembly system. For this purpose, a solution of **B** and a five-fold excess of  $o\text{-(NC)}_2\text{C}_6\text{H}_4$  with respect to the bulkier **B** in a 1:2 ratio of toluene/hexane ( $3 \text{ mmol L}^{-1}$ ) was stirred, filtered, and then layered on the mixture of  $\text{CH}_2\text{Cl}_2$  and toluene (2:1) and the already prepared solution of  $\text{AgSbF}_6$  in  $\text{CH}_2\text{Cl}_2$ . This one-pot reaction with the ratio of **B**:2Ag leads to the 1D coordination polymer of  $[\{B\}_3Ag_4(o\text{-(NC)}_2\text{C}_6\text{H}_4)_2]_n[\text{SbF}_6]_{4n}$  (**8**: brown prisms). The only possible way to obtain crystals with  $m\text{-(NC)}_2\text{C}_6\text{H}_4$

is to layer a solution of  $\text{AgSbF}_6$  in  $\text{CH}_2\text{Cl}_2$  with a mixture of  $\text{CH}_2\text{Cl}_2$  and toluene (2:1) as interlayer and afterwards with a solution of **B** in toluene and a 10-fold excess of the dinitrile with respect to **B** which leads to a 2D polymer of  $\{[\text{B}]_3\text{Ag}_3(m\text{-(NC)}_2\text{C}_6\text{H}_4)_n\}[\text{SbF}_6]_{3n}$  (**9**: green plates). Under the same reaction conditions, a 1D polymer of  $\{[\text{B}]_2\text{Ag}_2(p\text{-(NC)}_2\text{C}_6\text{H}_4)_n\}[\text{SbF}_6]_{2n}$  (**10**: green plates) is obtained in the reaction with  $p\text{-(NC)}_2\text{C}_6\text{H}_4$ . In all reactions, colorless crystals of a compound containing only  $\text{AgSbF}_6$  and the respective dinitrile co-crystallize as a byproduct and can be separated manually.



**Scheme 5.2.** One-pot self-assembly reactions of **B**,  $\text{AgSbF}_6$ , and isomers of aromatic  $o\text{-}/m\text{-}/p\text{-(NC)}_2\text{C}_6\text{H}_4$ . Isolated crystalline yields are given in parentheses. a) hexameric repeating unit in **8**, b) cationic 1D polymeric strand; c) hexameric  $\{[\text{B}]_3\text{Ag}_3\}_n^{3n+}$  and d) section of the infinite cationic 2D network in **9**; e)  $\{[\text{B}]_2\text{Ag}_2\}_n^{2n+}$  subunits comprising; f) 1D polymeric structure of **10**. H atoms are omitted for clarity.

The 1D polymeric structure of **8** is severely disordered (see SI for details); the major part consists of  $\{[\text{B}]_3\text{Ag}_4\}_n^{4n+}$  with the *cyclo*- $\text{P}_5$  ligands coordinating to Ag atoms in 1,2,3- or 1,2,3,4-coordination modes (Scheme 5.2a,b). The dinitrile ligands bridge Ag atoms of the strands. There are four different types of Ag atoms in the crystal structure, one is trigonally coordinated to one linker and two *cyclo*- $\text{P}_5$  ligands. The other three are tetrahedrally coordinated; one silver cation coordinates to two different linker molecules and two *cyclo*- $\text{P}_5$  ligands, another to one linker and three *cyclo*- $\text{P}_5$  ligands, whereas one more  $\text{Ag}^+$  binds two *cyclo*- $\text{P}_5$  ligands in a  $\sigma$ -mode and is  $\eta^{1:1:3}$ -coordinated to one more *cyclo*- $\text{P}_5$  ligand.

For the linker  $m\text{-(NC)}_2\text{C}_6\text{H}_4$ , the resulting 2D polymer **9** is built up by 1D strands of repeating units of  $\{[\text{B}]_3\text{Ag}_3\}_n^{3n+}$ . These parallel strands are connected *via* the rigid aromatic linkers to give a double square net (Scheme 5.2c,d). Two *cyclo*- $\text{P}_5$  ligands coordinate in a 1,2-mode to a trigonally coordinated Ag atom and therefore build a six-membered ring of  $\{\text{P}_4\text{Ag}_2\}$ . The remaining four *cyclo*- $\text{P}_5$  ligands build pincer-like 12-membered rings of  $\{\text{P}_8\text{Ag}_4\}$  for steric reasons of accommodating bulky Cp'' ligands in a 2D framework (see SI for detail). Therefore, these seemingly large channels provide in fact only little space within the in-layer cavities for one outer sphere  $\text{SbF}_6^-$  anion per cavity. The

*cyclo*-P<sub>5</sub> ligands in the ring are coordinated in a 1,2,3- or 1,2-coordination mode to an Ag atom in a pseudo-tetrahedral environment. There are no specific interactions between the layers that are interlaid by disordered counter anions and toluene and CH<sub>2</sub>Cl<sub>2</sub> solvent molecules.

The 1D polymer **10** with the linker *p*-(NC)<sub>2</sub>C<sub>6</sub>H<sub>4</sub> is built up by dimeric nodes [**B**]<sub>2</sub>Ag<sub>2</sub>]<sub>n</sub><sup>2n+</sup>, with the *cyclo*-P<sub>5</sub> ligands coordinating to trigonally coordinated Ag atoms and therefore building six-membered rings {P<sub>4</sub>Ag<sub>2</sub>} (Scheme 5.2e,f). Each Ag atom has a coordinated linker which interconnects the dimeric nodes to the 1D polymer.

According to the X-ray diffraction, the polymeric compounds built-up by **B**, AgSbF<sub>6</sub> and the isomers of (NC)<sub>2</sub>C<sub>6</sub>H<sub>4</sub> have a 1D or 2D dimensionality. These polymers **8-10** consist of finite subunits and 1D chains formed by *cyclo*-P<sub>5</sub> building blocks and Ag cations. The nodes consisting of the six-membered rings {P<sub>4</sub>Ag<sub>2</sub>} are interconnected by linear *para* linkers that lead to the formation of a 1D polymeric motif in **10** as expected. The 1D strand formed by P<sub>5</sub> rings and silver cations comprises a backbone of the 1D polymer **8**, in which the *ortho*-dinitrile ligands block all silver cations at the sides of the chain from further coordination. 1D strands can also act as subunits connected with the *meta*-isomer of an aromatic dinitrile to an infinite 2D polymer **9**.

### 5.3 Conclusion

The chosen self-assembly system consisting of [Cp\*Fe(η<sup>5</sup>-P<sub>5</sub>)] (**A**) or [Cp<sup>R</sup>Fe(η<sup>5</sup>-P<sub>5</sub>)] (**B**), AgSbF<sub>6</sub> and *o/m/p*-(NC)<sub>2</sub>C<sub>6</sub>H<sub>4</sub> gives a remarkable insight into the versatility of rigid aromatic dinitriles and the influence of pentaphosphaferrocenes with different steric demands for the obtained coordination products. The required free coordination sites at the Ag cations for the coordination of an N-donor ligand besides the polyphosphorus organometallic building blocks **A** and **B** are predesigned by utilizing the weakly coordinating anion SbF<sub>6</sub><sup>-</sup> of the respective Ag salt. Using the less sterically demanding **A** clearly led to an increased, but less selective number of coordination products (**1-7**), whereas the same reactions with the sterically bulkier **B** are more selective (**8-10**). In the systems containing **A**, various coordination polymers with different dimensionalities of up to 3D (**7**) can be isolated, while, for **B**, the formation of coordination polymers is limited by the formation of maximally 2D assemblies (**9**). This may be assumed to depend on the bulkiness of the Cp<sup>R</sup> ligand as well as on a better solubility of **B**. Besides this, the used dinitrile plays a crucial role in these systems.

A systematic study with these building blocks highlighted the variability of the configurations of the aromatic dinitrile by changing only one component. For *o*-(NC)<sub>2</sub>C<sub>6</sub>H<sub>4</sub>, mostly 1D polymers (**1,3** and **8**) were observed, as the dinitrile molecules themselves chelate the Ag cations of the polymeric arrangements and block their further growth. The only realizable 2D polymer (**2**) was obtained

using **A**, as, due to the increased sterical demand of the Cp<sup>R</sup> ligand **B**, a crosslinking between the 1D strands seems to be hampered. Small 0D subunits that are connected *via* *p*-(NC)<sub>2</sub>C<sub>6</sub>H<sub>4</sub> to give the 1D polymer **10** are also achievable as well as the extended 3D polymeric network **7** introducing a higher sterical demand by using **B** instead of **A**. The structural motifs of **4**, **5** and **9** based on *m*-(NC)<sub>2</sub>C<sub>6</sub>H<sub>4</sub> are similar and composed of 2D polymers with the dinitriles crosslinking the 1D subunits. Interestingly, the 1D strands formed by different pentaphosphaferrocenes consist of a similar motif with parallel slipped *cyclo*-P<sub>5</sub> ligands, but, in the case of **B**, the connectivity sequence is interrupted by a parallel directed *cyclo*-P<sub>5</sub> unit and a trigonal (not tetrahedral) coordination sphere of the adjacent Ag site. The used different isomeric aromatic dinitriles with their different angles between the nitrile-groups still give the three-component self-assembly system enough flexibility within the scope of fixed angles to achieve up to multi-dimensional networks.

These results with rigid dinitriles leading to various polymeric products as well as the previously obtained results with aliphatic flexible dinitriles yielding different 1D/2D/3D polymeric networks and supramolecular networks of host-guest able nodes<sup>[15]</sup> encourage us to use larger and therefore sterically significantly more demanding polyphosphorus complexes as a next step in further restricting the three-component self-assembly system to study factors leading to the formation of host-guest able nodes connected in a supramolecular network.

## 5.4 Experimental Part

### General Remarks

All reactions were performed under an inert atmosphere of dry nitrogen with standard vacuum, Schlenk and glove-box techniques. Solvents were purified, dried, and degassed prior to use by standard procedures. [Cp\*Fe(η<sup>5</sup>-P<sub>5</sub>)]<sup>[17]</sup>, Cp<sup>''</sup>Fe(η<sup>5</sup>-P<sub>5</sub>)]<sup>[18]</sup> were synthesized following reported procedures. Commercially available chemicals (AgSbF<sub>6</sub>, 1,2-Dicyanobenzene, 1,3-Dicyanobenzene, 1,4-Dicyanobenzene) were used without further purification. Solution NMR spectra were recorded on Bruker Avance 300 or 400 spectrometer. The corresponding ESI-MS spectra were acquired on a ThermoQuest Finnigan MAT TSQ 7000 mass spectrometer. CHN Elemental analysis were performed on a Vario El III apparatus.

In all reactions with [Cp\*Fe(η<sup>5</sup>-P<sub>5</sub>)] and AgSbF<sub>6</sub> the co-crystallization of the byproduct [(Cp\*Fe(η<sup>5:2:1</sup>-P<sub>5</sub>))<sub>2</sub>Ag]<sub>n</sub>[SbF<sub>6</sub>]<sub>n</sub><sup>[15]</sup> was observed. All obtained crystal mixtures, were sorted out manually under the microscope by shape, color or at diffractometer by the measurement of the unit cell constants. Due to the insolubility of all products in common solvents, all NMR and ESI-MS measurements were performed with CH<sub>3</sub>CN under destruction of the structure. For all used organic



ligands (1,2-Dicyanobenzene, 1,3-Dicyanobenzene, 1,4-Dicyanobenzene) stock solutions with different concentrations (0.2 M or 0.4M) were prepared in dichloromethane.

#### Analytical data of AgSbF<sub>6</sub> and o/m/p-(NC)<sub>2</sub>C<sub>6</sub>H<sub>4</sub> (I/II/III)

In all following reactions colourless clear crystals of AgSbF<sub>6</sub> with a different amount of o/m/p-(NC)<sub>2</sub>C<sub>6</sub>H<sub>4</sub> (I/II/III) co-crystallize as byproduct.

Analytical data of [Ag<sub>x</sub>(o-(NC)<sub>2</sub>C<sub>6</sub>H<sub>4</sub>)<sub>y</sub>][SbF<sub>6</sub>]<sub>x</sub> (I)

**Yield:** varies seriously

<sup>1</sup>H NMR (CD<sub>3</sub>CN): δ [ppm] = 7.82 (m, C<sub>8</sub>H<sub>4</sub>N<sub>2</sub>), 7.93 (m, C<sub>8</sub>H<sub>4</sub>N<sub>2</sub>)

<sup>19</sup>F NMR (CD<sub>3</sub>CN): no signal was detected.

**Positive ion ESI-MS** (CH<sub>3</sub>CN): *m/z* (%) = 124.91 [Ag(H<sub>2</sub>O)]<sup>+</sup>, 768.93 [Ag<sub>2</sub>(C<sub>8</sub>H<sub>4</sub>N<sub>2</sub>)<sub>4</sub>(CH<sub>3</sub>CN)]<sup>+</sup>

**Negative ion ESI-MS** (CH<sub>3</sub>CN): *m/z* (%) = 234.89 [SbF<sub>6</sub>]<sup>-</sup>.

**Elemental analysis:** Calculated (%) for [(o-(NC)<sub>2</sub>C<sub>6</sub>H<sub>4</sub>)<sub>3</sub>Ag<sub>2</sub>(C<sub>7</sub>H<sub>8</sub>)]<sub>n</sub>[SbF<sub>6</sub>]<sub>2n</sub> (1163.76 g/mol): 31.99 C, 1.73 H, 7.22 N; found: 31.62 C, 2.20 H, 8.00 N.

Analytical data of [Ag<sub>x</sub>(m-(NC)<sub>2</sub>C<sub>6</sub>H<sub>4</sub>)<sub>y</sub>][SbF<sub>6</sub>]<sub>x</sub> (II)

**Yield:** varies seriously

<sup>1</sup>H NMR (CD<sub>3</sub>CN): δ [ppm] = 7.71 (t, C<sub>8</sub>H<sub>4</sub>N<sub>2</sub>), 8.00 (d, C<sub>8</sub>H<sub>4</sub>N<sub>2</sub>), 8.12 (s, C<sub>8</sub>H<sub>4</sub>N<sub>2</sub>)

<sup>19</sup>F NMR (CD<sub>3</sub>CN): δ [ppm] = -123 (m, SbF<sub>6</sub><sup>-</sup>)

**Positive ion ESI-MS** (CH<sub>3</sub>CN): *m/z* (%) = 147.93 [Ag<sub>2</sub>(CH<sub>3</sub>CN)]<sup>2+</sup>, 188.95 [Ag<sub>2</sub>(CH<sub>3</sub>CN)]<sup>+</sup>, 652.56 [Ag<sub>5</sub>(CH<sub>3</sub>CN)<sub>2</sub>O<sub>2</sub>]<sup>+</sup>, 768.98 [Ag<sub>2</sub>(C<sub>8</sub>H<sub>4</sub>N<sub>2</sub>)<sub>4</sub>(CH<sub>3</sub>CN)]<sup>+</sup>, 1112.83 [Ag<sub>4</sub>(C<sub>8</sub>H<sub>4</sub>N<sub>2</sub>)<sub>5</sub>(CH<sub>3</sub>CN)<sub>2</sub>]<sup>+</sup>

**Negative ion ESI-MS** (CH<sub>3</sub>CN): *m/z* (%) = 234.89 [SbF<sub>6</sub>]<sup>-</sup>.

**Elemental analysis:** Calculated (%) for [(m-(NC)<sub>2</sub>C<sub>6</sub>H<sub>4</sub>)<sub>2</sub>Ag(CH<sub>2</sub>Cl<sub>2</sub>)<sub>2</sub>]<sub>n</sub>[SbF<sub>6</sub>]<sub>n</sub> (684.81 g/mol): 29.82 C, 1.47 H, 8.18 N; found: 29.78 C, 1.41 H, 8.18 N.

Analytical data of [Ag<sub>x</sub>(p-(NC)<sub>2</sub>C<sub>6</sub>H<sub>4</sub>)<sub>y</sub>][SbF<sub>6</sub>]<sub>x</sub> (III)

**Yield:** varies seriously

<sup>1</sup>H NMR (CD<sub>3</sub>CN): δ [ppm] = 7.87 (s, C<sub>8</sub>H<sub>4</sub>N<sub>2</sub>).

<sup>19</sup>F NMR (CD<sub>3</sub>CN): δ [ppm] = -123 (m, SbF<sub>6</sub><sup>-</sup>)

**Positive ion ESI-MS** (CH<sub>3</sub>CN): *m/z* (%) = 147.93 [Ag(CH<sub>3</sub>CN)]<sup>+</sup>, 188.95 [Ag(CH<sub>3</sub>CN)<sub>2</sub>]<sup>+</sup>, 229.98 [Ag(CH<sub>3</sub>CN)<sub>3</sub>]<sup>+</sup>, 271.01 [Ag(CH<sub>3</sub>CN)<sub>4</sub>]<sup>+</sup>.

**Negative ion ESI-MS** (CH<sub>3</sub>CN): *m/z* (%) = 234.89 [SbF<sub>6</sub>]<sup>-</sup>.

**Elemental analysis:** Calculated (%) for  $[(p\text{-}(\text{NC})_2\text{C}_6\text{H}_4)_2\text{Ag}(\text{CH}_2\text{Cl}_2)]_n[\text{SbF}_6]_n$  (589.91 g/mol): 29.82 C, 1.74 H, 8.18 N ; found: 28.89 C, 1.60 H, 8.09 N.

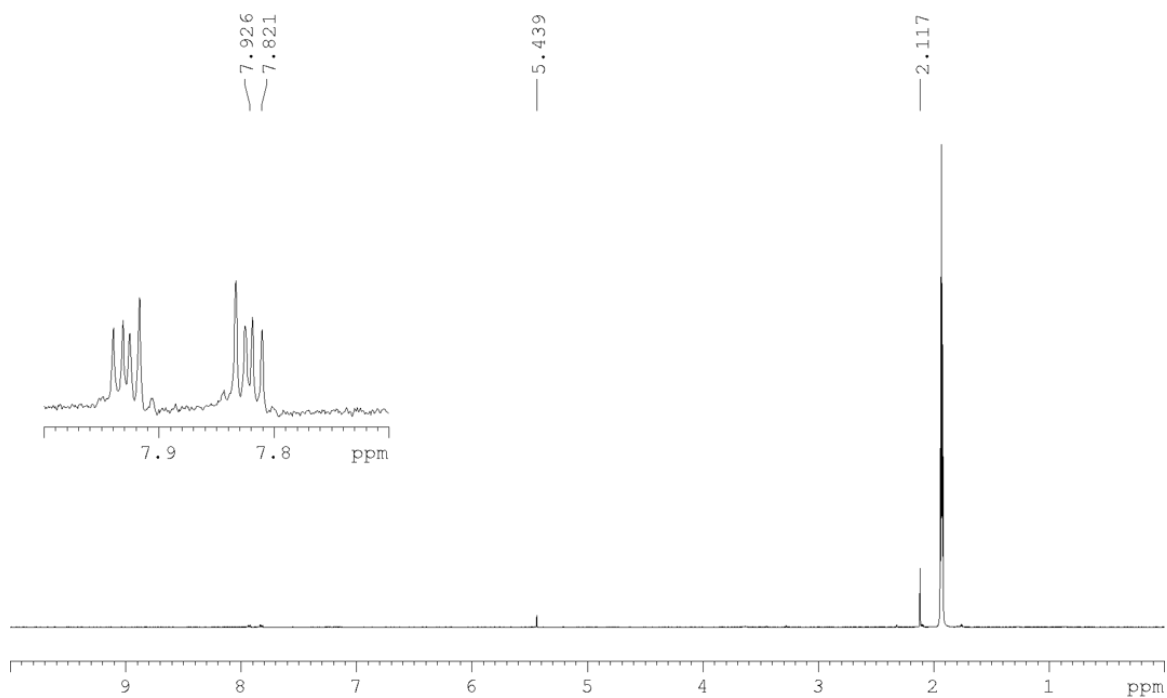


**Figure 5.8.**  $^1\text{H}$  NMR spectrum of I. (1.93  $\text{CH}_3\text{CN}$ , 2.12  $\text{H}_2\text{O}$ , 5.44  $\text{CH}_2\text{Cl}_2$ )

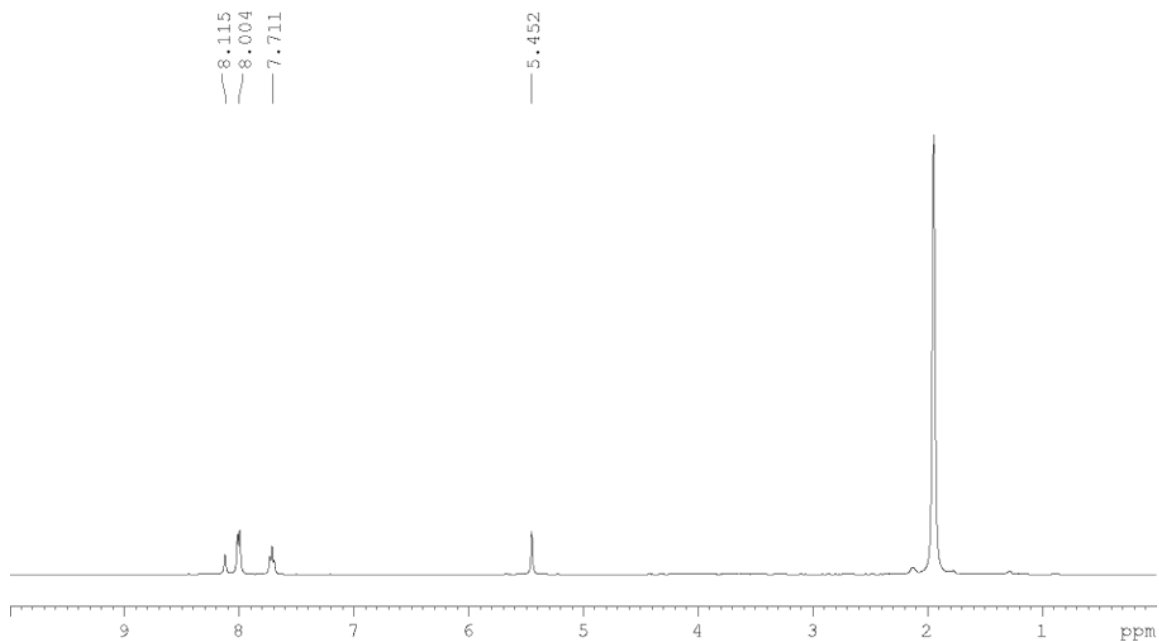


**Figure 5.9.**  $^1\text{H}$  NMR spectrum of II. (1.93  $\text{CH}_3\text{CN}$ , 2.12  $\text{H}_2\text{O}$ , 5.44  $\text{CH}_2\text{Cl}_2$ )

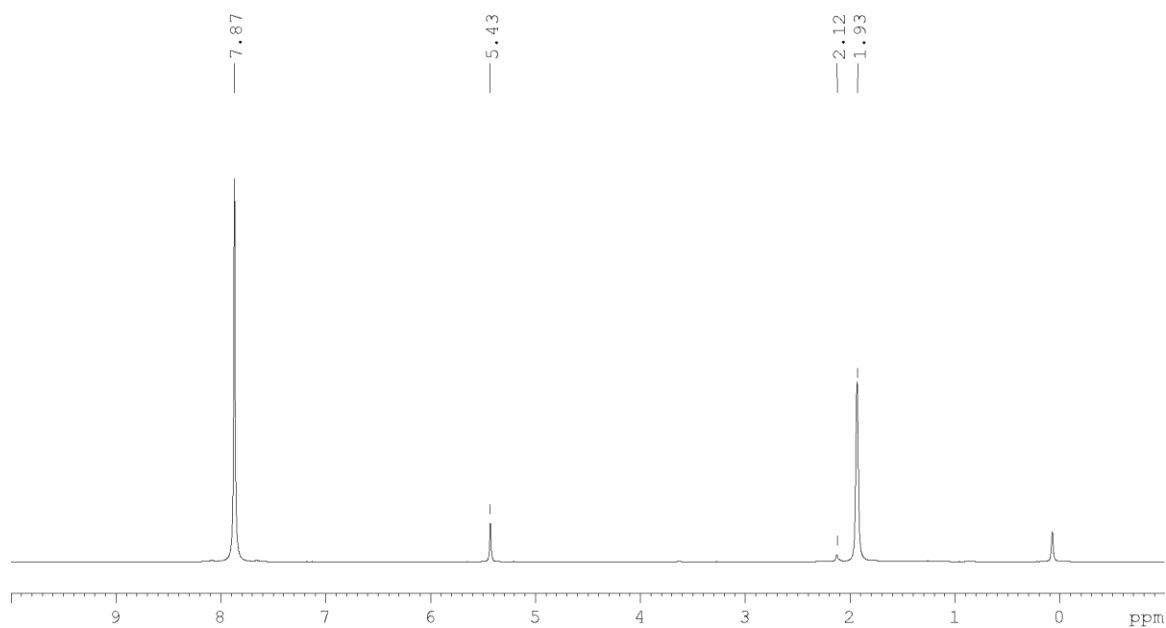


Figure 5.10.  $^1\text{H}$  NMR spectrum of III. (1.93  $\text{CH}_3\text{CN}$ , 2.12  $\text{H}_2\text{O}$ , 5.43  $\text{CH}_2\text{Cl}_2$ )

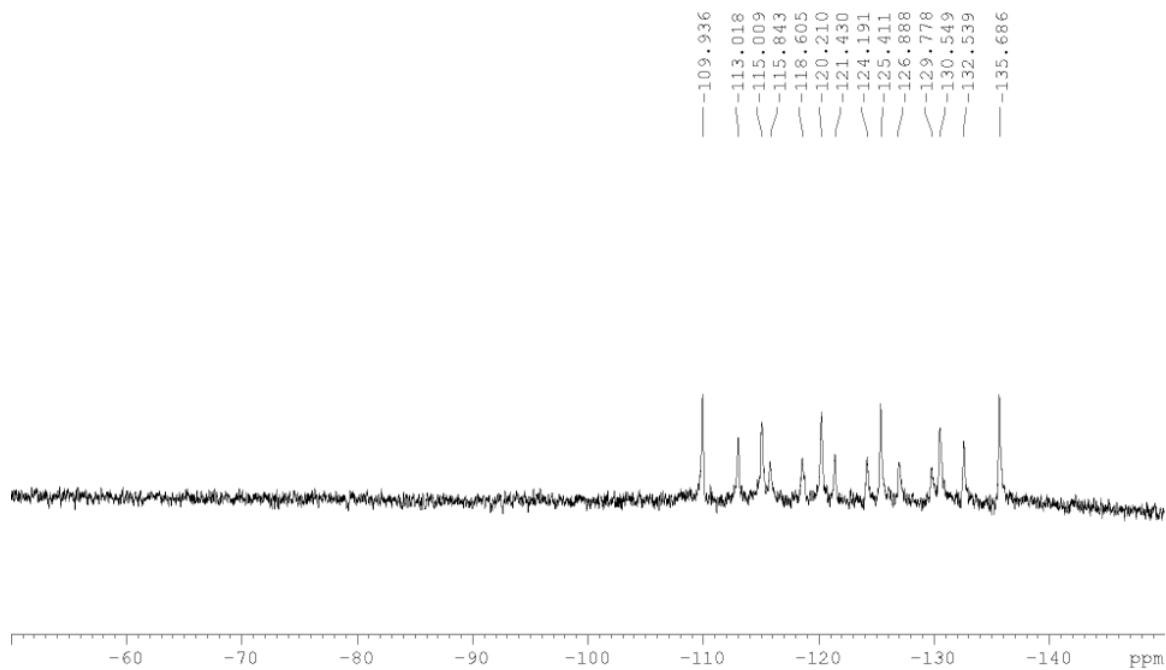


Figure 5.11.  $^{19}\text{F}$  NMR spectrum of II.

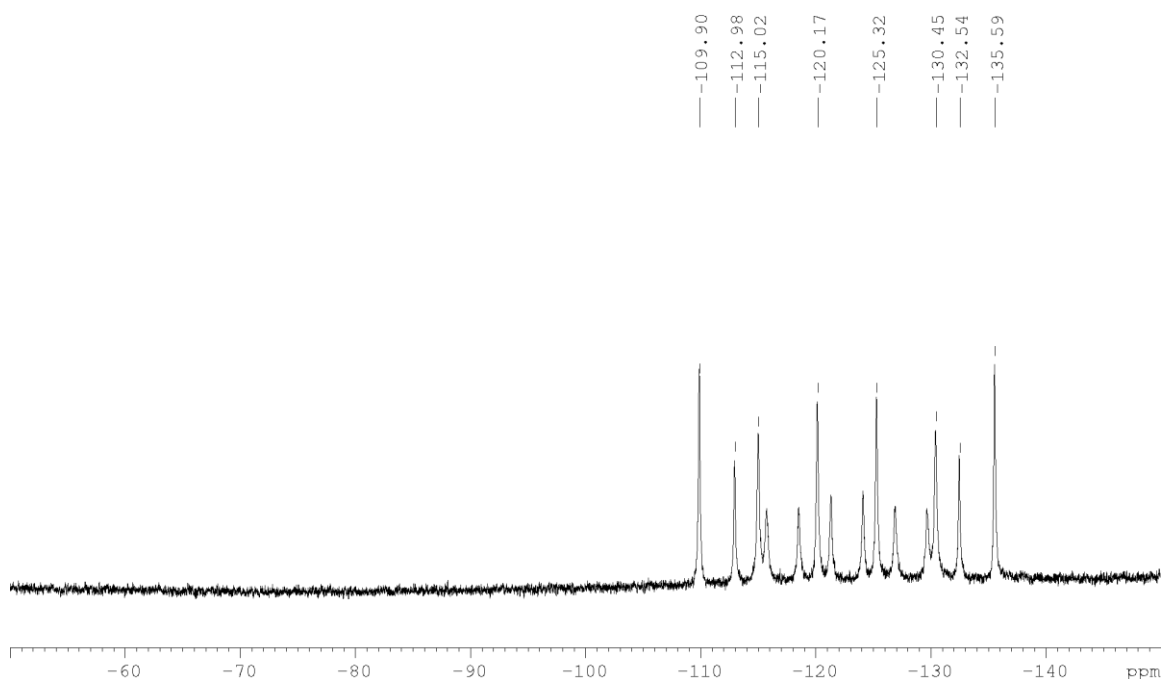


Figure 5.12.  $^{19}\text{F}$  NMR spectrum of III.

Synthesis of  $[\{\text{Cp}^*\text{Fe}(\eta^5\text{-P}_5)\}_2\text{Ag}_3(o\text{-(NC)}_2\text{C}_6\text{H}_4)_2\text{]}_n[\text{SbF}_6]_{3n}$  (**1**),  $[\{\text{Cp}^*\text{Fe}(\eta^5\text{-P}_5)\}_2\text{Ag}_4(o\text{-(NC)}_2\text{C}_6\text{H}_4)_4(\text{C}_7\text{H}_8)_{1.3}(\text{CH}_2\text{Cl}_2)_{0.65}\text{]}_n[\text{SbF}_6]_{4n}$  (**2**) and  $[\{\text{Cp}^*\text{Fe}(\eta^5\text{-P}_5)\}_3\text{Ag}_4(o\text{-(NC)}_2\text{C}_6\text{H}_4)_2\text{]}_n[\text{SbF}_6]_{4n}$  (**3**)

In a Schlenk tube a solution of  $\text{AgSbF}_6$  (28 mg, 0.08 mmol) in  $\text{CH}_2\text{Cl}_2$  (20 mL) is carefully layered first with a solvent mixture of  $\text{CH}_2\text{Cl}_2$ /toluene (5 mL, 2:1) and then with a green solution of  $[\text{Cp}^*\text{Fe}(\eta^5\text{-P}_5)]$  (14 mg, 0.04 mmol) and  $o\text{-(NC)}_2\text{C}_6\text{H}_4$  (1 mL, 0.4 M in  $\text{CH}_2\text{Cl}_2$ ) in toluene (20 mL). After a few hours, the phase boundary turns yellow and after one day, the formation of brown blocks of **1** at the phase boundary, yellow plates of **2** and brown laths of **3** can be observed slightly below the phase boundary. After complete diffusion the colorless mother liquor is decanted, the crystals are washed with hexane ( $3 \times 10$  mL) and dried *in vacuo*. The crystals of **1**, **2** and **3** were separated manually.

Analytical data of **1**

**Yield:** 36 mg (0.0182 mmol, 45% referred to  $[\text{Cp}^*\text{Fe}(\eta^5\text{-P}_5)]$ )

$^1\text{H}$  NMR ( $\text{CD}_3\text{CN}$ ):  $\delta$  [ppm] = 1.45 (s,  $[\text{Cp}^*\text{Fe}(\eta^5\text{-P}_5)]$ ), 7.82 (d,  $o\text{-(NC)}_2\text{C}_6\text{H}_4$ ).

$^{31}\text{P}\{^1\text{H}\}$  NMR ( $\text{CD}_3\text{CN}$ ):  $\delta$  [ppm] = 139.0 (s,  $[\text{Cp}^*\text{Fe}(\eta^5\text{-P}_5)]$ ).

$^{19}\text{F}$  NMR ( $\text{CD}_3\text{CN}$ ):  $\delta$  [ppm] = -126.0 (m,  $\text{SbF}_6$ )

**Positive ion ESI-MS** ( $\text{CH}_3\text{CN}$ ):  $m/z$  (%) = 106.9  $\text{Ag}^+$ , 130.2  $[o\text{-NC}(\text{C}_6\text{H}_4)\text{CN}]^{2+}$ , 147.9  $[\text{Ag}(\text{CH}_3\text{CN})]^+$ , 452.8  $[\{\text{Cp}^*\text{Fe}(\eta^5\text{-P}_5)\}\text{Ag}]^+$ , 493.9  $[\{\text{Cp}^*\text{Fe}(\eta^5\text{-P}_5)\}\text{Ag}(\text{CH}_3\text{CN})]^+$ , 534.9  $[\{\text{Cp}^*\text{Fe}(\eta^5\text{-P}_5)\}\text{Ag}(\text{CH}_3\text{CN})_2]^+$ , 798.7  $[\{\text{Cp}^*\text{Fe}(\eta^5\text{-P}_5)\}_2\text{Ag}]^+$ , 1142.5  $[\{\text{Cp}^*\text{Fe}(\eta^5\text{-P}_5)\}_2\text{Ag}_2(\text{SbF}_6)]^+$ , 1832.3  $[\{\text{Cp}^*\text{Fe}(\eta^5\text{-P}_5)\}_3\text{Ag}_3(\text{SbF}_6)_2]^+$ , 2178.2  $[\{\text{Cp}^*\text{Fe}(\eta^5\text{-P}_5)\}_4\text{Ag}_4(\text{SbF}_6)_2]^+$ .

**Negative ion ESI-MS** (CH<sub>3</sub>CN):  $m/z$  (%) = 234.9 [SbF<sub>6</sub>]<sup>-</sup>.

**Elemental analysis:** Calculated (%) for [{Cp\*Fe(η<sup>5</sup>-P<sub>5</sub>)<sub>2</sub>Ag<sub>3</sub>(*o*-(NC)<sub>2</sub>C<sub>6</sub>H<sub>4</sub>)<sub>2</sub>][SbF<sub>6</sub>]<sub>3</sub> (1978.99 g/mol): 21.85 C, 1.94 H, 2.83 N; found: 22.22 C, 2.11 H, 2.70 N.

Analytical data of **2**

**Yield:** 14 mg (0.0054 mmol, 14% referred to [Cp\*Fe(η<sup>5</sup>-P<sub>5</sub>)])

**<sup>1</sup>H NMR** (CD<sub>3</sub>CN): δ [ppm] = 1.46 (s, [Cp\*Fe(η<sup>5</sup>-P<sub>5</sub>)]), 7.82 (d, *o*-(NC)<sub>2</sub>C<sub>6</sub>H<sub>4</sub>)

**<sup>31</sup>P{<sup>1</sup>H} NMR** (CD<sub>3</sub>CN): δ [ppm] = 137.77 (s, [Cp\*Fe(η<sup>5</sup>-P<sub>5</sub>)]).

**<sup>19</sup>F NMR** (CD<sub>3</sub>CN): δ [ppm] = -126.0 (m, SbF<sub>6</sub>).

**Positive ion ESI-MS** (CH<sub>3</sub>CN):  $m/z$  (%) = 106.9 Ag<sup>+</sup>, 130.2 [*o*-(NC)(C<sub>6</sub>H<sub>4</sub>)CN]<sup>2+</sup>, 147.9 [Ag(CH<sub>3</sub>CN)]<sup>+</sup>, 493.9 [{Cp\*Fe(η<sup>5</sup>-P<sub>5</sub>)}Ag(CH<sub>3</sub>CN)]<sup>+</sup>, 798.7 [{Cp\*Fe(η<sup>5</sup>-P<sub>5</sub>)<sub>2</sub>Ag]<sup>+</sup>, 1142.5 [{Cp\*Fe(η<sup>5</sup>-P<sub>5</sub>)<sub>2</sub>Ag<sub>2</sub>(SbF<sub>6</sub>)]<sup>+</sup>, 1486.3 [{Cp\*Fe(η<sup>5</sup>-P<sub>5</sub>)<sub>2</sub>Ag<sub>3</sub>(SbF<sub>6</sub>)<sub>2</sub>]<sup>+</sup>, 1645.4 Ag<sub>4</sub>(SbF<sub>6</sub>)<sub>3</sub>(*o*-(NC)<sub>2</sub>C<sub>6</sub>H<sub>4</sub>)<sub>3</sub>(CH<sub>3</sub>CN)<sub>3</sub><sup>+</sup>, 1832.3 [{Cp\*Fe(η<sup>5</sup>-P<sub>5</sub>)<sub>3</sub>Ag<sub>3</sub>(SbF<sub>6</sub>)<sub>2</sub>]<sup>+</sup>.

**Negative ion ESI-MS** (CH<sub>3</sub>CN):  $m/z$  (%) = 234.9 [SbF<sub>6</sub>]<sup>-</sup>.

**Elemental analysis:** Calculated (%) for [{Cp\*Fe(η<sup>5</sup>-P<sub>5</sub>)<sub>2</sub>Ag<sub>4</sub>(*o*-(NC)<sub>2</sub>C<sub>6</sub>H<sub>4</sub>)<sub>4</sub>][SbF<sub>6</sub>]<sub>4</sub> (2578.86 g/mol) = 24.22 C, 1.80 H, 4.35 N; found = 24.60 C, 2.17 H, 4.34 N.

Analytical data of **3**

**Yield:** 23 mg (0.0086 mmol, 22% referred to [Cp\*Fe(η<sup>5</sup>-P<sub>5</sub>)])

**<sup>1</sup>H NMR** (CD<sub>3</sub>CN): δ [ppm] = 1.46 (s, [Cp\*Fe(η<sup>5</sup>-P<sub>5</sub>)]), 7.82 (d, *o*-(NC)<sub>2</sub>C<sub>6</sub>H<sub>4</sub>).

**<sup>31</sup>P{<sup>1</sup>H} NMR** (CD<sub>3</sub>CN): δ [ppm] = 136.44 (s, [Cp\*Fe(η<sup>5</sup>-P<sub>5</sub>)]).

**<sup>19</sup>F NMR** (CD<sub>3</sub>CN): δ [ppm] = -126.0 (m, SbF<sub>6</sub>).

**Positive ion ESI-MS** (CH<sub>3</sub>CN):  $m/z$  (%) = 106.9 Ag<sup>+</sup>, 147.9 [Ag(CH<sub>3</sub>CN)]<sup>+</sup>, 452.8 [{Cp\*Fe(η<sup>5</sup>-P<sub>5</sub>)}Ag]<sup>+</sup>, 493.9 [{Cp\*Fe(η<sup>5</sup>-P<sub>5</sub>)}Ag(CH<sub>3</sub>CN)]<sup>+</sup>, 798.7 [{Cp\*Fe(η<sup>5</sup>-P<sub>5</sub>)<sub>2</sub>Ag]<sup>+</sup>, 1142.5 [{Cp\*Fe(η<sup>5</sup>-P<sub>5</sub>)<sub>2</sub>Ag<sub>2</sub>(SbF<sub>6</sub>)]<sup>+</sup>, 1486.3 [{Cp\*Fe(η<sup>5</sup>-P<sub>5</sub>)<sub>2</sub>Ag<sub>3</sub>(SbF<sub>6</sub>)<sub>2</sub>]<sup>+</sup>, 1645.4 Ag<sub>4</sub>(SbF<sub>6</sub>)<sub>3</sub>(*o*-(NC)<sub>2</sub>C<sub>6</sub>H<sub>4</sub>)<sub>3</sub>(CH<sub>3</sub>CN)<sub>3</sub><sup>+</sup>, 1832.3 [{Cp\*Fe(η<sup>5</sup>-P<sub>5</sub>)<sub>3</sub>Ag<sub>3</sub>(SbF<sub>6</sub>)<sub>2</sub>]<sup>+</sup>, 2176.06 [{Cp\*Fe(η<sup>5</sup>-P<sub>5</sub>)<sub>3</sub>Ag<sub>4</sub>(SbF<sub>6</sub>)<sub>3</sub>]<sup>+</sup>, 2521.9 [{Cp\*Fe(η<sup>5</sup>-P<sub>5</sub>)<sub>4</sub>Ag<sub>4</sub>(SbF<sub>6</sub>)<sub>3</sub>]<sup>+</sup>.

**Negative ion ESI-MS** (CH<sub>3</sub>CN):  $m/z$  (%) = 234.9 [SbF<sub>6</sub>]<sup>-</sup>.

**Elemental analysis:** Calculated (%) for [{Cp\*Fe(η<sup>5</sup>-P<sub>5</sub>)<sub>3</sub>Ag<sub>4</sub>(*o*-(NC)<sub>2</sub>C<sub>6</sub>H<sub>4</sub>)<sub>2</sub>][SbF<sub>6</sub>]<sub>4</sub> (2668.55 g/mol): 20.70 C, 2.00 H, 2.10 N; found: 21.44 C, 2.55 H, 2.08 N.

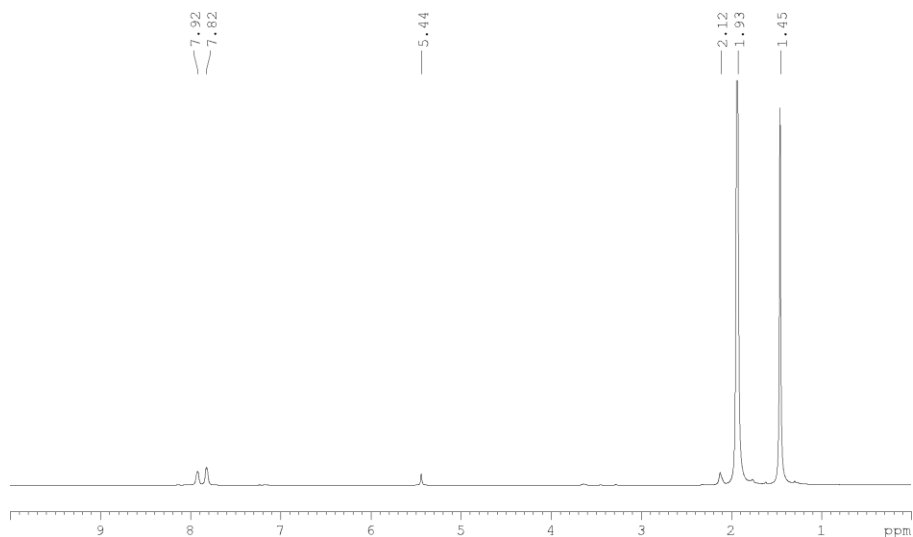


Figure 5.13.  $^1\text{H}$  NMR spectrum of **1**. (1.93  $\text{CH}_3\text{CN}$ , 2.12  $\text{H}_2\text{O}$ , 5.44  $\text{CH}_2\text{Cl}_2$ )

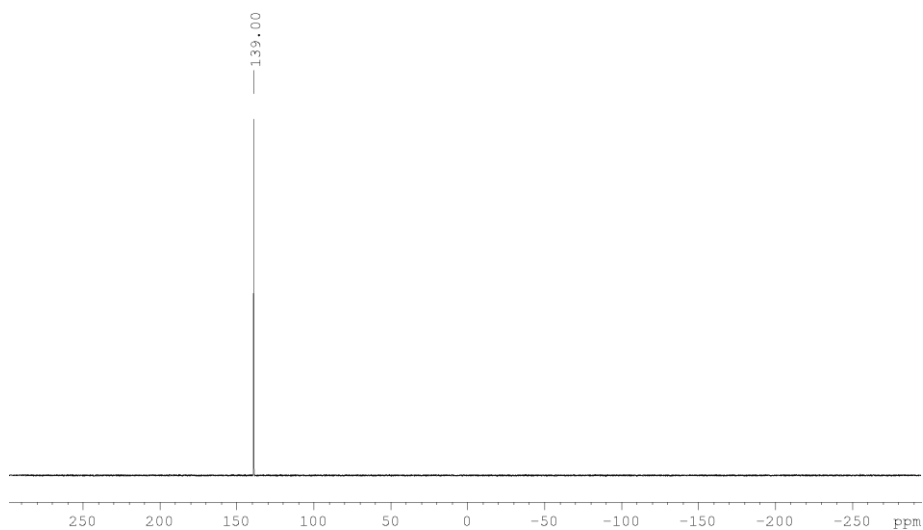


Figure 5.14.  $^{31}\text{P}\{^1\text{H}\}$  NMR spectrum of **1**.

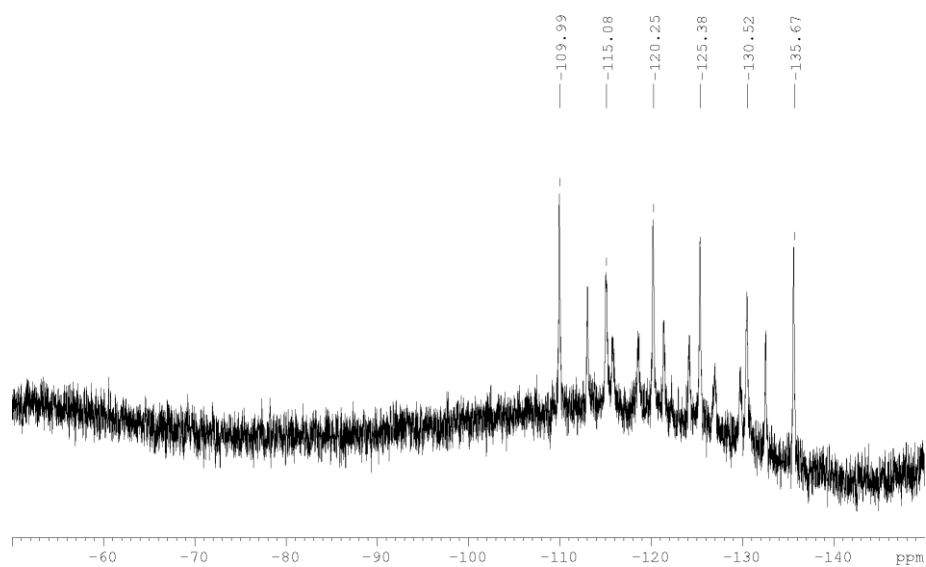


Figure 5.15.  $^{19}\text{F}$  NMR spectrum of **1**.

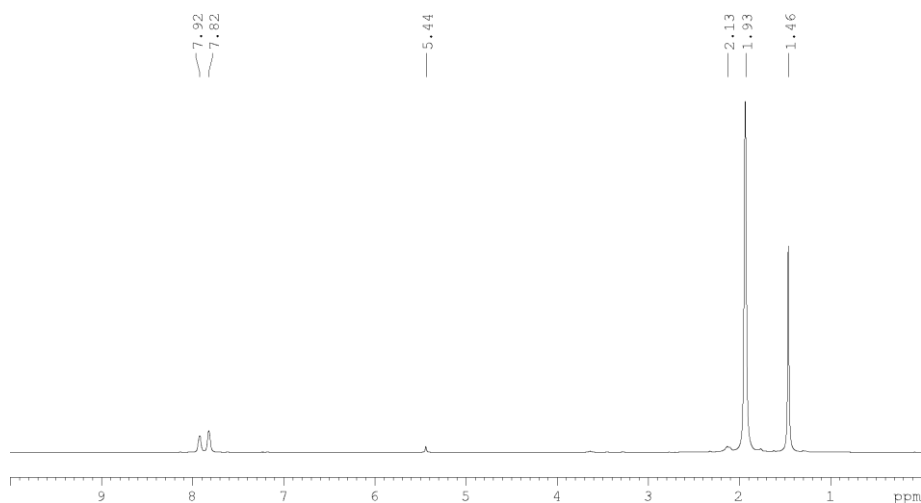


Figure 5.16.  $^1\text{H}$  NMR spectrum of **2** (1.93  $\text{CH}_3\text{CN}$ , 2.13  $\text{H}_2\text{O}$ , 5.44  $\text{CH}_2\text{Cl}_2$ )

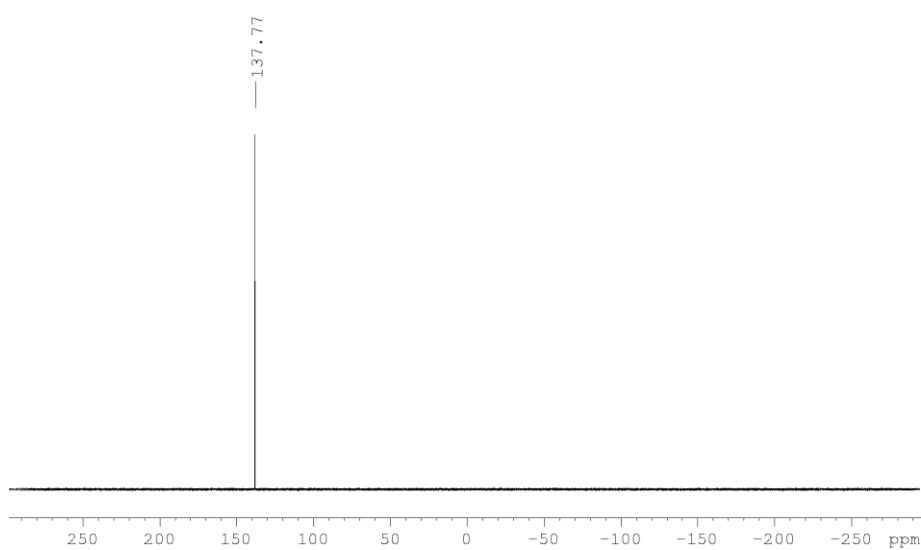


Figure 5.17.  $^{31}\text{P}\{^1\text{H}\}$  NMR spectrum of **2**.

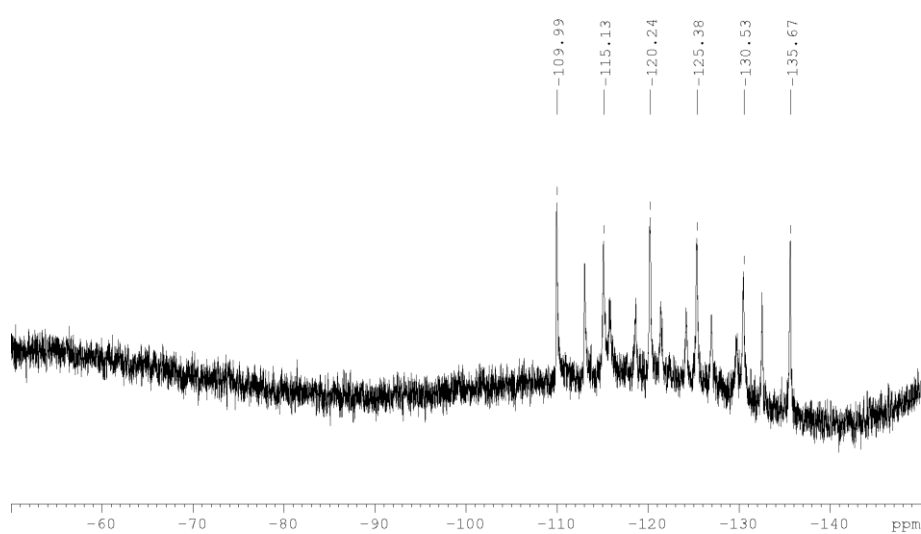


Figure 5.18.  $^{19}\text{F}$  NMR spectrum of **2**.

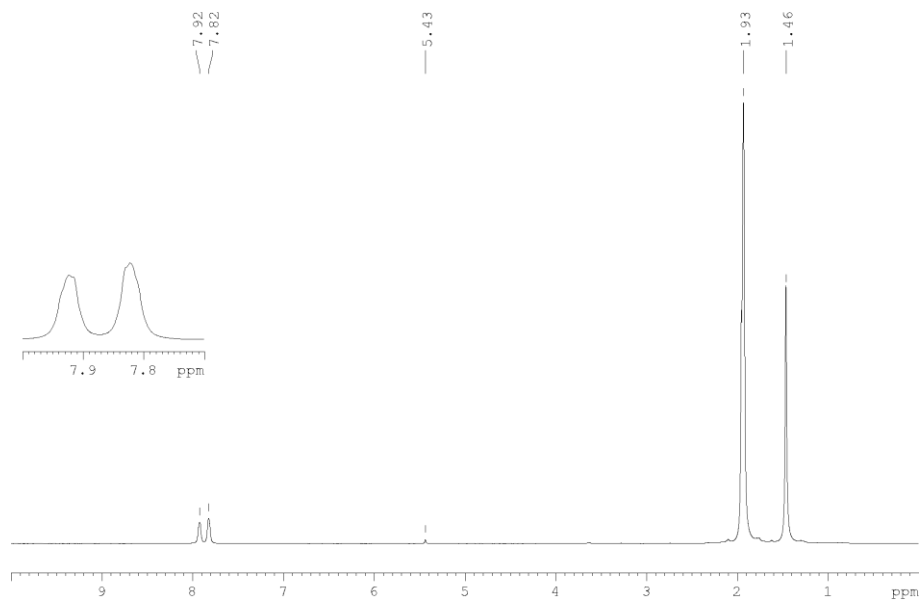


Figure 5.19.  $^1\text{H}$  NMR spectrum of **3**. (1.93  $\text{CH}_3\text{CN}$ , 5.43  $\text{CH}_2\text{Cl}_2$ ).

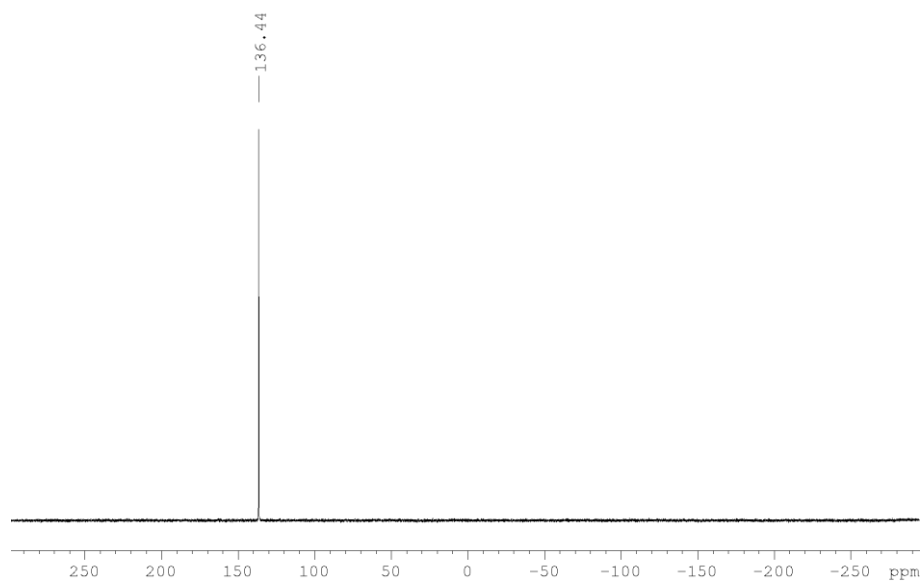


Figure 5.20.  $^{31}\text{P}\{^1\text{H}\}$  NMR spectrum of **3**.



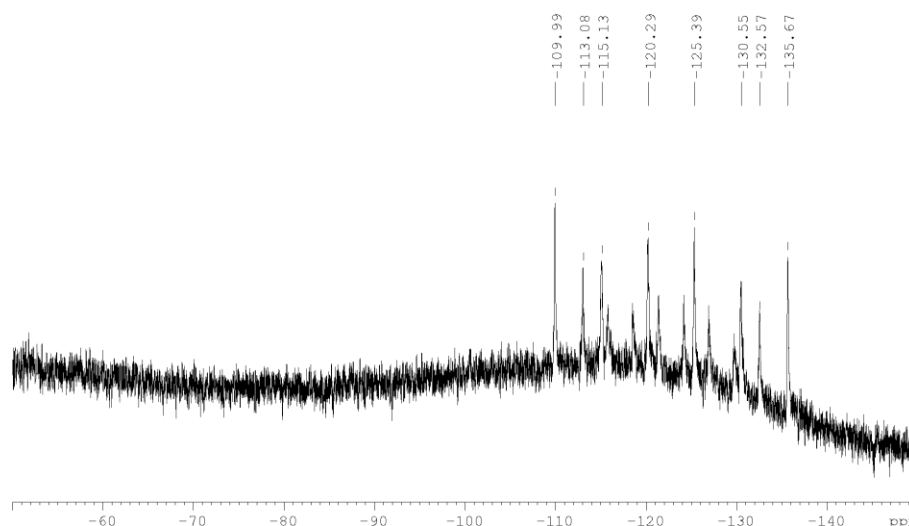


Figure 5.21.  $^{19}\text{F}$  NMR spectrum of **3**.

**Synthesis of  $[\{\text{Cp}^*\text{Fe}(\eta^5\text{-P}_5)\}_2\text{Ag}_2(m\text{-}(\text{NC})_2\text{C}_6\text{H}_4)(\text{C}_7\text{H}_8)_{0.5}(\text{CH}_2\text{Cl}_2)_{0.5}]_n[\text{SbF}_6]_{2n}$  (**4**) and  $[\{\text{Cp}^*\text{Fe}(\eta^5\text{-P}_5)\}_2\text{Ag}_2(m\text{-}(\text{NC})_2\text{C}_6\text{H}_4)(\text{C}_7\text{H}_8)_{0.5}(\text{CH}_2\text{Cl}_2)_{0.85}]_n[\text{SbF}_6]_{2n}$  (**5**)**

In a Schlenk tube a solution of  $\text{AgSbF}_6$  (28 mg, 0.08 mmol) in  $\text{CH}_2\text{Cl}_2$  (20 mL) is carefully layered first with a solvent mixture of  $\text{CH}_2\text{Cl}_2$ /toluene (5 mL, 2:1) and then with a green solution of  $[\text{Cp}^*\text{Fe}(\eta^5\text{-P}_5)]$  (14 mg, 0.04 mmol) and  $m\text{-}(\text{NC})_2\text{C}_6\text{H}_4$  (1 mL, 0.4 M in  $\text{CH}_2\text{Cl}_2$ ) in toluene (20 mL). After few hours, the phase boundary turns yellow and after one day, the formation of yellow plates of **4** and brown lath of **5** at the phase boundary can be observed. After complete diffusion the colorless mother liquor is decanted, the crystals are washed with hexane ( $3 \times 10$  mL) and dried *in vacuo*. The products can be separated manually.

Analytical data of **4**

**Yield:** 43 mg (0.0269 mmol, 67% referred to  $[\text{Cp}^*\text{Fe}(\eta^5\text{-P}_5)]$ )

$^1\text{H}$  NMR ( $\text{CD}_3\text{CN}$ ):  $\delta$  [ppm] = 1.46 (s,  $[\text{Cp}^*\text{Fe}(\eta^5\text{-P}_5)]$ ), 7.70 (t,  $m\text{-}(\text{NC})_2\text{C}_6\text{H}_4$ ), 7.98 (d,  $m\text{-}(\text{NC})_2\text{C}_6\text{H}_4$ ), 8.00 (s,  $m\text{-}(\text{NC})_2\text{C}_6\text{H}_4$ ).

$^{31}\text{P}\{^1\text{H}\}$  NMR ( $\text{CD}_3\text{CN}$ ):  $\delta$  [ppm] = 139.14 (s,  $[\text{Cp}^*\text{Fe}(\eta^5\text{-P}_5)]$ ).

$^{19}\text{F}$  NMR ( $\text{CD}_3\text{CN}$ ):  $\delta$  [ppm] = -125.36 (m,  $\text{SbF}_6$ ).

**Positive ion ESI-MS** ( $\text{CH}_3\text{CN}$ ):  $m/z$  (%) = 106.9  $\text{Ag}^+$ , 130.2  $[m\text{-}(\text{NC})_2\text{C}_6\text{H}_4\text{CN}]^{2+}$ , 147.9  $[\text{Ag}(\text{CH}_3\text{CN})]^+$ , 452.8  $[\{\text{Cp}^*\text{Fe}(\eta^5\text{-P}_5)\}_2\text{Ag}]^+$ , 493.9  $[\{\text{Cp}^*\text{Fe}(\eta^5\text{-P}_5)\}_2\text{Ag}(\text{CH}_3\text{CN})]^+$ , 534.9  $[\{\text{Cp}^*\text{Fe}(\eta^5\text{-P}_5)\}_2\text{Ag}(\text{CH}_3\text{CN})_2]^+$ , 798.7  $[\{\text{Cp}^*\text{Fe}(\eta^5\text{-P}_5)\}_2\text{Ag}]^+$ , 1142.5  $[\{\text{Cp}^*\text{Fe}(\eta^5\text{-P}_5)\}_2\text{Ag}_2(\text{SbF}_6)]^+$ , 1832.3  $[\{\text{Cp}^*\text{Fe}(\eta^5\text{-P}_5)\}_3\text{Ag}_3(\text{SbF}_6)_2]^+$ , 2180.2  $[\{\text{Cp}^*\text{Fe}(\eta^5\text{-P}_5)\}_5\text{Ag}_2(\text{SbF}_6)]^+$ , 2303.1  $[\{\text{Cp}^*\text{Fe}(\eta^5\text{-P}_5)\}_3\text{Ag}_4(\text{SbF}_6)_3(m\text{-}(\text{NC})_2\text{C}_6\text{H}_4)]^+$ , 2521.9  $[\{\text{Cp}^*\text{Fe}(\eta^5\text{-P}_5)\}_4\text{Ag}_4(\text{SbF}_6)_3]^+$ .

**Negative ion ESI-MS**( $\text{CH}_3\text{CN}$ ):  $m/z$  (%) = 234.9  $[\text{SbF}_6]^-$ .

**Elemental analysis:** Calculated (%) for  $\{[\text{Cp}^*\text{Fe}(\eta^5\text{-P}_5)]_2\text{Ag}_2(m\text{-(NC)}_2\text{C}_6\text{H}_4)(\text{C}_7\text{H}_8)_{0.5}(\text{CH}_2\text{Cl}_2)_{0.5}\}[\text{SbF}_6]_2$  (1595.7805 g/mol): 24.09 C, 2.46 H, 1.76 N; found: 23.84 C, 2.59 H, 2.23 N.

Analytical data of **5**

**Yield:** 11 mg (0.0075 mmol, 19 % referred to  $[\text{Cp}^*\text{Fe}(\eta^5\text{-P}_5)]$ )

$^1\text{H NMR}$  ( $\text{CD}_3\text{CN}$ ):  $\delta$  [ppm] = 1.45 (s,  $[\text{Cp}^*\text{Fe}(\eta^5\text{-P}_5)]$ ), 7.70 (t,  $m\text{-(NC)}_2\text{C}_6\text{H}_4$ ), 7.98 (d,  $m\text{-(NC)}_2\text{C}_6\text{H}_4$ ), 8.11 (s,  $m\text{-(NC)}_2\text{C}_6\text{H}_4$ ).

$^{31}\text{P}\{^1\text{H}\}$  NMR ( $\text{CD}_3\text{CN}$ ):  $\delta$  [ppm] = 138.93 (s,  $[\text{Cp}^*\text{Fe}(\eta^5\text{-P}_5)]$ ).

$^{19}\text{F}$  NMR ( $\text{CD}_3\text{CN}$ ):  $\delta$  [ppm] = -125.37 (m,  $\text{SbF}_6$ ).

**Positive ion ESI-MS** ( $\text{CH}_3\text{CN}$ ):  $m/z$  (%) = 106.9  $\text{Ag}^+$ , 130.2  $[m\text{-NC}(\text{C}_6\text{H}_4)\text{CN}]^{2+}$ , 452.8  $[\{\text{Cp}^*\text{Fe}(\eta^5\text{-P}_5)\}\text{Ag}]^+$ , 493.9  $[\{\text{Cp}^*\text{Fe}(\eta^5\text{-P}_5)\}\text{Ag}(\text{CH}_3\text{CN})]^+$ , 534.9  $[\{\text{Cp}^*\text{Fe}(\eta^5\text{-P}_5)\}\text{Ag}(\text{CH}_3\text{CN})_2]^+$ , 798.7  $[\{\text{Cp}^*\text{Fe}(\eta^5\text{-P}_5)\}_2\text{Ag}]^+$ , 1142.5  $[\{\text{Cp}^*\text{Fe}(\eta^5\text{-P}_5)\}_2\text{Ag}_2(\text{SbF}_6)]^+$ , 1486.3  $[\{\text{Cp}^*\text{Fe}(\eta^5\text{-P}_5)\}_2\text{Ag}_3(\text{SbF}_6)_2]^+$ , 1645.4  $\text{Ag}_4(\text{SbF}_6)_3(m\text{-(NC)}_2\text{C}_6\text{H}_4)_3(\text{CH}_3\text{CN})_3]^+$ , 1832.3  $[\{\text{Cp}^*\text{Fe}(\eta^5\text{-P}_5)\}_3\text{Ag}_3(\text{SbF}_6)_2]^+$ , 2178.2  $[\{\text{Cp}^*\text{Fe}(\eta^5\text{-P}_5)\}_4\text{Ag}_3(\text{SbF}_6)_2]^+$ , 2303.1  $[\{\text{Cp}^*\text{Fe}(\eta^5\text{-P}_5)\}_3\text{Ag}_4(\text{SbF}_6)_3(m\text{-(NC)}_2\text{C}_6\text{H}_4)]^+$ .

**Negative ion ESI-MS** ( $\text{CH}_3\text{CN}$ ):  $m/z$  (%) = 234.9  $[\text{SbF}_6]^-$ .

**Elemental analysis:** Calculated (%) for  $\{[\text{Cp}^*\text{Fe}(\eta^5\text{-P}_5)]_2\text{Ag}_2(m\text{-(NC)}_2\text{C}_6\text{H}_4)_2(\text{C}_7\text{H}_8)(\text{CH}_2\text{Cl}_2)\}[\text{SbF}_6]_2$  (1466.51 g/mol): C 27.85, H 2.27, N 3.82; found: C 27.62, H 2.48, N 3.71.

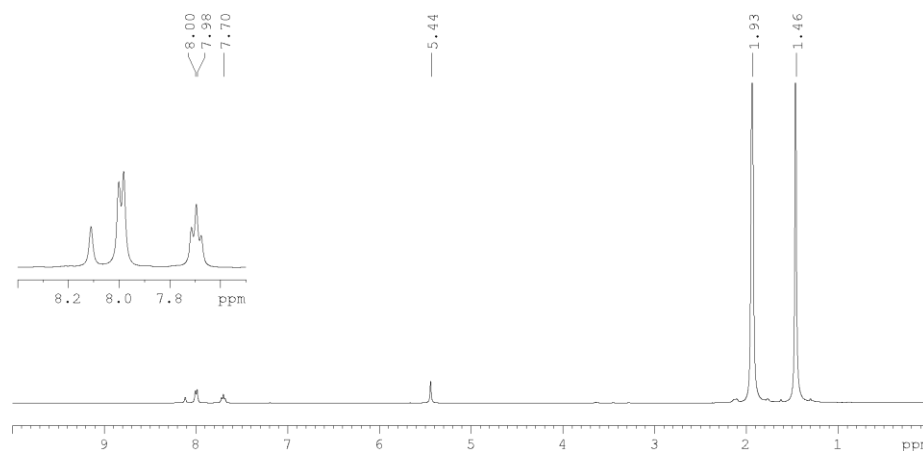


**Figure 5.22.**  $^1\text{H NMR}$  spectrum of **4**. (1.93  $\text{CH}_3\text{CN}$ , 5.44  $\text{CH}_2\text{Cl}_2$ )

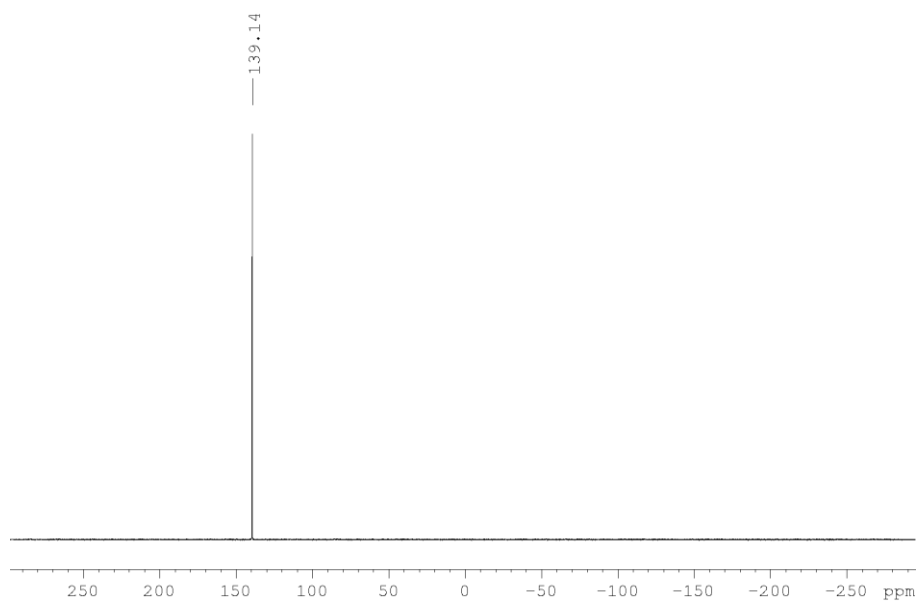


Figure 5.23.  $^{31}\text{P}\{^1\text{H}\}$  NMR spectrum of 4.

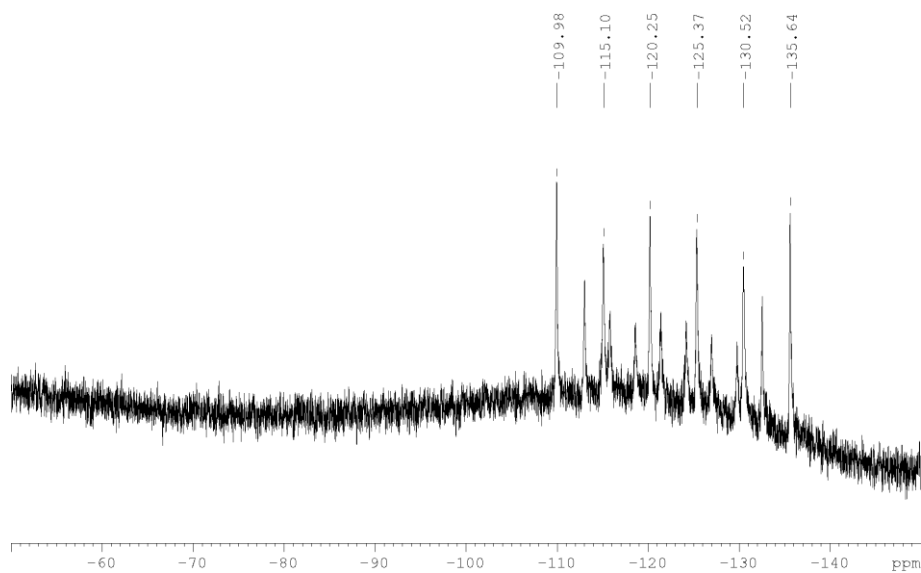


Figure 5.24.  $^{19}\text{F}$  NMR spectrum of 4.

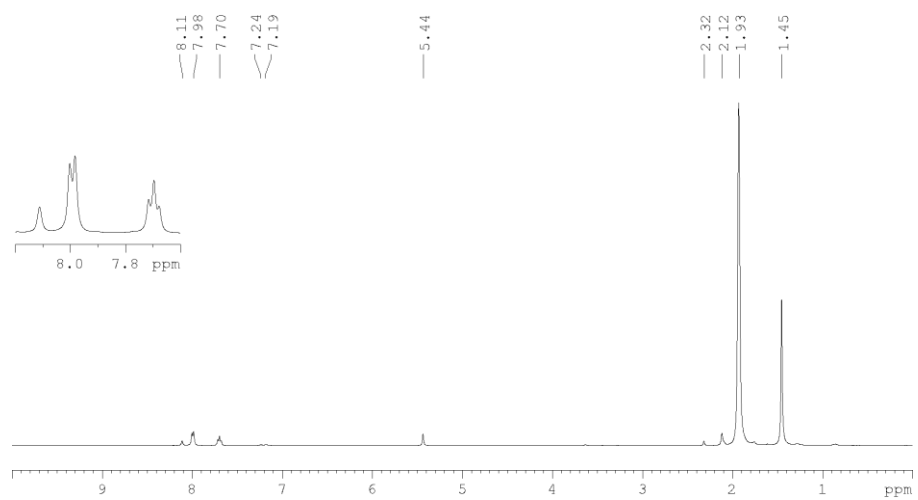


Figure 5.25.  $^1\text{H}$  NMR spectrum of 5 (1.93  $\text{CH}_3\text{CN}$ , 2.12  $\text{H}_2\text{O}$ , 2.32 Toluene, 5.44  $\text{CH}_2\text{Cl}_2$ , 7.19-7.24 Toluene).

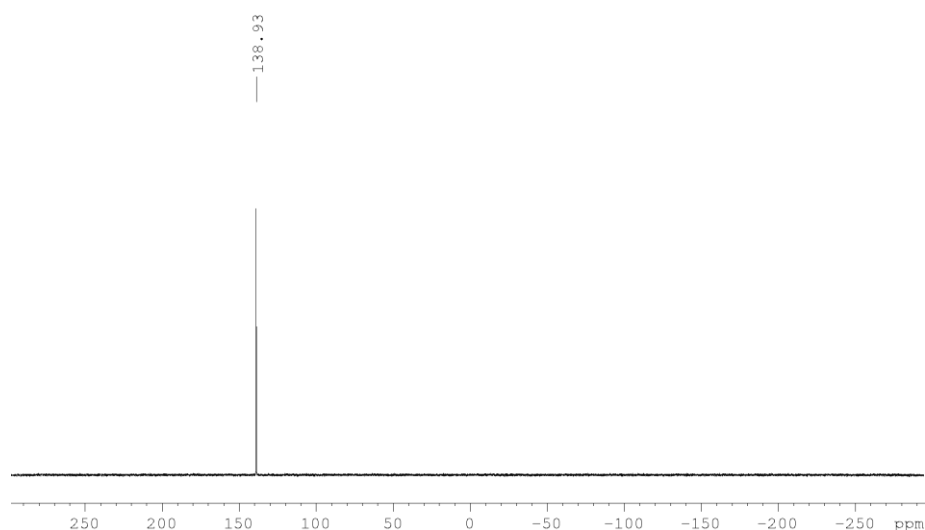


Figure 5.26.  $^{31}\text{P}\{^1\text{H}\}$  NMR spectrum of **5**.

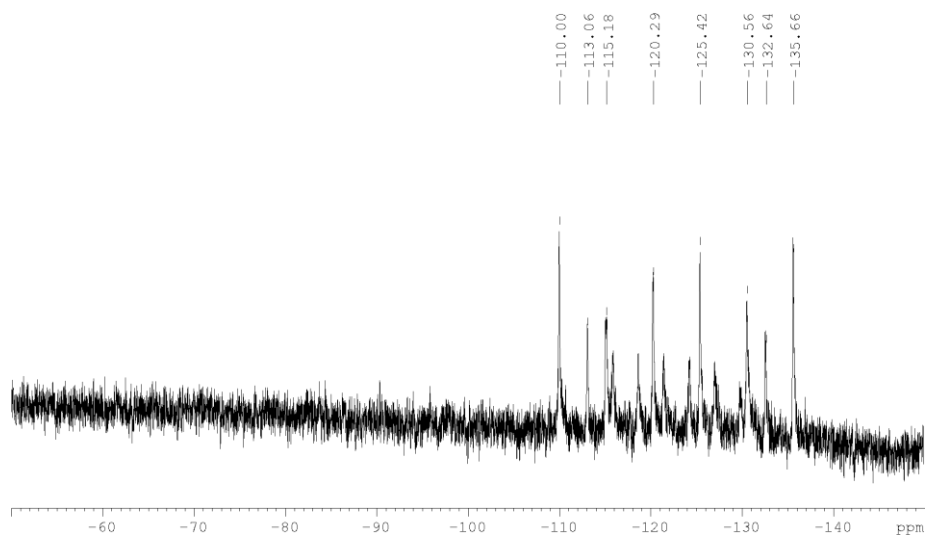


Figure 5.27.  $^{19}\text{F}$  NMR spectrum of **5**.

### Synthesis of $[\{\text{Cp}^*\text{Fe}(\eta^5\text{-P}_5)\}\text{Ag}_2(p\text{-(NC)}_2\text{C}_6\text{H}_4)]_n[\text{SbF}_6]_{2n}$ (**6a**) and $[\{\text{Cp}^*\text{Fe}(\eta^5\text{-P}_5)\}\text{Ag}_2(p\text{-(NC)}_2\text{C}_6\text{H}_4)(\text{C}_7\text{H}_8)_{0.7}(\text{CH}_2\text{Cl}_2)_{0.3}]_n[\text{SbF}_6]_{2n}$ (**6b**)

In a Schlenk tube a solution of  $\text{AgSbF}_6$  (28 mg, 0.04 mmol) in  $\text{CH}_2\text{Cl}_2$  (10 mL) is carefully layered first with a solvent mixture of  $\text{CH}_2\text{Cl}_2$ /toluene (3 mL, 2:1) and then with a green solution of  $[\text{Cp}^*\text{Fe}(\eta^5\text{-P}_5)]$  (14 mg, 0.04 mmol) and  $p\text{-(NC)}_2\text{C}_6\text{H}_4$  (1 mL, 0.2 M in DCM) in toluene (10 mL). After few hours, the phase boundary turns yellow and after one day, the formation of brown blocks of **6a** at the phase boundary can be observed. After complete diffusion yellow needles of **6b** can be found in the bottom of the Schlenk tube. The colourless mother liquor is decanted, the crystals are washed with hexane ( $3 \times 10$  mL) and dried *in vacuo*. The crystals were sorted manually.

Analytical data of **6a**

**Yield:** 22 mg (0.018 mmol, 45% referred to [Cp\*Fe( $\eta^5$ -P<sub>5</sub>)])

**<sup>1</sup>H NMR** (CD<sub>3</sub>CN):  $\delta$  [ppm] = 1.46 (s, [Cp\*Fe( $\eta^5$ -P<sub>5</sub>)]), 7.88 (s, *p*-(NC)<sub>2</sub>C<sub>6</sub>H<sub>4</sub>).

**<sup>31</sup>P{<sup>1</sup>H} NMR** (CD<sub>3</sub>CN):  $\delta$  [ppm] = 136.78 (s, [Cp\*Fe( $\eta^5$ -P<sub>5</sub>)]).

**<sup>19</sup>F NMR** (CD<sub>3</sub>CN):  $\delta$  [ppm] = -125.37 (m, SbF<sub>6</sub>).

**Positive ion ESI-MS** (CH<sub>3</sub>CN): *m/z* (%) = 106.9 Ag<sup>+</sup>, 147.9 [Ag(CH<sub>3</sub>CN)]<sup>+</sup>, 188.9 [Ag(CH<sub>3</sub>CN)<sub>2</sub>]<sup>+</sup>, 452.8 [Cp\*Fe( $\eta^5$ -P<sub>5</sub>)]Ag<sup>+</sup>, 493.9 [Cp\*Fe( $\eta^5$ -P<sub>5</sub>)]Ag(CH<sub>3</sub>CN)<sup>+</sup>, 534.9 [Cp\*Fe( $\eta^5$ -P<sub>5</sub>)]Ag(CH<sub>3</sub>CN)<sub>2</sub><sup>+</sup>, 798.7 [Cp\*Fe( $\eta^5$ -P<sub>5</sub>)<sub>2</sub>Ag]<sup>+</sup>, 1142.5 [Cp\*Fe( $\eta^5$ -P<sub>5</sub>)<sub>2</sub>Ag<sub>2</sub>(SbF<sub>6</sub>)]<sup>+</sup>, 1486.3 [Cp\*Fe( $\eta^5$ -P<sub>5</sub>)<sub>2</sub>Ag<sub>3</sub>(SbF<sub>6</sub>)<sub>2</sub>]<sup>+</sup>, 1645.42 Ag<sub>4</sub>(SbF<sub>6</sub>)<sub>3</sub>(*p*-(NC)<sub>2</sub>C<sub>6</sub>H<sub>4</sub>)<sub>3</sub>(CH<sub>3</sub>CN)<sub>3</sub><sup>+</sup>, 1832.3 [Cp\*Fe( $\eta^5$ -P<sub>5</sub>)<sub>3</sub>Ag<sub>3</sub>(SbF<sub>6</sub>)<sub>2</sub>]<sup>+</sup>, 2176.06 [Cp\*Fe( $\eta^5$ -P<sub>5</sub>)<sub>3</sub>Ag<sub>4</sub>(SbF<sub>6</sub>)<sub>3</sub>]<sup>+</sup>.

**Negative ion ESI-MS** (CH<sub>3</sub>CN): *m/z* (%) = 234.9 [SbF<sub>6</sub>]<sup>-</sup>.

**Elemental analysis:** Calculated (%) for [Cp\*Fe( $\eta^5$ -P<sub>5</sub>)]Ag<sub>2</sub>(*p*-(NC)<sub>2</sub>C<sub>6</sub>H<sub>4</sub>)(CH<sub>2</sub>Cl<sub>2</sub>)<sub>0.7</sub><sub>n</sub>[SbF<sub>6</sub>]<sub>2n</sub>: (1224.16 g/mol): C 18.39, H 1.69, N 2.29; found: C 17.97, H 2.07, N 2.10.

Analytical data of **6b**

**Yield:** 27 mg (0.0116 mmol, 29% referred to [Cp\*Fe( $\eta^5$ -P<sub>5</sub>)])

**<sup>1</sup>H NMR** (CD<sub>3</sub>CN):  $\delta$  [ppm] = 1.46 (s, [Cp\*Fe( $\eta^5$ -P<sub>5</sub>)]), 7.88 (s, *p*-(NC)<sub>2</sub>C<sub>6</sub>H<sub>4</sub>).

**<sup>31</sup>P{<sup>1</sup>H} NMR** (CD<sub>3</sub>CN):  $\delta$  [ppm] = 135.45 (s, [Cp\*Fe( $\eta^5$ -P<sub>5</sub>)]).

**<sup>19</sup>F NMR** (CD<sub>3</sub>CN):  $\delta$  [ppm] = -125.36 (m, SbF<sub>6</sub>).

**Positive ion ESI-MS** (CH<sub>3</sub>CN): *m/z* (%) = 106.9 Ag<sup>+</sup>, 147.9 [Ag(CH<sub>3</sub>CN)]<sup>+</sup>, 188.9 [Ag(CH<sub>3</sub>CN)<sub>2</sub>]<sup>+</sup>, 452.8 [Cp\*Fe( $\eta^5$ -P<sub>5</sub>)]Ag<sup>+</sup>, 493.9 [Cp\*Fe( $\eta^5$ -P<sub>5</sub>)]Ag(CH<sub>3</sub>CN)<sup>+</sup>, 534.9 [Cp\*Fe( $\eta^5$ -P<sub>5</sub>)]Ag(CH<sub>3</sub>CN)<sub>2</sub><sup>+</sup>, 798.7 [Cp\*Fe( $\eta^5$ -P<sub>5</sub>)<sub>2</sub>Ag]<sup>+</sup>, 1142.5 [Cp\*Fe( $\eta^5$ -P<sub>5</sub>)<sub>2</sub>Ag<sub>2</sub>(SbF<sub>6</sub>)]<sup>+</sup>, 1486.3 [Cp\*Fe( $\eta^5$ -P<sub>5</sub>)<sub>2</sub>Ag<sub>3</sub>(SbF<sub>6</sub>)<sub>2</sub>]<sup>+</sup>, 1645.42 [Ag<sub>4</sub>(SbF<sub>6</sub>)<sub>3</sub>(*p*-(NC)<sub>2</sub>C<sub>6</sub>H<sub>4</sub>)<sub>3</sub>(CH<sub>3</sub>CN)<sub>3</sub>]<sup>+</sup>, 1832.3 [Cp\*Fe( $\eta^5$ -P<sub>5</sub>)<sub>3</sub>Ag<sub>3</sub>(SbF<sub>6</sub>)<sub>2</sub>]<sup>+</sup>, 2176.06 [Cp\*Fe( $\eta^5$ -P<sub>5</sub>)<sub>3</sub>Ag<sub>4</sub>(SbF<sub>6</sub>)<sub>3</sub>]<sup>+</sup>, 2335.14 [Cp\*Fe( $\eta^5$ -P<sub>5</sub>)]Ag<sub>5</sub>(SbF<sub>6</sub>)<sub>4</sub>(*p*-(NC)<sub>2</sub>C<sub>6</sub>H<sub>4</sub>)<sub>3</sub>(CH<sub>3</sub>CN)<sub>3</sub><sup>+</sup>, 2521.9 [Cp\*Fe( $\eta^5$ -P<sub>5</sub>)<sub>4</sub>Ag<sub>4</sub>(SbF<sub>6</sub>)<sub>3</sub>]<sup>+</sup>.

**Negative ion ESI-MS**(CH<sub>3</sub>CN): *m/z* (%) = 234.9 [SbF<sub>6</sub>]<sup>-</sup>.

**Elemental analysis:** Calculated (%) for [Cp\*Fe( $\eta^5$ -P<sub>5</sub>)]Ag<sub>2</sub>(*p*-(NC)<sub>2</sub>C<sub>6</sub>H<sub>4</sub>)<sub>n</sub>[SbF<sub>6</sub>]<sub>2n</sub> (2322.63 g/mol): 18.62 C, 1.65 H, 2.41 N; found: 19.08 C, 2.21 H, 2.37 N.

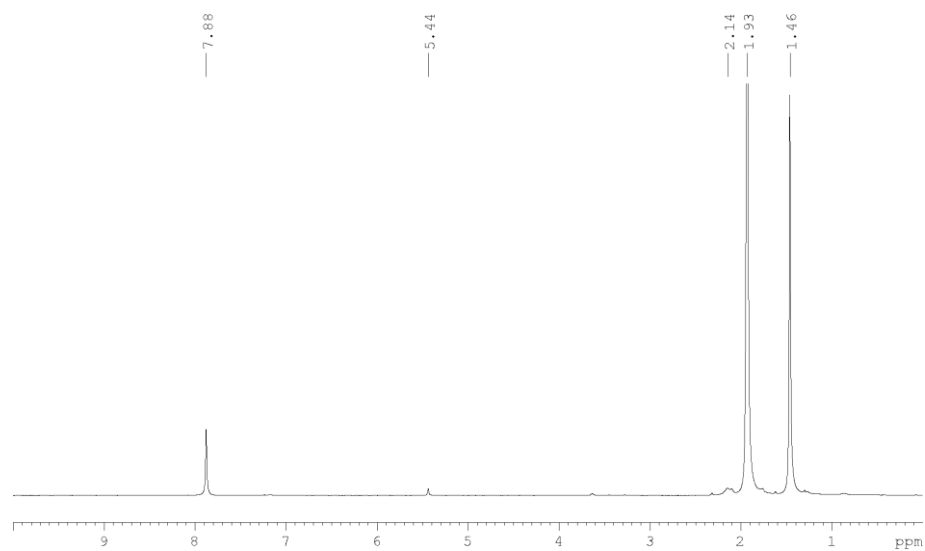


Figure 5.28.  $^1\text{H}$  NMR spectrum of **6a**. (1.93  $\text{CH}_3\text{CN}$ , 2.14  $\text{H}_2\text{O}$ , 5.44  $\text{CH}_2\text{Cl}_2$ )

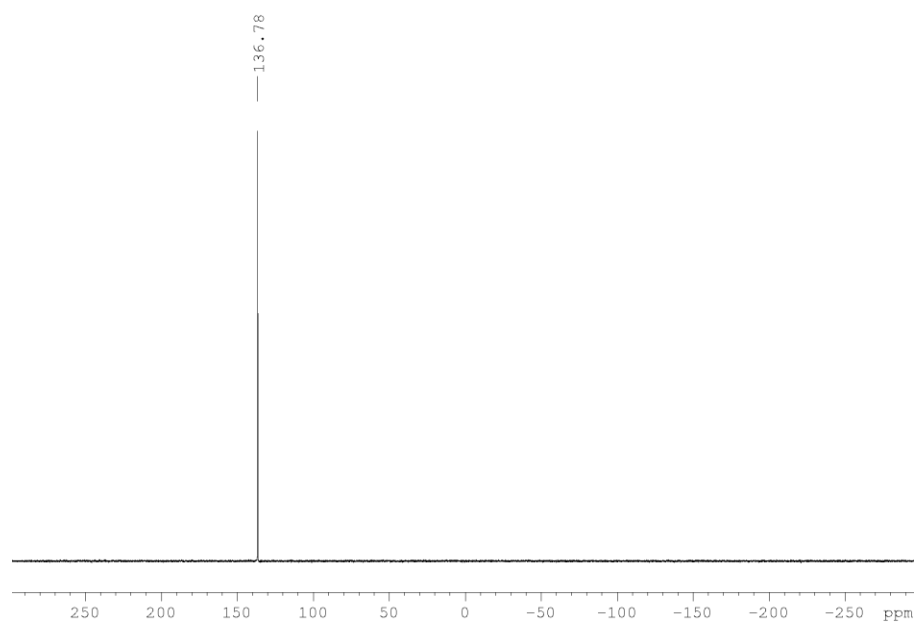


Figure 5.29.  $^{31}\text{P}\{^1\text{H}\}$  NMR spectrum of **6a**.

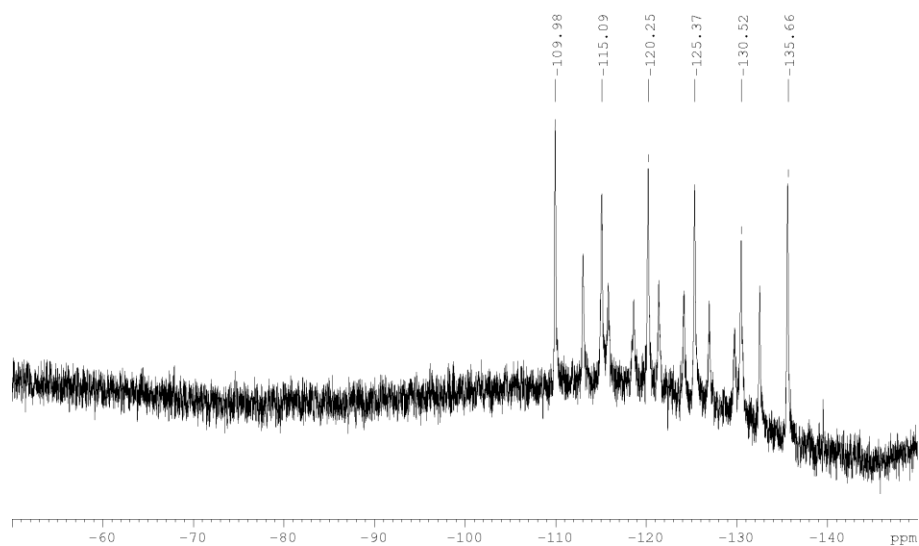


Figure 5.30.  $^{19}\text{F}$  NMR spectrum of **6a**.

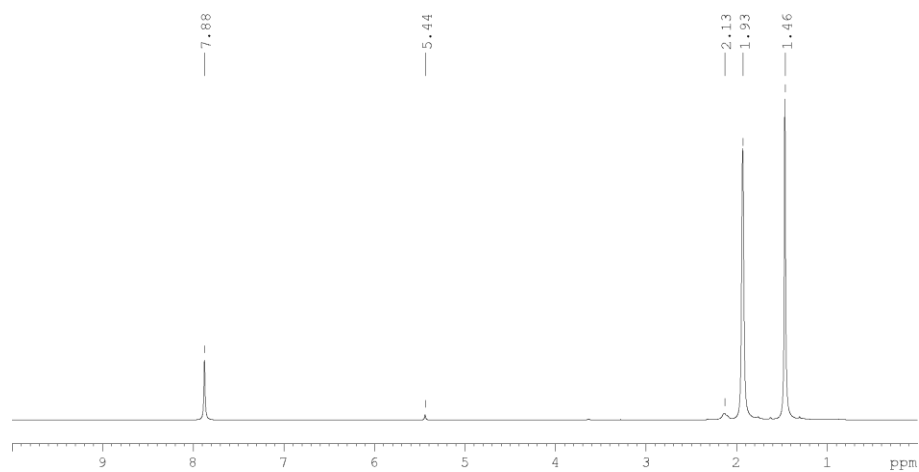


Figure 5.31.  $^1\text{H}$  NMR spectrum of **6b** (1.93  $\text{CH}_3\text{CN}$ , 2.13  $\text{H}_2\text{O}$ , 5.44  $\text{CH}_2\text{Cl}_2$ )

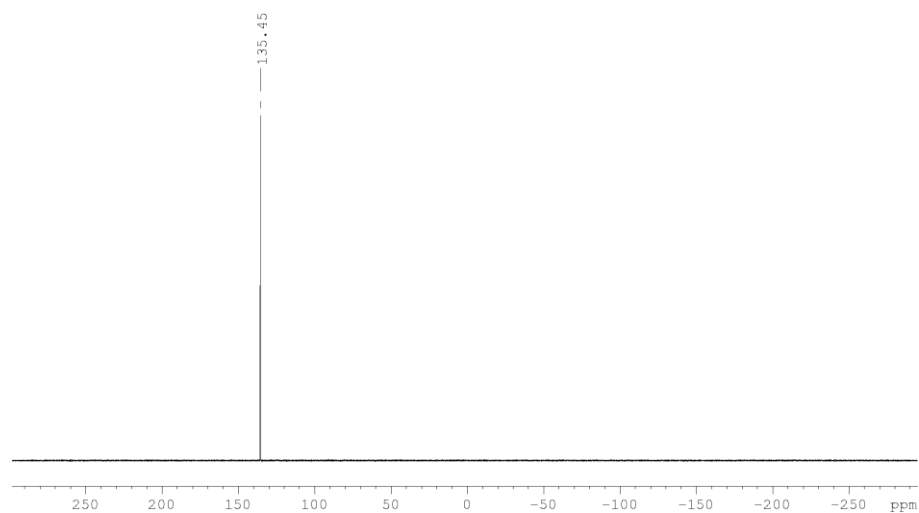


Figure 5.32.  $^{31}\text{P}\{^1\text{H}\}$  NMR spectrum of **6b**.

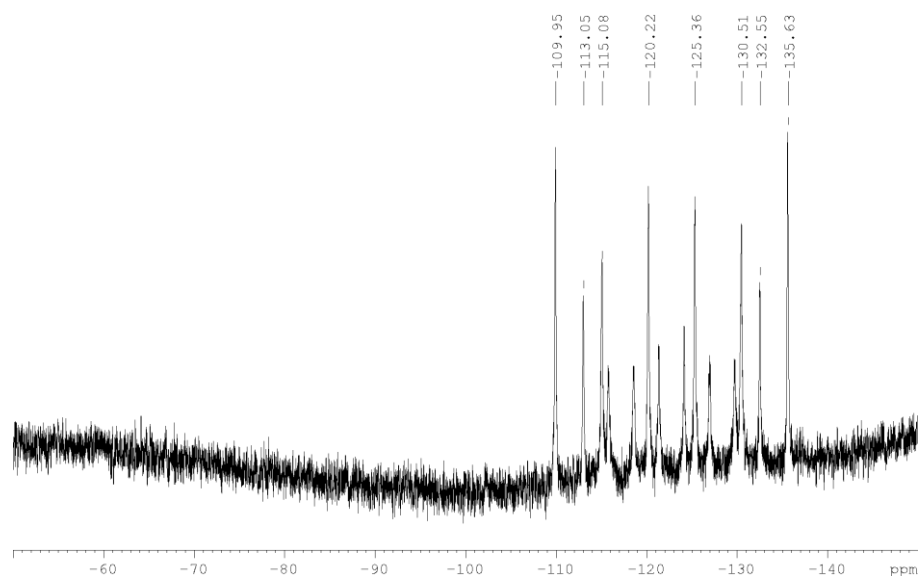


Figure 5.33.  $^{19}\text{F}$  NMR spectrum of **6b**.

### Synthesis of $[\{\text{Cp}^*\text{Fe}(\eta^5\text{-P}_5)\}_2\text{Ag}_2(p\text{-}(\text{NC})_2\text{C}_6\text{H}_4)]_n[\text{SbF}_6]_{2n}$ (**7**)

In a Schlenk tube a solution of  $\text{AgSbF}_6$  (14 mg, 0.04 mmol) in  $\text{CH}_2\text{Cl}_2$  (8 mL) is carefully layered first with a solvent mixture of  $\text{CH}_2\text{Cl}_2$ /toluene (2 mL, 2:1) and then with a green solution of  $[\text{Cp}^*\text{Fe}(\eta^5\text{-P}_5)]$  (14 mg, 0.04 mmol) and  $p\text{-}(\text{NC})_2\text{C}_6\text{H}_4$  (51 mg, 0.4 mmol) in toluene (8 mL). After few hours, the phase boundary turns yellow and after one day, the formation of brown prism **7** at the phase boundary can be observed. After complete diffusion the light green mother liquor is decanted, the crystals are washed with hexane ( $3 \times 10$  mL) and dried *in vacuo*.

Analytical data of **7**

**Yield:** 36 mg, (0.024 mmol, 60% referred to  $[\text{Cp}^*\text{Fe}(\eta^5\text{-P}_5)]$ )

$^1\text{H}$  NMR ( $\text{CD}_3\text{CN}$ ):  $\delta$  [ppm] = 1.44 (s,  $[\text{Cp}^*\text{Fe}(\eta^5\text{-P}_5)]$ ), 7.87 (s,  $p\text{-}(\text{NC})_2\text{C}_6\text{H}_4$ ).

$^{31}\text{P}\{^1\text{H}\}$  NMR ( $\text{CD}_3\text{CN}$ ):  $\delta$  [ppm] = 141.424 (s,  $[\text{Cp}^*\text{Fe}(\eta^5\text{-P}_5)]$ ).

$^{19}\text{F}$  NMR ( $\text{CD}_3\text{CN}$ ):  $\delta$  [ppm] = -125.38 (m,  $\text{SbF}_6$ )

**Positive ion ESI-MS** ( $\text{CH}_3\text{CN}$ ):  $m/z$  (%) = 106.9  $\text{Ag}^+$ , 130.2  $[p\text{-}(\text{NC})_2\text{C}_6\text{H}_4\text{CN}]^{2+}$ , 147.9  $[\text{Ag}(\text{CH}_3\text{CN})]^+$ , 452.8  $[\{\text{Cp}^*\text{Fe}(\eta^5\text{-P}_5)\}\text{Ag}]^+$ , 493.9  $[\{\text{Cp}^*\text{Fe}(\eta^5\text{-P}_5)\}\text{Ag}(\text{CH}_3\text{CN})]^+$ , 534.9  $[\{\text{Cp}^*\text{Fe}(\eta^5\text{-P}_5)\}\text{Ag}(\text{CH}_3\text{CN})_2]^+$ , 798.7  $[\{\text{Cp}^*\text{Fe}(\eta^5\text{-P}_5)\}_2\text{Ag}]^+$ , 1142.5  $[\{\text{Cp}^*\text{Fe}(\eta^5\text{-P}_5)\}_2\text{Ag}_2(\text{SbF}_6)]^+$ , 1486.3  $[\{\text{Cp}^*\text{Fe}(\eta^5\text{-P}_5)\}_2\text{Ag}_3(\text{SbF}_6)_2]^+$ , 1832.3  $[\{\text{Cp}^*\text{Fe}(\eta^5\text{-P}_5)\}_3\text{Ag}_3(\text{SbF}_6)_2]^+$ , 2180.2  $[\{\text{Cp}^*\text{Fe}(\eta^5\text{-P}_5)\}_5\text{Ag}_2(\text{SbF}_6)]^+$ .

**Negative ion ESI-MS** ( $\text{CH}_3\text{CN}$ ):  $m/z$  (%) = 234.9  $[\text{SbF}_6]^-$ .

**Elemental analysis:** Calculated (%) for  $[\{\text{Cp}^*\text{Fe}(\eta^5\text{-P}_5)\}_2\text{Ag}_2(p\text{-}(\text{NC})_2\text{C}_6\text{H}_4)]_n[\text{SbF}_6]_{2n}$  (1507.2438 g/mol): 22.31 C, 2.27 H, 1.86 N; found: 22.39 C, 2.27 H, 1.75 N.



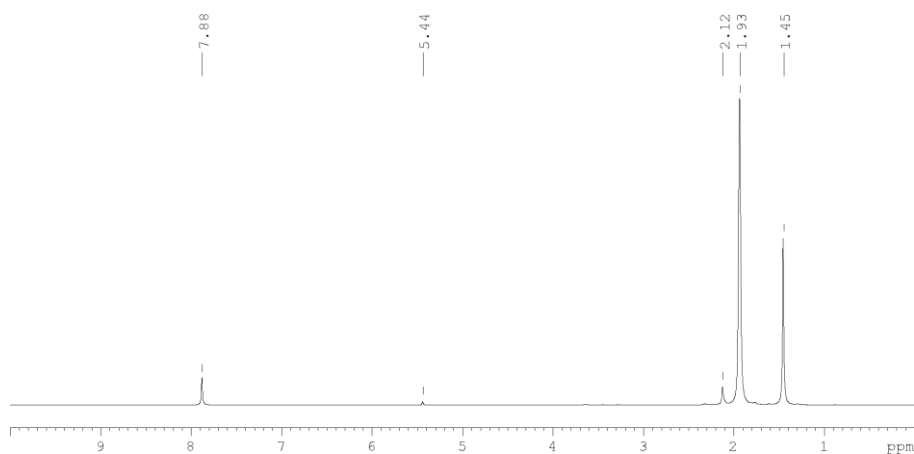


Figure 5.34.  $^1\text{H}$  NMR spectrum of **7**. (1.93  $\text{CH}_3\text{CN}$ , 2.12  $\text{H}_2\text{O}$ , 5.44  $\text{CH}_2\text{Cl}_2$ )

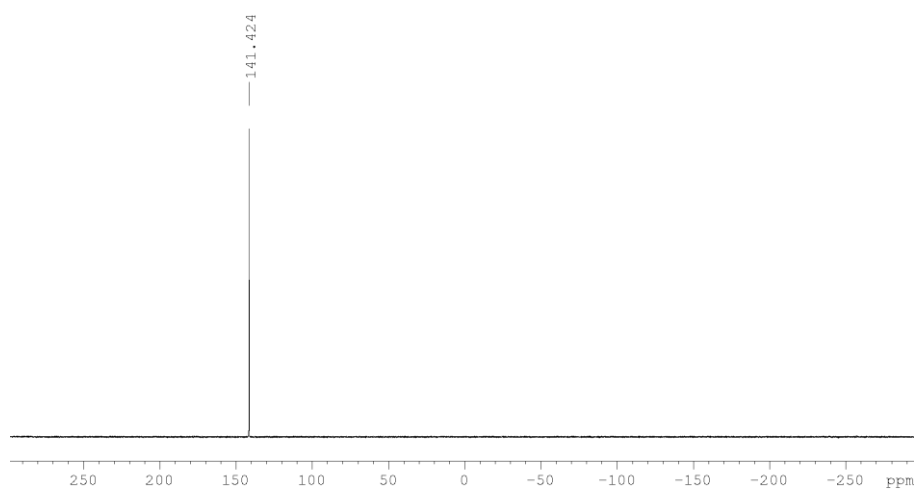


Figure 5.35.  $^{31}\text{P}\{^1\text{H}\}$  NMR spectrum of **7**.

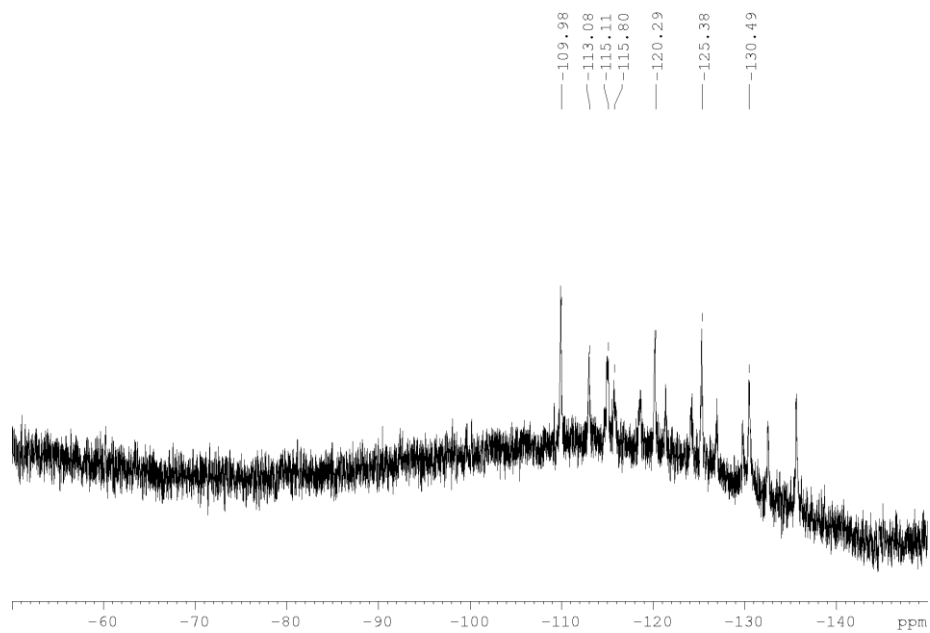


Figure 5.36.  $^{19}\text{F}$  NMR spectrum of **7**.

**Synthesis of  $[\{\text{Cp}''\text{Fe}(\eta^5\text{-P}_5)\}_3\text{Ag}_4(o\text{-(NC)}_2\text{C}_6\text{H}_4)_2\}_n[\text{SbF}_6]_{4n}$  (**8**)**

A solution of  $[\text{Cp}''\text{Fe}(\eta^5\text{-P}_5)]$  (15.5 mg, 0.04 mmol) and *ortho*- $\text{C}_8\text{H}_4\text{N}_2$  (1 mL, 0.2 M in  $\text{CH}_2\text{Cl}_2$ ) in a 1:2 mixture of toluene/hexane (15 mL) is stirred for 3 h at room temperature. Afterwards the reaction mixture is filtered. A solution of  $\text{AgSbF}_6$  (27.5 mg, 0.08 mmol) in  $\text{CH}_2\text{Cl}_2$  (15 mL) is first carefully layered by a solvent mixture of  $\text{CH}_2\text{Cl}_2$ /toluene (4 mL, 2:1) and then by the mixture of  $[\text{Cp}''\text{Fe}(\eta^5\text{-P}_5)]$  and *ortho*- $\text{C}_8\text{H}_4\text{N}_2$ . After one day the formation of light brown blocks of **8** at the phase boundary were observed. The light brownish mother liquor is decanted, the crystals are washed with hexane ( $3 \times 15$  mL) and  $\text{CH}_2\text{Cl}_2$  ( $4 \times 15$  mL) and dried *in vacuo*.

Analytical data of **8**

**Yield:** 59 mg (53%, referred to  $[\text{Cp}''\text{Fe}(\eta^5\text{-P}_5)]$ )

**$^1\text{H}$  NMR** ( $\text{CD}_3\text{CN}$ ):  $\delta$  [ppm] = 1.19 (s,  $\text{C}_5\text{H}_3^t\text{Bu}_2$ ), 4.23 (s,  $\text{C}_5\text{H}_3^t\text{Bu}_2$ ), 4.28 (s,  $\text{C}_5\text{H}_3^t\text{Bu}_2$ ), 7.87 (m,  $\text{C}_8\text{H}_4\text{N}_2$ )

**$^{31}\text{P}\{^1\text{H}\}$  NMR** ( $\text{CD}_3\text{CN}$ ):  $\delta$  [ppm] = 149.6 (s,  $[\text{Cp}''\text{Fe}(\eta^5\text{-P}_5)]$ )

**$^{19}\text{F}$  NMR** ( $\text{CD}_3\text{CN}$ ):  $\delta$  [ppm] = -122.8 (m,  $\text{SbF}_6^-$ )

**Positive ion ESI-MS** ( $\text{CH}_3\text{CN}$ ):  $m/z$  (%) = 124.91  $[\text{Ag}(\text{H}_2\text{O})]^+$ , 535.89  $[\text{C}_{13}\text{H}_{21}\text{FeP}_5\text{AgCH}_3\text{CN}]^+$ , 882.84  $[(\text{C}_{13}\text{H}_{21}\text{FeP}_5)_2\text{Ag}]^+$ , 1026.71  $[\text{Ag}_4(\text{C}_8\text{H}_4\text{N}_2)_4(\text{CH}_3\text{CN})_2]^+$ .

**Negative ion ESI-MS** ( $\text{CH}_3\text{CN}$ ):  $m/z$  (%) = 234.89  $[\text{SbF}_6]^-$

**Elemental analysis:** Calculated (%) for  $[\{\text{Cp}''\text{Fe}(\eta^5\text{-P}_5)\}_3\text{Ag}_4(o\text{-(NC)}_2\text{C}_6\text{H}_4)_2\}_n[\text{SbF}_6]_{4n}$  (2794.78 g/mol): 23.64 C, 2.56 H, 2.00 N; found: 23.89 C, 2.81 H, 2.65 N.

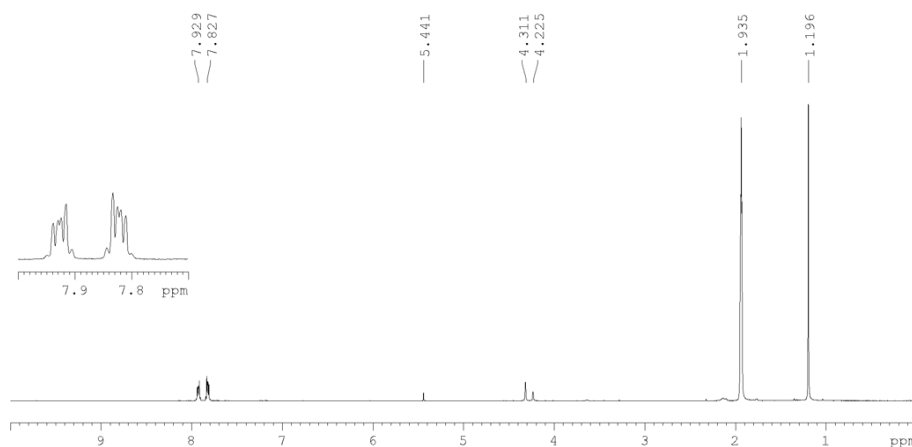


**Figure 5.37.**  $^1\text{H}$  NMR spectrum of **8**. (1.93  $\text{CH}_3\text{CN}$ , 2.18  $\text{H}_2\text{O}$ , 5.44  $\text{CH}_2\text{Cl}_2$ )

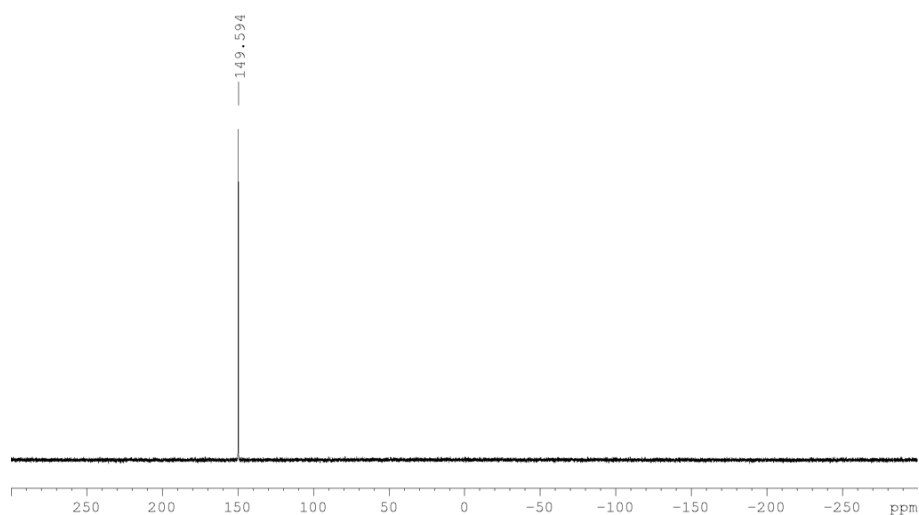


Figure 5.38.  $^{31}\text{P}\{^1\text{H}\}$  NMR spectrum of **8**.

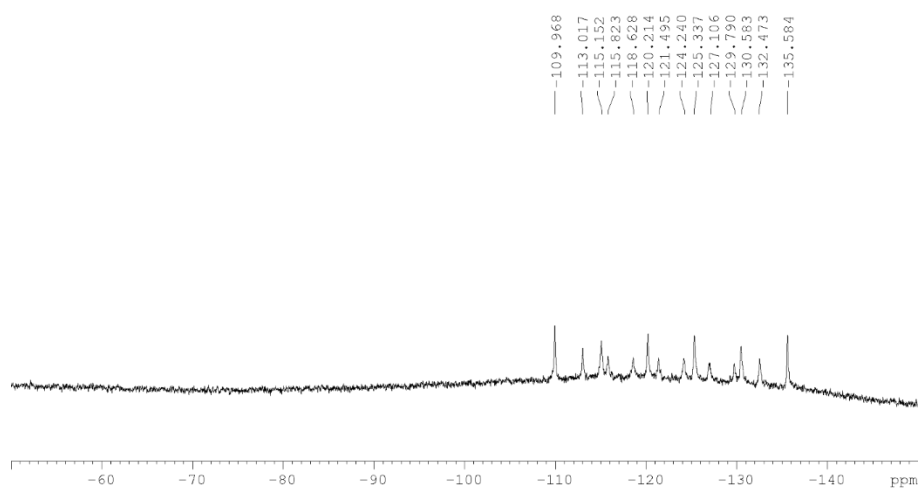


Figure 5.39.  $^{19}\text{F}$  NMR spectrum of **8**.

### Synthesis of $[(\text{Cp}''\text{Fe}(\eta^5\text{-P}_5))_3\text{Ag}_3(m\text{-}(\text{NC})_2\text{C}_6\text{H}_4)][\text{SbF}_6]_3 \cdot (\text{CH}_2\text{Cl}_2)_{2.5n}(\text{C}_7\text{H}_8)_{1.475n}$ (**9**)

In a Schlenk tube a solution of  $\text{AgSbF}_6$  (27.5 mg, 0.08 mmol) in  $\text{CH}_2\text{Cl}_2$  (15 mL) is carefully layered first with a solvent mixture of  $\text{CH}_2\text{Cl}_2$ /toluene (4 mL, 2:1) and then with a green solution of  $[\text{Cp}''\text{Fe}(\eta^5\text{-P}_5)]$  (15.5 mg, 0.04 mmol) and *meta*- $\text{C}_8\text{H}_4\text{N}_2$  (1 mL, 0.4 M in  $\text{CH}_2\text{Cl}_2$ ) in toluene (15 mL). After one day, the formation of green plates of **9** at the phase boundary were observed. The brownish mother liquor is decanted, the crystals are washed with  $\text{CH}_2\text{Cl}_2$  (2  $\times$  5 mL) and pentane (2  $\times$  5 mL) and dried *in vacuo*.

Analytical data of **9**

**Yield:** 32 mg (0.033 mmol), 81% referred to  $[\text{Cp}''\text{Fe}(\eta^5\text{-P}_5)]$

$^1\text{H}$  NMR ( $\text{CD}_3\text{CN}$ ):  $\delta$  [ppm] = 1.19 (s,  $\text{C}_5\text{H}_3^t\text{Bu}_2$ ), 4.24 (s,  $\text{C}_5\text{H}_3^t\text{Bu}_2$ ), 4.33 (s,  $\text{C}_5\text{H}_3^t\text{Bu}_2$ ), 7.27-7.13 (m,  $\text{C}_8\text{H}_4\text{N}_2$ )

$^{31}\text{P}\{^1\text{H}\}$  NMR ( $\text{CD}_3\text{CN}$ ):  $\delta$  [ppm] = 147.4 (s,  $[\text{Cp}''\text{Fe}(\eta^5\text{-P}_5)]$ )

$^{19}\text{F}$  NMR ( $\text{CD}_3\text{CN}$ ):  $\delta$  [ppm] = -78.04 (s,  $\text{SbF}_6^-$ )

**Positive ion ESI-MS** ( $\text{CH}_3\text{CN}$ ):  $m/z$  (%) = 535.89  $[\text{C}_{13}\text{H}_{21}\text{FeP}_5\text{AgCH}_3\text{CN}]^+$ , 576.92  $[\text{C}_{13}\text{H}_{21}\text{FeP}_5\text{Ag}(\text{CH}_3\text{CN})_2]^+$ , 882.84  $[(\text{C}_{13}\text{H}_{21}\text{FeP}_5)_2\text{Ag}]^+$ , 1026.71  $[\text{Ag}_4(\text{C}_8\text{H}_4\text{N}_2)_4(\text{CH}_3\text{CN})_2]^+$ , 1108.99  $[\text{Ag}_4(\text{C}_8\text{H}_4\text{N}_2)_4(\text{CH}_3\text{CN})_4]^+$ .

**Negative ion ESI-MS** ( $\text{CH}_3\text{CN}$ ):  $m/z$  (%) = 234.89  $[\text{SbF}_6]^-$

**Elemental analysis:** Calculated (%) for  $[\{\text{Cp}''\text{Fe}(\eta^5\text{-P}_5)\}_3\text{Ag}_3(m\text{-}(\text{NC})_2\text{C}_6\text{H}_4)]_n[\text{SbF}_6]_{3n}$  (1957.79 g/mol): 24.30 C, 2.91 H, 1.21 N; found: 24.41 C, 2.55 H, 0.99 N.

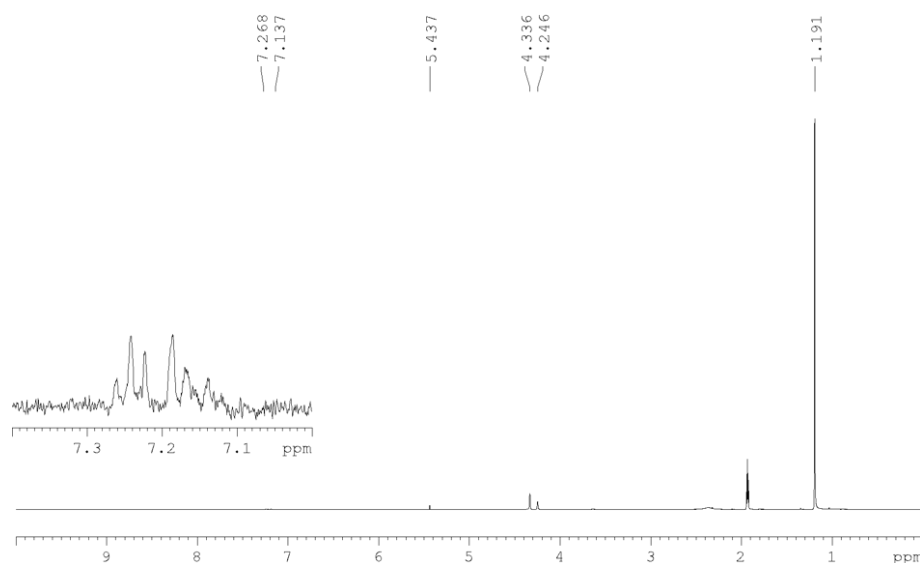


Figure 5.40.  $^1\text{H}$  NMR spectrum of **9** (1.93  $\text{CH}_3\text{CN}$ , 5.43  $\text{CH}_2\text{Cl}_2$ )

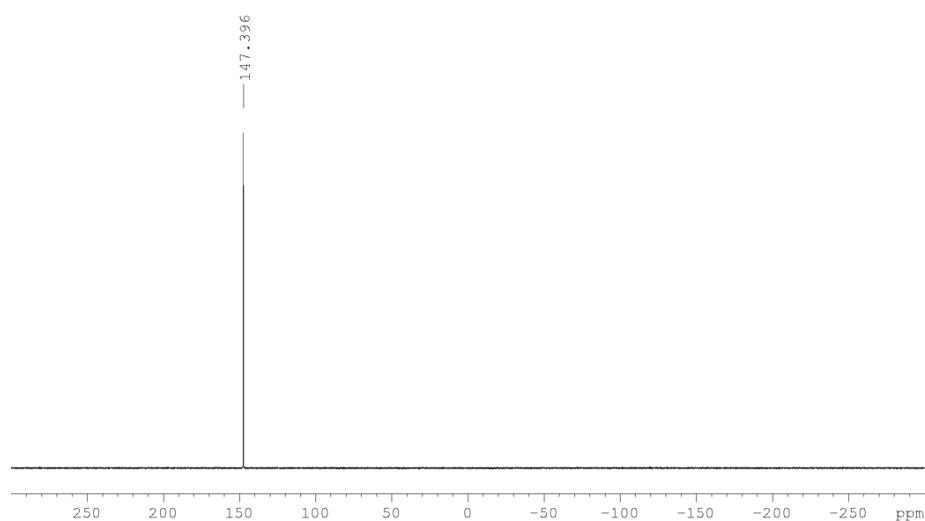


Figure 5.41.  $^{31}\text{P}\{^1\text{H}\}$  NMR spectrum of **9**.

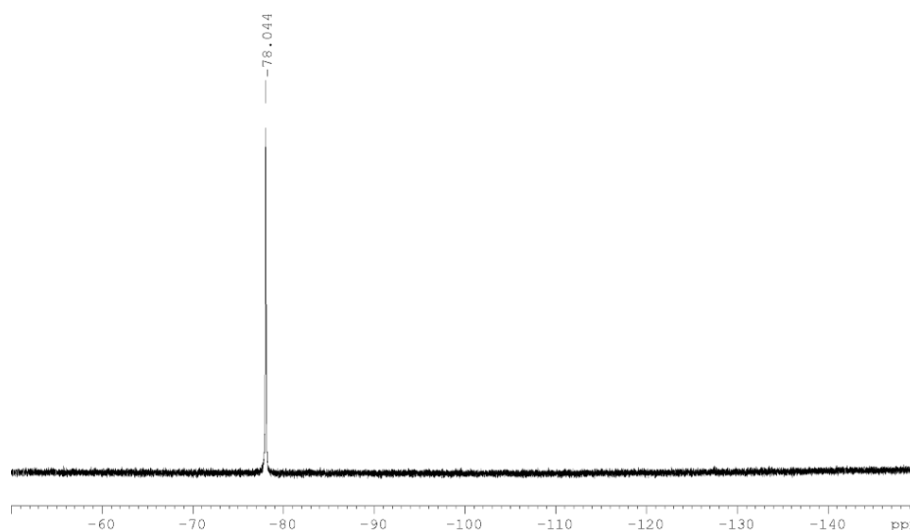


Figure 5.42.  $^{19}\text{F}$  NMR spectrum of **9**.

### Synthesis of $[(\text{Cp}''\text{Fe}(\eta^5\text{-P}_5))_2\text{Ag}_2(p\text{-(NC)}_2\text{C}_6\text{H}_4)]_n(\text{SbF}_6)_{2n}$ (**10**)

In a Schlenk tube a solution of  $\text{AgSbF}_6$  (27.5 mg, 0.08 mmol) in  $\text{CH}_2\text{Cl}_2$  (15 mL) is carefully layered first with a solvent mixture of  $\text{CH}_2\text{Cl}_2$ /toluene (4 mL, 2:1) and then with a green solution of  $[\text{Cp}''\text{Fe}(\eta^5\text{-P}_5)]$  (15.5 mg, 0.04 mmol) and *para*- $\text{C}_8\text{H}_4\text{N}_2$  (1 mL, 0.4 M in  $\text{CH}_2\text{Cl}_2$ ) in toluene (15 mL). After one day, the formation of green plates of **10** at the phase boundary were observed. The crystals were washed with pentane ( $3 \times 5$  mL) and dried *in vacuo*.

Analytical data of **10**

**Yield:** 21 mg (0.024 mmol, 60% referred to  $[\text{Cp}''\text{Fe}(\eta^5\text{-P}_5)]$ )

$^1\text{H}$  NMR ( $\text{CD}_3\text{CN}$ ):  $\delta$  [ppm] = 1.19 (s,  $\text{C}_5\text{H}_3^t\text{Bu}_2$ ), 4.17 (s,  $\text{C}_5\text{H}_3^t\text{Bu}_2$ ), 4.25 (s,  $\text{C}_5\text{H}_3^t\text{Bu}_2$ ), 7.89 (s,  $\text{C}_8\text{H}_4\text{N}_2$ )

$^{31}\text{P}\{^1\text{H}\}$  NMR ( $\text{CD}_3\text{CN}$ ):  $\delta$  [ppm] = 158.8 (s,  $[\text{Cp}''\text{Fe}(\eta^5\text{-P}_5)]$ )

$^{19}\text{F}$  NMR ( $\text{CD}_3\text{CN}$ ):  $\delta$  [ppm] = no signal was detected.

**Positive ion ESI-MS** ( $\text{CH}_3\text{CN}$ ):  $m/z$  (%) = 124.08  $[\text{Ag}(\text{H}_2\text{O})]^+$ , 535.89  $[\text{C}_{13}\text{H}_{21}\text{FeP}_5\text{AgCH}_3\text{CN}]^+$ , 882.84  $[(\text{C}_{13}\text{H}_{21}\text{FeP}_5)_2\text{Ag}]^+$ , 1026.71  $[\text{Ag}_4(\text{C}_8\text{H}_4\text{N}_2)_4(\text{CH}_3\text{CN})_2]^+$

**Negative ion ESI-MS** ( $\text{CH}_3\text{CN}$ ):  $m/z$  (%) = 234.89  $[\text{SbF}_6]^-$

**Elemental analysis:** Calculated (%) for  $[(\text{Cp}''\text{Fe}(\eta^5\text{-P}_5))_2\text{Ag}(p\text{-(NC)}_2\text{C}_6\text{H}_4)_{0.5}(\text{CH}_2\text{Cl}_2)]_n[\text{SbF}_6]_n$  (880.64 g/mol): 24.55 C, 2.86 H, 1.59 N; found: 24.17 C, 3.11 H, 0.98 N.

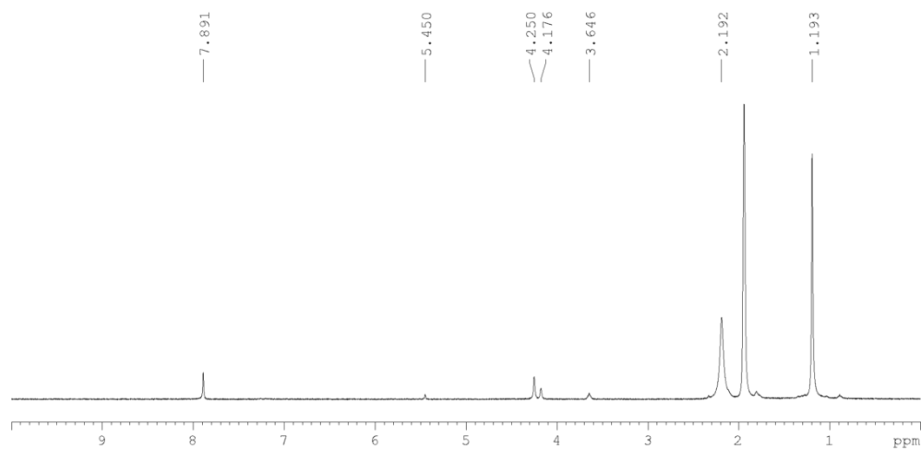


Figure 5.43.  $^1\text{H}$  NMR spectrum of **10** (1.93  $\text{CH}_3\text{CN}$ , 2.19  $\text{H}_2\text{O}$ , 5.45  $\text{CH}_2\text{Cl}_2$ ).

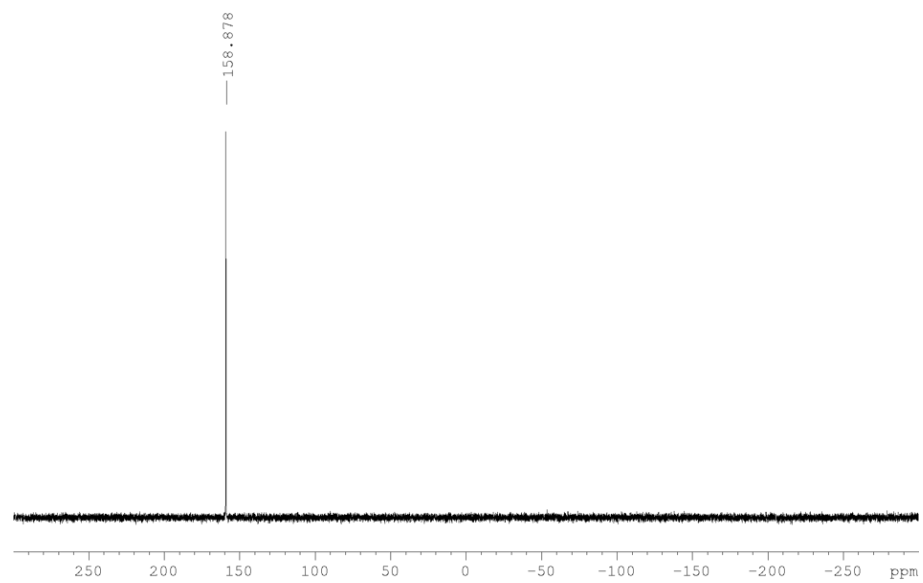


Figure 5.44.  $^{31}\text{P}\{^1\text{H}\}$  NMR spectrum of **10**.

## 5.5 Crystallographic Details and Structure Refinement

### Experimental

Crystals of compounds **1**, **2**, **3**, **4**, **5**, **6a**, **7**, **8** were taken from a Schlenk flask under a stream of argon and immediately covered with perfluorinated Fomblin® mineral oil to prevent decomposition or/and a loss of solvent. The chosen single crystals covered by a drop of the oil were quickly mounted on a CryoMount® attached to a magnetic base and placed on into a stream of cold nitrogen on the pre-centered magnetic goniometer head attached to the goniometer of a diffractometer.

The diffraction data for **2**, **3**, **7** were collected on a Rigaku SuperNova Dualflex diffractometer equipped with a Titan<sup>S2</sup> CCD detector and a CuK $\alpha$  microfocus source using either 1°  $\omega$  scans depending mostly on the unit cell constants at T = 123 K. The diffraction data for **1**, **4**, **8** were collected on a Rigaku XtaLAB Synergy R diffractometer equipped with a HyPix-Arc 150 detector and a CuK $\alpha$  rotating-anode X-ray source using 0.5° (for **1**, **4**) or 1° (for **8**)  $\omega$  scans at 100 (for **1**, **4**) or 123 K (for **8**).

The single crystals of **6a** and **6b** were carefully selected, mounted on a magnetic holder, checked for quality and placed into a Dewar vessel in liquid nitrogen using standard cryo crystallography tools. After a few weeks it was taken to the DESY PETRA III synchrotron. Using standard procedures, the crystals were placed into a vessel filled with liquid nitrogen among others. A robotic mounting/demounting was used for further manipulations in the P11 beamline hutch for **6a** and **6b**.<sup>[19]</sup> X-ray diffraction experiments were measured at wavelength  $\lambda = 0.6199 \text{ \AA}$  (20 keV) using one-circle diffractometer and DECTRIS Eiger2 X 16M pixel array detector at 90.0(2) K. The data for **6a** were acquired by 360°  $\phi$ -rotation with 0.1° and exposure 0.1 s per readout. The data for **6b** were acquired by 360°  $\phi$ -rotation with 0.2° and exposure 0.2 s per readout.

X-ray diffraction experiment for **9** and **10** were measured at 18-20(2) K at beamline P24<sup>[20]</sup> at DESY PETRA III synchrotron equipped with Huber 3-cycle diffractometer and Pilatus3 CdTe 1M detector and an open-flow He LT system. Data collection for was performed by 360°  $\phi$ -rotation with 0.1° and exposure 1.5 s (for **9**) or 0.5 s (for **10**) per readout at a wavelength  $\lambda = 0.56002 \text{ \AA}$  (22.139 keV).

Data reduction for all crystal structures, except for **6a**, was performed with CrysAlisPro software.<sup>[21]</sup> Analytical absorption correction for **1**, **2**, **4**, **5**, **6a**, **7**, **8** was applied based on crystal faces. For **9** and **10** empirical based on equivalent reflections was applied, whereas for **6a**, no absorption correction with respect to small absorption coefficient.

## Structure refinement

The structures were solved by direct methods with *SHELXT* and were refined by full-matrix least-squares method against  $F^2$  in anisotropic approximation using multiprocessor variable memory versions of *SHELXL (2014-2018)*.<sup>[22]</sup> All non-hydrogen atoms were refined anisotropically, while the hydrogen atoms were refined riding on pivot atoms.

In **2**, **4**, **5**, **6a** and **8**, the  $\text{SbF}_6^-$  counter-anions are disordered over two or more close positions. The occupation factors for disordered positions of Sb atoms were refined with fixed isotropic  $U_{\text{iso}}$  similar to the average  $U_{\text{iso}}$  (usually 0.025-0.035  $\text{\AA}^{-2}$ ) for the fully occupied heavy atoms in the corresponding structure. In some cases, the disorder is so severe, that for some minor disordered positions of the  $\text{SbF}_6^-$  anions, not all fluorine atoms could be located from the difference Fourier map. For the same reason, the fluorine atoms in very close positions were refined using restraint a.d.p. parameters. In case of small occupancy, F atoms were refined isotropically. If the disorder pattern did not allow a free refinement, the refinement of the disordered counter anions  $\text{SbF}_6^-$  over multiple positions was performed as a rigid body refinement in **5**, **6a** and **8**. The geometry of the ideal octahedral structure was transferred from CSD<sup>[23]</sup> the crystal structure of 3,4-diphenylquinolinium hexafluoro-antimony deposited under RefCode JABWAN.<sup>[24]</sup>

The solvent molecules also showed a strong tendency for disorder in the interstitial space or were following the disorder pattern of the major structural components. The molecular site occupancy factors (equal s.o.f.'s for all atoms of a molecule) were refined using the FVAR instruction of SHELX with isotropic displacement parameters fixed typically at  $U_{\text{iso}} = 0.05 \text{ \AA}^{-2}$ . The resulting occupancies were fixed and the atoms with occupancies of more than 0.5 were refined in anisotropic approximation. Some toluene molecules were refined with restraint geometry. The restraints were removed at the final stage of the refinement when possible. The disorder of the solvent molecules  $\text{CH}_2\text{Cl}_2$  was treated in a similar way.

All ORTEP drawings were made in Olex2.<sup>[25]</sup> Crystallographic data and details of the diffraction experiments are given in table 5.1-5.5, bond lengths and angles are listed in and molecular structures are depicted in the published SI of the manuscript.

## Data Deposition

CIF files with comprehensive information on the details of the diffraction experiments and full tables of bond lengths and angles for **1** - **10** are deposited in Cambridge Crystallographic Data Centre under the deposition codes CCDC-2213602 (**1**), CCDC-2213601 (**2**), CCDC-2213604 (**3**), CCDC-2213600 (**4**), CCDC-2213608 (**5**), CCDC-2213603 (**6a**), CCDC-2213606 (**6b**), CCDC-2213605 (**7**), CCDC-2213609 (**8**), CCDC-2213610 (**9**), CCDC-2213607 (**10**).



**Table 5.1.** Experimental details for **1 – 3**.

Crystal data	1	2	3
CCDC Code	CCDC-2213602	CCDC-2213601	CCDC-2213604
Chemical formula	$C_{36}H_{38}Ag_3Fe_2N_4P_{10} \cdot (SbF_6)_3$	$C_{52}H_{46}Ag_4Fe_2N_8P_{10}(SbF_6)_4 \cdot 1.3$ $C_7H_8 \cdot 0.65CH_2Cl_2$	$C_{46}H_{53}Ag_4F_{24}Fe_3N_4P_{15}Sb_4$
$M_r$	1978.96	2753.82	2668.50
Crystal system, space group	Triclinic, $P1$	Monoclinic, $P2_1/n$	Triclinic, $P1$
Temperature(K)	100	123	123
$a, b, c(\text{\AA})$	14.6319(4), 15.3881(4), 15.4157(4)	13.41330(13), 23.4055(2)	14.5378(3), 15.8390(4), 18.4931(4)
$\alpha, \beta, \gamma(^{\circ})$	102.144(2), 116.125(3), 99.352(2)	90.2256(9)	92.0303(16), 111.0035(17), 97.4659(16)
$V(\text{\AA}^3)$	2915.06(14)	9088.07(15)	3926.16(14)
$Z$	2	4	2
$F(000)$	1880	5265	2536
$D_x(\text{Mg m}^{-3})$	2.255	2.013	2.257
Radiation type	Cu $K\alpha$	Cu $K\alpha$	Cu $K\alpha$
$\mu(\text{mm}^{-1})$	26.06	21.33	26.58
Crystal shape and colour	yellow thick plate	yellow plate	brown elongated prism
Crystal size(mm)	0.24 × 0.16 × 0.05	0.16 × 0.11 × 0.01	0.28 × 0.07 × 0.03
Data collection			
Diffractometer	XtaLAB Synergy R, DW	SuperNova, Dualflex, Titan <sup>S2</sup>	SuperNova, Dualflex, Titan <sup>S2</sup>
Absorption correction	Gaussian	Gaussian	Gaussian
$T_{\min}, T_{\max}$	0.038, 0.572	0.103, 0.888	0.210, 1.000
No. of measured independent and observed [ $I > 2\sigma(I)$ ] reflections	41508, 11622, 11179	46999, 15185, 12037	70354, 13848, 12217
$R_{\text{int}}$	0.071	0.044	0.058
$(\sin \theta/\lambda)_{\text{max}}(\text{\AA}^{-1})$	0.627	0.595	0.596
Range of $h, k, l$	$h = -16 \rightarrow 18, k = -19 \rightarrow 16,$ $l = -19 \rightarrow 19$	$h = -15 \rightarrow 15, k = -34 \rightarrow 34, l = -$ $26 \rightarrow 27$	$h = -17 \rightarrow 17, k = -18 \rightarrow 18, l =$ $-18 \rightarrow 21$
Refinement			
$R[F^2 > 2\sigma(F^2)], wR(F^2), S$	0.053, 0.155, 1.06	0.043, 0.119, 1.00	0.030, 0.076, 0.98
No. of reflections	11622	15185	13848
No. of parameters	695	1182	977
No. of restraints	0	138	0
H-atom treatment	H-atom parameters constrained	H-atom parameters constrained	H-atom parameters constrained
$\Delta_{\text{max}}, \Delta_{\text{min}}(\text{e \AA}^{-3})$	2.21, -1.91	2.08, -1.84	1.00, -1.48

Computer programs: CrysAlis PRO 1.171.41.93a (Rigaku OD, 2020) (**1**, **2**), CrysAlis PRO 1.171.42.43a (Rigaku OD, 2022) (**3**), SHELXT2018/5 (Sheldrick, 2018), SHELXL2018/3 (Sheldrick, 2018).

**Table 5.2.** Experimental details for **4** and **5**.

Crystal data	4	5
CCDC Code	CCDC-2213600	CCDC-2213608
Chemical formula	C <sub>28</sub> H <sub>34</sub> Ag <sub>2</sub> Fe <sub>2</sub> N <sub>2</sub> P <sub>10</sub> ·2(SbF <sub>6</sub> )·0.5(C <sub>7</sub> H <sub>8</sub> )·0.5(CH <sub>2</sub> Cl <sub>2</sub> )	C <sub>26</sub> H <sub>23</sub> Ag <sub>2</sub> FeN <sub>4</sub> P <sub>5</sub> ·2(SbF <sub>6</sub> )·0.85(CH <sub>2</sub> Cl <sub>2</sub> )·0.5(C <sub>7</sub> H <sub>8</sub> )
<i>M<sub>r</sub></i>	1595.74	1407.68
Crystal system, space group	Triclinic, <i>P</i> 1	Monoclinic, <i>C</i> 2/ <i>m</i>
Temperature(K)	100	123
<i>a</i> , <i>b</i> , <i>c</i> (Å)	12.2750(2), 15.1740(3), 15.2342(4)	26.3937 (8), 13.3736 (3), 14.5566 (4)
$\alpha$ , $\beta$ , $\gamma$ (°)	84.1802(18), 71.9806(19), 67.3478(19)	105.432 (3)
<i>V</i> (Å <sup>3</sup> )	2489.70(10)	4952.9 (2)
<i>Z</i>	2	4
<i>F</i> (000)	1536	2691
<i>D<sub>x</sub></i> (Mg m <sup>-3</sup> )	2.129	1.888
Radiation type	Cu <i>K</i> α	Cu <i>K</i> α
$\mu$ (mm <sup>-1</sup> )	23.43	20.10
Crystal shape and colour	light yellow plate	Clear yellow prism
Crystal size(mm)	0.23 × 0.10 × 0.02	0.30 × 0.06 × 0.02
Data collection		
Diffractometer	XtLAB Synergy R, DW system, HyPix-Arc	SuperNova, Dualflex, Titan <sup>S2</sup>
Absorption correction	Gaussian	Gaussian
<i>T<sub>min</sub></i> , <i>T<sub>max</sub></i>	0.055, 0.715	0.186, 1.000
No. of measured, independent and observed [ <i>I</i> > 2σ( <i>I</i> )] reflections	51310, 10025, 9172	39393, 4578, 4026
<i>R<sub>int</sub></i>	0.052	0.059
(sin $\theta/\lambda$ ) <sub>max</sub> (Å <sup>-1</sup> )	0.625	0.597
Range of <i>h</i> , <i>k</i> , <i>l</i>	<i>h</i> = -15→14, <i>k</i> = -18→18, <i>l</i> = -18→19	<i>h</i> = -31→30, <i>k</i> = -15→13, <i>l</i> = -15→17
Refinement		
<i>R</i> [ <i>F</i> <sup>2</sup> > 2σ( <i>F</i> <sup>2</sup> )], <i>wR</i> ( <i>F</i> <sup>2</sup> ), <i>S</i>	0.032, 0.085, 1.03	0.050, 0.146, 1.13
No. of reflections	10025	4578
No. of parameters	701	333
No. of restraints	0	8
H-atom treatment	H-atom parameters constrained	H-atom parameters constrained
$\Delta$ <sub>max</sub> , $\Delta$ <sub>min</sub> (e Å <sup>-3</sup> )	1.40, -1.44	2.35, -1.77

Computer programs: *CrysAlis PRO* 1.171.41.93a (Rigaku OD, 2020), *SHELXT2018/5* (Sheldrick, 2018), *SHELXL2018/3* (Sheldrick, 2018).

**Table 5.3.** Experimental details for **6a** and **6b**.

Crystal data	6a	6b
CCDC Code	CCDC-2213603	CCDC-2213606
Chemical formula	C <sub>18</sub> H <sub>19</sub> Ag <sub>2</sub> FeN <sub>2</sub> P <sub>5</sub> ·2(SbF <sub>6</sub> )·0.7375(CH <sub>2</sub> Cl <sub>2</sub> )	C <sub>18</sub> H <sub>19</sub> Ag <sub>2</sub> FeN <sub>2</sub> P <sub>5</sub> ·(SbF <sub>6</sub> ) <sub>2</sub> ·0.35C <sub>7</sub> H <sub>8</sub> ·0.15CH <sub>2</sub> Cl <sub>2</sub>
<i>M<sub>r</sub></i>	1223.92	1206.28
Crystal system, space group	Monoclinic, <i>C2/c</i>	Triclinic, <i>P1</i>
Temperature(K)	80	90
<i>a, b, c</i> (Å)	32.2183(18), 18.4025(7), 13.0875(7)	10.754(2), 12.748(3), 13.237(3)
$\alpha, \beta, \gamma$ (°)	98.686 (6)	72.44(3), 83.95(3), 84.04(3)
<i>V</i> (Å <sup>3</sup> )	7670.5 (7)	1715.5(7)
<i>Z</i>	8	2
<i>F</i> (000)	4616	1140
<i>D<sub>x</sub></i> (Mg m <sup>-3</sup> )	2.120	2.335
Radiation type	Synchrotron, $\lambda = 0.6199$ Å	Synchrotron, $\lambda = 0.6199$ Å
$\mu$ (mm <sup>-1</sup> )	2.14	2.37
Crystal shape and colour	Green-brown rod	Green-brown rod
Crystal size(mm)	0.1 × 0.1 × 0.1	0.20 × 0.03 × 0.03
<b>Data collection</b>		
Diffractometer	P11 beamline, PETRA III, DESY, Eiger2 X 16M	P11 beamline, PETRA III, DESY, Eiger2 X 16M
Absorption correction	–	–
<i>T<sub>min</sub>, T<sub>max</sub></i>	–	–
No. of measured, independent and observed [ <i>I</i> > 2σ( <i>I</i> )] reflections	13295, 13295, 9699	18866, 5117, 4715
<i>R<sub>int</sub></i>	0.0736	0.036
(sin $\theta$ /λ) <sub>max</sub> (Å <sup>-1</sup> )	0.633	0.585
Range of <i>h, k, l</i>	<i>h</i> = -40→40, <i>k</i> = -23→23, <i>l</i> = -16→16	<i>h</i> = -12→12, <i>k</i> = -14→14, <i>l</i> = -15→15
<b>Refinement</b>		
<i>R</i> [ <i>F</i> <sup>2</sup> > 2σ( <i>F</i> <sup>2</sup> )], <i>wR</i> ( <i>F</i> <sup>2</sup> ), <i>S</i>	0.089, 0.295, 1.19	0.044, 0.133, 1.17
No. of reflections	13295	5117
No. of parameters	307	455
No. of restraints	1	4
H-atom treatment	H-atom parameters constrained	H-atom parameters constrained
$\Delta$ <sub>max</sub> , $\Delta$ <sub>min</sub> (e Å <sup>-3</sup> )	3.12, -2.88	1.03, -1.81

Computer programs: CrysAlis PRO 1.171.42.43a (Rigaku OD, 2022) (6a); XDS (Kabsch, 2010) (6b); local software (Crystal Control) at P11 beamline, PETRA III, DESY; SHELXT2018/5 (Sheldrick, 2018), SHELXL2018/3 (Sheldrick, 2018).

**Table 5.4.** Experimental details for **7** and **8**.

Crystal data	<b>7</b>	<b>8</b>
CCDC Code	CCDC-2213605	CCDC-2213609
Chemical formula	C <sub>28</sub> H <sub>34</sub> Ag <sub>2</sub> Fe <sub>2</sub> N <sub>2</sub> P <sub>10</sub> ·2(SbF <sub>6</sub> )	C <sub>55</sub> H <sub>71</sub> Ag <sub>4</sub> Fe <sub>3</sub> N <sub>4</sub> P <sub>15</sub> ·4(SbF <sub>6</sub> )·1.075CH <sub>2</sub> Cl <sub>2</sub> ·0.375C <sub>7</sub> H <sub>8</sub>
<i>M<sub>r</sub></i>	1507.21	2920.58
Crystal system, space group	Triclinic, <i>P</i> 1	Triclinic, <i>P</i> 1
Temperature(K)	123	123
<i>a</i> , <i>b</i> , <i>c</i> (Å)	12.5363(3), 14.7029(4), 14.9194(4)	14.7297(3), 18.3736(3), 18.5896(2)
$\alpha$ , $\beta$ , $\gamma$ (°)	64.664(3), 86.294(2), 73.696(2)	76.6156(12), 87.0804(16), 81.8419(16)
<i>V</i> (Å <sup>3</sup> )	2380.59(12)	4844.02(13)
<i>Z</i>	2	2
<i>F</i> (000)	1444	2808
<i>D<sub>x</sub></i> (Mg m <sup>-3</sup> )	2.103	2.002
Radiation type	Cu <i>K</i> $\alpha$	Cu <i>K</i> $\alpha$
$\mu$ (mm <sup>-1</sup> )	23.89	22.32
Crystal shape and colour	dark brown elongated plate	light brown prism
Crystal size(mm)	0.30 × 0.10 × 0.06	0.23 × 0.14 × 0.02
Data collection		
Diffractometer	SuperNova, Dualflex, Titan <sup>S2</sup>	XtaLAB Synergy R, DW system, HyPix-Arc 150
Absorption correction	Gaussian	Gaussian
<i>T<sub>min</sub></i> , <i>T<sub>max</sub></i>	0.073, 0.438	0.045, 1.000
No. of measured, independent and observed [ <i>I</i> > 2 $\sigma$ ( <i>I</i> )] reflections	35067, 8379, 7174	88379, 19374, 14714
<i>R<sub>int</sub></i>	0.055	0.097
( <i>sin</i> $\theta$ / $\lambda$ ) <sub>max</sub> (Å <sup>-1</sup> )	0.595	0.628
Range of <i>h</i> , <i>k</i> , <i>l</i>	<i>h</i> = -12→14, <i>k</i> = -16→17, <i>l</i> = -17→17	<i>h</i> = -18→15, <i>k</i> = -22→22, <i>l</i> = -22→23
Refinement		
<i>R</i> [ <i>F</i> <sup>2</sup> > 2 $\sigma$ ( <i>F</i> <sup>2</sup> )], <i>wR</i> ( <i>F</i> <sup>2</sup> ), <i>S</i>	0.029, 0.073, 0.97	0.077, 0.231, 1.04
No. of reflections	8379	19374
No. of parameters	533	1347
No. of restraints	0	18
H-atom treatment	H-atom parameters constrained	H-atom parameters constrained
$\Delta$ <sub>max</sub> , $\Delta$ <sub>min</sub> (e Å <sup>-3</sup> )	0.75, -1.13	1.61, -1.69

Computer programs: Computer programs: *CrysAlis PRO* 1.171.42.43a (Rigaku OD, 2022), *SHELXT2018/5* (Sheldrick, 2018), *SHELXL2018/3* (Sheldrick, 2018).

**Table 5.5.** Experimental details for **9** and **10**.

Crystal data	9	10
CCDC Code	CCDC-2213610	CCDC-2213607
Chemical formula	C <sub>47</sub> H <sub>72</sub> Ag <sub>3</sub> Fe <sub>3</sub> N <sub>2</sub> P <sub>15</sub> ·(SbF <sub>6</sub> ) <sub>3</sub> ·2.5(CH <sub>2</sub> Cl <sub>2</sub> )·1.4 75(C <sub>7</sub> H <sub>8</sub> )	C <sub>34</sub> H <sub>46</sub> Ag <sub>2</sub> Fe <sub>2</sub> N <sub>2</sub> P <sub>10</sub> ·2(SbF <sub>6</sub> )
<i>M<sub>r</sub></i>	2671.19	1591.37
Crystal system, space group	Monoclinic, <i>P</i> <sub>2</sub> <sub>1</sub> / <i>n</i>	Monoclinic, <i>P</i> <sub>2</sub> <sub>1</sub> / <i>n</i>
Temperature(K)	18	20
<i>a</i> , <i>b</i> , <i>c</i> (Å)	17.61292(11), 38.18946(18), 28.7137(3)	10.7985(4), 16.9711(4), 14.2483(5)
$\alpha$ , $\beta$ , $\gamma$ (°)	103.7019(8)	96.487(3)
<i>V</i> (Å <sup>3</sup> )	18764.0(2)	2594.47(14)
<i>Z</i>	8	2
<i>F</i> (000)	10406	1540
<i>D<sub>x</sub></i> (Mg m <sup>-3</sup> )	1.891	2.037
Radiation type	Synchrotron, $\lambda$ = 0.56002 Å	Synchrotron, $\lambda$ = 0.56002 Å
$\mu$ (mm <sup>-1</sup> )	1.25	1.41
Crystal shape and colour	brown green plate	green elongated plate
Crystal size(mm)	0.25 × 0.15 × 0.05	0.30 × 0.10 × 0.02
Data collection		
Diffractionmeter	P24 beamline, Huber diffractometer, Pilatus3 CdTe 1M	P24 beamline, Huber diffractometer, Pilatus3 CdTe 1M
Absorption correction	Multi-scan	Multi-scan
<i>T<sub>min</sub></i> , <i>T<sub>max</sub></i>	0.508, 1.000	0.810, 1.000
No. of measured, independent and observed [ <i>I</i> > 2σ( <i>I</i> )] reflections	258361, 45637, 42791	35249, 6350, 5830
<i>R<sub>int</sub></i>	0.036	0.047
(sin $\theta$ / $\lambda$ ) <sub>max</sub> (Å <sup>-1</sup> )	0.734	0.733
Range of <i>h</i> , <i>k</i> , <i>l</i>	<i>h</i> = -25→25, <i>k</i> = -54→55, <i>l</i> = -38→38	<i>h</i> = -15→15, <i>k</i> = -24→24, <i>l</i> = -20→20
Refinement		
<i>R</i> [ <i>F</i> <sup>2</sup> > 2σ( <i>F</i> <sup>2</sup> )], <i>wR</i> ( <i>F</i> <sup>2</sup> ), <i>S</i>	0.040, 0.108, 1.08	0.026, 0.072, 1.06
No. of reflections	45637	6350
No. of parameters	2463	295
No. of restraints	24	0
H-atom treatment	H-atom parameters constrained	H-atom parameters constrained
$\Delta$ <sub>max</sub> , $\Delta$ <sub>min</sub> (e Å <sup>-3</sup> )	2.59, -1.77	1.81, -0.57

Computer programs: local software, *CrysAlis PRO* 1.171.41.83a (Rigaku OD, 2020), *SHELXT2018/5* (Sheldrick, 2018), *SHELXL2018/3* (Sheldrick, 2018).

## 5.6 Author Contribution

- ❖ The synthesis and characterization of compound **1-7** was performed by K. Grill.
- ❖ The synthesis and characterization of compound **8-10** was performed by S. Dinauer.
- ❖ The byproduct of **I-III** was in all reactions present. The characterization was performed by K. Grill and S. Dinauer.
- ❖ The publication and experimental part were written by K. Grill.
- ❖ The section “crystallographic details and structure refinement” was written by Dr. E. Peresykina
- ❖ The X-ray structure analyses for compound **1-5** and **7** was performed by K. Grill.
- ❖ The X-ray structure analyses for compound **8** was performed by S. Dinauer.
- ❖ All Synchrotron (**6a**, **6b**, **9**, **10**) measurements were performed by Dr. E. Peresykina and A. V. Virovets, including sample preparation.
- ❖ The data reduction and all calculations were performed by Dr. E. Peresykina and A. V. Virovets.

## 5.7 References

- [1] J. Mohanty, S. D. Choudhury, N. Barooah, H. Pal, A. C. Bhasikuttan in *Comprehensive supramolecular chemistry II* (Ed.: J. L. Atwood), Elsevier, Amsterdam, **2017**, pp. 435–457.
- [2] a) H.-J. Schneider, A. K. Yatsimirsky, *Principles and methods in supramolecular chemistry*, Wiley, Chichester, **2000**; b) J. W. Steed, D. R. Turner, K. J. Wallace, *Core concepts in supramolecular chemistry and nanochemistry*, Wiley, Hoboken, NJ, **2007**.
- [3] a) K. Tiefenbacher, D. Ajami, J. Rebek, *Angew. Chem. Int. Ed.* **2011**, *50*, 12003; b) L. R. MacGillivray, J. L. Atwood, *Nature* **1997**, *389*, 469; c) W. Wei, W. Li, Z. Li, W. Su, M. Hong, *Chem. Eur. J.* **2013**, *19*, 469; d) D. Niu, Y. Jiang, L. Ji, G. Ouyang, M. Liu, *Angew. Chem. Int. Ed.* **2019**, *58*, 5946.
- [4] M. D. Pluth, K. N. Raymond, *Chem. Soc. Rev.* **2007**, *36*, 161.
- [5] a) T. Kreckmann, C. Diedrich, T. Pape, H. V. Huynh, S. Grimme, F. E. Hahn, *J. Am. Chem. Soc.* **2006**, *128*, 11808; b) A. V. Virovets, E. Peresykina, M. Scheer, *Chem. Rev.* **2021**, *121*, 14485.
- [6] a) S. Sevim, A. Sorrenti, C. Franco, S. Furukawa, S. Pané, A. J. deMello, J. Puigmartí-Luis, *Chem. Soc. Rev.* **2018**, *47*, 3788; b) K. Suzuki, M. Kawano, M. Fujita, *Angew. Chem.* **2007**, *46*, 2819; c) V. Patroniak, M. Kubicki, A. Mondry, J. Lisowski, W. Radecka-Paryzek, *Dalton Trans.* **2004**, 3295; d) Y. Chu, A. Saad, P. Yin, J. Wu, O. Oms, A. Dolbecq, P. Mialane, T. Liu, *Chem. Eur. J.* **2016**, *22*, 11756.
- [7] M. Fujita, J. Yazaki, K. Ogura, *J. Am. Chem. Soc.* **1990**, *112*, 5645.

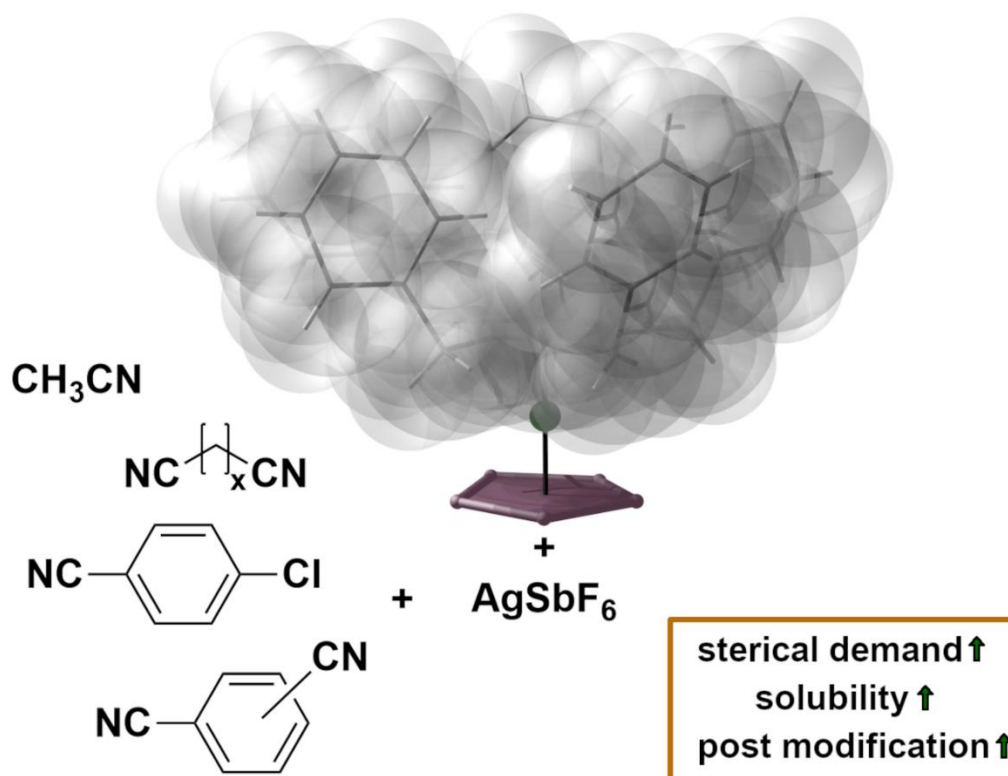
- [8] a) P. J. Stang, D. H. Cao, S. Saito, A. M. Arif, *J. Am. Chem. Soc.* **1995**, *117*, 6273; b) C. A. Hunter, *Angew. Chem. Int. Ed.* **1995**, *34*, 1079.
- [9] a) M. Fujita, Y. J. Kwon, S. Washizu, K. Ogura, *J. Am. Chem. Soc.* **1994**, *116*, 1151; b) M. Fujita, *J. Syn. Org. Chem., Jpn.* **1996**, *54*, 953.
- [10] M. Fujita, Y. J. Kwon, O. Sasaki, K. Yamaguchi, K. Ogura, *J. Am. Chem. Soc.* **1995**, *117*, 7287.
- [11] a) V. Guillerme, D. Maspoch, *J. Am. Chem. Soc.* **2019**, *141*, 16517; b) S. M. Cohen, Z. Zhang, J. A. Boissonnault, *Inorg. Chem.* **2016**, *55*, 7281; c) H. Kim, C. S. Hong, *CrystEngComm* **2021**, *23*, 1377; d) B. Attenberger, E. V. Peresyphkina, M. Scheer, *Inorg. Chem.* **2015**, *54*, 7021; e) M. Elsayed Moussa, B. Attenberger, E. V. Peresyphkina, M. Fleischmann, G. Balázs, M. Scheer, *Chem. Commun.* **2016**, *52*, 10004.
- [12] H. Brake, E. Peresyphkina, A. V. Virovets, W. Kremer, C. Klimas, C. Schwarzmaier, M. Scheer, *Inorg. Chem.* **2021**, *60*, 6027.
- [13] a) A. Lennartson, P. Southon, N. F. Sciortino, C. J. Kepert, C. Frandsen, S. Mørup, S. Piligkos, C. J. McKenzie, *Chem. Eur. J.* **2015**, *21*, 16066; b) L. Carlucci, G. Ciani, D. M. Proserpio, S. Rizzato, *CrystEngComm* **2002**, *4*, 413; c) E. Peresyphkina, M. Bielmeier, A. Virovets, M. Scheer, *Chem. Sci.* **2020**, *11*, 9067.
- [14] a) F. Dielmann, M. Fleischmann, C. Heindl, E. V. Peresyphkina, A. V. Virovets, R. M. Gschwind, M. Scheer, *Chem. Eur. J.* **2015**, *21*, 6208; b) E. Peresyphkina, C. Heindl, A. Virovets, H. Brake, E. Mädl, M. Scheer, *Chem. Eur. J.* **2018**, *24*, 2503; c) C. Heindl, E. Peresyphkina, A. V. Virovets, I. S. Bushmarinov, M. G. Medvedev, B. Krämer, B. Dittrich, M. Scheer, *Angew. Chem. Int. Ed.* **2017**, *56*, 13237; d) C. Heindl, E. Peresyphkina, A. V. Virovets, I. S. Bushmarinov, M. G. Medvedev, B. Krämer, B. Dittrich, M. Scheer, *Angew. Chem.* **2017**, *129*, 13420; e) M. Scheer, A. Schindler, R. Merkle, B. P. Johnson, M. Linseis, R. Winter, C. E. Anson, A. V. Virovets, *J. Am. Chem. Soc.* **2007**, *129*, 13386.
- [15] E. Peresyphkina, K. Grill, B. Hiltl, A. V. Virovets, W. Kremer, J. Hilgert, W. Tremel, M. Scheer, *Angew. Chem. Int. Ed.* **2021**, *60*, 12132-12142.
- [16] E. Peresyphkina, A. Virovets, M. Scheer, *Coord. Chem. Rev.* **2021**, *446*, 213995.
- [17] a) M. Detzel, G. Friedrich, O. J. Scherer, G. Wolmershäuser, *Angew. Chem. Int. Ed.* **1995**, *34*, 1321; b) S. Reichl, E. Mädl, F. Riedelberger, M. Piesch, G. Balázs, M. Seidl, M. Scheer, *Nat. Commun.* **2021**, *12*, 5774.
- [18] a) M. Fleischmann, J. S. Jones, F. P. Gabbai, M. Scheer, *Chem. Sci.* **2015**, *6*, 132. b) O. J. Scherer, H. Sitzmann, G. Wolmershäuser, *J. Organomet. Chem.* **1984**, *268*, C9-C12.
- [19] Burkhardt, A.; Pakendorf, T.; Reime, B. et al, *Eur. Phys. J. Plus* **2016**, *131*, 56-64.

- [20] [https://photon-science.desy.de/facilities/petra\\_iii/beamlines/p24-crystallography/eh2/index\\_eng.html](https://photon-science.desy.de/facilities/petra_iii/beamlines/p24-crystallography/eh2/index_eng.html) chemical
- [21] CrysAlisPro, different versions (Rigaku OD).
- [22] Sheldrick, G. M. *Acta Cryst. sect. C* **2015**, *C71*, 3.
- [23] Groom, C.R.; Bruno, I.J.; Lightfoot, M.P.; Ward S.C., *Acta Cryst. B72* (2016) 171-179.
- [24] Luo, C.-Z.; Gandeepan, P.; Wu, Y.-C.; Tsai, C.-H.; Cheng, C.-H., *ACS Catalysis*, 2015, 5, 4837.
- [25] O. V. Dolomanov, L. J. Bourhis, R. J. Gildea, J. A. K. Howard, H. Puschmann, *J. Appl. Cryst.* **2009**, *42*, 339-341.



## 6. Organic nitriles matter: A way to modify and connect discrete supramolecules based on bulky pentaphosphaferrocenes and Ag(I)

Kevin Grill, Eugenia Peresyphkina, Barbara Hiltl, Alexander V. Virovets and Manfred Scheer



**Abstract:** Over the years, numerous coordination polymers (CP) and supramolecular aggregates have been obtained from multi-component self-assembly reactions with pentaphosphaferrocenes, coinage metal salts of weakly coordinating anions such as  $\text{AgSbF}_6$  and organic ligands. Sterically less demanding pentaphosphaferrocenes such as  $[\text{Cp}^{\text{R}}\text{Fe}(\eta^5\text{-P}_5)]$  ( $\text{Cp}^{\text{R}} = \text{Cp}^* (\eta^5\text{-C}_5\text{Me}_5)$ ,  $\text{Cp}'' (\eta^5\text{-C}_5\text{H}_3\text{tBu}_{2-1,3})$ ) led to coordination products that were insoluble in common solvents or decomposed in coordinating ones, that considerably hampered applications and subsequent chemistry. A transfer of the approach of previous multi-component self-assembly to one of the most sterically demanding  $[\text{Cp}^{\text{Bn}}\text{Fe}(\eta^5\text{-P}_5)]$  ( $\text{Cp}^{\text{Bn}} = \eta^5\text{-C}_5(\text{CH}_2\text{Ph})_5$ ) (**1**) pentaphosphaferrocenes so far is reported and the influence of the  $\text{Cp}^{\text{Bn}}$  ligand on the system is demonstrated. In addition, the crucial influence of nitriles  $\text{CH}_3\text{CN}$ ,  $p\text{-NC}(\text{C}_6\text{H}_4)\text{Cl}$  and dinitriles  $\text{NC}(\text{CH}_2)_x\text{CN}$  ( $x = 8\text{-}10$ ),  $o\text{-}/m\text{-}/p\text{-}(\text{NC})_2\text{C}_6\text{H}_4$  on the self-assembly system with **1** and  $\text{AgSbF}_6$  is also highlighted. Furthermore, the use of  $p\text{-NC}(\text{C}_6\text{H}_4)\text{Cl}$  opens up an unprecedented possibility for the future post-synthetic modifications due to the chlorine group. All obtained coordination products were characterised by NMR-spectroscopy, mass spectrometry, elemental analysis, and X-ray crystallography.

## 6.1 Introduction

In recent decades, supramolecular chemistry has become one of the most fascinating and rapidly growing topics of contemporary research due to interdisciplinary influence of chemistry and biology. Its principles are based on the concepts of molecular self-assembly and recognition and focuses on rather weak interactions like van der Waals,  $\pi$ - $\pi$  interactions, or hydrogen bonding.<sup>[1,2]</sup> Furthermore, the introduction of metal-ligand bonding in the self-assembly gave rise to the so called 'metallo-supramolecular chemistry' which is distinguished by a better control over the self-assembly and can provide a more direct synthesis.<sup>[2]</sup> All this combined provides a fertile soil for a wide range of applications in different fields, e.g. of catalysis, sensing and capacitors.<sup>[3]</sup>

First results in the field of metallo-supramolecular chemistry were obtained by the groups of Stang<sup>[4]</sup>, Fujita<sup>[5]</sup> and Verkada<sup>[6]</sup> when with metal ions (Lewis acid) and organic ligands (Lewis base) stunning homo- and heterometallic coordination macrocycles and polymeric architectures were obtained. A noticeable aspect of these complexes is that coordination sites of the metal atom are blocked by coordinating chelating ligands such as ethylenediamine or 1,3-bis(diphenylphosphino)propane. By controlling possible coordination sites *via* such Lewis bases, the subsequent self-assembly with further Lewis bases can be skilfully controlled, thus predetermining whether the product obtained is a discrete or polymeric assembly.

Already in 1978, Sacconi succeeded in synthesizing a metal complex with an  $\eta^3$ -P<sub>3</sub> ligand (Lewis base) and a Co or Ni atom (Lewis acid).<sup>[7]</sup> This approach was quickly developed by using organic conjugated systems (e.g. arenes or cyclopentadienyl substituents) to introduce carbon based ligands. These ligands act rather as spectator ligands and be relatively inert in substitution reactions, but can be used to finetune the solubility and redox properties of the complexes.<sup>[8]</sup> Scherer successfully combined a Cp<sup>R</sup> ligand and an  $\eta^5$ -P<sub>5</sub> ligands by thermolysis or photolysis of a respective carbonyl complex of iron with white phosphorus making the obtained building block a Lewis base.<sup>[9]</sup>

With these in mind, we have already demonstrated that polyphosphorus complexes [Cp<sup>R</sup>Fe( $\eta^5$ -P<sub>5</sub>)] (Cp<sup>R</sup> = Cp\* ( $\eta^5$ -C<sub>5</sub>Me<sub>5</sub>), Cp<sup>Bn</sup> =  $\eta^5$ -C<sub>5</sub>(CH<sub>2</sub>Ph)<sub>5</sub> (**1**)) have excellent Lewis base properties due to their substituent-free P atoms and are thus exclusively bound to other P or metal atoms. In addition, the chosen Cp<sup>R</sup> ligands actively influence self-assembly through for example high sterical demand, as in **1**, whereby coordination sites can be blocked and also interactions to other Lewis acids. This in turn creates a unique coordination chemistry as shown for self-assembly with Cu(I), Cu(II) halides and triflates.<sup>[10,11-13]</sup> As Ag halides are insoluble in common solvents, this approach was successfully transferred to AgSbF<sub>6</sub>.<sup>[14,15]</sup>

The introduction of silver salts of non-coordinating anions allows the use of coordination sites at metal cations for further coordination and therefore introduces the possibility of dinitriles into a self-assembly with  $[\text{Cp}^{\text{R}}\text{Fe}(\eta^5\text{-P}_5)]$  ( $\text{Cp}^{\text{R}} = \text{Cp}^*$ ,  $\text{Cp}''$  ( $\eta^5\text{-C}_5\text{H}_3\text{tBu}_{2-1,3}$ )) as the third component. Among them, rigid aromatic dinitriles *o-/m-/p*-NC(C<sub>6</sub>H<sub>4</sub>)CN (**x-BDN**,  $x = o-/m-/p-$ ) with a certain length and fixed bite angles lead to the formation of only simple coordination polymers with various dimensionality.<sup>[14]</sup> For flexible aliphatic dinitriles NC(CH<sub>2</sub>)<sub>x</sub>CN (**DNx**,  $x = 1-10$ ), simple 1D-3D coordination polymers for shorter chained **DNx** ( $x \leq 6$ ) and spectacular 3D supramolecular coordination networks of nanosized organometallic spherical host-guest assemblies for longer chained **DNx** ( $x \geq 7$ ) were obtained.<sup>[15]</sup>

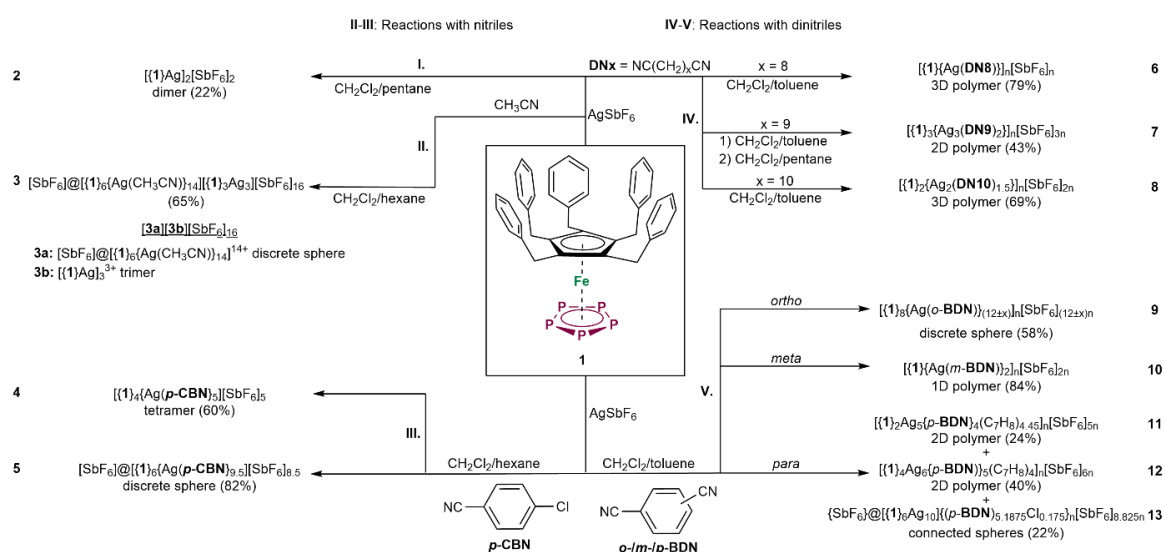
In view of the so far obtained results, the question arises as to how sterically more demanding pentaphosphaferrocenes will change the behavior of a multi-component self-assembly with different organic nitriles and AgSbF<sub>6</sub>. As already shown, bulky Cp<sup>R</sup> ligands also dramatically increase the solubility of the polyphosphorus complexes.<sup>[11-13]</sup> With these considerations in mind, we systematically investigated the behavior of  $[\text{Cp}^{\text{Bn}}\text{Fe}(\eta^5\text{-P}_5)]$  ( $\text{Cp}^{\text{Bn}} = \eta^5\text{-C}_5(\text{CH}_2\text{Ph})_5$ ) (**1**) in a self-assembly reaction with AgSbF<sub>6</sub> and various organic nitriles CH<sub>3</sub>CN, *p*-NC(C<sub>6</sub>H<sub>4</sub>)Cl (**p-CBN**), NC(CH<sub>2</sub>)<sub>x</sub>CN (**DNx**,  $x = 8-10$ ) or *o-/m-/p*-(NC)<sub>2</sub>(C<sub>6</sub>H<sub>4</sub>) (**o-/m-/p-BDN**) since the accessibility of the leaving group for future reactions does not have to be considered as is in the case of **p-CBN**. With the intention to obtain spherical supramolecules, we have selected only longer flexible aliphatic dinitriles **DNx** ( $x = 8-10$ ) to overcome the size of Cp<sup>Bn</sup> ligand. The resulting various coordination polymers and supramolecular assemblies show, on the one hand, the influence of the Cp<sup>Bn</sup> ligand on multi-component self-assembly systems and, on the other hand, demonstrate the dependence of the resulting coordination product on variable nitriles from the smallest possible nitrile to flexible and rigid dinitriles. Furthermore, the controllability of the self-assembly system with the *p*-NC(C<sub>6</sub>H<sub>4</sub>)Cl ligand and paving the way for the first post-synthesis reactions of this chemistry is demonstrated.

## 6.2 Results and Discussion

### Two-Component Self-Assembly

The behaviour of  $[\text{Cp}^{\text{Bn}}\text{Fe}(\eta^5\text{-P}_5)]$  (**1**) and AgSbF<sub>6</sub> with coordinating and non-coordinating solvents was investigated to determine whether free coordination sites can be created on the silver cation with the heavy sterically demanding Cp ligand (Scheme 6.1-I,II). Henceforth, all reactions were controlled via concentration and ratio of the components. In a one pot reactions, a reaction solution with a 1:1 ratio was prepared by adding a 20 mmol·L<sup>-1</sup> solution of **1** in CH<sub>2</sub>Cl<sub>2</sub> dropwise to a 13.3 mmol·L<sup>-1</sup> solution of AgSbF<sub>6</sub> in CH<sub>2</sub>Cl<sub>2</sub>. The resulting mixture was stirred for 1h at room

temperature and then layered with pentane. After few hours, the formation of dark green prisms of the dimer  $[\{1\}Ag]_2[SbF_6]_2$  (**2**) (Figure 6.1) at the phase boundary is observed. A reaction mixture was prepared by adding a 24 mmol·L<sup>-1</sup> solution of AgSbF<sub>6</sub> in CH<sub>3</sub>CN dropwise to a 10 mmol·L<sup>-1</sup> solution of **1** in CH<sub>2</sub>Cl<sub>2</sub> in a ratio of 3:1. The reaction mixture was then stirred for 1h and then layered with hexane. After three days brown polyhedras of discrete supramolecular complex of  $[SbF_6]@[\{1\}_6(Ag(CH_3CN)_{14})][SbF_6]_{13}$  (**3**) are formed at the phase boundary (Figure 6.2). According to X-ray structure analysis, the dimer  $[\{1\}Ag_2]^{2+}$  (**2**) is built up by two *cyclo*-P<sub>5</sub> ligands coordinated in a η<sup>3:1</sup>-mode to Ag atoms (Figure 6.1, Table 6.1). Ag atoms are pseudo-trigonally coordinated to two different *cyclo*-P<sub>5</sub> ligand complexes. In addition, the Ag atom forms an asymmetric π-contact with one of the Cp<sup>Bn</sup> residues.



**Scheme 6.1.** One-pot two-component (I.) and three-component (II-V.) self-assembly reactions of **1**, AgSbF<sub>6</sub>, and various organic nitriles (II-III: nitriles; IV-V: dinitriles). Isolated crystalline yields are given in parentheses.

Comparing this with the earlier obtained 1D polymer  $[\{Cp^*Fe(\eta^5-P_5)\}_2Ag]_n[SbF_6]_n$ , the sterically more demanding Cp<sup>Bn</sup> ligands block accessible coordination sites of the Ag atoms and thus no further coordination is possible in this case.<sup>[15,16]</sup>

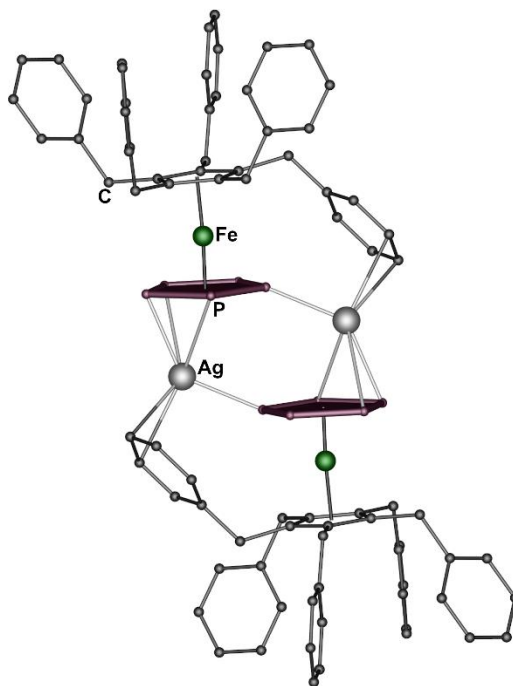


**Figure 6.1.** Cationic dimer  $[\{1\}_2\text{Ag}_2]^{2+}$  of **2**. H atoms and counterions are omitted for clarity.

Compound **3** consists of a discrete polycationic assemblies of  $[\text{SbF}_6]@[\{1\}_6\{\text{Ag}(\text{CH}_3\text{CN})\}_{14}][\{1\}_3\text{Ag}_3][\text{SbF}_6]_{16}$  in one unit cell, according to preliminary data. In the cationic sphere  $[\text{SbF}_6]@[\{1\}_6\{\text{Ag}(\text{CH}_3\text{CN})\}_{14}]^{13+}$  **3a** all *cyclo*-P<sub>5</sub> ligands are coordinated in a 1,2,4-fashion to Ag atoms, forming 9-membered  $\{\text{Ag}_3\text{P}_6\}$  and 16-membered  $\{\text{Ag}_4\text{P}_{12}\}$  rings that build up the spherical inorganic scaffold (Figure 6.2). All Ag atoms are coordinatively saturated by CH<sub>3</sub>CN ligands. The sphere acts as a host for one SbF<sub>6</sub><sup>-</sup> anion. The centroids of the *cyclo*-P<sub>5</sub> ligands form a hexagonal prism with an inner diameter of about 1.03 nm. The sphere **3a** co-crystallizes with the trimer **3b**  $[\{1\}_3\text{Ag}]_3^{3+}$ . The latter consists of three *cyclo*-P<sub>5</sub> ligands coordinated in a 1,3 motif to Ag atoms, each supported by two extra  $\pi$  contacts (Table 6.1). Surprisingly, no CH<sub>3</sub>CN are coordinated to the trimer. In order to separate the sphere from the trimer, several attempts were made to further slow down the diffusion of the layering. Since even the thinnest of the Schlenks were used to obtain crystals at all, reactions were carried out at 0°C and CH<sub>2</sub>Cl<sub>2</sub> was replaced with CHCl<sub>3</sub>, whereby no crystallisation took place in the former and in the latter a black solid precipitated. Due to the preliminary data, no information about bond lengths and distances can be given. Interestingly, the dimer  $[\{\text{Cp}^*\text{Fe}(\eta^5\text{-P}_5)\}\text{Ag}(\text{CH}_3\text{CN})_2]_2[\text{SbF}_6]_2$ , could be obtained for sterically less demanding  $[\text{Cp}^*\text{Fe}(\eta^5\text{-P}_5)]$ , whereby coordinating CH<sub>3</sub>CN molecules block further polymerization.<sup>[15]</sup> Since if one compares **3** with previous results on dimeric structures the only changing factor is the sterically more demanding **1** and the resulting blocking of the free coordination sites at the Ag atom by it. In addition, the large Cp<sup>Bn</sup> ligand increases the overall solubility, which results in a significantly slower crystallization of Cp<sup>Bn</sup> derivatives compared to those of Cp\* ones.

The formation of **2** shows that free coordination sites at the Ag atoms can be created even without additional blocking ligands and sterically demanding ligands such as Cp<sup>Bn</sup> can be used for this purpose. Similar effect is achieved with weakly coordinating molecules such as CH<sub>3</sub>CN.

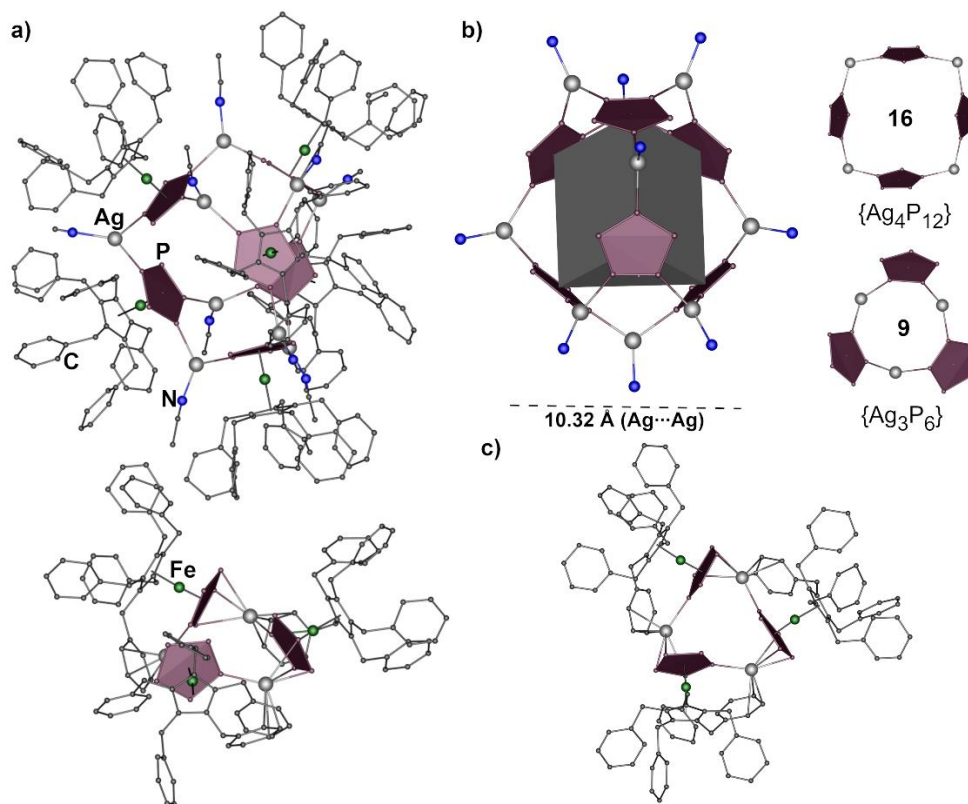


**Figure 6.2.** a) Cationic assemblies  $[\{1\}_6\{Ag(CH_3CN)\}_{14}][\{1\}_3Ag_3]^{17+}$  in **3**, b) inorganic spherical scaffold  $[\{1\}_6\{Ag(CH_3CN)\}_{14}]^{14+}$  (**3a**), c) trimer  $[\{1\}_3Ag_3]^{3+}$  (**3b**). H atoms and counterions are omitted for clarity.

### Three-Component Self-Assembly with *p*-NC(C<sub>6</sub>H<sub>4</sub>)Cl (*p*-CBN)

Since spherical supramolecules are already formed with acetonitrile, the smallest possible nitrile as a third component in the self-assembly of AgSbF<sub>6</sub> and **1**, the next step would be to introduce higher functionality compared to acetonitrile to a supramolecule and thus enable post-modification. For this purpose, *p*-NC(C<sub>6</sub>H<sub>4</sub>)Cl (*p*-CBN) was chosen because it possesses a rigid linear structure as acetonitrile and has a chlorine atom in *para*-position as a potential leaving group. Being unhindered by Cp<sup>Bn</sup> ligands of **1** due to an overall ligand length of 6.96–7.08 Å, it is available for e.g. substitution reactions.

A mixture of **1** and *p*-CBN in CH<sub>2</sub>Cl<sub>2</sub> was added dropwise to an 8 mmol·L<sup>-1</sup> AgSbF<sub>6</sub> solution in CH<sub>2</sub>Cl<sub>2</sub>, stirred for 20 min and layered with pentane or hexane. In an alternative procedure the dimer **2** in CH<sub>2</sub>Cl<sub>2</sub> is added dropwise to a solution of AgSbF<sub>6</sub> and *p*-CBN in CH<sub>2</sub>Cl<sub>2</sub>, stirred for 20h and layered with hexane (Scheme 6.2). Both ways lead to crystallization of the tetramer  $[\{1\}_4\{Ag(p\text{-CBN})\}_5][SbF_6]_5$  (**4**; green rods) (Figure 6.3). X-ray structure analysis reveals a curved shell of tetrameric cation  $[\{1\}_4Ag_5]^{5+}$ , whereby two fused  $\{Ag_3P_6\}$  rings are formed. The two *cyclo*-P<sub>5</sub> ligands

on the side apexes coordinate Ag atoms in a 1,2-fashion, whereas the middle two *cyclo*-P<sub>5</sub> ligands show a 1,2,3-coordination mode (Table 6.1). All Ag atoms coordinate one *p*-CBN ligand and complete their planar trigonal coordination environment. The widest inner diameter amounts to 12.34 Å (P...P) and 8.19 Å (Ag...Ag) at the narrowest point.

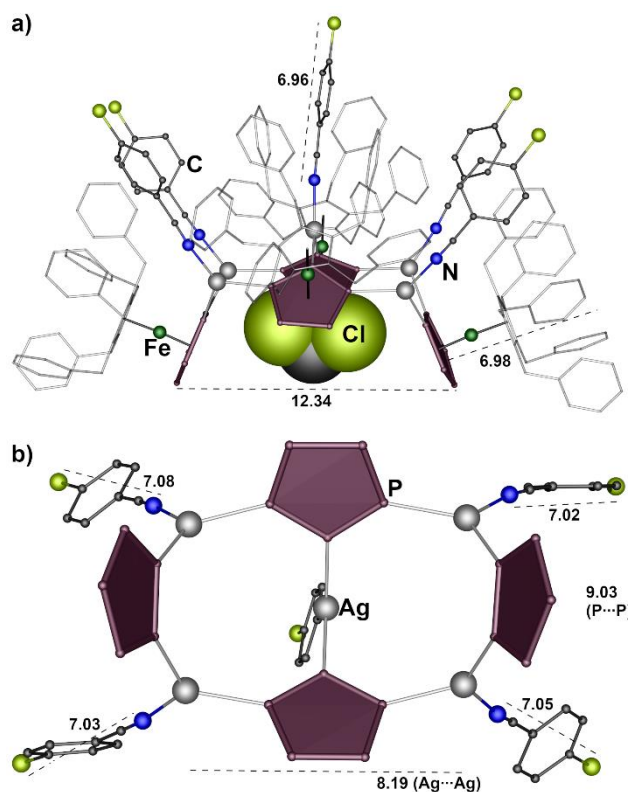


**Figure 6.3.** a) Tetrameric structural motif  $[{\{1\}}_4\text{Ag}_5(\text{p-CBN})_5]^{5+}$  of **4**, b) two nine membered rings of  $\{\text{Ag}_3\text{P}_6\}$ . H atoms and counterions are omitted for clarity.

Under more diluted conditions a mixture of 4  $\text{mmol}\cdot\text{L}^{-1}$  solution of **1** and *p*-CBN in toluene/pentane was layered on a 4  $\text{mmol}\cdot\text{L}^{-1}$  solution of  $\text{AgSbF}_6$  in  $\text{CH}_2\text{Cl}_2$ . After complete diffusion hexane was layered on the mixture that led to crystallization of red blocks with an average formula  $[\text{SbF}_6]@[\{1\}_6\{\text{Ag}(\text{p-CBN})_{9.5}\}[\text{SbF}_6]_{8.5}]$  (**5**). Compound **5** reveals the discrete spherical aggregate  $[\text{SbF}_6]@[\{1\}_6\{\text{Ag}(\text{p-CBN})_{9.5}\}]^{8.5+}$ . Its inorganic core is formed by six units of **1** arranged in a distorted trigonal antiprism which are connected by  $[\text{Ag}\{\text{p-CBN}\}]^+$  fragments (Figure 6.4). The ideal core would provide 14 positions accessible for Ag atoms, most of which are however only partly occupied resulting in an overall Ag amount of 9.5 Ag atoms. This implies that crystals of **5** contain different forms of supramolecules with a similar core, but different Ag content. As they overlap in the same crystallographic position, the arising disorder does not allow to distinguish each type of co-crystallized core.

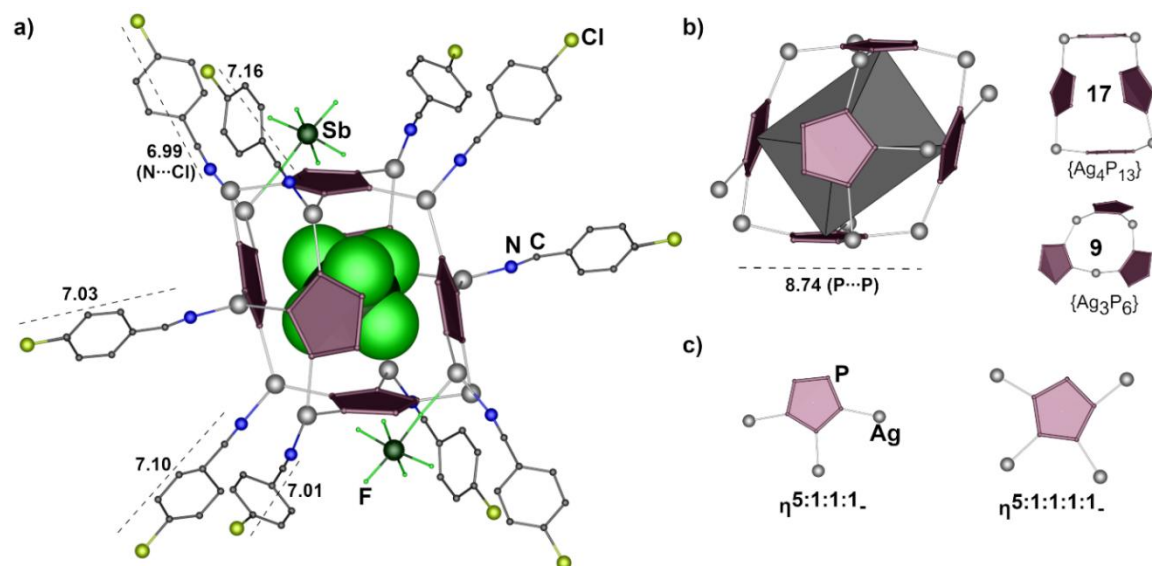


**Figure 6.4.** a) Supramolecular sphere  $[SbF_6]@[1]_6\{Ag(p-CBN)_{9.5}\}^{6.5+}$  **5** with  $SbF_6^-$  anion encapsulated; b) inorganic core based on 9- and 17- membered rings with trigonal antiprism formed by centres of cyclo- $P_5$  ligands c) coordination motifs of cyclo- $P_5$  ligands of **1**. H atoms and counterions are omitted for clarity.

For example, a mixture of 50%  $[[1]_6\{Ag\}_9]^{9+}$  and 50%  $[[1]_6\{Ag\}_{10}]^{10+}$  would give the sum formula. Considering the core  $[[1]_6\{Ag\}_{10}]^{10+}$  which includes the 10 Ag cations with major occupancies, which has at least 50% content in the solid solution, four ligands **1** coordinate in a 1,2,3- and two ligands in a 1,2,3,4-mode to the Ag atoms. Eight of the ten considered Ag atoms show a trigonal coordination environment of two units **1** and one *p*-CBN. However, two Ag atoms are in a pseudo tetrahedral coordination of one *cyclo*- $P_5$  ligand of **1**, one *p*-CBN, one  $SbF_6^-$  anion and aromatic C-C bond of one Bn residue. Therefore, due to the arrangement of the *cyclo*- $P_5$  ligands of **1** and the coordination environment of Ag atoms, the sphere thus consists of two large  $\{Ag_4P_{13}\}$  and four  $\{Ag_3P_6\}$ . In the resulting inner void of the sphere with a diameter of 8.74 Å, a  $SbF_6^-$  anion (diameter of 6.96 Å) is encapsulated, which acts as a guest for the scaffold. All remaining anions are in the outer sphere. Due to the long terminal *p*-CBN ligands coordinated to the Ag atoms and the bulky  $Cp^{Bn}$  residues, the supramolecular assembly **5** reaches an outer diameter of 3.5 nm. Interestingly, the structural motif of **4** can be found in the inorganic scaffold of **5** as a half shell of the sphere if minor occupied Ag positions are considered as well. Therefore, the pentanuclear complex **4** can be regarded as a possible intermediate towards spherical supramolecular assemblies, that can be formed in this highly labile self-assembly system. Furthermore, this pentanuclear moiety  $[[1]_4\{Ag\}_5]^{5+}$  is reminiscent of the structural fragments in other known supramolecules as  $[[1]_{12}\{CuSO_3CF_3\}_{19.6}]^{13}$ .

### Three-Component Self Assembly with flexible dinitrile ligands DN<sub>x</sub> (x = 8-10)

The next logical step was to use organic ligands with two nitrile groups in order to link supposed supramolecules to polymeric networks as it was demonstrated with flexible aliphatic dinitriles DN<sub>x</sub>



( $x = 1 - 10$ ) in the case of polyphosphorus complex  $[\text{Cp}^*\text{Fe}(\eta^5\text{-P}_5)]$ .<sup>[15]</sup> As the shorter dinitriles will be screened by steric requirements of the  $\text{Cp}^{\text{Bn}}$  ligand, we have chosen only the longest dinitriles **DN $x$**  ( $x = 8 - 10$ ) whose lengths exceed 13 Å and are compared to twice the length of *p*-CBN ligand.

All reactions were performed in a 1:1 ratio, the same concentrations and a 10-fold excess of linker with respect to **1** to prohibit restrictions by the amount of organic ligand in the form of stock solutions. Other ratios and concentrations proved to result in lower yields and poorer quality of the same crystalline products. For the reaction with **DN8**, a 10 mmol L<sup>-1</sup> AgSbF<sub>6</sub> solution in CH<sub>2</sub>Cl<sub>2</sub> was prepared and layered with a mixture of a 10 mmol L<sup>-1</sup> green solution of **1** in toluene and 0.4 mmol L<sup>-1</sup> **DN8** in CH<sub>2</sub>Cl<sub>2</sub>. After a few days, the brown-green plates of 3D polymer  $[\{\mathbf{1}\}\{\text{Ag}(\text{DN8})\}]_n[\text{SbF}_6]_n$  (**6**) (Figure 6.5 a, d) were obtained. With the same equimolar ratio and concentrations used but with an interlayer of CH<sub>2</sub>Cl<sub>2</sub>/toluene (2:1) between the CH<sub>2</sub>Cl<sub>2</sub> and toluene solution the reaction with **DN9** was prepared. As no crystallization was observed after complete diffusion, the mother liquor was removed, the residue dissolved in CH<sub>2</sub>Cl<sub>2</sub> and layered with pentane. In a month the formation of green needles of a 2D polymer  $[\{\mathbf{1}\}_3\{\text{Ag}_3(\text{DN9})_2\}]_n[\text{SbF}_6]_{3n}$  (**7**) (Figure 6.5b, e) was observed. In the case of **DN10**, under the same reaction conditions as for **8** brown-green plates of the 3D polymer  $[\{\mathbf{1}\}_4\{\text{Ag}_2(\text{DN10})_3\}]_n[\text{SbF}_6]_{4n}$  (**8**) were formed after a few days (Figure 6.5 c, f).

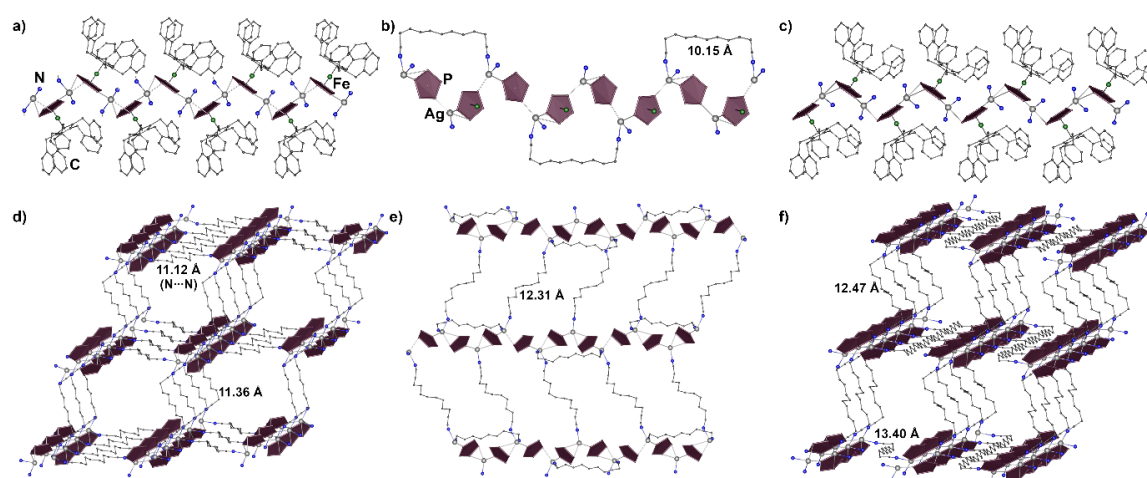
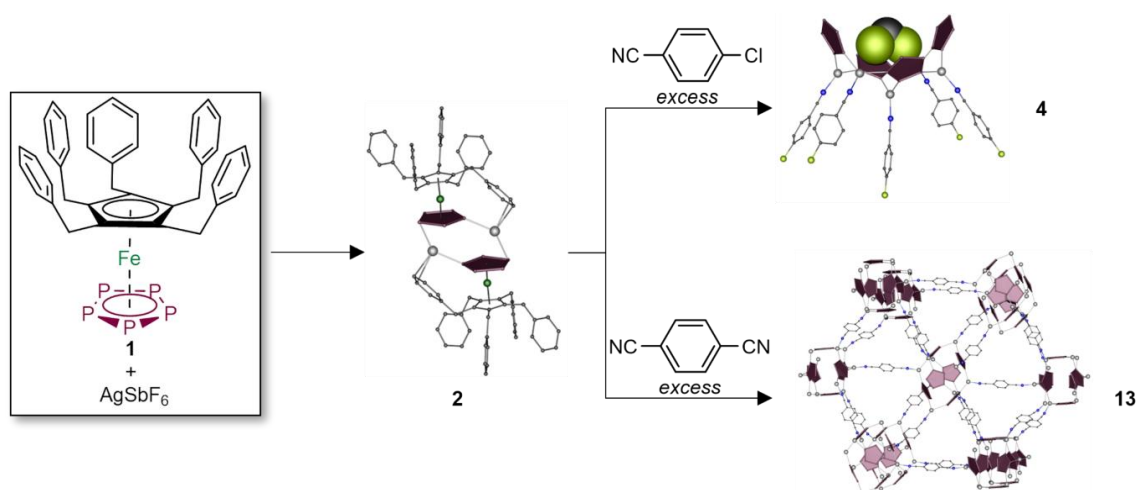


**Figure 6.5.** Cationic fragments in solid-state structures of compounds based on flexible dinitriles **DN $x$**  in a) **6**: ( $x = 8$ ), b) **7** ( $x = 9$ ), c) **8** ( $x = 10$ ): chain fragments  $[\{\mathbf{1}\}\text{Ag}]_n^{n+}$  and coordination networks based on them. d) 3D polymeric network of **6**, e) cationic 2D polymer of **7** with lateral coordinated **DN9**, f) 3D aggregate of **8**. H atoms and counterions are omitted for clarity.

According to single crystal X-ray structure analysis, the coordination polymers based on **1**, AgSbF<sub>6</sub> and flexible dinitriles **DN $x$**  ( $x = 8-10$ ) (Figure 6.5) do not form supramolecular nodes as in the case of  $[\text{Cp}^*\text{Fe}(\eta^5\text{-P}_5)]$  and consist of similar infinite 1D subunits  $[\{\mathbf{1}\}\text{Ag}]_n^{n+}$ , which are joined by **DN $x$**  linkers in either 2D (**7**) or 3D (**6**, **8**) networks. In the 1D strands, the *cyclo*-P<sub>5</sub> ligands are coordinated in a 1,3-mode to two different Ag atoms in a tetrahedral or pseudo-tetrahedral coordination

environment (Figure 6.5). All *cyclo*-P<sub>5</sub> ligands are additionally coordinated in a  $\eta^{2:1}$ -coordination (Figure 6.5a,c,e). The difference between the polymers (**6-8**) relies in the way of linking of the 1D strands. While the framework of the 3D polymers **6** (**DN8**) and **8** (**DN10**) is the same, the distance between the 1D strands of **6** significantly smaller than that in **8** (Table 6.1). Although the longer linker **DN10** is used in **8**, this does not necessarily lead to larger distances between the 1D strands due to the ligand folding. While in one direction the distance between two strands is significantly larger than that in **6**, another **DN10** ligand does not coordinate to the next Ag atom with free coordination sites as usual, but to the one after next, which results in closer 1D strands in the other direction than in **6** (Figure 6.5f). While one part of **DN9** linkers coordinates on the side of the 1D strand, the others link the strands to form a 2D polymer. In summary, in contrast to self-assembly system with [Cp\*Fe( $\eta^5$ -P<sub>5</sub>)], only simple 2D/3D coordination polymers were obtained even with the longest dinitriles **DNx** (x = 8-10) used. The formation of **6-8** shows that although **DNx** as linkers can link silver atoms despite steric demand of **1**, the formation of the spherical assemblies is hampered in this case.



**Scheme 6.2.** Alternative procedure and post-synthetic approach of compound **2** to obtain **4** and **13**.

### Three-Component Self-Assembly with rigid *o*-/*m*-/*p*-(NC)<sub>2</sub>(C<sub>6</sub>H<sub>4</sub>) (*o*-/*m*-/*p*-BDN) linkers

In previous sections, we have already demonstrated the availability of linkage of aggregates via dinitriles. Due to the known size of *o*-/*m*-/*p*-BDN as well as the predefined angles, we could already control a three-component self-assembly system with AgSbF<sub>6</sub> and less sterically demanding Cp<sup>R</sup>Fe( $\eta^5$ -P<sub>5</sub>) (Cp<sup>R</sup> = Cp\*, Cp'' ( $\eta^5$ -C<sub>5</sub>H<sub>3</sub>tBu<sub>2</sub>-1,3)).<sup>[14]</sup> An 8 mmol L<sup>-1</sup> AgSbF<sub>6</sub> solution in CH<sub>2</sub>Cl<sub>2</sub> is prepared in a one pot reaction using a 2:1 molar ratio of CH<sub>2</sub>Cl<sub>2</sub>/toluene interlayer, which is then covered with a mixture of **1** and *o*-BDN in toluene. This leads to brown blocks of molecular spherical aggregate  $[\{1\}_8\{\text{Ag}(\textit{o}\text{-BDN})\}_{(12\pm x)}]_n[\text{SbF}_6]_{(12\pm x)n}$  (preliminary structural characterization) (**9**) (Figure 6.6). Under the same conditions but with *m*-BDN green needles of the 1D polymer of  $[\{1\}\text{Ag}\{\textit{m}$ -

$\text{BDN}]_2]_n[\text{SbF}_6]_{2n}$  (**10**) were obtained (Figure 6.7). Changing to *p*-BDN, the reaction afforded three products crystallizing, green needles of the 2D polymer  $[\{1\}_2\text{Ag}_5\{p\text{-BDN}\}_4(\text{C}_7\text{H}_8)_{4.45}]_n[\text{SbF}_6]_{5n}$  (**11**) and the 2D polymer  $[\{1\}_4\text{Ag}_6\{p\text{-BDN}\}_4(\text{C}_7\text{H}_8)_4]_n[\text{SbF}_6]_{6n}$  (**12**) (Figure 6.8) and green prisms of the 3D polymer  $[\{1\}_6\text{Ag}_{10}\{p\text{-BDN}\}_5]_n[\text{SbF}_6]_{10n}$  (**13**) (Figure 6.9). An alternative procedure is to dissolve the dimer **2** in  $\text{CH}_2\text{Cl}_2$ , add a 10-fold excess of *p*-BDN, stir this mixture for 24h at r.t. and layer hexane over the reaction solution. After 30 days green prisms of **13** were isolated (Scheme 6.2). The supramolecular aggregate **9** is formed by using *o*-BDN in a one pot reaction with **1** and  $\text{AgSbF}_6$ . This preliminary solid-state structure is built up by a node of  $[\{1\}_6\text{Ag}_{12\pm x}]^{(12\pm x)+}$  and three *o*-BDN linkers which link the node to nearby units of  $[\{1\}\text{Ag}_3]^{3+}$  (Figure 6.6). Due to the small distance/angle between the nitrile groups, it is the shortest BDN used and thus has the most limited coordination possibilities compared to *m*-/*p*-BDN (table 6.1). As this crystal structure needs to be further refined, no details can be made about connectivity peculiarities, total number of Ag atoms and counterion, or about bond lengths and atom distances.

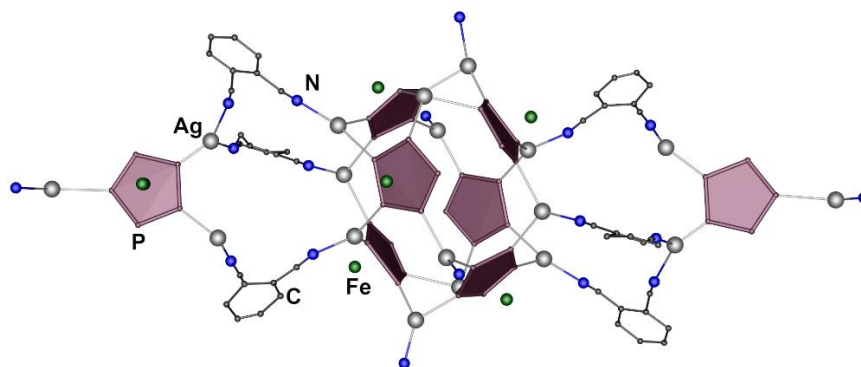


**Figure 6.6.** Inorganic scaffold of **9**. H atoms and counterions are omitted for clarity.

**Table 6.1.** Selected structural characteristics of all compounds.

Structure	Node	<i>cyclo</i> -P <sub>5</sub> coordination	N...N/C <sup>[a]</sup>	Ag-P <sup>[b]</sup>	Ag-C <sup>[b]</sup>
<b>2</b> (dimer)	$[\{1\}\text{Ag}_2]^{2+}$	1,3	-	2.54-2.62 ( $\sigma$ ); 2.95-3.05 ( $\pi$ )	2.52-2.75 ( $\pi$ )
<b>3a</b> (sphere)	$[\{1\}_6\{\text{Ag}(\text{CH}_3\text{CN})_{14}\}]^{14+}$	1,2,3,4,5; 1,2,3,4	-	2.46- 2.47*	- *
<b>3b</b> (trimer)	$[\{1\}\text{Ag}_3]^{3+}$	1,2,4	-	2.44, 2.56 ( $\sigma$ ); 2.96 ( $\pi$ ) *	- *
<b>4</b> (tetramer)	$[\{1\}_4\text{Ag}_5]^{5+}$	1,2; 1,2,3	7.02-7.08	2.45-2.49	-
<b>5</b> (sphere)	$[\{1\}_6\text{Ag}_{9.5}]^{9.5+}$	1,2,3; 1,2,4	6.99-7.16	2.25-2.51	2.53-2.70 ( $\pi$ ) , 2.24
<b>6</b> (polymer)	$[\{1\}\text{Ag}]_n^{n+}$	1,3	11.12, 11.36	2.44 ( $\sigma$ ); 2.66, 2.75 ( $\pi$ )	-
<b>7</b> (polymer)	$[\{1\}_3\text{Ag}_3]_n^{3n+}$	1,3	10.15, 12.31	2.32-2.55 ( $\sigma$ ); 2.64-2.93 ( $\pi$ )	-
<b>8</b> (polymer)	$[\{1\}_4\text{Ag}_2]_n^{2n+}$	1,3	12.47, 13.40	2.41-2.47 ( $\sigma$ ); 2.84-2.94 ( $\pi$ )	-

<b>9</b> (sphere)	$[\{1\}_6\text{Ag}_{12x}]^{(12+x)+}$	1,2,3; 1,2,3,4	3.76-4.14*	- *	- *
<b>10</b> (polymer)	$[\{1\}\text{Ag}]^+$	1	6.82	2.42	-
<b>11</b> (polymer)	$[\{1\}_2\text{Ag}_5]^{5+}$	1,2,4	7.88, 7.89	2.39-2.47	2.47-2.67 ( $\pi$ )
<b>12</b> (polymer)	$[\{1\}_2\text{Ag}_3]^{3+}$	1,2	7.77	2.36, 2.45	2.54-2.67 ( $\pi$ )
<b>13</b> (polymer)	$[\{1\}_6\text{Ag}_{10}]^{10+}$	1,2,3; 1,2,4; 1,2,3,4	7.82-7.88	2.35-2.49 ( $\sigma$ ); 2.72-3.03 ( $\pi$ )	2.44-2.55 ( $\pi$ )

[a] Range of intramolecular distances between donor atoms in (di)nitriles (in Å). [b] Range of bond distances (in Å). \*Preliminary results, no exact data can be given.

By using *m*-BDN the ladderlike 1D polymer **10** consisting of  $[\{1\}\text{Ag}]^+$  units are built up (Figure 6.7). The *cyclo*-P<sub>5</sub> ligand is coordinated in a 1,2-mode to Ag atoms which coordinate two dinitriles and form a trigonal coordination environment.

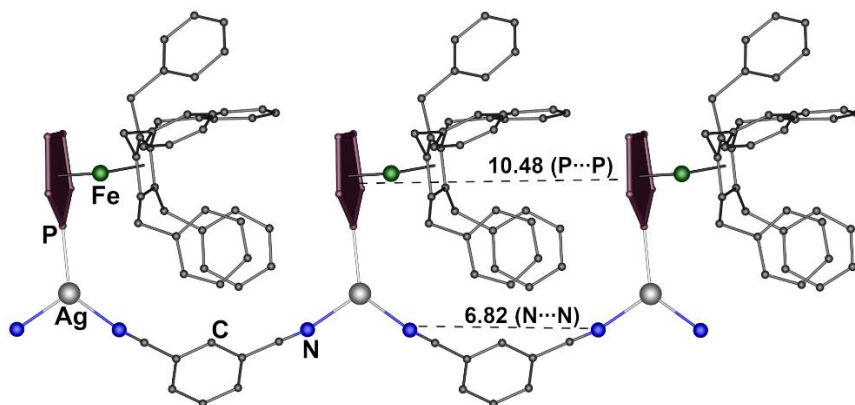


**Figure 6.7.** Cationic ladder-like 1D polymer of **10** consisting of  $[\{1\}\text{Ag}]^+$  units and *m*-BDN molecules. H atoms and counterions are omitted for clarity.

The polymers **11-13** are obtained with *p*-BDN by fractional crystallization. Crystals of **11** and **12** growing side by side at the former phase boundary after days while crystals of **13** are observed after a week in the bottom of the Schlenk. X-ray crystallography elucidates compound **11** as a 2D polymeric structure which can be considered as consisting of dimeric nodes of  $[\{1\}_2\text{Ag}_5]^{5+}$  with *cyclo*-P<sub>5</sub> ligands coordinating in a 1,2,4 coordination mode to Ag atoms (Figure 6.8a). All Ag atoms coordinate two different dinitrile ligands to give trigonal planar environment, except for the Ag atoms coordinated additionally to the *cyclo*-P<sub>5</sub> ligands in the position 3 which is coordinated to both a dinitrile ligand and asymmetrically to a  $\pi$ -bond of a toluene molecule (Table 6.1). Starting from one node, eight dinitriles link to four adjacent nodes and thus build up a 2D coordination polymer. The eight dinitriles interconnect four adjacent nodes (Figure 6.8a). The architecture **12** consists of dimeric nodes of  $[\{1\}_2\text{Ag}_3]^{3+}$  with *cyclo*-P<sub>5</sub> ligands coordinating to Ag atoms in a 1,3-coordination mode, with tetrahedrally or trigonally coordinated Ag atoms (Figure 6.8b). The environment of a tetrahedral Ag cation is formed by two *cyclo*-P<sub>5</sub> and two *p*-BDN ligands. The Ag cation in trigonal environment coordinates one *cyclo*-P<sub>5</sub> ligand, one dinitrile linker and a  $\pi$ -bond of a toluene

molecule (Table 6.1). The linkers interconnect four different neighbouring dimeric nodes and give rise to a 2D coordination polymer (Figure 6.8b). Interestingly, the nodes of **1** (orange + yellow) and **12** (orange) have a similar node structure, except that **11** has two more silver atoms coordinating the *cyclo*-P<sub>5</sub> ligand (position 2) (Figure 6.8c). This leads to more connections between the nodes through *p*-BDN, but not to a higher dimensionality. The coordinated toluene molecules occupy coordination sites on the outer silver atoms, which in turn limits the dimensionality of the polymer. These toluene molecules cannot be substituted by carrying out the reaction with an even larger excess of *p*-BDN.

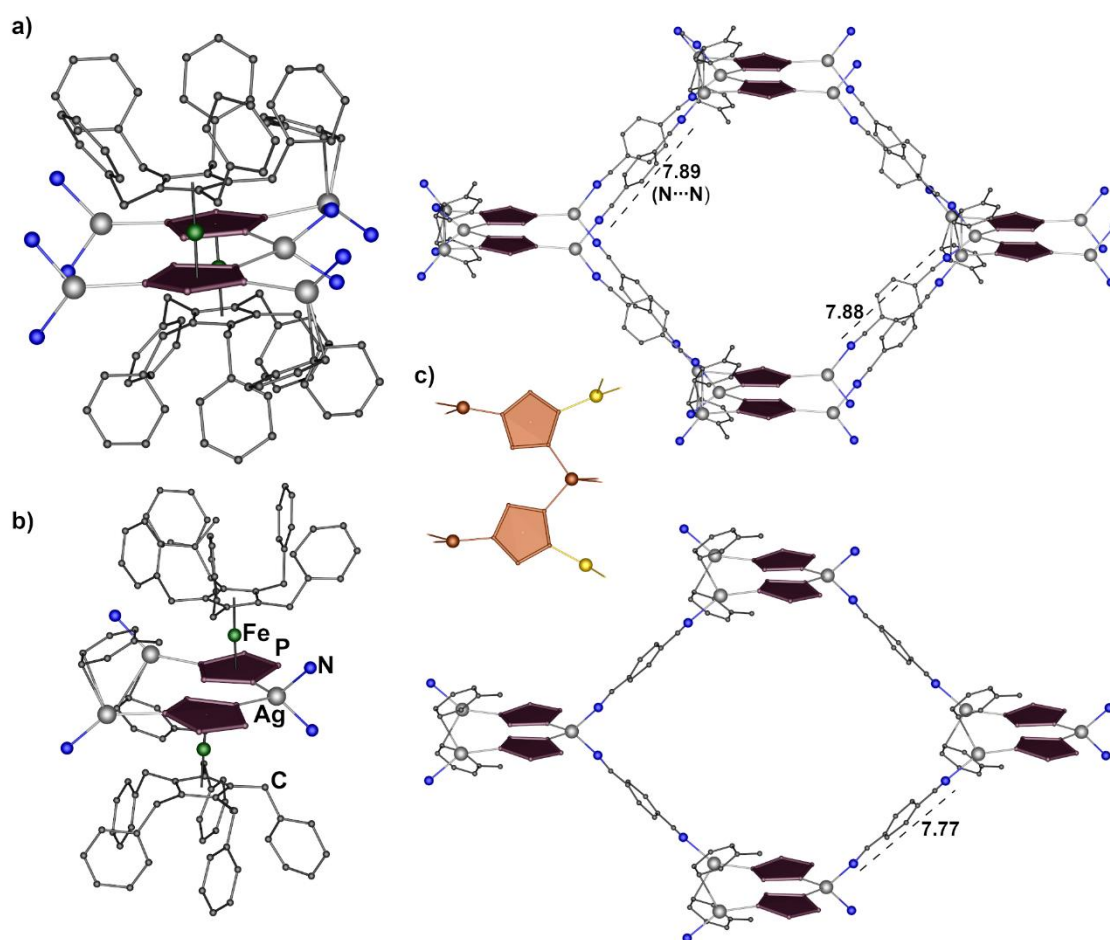


**Figure 6.8.** Crystal structure of compound **11** and **12**. a) Dimeric nodes  $[\{1\}_2\text{Ag}_5(\text{tol})_2]^{5+}$  in **11** and 2D cationic network in **11**, b) Dimeric node of **12** with the motif  $[\{1\}_2\text{Ag}_3(\text{tol})_2]^{6+}$  and 2D polymeric network. c) structural similarity of the repeating units in **11** (orange and yellow) and **12** (orange). H atoms and counterions are omitted for clarity.

Compound **13** is surprisingly a coordination network built up by polycationic spherical nodes of  $[\{1\}_6\text{Ag}_{10}]^{10+}$  (Figure 6.9) that are linked in a 3D polymeric network by *p*-BDN ligands. The node is formed by six *cyclo*-P<sub>5</sub> ligands that are coordinated by silver cations in 1,2,3-, 1,2,4- and 1,2,3,4- coordination mode (Figure 6.9c). This creates a nine-membered ring  $\{\text{Ag}_3\text{P}_6\}$  and a fourteen-membered ring  $\{\text{Ag}_4\text{P}_{10}\}$  (Figure 6.9a). The trigonal coordination environment of the Ag atoms is completed by one coordinated *p*-BDN molecule (Table 6.1), which links two neighbouring

supramolecular nodes and therefore one node is linked to ten nearby nodes to give a 3D polymeric network (Figure 6.9d). A node has an inner diameter of 8.62 Å and an outer diameter of 2.26 nm. In each inorganic core a  $\text{SbF}_6$  anion is encapsulated, while all other counterions are in outer sphere.

By controlling the three-component self-assembly system with **1**,  $\text{AgSbF}_6$  and *o*-/*m*-/*p*-BDN we succeeded to obtain unprecedented polymers consisting of spherical nodes in addition to simple coordination polymers. This novel type of polymers for pentaphosphaferrocene chemistry was obtained for the first time in the three-component self-assembly systems with various aliphatic  $\text{DN}_x$  ( $x = 7-10$ ),  $\text{AgSbF}_6$  and  $[\text{Cp}^*\text{Fe}(\eta^5\text{-P}_5)]$ . In our opinion the flexibility and length of the aliphatic dinitriles were one of the decisive factors of success in this case.<sup>[15]</sup> Since with shorter  $\text{DN}_x$  ( $x = 1 - 6$ ) and sterically less demanding  $[\text{Cp}^R\text{Fe}(\eta^5\text{-P}_5)]$  ( $\text{Cp}^R = \text{Cp}^*, \text{Cp}''$ ) compared to **1**, only simple coordination polymers could be obtained. With the results with **1**,  $\text{AgSbF}_6$  and *o*-/*m*-/*p*-BDN the self-assembly system seems to change and at the same time starts to become more unpredictable, which is why further investigations of the system are necessary.

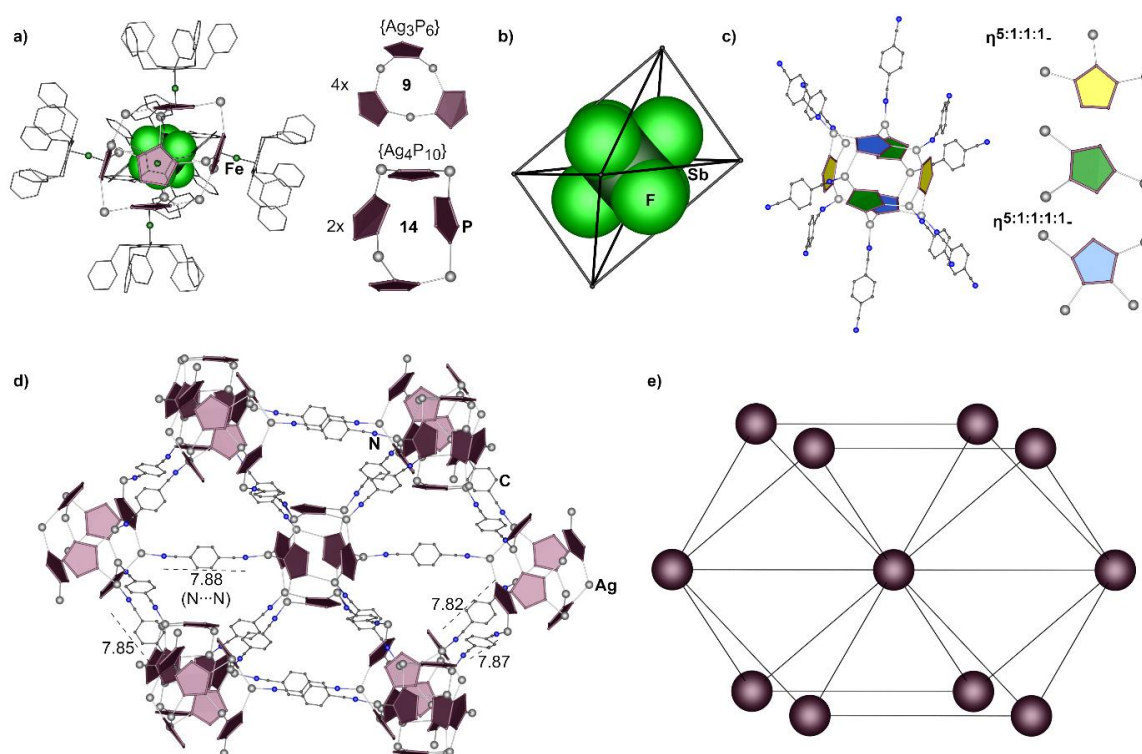


**Figure 6.9.** Polymer **13** with supramolecular assemblies as nodes. a) A  $(\text{SbF}_6)@[1]_6\text{Ag}_{10}^{10+}$  node based on 9- and 14-membered rings; b) trigonal antiprism formed by the centres of cyclo-P<sub>5</sub> rings; c) different coordination modes of the cyclo-P<sub>5</sub> ligands; d) section of the 3D cationic network, e) simplified network of **13**. H atoms, counterions and  $\text{Cp}^{\text{Bn}}$  ligands are omitted for clarity.

### 6.3 Conclusion

By turning from less sterically demanding pentaphosphaferrocenes, to one of the most sterically demanding pentaphosphaferrocene [Cp<sup>Bn</sup>Fe( $\eta^5$ -P<sub>5</sub>)] (**1**), we were able not only to highlight the drastic influence of the Cp<sup>Bn</sup> ligand on self-assembly using multi-component systems with AgSbF<sub>6</sub> and various organic nitriles CH<sub>3</sub>CN, *p*-CBN and dinitriles DN<sub>x</sub> (x = 8-10) or *o*-/*m*-/*p*-BDN but also to give a broad overview of the influence of the used organic linkers on the self-assembly process.

Despite the large Cp<sup>Bn</sup> ligand with its conformational flexibility of the Bn residues and the associated steric effects, free coordination sites on the Ag atoms could be obtained (**2**) and utilized by using non-coordination SbF<sub>6</sub><sup>-</sup> anions from the respective Ag salt. These sites could be used for the coordination of the smallest possible coordinating nitrile CH<sub>3</sub>CN and thus, unlike the chemistry of other [Cp<sup>R</sup>Fe( $\eta^5$ -P<sub>5</sub>)] derivatives, the first discrete spherical supramolecule **3** could be obtained. With only six *cyclo*-P<sub>5</sub> ligands of **1** the cationic supramolecule represents the smallest possible scaffold which is also able to encapsulate a small SbF<sub>6</sub><sup>-</sup> anion.

With *p*-CBN, it was possible to show that sterically more demanding terminal ligands can lead to tetramer **4** and spherical aggregate **5**, but also for the first time introduced a functional group in form of a good leaving group (Cl) into a self-assembly system based on P<sub>n</sub> ligand complexes. The para configuration in this case is necessary for better accessibility of the functional group for future substitution or other post-synthetic reactions.

By using aliphatic dinitriles DN<sub>x</sub> (x = 8-10) 2D (**7**) and 3D coordination polymers (**6**, **8**) were obtained. These have a similarly constructed 1D strand that is linked differently by the dinitriles used so that the distance between the strands grow with increasing length of DN<sub>x</sub> used, but with unforeseen exceptions between **6** and **8**, whereby in one direction the strands are closer in **8** (DN<sub>10</sub>) as in **6** (DN<sub>8</sub>). The 2D polymer **7**, results from DN<sub>9</sub> linkers coordinated on the side of the 1D strands blocking coordination sites on the Ag atom and therefore reducing the possible dimensionality compared to **6** and **8**.

These results from multicomponent self-assembly show the significant influence of the large steric demand of Cp<sup>Bn</sup> compared to previous results. Nevertheless, spherical polyphosphorus supramolecules assembled without additional stimuli, which, in combination with the increased solubility of the obtained scaffolds caused by the Cp<sup>Bn</sup> ligands, represents a novelty for supramolecular chemistry with P<sub>5</sub> ligand complexes and opens new perspectives in host-guest chemistry. Thus, based on our previous experience, targeted inclusion, and subsequent exclusion without damaging the inorganic framework seems to be possible, which represents the next step in this research and offers extensive perspectives for further adaptations of the structure. In

addition, the increased solubility offers completely new approaches in post-synthetic modifications for  $P_n$  ligand complexes in coordination compounds.

## 6.4 Exerimental Part

### General Remarks

All reactions were performed under an inert atmosphere of dry nitrogen with standard vacuum, Schlenk and glove-box techniques. Solvents were purified, dried, and degassed prior to use by standard procedures.  $[Cp^{Bn}Fe(\eta^5-P_5)]^{[18]}(\mathbf{1})$  was synthesized following reported procedures. Commercially available chemicals (AgSbF<sub>6</sub>, 1,2-Dicyanobenzene, 1,3-Dicyanobenzene, 1,4-Dicyanobenzene, 4-Chlorobenzonitrile) were used without further purification. Solution NMR spectra were recorded on Bruker Avance 300 or 400 spectrometer. The corresponding ESI-MS spectra were acquired on a ThermoQuest Finnigan MAT TSQ 7000 mass spectrometer. CHN elemental analyses were performed on a Vario EL III apparatus, whereas all other elements were determined by the Catalysis Research Center of the Technical University Munich by photometry, atomic absorption spectroscopy or titrimetry.

Due to the poor solubility of some products of  $[Cp^{Bn}Fe(\eta^5-P_5)]$  in common solvents, these NMR measurements were performed in CD<sub>3</sub>CN or were treated first with few amounts of pyridine and afterwards dissolved in CD<sub>2</sub>Cl<sub>2</sub>. Both techniques lead to a destruction of the compound, whereby only signals of the starting material can be observed in the respective NMR measurements.

### Synthesis of $[{Cp^{Bn}Fe(\eta^{5:1:1}-P_5)}Ag]_2[SbF_6]_2$ (**2**)

A solution of  $[Cp^{Bn}Fe(\eta^5-P_5)]$  (30 mg, 0.04 mmol) in CH<sub>2</sub>Cl<sub>2</sub> (2 mL) was dropped to a solution of AgSbF<sub>6</sub> (14 mg, 0.04 mmol) in CH<sub>2</sub>Cl<sub>2</sub> (3 mL). After stirring for 1h at r.t. the resulting red solution was layered with pentane. The formation of dark green prisms of **2** can be observed at the phase boundary after several hours. After complete diffusion, the mother liquor is decanted, the crystals are washed with hexane (3 × 10 mL) and dried *in vacuo*.

Analytical data of **2**

**Yield:** 20 mg (0.009 mmol, 22 % referred to  $[Cp^{Bn}Fe(\eta^5-P_5)]$ )

**<sup>1</sup>H NMR** (C<sub>6</sub>D<sub>6</sub>):  $\delta$  [ppm] = 3.77 (s,  $[Cp^{Bn}Fe(\eta^5-P_5)]$ ), 6.39 (d,  $[Cp^{Bn}Fe(\eta^5-P_5)]$ ), 6.67 (t,  $[Cp^{Bn}Fe(\eta^5-P_5)]$ ), 6.73 (t,  $[Cp^{Bn}Fe(\eta^5-P_5)]$ ).

**<sup>31</sup>P{<sup>1</sup>H} NMR** (C<sub>6</sub>D<sub>6</sub>):  $\delta$  [ppm] = 147.87 (s,  $[Cp^{Bn}Fe(\eta^5-P_5)]$ ).

**Positive ion ESI-MS** (CH<sub>2</sub>Cl<sub>2</sub>/CH<sub>3</sub>CN):  $m/z$  (%) = 191.29  $[Ag(CH_3CN)_2]^+$ , 834.44  $[{Cp^{Bn}Fe(\eta^5-P_5)}Ag]^+$ , 877.54  $[{Cp^{Bn}Fe(\eta^5-P_5)}Ag(CH_3CN)]^+$ , 1563.75  $[{Cp^{Bn}Fe(\eta^5-P_5)}_2Ag]^+$ .



**Negative ion ESI-MS** (CH<sub>2</sub>Cl<sub>2</sub>/CH<sub>3</sub>CN):  $m/z$  (%) = 234.52 [SbF<sub>6</sub>]<sup>-</sup>.

**Elemental analysis:** Calculated (%) for [{Cp<sup>Bn</sup>Fe(η<sup>5</sup>-P<sub>5</sub>)}]Ag<sub>2</sub>[SbF<sub>6</sub>]<sub>2</sub>·(CH<sub>2</sub>Cl<sub>2</sub>)<sub>2</sub> (2309.95 g/mol): C 42.64, H 3.3; found: C 42.73, H 3.35.

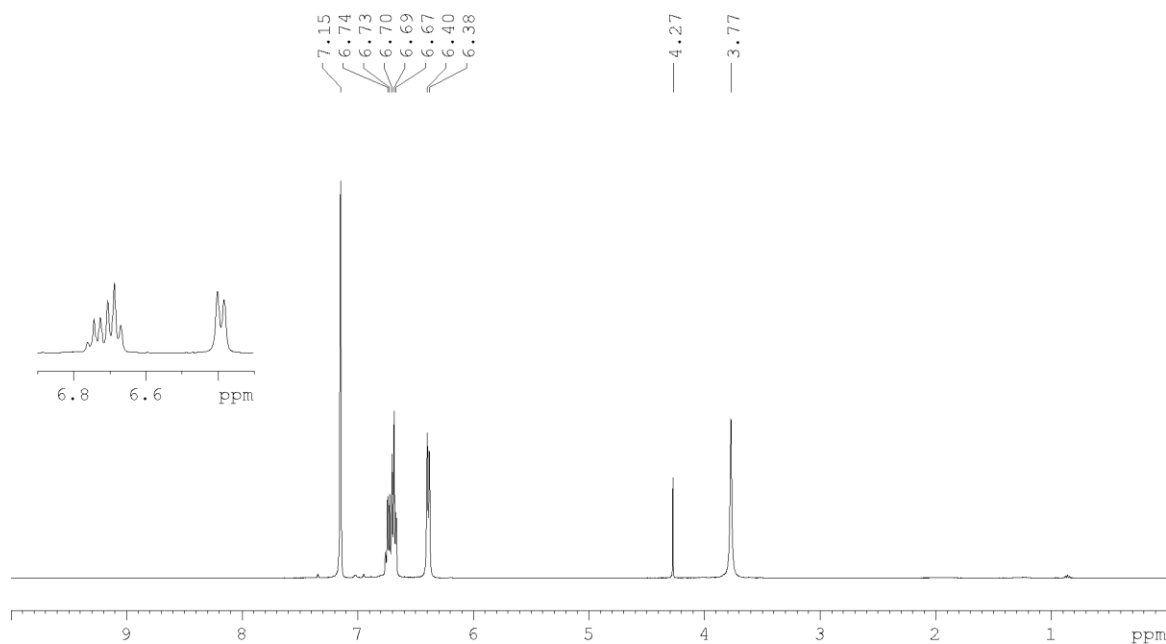


**Figure 6.10.** <sup>1</sup>H NMR spectrum of **2**. (4.27 CH<sub>2</sub>Cl<sub>2</sub>, 7.15 C<sub>6</sub>H<sub>6</sub>).

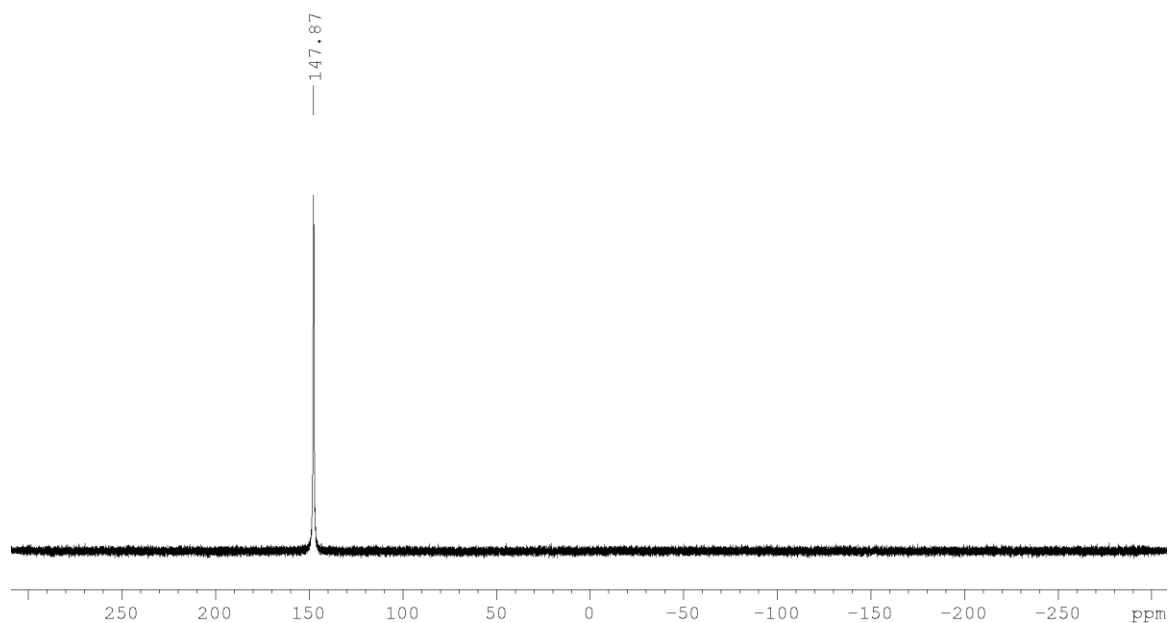


**Figure 6.11.** <sup>31</sup>P{<sup>1</sup>H} NMR spectrum of **2**.

### Synthesis of [SbF<sub>6</sub>]<sub>3</sub>@[{Cp<sup>Bn</sup>Fe(η<sup>5</sup>-P<sub>5</sub>)}]<sub>6</sub>(AgCH<sub>3</sub>CN)<sub>14</sub> [{Cp<sup>Bn</sup>Fe(η<sup>5</sup>-P<sub>5</sub>)}]<sub>3</sub>Ag<sub>3</sub>[SbF<sub>6</sub>]<sub>16</sub> (**3**)

In a thin Schlenk tube a solution of AgSbF<sub>6</sub> (41 mg, 0.12 mmol) in CH<sub>3</sub>CN (2 mL) was added to a green solution of [Cp<sup>Bn</sup>Fe(η<sup>5</sup>-P<sub>5</sub>)] (30 mg, 0.04 mmol) CH<sub>2</sub>Cl<sub>2</sub> (4 mL), stirred for 1h and layered with hexane (8 mL). After complete diffusion the mother liquor was removed, and the residue dissolved

in CH<sub>2</sub>Cl<sub>2</sub> (10 mL) and layered with hexane (10 mL). After one week the formation of green prism can (3) can be observed. After complete diffusion, the mother liquor is decanted, and the crystals were washed with hexane (3 × 5 mL) and dried *in vacuo*.

Analytical data of 3:

**Yield:** 25 mg (0.19 μmol, 4.8 % for an assumed composition of (C<sub>40</sub>H<sub>35</sub>FeP<sub>5</sub>)<sub>9</sub>(AgSbF<sub>6</sub>)<sub>17</sub>(CH<sub>3</sub>CN)<sub>14</sub>, 12954.01 g/mol)

**<sup>1</sup>H NMR** (CD<sub>2</sub>Cl<sub>2</sub>): δ [ppm] = 2.05 (s, CH<sub>3</sub>CN), 3.66 (s, [Cp<sup>Bn</sup>Fe(η<sup>5</sup>-P<sub>5</sub>)]), 6.36 (d, [Cp<sup>Bn</sup>Fe(η<sup>5</sup>-P<sub>5</sub>)]), 6.86 (t, [Cp<sup>Bn</sup>Fe(η<sup>5</sup>-P<sub>5</sub>)]), 6.99 (t, [Cp<sup>Bn</sup>Fe(η<sup>5</sup>-P<sub>5</sub>)]).

**<sup>31</sup>P{<sup>1</sup>H} NMR** (CD<sub>2</sub>Cl<sub>2</sub>): δ [ppm] = 142.37 (s, [Cp<sup>Bn</sup>Fe(η<sup>5</sup>-P<sub>5</sub>)]).

**Positive ion ESI-MS** (CH<sub>2</sub>Cl<sub>2</sub>/CH<sub>3</sub>CN): *m/z* (%) = 106.9 [Ag]<sup>+</sup>, 147.9 [Ag(CH<sub>3</sub>CN)]<sup>+</sup>, 188.9 [Ag(CH<sub>3</sub>CN)<sub>2</sub>]<sup>+</sup>, 832.9 [{Cp<sup>Bn</sup>Fe(η<sup>5</sup>-P<sub>5</sub>)}Ag]<sup>+</sup>, 1176.7 [{Cp<sup>Bn</sup>Fe(η<sup>5</sup>-P<sub>5</sub>)}Ag<sub>2</sub>(SbF<sub>6</sub>)]<sup>+</sup>, 1520.6 [{Cp<sup>Bn</sup>Fe(η<sup>5</sup>-P<sub>5</sub>)}Ag<sub>3</sub>(SbF<sub>6</sub>)<sub>2</sub>]<sup>+</sup>, 1561.1 [{Cp<sup>Bn</sup>Fe(η<sup>5</sup>-P<sub>5</sub>)<sub>2</sub>Ag]<sup>+</sup>.

**Negative ion ESI-MS** (CH<sub>2</sub>Cl<sub>2</sub>/CH<sub>3</sub>CN): *m/z* (%) = 234.9 [SbF<sub>6</sub>]<sup>-</sup>

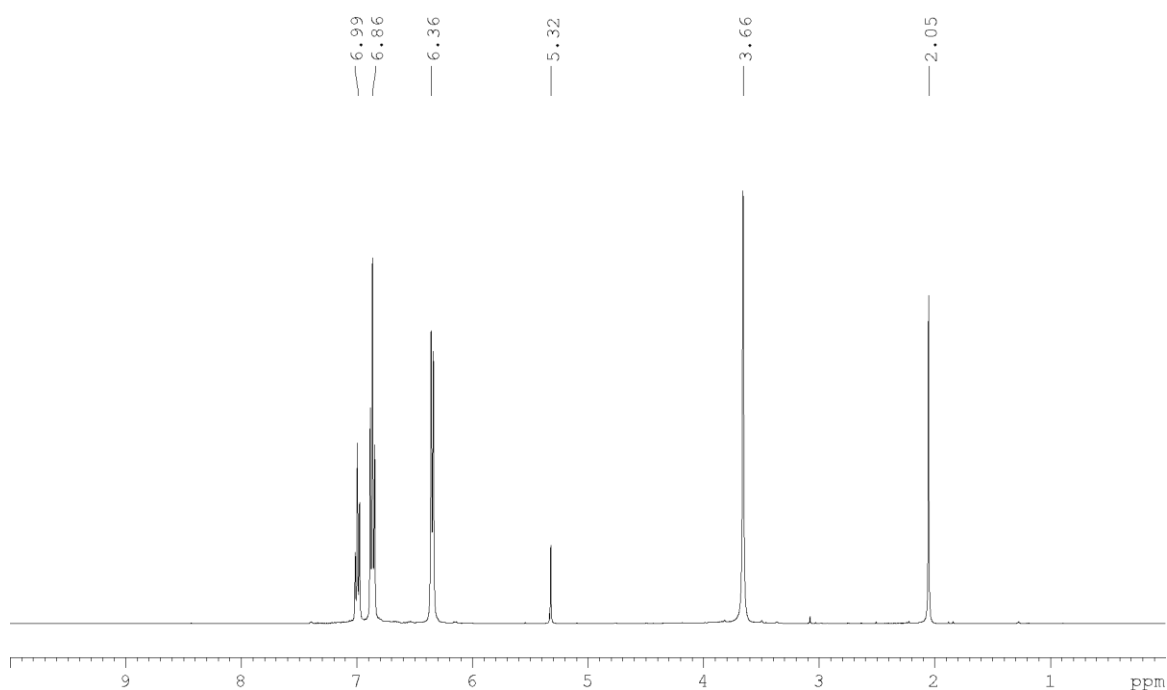


Figure 6.12. <sup>1</sup>H NMR spectrum of 3.

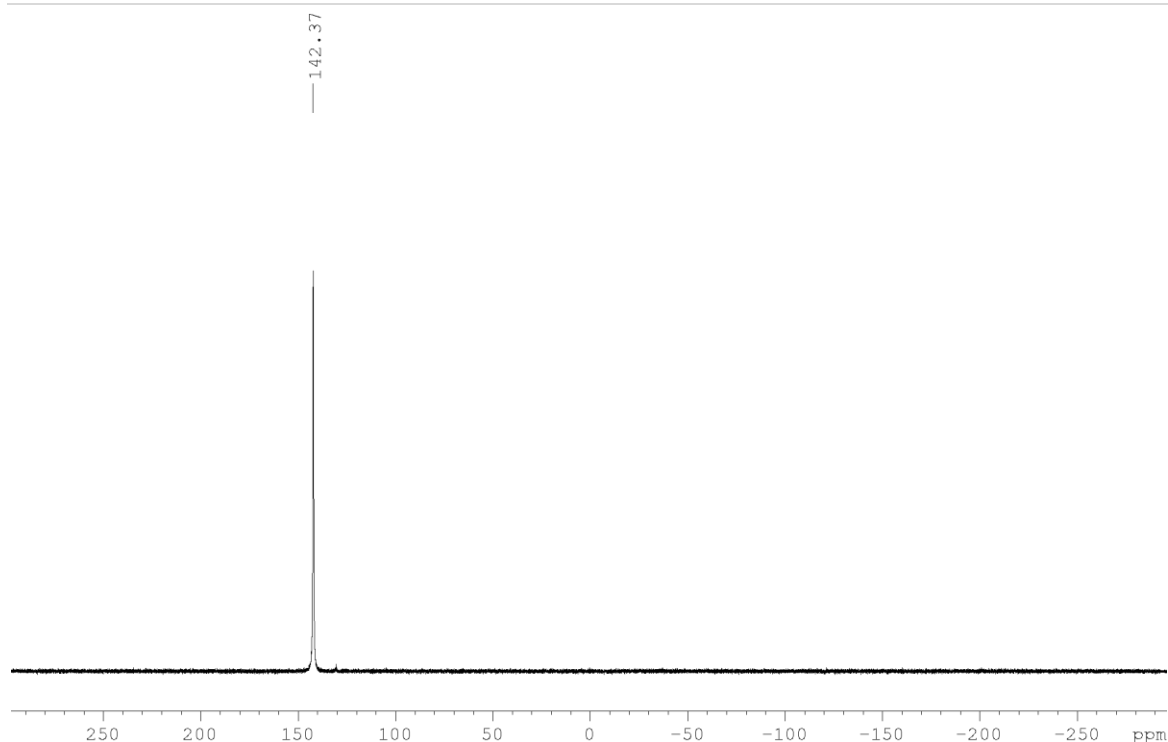


Figure 6.13.  $^{31}\text{P}\{^1\text{H}\}$  NMR spectrum of **3**.

#### Synthesis of $[\{\text{Cp}^{\text{Bn}}\text{Fe}(\eta^5\text{-P}_5)\}_4\{\text{Ag}(\text{NC}(\text{C}_6\text{H}_4)\text{Cl})\}_5\{\text{SbF}_6\}_5]$ (**4**)

A mixture of **1** (30 mg, 0.04 mmol) and *p*-Cl(C<sub>6</sub>H<sub>4</sub>)CN (55 mg, 0.4 mmol) in CH<sub>2</sub>Cl<sub>2</sub> (5 mL) was added dropwise to a solution of AgSbF<sub>6</sub> (15 mg, 0.04 mmol) in CH<sub>2</sub>Cl<sub>2</sub> (5 mL), stirred for 20 min and layered with hexane. One alternative procedure is to layer a solution of **1** in hexane (5 mL) on a mixture of AgSbF<sub>6</sub> and *p*-Cl(C<sub>6</sub>H<sub>4</sub>)CN in CH<sub>2</sub>Cl<sub>2</sub> (5 mL). Another procedure is to solve the dimer **2** (10 mg, 0.04 mmol) in CH<sub>2</sub>Cl<sub>2</sub> (5 mL) and drop a solution of *p*-Cl(C<sub>6</sub>H<sub>4</sub>)CN (55 mg, 0.4 mmol) in CH<sub>2</sub>Cl<sub>2</sub> (5 mL) to the dimer **2**, stir the mixture for 20h and layer hexane on the mixture. In all cases, the growth of green rods of **4** can be observed at the phase boundary after one day. After complete diffusion, the mother liquor is decanted, the crystals are washed with hexane (3 × 5 mL) and dried *in vacuo*.

Analytical data of **4**:

**Yield:** 26 mg (0.005 mmol, 60 % referred to [Cp<sup>Bn</sup>Fe(η<sup>5</sup>-P<sub>5</sub>)])

**$^1\text{H}$  NMR** (CH<sub>3</sub>CN):  $\delta$  [ppm] = 3.68 (s, [Cp<sup>Bn</sup>Fe(η<sup>5</sup>-P<sub>5</sub>)]), 6.27 (m, [Cp<sup>Bn</sup>Fe(η<sup>5</sup>-P<sub>5</sub>)]), 6.78 (m, [Cp<sup>Bn</sup>Fe(η<sup>5</sup>-P<sub>5</sub>)]), 6.93 (m, [Cp<sup>Bn</sup>Fe(η<sup>5</sup>-P<sub>5</sub>)]), 7.58 (dt, Cl-C<sub>6</sub>H<sub>4</sub>-CN), 7.71 (dt, Cl-C<sub>6</sub>H<sub>4</sub>-CN).

**$^{31}\text{P}\{^1\text{H}\}$  NMR** (CD<sub>2</sub>Cl<sub>2</sub>, 293 K):  $\delta$  [ppm] = 104.03 (s,  $\omega$  = 1170 Hz, [Cp<sup>Bn</sup>Fe(η<sup>5</sup>-P<sub>5</sub>)]), 146.56 (s,  $\omega$  = 578 Hz, [Cp<sup>Bn</sup>Fe(η<sup>5</sup>-P<sub>5</sub>)]).

**$^{31}\text{P}\{^1\text{H}\}$  NMR** (CD<sub>2</sub>Cl<sub>2</sub>, 193 K):  $\delta$  [ppm] = 104.20 (m(br)), 151.30 (m(br)).

**$^{19}\text{F}$  NMR** (C<sub>6</sub>D<sub>6</sub>):  $\delta$  [ppm] = -114.94 [SbF<sub>6</sub>]<sup>-</sup>.

**Positive ion ESI-MS** ( $\text{CH}_2\text{Cl}_2/\text{CH}_3\text{CN}$ ):  $m/z$  (%) = 190.9  $[\text{Ag}(\text{CH}_3\text{CN})_2]^+$ , 245.9  $[\text{Ag}(\text{NC}(\text{C}_6\text{H}_4)\text{Cl})]^+$ , 286.9  $[\text{Ag}(\text{CH}_3\text{CN})(\text{CN}(\text{C}_6\text{H}_4)\text{Cl})]^+$ , 382.9  $[\text{Ag}(\text{NC}(\text{C}_6\text{H}_4)\text{Cl})_2]^+$ , 832.9  $[\{\text{Cp}^{\text{Bn}}\text{Fe}(\eta^5\text{-P}_5)\text{Ag}\}]^+$ , 875.4  $[\{\text{Cp}^{\text{Bn}}\text{Fe}(\eta^5\text{-P}_5)\text{Ag}(\text{CH}_3\text{CN})\}]^+$ , 971.9  $[\{\text{Cp}^{\text{Bn}}\text{Fe}(\eta^5\text{-P}_5)\text{Ag}(\text{NC}(\text{C}_6\text{H}_4)\text{Cl})\}]^+$ , 1176.7  $[\{\text{Cp}^{\text{Bn}}\text{Fe}(\eta^5\text{-P}_5)\text{Ag}_2(\text{SbF}_6)\}]^+$ , 1218.9  $[\{\text{Cp}^{\text{Bn}}\text{Fe}(\eta^5\text{-P}_5)\text{Ag}_2(\text{SbF}_6)(\text{CH}_3\text{CN})\}]^+$ , 1904.6  $[\{\text{Cp}^{\text{Bn}}\text{Fe}(\eta^5\text{-P}_5)\text{Ag}_2(\text{SbF}_6)\}]^+$ , 2248.3  $[\{\text{Cp}^{\text{Bn}}\text{Fe}(\eta^5\text{-P}_5)\text{Ag}_3(\text{SbF}_6)_2\}]^+$ .

**Negative ion ESI-MS** ( $\text{CH}_2\text{Cl}_2/\text{CH}_3\text{CN}$ ):  $m/z$  (%) = 234.7  $[\text{SbF}_6]^-$ .

**Elemental analysis:** Calculated (%) for  $[\{\text{Cp}^{\text{Bn}}\text{Fe}(\eta^5\text{-P}_5)\}_4\{\text{Ag}(\text{NC}(\text{C}_6\text{H}_4)\text{Cl})\}_5][\text{SbF}_6]_5 \cdot (\text{CH}_2\text{Cl}_2)$  (5396.56 g/mol): C 43.64, H 3.03, N 1.30 ; found: C 43.11, H 3.12, N 1.20.

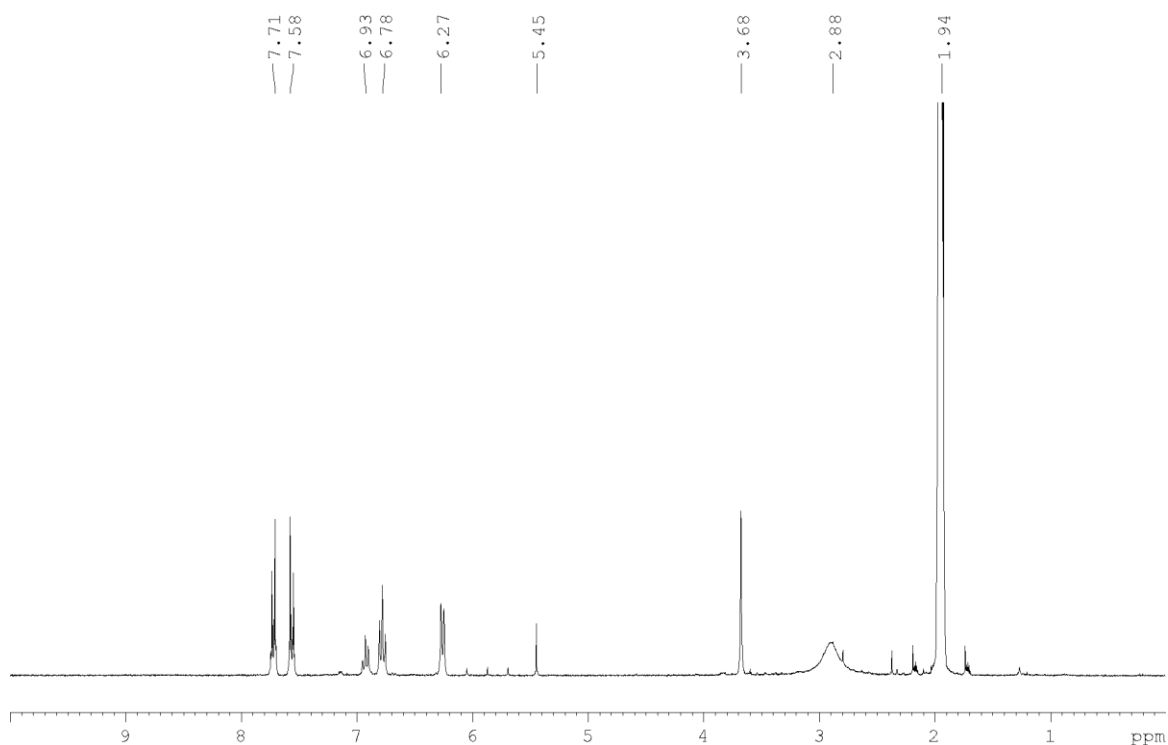


**Figure 6.14.**  $^1\text{H}$  NMR spectrum of **4**. (1.94  $\text{CH}_3\text{CN}$ , 2.88 organic residue)

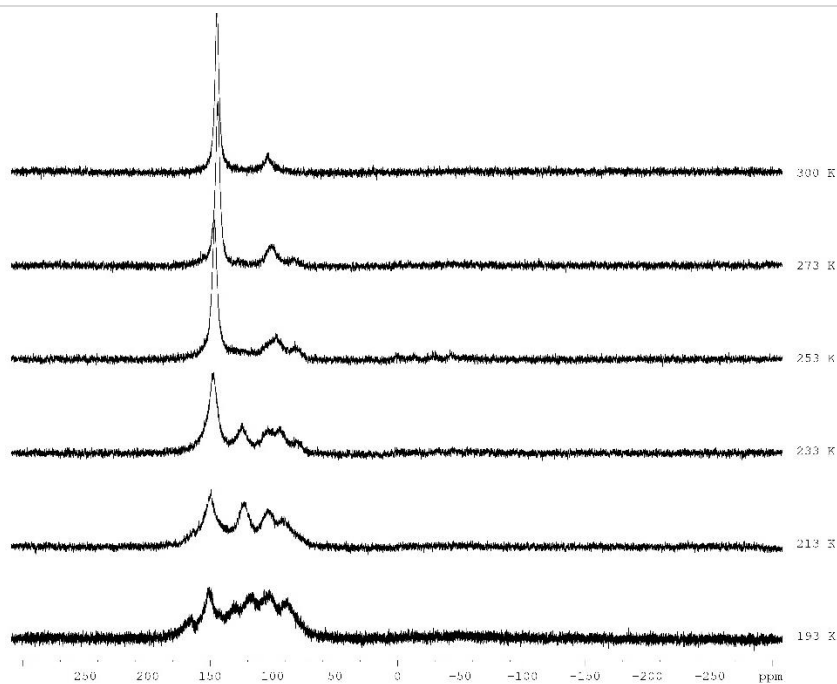


Figure 6.15.  $^{31}\text{P}\{^1\text{H}\}$  NMR spectrum of **4** in  $\text{CD}_2\text{Cl}_2$  at variable temperatures.

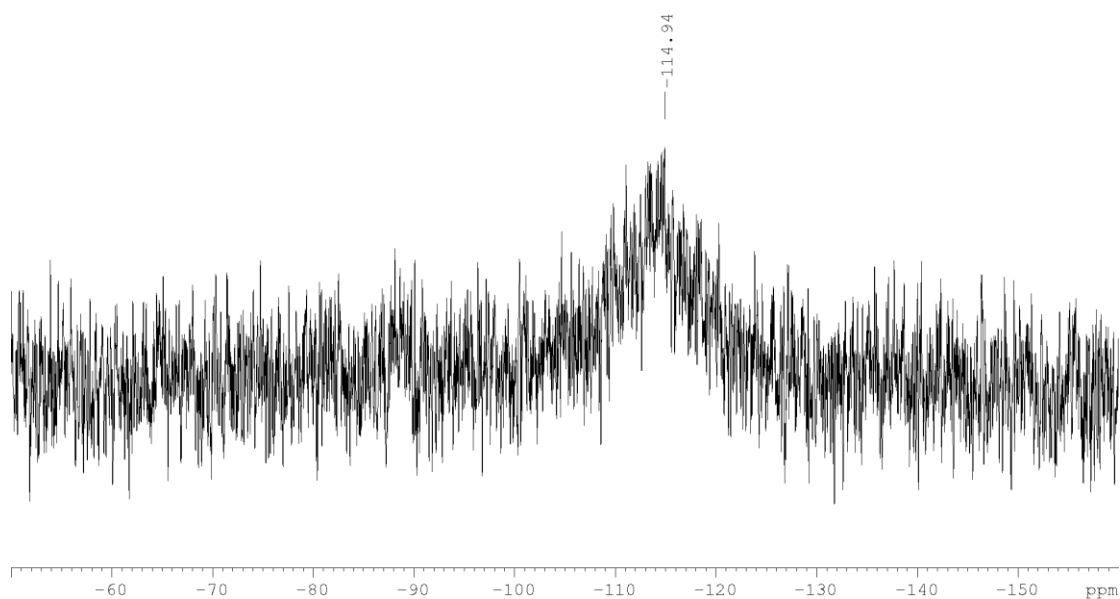


Figure 6.16.  $^{19}\text{F}\{^1\text{H}\}$  NMR spectrum of **4**.

#### Synthesis of $[\text{SbF}_6]@[\{\text{Cp}^{\text{Bn}}\text{Fe}(\eta^5\text{-P}_5)\}_6\{\text{Ag}(\text{NC}(\text{C}_6\text{H}_4)\text{Cl})\}_{9.55}][\text{SbF}_6]_{8.55}$ (**5**)

A mixture of **1** (30 mg, 0.04 mmol) and *p*-Cl( $\text{C}_6\text{H}_4$ )CN (55 mg, 0.4 mmol) in toluene/pentane (1:1, 10 mL) was layered on a solution of  $\text{AgSbF}_6$  (15 mg, 0.04 mmol) in  $\text{CH}_2\text{Cl}_2$  (10 mL). After complete diffusion, the reaction mixture was layered with hexane. The growth of red blocks of **5** can be observed in both procedures at the phase boundary after one day. After complete diffusion, the mother liquor is decanted, the crystals are washed with hexane ( $3 \times 5$  mL) and dried *in vacuo*.

Analytical data of **5**:

**Yield:** 49 mg (0.0055 mmol, 82 % referred to [Cp<sup>Bn</sup>Fe(η<sup>5</sup>-P<sub>5</sub>)])

**<sup>1</sup>H NMR** (CD<sub>2</sub>Cl<sub>2</sub>): δ [ppm] = 3.95 (m, [Cp<sup>Bn</sup>Fe(η<sup>5</sup>-P<sub>5</sub>)]), 6.40 (m, [Cp<sup>Bn</sup>Fe(η<sup>5</sup>-P<sub>5</sub>)]), 6.69 (m, [Cp<sup>Bn</sup>Fe(η<sup>5</sup>-P<sub>5</sub>)]), 6.90 (m, [Cp<sup>Bn</sup>Fe(η<sup>5</sup>-P<sub>5</sub>)]), 7.30 (m, Cl-C<sub>6</sub>H<sub>4</sub>-CN).

**<sup>31</sup>P{<sup>1</sup>H} NMR** (CD<sub>2</sub>Cl<sub>2</sub>, 293 K): δ [ppm] = 104.46 (s), 140.33 (s).

**<sup>31</sup>P{<sup>1</sup>H} NMR** (CD<sub>2</sub>Cl<sub>2</sub>, 193 K): δ [ppm] = -46.58 (m(br), ω<sub>1/2</sub> = 6000 Hz), 83.24 (m(br), ω<sub>1/2</sub> = 7000 Hz).

**Positive ion ESI-MS** (CH<sub>2</sub>Cl<sub>2</sub>/CH<sub>3</sub>CN): *m/z* (%) = 832.90 [(Cp<sup>Bn</sup>Fe(η<sup>5</sup>-P<sub>5</sub>))Ag]<sup>+</sup>, 1904.82 [(Cp<sup>Bn</sup>Fe(η<sup>5</sup>-P<sub>5</sub>))<sub>2</sub>Ag<sub>2</sub>(SbF<sub>6</sub>)]<sup>+</sup>.

**Negative ion ESI-MS** (CH<sub>2</sub>Cl<sub>2</sub>/CH<sub>3</sub>CN): *m/z* (%) = 234.90 [SbF<sub>6</sub>]<sup>-</sup>.

**Elemental analysis:** Calculated (%) for [SbF<sub>6</sub>]<sub>10</sub>[(Cp<sup>Bn</sup>Fe(η<sup>5</sup>-P<sub>5</sub>))<sub>6</sub>(Ag(NC(C<sub>6</sub>H<sub>4</sub>)Cl))] [SbF<sub>6</sub>]<sub>10</sub> (9170.39 g/mol): C 40.60, H 2.75, N 1.53, Ag 11.76, Fe 3.65, Cl 3.87, P 10.13; found: C 38.93, H 2.74, N 1.72, Ag 11.80, Fe 3.30, Cl 3.61, P 9.38.

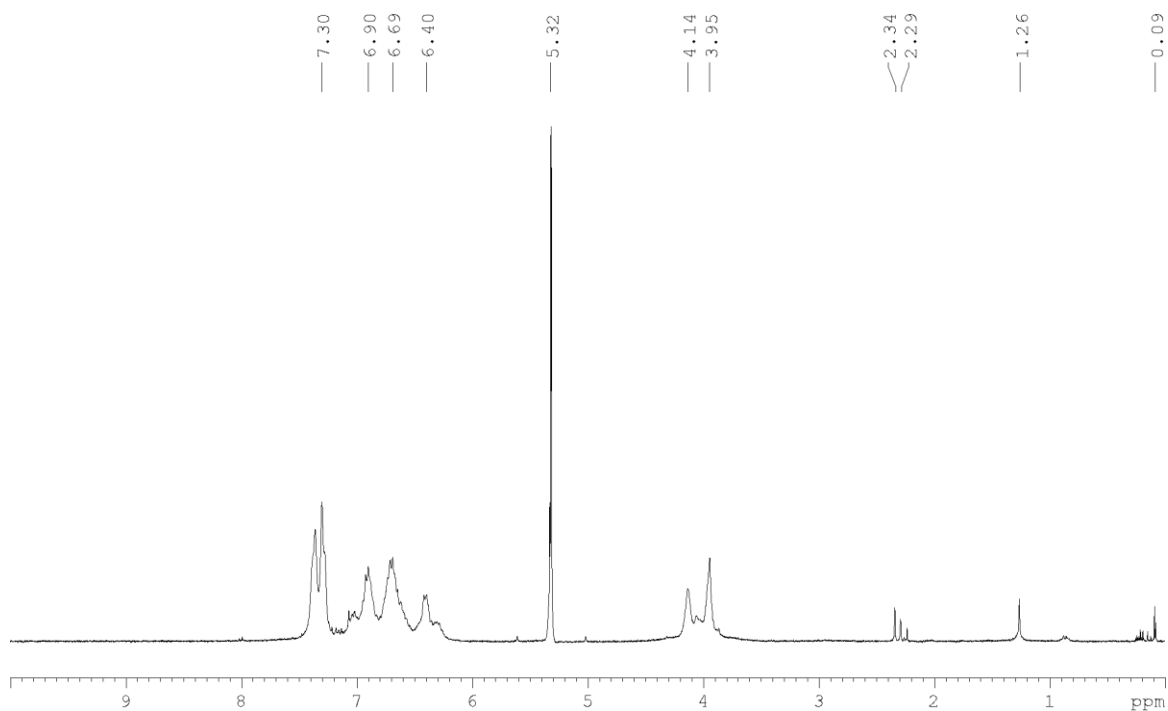


**Figure 6.17.** <sup>1</sup>H NMR spectrum of **5**. (0.09 grease, 0.89 hexane, 1.27 hexane, 2.29 solvent residues, 2.34 toluene)

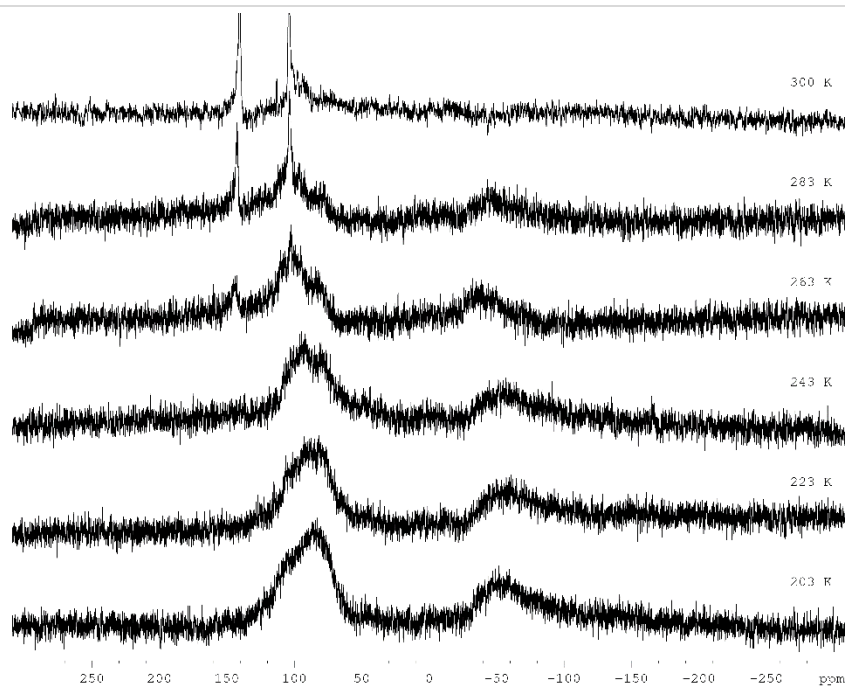


Figure 6.18.  $^{31}\text{P}\{^1\text{H}\}$  NMR spectrum of **5** in  $\text{CD}_2\text{Cl}_2$  at variable temperatures.

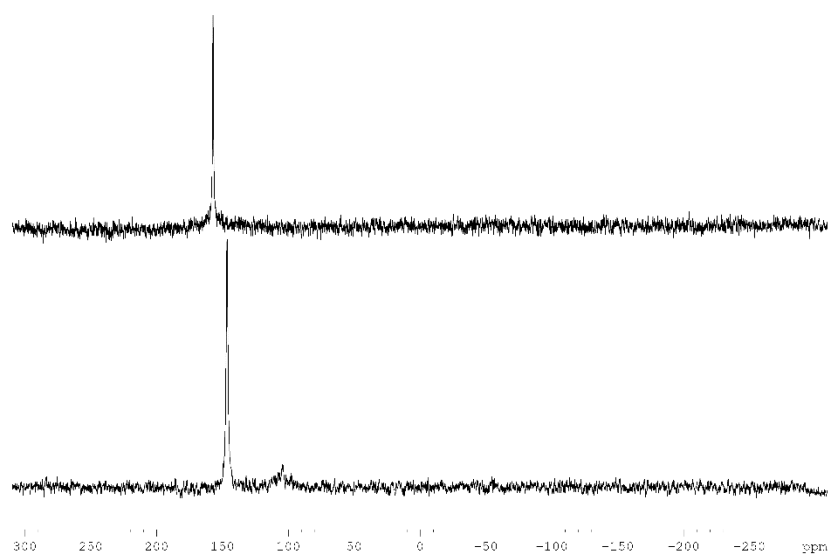


Figure 6.19.  $^{31}\text{P}\{^1\text{H}\}$  NMR spectrum of crystals of **5** in  $\text{CD}_2\text{Cl}_2$  after 24 h in solution (bottom) and after one week in solution (top). No precipitate or colour change was observed.

#### Synthesis of $[\{\text{Cp}^{\text{Bn}}\text{Fe}(\eta^5\text{-P}_5)\}\{\text{Ag}(\text{NC}(\text{CH}_2)_8\text{CN})\}]_n[\text{SbF}_6]_n$ (**6**)

In a Schlenk tube a solution of  $\text{AgSbF}_6$  (17 mg, 0.05 mmol) in  $\text{CH}_2\text{Cl}_2$  (5 mL) is carefully layered with a green solution of  $[\text{Cp}^{\text{Bn}}\text{Fe}(\eta^5\text{-P}_5)]$  (40 mg, 0.05 mmol) and  $\text{NC}(\text{CH}_2)_8\text{CN}$  (1 mL, 0.4 mmol, 0.4 mmol/mL in  $\text{CH}_2\text{Cl}_2$ ) in toluene (5 mL). Thereby, the phase boundary turns yellow. After a few days, the formation of brown-green plates of **6** at the phase boundary was observed. After complete diffusion, the light green mother liquor is decanted, the crystals are washed with hexane ( $3 \times 10$  mL) and dried *in vacuo*.

Analytical data of **6**:

**Yield:** 48 mg (0.039 mmol, 79% based on  $[\text{Cp}^{\text{Bn}}\text{Fe}(\eta^5\text{-P}_5)]$ ).

**$^1\text{H}$  NMR** ( $\text{CD}_2\text{Cl}_2$ ):  $\delta$  [ppm] = 1.39 (m,  $\text{NC}(\text{CH}_2)_8\text{CN}$ ), 1.49 (m,  $\text{NC}(\text{CH}_2)_8\text{CN}$ ), 1.73 (m,  $\text{NC}(\text{CH}_2)_8\text{CN}$ ), 2.79 (s,  $\text{NC}(\text{CH}_2)_8\text{CN}$ ), 3.62 (s,  $[\text{Cp}^{\text{Bn}}\text{Fe}(\eta^5\text{-P}_5)]$ ), 6.28 (d,  $[\text{Cp}^{\text{Bn}}\text{Fe}(\eta^5\text{-P}_5)]$ ), 6.83 (m,  $[\text{Cp}^{\text{Bn}}\text{Fe}(\eta^5\text{-P}_5)]$ ), 6.97 (m,  $[\text{Cp}^{\text{Bn}}\text{Fe}(\eta^5\text{-P}_5)]$ ).

**$^1\text{H}$  NMR** ( $\text{CD}_2\text{Cl}_2/\text{pyridine}$ ):  $\delta$  [ppm] = 1.34 (m,  $\text{NC}(\text{CH}_2)_8\text{CN}$ ), 1.44 (m,  $\text{NC}(\text{CH}_2)_8\text{CN}$ ), 1.65 (m,  $\text{NC}(\text{CH}_2)_8\text{CN}$ ), 2.38 (s,  $\text{NC}(\text{CH}_2)_8\text{CN}$ ), 3.63 (s,  $[\text{Cp}^{\text{Bn}}\text{Fe}(\eta^5\text{-P}_5)]$ ), 6.18 (d,  $[\text{Cp}^{\text{Bn}}\text{Fe}(\eta^5\text{-P}_5)]$ ), 6.75 (m,  $[\text{Cp}^{\text{Bn}}\text{Fe}(\eta^5\text{-P}_5)]$ ), 6.90 (m,  $[\text{Cp}^{\text{Bn}}\text{Fe}(\eta^5\text{-P}_5)]$ ).

**$^{31}\text{P}\{^1\text{H}\}$  NMR** ( $\text{CD}_2\text{Cl}_2$ ):  $\delta$  [ppm] = 145.05 (s,  $[\text{Cp}^{\text{Bn}}\text{Fe}(\eta^5\text{-P}_5)]$ ).

**$^{31}\text{P}\{^1\text{H}\}$  NMR** ( $\text{CD}_2\text{Cl}_2/\text{pyridine}$ ):  $\delta$  [ppm] = 152.6 (s,  $[\text{Cp}^{\text{Bn}}\text{Fe}(\eta^5\text{-P}_5)]$ ).

**Positive ion ESI-MS** ( $\text{CH}_2\text{Cl}_2$ ):  $m/z$  (%) = 271.0  $[\text{Ag}(\text{NC}(\text{CH}_2)_8\text{CN})]^+$ , 435.1  $[\text{Ag}(\text{NC}(\text{CH}_2)_8\text{CN})_2]^+$ , 832.9  $\{[\text{Cp}^{\text{Bn}}\text{Fe}(\eta^5\text{-P}_5)]\text{Ag}\}^+$ , 997.0  $\{[\text{Cp}^{\text{Bn}}\text{Fe}(\eta^5\text{-P}_5)]\text{Ag}(\text{NC}(\text{CH}_2)_8\text{CN})\}^+$ , 1175  $\{[\text{Cp}^{\text{Bn}}\text{Fe}(\eta^5\text{-P}_5)]\text{Ag}_2\text{SbF}_6\}^+$ , 1340.8  $\{[\text{Cp}^{\text{Bn}}\text{Fe}(\eta^5\text{-P}_5)]\text{Ag}_2\text{SbF}_6(\text{NC}(\text{CH}_2)_8\text{CN})\}^+$ , 1560.9  $\{[\text{Cp}^{\text{Bn}}\text{Fe}(\eta^5\text{-P}_5)]_2\text{Ag}\}^+$ .

**Negative ion ESI-MS** ( $\text{CH}_2\text{Cl}_2$ ):  $m/z$  (%) = 234.7  $[\text{SbF}_6]^-$ .

**Elemental analysis:** Calculated (%) for  $\{[\text{Cp}^{\text{Bn}}\text{Fe}(\eta^5\text{-P}_5)]\{\text{AgSbF}_6\}(\text{NC}(\text{CH}_2)_8\text{CN})\}$  (1234.29 g/mol): C 48.66, H 4.16, N 2.27; found: C 48.64, H 4.19, N 2.24.

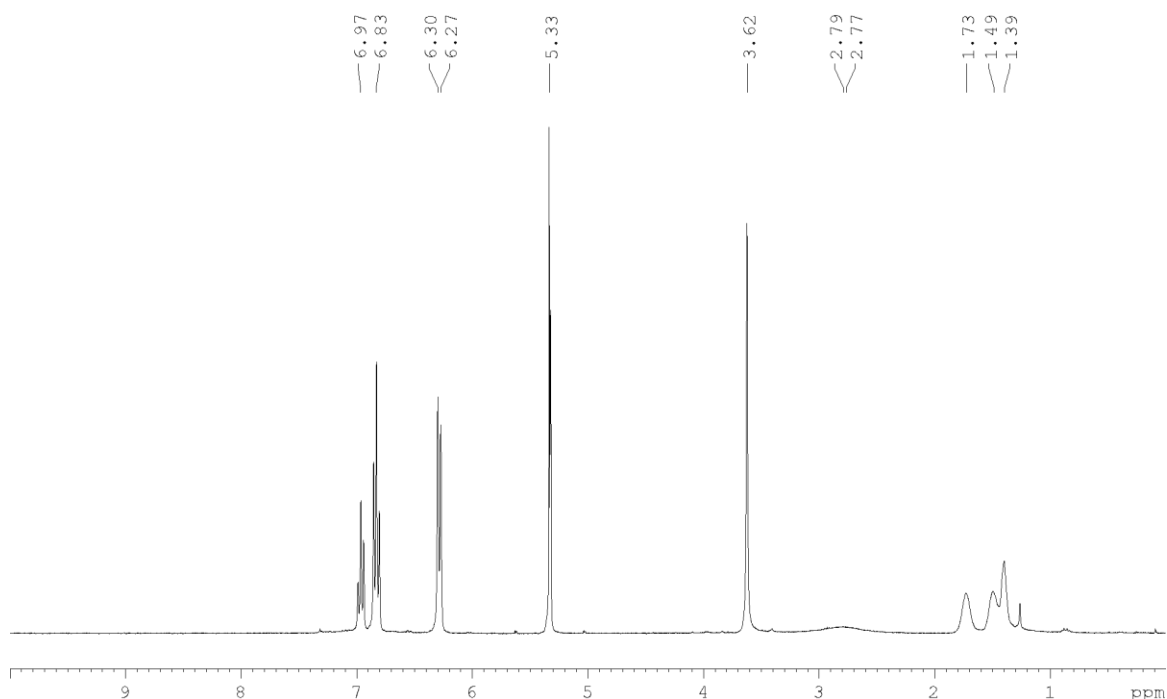


**Figure 6.20.**  $^1\text{H}$  NMR spectrum of **6** in  $\text{CD}_2\text{Cl}_2$ . (5.33  $\text{CH}_2\text{Cl}_2$ )



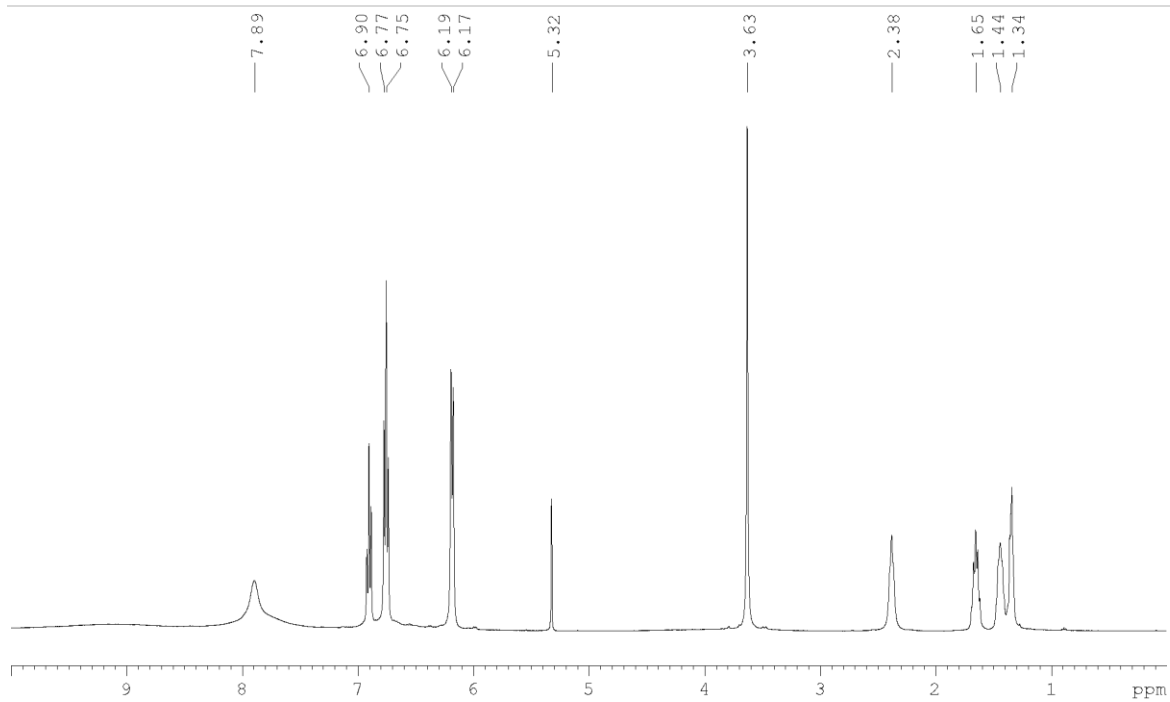


Figure 6.21.  $^1\text{H}$  NMR spectrum of **6** in  $\text{CD}_2\text{Cl}_2/\text{pyridine}$ . (5.32  $\text{CH}_2\text{Cl}_2$ , 7.89 pyridine)

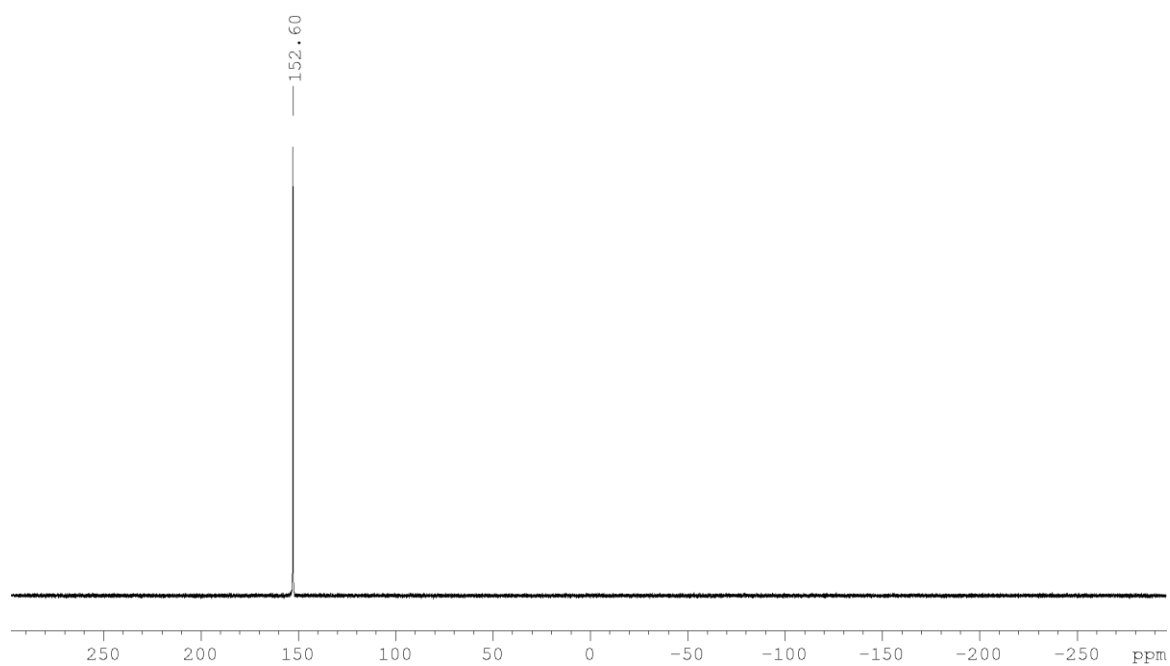
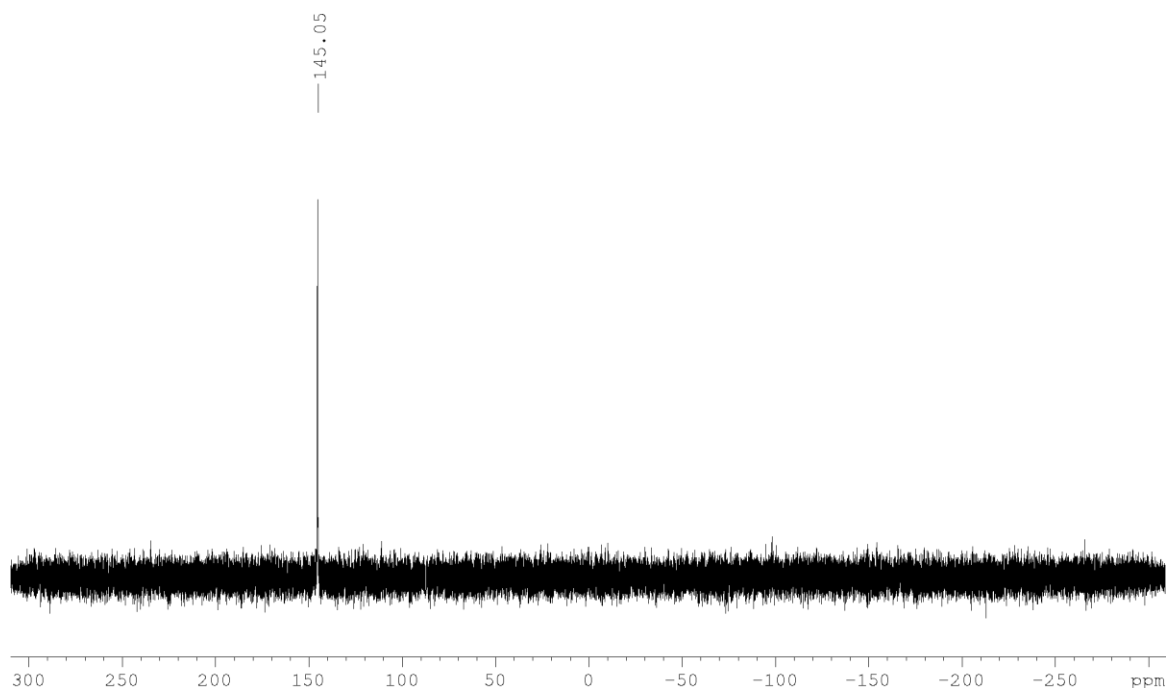


Figure 6.22.  $^{31}\text{P}\{^1\text{H}\}$  NMR spectrum of **6** in  $\text{CD}_2\text{Cl}_2/\text{pyridine}$ .



**Figure 6.23.**  $^{31}\text{P}\{^1\text{H}\}$  NMR spectrum of **6** in  $\text{CD}_2\text{Cl}_2$ .

### Synthesis of $[\{\text{Cp}^{\text{Bn}}\text{Fe}(\eta^5\text{-P}_5)\}_3(\text{Ag}_3(\text{NC}(\text{CH}_2)_9\text{CN})_2)]_n[\text{SbF}_6]_{3n}$ (**7**)

In a Schlenk tube a solution of  $\text{AgSbF}_6$  (17 mg, 0.05 mmol) in  $\text{CH}_2\text{Cl}_2$  (5 mL) is carefully layered first with a solvent mixture of  $\text{CH}_2\text{Cl}_2$ /toluene (2 mL, 2:1) and then with a green solution of  $[\text{Cp}^{\text{Bn}}\text{Fe}(\eta^5\text{-P}_5)]$  (40 mg, 0.05 mmol) and  $\text{NC}(\text{CH}_2)_9\text{CN}$  (1 mL, 0.4 mmol, 0.4 M in  $\text{CH}_2\text{Cl}_2$ ) in toluene (5 mL). After complete diffusion, the green mother liquor is removed, the solid is dissolved in  $\text{CH}_2\text{Cl}_2$  (5 mL), filtered, and carefully layered with pentane (5 mL). During the layering a brownish turbidity can be observed at the phase boundary. One month later the formation of green needles of **7** can be observed. After complete diffusion, the yellow-green mother liquor is decanted, the crystals are washed with pentane ( $3 \times 10$  mL) and dried *in vacuo*.

Analytical data of **7**

**Yield:** 75.9 mg (0.021 mmol, 43% referred to  $[\text{Cp}^{\text{Bn}}\text{Fe}(\eta^5\text{-P}_5)]$ )

$^1\text{H}$  NMR ( $\text{CD}_3\text{CN}/\text{pyridine}$ ):  $\delta$  [ppm] = 1.31 (m,  $\text{NC}(\text{CH}_2)_9\text{CN}$ ), 1.40 (m,  $\text{NC}(\text{CH}_2)_9\text{CN}$ ), 1.61 (m,  $\text{NC}(\text{CH}_2)_9\text{CN}$ ), 2.37 (t,  $\text{NC}(\text{CH}_2)_9\text{CN}$ ), 3.66 (m,  $[\text{Cp}^{\text{Bn}}\text{Fe}(\eta^5\text{-P}_5)]$ ), 6.25 (m,  $[\text{Cp}^{\text{Bn}}\text{Fe}(\eta^5\text{-P}_5)]$ ), 6.76 (m,  $[\text{Cp}^{\text{Bn}}\text{Fe}(\eta^5\text{-P}_5)]$ ), 6.91 (m,  $[\text{Cp}^{\text{Bn}}\text{Fe}(\eta^5\text{-P}_5)]$ ).

$^{31}\text{P}\{^1\text{H}\}$  NMR ( $\text{CD}_3\text{CN}/\text{pyridine}$ ):  $\delta$  [ppm] = 151.2 (s,  $[\text{Cp}^{\text{Bn}}\text{Fe}(\eta^5\text{-P}_5)]$ ).

$^{19}\text{F}$  NMR ( $\text{CD}_3\text{CN}/\text{pyridine}$ ):  $\delta$  [ppm] = -125.34 (m,  $\text{SbF}_6$ ).

**Positive ion ESI-MS** ( $\text{CH}_3\text{CN}/\text{CH}_2\text{Cl}_2$ ):  $m/z$  (%) = 531.2  $[\text{Cp}^{\text{Bn}}\text{O}]^+$ .

**Negative ion ESI-MS** ( $\text{CH}_3\text{CN}$ ):  $m/z$  (%) = 234.9  $[\text{SbF}_6]^-$ .

**Elemental analysis:** Calculated (%) for  $\{\text{Cp}^{\text{Bn}}\text{Fe}(\eta^5\text{-P}_5)\}_3(\text{AgSbF}_6)_3(\text{NC}(\text{CH}_2)_9\text{CN})_2$  (3566.69 g/mol) = C 47.82, H 3.98, N 1.57; found: C 47.81, H 4.15, N 1.75.

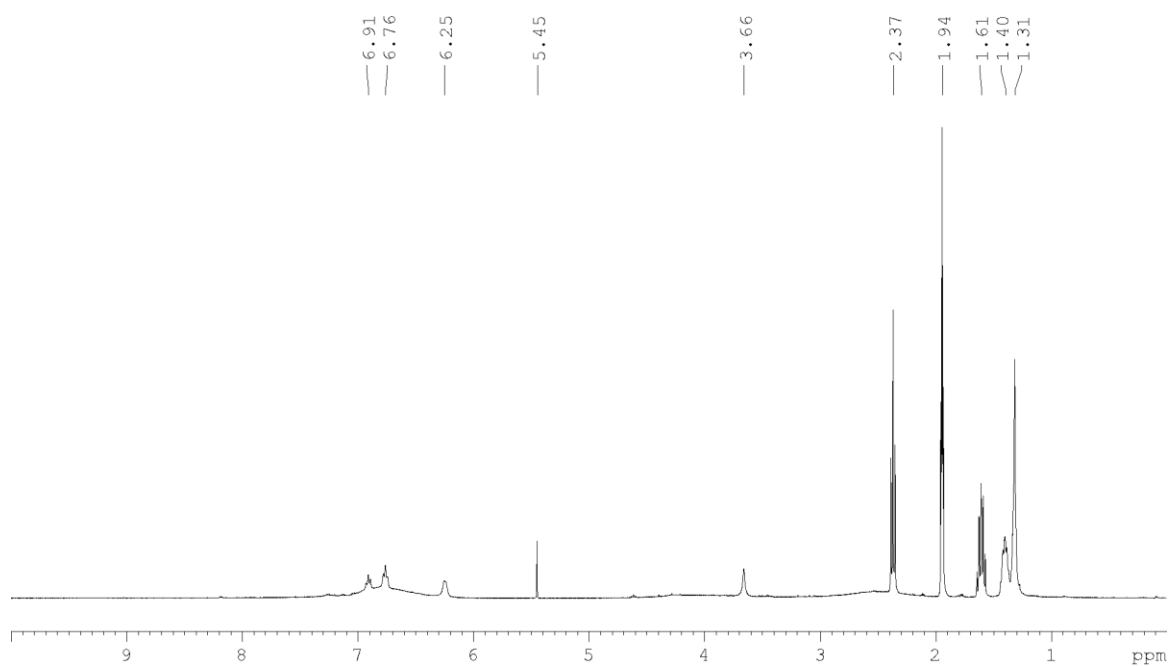


**Figure 6.24.**  $^1\text{H}$  NMR spectrum of **7** (1.94  $\text{CH}_3\text{CN}$ , 5.45  $\text{CH}_2\text{Cl}_2$ ).

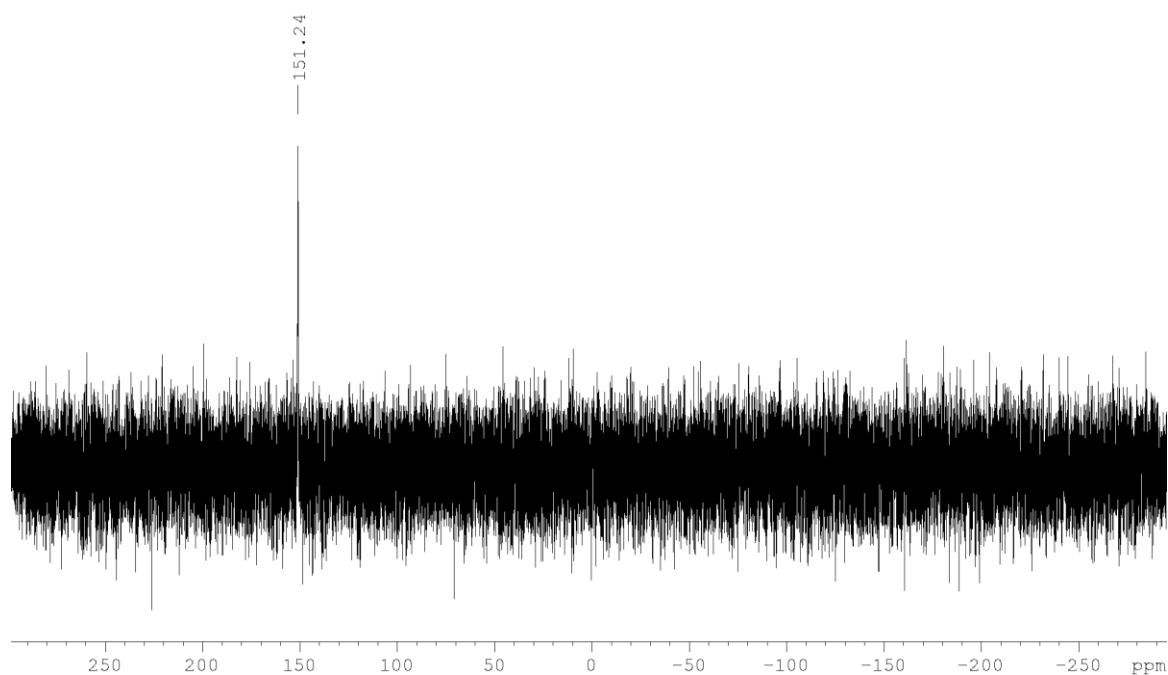


**Figure 6.25.**  $^{31}\text{P}\{^1\text{H}\}$  NMR spectrum of **7**.

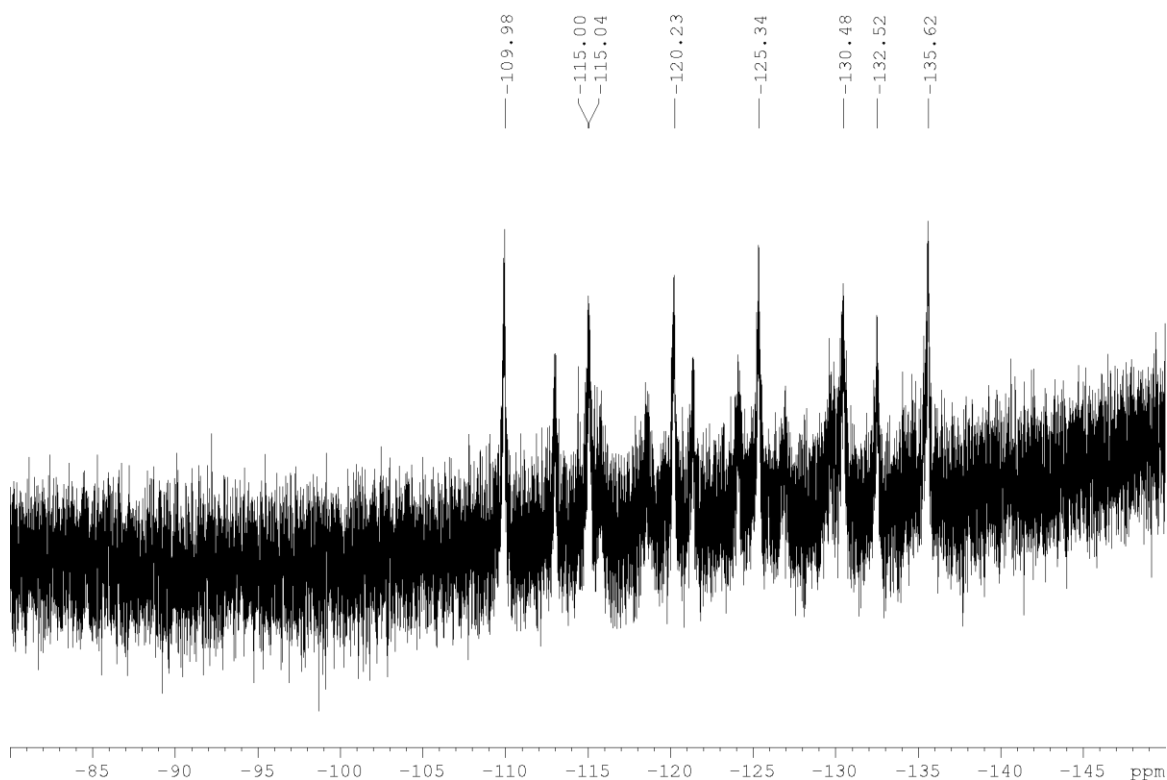


Figure 6.26.  $^{19}\text{F}\{^1\text{H}\}$  NMR spectrum of **7**.

#### Synthesis of $[\{\text{Cp}^{\text{Bn}}\text{Fe}(\eta^5\text{-P}_5)\}_2\{\text{Ag}_2(\text{NC}(\text{CH}_2)_{10}\text{CN})_{1.5}\}_n\{\text{SbF}_6\}_{2n}(\text{CH}_2\text{Cl}_2)_{0.5n}$ (**8**)

In a Schlenk tube a solution of  $\text{AgSbF}_6$  (17 mg, 0.05 mmol) in  $\text{CH}_2\text{Cl}_2$  (5 mL) is carefully layered with a green solution of  $[\text{Cp}^{\text{Bn}}\text{Fe}(\eta^5\text{-P}_5)]$  (40 mg, 0.05 mmol) and  $\text{NC}(\text{CH}_2)_{10}\text{CN}$  (0.4 mmol/mL in  $\text{CH}_2\text{Cl}_2$ ) in toluene (5 mL). Thereby, the phase boundary turns yellow. After a few days, the formation of brown-green elongated plates of **8** at the phase boundary was observed. After complete diffusion, the light green mother liquor is decanted, the crystals are washed with hexane ( $3 \times 10$  mL) and dried *in vacuo*.

Analytical data of **8**:

**Yield:** 42 mg (0.017 mmol, 69% based on  $[\text{Cp}^{\text{Bn}}\text{Fe}(\eta^5\text{-P}_5)]$ ).

$^1\text{H}$  NMR ( $\text{CD}_2\text{Cl}_2$ ):  $\delta$  [ppm] = 1.30 (s,  $\text{NC}(\text{CH}_2)_8\text{CN}$ ), 1.40 (m,  $\text{NC}(\text{CH}_2)_8\text{CN}$ ), 1.62 (m,  $\text{NC}(\text{CH}_2)_8\text{CN}$ ), 2.44 (m, 4H,  $\text{NC}(\text{CH}_2)_8\text{CN}$ ), 3.61 (s,  $[\text{Cp}^{\text{Bn}}\text{Fe}(\eta^5\text{-P}_5)]$ ), 6.28 (d,  $[\text{Cp}^{\text{Bn}}\text{Fe}(\eta^5\text{-P}_5)]$ ), 6.83 (m,  $[\text{Cp}^{\text{Bn}}\text{Fe}(\eta^5\text{-P}_5)]$ ), 6.97 (m,  $[\text{Cp}^{\text{Bn}}\text{Fe}(\eta^5\text{-P}_5)]$ ).

$^1\text{H}$  NMR ( $\text{CD}_2\text{Cl}_2/\text{pyridine}$ ):  $\delta$  [ppm] = 1.31 (s,  $\text{NC}(\text{CH}_2)_8\text{CN}$ ), 1.42 (m,  $\text{NC}(\text{CH}_2)_8\text{CN}$ ), 1.63 (m,  $\text{NC}(\text{CH}_2)_8\text{CN}$ ), 2.33 (t,  $\text{NC}(\text{CH}_2)_8\text{CN}$ ), 3.63 (s,  $[\text{Cp}^{\text{Bn}}\text{Fe}(\eta^5\text{-P}_5)]$ ), 6.20 (d,  $[\text{Cp}^{\text{Bn}}\text{Fe}(\eta^5\text{-P}_5)]$ ), 6.76 (m,  $[\text{Cp}^{\text{Bn}}\text{Fe}(\eta^5\text{-P}_5)]$ ), 6.90 (m,  $[\text{Cp}^{\text{Bn}}\text{Fe}(\eta^5\text{-P}_5)]$ ).

$^{31}\text{P}\{^1\text{H}\}$  NMR ( $\text{CD}_2\text{Cl}_2$ ):  $\delta$  [ppm] = 149.05 (s,  $[\text{Cp}^{\text{Bn}}\text{Fe}(\eta^5\text{-P}_5)]$ ).

$^{31}\text{P}\{^1\text{H}\}$  NMR ( $\text{CD}_2\text{Cl}_2/\text{pyridine}$ ):  $\delta$  [ppm] = 155.14 (s,  $[\text{Cp}^{\text{Bn}}\text{Fe}(\eta^5\text{-P}_5)]$ ).

**Positive ion ESI-MS** ( $\text{CH}_2\text{Cl}_2$ ):  $m/z$  (%) = 301.1  $[\text{Ag}(\text{NC}(\text{CH}_2)_{10}\text{CN})]^+$ , 491.4  $[\text{Ag}(\text{NC}(\text{CH}_2)_{10}\text{CN})_2]^+$ , 835.2  $[\text{Cp}^{\text{Bn}}\text{Fe}(\eta^5\text{-P}_5)\text{Ag}]^+$ , 877  $[\text{Ag}(\text{NC}(\text{CH}_2)_{10}\text{CN})_4]^+$ , 1027.5  $[\{\text{Cp}^{\text{Bn}}\text{Fe}(\eta^5\text{-P}_5)\}\text{Ag}(\text{NC}(\text{CH}_2)_{10}\text{CN})]^+$ , 1181.3  $[\{\text{Cp}^{\text{Bn}}\text{Fe}(\eta^5\text{-P}_5)\}\text{Ag}_2\text{SbF}_6]^+$ , 1561.6  $[\{\text{Cp}^{\text{Bn}}\text{Fe}(\eta^5\text{-P}_5)\}_2\text{Ag}]^+$ .

**Negative ion ESI-MS** ( $\text{CH}_2\text{Cl}_2$ ):  $m/z$  (%) = 234.7  $[\text{SbF}_6]^-$ .

**Elemental analysis:** Calculated (%) for  $[\{\text{Cp}^{\text{Bn}}\text{Fe}(\eta^5\text{-P}_5)\}_2\{\text{AgSbF}_6\}_2(\text{CN}(\text{CH}_2)_{10}\text{CN})_{1.5}(\text{CH}_2\text{Cl}_2)_{0.5}]$  (2428.93 g/mol): C 47.88, H 4.12, N 1.70; found: C 47.94, H 4.12, N 1.56.

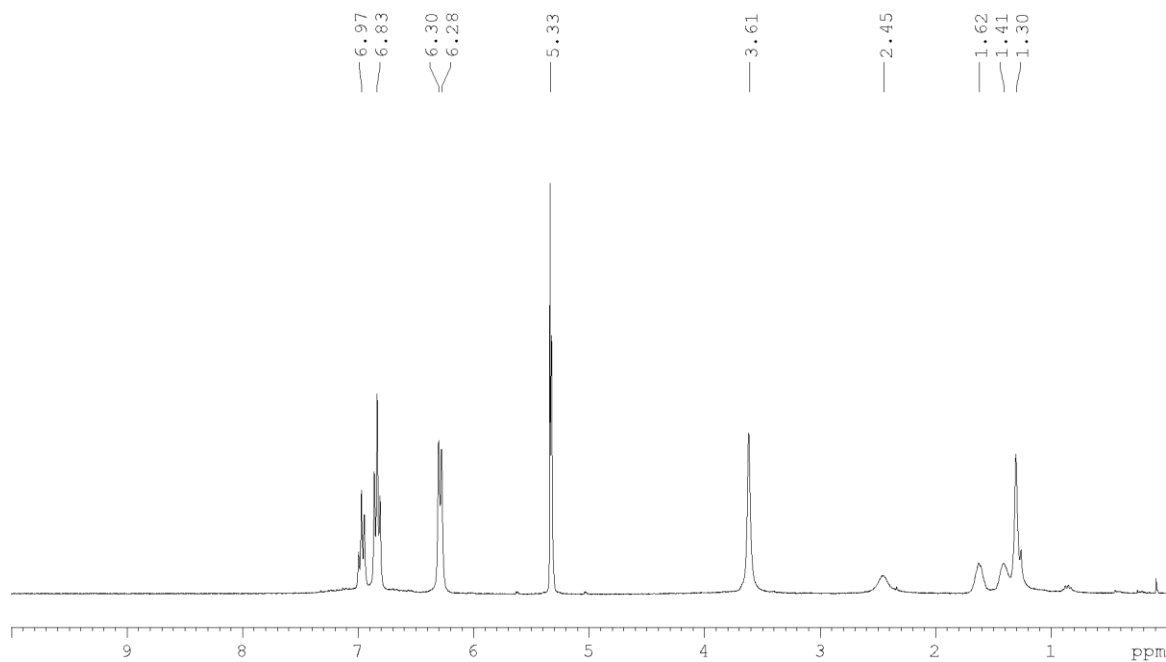


**Figure 6.27.**  $^1\text{H}$  NMR spectrum of **8** in  $\text{CD}_2\text{Cl}_2$  (5.33  $\text{CH}_2\text{Cl}_2$ ).

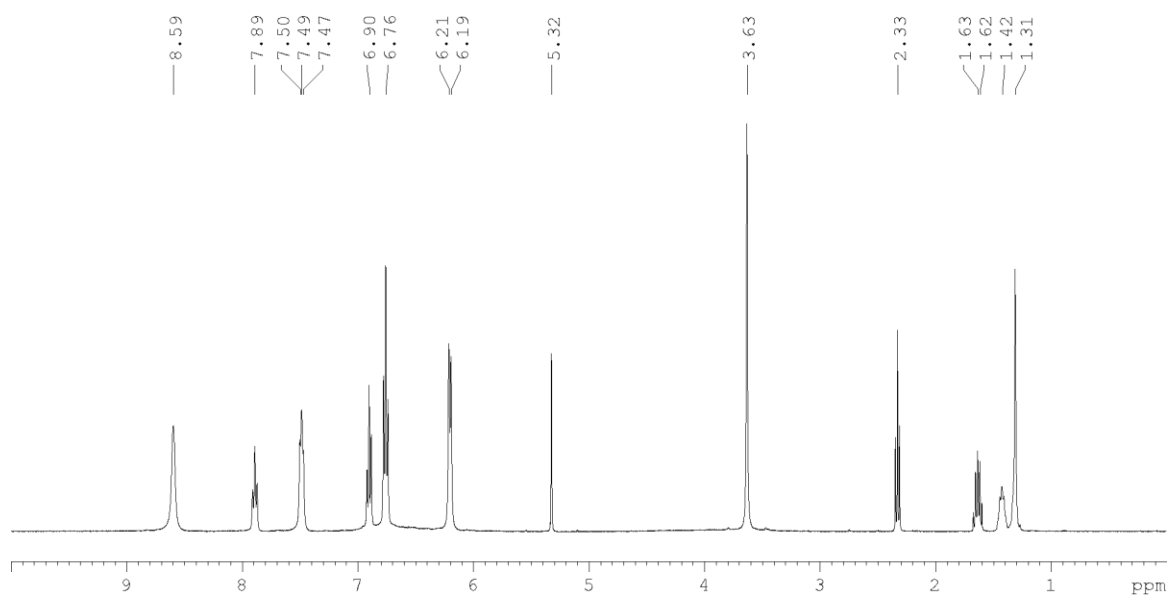


**Figure 6.28.**  $^1\text{H}$  NMR spectrum of **8** in  $\text{CD}_2\text{Cl}_2$ /pyridine (5.32  $\text{CH}_2\text{Cl}_2$ , 7.50 pyridine, 7.89 pyridine, 8.59 pyridine).

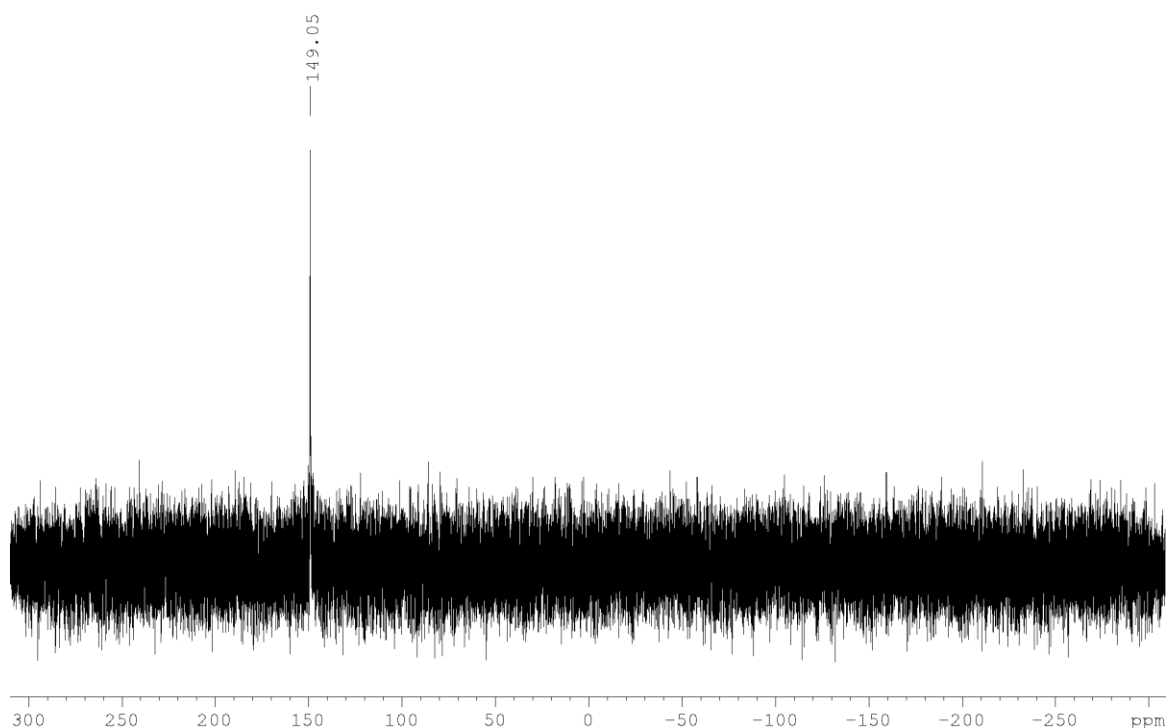


Figure 6.29.  $^{31}\text{P}\{^1\text{H}\}$  NMR spectrum of **8** in  $\text{CD}_2\text{Cl}_2$ .

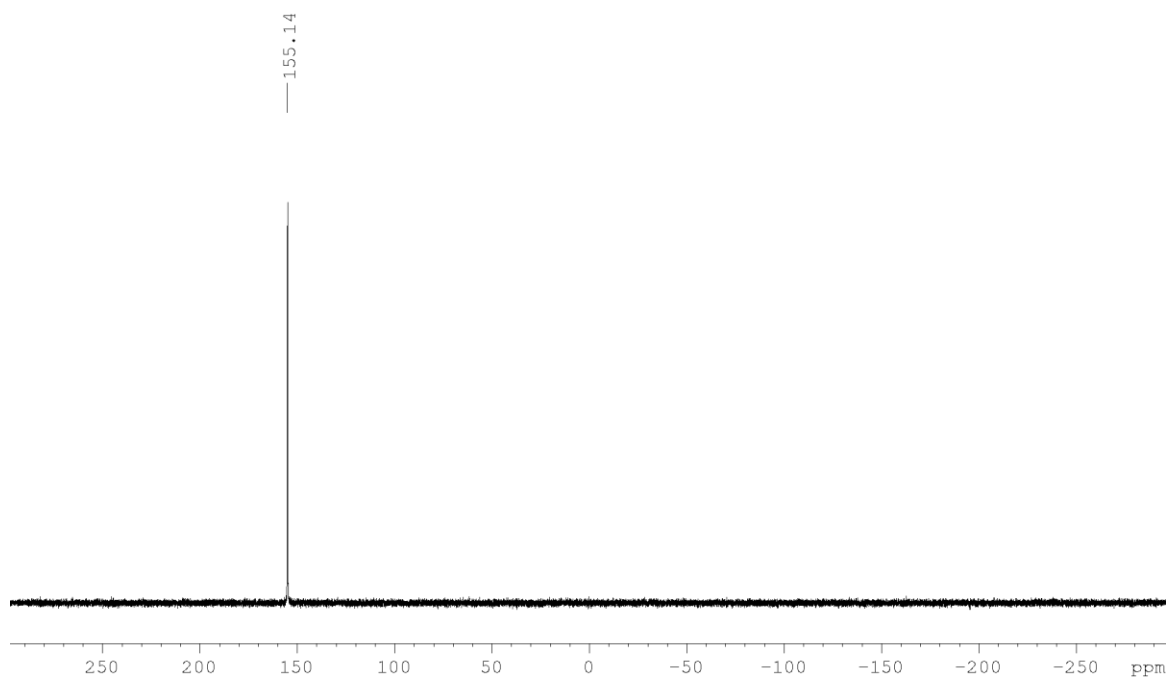


Figure 6.30.  $^{31}\text{P}\{^1\text{H}\}$  NMR spectrum of **8** in  $\text{CD}_2\text{Cl}_2/\text{pyridine}$ .

### Synthesis of $[(\text{Cp}^{\text{Bn}}\text{Fe}(\eta^5\text{-P}_5))_8\{\text{Ag}(o\text{-NC}(\text{C}_6\text{H}_4)\text{CN})\}_{(12\pm x)}]_n[\text{SbF}_6]_{(12\pm x)n}$ (**9**)

In a Schlenk tube a solution of  $\text{AgSbF}_6$  (28 mg, 0.04 mmol) in  $\text{CH}_2\text{Cl}_2$  (15 mL) is carefully layered first with a solvent mixture of  $\text{CH}_2\text{Cl}_2/\text{toluene}$  (2 mL, 2:1) and then with a green solution of  $[\text{Cp}^{\text{Bn}}\text{Fe}(\eta^5\text{-P}_5)]$  (28 mg, 0.04 mmol) and  $o\text{-(NC)}_2\text{C}_6\text{H}_4$  (1 mL, 0.2 M in DCM) in toluene (15 mL). After

complete diffusion the mother liquor is layered with pentane whereby brown blocks of **9** can be observed after three days. The crystals are washed with hexane (3 × 10 mL) and dried *in vacuo*.

Analytical data of **9**

**Yield:** 71 mg (0.023 mmol, 58% referred to [Cp<sup>Bn</sup>Fe(η<sup>5</sup>-P<sub>5</sub>)])

**<sup>1</sup>H NMR** (CD<sub>2</sub>Cl<sub>2</sub>): δ [ppm] = 3.77 (m, [Cp<sup>Bn</sup>Fe(η<sup>5</sup>-P<sub>5</sub>)]), 6.38 (m, [Cp<sup>Bn</sup>Fe(η<sup>5</sup>-P<sub>5</sub>)]), 6.81-6.97 (m, [Cp<sup>Bn</sup>Fe(η<sup>5</sup>-P<sub>5</sub>)]), 7.70 (m, *o*-(NC)<sub>2</sub>C<sub>6</sub>H<sub>4</sub>)

**<sup>31</sup>P{<sup>1</sup>H} NMR** (CD<sub>2</sub>Cl<sub>2</sub>): δ [ppm] = 137.20 (br, [Cp<sup>Bn</sup>Fe(η<sup>5</sup>-P<sub>5</sub>)])

**Positive ion ESI-MS** (CH<sub>3</sub>CN): *m/z* (%) = 832.9 [(Cp<sup>Bn</sup>Fe(η<sup>5</sup>-P<sub>5</sub>))Ag]<sup>+</sup>, 1558.9 [(Cp<sup>Bn</sup>Fe(η<sup>5</sup>-P<sub>5</sub>))<sub>2</sub>Ag]<sup>+</sup>, 1902.75 [(Cp<sup>Bn</sup>Fe(η<sup>5</sup>-P<sub>5</sub>))<sub>2</sub>Ag<sub>2</sub>(SbF<sub>6</sub>)]<sup>+</sup>, 2286.9 [(Cp<sup>Bn</sup>Fe(η<sup>5</sup>-P<sub>5</sub>))<sub>2</sub>Ag<sub>2</sub>(SbF<sub>6</sub>)(*o*-(NC)<sub>2</sub>C<sub>6</sub>H<sub>4</sub>)<sub>3</sub>]<sup>+</sup>, 2630.8 [(Cp<sup>Bn</sup>Fe(η<sup>5</sup>-P<sub>5</sub>))<sub>3</sub>Ag<sub>2</sub>(SbF<sub>6</sub>)]<sup>+</sup>.

**Negative ion ESI-MS** (CH<sub>3</sub>CN): *m/z* (%) = 234.9 [SbF<sub>6</sub>]<sup>-</sup>.

**Elemental analysis:** Calculated (%) for C<sub>96</sub>H<sub>78</sub>Ag<sub>4</sub>F<sub>24</sub>Fe<sub>2</sub>N<sub>4</sub>P<sub>10</sub>Sb<sub>4</sub> (3083.58 g/mol): 37.39 C, 2.55 H, 1.82 N; found: 37.87 C, 2.91 H, 1.20 N.

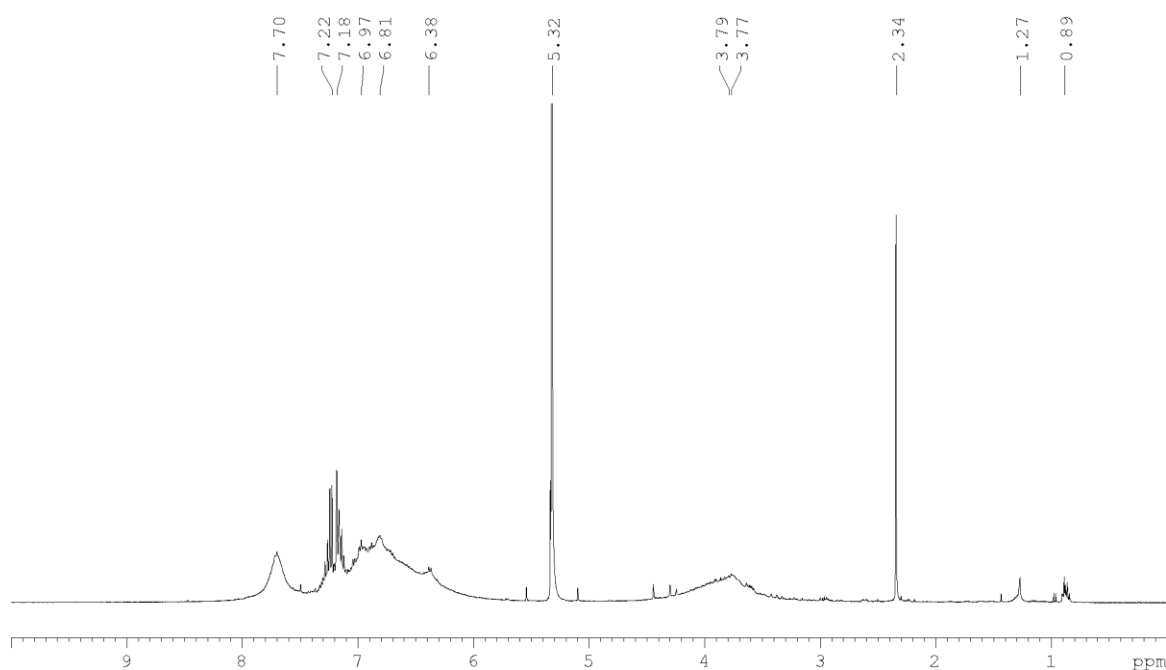


**Figure 6.31.** <sup>1</sup>H NMR spectrum of **9**. (0.89 and 1.27 grease; 2.34, 7.18 and 7.22 toluene)

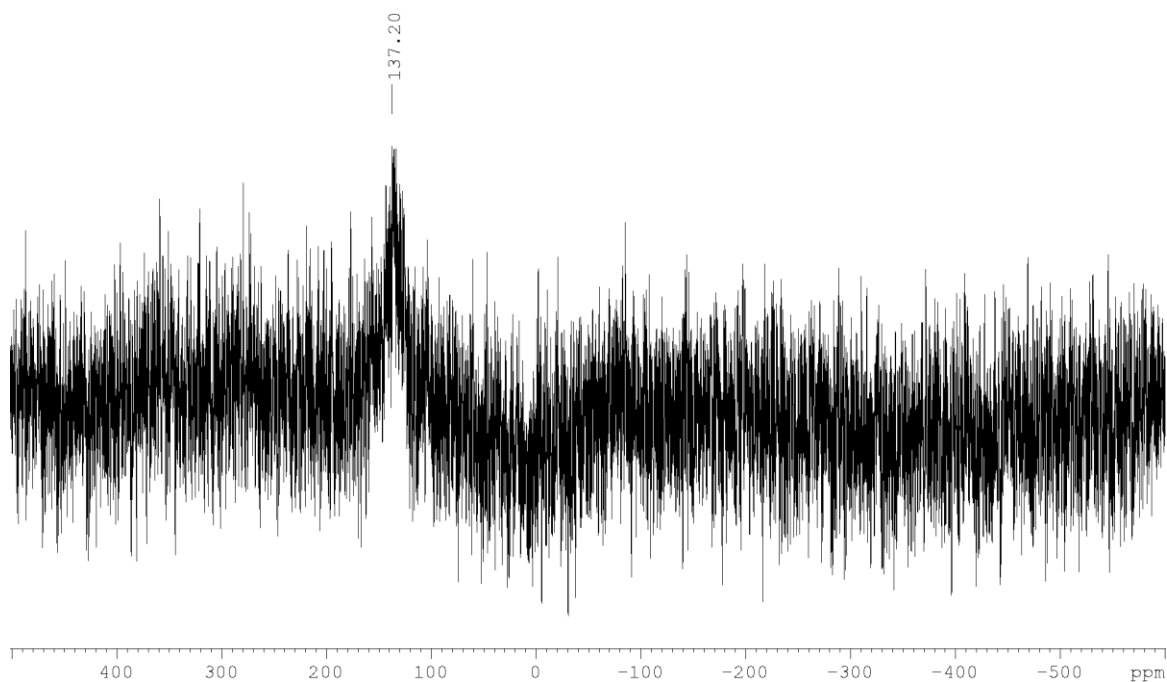


Figure 6.32.  $^{31}\text{P}\{^1\text{H}\}$  NMR spectrum of **9**.

### Synthesis of $[\{\text{Cp}^{\text{Bn}}\text{Fe}(\eta^5\text{-P}_5)\}\{\text{Ag}(m\text{-NC}(\text{C}_6\text{H}_4)\text{CN})\}_2]_n[\text{SbF}_6]_{2n} \cdot (\text{C}_7\text{H}_8)$ (**10**)

In a Schlenk tube a solution of  $\text{AgSbF}_6$  (28 mg, 0.08 mmol) in  $\text{CH}_2\text{Cl}_2$  (10 mL) is carefully layered first with a solvent mixture of  $\text{CH}_2\text{Cl}_2$ /toluene (2 mL, 2:1) and then with a green solution of  $[\text{Cp}^{\text{Bn}}\text{Fe}(\eta^5\text{-P}_5)]$  (28 mg, 0.04 mmol) and  $m\text{-(NC)}_2\text{C}_6\text{H}_4$  (1 mL, 0.4 M in DCM) in toluene (10 mL). One day later green needles of **10** can be observed on the phase boundary. After complete diffusion the colorless mother liquor is decanted, the crystals are washed with hexane (3 x 10 mL) and dried *in vacuo*.

Analytical data of **10**

**Yield:** 59 mg (0.033 mmol, 84 % referred to  $[\text{Cp}^{\text{Bn}}\text{Fe}(\eta^5\text{-P}_5)]$ )

$^1\text{H}$  NMR ( $\text{CD}_2\text{Cl}_2$ ):  $\delta$  [ppm] = 3.66 (s,  $[\text{Cp}^{\text{Bn}}\text{Fe}(\eta^5\text{-P}_5)]$ ), 6.24 (d,  $[\text{Cp}^{\text{Bn}}\text{Fe}(\eta^5\text{-P}_5)]$ ), 6.76 (t,  $[\text{Cp}^{\text{Bn}}\text{Fe}(\eta^5\text{-P}_5)]$ ), 6.91 (t,  $[\text{Cp}^{\text{Bn}}\text{Fe}(\eta^5\text{-P}_5)]$ ), 7.70 (t,  $m\text{-(NC)}_2\text{C}_6\text{H}_4$ ), 7.98 (d,  $m\text{-(NC)}_2\text{C}_6\text{H}_4$ ), 8.11 (s,  $m\text{-(NC)}_2\text{C}_6\text{H}_4$ ).

$^{31}\text{P}\{^1\text{H}\}$  NMR ( $\text{CD}_2\text{Cl}_2$ /pyridine):  $\delta$  [ppm] = 150.66 (s,  $[\text{Cp}^{\text{Bn}}\text{Fe}(\eta^5\text{-P}_5)]$ )

**Positive ion ESI-MS** ( $\text{CH}_3\text{CN}$ ):  $m/z$  (%) = 106.9  $[\text{Ag}]^+$ , 147.9  $[\text{Ag}(\text{CH}_3\text{CN})]^+$ , 188.9  $[\text{Ag}(\text{CH}_3\text{CN})_2]^+$ , 229.9  $[\text{Ag}(\text{CH}_3\text{CN})_3]^+$ , 271.1  $[\text{Ag}(\text{CH}_3\text{CN})_4]^+$ , 832.9  $[\{\text{Cp}^{\text{Bn}}\text{Fe}(\eta^5\text{-P}_5)\}\text{Ag}]^+$ , 915.0  $[\{\text{Cp}^{\text{Bn}}\text{Fe}(\eta^5\text{-P}_5)\}\text{Ag}(\text{CH}_3\text{CN})_2]^+$ , 1176.7  $[\{\text{Cp}^{\text{Bn}}\text{Fe}(\eta^5\text{-P}_5)\}\text{Ag}_2(\text{SbF}_6)]^+$ , 1559.0  $[\{\text{Cp}^{\text{Bn}}\text{Fe}(\eta^5\text{-P}_5)\}_2\text{Ag}]^+$ , 1904.8  $[\{\text{Cp}^{\text{Bn}}\text{Fe}(\eta^5\text{-P}_5)\}_2\text{Ag}_2(\text{SbF}_6)]^+$ , 2287.1  $[\{\text{Cp}^{\text{Bn}}\text{Fe}(\eta^5\text{-P}_5)\}_2\text{Ag}_2(\text{SbF}_6)_1(m\text{-(NC)}_2\text{C}_6\text{H}_4)_3]^+$ , 2246.6  $[\{\text{Cp}^{\text{Bn}}\text{Fe}(\eta^5\text{-P}_5)\}_2\text{Ag}_3(\text{SbF}_6)_2]^+$ ,

**Negative ion ESI-MS** ( $\text{CH}_3\text{CN}$ ):  $m/z$  (%) = 234.9  $[\text{SbF}_6]^-$ .

**Elemental analysis:** Calculated (%) for  $\text{C}_{63}\text{H}_{51}\text{Ag}_2\text{F}_{12}\text{FeN}_4\text{P}_5\text{Sb}_2$  (1762.06 g/mol): 42.94 C, 2.92 H, 3.18 N; found: 42.78 C, 3.04 H, 3.30 N.



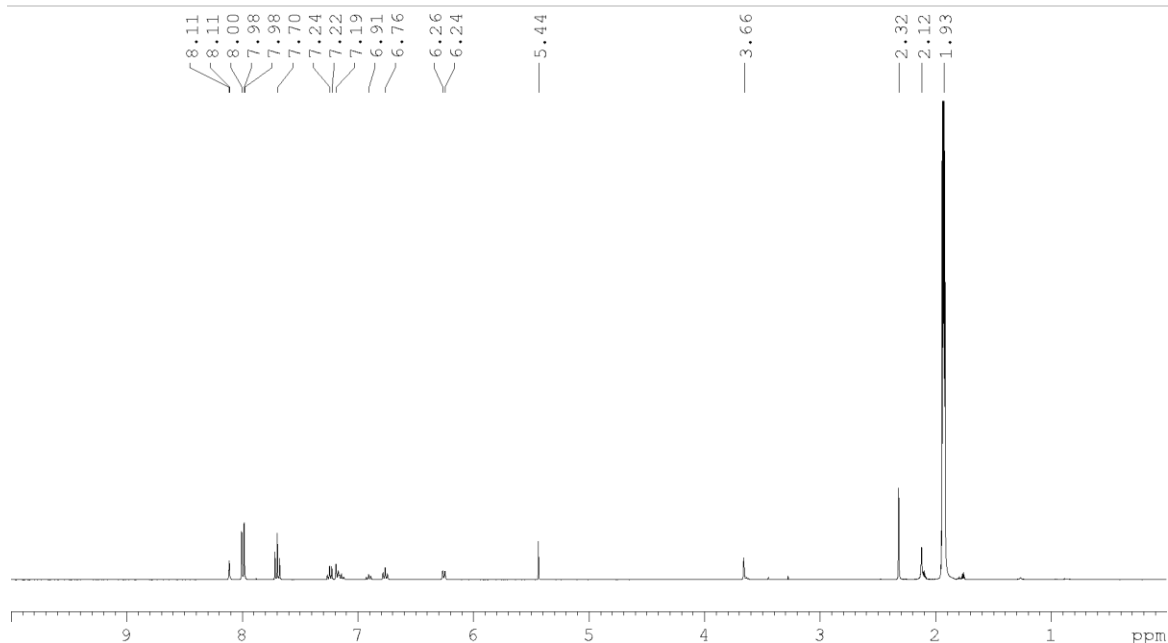


Figure 6.33.  $^1\text{H}$  NMR spectrum of **10**. (2.12 water, 2.32 toluene, 5.44  $\text{CH}_2\text{Cl}_2$ , 7.19 toluene, 7.24 toluene).

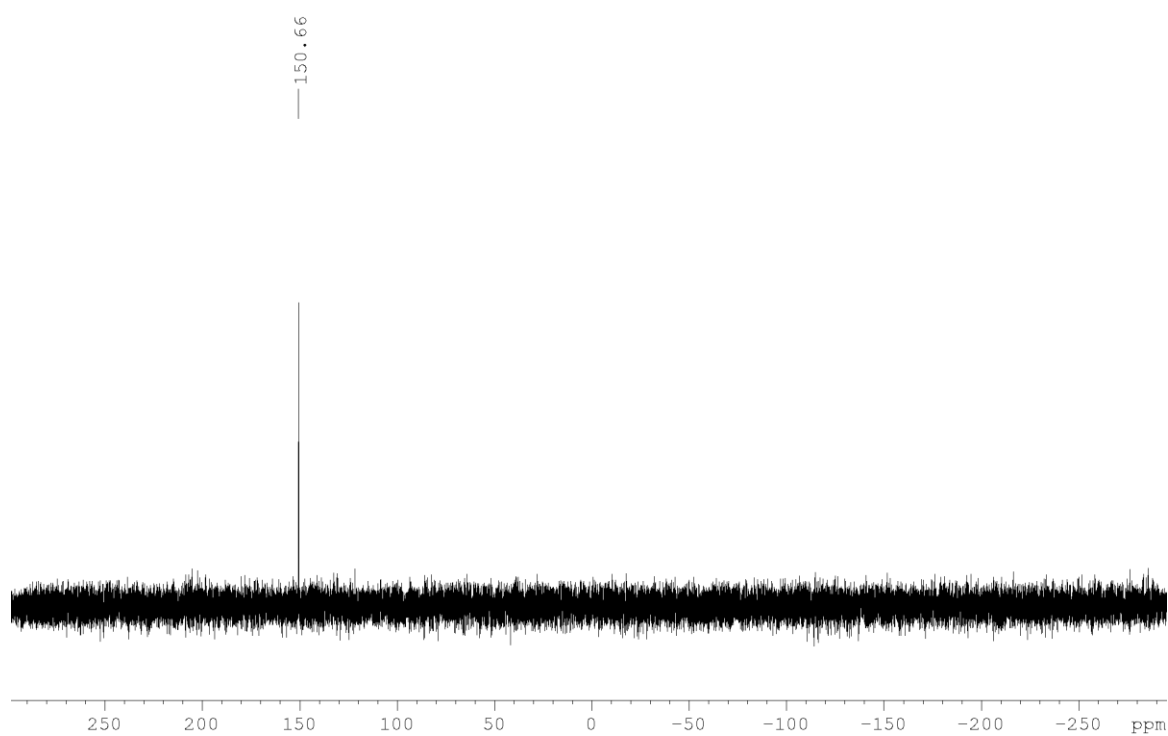


Figure 6.34.  $^{31}\text{P}\{^1\text{H}\}$  NMR spectrum of **10**.

Synthesis of  $[\{\text{Cp}^{\text{Bn}}\text{Fe}(\eta^5\text{-P}_5)\}_2\text{Ag}_5\{\textit{p}\text{-NC}(\text{C}_6\text{H}_4)\text{CN}\}_4(\text{C}_7\text{H}_8)_{4.45}\text{]}_n[\text{SbF}_6]_{5n}$  (**11**),  $[\{\text{Cp}^{\text{Bn}}\text{Fe}(\eta^5\text{-P}_5)\}_4\text{Ag}_6\{\textit{p}\text{-NC}(\text{C}_6\text{H}_4)\text{CN}\}_4(\text{C}_7\text{H}_8)_4]_n[\text{SbF}_6]_{6n}\cdot(\text{CH}_2\text{Cl}_2)_3$  (**12**) and  $\{\text{SbF}_6\}@[\{\text{Cp}^{\text{Bn}}\text{Fe}(\eta^5\text{-P}_5)\}_6\text{Ag}_{10}\{\textit{p}\text{-NC}(\text{C}_6\text{H}_4)\text{CN}\}_{5.1875}\text{Cl}_{0.175}\text{]}_n[\text{SbF}_6]_{8.825n}$  (**13**)

In a Schlenk tube a solution of AgSbF<sub>6</sub> (28 mg, 0.08 mmol) in CH<sub>2</sub>Cl<sub>2</sub> (10 mL) is carefully layered first with a solvent mixture of CH<sub>2</sub>Cl<sub>2</sub>/toluene (2 mL, 2:1) and then with a green solution of [Cp<sup>Bn</sup>Fe(η<sup>5</sup>-P<sub>5</sub>)] (29 mg, 0.04 mmol) and *p*-(NC)<sub>2</sub>C<sub>6</sub>H<sub>4</sub> (1 mL, 0.2 M in DCM) in toluene (10 mL). While after one day green needles of **11** and **12** are observed at the phase boundary, small green prisms of **13** crystalize at the pat the bottom of the Schlenk after a week. An alternative procedure for **13** is to dissolve dimer **2** (10 mg, 0.04 mmol) in CH<sub>2</sub>Cl<sub>2</sub> (10 mL), add *p*-(NC)<sub>2</sub>C<sub>6</sub>H<sub>4</sub> (1 mL, 0.2 M in DCM), stir this mixture 24h at r.t. and layer the reaction mixture with hexane. After 30 days crystals of 13 appear in the bottom of the Schlenk. After complete diffusion the colorless mother liquor is decanted, the crystals are washed with hexane (3x 10 mL) and dried *in vacuo*. The products are sorted out manually.

Analytical data of **11**

**Yield:** 37 mg (0.0098 mmol, 24% referred to [Cp<sup>Bn</sup>Fe(η<sup>5</sup>-P<sub>5</sub>)]).

**<sup>1</sup>H NMR** (CD<sub>2</sub>Cl<sub>2</sub>/pyridine): δ [ppm] = 3.62 (s, [Cp<sup>Bn</sup>Fe(η<sup>5</sup>-P<sub>5</sub>)]), 6.20 (d, [Cp<sup>Bn</sup>Fe(η<sup>5</sup>-P<sub>5</sub>)]), 6.75 (m, [Cp<sup>Bn</sup>Fe(η<sup>5</sup>-P<sub>5</sub>)]), 7.07 (m, [Cp<sup>Bn</sup>Fe(η<sup>5</sup>-P<sub>5</sub>)]), 7.79 (*p*-(NC)<sub>2</sub>C<sub>6</sub>H<sub>4</sub>/pyridine).

**<sup>31</sup>P{<sup>1</sup>H} NMR** (CD<sub>2</sub>Cl<sub>2</sub>/pyridine): δ [ppm] = 153.63 (s, [Cp<sup>Bn</sup>Fe(η<sup>5</sup>-P<sub>5</sub>)]).

**<sup>19</sup>F NMR** (CD<sub>2</sub>Cl<sub>2</sub>/pyridine): no signal was detected.

**Positive ion ESI-MS** (CH<sub>3</sub>CN): *m/z* (%) = 106.9 [Ag]<sup>+</sup>, 147.9 [Ag(CH<sub>3</sub>CN)]<sup>+</sup>, 188.9 [Ag(CH<sub>3</sub>CN)<sub>2</sub>]<sup>+</sup>, 229.9 [Ag(CH<sub>3</sub>CN)<sub>3</sub>]<sup>+</sup>, 271.1 [Ag(CH<sub>3</sub>CN)<sub>4</sub>]<sup>+</sup>, 832.9 [(Cp<sup>Bn</sup>Fe(η<sup>5</sup>-P<sub>5</sub>))Ag]<sup>+</sup>, 915.0 [(Cp<sup>Bn</sup>Fe(η<sup>5</sup>-P<sub>5</sub>))Ag(CH<sub>3</sub>CN)<sub>2</sub>]<sup>+</sup>, 1176.7 [(Cp<sup>Bn</sup>Fe(η<sup>5</sup>-P<sub>5</sub>))Ag<sub>2</sub>(SbF<sub>6</sub>)]<sup>+</sup>, 1559.0 [(Cp<sup>Bn</sup>Fe(η<sup>5</sup>-P<sub>5</sub>))<sub>2</sub>Ag]<sup>+</sup>, 1904.6 [(Cp<sup>Bn</sup>Fe(η<sup>5</sup>-P<sub>5</sub>))<sub>2</sub>Ag<sub>2</sub>(SbF<sub>6</sub>)]<sup>+</sup>, 2073.76 [(Cp<sup>Bn</sup>Fe(η<sup>5</sup>-P<sub>5</sub>))<sub>1</sub>Ag<sub>3</sub>(SbF<sub>6</sub>)<sub>2</sub>(*p*-(NC)<sub>2</sub>C<sub>6</sub>H<sub>4</sub>)<sub>2</sub>(CH<sub>3</sub>CN)]<sup>+</sup>, 2248.3 [(Cp<sup>Bn</sup>Fe(η<sup>5</sup>-P<sub>5</sub>))<sub>2</sub>Ag<sub>3</sub>(SbF<sub>6</sub>)<sub>2</sub>]<sup>+</sup>.

**Negative ion ESI-MS** (CH<sub>3</sub>CN): *m/z* (%) = 234.9 [SbF<sub>6</sub>]<sup>-</sup>.

**Elemental analysis:** Calculated (%) for C<sub>119</sub>H<sub>94</sub>Ag<sub>5</sub>F<sub>30</sub>Fe<sub>2</sub>N<sub>8</sub>P<sub>10</sub>Sb<sub>5</sub> (3775.59 g/mol) = 37.85 C, 2.51 H, 2.97 N; found = 37.54 C, 2.90 H, 2.85 N.

Analytical data of **12**

**Yield:** 97 mg (0.016 mmol, 40% referred to [Cp<sup>Bn</sup>Fe(η<sup>5</sup>-P<sub>5</sub>)])

**<sup>1</sup>H NMR** (CD<sub>2</sub>Cl<sub>2</sub>/pyridine): δ [ppm] = 3.64 (s, [Cp<sup>Bn</sup>Fe(η<sup>5</sup>-P<sub>5</sub>)]), 6.18 (d, [Cp<sup>Bn</sup>Fe(η<sup>5</sup>-P<sub>5</sub>)]), 6.75 (m, [Cp<sup>Bn</sup>Fe(η<sup>5</sup>-P<sub>5</sub>)]), 6.90 (m, [Cp<sup>Bn</sup>Fe(η<sup>5</sup>-P<sub>5</sub>)]), 7.79 (*p*-(NC)<sub>2</sub>C<sub>6</sub>H<sub>4</sub>).

**<sup>31</sup>P{<sup>1</sup>H} NMR** (CD<sub>2</sub>Cl<sub>2</sub>/pyridine): δ [ppm] = 157.28 (s, [Cp<sup>Bn</sup>Fe(η<sup>5</sup>-P<sub>5</sub>)])

**<sup>19</sup>F NMR** (CD<sub>2</sub>Cl<sub>2</sub>/pyridine): no signal was detected.

**Positive ion ESI-MS** (CH<sub>2</sub>Cl<sub>2</sub>): *m/z* (%) = 106.9 [Ag]<sup>+</sup>, 130.2 [*p*-(NC)<sub>2</sub>C<sub>6</sub>H<sub>4</sub>]<sup>2+</sup>, 147.9 [Ag(CH<sub>3</sub>CN)]<sup>+</sup>, 188.9 [Ag(CH<sub>3</sub>CN)<sub>2</sub>]<sup>+</sup>, 229.9 [Ag(CH<sub>3</sub>CN)<sub>3</sub>]<sup>+</sup>, 271.1 [Ag(CH<sub>3</sub>CN)<sub>4</sub>]<sup>+</sup>, 832.9 [(Cp<sup>Bn</sup>Fe(η<sup>5</sup>-P<sub>5</sub>))Ag]<sup>+</sup>, 915.0 [(Cp<sup>Bn</sup>Fe(η<sup>5</sup>-P<sub>5</sub>))Ag(CH<sub>3</sub>CN)<sub>2</sub>]<sup>+</sup>, 1559.0 [(Cp<sup>Bn</sup>Fe(η<sup>5</sup>-P<sub>5</sub>))<sub>2</sub>Ag]<sup>+</sup>, 2248.3 [(Cp<sup>Bn</sup>Fe(η<sup>5</sup>-P<sub>5</sub>))<sub>2</sub>Ag<sub>3</sub>(SbF<sub>6</sub>)<sub>2</sub>]<sup>+</sup>.

**Negative ion ESI-MS** (CH<sub>2</sub>Cl<sub>2</sub>):  $m/z$  (%) = 234.9 [SbF<sub>6</sub>]<sup>-</sup>.

**Elemental analysis:** Calculated (%) for C<sub>223</sub>H<sub>194</sub>Ag<sub>6</sub>Cl<sub>6</sub>F<sub>36</sub>Fe<sub>4</sub>N<sub>8</sub>P<sub>20</sub>Sb<sub>6</sub> (6103.29 g/mol) = 43.89 C, 3.20 H, 1.84 N; found = 43.70 C, 3.14 H, 2.21 N.

Analytical data of **13**

**Yield:** 72 mg (0.0087 mmol, 22% referred to [Cp<sup>Bn</sup>Fe(η<sup>5</sup>-P<sub>5</sub>)]).

**<sup>1</sup>H NMR** (CD<sub>2</sub>Cl<sub>2</sub>/pyridine): δ [ppm] = 3.63 (s, [Cp<sup>Bn</sup>Fe(η<sup>5</sup>-P<sub>5</sub>)]), 6.18 (d, [Cp<sup>Bn</sup>Fe(η<sup>5</sup>-P<sub>5</sub>)]), 6.75 (m, [Cp<sup>Bn</sup>Fe(η<sup>5</sup>-P<sub>5</sub>)]), 6.89 (m, [Cp<sup>Bn</sup>Fe(η<sup>5</sup>-P<sub>5</sub>)]), 7.79 (*p*-(NC)<sub>2</sub>C<sub>6</sub>H<sub>4</sub>).

**<sup>31</sup>P{<sup>1</sup>H} NMR** (CD<sub>2</sub>Cl<sub>2</sub>/pyridine): δ [ppm] = 154.99 (s, [Cp<sup>Bn</sup>Fe(η<sup>5</sup>-P<sub>5</sub>)]).

**<sup>19</sup>F NMR** (CD<sub>2</sub>Cl<sub>2</sub>/pyridine): no signal was detected.

**Positive ion ESI-MS** (CH<sub>2</sub>Cl<sub>2</sub>):  $m/z$  (%) = 833.0 [(Cp<sup>Bn</sup>Fe(η<sup>5</sup>-P<sub>5</sub>))Ag]<sup>+</sup>, 1559.2 [(Cp<sup>Bn</sup>Fe(η<sup>5</sup>-P<sub>5</sub>))<sub>2</sub>Ag]<sup>+</sup>, 2287.5 [(Cp<sup>Bn</sup>Fe(η<sup>5</sup>-P<sub>5</sub>))<sub>2</sub>Ag<sub>2</sub>(SbF<sub>6</sub>)<sub>1</sub>(*p*-(NC)<sub>2</sub>C<sub>6</sub>H<sub>4</sub>)<sub>3</sub>]<sup>+</sup>,

**Negative ion ESI-MS** (CH<sub>2</sub>Cl<sub>2</sub>):  $m/z$  (%) = 234.9 [SbF<sub>6</sub>]<sup>-</sup>.

**Elemental analysis:** Calculated (%) for C<sub>315</sub>H<sub>268</sub>Ag<sub>10</sub>F<sub>60</sub>Fe<sub>6</sub>N<sub>10</sub>P<sub>30</sub>Sb<sub>10</sub> (8238.05 g/mol) = 42.53 C, 3.06 H, 1.57 N; found = 43.02 C, 3.24 H, 2.10 N.

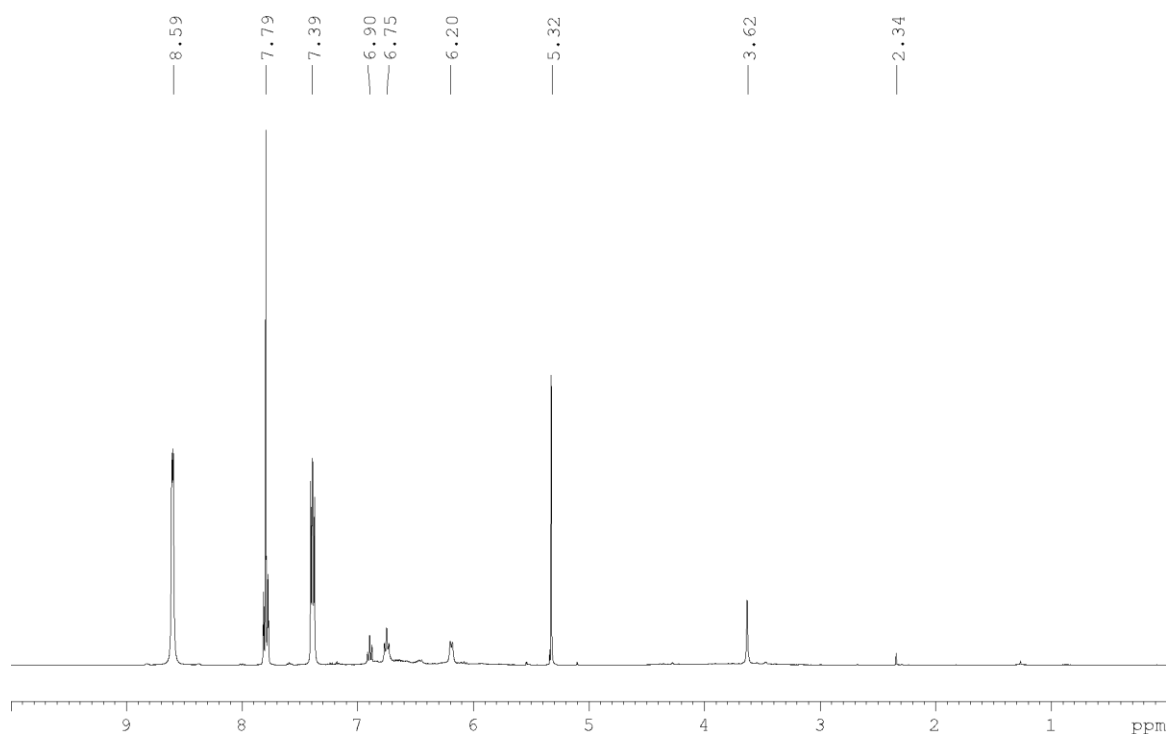


**Figure 6.35.** <sup>1</sup>H NMR spectrum of **11**. (2.34 toluene, 5.32 CH<sub>2</sub>Cl<sub>2</sub>, 7.39 pyridine, 8.59 pyridine)

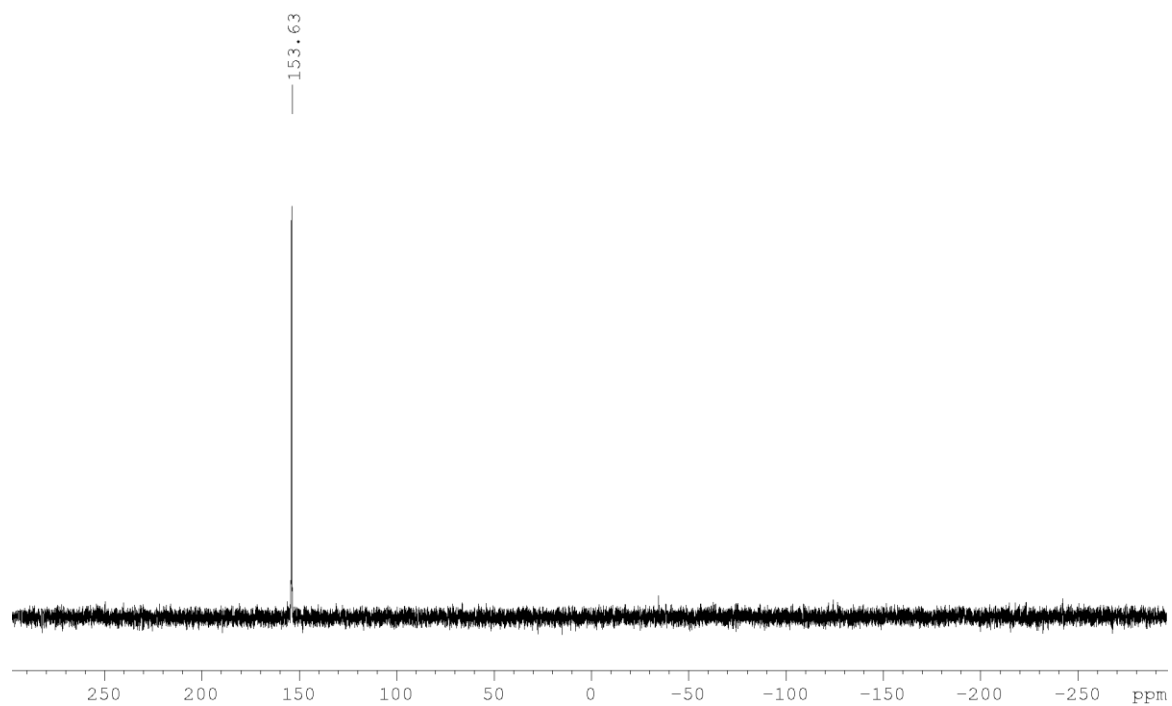


Figure 6.36.  $^{31}\text{P}\{^1\text{H}\}$  NMR spectrum of **11**.

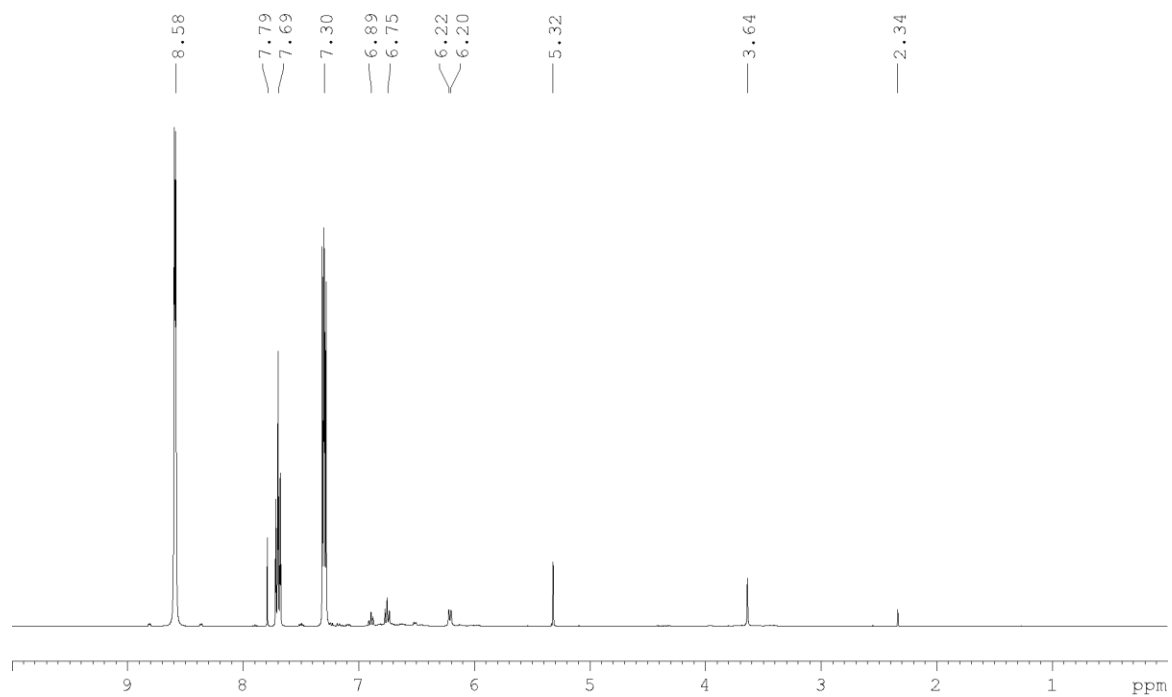


Figure 6.37.  $^1\text{H}$  NMR spectrum of **12**. (2.34 toluene, 5.32  $\text{CH}_2\text{Cl}_2$ , 7.30 pyridine, 7.69 pyridine, 8.58 pyridine)

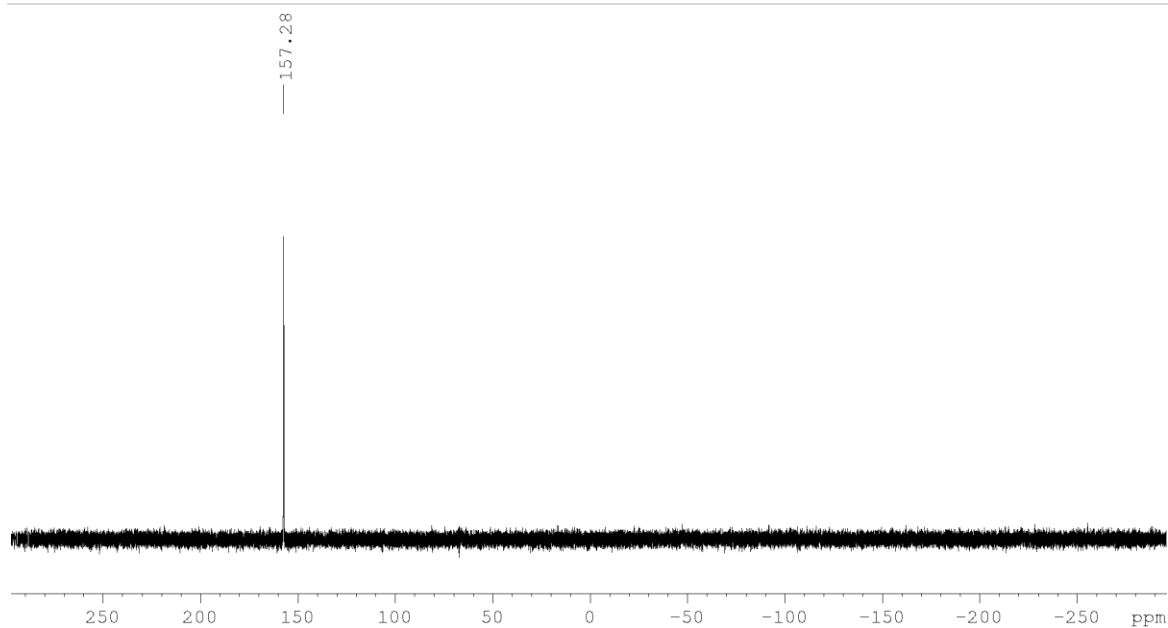


Figure 6.38.  $^{31}\text{P}\{^1\text{H}\}$  NMR spectrum of **12**.

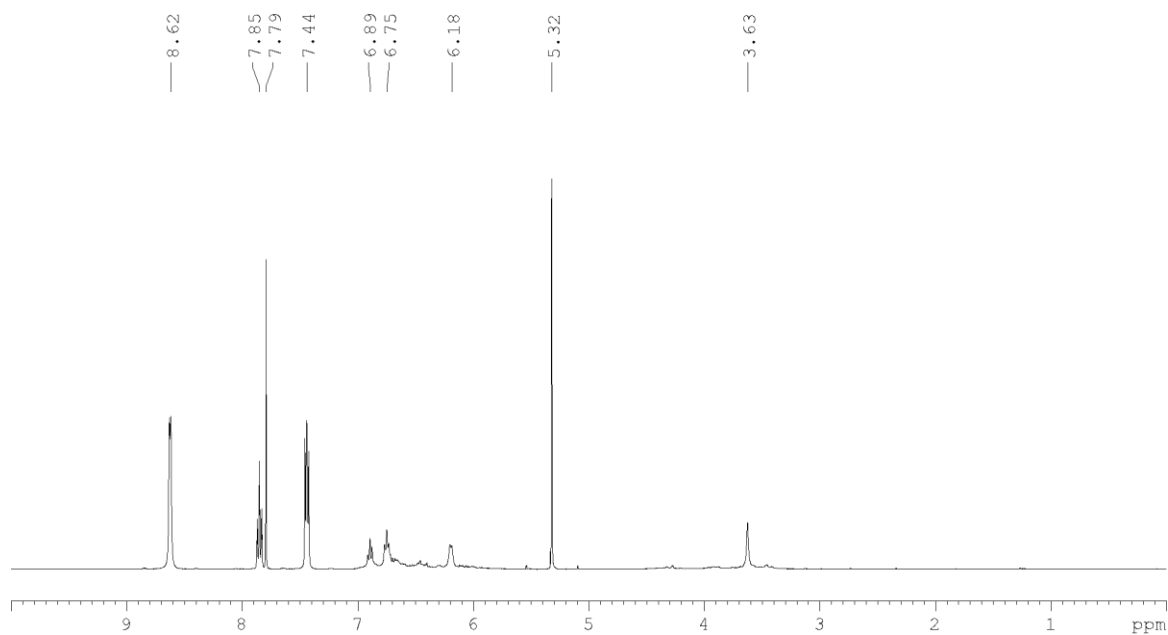


Figure 6.39.  $^1\text{H}$  NMR spectrum of **13**. (5.32  $\text{CH}_2\text{Cl}_2$ , 7.44 pyridine, 7.85 pyridine, 8.62 pyridine)

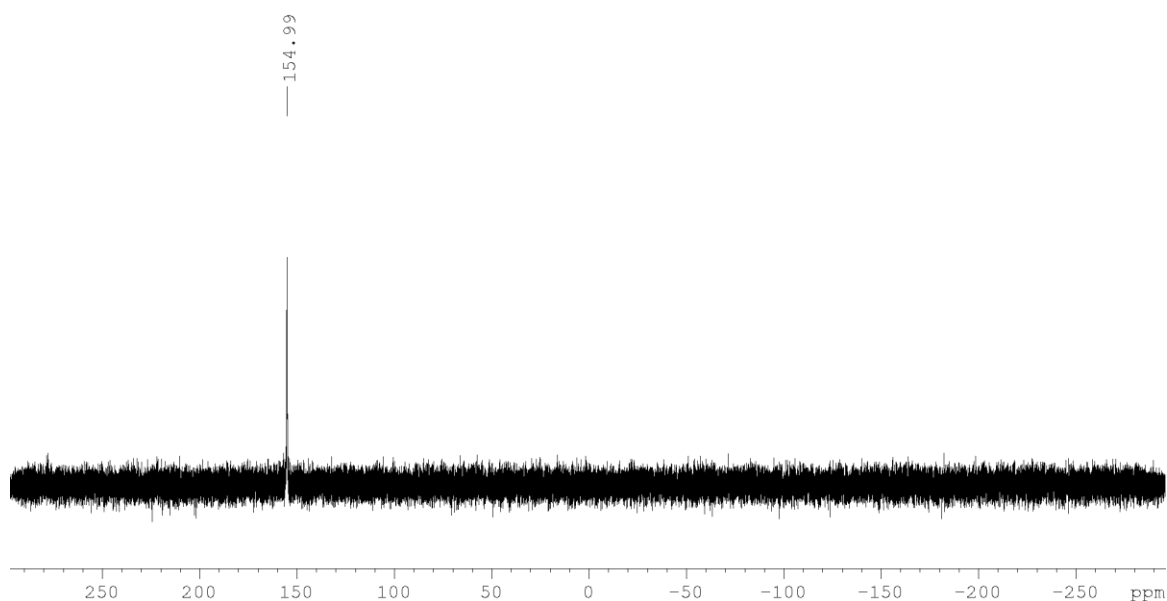


Figure 6.40.  $^{31}\text{P}\{^1\text{H}\}$  NMR spectrum of **13**.

## 6.5 Crystallographic Details and Structure Refinement

### Experimental

Crystals of **2-13** were taken from a Schlenk flask under a stream of argon and immediately covered with perfluorinated Fomblin<sup>®</sup> mineral oil to prevent decomposition and a loss of solvent. The quickly chosen single crystals covered by a drop of the oil were directly placed into a stream of cold nitrogen with the pre-centered goniometer head with CryoMount<sup>®</sup> and attached to the goniometer of a diffractometer. The single crystals of **10** were carefully selected, mounted on a magnetic holders and placed into a Dewar vessel in liquid nitrogen using standard cryocrystallography tools. After a week it was taken to the DESY PETRA III synchrotron. Using standard procedures, single crystals were placed into a vessel filled with liquid nitrogen among other crystals. A robotic mounting/demounting was used for further manipulations in the P11 beamline hutch for **10**.<sup>[19]</sup>

The diffraction data for **2** were collected on a Gemini Rigaku diffractometer equipped with an Atlas<sup>S2</sup> detector and a SuperNova CuK $\alpha$  microfocus source using either 1 $^\circ$   $\omega$  scans at 123 K. X-ray diffraction experiments for **3-5**, **9**, **10** and **12** at beamline P24 (DESY PETRA III synchrotron)<sup>[20]</sup> equipped with Huber 3-cycle diffractometer and PILATUS CdTe 1M photon counting detector. X-ray diffraction experiments for **9**, **11** and **12 (20 K)** an open-flow He LT system were measured at 20 K. Data collection for was performed by 360 $^\circ$   $\phi$ -rotation with 0.25-0.50 $^\circ$  scan width and exposure times of a few seconds per frame at a wavelength  $\lambda = 0.56002 \text{ \AA}$ . The diffraction data for **6-8** were collected on a Rigaku diffractometer equipped with a Titan<sup>S2</sup> CCD detector and a SuperNova CuK $\alpha$  microfocus source using either 1 $^\circ$  or 0.5 $^\circ$   $\omega$  scans depending on the unit cell constants.

The diffraction data for **13** were collected on a Rigaku XtaLAB Synergy R diffractometer equipped with a HyPix-Arc 150 detector and a CuK $\alpha$  rotating-anode X-ray source using 0.5°  $\omega$  scans at 100 K.

X-ray diffraction experiments for **10** for were measured at 100 K at the beamline P11 (DESY PETRA III synchrotron) using robotic mounting.<sup>[21]</sup> Data collection for was performed by 360°  $\phi$ -rotation with 0.2° scan width and exposure 0.12 s per frame at wavelength  $\lambda = 0.6199 \text{ \AA}$  (20 keV).

Data reduction for all crystal structures was performed with CrysAlisPro software.<sup>[22]</sup> Analytical absorption correction for **2**, **6-8**, **11** and **13** was applied based on crystal faces. For **3-5** and **9-13** empirical absorption correction based on equivalent reflections was used.

### Structure refinement

The structures were solved by direct methods with *SHELXT* and were refined by full-matrix least-squares method against  $F^2$  in anisotropic approximation using multiprocessor variable memory versions of *SHELXL (2014-2015)*.<sup>[23]</sup> All non-hydrogen atoms were refined anisotropically, while the hydrogen atoms were refined riding on pivot atoms.

In most of the crystal structures the SbF<sub>6</sub><sup>-</sup> counter-anions are disordered over two or more close positions. The occupation factors for disordered positions of Sb atoms were refined with fixed isotropic  $U_{\text{iso}}$  similar to the average  $U_{\text{iso}}$  (usually 0.025-0.035  $\text{\AA}^2$ ) for the fully occupied heavy atoms in the corresponding structure. The refinement of the disordered counter-anions SbF<sub>6</sub><sup>-</sup> was performed using idealized octahedral geometry. The fluorine atoms in very close positions were refined using equalized a.d.p. parameters. In case of small occupancy (<50%), F atoms were refined isotropically.

The flexible linker molecule DN9 also showed a strong tendency for conformational disorder in **5**. The dinitrile molecules were disordered over two or three close positions with different occupancies. In **6**, positional disorder of **DN10** linker molecule takes place. Their molecular site occupancy factors (equal s.o.f.'s for all atoms of a molecule) were refined using the FVAR instruction of SHELX with isotropic displacement parameters fixed at  $U_{\text{iso}} = 0.05 \text{ \AA}^2$ . The resulting occupancies were fixed and the C and N atoms with occupancies of more than 0.5 were refined in anisotropic approximation. Some minor positions of the linker molecules were refined with restraint geometry. The restraints were removed at the final stage of the refinement when possible. The disorder of the solvent molecules CH<sub>2</sub>Cl<sub>2</sub> was treated in a similar way.

**Table 6.2.** Experimental details for crystal structures **2** and **3**

Crystal data	<b>2</b>	<b>3</b> (preliminary data)
Chemical formula	C <sub>80</sub> H <sub>70</sub> Ag <sub>2</sub> Fe <sub>2</sub> P <sub>10</sub> ·2(SbF <sub>6</sub> )·2(CH <sub>2</sub> Cl <sub>2</sub> )	C <sub>388</sub> H <sub>357</sub> Ag <sub>17</sub> F <sub>102</sub> Fe <sub>9</sub> N <sub>14</sub> P <sub>45</sub> Sb <sub>17</sub>
Structural formula	[(C <sub>40</sub> H <sub>35</sub> FeP <sub>5</sub> )Ag] <sub>2</sub> (SbF <sub>6</sub> ) <sub>2</sub>	[SbF <sub>6</sub> ] <sub>2</sub> @[(C <sub>40</sub> H <sub>35</sub> FeP <sub>5</sub> ) <sub>6</sub> (AgCH <sub>3</sub> CN) <sub>14</sub> ][{(C <sub>40</sub> H <sub>35</sub> FeP <sub>5</sub> ) <sub>3</sub> Ag <sub>3</sub> ][SbF <sub>6</sub> ] <sub>16</sub>
<i>M<sub>r</sub></i>	2309.85	> 32069.12
Crystal system, space group	Monoclinic, <i>P</i> 2 <sub>1</sub> / <i>c</i>	Hexagonal, <i>P</i> 6 <sub>3</sub> / <i>m</i>
Temperature (K)	123	100
<i>a</i> , <i>b</i> , <i>c</i> (Å)	20.34757(15), 10.97815(8), 19.23413(15)	22.74410(16), 22.74410(16), 72.0649(5)
$\alpha, \beta, \gamma$ (°)	90, 96.8959(7), 90	90, 90, 120
<i>V</i> (Å <sup>3</sup> )	4265.41(6)	32284.3(4)
<i>Z</i>	2	1
<i>F</i> (000)	2280	>15839
<i>D<sub>x</sub></i> (Mg m <sup>-3</sup> )	1.798	>1.649
Radiation type	Cu <i>K</i> $\alpha$	synchrotron
$\mu$ (mm <sup>-1</sup> )	14.74	> 0.812
Crystal shape and colour	Dark green prism	Green hexagonal prism
Crystal size (mm)	0.20 × 0.10 × 0.08	0.12 × 0.12 × 0.15
Data collection		
Diffractionmeter	Xcalibur, Atlas <sup>S2</sup> , Gemini ultra	P24 beamline, Huber diffractometer, Pilatus3 CdTe 1M, DESY
Absorption correction	Analytical	multi-scan
<i>T<sub>min</sub></i> , <i>T<sub>max</sub></i>	0.201, 0.446	0.139, 1
No. of measured, independent and observed [ <i>I</i> > 2 $\sigma$ ( <i>I</i> )] reflections	27466, 7486, 6522	177670, 19875,
<i>R<sub>int</sub></i>	0.027	0.0596
( <i>sin</i> $\theta$ / $\lambda$ ) <sub>max</sub> (Å <sup>-1</sup> )	0.596	
Range of <i>h</i> , <i>k</i> , <i>l</i>	<i>h</i> = -19→24, <i>k</i> = -12→13, <i>l</i> = -22→22	<i>h</i> = -27→27, <i>k</i> = -26→26, <i>l</i> = -86→86
Refinement		
<i>R</i> [ <i>F</i> <sup>2</sup> > 2 $\sigma$ ( <i>F</i> <sup>2</sup> )], <i>wR</i> ( <i>F</i> <sup>2</sup> ), <i>S</i>	0.022, 0.053, 1.03	0.0854, 0.2800, 1.033
No. of reflections	7486	19875
No. of parameters	514	>1226
No. of restraints	0	0
H-atom treatment	H-atom parameters constrained	H-atom parameters constrained
$\Delta$ <sub>max</sub> , $\Delta$ <sub>min</sub> (e Å <sup>-3</sup> )	0.58, -0.67	7.692, -1.928

Computer programs for **2**: *CrysAlis PRO* 1.171.38.41 (Rigaku OD, 2015), *SHELXT2014* (Sheldrick, 2014), *SHELXL2014/7* (Sheldrick, 2014); for **3**: Computer programs: *CrysAlis PRO* 1.171.42.43a (Rigaku OD, 2022), *SHELXT2018/5* (Sheldrick, 2018), *SHELXL2018/3* (Sheldrick, 2018).



**Table 6.3.** Experimental details for crystal structures **4** and **5**.

Crystal data	4	5
Chemical formula	C <sub>200.90</sub> H <sub>168.10</sub> Ag <sub>4.95</sub> Cl <sub>7.75</sub> F <sub>29.10</sub> Fe <sub>4</sub> N <sub>4.95</sub> P <sub>2</sub> oSb <sub>4.85</sub>	C <sub>306.15</sub> H <sub>247.80</sub> Ag <sub>9.50</sub> Cl <sub>9.45</sub> Fe <sub>6</sub> N <sub>9.45</sub> P <sub>30</sub> · (SbF <sub>6</sub> ) <sub>9.5</sub> ·(CH <sub>2</sub> Cl <sub>2</sub> ) <sub>1.75</sub> ·C <sub>7</sub> H <sub>8</sub>
Structural formula	[(C <sub>40</sub> H <sub>35</sub> FeP <sub>5</sub> ) <sub>4</sub> Ag(CN(C <sub>6</sub> H <sub>4</sub> )Cl)] <sub>4.95</sub> (SbF <sub>6</sub> ) <sub>4.85</sub> Cl <sub>0.1</sub> ·(CH <sub>2</sub> Cl <sub>2</sub> ) <sub>1.35</sub> ·(C <sub>7</sub> H <sub>8</sub> ) <sub>0.7</sub>	[SbF <sub>6</sub> ]@[[(C <sub>40</sub> H <sub>35</sub> FeP <sub>5</sub> ) <sub>6</sub> (Ag(CN(C <sub>6</sub> H <sub>4</sub> )Cl)] <sub>9.5</sub> )] [SbF <sub>6</sub> ] <sub>8.5</sub> ·(CH <sub>2</sub> Cl <sub>2</sub> ) <sub>1.75</sub> ·C <sub>7</sub> H <sub>8</sub>
<i>M<sub>r</sub></i>	5446.47	9163.37
Crystal system, space group	Orthorhombic, <i>P</i> 2 <sub>1</sub> 2 <sub>1</sub> 2 <sub>1</sub>	Triclinic, <i>P</i> 1
Temperature (K)	100	100
<i>a</i> , <i>b</i> , <i>c</i> (Å)	23.86575(17), 26.3064(2), 34.2857(3)	20.08181(16), 23.25396(16), 24.09127(14)
$\alpha$ , $\beta$ , $\gamma$ (°)	90	98.8155 (5), 112.9049 (7), 112.7662 (7)
<i>V</i> (Å <sup>3</sup> )	21525.3 (3)	8923.33 (12)
<i>Z</i>	4	1
<i>F</i> (000)	10743	4485
<i>D<sub>x</sub></i> (Mg m <sup>-3</sup> )	1.681	1.705
Radiation type	Synchrotron, $\lambda$ = 0.56002 Å	Synchrotron, $\lambda$ = 0.56002 Å
$\mu$ (mm <sup>-1</sup> )	0.84	0.91
Crystal shape and colour	Green needle	Brown polyhedron
Crystal size (mm)	0.20 × 0.01 × 0.01	0.15 × 0.15 × 0.10
Data collection		
Diffractometer	P24 beamline, Huber diffractometer, Pilatus3 CdTe 1M, DESY	P24 beamline, Huber diffractometer, Pilatus3 CdTe 1M, DESY
Absorption correction	Multi-scan	Multi-scan
<i>T<sub>min</sub></i> , <i>T<sub>max</sub></i>	0.566, 1.000	0.946, 1.000
No. of measured, independent and observed [ <i>i</i> > 2σ( <i>I</i> )] reflections	265158, 40806, 31639	119019, 43619, 39732
<i>R<sub>int</sub></i>	0.093	0.020
(sin θ/λ) <sub>max</sub> (Å <sup>-1</sup> )	0.610	0.741
Range of <i>h</i> , <i>k</i> , <i>l</i>	<i>h</i> = -29→29, <i>k</i> = -32→32, <i>l</i> = -41→41	<i>h</i> = -29→29, <i>k</i> = -31→31, <i>l</i> = -34→34
Refinement		
<i>R</i> [ <i>F</i> <sup>2</sup> > 2σ( <i>F</i> <sup>2</sup> )], <i>wR</i> ( <i>F</i> <sup>2</sup> ), <i>S</i>	0.035, 0.075, 0.92	0.055, 0.168, 1.02
No. of reflections	40806	43619
No. of parameters	2516	2686
No. of restraints	10	11
H-atom treatment	H-atom parameters constrained	H atoms treated by a mixture of independent and constrained refinement
$\Delta$ <sub>max</sub> , $\Delta$ <sub>min</sub> (e Å <sup>-3</sup> )	0.85, -1.14	3.00, -2.00
Absolute structure parameter	0.448 (18)	-

Computer programs for **4**: beamline software, *CrysAlis PRO* 1.171.42.43a (Rigaku OD, 2022), *SHELXT2018/5* (Sheldrick, 2018), *SHELXL2018/3* (Sheldrick, 2018).

**Table 6.4.** Experimental details for crystal structures **6** and **7**.

Crystal data	6	7
Chemical formula	C <sub>50</sub> H <sub>51</sub> AgFeN <sub>2</sub> P <sub>5</sub> SbF <sub>6</sub>	C <sub>295</sub> H <sub>300</sub> Ag <sub>6</sub> F <sub>36</sub> Fe <sub>6</sub> N <sub>10</sub> P <sub>30</sub> Sb <sub>6</sub> ·(CH <sub>2</sub> Cl <sub>2</sub> ) <sub>0.8</sub>
Structural formula	[(C <sub>40</sub> H <sub>35</sub> FeP <sub>5</sub> )Ag(NC(CH <sub>2</sub> ) <sub>8</sub> CN)](SbF <sub>6</sub> )	(C <sub>40</sub> H <sub>35</sub> FeP <sub>5</sub> ) <sub>6</sub> Ag <sub>6</sub> (NC(CH <sub>2</sub> ) <sub>9</sub> CN) <sub>5</sub> [(SbF <sub>6</sub> ) <sub>6</sub> ·0.8(CH <sub>2</sub> Cl <sub>2</sub> )
<i>M<sub>r</sub></i>	1234.24	7379.29
Crystal system, space group	Monoclinic, <i>P</i> 2 <sub>1</sub> / <i>n</i>	Monoclinic, <i>P</i> 2 <sub>1</sub> / <i>n</i>
Temperature (K)	123	90
<i>a</i> , <i>b</i> , <i>c</i> (Å)	18.2093(3), 9.5766(2), 28.3305(5)	17.99395 (11), 30.78118 (19), 27.03445 (16)
β (°)	95.8409(18)	101.7520 (6)
<i>V</i> (Å <sup>3</sup> )	4914.71(17)	14659.83 (16)
<i>Z</i>	4	2
<i>F</i> (000)	2472	7383
<i>D<sub>x</sub></i> (Mg m <sup>-3</sup> )	1.668	1.672
Radiation type	Cu Kα	Cu Kα
μ (mm <sup>-1</sup> )	11.86	12.07
Crystal shape and colour	Green-brown rod	Green rod
Crystal size (mm)	0.72 × 0.33 × 0.06	0.34 × 0.11 × 0.07
Data collection		
Diffractometer	SuperNova, Titan <sup>S2</sup>	SuperNova, Titan <sup>S2</sup>
Absorption correction	Gaussian	Gaussian
<i>T<sub>min</sub></i> , <i>T<sub>max</sub></i>	0.029, 0.514	0.075, 0.627
No. of measured, independent and observed [ <i>I</i> > 2σ( <i>I</i> )] reflections	22717, 9531, 8185	80909, 29405, 23008
<i>R<sub>int</sub></i>	0.056	0.030
(sin θ/λ) <sub>max</sub> (Å <sup>-1</sup> )	0.622	0.624
Range of <i>h</i> , <i>k</i> , <i>l</i>	<i>h</i> = -22→17, <i>k</i> = -11→10, <i>l</i> = -30→34	<i>h</i> = -22→14, <i>k</i> = -28→38, <i>l</i> = -31→33
Refinement		
<i>R</i> [ <i>F</i> <sup>2</sup> > 2σ( <i>F</i> <sup>2</sup> )], <i>wR</i> ( <i>F</i> <sup>2</sup> ), <i>S</i>	0.040, 0.103, 0.98	0.044, 0.128, 0.99
No. of reflections	9531	29405
No. of parameters	595	2094
No. of restraints	0	214
H-atom treatment	H-atom parameters constrained	H-atom parameters constrained
Δ <sub>max</sub> , Δ <sub>min</sub> (e Å <sup>-3</sup> )	1.52, -1.41	1.99, -1.61

Computer programs for **6**: *CrysAlis PRO* 1.171.38.41 (Rigaku OD, 2015), *SHELXT2014* (Sheldrick, 2014), *SHELXL2014/7* (Sheldrick, 2014); Computer programs for **7**: *CrysAlis PRO* 1.171.40.14a (Rigaku OD, 2018), *SHELXT2018/5* (Sheldrick, 2018), *SHELXL2018/3* (Sheldrick, 2018).

**Table 6.5.** Experimental details for crystal structures **8** and **9**.

Crystal data	<b>8</b>	<b>9</b> (preliminary data)
Chemical formula	C <sub>196</sub> H <sub>200</sub> N <sub>6</sub> Ag <sub>4</sub> Fe <sub>4</sub> P <sub>20</sub> ·4(F <sub>6</sub> Sb)·2(CH <sub>2</sub> Cl <sub>2</sub> )	C <sub>416</sub> H <sub>328</sub> Ag <sub>12±x</sub> F <sub>72±x</sub> Fe <sub>8</sub> N <sub>24±x</sub> P <sub>40</sub> Sb <sub>12±x</sub>
Structural formula	[(C <sub>40</sub> H <sub>35</sub> FeP <sub>5</sub> ) <sub>4</sub> Ag <sub>4</sub> (CN(CH <sub>2</sub> ) <sub>10</sub> CN) <sub>3</sub> ](SbF <sub>6</sub> ) <sub>4</sub> ·C H <sub>2</sub> Cl <sub>2</sub>	[(Cp <sup>Bn</sup> Fe(η <sup>5</sup> -P <sub>5</sub> )) <sub>8</sub> {Ag(o- NC(C <sub>6</sub> H <sub>4</sub> )CN)} <sub>12±x</sub> ] <sub>n</sub> [SbF <sub>6</sub> ] <sub>(12±x)n</sub>
<i>M<sub>r</sub></i>	4941.81	>6816.78
Crystal system, space group	Monoclinic, <i>P</i> 2 <sub>1</sub> / <i>n</i>	Triclinic, <i>P</i> 1
Temperature (K)	123	100 K
<i>a</i> , <i>b</i> , <i>c</i> (Å)	18.0693(7), 10.2568(4), 26.9826(10)	20.11079(10), 25.29490(16), 28.57211(14)
$\alpha$ , $\beta$ , $\gamma$ (°)	101.848(4)	90.7163(4), 107.4372(4), 98.4411(5)
<i>V</i> (Å <sup>3</sup> )	4894.2(3)	13691.91(13)
<i>Z</i>	1	2
<i>F</i> (000)	2472	6765
<i>D<sub>x</sub></i> (Mg m <sup>-3</sup> )	1.677	1.653
Radiation type	Cu K $\alpha$	Synchrotron, $\lambda$ = 0.6199 Å
$\mu$ (mm <sup>-1</sup> )	12.16	>0.962
Crystal shape and colour	Brown-green elongated plate	green plate
Crystal size (mm)	1.08 × 0.15 × 0.02	0.1 × 0.1 × 0.02
Data collection		
Diffractometer	SuperNova, Titan <sup>S2</sup>	P11 beamline, Eiger, DESY
Absorption correction	Gaussian	Multi-scan
<i>T<sub>min</sub></i> , <i>T<sub>max</sub></i>	0.069, 0.793	0.701, 1
No. of measured, independent and observed [ <i>I</i> > 2 $\sigma$ ( <i>I</i> )] reflections	20020, 9587, 7407	229516, 64214, 40739
<i>R<sub>int</sub></i>	0.032	0.0341
(sin $\theta$ / $\lambda$ ) <sub>max</sub> (Å <sup>-1</sup> )	0.623	
Range of <i>h</i> , <i>k</i> , <i>l</i>	<i>h</i> = -22→22, <i>k</i> = -8→12, <i>l</i> = -33→24	<i>h</i> = -30→29, <i>k</i> = -32→32, <i>l</i> = -43→42
Refinement		
<i>R</i> [ <i>F</i> <sup>2</sup> > 2 $\sigma$ ( <i>F</i> <sup>2</sup> )], <i>wR</i> ( <i>F</i> <sup>2</sup> ), <i>S</i>	0.036, 0.093, 0.97	0.1398, 0.4250, 1.662
No. of reflections	9587	229516
No. of parameters	723	> 2189
No. of restraints	0	0
H-atom treatment	H-atom parameters constrained	H-atom parameters constrained
$\Delta$ <sub>max</sub> , $\Delta$ <sub>min</sub> (e Å <sup>-3</sup> )	0.58, -0.73	4.346, -2.776

Computer programs for **8**: *CrysAlis PRO* 1.171.38.41 (Rigaku OD, 2015), *SHELXT2014/7* (Sheldrick, 2014), *SHELXL2014/7* (Sheldrick, 2014).

**Table 6.6.** Experimental details for crystal structure **10** measured at 20K and 200K.

Crystal data	<b>10</b> (20K)	<b>10</b> (200K)
Chemical formula	(C <sub>56</sub> H <sub>43</sub> Ag <sub>2</sub> FeN <sub>4</sub> P <sub>5</sub> ) <sub>2</sub> ·2(SbF <sub>6</sub> )·C <sub>7</sub> H <sub>8</sub>	(C <sub>56</sub> H <sub>43</sub> Ag <sub>2</sub> FeN <sub>4</sub> P <sub>5</sub> ) <sub>2</sub> (SbF <sub>6</sub> )·C <sub>7</sub> H <sub>8</sub>
Structural formula	[(C <sub>40</sub> H <sub>35</sub> FeP <sub>5</sub> )Ag <sub>2</sub> (C <sub>6</sub> H <sub>4</sub> (CN) <sub>2</sub> ) <sub>2</sub> ](SbF <sub>6</sub> ) <sub>2</sub> ·C <sub>7</sub> H <sub>8</sub>	[(C <sub>40</sub> H <sub>35</sub> FeP <sub>5</sub> )Ag <sub>2</sub> (C <sub>6</sub> H <sub>4</sub> (CN) <sub>2</sub> ) <sub>2</sub> ](SbF <sub>6</sub> ) <sub>2</sub> ·C <sub>7</sub> H <sub>8</sub>
<i>M<sub>r</sub></i>	1762.01	1762.01
Crystal system, space group	Monoclinic, P21/m	Monoclinic, P21/m
Temperature (K)	20	200
<i>a</i> , <i>b</i> , <i>c</i> (Å)	10.4551(3), 25.2797(7), 12.3341(10)	10.4835(3), 25.4904(7), 12.4536(8)
$\alpha$ , $\beta$ , $\gamma$ (°)	95.458(4)	95.499(3)
<i>V</i> (Å <sup>3</sup> )	3245.2(3)	3312.7(2)
<i>Z</i>	2	2
<i>F</i> (000)	1724	1724
<i>D<sub>x</sub></i> (Mg m <sup>-3</sup> )	1.803	1.766
Radiation type	Synchrotron, $\lambda$ = 0.56002 Å	Synchrotron, $\lambda$ = 0.56002 Å
$\mu$ (mm <sup>-1</sup> )	0.97	0.95
Crystal shape and colour	Green plate	Green plate
Crystal size (mm)	0.20 × 0.20 × 0.03	0.20 × 0.20 × 0.03
Data collection		
Diffractionmeter	P24 beamline, Huber diffractometer, PILATUS CdTe 1M	P24 beamline, Huber diffractometer, PILATUS CdTe 1M
Absorption correction	Multi-scan	Multi-scan
<i>T<sub>min</sub></i> , <i>T<sub>max</sub></i>	0.455, 1.000	0.213, 1.000
No. of measured, independent and observed [ <i>I</i> > 2σ( <i>I</i> )] reflections	44710, 8626, 8053	46659, 8859, 7615
<i>R<sub>int</sub></i>	0.023	0.022
(sin θ/λ) <sub>max</sub> (Å <sup>-1</sup> )	0.733	0.732
Range of <i>h</i> , <i>k</i> , <i>l</i>	<i>h</i> = -15*15, <i>k</i> = -36*36, <i>l</i> = -16*16	<i>h</i> = -15*15, <i>k</i> = -36*37, <i>l</i> = -17*17
Refinement		
<i>R</i> [ <i>F</i> <sup>2</sup> > 2σ( <i>F</i> <sup>2</sup> )], <i>wR</i> ( <i>F</i> <sup>2</sup> ), <i>S</i>	0.066, 0.162, 1.09	0.048, 0.138, 1.06
No. of reflections	8626	8859
No. of parameters	726	726
No. of restraints	0	0
H-atom treatment	H-atom parameters constrained	H-atom parameters constrained
$\Delta$ <sub>max</sub> , $\Delta$ <sub>min</sub> (e Å <sup>-3</sup> )	1.26, -0.99	0.57, -0.61

Computer programs for **10** at 20K: *CrysAlis PRO* 1.171.41.83a (Rigaku OD, 2020), *SHELXT2018/5* (Sheldrick, 2018), *SHELXL2018/3* (Sheldrick, 2018); for **10** at 200K: *CrysAlis PRO* 1.171.41.83a (Rigaku OD, 2020), *SHELXT2018/5* (Sheldrick, 2018), *SHELXL2018/3* (Sheldrick, 2018).

**Table 6.7.** Experimental details for crystal structures **11** and **12**.

Crystal data	11	12
Chemical formula	(C <sub>126</sub> H <sub>102</sub> Ag <sub>5</sub> Fe <sub>2</sub> N <sub>8</sub> P <sub>10</sub> )·5(SbF <sub>6</sub> ) <sub>4.45</sub> (C <sub>7</sub> H <sub>8</sub> )	(C <sub>110</sub> H <sub>94</sub> Ag <sub>3</sub> F <sub>12</sub> Fe <sub>2</sub> N <sub>4</sub> P <sub>10</sub> Sb <sub>2</sub> )·3(F <sub>6</sub> Sb)·2(C <sub>7</sub> H <sub>8</sub> )·1.5(CH <sub>2</sub> Cl <sub>2</sub> )
Structural formula	[(C <sub>40</sub> H <sub>35</sub> FeP <sub>5</sub> ) <sub>2</sub> Ag <sub>5</sub> ((NC) <sub>2</sub> C <sub>6</sub> H <sub>4</sub> ) <sub>4</sub> (C <sub>7</sub> H <sub>8</sub> ) <sub>4.45</sub> ][SbF <sub>6</sub> ] <sub>5</sub>	[(C <sub>40</sub> H <sub>35</sub> FeP <sub>5</sub> ) <sub>4</sub> Ag <sub>6</sub> ((NC) <sub>2</sub> C <sub>6</sub> H <sub>4</sub> ) <sub>5</sub> (C <sub>7</sub> H <sub>8</sub> ) <sub>4</sub> ][SbF <sub>6</sub> ] <sub>6</sub>
<i>M<sub>r</sub></i>	4093.38	6103.07
Crystal system, space group	Monoclinic, C2/c	Monoclinic, C2/c
Temperature (K)	20	20
<i>a</i> , <i>b</i> , <i>c</i> (Å)	19.75958(18), 30.9316(3), 25.8753(3)	17.5939 (2), 28.7379 (2), 24.6493 (5)
$\alpha$ , $\beta$ , $\gamma$ (°)	90, 102.1189(10), 90	105.2371 (15)
<i>V</i> (Å <sup>3</sup> )	15462.4 (3)	12024.9 (3)
<i>Z</i>	4	2
<i>F</i> (000)	7994	6012
<i>D<sub>x</sub></i> (Mg m <sup>-3</sup> )	1.758	1.686
Radiation type	Synchrotron, <i>l</i> = 0.560 Å	Synchrotron, <i>l</i> = 0.560 Å
$\mu$ (mm <sup>-1</sup> )	0.98	0.87
Crystal shape and colour	Green prism	Green lath-shaped plate
Crystal size (mm)	0.1 × 0.1 × 0.1	0.25 × 0.05 × 0.03
Data collection		
Diffractometer	P24 beamline, Huber diffractometer, PILATUS CdTe 1M	P24 beamline, Huber diffractometer, PILATUS CdTe 1M
Absorption correction	Multi-scan	Multi-scan
<i>T<sub>min</sub></i> , <i>T<sub>max</sub></i>	0.907, 1.000	0.866, 1.000
No. of measured, independent and observed [ <i>I</i> > 2σ( <i>I</i> )] reflections	96108, 20031, 16101	70624, 11768, 11443
<i>R<sub>int</sub></i>	0.053	0.043
(sin θ/ <i>λ</i> ) <sub>max</sub> (Å <sup>-1</sup> )	0.694	0.625
Range of <i>h</i> , <i>k</i> , <i>l</i>	<i>h</i> = -27*27, <i>k</i> = -42*42, <i>l</i> = -34*34	<i>h</i> = -21*21, <i>k</i> = -35*35, <i>l</i> = -29*29
Refinement		
<i>R</i> [ <i>F</i> <sup>2</sup> > 2σ( <i>F</i> <sup>2</sup> )], <i>wR</i> ( <i>F</i> <sup>2</sup> ), <i>S</i>	0.064, 0.186, 1.03	0.056, 0.168, 1.03
No. of reflections	20031	11768
No. of parameters	1271	827
No. of restraints	3	11
H-atom treatment	H-atom parameters constrained	H-atom parameters constrained
$\Delta$ <sub>max</sub> , $\Delta$ <sub>min</sub> (e Å <sup>-3</sup> )	2.87, -1.38	1.11, -1.20

Computer programs: SHELXL2018/3 (Sheldrick, 2018), SHELXT2018/5 (Sheldrick, 2018); for **11**: CrysAlis PRO 1.171.41.83a (Rigaku OD, 2020), SHELXT2018/5 (Sheldrick, 2018), SHELXL2018/3 (Sheldrick, 2018); for **12**: CrysAlis PRO 1.171.41.83a (Rigaku OD, 2020).

**Table 6.8.** Experimental details for crystal structure **13**.

Crystal data	<b>13</b>
Chemical formula	$(C_{243}H_{211.5}Ag_{10}Cl_{0.35}Fe_6No_{0.75}P_{30})(C_{240}H_{210}Ag_{10}Fe_6P_{30})(C_8H_4N_2)_{10} \cdot 19.65(SbF_6) \cdot 7.69(CH_2Cl_2) \cdot 5.8(C_7H_8)$
Structural formula	$[SbF_6]@[C_{40}H_{35}FeP_5]_6Ag_{10}[(NC)_2C_6H_4]_{5.1875}Cl_{0.175}[SbF_6]_{8.825}$
$M_r$	18035.65
Crystal system, space group	Monoclinic, $P2_1/c$
Temperature (K)	123
$a, b, c$ (Å)	37.6522 (5), 25.7823 (3), 37.8829 (5)
$\alpha, \beta, \gamma$ (°)	109.7959 (14)
$V$ (Å <sup>3</sup> )	34601.9 (8)
$Z$	2
$F(000)$	17638
$D_x$ (Mg m <sup>-3</sup> )	1.731
Radiation type	Mo $K\alpha$
$\mu$ (mm <sup>-1</sup> )	1.83
Crystal shape and colour	Dark green prism
Crystal size (mm)	0.13 × 0.10 × 0.08
Data collection	
Diffractometer	XtaLAB Synergy R, DW system, HyPix-Arc 150
Absorption correction	Gaussian
$T_{min}, T_{max}$	0.920, 0.976
No. of measured, independent and observed [ $I > 2\sigma(I)$ ] reflections	312803, 76033, 52852
$R_{int}$	0.048
$(\sin \theta/\lambda)_{max}$ (Å <sup>-1</sup> )	0.641
Range of $h, k, l$	$h = -48 \rightarrow 48, k = -33 \rightarrow 33, l = -48 \rightarrow 48$
Refinement	
$R[F^2 > 2\sigma(F^2)], wR(F^2), S$	0.044, 0.125, 1.01
No. of reflections	76033
No. of parameters	4348
No. of restraints	61
H-atom treatment	H-atom parameters constrained
$\Delta_{max}, \Delta_{min}$ (e Å <sup>-3</sup> )	2.76, -1.42

Computer programs for **13**: Computer programs: CrysAlis PRO 1.171.42.43a (Rigaku OD, 2022), SHELXT2018/5 (Sheldrick, 2018), SHELXL2018/3 (Sheldrick, 2018).

## 6.6 Author Contributions

- ❖ The synthesis and characterization of compound **2,6,8** was performed by Dr. B. Hiltl and was also part of the PhD-Thesis of Dr. B. Hiltl.
- ❖ The synthesis of **4** and **5** was performed by Dr. B. Hiltl and K. Grill and was also part of the PhD-Thesis of Dr. B. Hiltl. The characterization was performed of Dr. B. Hiltl. Crystals for a solid-state structure were provided by K. Grill.
- ❖ The description of **2,4,5,6,8** was done by Dr. B. Hiltl and K. Grill
- ❖ The synthesis and characterization of compound **3,7** and **9-13** was performed by K. Grill.
- ❖ The manuscript (Abstract, Introduction, Results and Discussion, Conclusion, Experimental Part, References) was written by K. Grill.
- ❖ The section “crystallographic details and structure refinement” was written by Dr. E. Peresykina.
- ❖ The X-ray structure analyses for structures **2-12** are performed by Dr. E. Peresykina and Dr. Sc. A. V. Virovets including the sample preparation.
- ❖ The X-ray structure analysis for structure **13** is performed by K. Grill.
- ❖ All data reductions were performed by Dr. Sc. A. V. Virovets and all calculations by Dr. E. Peresykina.

## 6.7 References

- [1] J. W. Steed, D. R. Turner, K. J. Wallace, *Core concepts in supramolecular chemistry and nanochemistry*, John Wiley, Chichester, England, Hoboken, NJ, **2007**.
- [2] R. Chakrabarty, P. S. Mukherjee, P. J. Stang, *Chem. Rev.* **2011**, *111*, 6810.
- [3] a) A. V. Baskar, M. R. Benzigar, S. N. Talapaneni, G. Singh, A. S. Karakoti, J. Yi, A. H. Al-Muhtaseb, K. Ariga, P. M. Ajayan, A. Vinu, *Adv. Funct. Mater.* **2022**, *32*, 2106924; b) J. L. Atwood (Ed.) *Comprehensive supramolecular chemistry II*, Elsevier, **2017**.
- [4] P. J. Stang, D. H. Cao, *J. Am. Chem. Soc.* **1994**, *116*, 4981.
- [5] M. Fujita, J. Yazaki, K. Ogura, *J. Am. Chem. Soc.* **1990**, *112*, 5645.
- [6] P. Stricklen, J. Verkade, *J. Am. Chem. Soc.* **1983**, *105*, 2494.
- [7] M. Di Vaira, C. A. Ghilardi, S. Midollini, L. Sacconi, *J. Am. Chem. Soc.* **1978**, *100*, 2550.
- [8] a) K. Severin, *Chem. Commun.* **2006**, 3859; b) H. Suzuki, Y. Yamamoto, N. Tajima, K. Tatsumi, *Chem. Commun.* **2000**, 1801; c) M. Ramesh, T. B. Rauchfuss, *J. Organomet.- Chem.* **2004**, *689*, 1425.
- [9] O. J. Scherer, H. Sitzmann, G. Wolmershäuser, *J. Organomet. Chem.* **1984**, *268*, C9-C12.

- [10] a) J. Bai, A. V. Virovets, M. Scheer, *Science* **2003**, *300*, 781; b) S. Welsch, C. Gröger, M. Sierka, M. Scheer, *Angew. Chem. Int. Ed.* **2011**, *50*, 1435; c) M. Scheer, A. Schindler, R. Merkle, B. P. Johnson, M. Linseis, R. Winter, C. E. Anson, A. V. Virovets, *J. Am. Chem. Soc.* **2007**, *129*, 13386; d) E. Peresykina, C. Heindl, A. Virovets, H. Brake, E. Mädl, M. Scheer, *Eur. J. Chem.* **2018**, *24*, 2503; e) H. Brake, E. Peresykina, C. Heindl, A. V. Virovets, W. Kremer, M. Scheer, *Chem. Sci.* **2019**, *10*, 2940; f) A. Schindler, C. Heindl, G. Balázs, C. Gröger, A. V. Virovets, E. V. Peresykina, M. Scheer, *Eur. J. Chem.* **2012**, *18*, 829.
- [11] F. Dielmann, C. Heindl, F. Hastreiter, E. V. Peresykina, A. V. Virovets, R. M. Gschwind, M. Scheer, *Angew. Chem. Int. Ed.* **2014**, *53*, 13605.
- [12] F. Dielmann, M. Fleischmann, C. Heindl, E. V. Peresykina, A. V. Virovets, R. M. Gschwind, M. Scheer, *Eur. J. Chem.* **2015**, *21*, 6208.
- [13] C. Heindl, E. Peresykina, A. V. Virovets, I. S. Bushmarinov, M. G. Medvedev, B. Krämer, B. Dittrich, M. Scheer, *Angew. Chem. Int. Ed.* **2017**, *56*, 13237.
- [14] K. Grill, S. B. Dinauer, E. Peresykina, A. V. Virovets, M. Scheer, *Chem. Eur. J.* **2023**, *29*, e202203963.
- [15] E. Peresykina, K. Grill, B. Hiltl, A. V. Virovets, W. Kremer, J. Hilgert, W. Tremel, M. Scheer, *Angew. Chem. Int. Ed.* **2021**, *60*, 12132-12142.
- [16] M. Scheer, L. J. Gregoriades, A. V. Virovets, W. Kunz, R. Neueder, I. Krossing, *Angew. Chem.* **2006**, *118*, 5818.
- [17] The diameter was calculated considering the maximum distance between two F atoms plus twice the van der Waals radius of F (147 pm from A. Bondi, *J. Phys. Chem.* **1964**, *68*, 441-451).
- [18] F. Dielmann, R. Merkle, S. Heintl, M. Scheer, *Z. Naturforsch.* **2009**, *64*, 3.
- [19] A. Burkhardt, T. Pakendorf, B. Reime, *Eur. Phys. J. Plus* **2016**, *131*, 56-64.
- [20] [https://photon-science.desy.de/facilities/petra\\_iii/beamlines/p24\\_chemical\\_crystallography/eh2/index\\_eng.html](https://photon-science.desy.de/facilities/petra_iii/beamlines/p24_chemical_crystallography/eh2/index_eng.html)
- [21] POV-Ray. <https://www.povray.org>
- [22] CrysAlisPro, different versions (Rigaku OD) 2006-2022.
- [23] G.M. Sheldrick, *Acta Cryst. C* **2015**, *C71*, 3.



## 7. Conclusion

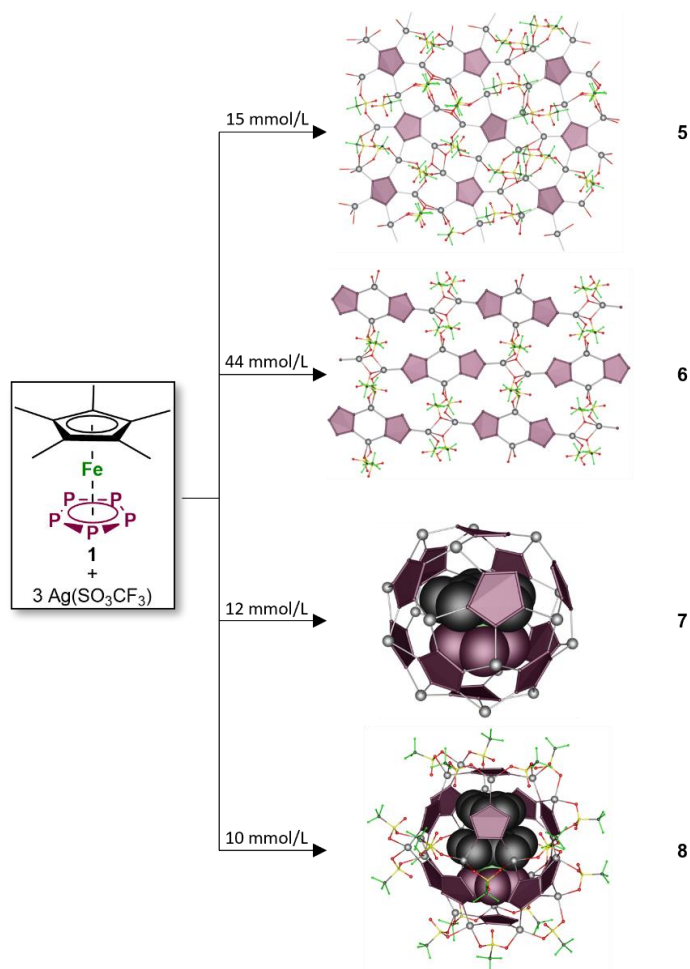
This work deals with multi-component reactions in supramolecular chemistry based on pentaphosphaferrocenes, Ag salts and different organic ligands. The introduction (chapter 1) gives an insight into the basic concepts of supramolecular chemistry as well as of self-assembly and finally focuses on the formation of discrete spherical aggregates and polymeric assembly based on polyphosphorus complexes in combination with coinage metal salts. The research objectives of this thesis are defined in chapter 2. The results regarding the research topics are listed in chapter 3-6.

The main topic of this thesis is the investigation of coordination behaviour of pentaphosphaferrocenes  $[\text{Cp}^{\text{R}}\text{Fe}\{\eta^5\text{-P}_5\}]$  towards Ag(I) salts. Thus, this is presented in chapter 3 devoted to pentaphosphaferrocenes with different sterical demands and AgOTf, an Ag(I) salt with a coordinating scaffold-constructing counterion. The change to the silver salt  $\text{AgSbF}_6$ , with a weakly coordinating anion (WCA), opened the possibility of introducing a third component into the self-assembly in the form of flexible aliphatic (Chapter 4) and rigid aromatic (Chapter 5) organic dinitrile ligands. The influence of one of the most sterically demanding Cp ligands ( $\text{Cp}^{\text{Bn}}$ ) on the coordination behaviour with terminal nitriles as well as dinitriles is described in chapter 6.

### **The influence of different sterically demanding $[\text{Cp}^{\text{R}}\text{Fe}\{\eta^5\text{-P}_5\}]$ ( $\text{Cp}^{\text{R}} = \text{Cp}^*$ , $\text{Cp}^{\text{x}}$ , $\text{Cp}''$ , $\text{Cp}^{\text{Bn}}$ ) on a two-component self-assembly with scaffold-constructing AgOTf.**

Due to excellent coordination behaviour of pentaphosphaferrocenes with copper halides and the resulting giant nano-sized hollow self-assembled aggregates with partial fullerene topology, they have proven to be an excellent building block in supramolecular chemistry. However, these pentaphosphaferrocenes-based supramolecules are not only limited to Cu halide (Cl, Br, I) derivatives and thus impressive aggregates could also be obtained with the use of CuOTf. The inserting bridging triflate ligands between the tetrahedrally coordinated copper cations in this instance expands the spherical framework and could thus reveal the true scaffold-constructing role of triflate. The scaffold-constructing behaviour of the triflate anion prompted a switch to other coinage metal salts, with AgOTf being the best choice for further investigation of coordination behaviour due to its higher coordination number than gold and the ability to adopt different coordination environments compared to copper. In order to acquire a full understanding of behaviour of AgOTf and pentaphosphaferrocene in self-assembly, numerous pentaphosphaferrocenes  $[\text{Cp}^{\text{R}}\text{Fe}\{\eta^5\text{-P}_5\}]$  ( $\text{Cp}^{\text{R}} = \text{Cp}^*$  (**1**),  $\text{Cp}^{\text{x}}$  (**2**),  $\text{Cp}''$  (**3**),  $\text{Cp}^{\text{Bn}}$  (**4**)) with varying steric demands were utilized in addition to the transfer of AgOTf.

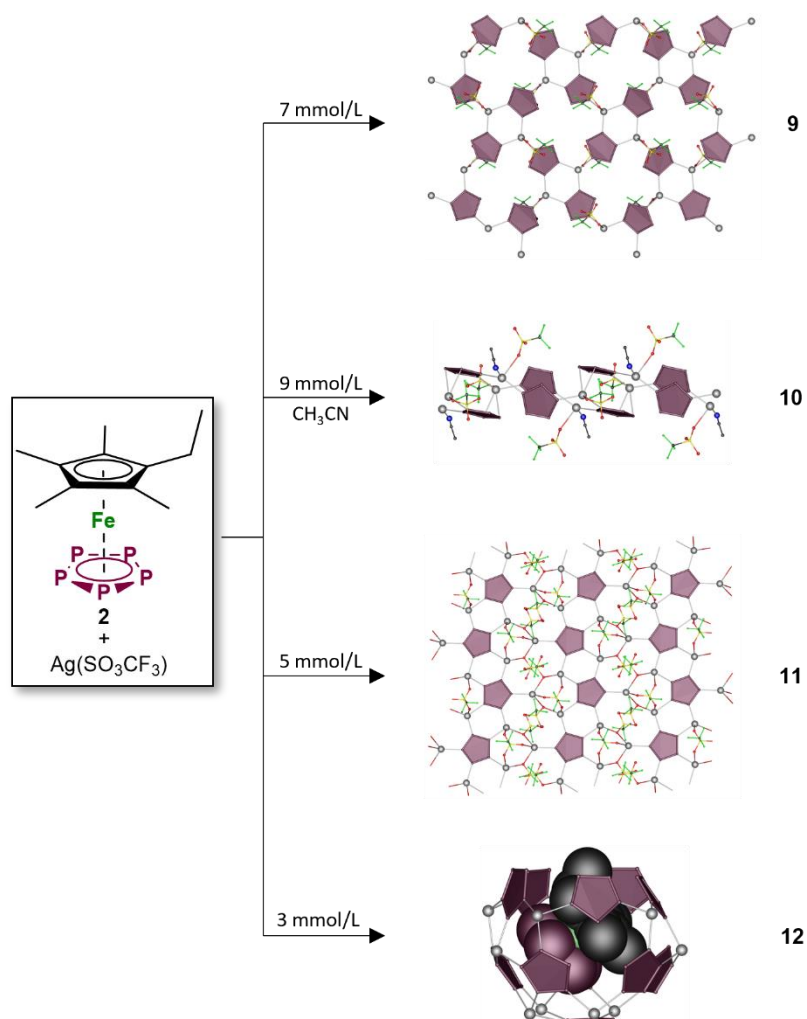
All the following coordination assemblies were obtained by using a AgOTf suspension in CH<sub>2</sub>Cl<sub>2</sub> which was subsequently layered with the respective pentaphosphaferrocene dissolved in toluene. These reactions were controlled by concentration of the reagents and their ratios, whereby reactions conditions were found, under which the respective products could be crystallised preferentially. With the highest AgOTf concentration and a ratio of 1:3 [Cp\*Fe(η<sup>5</sup>-P<sub>5</sub>):Ag(I)] the 2D polymer  $[\{\text{Cp}^*\text{Fe}\{\eta^5\text{-P}_5\}\{\text{Ag}(\text{SO}_3\text{CF}_3)\}_2]$  **6** (Scheme 7.1) could be obtained. By halving the concentration, the 2D polymer  $[\{\text{Cp}^*\text{Fe}\{\eta^5\text{-P}_5\}\{\text{Ag}(\text{SO}_3\text{CF}_3)\}_4(\text{CH}_2\text{Cl}_2)]$  **5** is formed. Here for the first time, pentacoordinated *cyclo*-P<sub>5</sub> ligands could be generated in a polymer, whereas this coordination configuration could previously only be observed in spherical pentaphosphaferrocene based spherical supramolecules. With further dilution to 12 mmol L<sup>-1</sup> AgOTf in CH<sub>2</sub>Cl<sub>2</sub> the spherical supramolecule  $[\{\text{Cp}^*\text{Fe}\{\eta^5\text{-P}_5\}\}@[\{\text{Cp}^*\text{Fe}\{\eta^5\text{-P}_5\}\}_{12}\{\text{Ag}(\text{SO}_3\text{CF}_3)\}_x]$  (x = ~10) **7** (preliminary structural characterization) were isolated. The scaffold obeys the isolated-pentagon-rule and shows a motif of an icosahedral Ag sphere, making it a carbon free I<sub>h</sub>-C<sub>80</sub> analogue (also called 80-vertex sphere). In addition, this sphere with its about 10 metal vacancies is among the most porous supramolecules in general and in the case of Ag, the most metal deficient host scaffold so far. Again, with further dilution the (90-10) vertex sphere  $[\{\text{Cp}^*\text{Fe}\{\eta^5\text{-P}_5\}\cdot\text{tol}\}@[\{\text{Cp}^*\text{Fe}\{\eta^5\text{-P}_5\}\}_{12}\{\text{Ag}(\text{SO}_3\text{CF}_3)\}_{20}]$  **8** is obtained. It is gratifying that it represents the first example of a spherical supramolecule based on pentaphosphaferrocenes and coinage metal salts that primarily exhibits ordering in the solid state. In addition, with the incorporation of **1** and a toluene molecule, it represents the first supramolecular assembly within a spherical supramolecular P<sub>n</sub> complex.



**Scheme 7.1.** Supramolecular aggregates based on AgOTf and **1**.

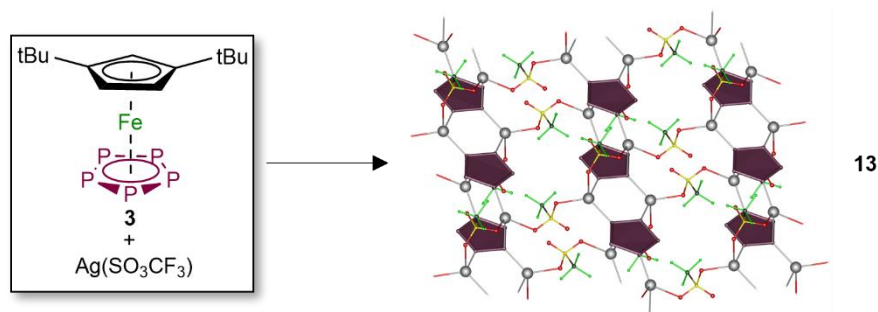
By minimally increasing the steric demand of the pentaphosphaferrocene by using **2** and AgOTf in an equimolar ratio, the highest used concentration of AgOTf in  $\text{CH}_2\text{Cl}_2$  of  $7 \text{ mmol L}^{-1}$  leads to the 2D polymer  $[\{\text{Cp}^x\text{Fe}\{\eta^5\text{-P}_5\}\}\{\text{Ag}(\text{SO}_3\text{CF}_3)\}]$  (**9**) (scheme 7.2). Using diluted reaction conditions ( $5 \text{ mmol L}^{-1}$ ), another 2D polymer  $[\{\text{Cp}^x\text{Fe}\{\eta^5\text{-P}_5\}\}\{\text{Ag}(\text{SO}_3\text{CF}_3)\}_3]$  (**11**) is obtained. In addition to **5**, **11** represents another coordination polymer with pentacoordinated *cyclo*- $\text{P}_5$  ligands towards AgOTf. By further dilution to  $3 \text{ mmol L}^{-1}$  one finally obtains in this self-assembly system novel bowl-like supramolecule  $[\{\text{Cp}^x\text{Fe}\{\eta^5\text{-P}_5\}\}]@[\{\text{Cp}^x\text{Fe}\{\eta^5\text{-P}_5\}\}_{12}\{\text{Ag}(\text{SO}_3\text{CF}_3)\}_{20}]$  (preliminary sum formula) **12** (scheme 7.2). Its skeleton is similar in structure to the 80-vertex sphere **8**, but with the crucial difference that the sticking out of the ethyl group of the  $\text{Cp}^x$  ligand of the guest molecule **2** prevents the coordination of the “lid” *cyclo*- $\text{P}_5$  ligand as in **8**. This is a first example of open architecture based on Ag(I) and *cyclo*- $\text{P}_5$  units. Further dilution or change of the ratio leads to mixtures of already obtained compounds in poorer yield and/or crystal quality. In order to investigate whether the coordination of small Lewis basic ligands is possible in addition to AgOTf or whether they compete for the same free coordination sites at the Ag atom as well as whether one of the two is preferentially coordinated, the reaction of **2** and AgOTf was carried out in toluene and  $\text{CH}_2\text{Cl}_2$  with

some amount of CH<sub>3</sub>CN. By this way the 1D polymer  $[\{\text{Cp}^x\text{Fe}\{\eta^5\text{-P}_5\}\}_2\{\text{Ag}(\text{SO}_3\text{CF}_3)\}_2\{\text{CH}_3\text{CN}\}]$  (**10**) was obtained. It shows in addition to terminally coordinated OTf<sup>-</sup> anions, there is also a CH<sub>3</sub>CN molecule on each Ag atom. These occupies a coordination site and limit the dimensionality of the structure.



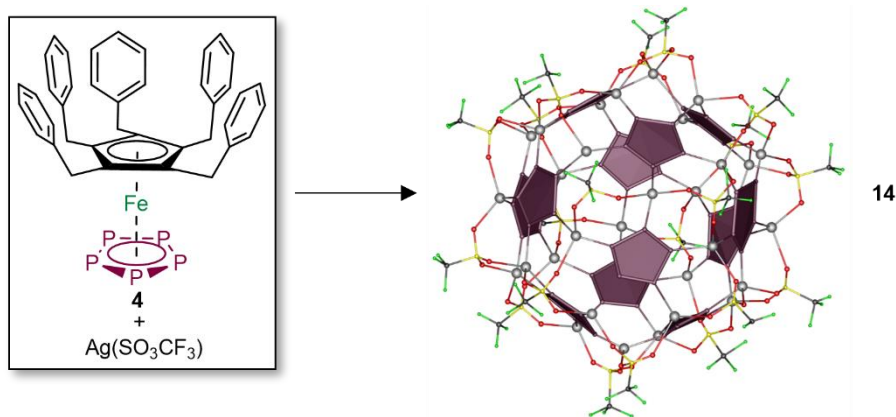
Scheme 7.2. Polymers and spherical aggregate obtained by self-assembly of **2** and AgOTf.

Interestingly, further increasing of the steric demand of the Cp ligand by 2 *t*Bu groups (**3**) leads to the only product 2D polymer  $[\{\text{Cp}^t\text{Fe}\{\eta^5\text{-P}_5\}\}\{\text{Ag}(\text{SO}_3\text{CF}_3)\}_2]$  (**13**) (Scheme 7.3) that can be obtained with AgOTf.



Scheme 7.3. Self-assembly of **3** and AgOTf leading to a 2D polymer.

The influence of the steric demand on the scaffold-constructing properties of the OTf-anion could be shown with an example of **4**, a very sterically demanding  $P_n$  ligand complex. In a reaction of **4** with a solution of AgOTf in  $\text{CH}_2\text{Cl}_2$  in a concentration of  $6.9 \text{ mmol L}^{-1}$  and a ratio of **4**:2Ag the (90-10) vertex sphere  $[\{\text{Cp}^{\text{Bn}}\text{Fe}\{\eta^5\text{-P}_5\}\}_{12}\{\text{Ag}(\text{CF}_3\text{SO}_3)\}_{20}]$  (**14**) was obtained. The sphere exhibits an idealized icosidodecahedral shape and has an average diameter of 2.7 nm.

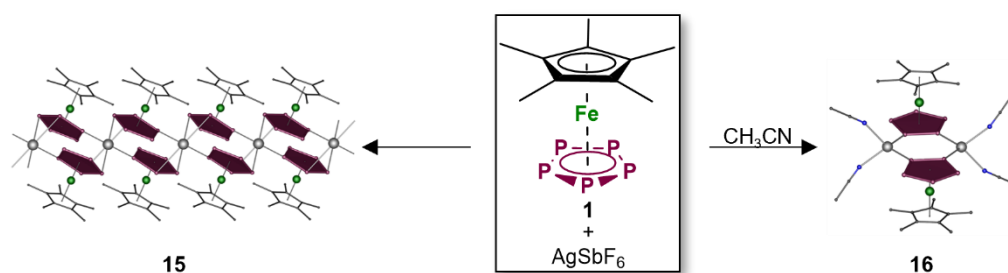


Scheme 7.4. Spherical aggregate consisting of **4** and AgOTf.

#### Multi-component self-assembly of $[\text{Cp}^{\text{R}}\text{Fe}\{\eta^5\text{-P}_5\}]$ ( $\text{Cp}^{\text{R}} = \text{Cp}^*, \text{Cp}^x, \text{Cp}^y, \text{Cp}^{\text{Bn}}$ ), $\text{AgSbF}_6$ and organic nitriles

Self-assembly of metal cations and Pentaphosphaferrocene has traditionally relied on coordination behaviour between Cu(I)/Ag(I) salts and coordinating counterions. These counterions obstruct potential coordination sites on the metal atom, limiting the system. Switching to the weakly coordinating/non-coordinating counterion  $\text{SbF}_6^-$ , Ag(I) salts give the best starting point for studying the coordination system without being limited by coordinating counterions. These coordination sites on the Ag atom can now be utilized for organic nitriles as a third component, allowing cross-linking across supramolecular aggregates.

The results of multicomponent self-assembly reactions can be fine-tuned by controlling the reaction conditions, that usually allows increasing the selectivity, crystal quality and yield of the products. The two-component reaction between  $[\{\text{Cp}^*\text{Fe}(\eta^5\text{-P}_5)\}]$  (**1**) and  $\text{AgSbF}_6$  leads to the 1D polymer  $[\{\text{Cp}^*\text{Fe}(\eta^{5:2:1}\text{-P}_5)\}_2\text{Ag}]_n[\text{SbF}_6]_n$  **15** (Scheme 7.5). In the presence of  $\text{CH}_3\text{CN}$ , however, free coordination sites on the silver are blocked faster than polymerisation can take place, resulting in the dimer  $[\{\text{Cp}^*\text{Fe}(\eta^{5:1:1}\text{-P}_5)\}\{\text{Ag}(\text{CH}_3\text{CN})_2\}]_2[\text{SbF}_6]_2$  **16** (Scheme 7.5).

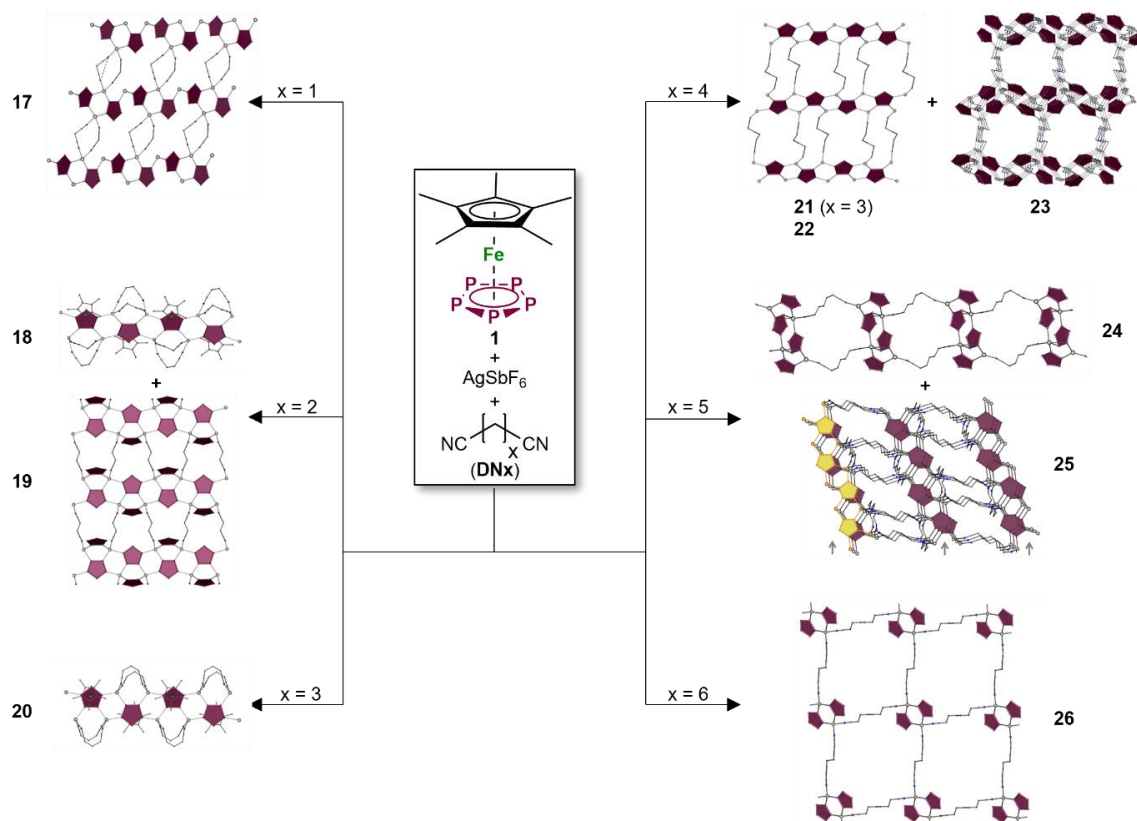


Scheme 7.5. Polymeric and dimeric assemblies obtained from self-assembly of  $[(\text{Cp}^*\text{Fe}(\eta^5\text{-P}_5))] (1)$  and  $\text{AgSbF}_6$ .

Interestingly, the observed coordination behaviour changes as in **16** when flexible dinitrile linker  $\text{NC}(\text{CH}_2)_x\text{CN}$  (**DN $x$** ) is introduced as a third component to **1** and  $\text{AgSbF}_6$ . If these are added in excess to the three-component one-pot reaction, the 2D polymer  $[(\text{Cp}^*\text{Fe}(\eta^5\text{-P}_5))_2\text{Ag}_3(\text{NC}(\text{CH}_2)\text{CN})_2(\text{C}_7\text{H}_8)]_n(\text{SbF}_6)_{3n}$  **17** can be obtained with **DN1** (Scheme 7.6). The coordination polymer is built up by 1D strands, which are in turn composed of *cyclo*- $\text{P}_5$  ligands of **1** and six-membered rings of  $\{\text{P}_4\text{Ag}_2\}$ . The dinitrile linkers link the 1D strands to form a periodic structure. This structural type of motif is also found in the compounds **19** with the formula  $[(\text{Cp}^*\text{Fe}(\eta^5\text{-P}_5))_2\text{Ag}_2\{(\text{NC}(\text{CH}_2)_2\text{CN})\}]_n[\text{SbF}_6]_{2n}$  (**DN2**),  $[(\text{Cp}^*\text{Fe}(\eta^5\text{-P}_5))\{\text{Ag}_2(\text{NC}(\text{CH}_2)_3\text{CN})\}]_n[\text{SbF}_6]_{2n}$  (**21**) (**DN3**),  $[(\text{Cp}^*\text{Fe}(\eta^5\text{-P}_5))_4\{\text{Ag}_4(\text{NC}(\text{CH}_2)_4\text{CN})_2\}]_n[\text{SbF}_6]_{4n}$  (**22**) (**DN4**),  $[(\text{Cp}^*\text{Fe}(\eta^5\text{-P}_5))_2\{\text{Ag}_2(\text{NC}(\text{CH}_2)_{10}\text{CN})\}]_n[\text{SbF}_6]_{2n}$  (**33**) (**DN10**) (Scheme 7.7) and in the 3D polymer **25** with the formula  $[(\text{Cp}^*\text{Fe}(\eta^5\text{-P}_5))\{\text{Ag}(\text{NC}(\text{CH}_2)_5\text{CN})\}]_n[\text{SbF}_6]_n$  (**DN5**) (Scheme 7.6). A 3D coordination polymer  $[(\text{Cp}^*\text{Fe}(\eta^5\text{-P}_5))\{\text{Ag}_2(\text{NC}(\text{CH}_2)_7\text{CN})\}]_n[\text{SbF}_6]_{2n}$  **29** (**DN7**) is similar to **22** and **25**, but forms alternating stacks. Interestingly, in the case of the simple polymers mentioned, only the dinitrile **DN $x$**  used changes and thus also the distance between the strands. Unexpectedly, however, the same motif of the structure is found for **DN2** (**19**) and **DN10** (**33**) despite the large difference in length of the dinitriles.

However, the dinitriles utilized do not have to coordinate to other 1D strands, and therefore coordination architectures are formed from these 1D strands, where the dinitriles coordinate to the next Ag atom and thereby saturate coordination sites. This type of side-on the strand coordinated dinitriles is found in compounds  $[(\text{Cp}^*\text{Fe}(\eta^5\text{-P}_5))\{\text{Ag}(\text{NC}(\text{CH}_2)_2\text{CN})\}]_n[\text{SbF}_6]_{2n}$  (**18**) (**DN2**) and  $[(\text{Cp}^*\text{Fe}(\eta^5\text{-P}_5))\{\text{Ag}(\text{NC}(\text{CH}_2)_3\text{CN})\}]_n[\text{SbF}_6]_{2n}$  (**20**) (**DN3**). The crystal structure of the compound **23**, however, is built up by tetrameric repeating units of *cyclo*- $\text{P}_5$  of **1** and Ag cations. As with the 1D strands, these puckered chains are linked by **DN4** and thus build up the 3D polymer  $[(\text{Cp}^*\text{Fe}(\eta^5\text{-P}_5))_2\{\text{Ag}_3(\text{NC}(\text{CH}_2)_4\text{CN})_2\}]_n[\text{SbF}_6]_{3n}$  **23** (**DN4**) (Scheme 7.6). In addition to the coordination patterns already mentioned, the discrete nodes consisting of **1** and Ag(I) can also form, to give a 1D polymer with linked tetrameric nodes forming in case of compound **24** with the formula  $[(\text{Cp}^*\text{Fe}(\eta^5\text{-P}_5))_4\{\text{Ag}_4(\text{NC}(\text{CH}_2)_5\text{CN})_2\}]_n[\text{SbF}_6]_{4n}$  (**DN5**) and 2D coordination polymers of linked dimeric nodes

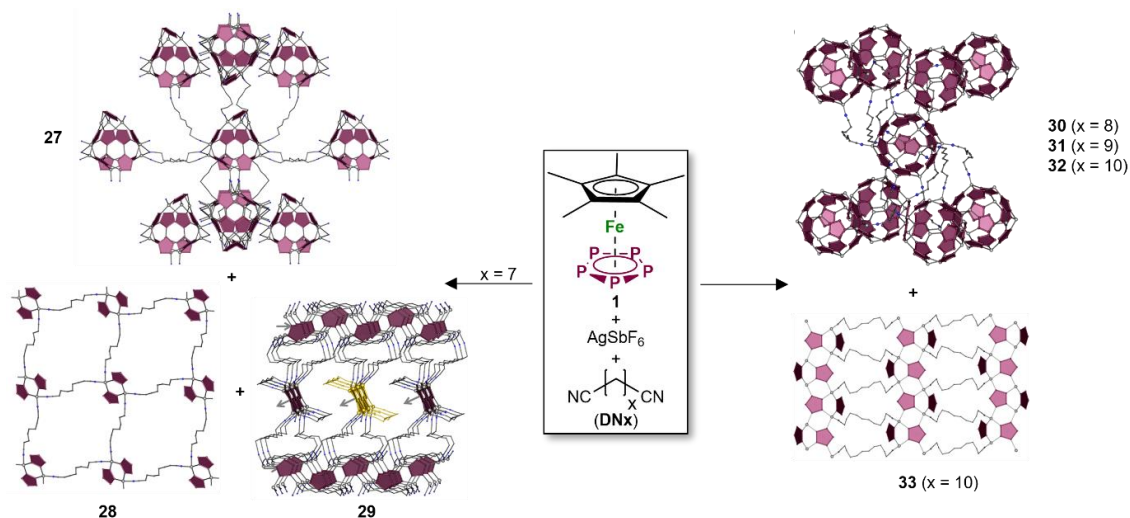
formed in compounds **26** and **28** with the formula  $[[\text{Cp}^*\text{Fe}(\eta^5\text{-P}_5)]\{\text{Ag}(\text{NC}(\text{CH}_2)_6\text{CN})\}]_n[\text{SbF}_6]_n$  (**DN6**) and  $[[\text{Cp}^*\text{Fe}(\eta^5\text{-P}_5)]\{\text{Ag}(\text{NC}(\text{CH}_2)_7\text{CN})\}]_n[\text{SbF}_6]_n$  (**DN7**), respectively.



**Scheme 7.6.** Coordination polymers obtained from **1**,  $\text{AgSbF}_6$  and  $\text{DN}_x$  ( $x = 1\text{-}6$ ).

Interestingly, the previously continuous three-component self-assembly of **1**,  $\text{AgSbF}_6$  and  $\text{DN}_x$  ( $x = 1\text{-}6, 10$ ) changes direction at  $x \geq 7$ . Compound **27** is the first representative of a novel class of 3D supramolecular coordination polymers based on polyphosphorus ligands, being the first example of a supersphere based on **1** and Ag (Scheme 7.7). The 3D polymeric structure  $[[\text{SbF}_6]@\{[\text{Cp}^*\text{Fe}(\eta^5\text{-P}_5)]_9\{\text{Ag}_{11}(\text{NC}(\text{CH}_2)_7\text{CN})_6\}\}]_n[\text{SbF}_6]_{10n}$  (**27**, **DN7**) consists of unprecedented 56-vertex polycationic assemblies that act as nodes with an outer diameter of 2.21 nm, which, to date, makes it the smallest spherical assembly based on five-fold symmetric building block **1**. In addition, each node acts as a molecular container for an  $\text{SbF}_6^-$  counterion. In comparison to **27**, with the longer chain lengths  $\text{DN}_x$  ( $x = 8\text{-}10$ ), 3D supramolecular coordination polymers  $[[\text{Cp}^*\text{Fe}(\eta^5\text{-P}_5)]@\{[\text{Cp}^*\text{Fe}(\eta^{5:1:1:1}\text{-P}_5)]_{12}\{\text{Ag}_{12}(\text{NC}(\text{CH}_2)_8\text{CN})_6\}\}]_n[\text{SbF}_6]_{12n}$  (**30**, **DN8**),  $[[\text{Cp}^*\text{Fe}(\eta^5\text{-P}_5)]@\{[\text{Cp}^*\text{Fe}(\eta^{5:1:1:1}\text{-P}_5)]_{12}\{\text{Ag}_{12}(\text{NC}(\text{CH}_2)_9\text{CN})_6\}\}]_n[\text{SbF}_6]_{12n}$  (**31**, **DN9**) and  $[[\text{Cp}^*\text{Fe}(\eta^5\text{-P}_5)]@\{[\text{Cp}^*\text{Fe}(\eta^{5:1:1:1}\text{-P}_5)]_{12}\{\text{Ag}_{12}(\text{NC}(\text{CH}_2)_{10}\text{CN})_6\}\}]_n[\text{SbF}_6]_{12n}$  (**32**, **DN10**) are also obtained from unique spherical polycationic nodes linked by the respective dinitriles, but the nodes show a completely different structure. These 72-vertex spheres have an outer diameter of 2.40-2.44 nm and serve as a container for molecule **1**. Furthermore, it was possible to visualise giant spherical

subunits using TEM techniques for the first time. In addition, all compounds were characterised by NMR spectroscopy, elemental analysis, X-ray spectroscopy and mass spectrometry.



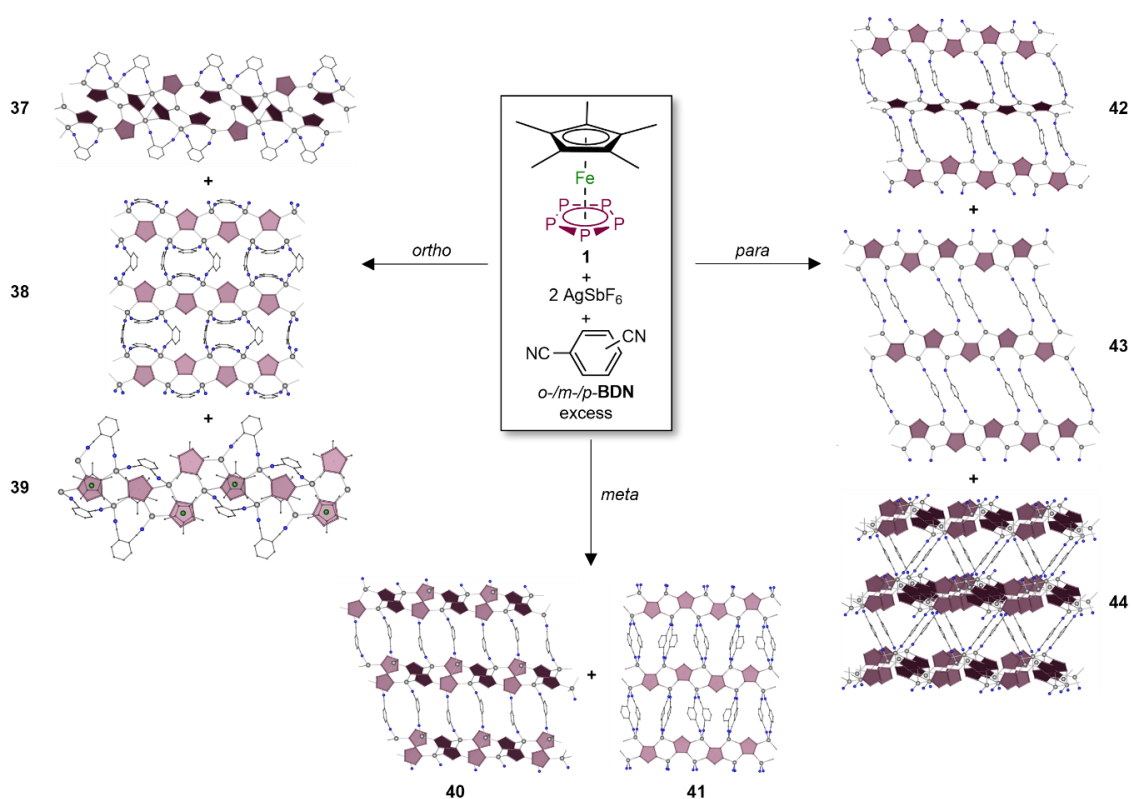
Scheme 7.7. Coordination polymers obtained in the self-assembly of **1**,  $\text{AgSbF}_6$  and  $\text{DN}_x$  ( $x = 7-10$ ).

Since with increasing the length of the aliphatic dinitrile and therefore giving the three-component self-assembly with **1**,  $\text{AgSbF}_6$  and  $\text{DN}_x$  more and more adjusting capabilities, the next step was to investigate how this system reacts when it is more restricted. It is possible to utilize more sterically demanding polyphosphorus complexes, which should influence the coordination capabilities of a metal cation because of the rising steric hinderance. The solubility of polyphosphorus complex will also alter, which will have an impact on the reaction conditions. In addition, more rigid aromatic linkers with fixed bite angles and a known arrangement of the donor groups can be used to make the self-assembly pathway/direction? more controllable. Here, the choice fell on  $[\text{Cp}^*\text{Fe}(\eta^5\text{-P}_5)]$  (**3**) in addition to **1** and *o*-/*m*-/*p*-( $\text{NC}$ ) $_2$ ( $\text{C}_6\text{H}_4$ ) (*o*-/*m*-/*p*-BDN) as a dinitrile.

However, to enable a direct comparison with flexible aliphatic dinitriles, the three-component self-assembly was performed with **1**,  $\text{AgSbF}_6$  and *o*-/*m*-/*p*-BDN. Besides all products with **1** or **3**,  $\text{AgSbF}_6$  and *o*-/*m*-/*p*-BDN, coordination polymers of  $\text{AgSbF}_6$  and *o*-/*m*-/*p*-BDN (**34**: *o*-BDN, **35**: *m*-BDN, **36**: *p*-BDN) were discovered as colourless crystals, which were analysed by elemental analysis, NMR spectrometry and mass spectrometry. The three-component self-assembly of **1**,  $\text{AgSbF}_6$  and *o*-BDN leads to the two 1D coordination polymers  $\{[\text{Cp}^*\text{Fe}(\eta^5\text{-P}_5)]_2\text{Ag}_3(\text{NC})_2\text{C}_6\text{H}_4\}_n[\text{SbF}_6]_{3n}$  (**37**) and  $\{[\text{Cp}^*\text{Fe}(\eta^5\text{-P}_5)]_3\text{Ag}_4(\text{NC})_2\text{C}_6\text{H}_4\}_n[\text{SbF}_6]_{4n}$  (**39**) as well as to a 2D polymer  $\{[\text{Cp}^*\text{Fe}(\eta^5\text{-P}_5)]_2\text{Ag}_4(\text{NC})_2\text{C}_6\text{H}_4\}_n(\text{C}_7\text{H}_8)_{1.3}(\text{CH}_2\text{Cl}_2)_{0.65}[\text{SbF}_6]_{4n}$  (**38**). The 1D polymers are built up from repeating rings formed by Ag atoms and *cyclo*- $\text{P}_5$  rings and differ in the coordination motif of the Ag atom and stoichiometry. The *o*-BDN molecules are coordinated on the chain and occupy coordination sites at the Ag atom. The 2D coordination polymer consists of 1D strands, but the linkers here join these 1D strands to form a 2D polymer. Similar coordination motifs are also



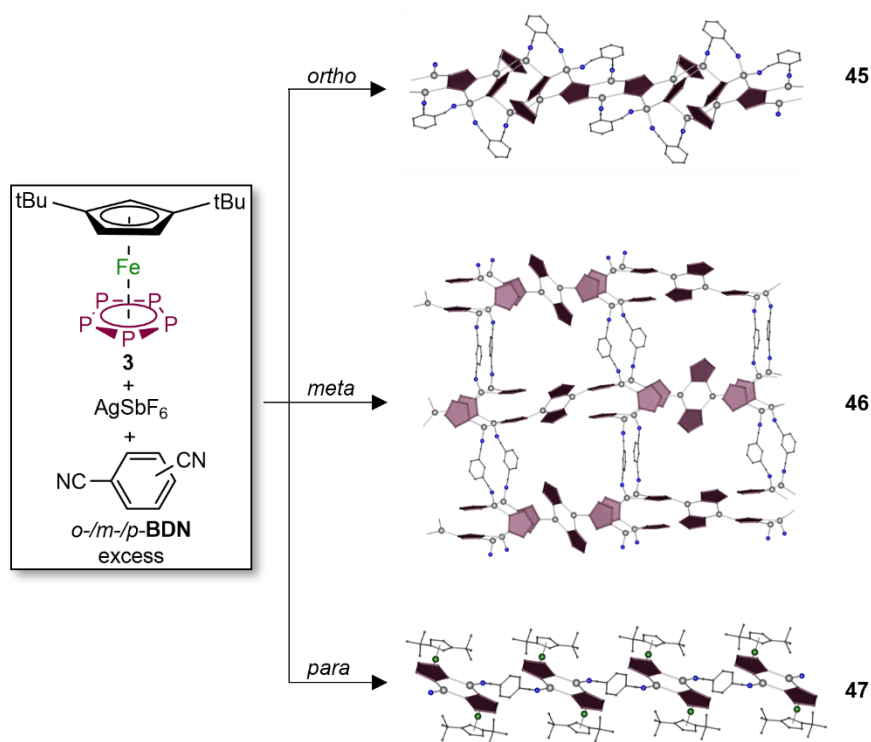
found in the 2D polymers  $[\{\text{Cp}^*\text{Fe}(\eta^5\text{-P}_5)\}\text{Ag}_2(m\text{-}(\text{NC})_2\text{C}_6\text{H}_4)(\text{C}_7\text{H}_8)_{0.5}(\text{CH}_2\text{Cl}_2)_{0.85}]_n[\text{SbF}_6]_{2n}$  (**41**, *m*-BDN),  $[\{\text{Cp}^*\text{Fe}(\eta^5\text{-P}_5)\}\text{Ag}_2(p\text{-}(\text{NC})_2\text{C}_6\text{H}_4)]_n[\text{SbF}_6]_{2n}$  (**42**, *p*-BDN) and  $[\{\text{Cp}^*\text{Fe}(\eta^5\text{-P}_5)\}\text{Ag}_2(p\text{-}(\text{NC})_2\text{C}_6\text{H}_4)(\text{C}_7\text{H}_8)_{0.7}(\text{CH}_2\text{Cl}_2)_{0.3}]_n[\text{SbF}_6]_{2n}$  (**43**, *p*-BDN) where the respective linker and thus also the distance between the 1D strands changes. The 2D polymer  $[\{\text{Cp}^*\text{Fe}(\eta^5\text{-P}_5)\}_2\text{Ag}_2(m\text{-}(\text{NC})_2\text{C}_6\text{H}_4)(\text{C}_7\text{H}_8)_{0.5}(\text{CH}_2\text{Cl}_2)_{0.5}]_n[\text{SbF}_6]_{2n}$  (**40**, *m*-BDN) also consists of 1D strands. However, unlike **41**, **42** and **43**, these are not almost planar but have a tubular structure with a narrow diameter of 3.41 Å which prevents the encapsulation of solvent molecules or counter ions. Tubular 1D rods are also found in the 3D polymer  $[\{\text{Cp}^*\text{Fe}(\eta^5\text{-P}_5)\}_2\text{Ag}_2(p\text{-}(\text{NC})_2\text{C}_6\text{H}_4)]_n[\text{SbF}_6]_{2n}$  (**44**). Here, the *p*-BDN linkers link the tubular strands to form a 3D coordination polymer, which is the only 3D structure among CPs for **1**, AgSbF<sub>6</sub> and *o*-/*m*-/*p*-BDN.



Scheme 7.8. Cationic coordination polymers obtained in three-component self-assembly reaction with **1**, AgSbF<sub>6</sub> and *o*-/*m*-/*p*-BDN.

The numerous polymers obtained from **1**, AgSbF<sub>6</sub> and *o*-/*m*-/*p*-BDN show that the freedom of three-component self-assembly is limited by the rigid linkers, but there is still enough flexibility to form architectures up to 3D. With a more sterically demanding Cp'' (**3**) and thus a further restriction for the three-component system by steric factors, the 1D polymer  $[\{\text{Cp}''\text{Fe}(\eta^5\text{-P}_5)\}_3\text{Ag}_4(o\text{-}(\text{NC})_2\text{C}_6\text{H}_4)_2]_n[\text{SbF}_6]_{4n}$  (**45**) is obtained with **3**, AgSbF<sub>6</sub> and *o*-BDN (Scheme 7.9). Here, the *o*-BDN molecules coordinated on the side to the 1D strand, similar to compound **37** and **39**. The 2D polymer  $[\{\text{Cp}''\text{Fe}(\eta^5\text{-P}_5)\}_3\text{Ag}_3(m\text{-}(\text{NC})_2\text{C}_6\text{H}_4)]_n[\text{SbF}_6]_{3n}(\text{CH}_2\text{Cl}_2)_{2.5n}(\text{C}_7\text{H}_8)_{1.475n}$  (**46**) consists of parallel 1D strands which are linked via *m*-BDN to form a 2D coordination polymer. For the first time for

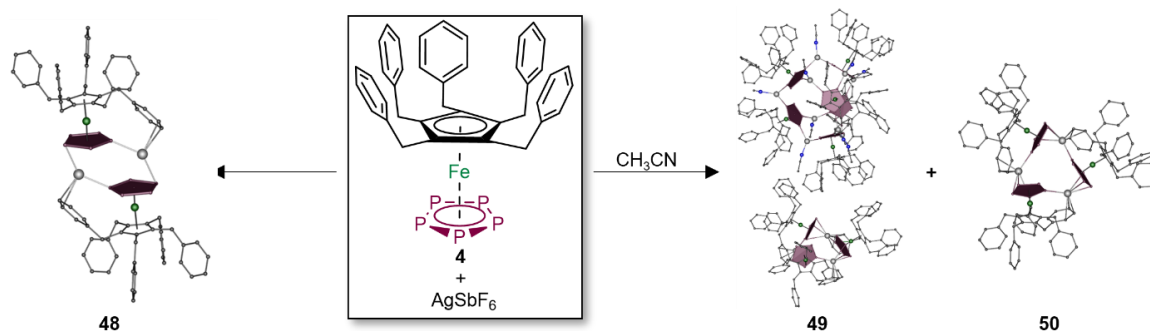
polyphosphorus based supramolecules, 1D strands consist of pincer-likers 12 membered rings  $\{P_8Ag_4\}$  in addition to the classical motif of six-membered  $\{P_4Ag_2\}$  rings and *cyclo*- $P_5$  rings to accommodate bulky  $Cp^Bn$  ligands in a 2D framework. The 2D polymer **46** possesses in the case of **3**,  $AgSbF_6$  and *o*-/*m*-/*p*-BDN the highest possible dimensionality. With *p*-BDN the 1D coordination polymer  $[\{Cp^BnFe(\eta^5-P_5)\}_2Ag_2(p-(NC)_2C_6H_4)]_n(SbF_6)_{2n}$  (**47**) is obtained. Compared to all other polymers with rigid aromatic *o*-/*m*-/*p*-BDN, it consists of dimeric nodes which are connected *via p*-BDN molecules.



Scheme 7.9. Coordination polymers in self-assembly of **3**,  $AgSbF_6$  and *o*-/*m*-/*p*-BDN.

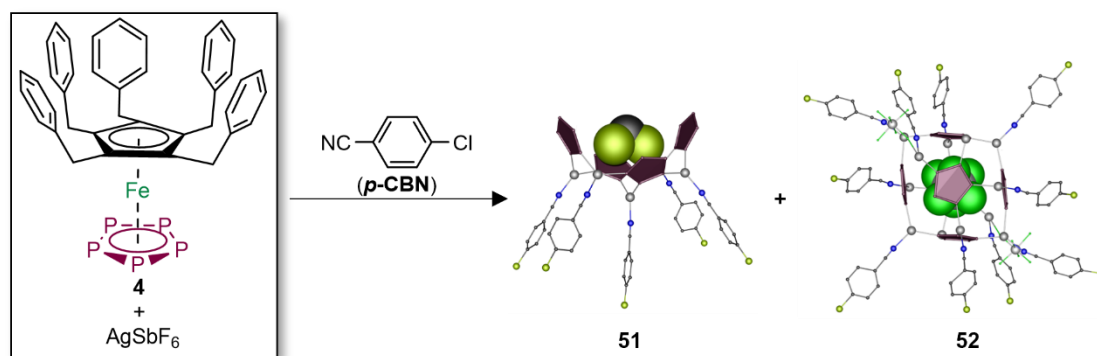
By increasing influence of the steric factor from building blocks **1** to **4** in the three-component self-assembly, considerable differences in the resulting products were observed. This changes the solubility of the products drastically and therefore makes the crystallization more difficult. In order to investigate the accessibility of pentaphosphaferrocenes in spite of a huge steric demand ( $Cp^{Bn}$ ), a reaction of **4** and  $AgSbF_6$  was first carried out and the dimer  $[\{Cp^{Bn}Fe(\eta^5-P_5)\}Ag]_2[SbF_6]_2$  (**48**) was obtained (Scheme 7.10). Interestingly, although this shows the possibility of silver-phosphorus coordination, a benzyl residue at the Cp ligand blocks coordination sites at the Ag atom, preventing polymerization. To test this behaviour of the  $Cp^{Bn}$  ligand, a reaction with acetonitrile was carried out. Due to its nitrile group, acetonitrile is able to compete against the benzyl residue over the coordination environment of the Ag atom. With the smallest possible nitrile, a spherical supramolecular aggregate  $[SbF_6]@[\{Cp^{Bn}Fe(\eta^5-P_5)\}_6\{Ag(CH_3CN)\}_{14}][\{Cp^{Bn}Fe(\eta^5-P_5)\}_3Ag_3][SbF_6]_{16}$  (**49**) and a trimer  $[\{Cp^{Bn}Fe(\eta^5-P_5)\}Ag_3][SbF_6]_3$  (**50**) were obtained co-crystallizing in the solid state

(Scheme 7.10). The sphere acts as a host for an  $\text{SbF}_6^-$  anion. Surprisingly, the trimer has no coordinated acetonitrile molecules. In the case of the supramolecular sphere, however, available coordination sites are occupied by acetonitrile ligands, so that polymerisation is not possible here either.



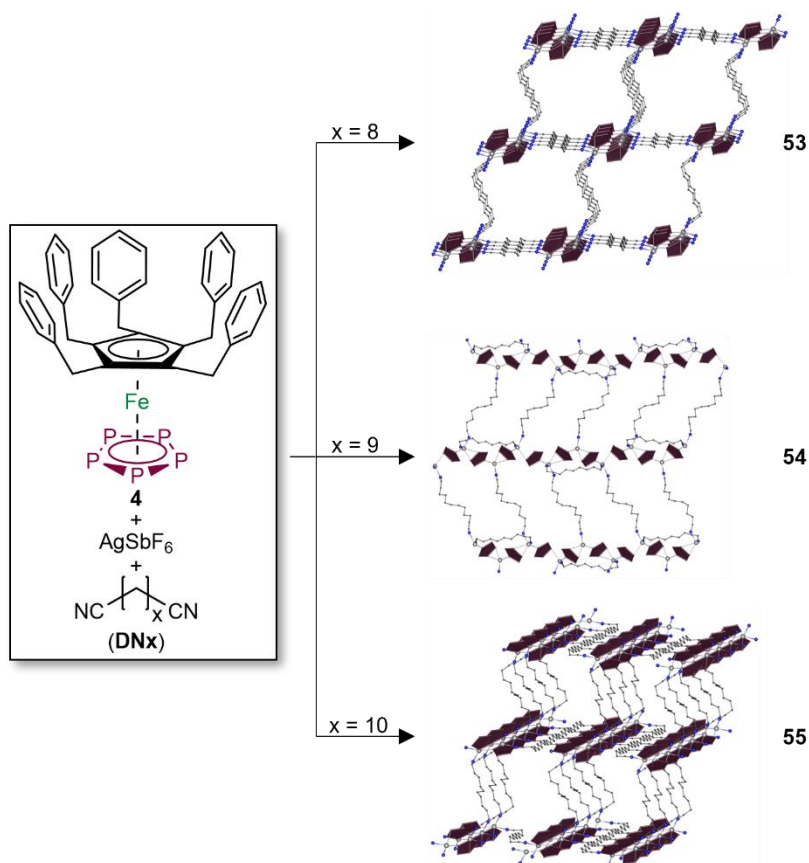
Scheme 7.10. Molecular aggregates obtained by self-assembly of **4** with  $\text{AgSbF}_6$ .

Since it was observed that spherical supramolecules with **4** are formed in presence of acetonitrile, the next idea was to introduce high functionality compared to the smallest possible nitriles. For this purpose, we have chosen *p*- $\text{NC}(\text{C}_6\text{H}_4)\text{Cl}$  (***p*-CBN**) because it has a rigid similar to acetonitrile linear structure and in addition features a chlorine atom in *para*-position as a possible leaving group to enable post-modifications. Due to the length of ***p*-CBN** (7.02–7.08 Å;  $\text{N}\cdots\text{Cl}$ ), the chlorine group is available for reactions like substitution since it is not screened by the  $\text{Cp}^{\text{Bn}}$  ligands of **4** (6.98 Å). A reaction with ***p*-CBN**, **4** and  $\text{AgSbF}_6$  leads to the tetrameric complex  $[\{\text{Cp}^{\text{Bn}}\text{Fe}(\eta^5\text{-P}_5)\}_4\{\text{Ag}(\textit{p}\text{-NC}(\text{C}_6\text{H}_4)\text{Cl})_5\}[\text{SbF}_6]_5$  (**51**) and the spherical supramolecule  $[\text{SbF}_6]@\{[\{\text{Cp}^{\text{Bn}}\text{Fe}(\eta^5\text{-P}_5)\}_6\{\text{Ag}(\textit{p}\text{-NC}(\text{C}_6\text{H}_4)\text{Cl})_{9.5}\}[\text{SbF}_6]_{8.5}$  (**52**) (Scheme 7.11). By fine-tuning the solvent mixtures, concentration and stirring time, the two components can be crystallized separately. Interestingly, the structural motif of **51** are found in the inorganic scaffold of **52** as a half shell of the sphere. Therefore, the pentanuclear complex **51** can be considered as a potential intermediate towards the spherical supramolecular assembly of **52**. The inner void of the sphere **52** has a diameter of 8.74 Å, and acts as host for an encapsulated  $\text{SbF}_6^-$  anion (6.96 Å). The outer diameter of the spherical supramolecular assembly reaches 3.5 nm. All Ag atoms coordinate a ***p*-CBN** ligand.



Scheme 7.11. Molecular assemblies obtained from self-assembly of **4**,  $\text{AgSbF}_6$  and ***p*-CBN**.

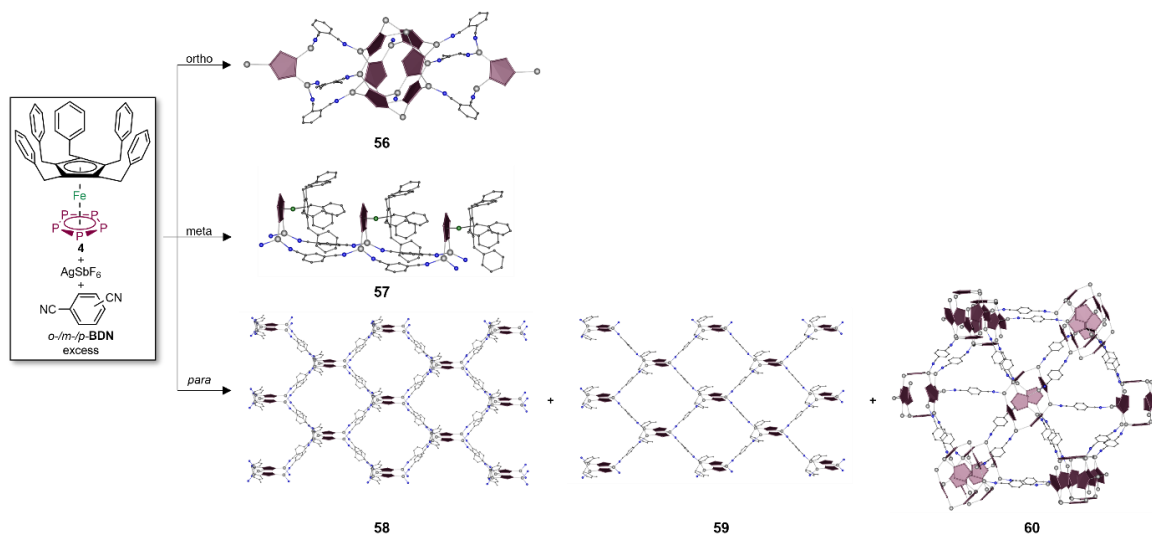
Since it has now been shown that larger nitriles can also be used in the three-component self-assembly system, the next logical step is to use organic ligands with two nitrile groups to investigate whether polymers and also spherical supramolecules can be linked by dinitriles. As it had already been demonstrated with flexible aliphatic dinitriles that both simple coordination polymers and polymers based on linked supramolecular spheres could be obtained, the choice fell on **DNx**. As the shorter dinitriles are shielded by the steric bulk of the Cp<sup>Bn</sup> ligand of **4**, we selected only the longest dinitriles **DNx** (x = 8 - 10) whose length is more than 13 Å in a linear confirmation and compared with the length of the *p*-**CBN** ligand (7.02-7.08 Å). In a reaction with **4**, AgSbF<sub>6</sub> and **DN8**, the 3D coordination polymer  $[\{\text{Cp}^{\text{Bn}}\text{Fe}(\eta^5\text{-P}_5)\}\{\text{Ag}(\text{NC}(\text{CH}_2)_8\text{CN})\}]_n[\text{SbF}_6]_n$  (**53**) was obtained (Scheme 7.12). When, however, **DN9** is used in a reaction, the 2D polymer  $[\{\text{Cp}^{\text{Bn}}\text{Fe}(\eta^5\text{-P}_5)\}\{\text{Ag}_3(\text{NC}(\text{CH}_2)_9\text{CN})_2\}]_n[\text{SbF}_6]_{3n}$  (**54**) is obtained. The reaction with **DN10** leads to the 3D polymer  $[\{\text{Cp}^{\text{Bn}}\text{Fe}(\eta^5\text{-P}_5)\}\{\text{Ag}_2(\text{NC}(\text{CH}_2)_{10}\text{CN})_3\}]_n[\text{SbF}_6]_{4n}$  (**55**) (Scheme 7.12). All these polymeric architectures are based on similarly constructed 1D strands, which are in turn linked to each other *via* the respective dinitriles. While in the 3D polymer **53**, **DN8** connects the next possible Ag atom of a neighbouring 1D strand, **55** has two different types of dinitriles. One links like **DN8** in **53** while the other coordinate to the next but one Ag atom, so that in **55** the distances between the 1D strands is in one direction smaller compared to **53**, although longer dinitriles were used. In the 2D polymer **54** with **DN9**, one type of dinitrile coordinates on the side of the 1D strand, occupying coordination sites and therefore limiting the dimensionality.



Scheme 7.12. Coordination polymers built up by **4**,  $\text{AgSbF}_6$  and  $\text{DN}_x$  ( $x = 8-10$ ).

In order to be able to better control the reactions, the next logical step was to use rigid ligands as linkers with a known length and rigid angles. The three-component system with *o*-/*m*-/*p*-BDN could already be controlled with Cp ligands with low steric demand and an extension to a Cp ligand with huge steric demand, **4** gives insight to the role of Cp ligands in the self-assembly. A reaction with *o*-BDN,  $\text{AgSbF}_6$  and **4** leads to the molecular assembly  $[\{\text{Cp}^{\text{Bn}}\text{Fe}(\eta^5\text{-P}_5)\}_8\{\text{Ag}(\text{o}-(\text{NC})_2(\text{C}_6\text{H}_4))\}_{(12\pm x)}]_n[\text{SbF}_6]_{(12\pm x)n}$  (preliminary structural characterization) (**56**). It consists of a spherical core of six molecules of **4** and about twelve Ag atoms that coordinates three *o*-BDN ligands on two sides to form an arrangement of **4** and Ag. Due to the small distance/angle between the nitrile groups, it is the shortest BDN with  $\sim 3.75 \text{ \AA}$  ( $\text{N}\cdots\text{N}$ ) used and thus has the most limited coordination possibilities compared to *m*-/*p*-BDN. With *m*-BDN ( $6.82 \text{ \AA}$ ), the ladder-like 1D polymer  $[\{\text{Cp}^{\text{Bn}}\text{Fe}(\eta^5\text{-P}_5)\}_2\text{Ag}\{m-(\text{NC})_2(\text{C}_6\text{H}_4)\}_2]_n[\text{SbF}_6]_{2n}$  (**57**) is obtained (Scheme 7.13.). With *p*-BDN ( $7.77-7.89 \text{ \AA}$ ), however, the two 2D polymers  $[\{\text{Cp}^{\text{Bn}}\text{Fe}(\eta^5\text{-P}_5)\}_2\text{Ag}_5\{p-(\text{NC})_2(\text{C}_6\text{H}_4)\}_4(\text{C}_7\text{H}_8)_{4.45}]_n[\text{SbF}_6]_{5n}$  (**58**) and  $[\{\text{Cp}^{\text{Bn}}\text{Fe}(\eta^5\text{-P}_5)\}_4\text{Ag}_6\{p-(\text{NC})_2(\text{C}_6\text{H}_4)\}_4(\text{C}_7\text{H}_8)_4]_n[\text{SbF}_6]_{6n}$  (**59**) as well as the 3D polymer  $[\{\text{Cp}^{\text{Bn}}\text{Fe}(\eta^5\text{-P}_5)\}_6\text{Ag}_{10}\{p-(\text{NC})_2(\text{C}_6\text{H}_4)\}_5]_n[\text{SbF}_6]_{10n}$  (**60**) consisting from linked spherical nodes can be obtained (Scheme 7.13). The 2D polymers are based on dimeric nodes of *cyclo*-P<sub>5</sub> ligands and three (**59**) or five (**58**) silver atoms. The nodes are similar, so that the structure with three Ag atoms can thus be found in the one with five. The used *p*-BDN linkers link nodes to build up honeycomb 2D

coordination polymers. Interestingly, toluene molecules in both 2D polymers occupy the remaining coordination sites at the Ag atom, blocking further polymerisation and thus higher dimensionality. The 3D polymer **60** consists of spherical nodes linked by *p*-BDN. The nodes have an inner diameter of 0.86 nm and an outer diameter of 2.26 nm and serve as a host for a  $\text{SbF}_6^-$  anion. Since a *p*-BDN ligand is coordinated to each Ag atom of a node, a node is linked to ten neighbouring nodes.



Scheme 7.13. Coordination polymers obtained from self-assembly of **4**,  $\text{AgSbF}_6$  and *o*-/*m*-/*p*-BDN.

## 8. Appendices

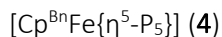
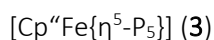
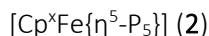
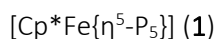
### 8.1 Alphabetic List of Abbreviations

$\sphericalangle$	angle
$\varnothing$	diameter
Å	Angström, $1 \text{ \AA} = 1 \cdot 10^{-10} \text{ m}$
°C	degree Celsius
1D	one-dimensional
2D	two-dimensional
3D	three-dimensional
bcc	body centered cubic
Bn	benzyl
br (NMR)	broad
<i>n</i> Bu	<i>n</i> -butyl
<i>t</i> Bu	<i>tert</i> -butyl
Cp	cyclopentadienyl, $\text{C}_5\text{H}_5$
Cp''	1,3-di- <i>tert</i> -butylcyclopentadienyl, $\text{C}_5\text{H}_3\text{tBu}_2$
Cp*	pentamethylcyclopentadienyl, $\text{C}_5(\text{CH}_3)_5$
Cp <sup>x</sup>	ethyltetramethylcyclopentadienyl, $\text{C}_5(\text{CH}_3)_4(\text{CH}_2\text{CH}_3)$
Cp <sup>BIG</sup>	pentakis-4- <i>n</i> butylphenylcyclopentadienyl, $\text{C}_5(\text{nBuC}_6\text{H}_4)_5$
Cp <sup>Bn</sup>	pentabenzylcyclopentadienyl, $\text{C}_5(\text{CH}_2\text{C}_6\text{H}_5)$
Cp <sup>R</sup>	substituted cyclopentadienyl ligand
d	day(s) or distance
d (NMR)	doublet
$\delta$	chemical shift
DFT	density functional theory
DIB	1,3-diisopropylbenzene
DOSY	diffusion ordered spectroscopy
ESI MS	electron spray ionization mass spectrometry
fcc	face centered cubic
h	hour(s)
Hz	Hertz
IR	infrared
J (NMR)	coupling constant
m (NMR)	multiplet
<i>m</i> -	meta-group
m (IR)	medium
M	metal
<i>m/z</i>	mass to charge ratio
MAS	magic angle spinning
min	minutes or minimum
max	maximum
MOF	Metal-Organic Framework
MOP	Metal-Organic Polyhedron
NMR	nuclear magnetic resonance

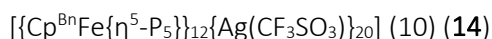
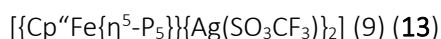
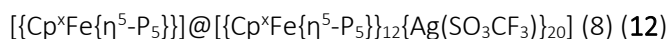
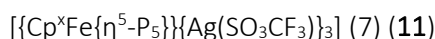
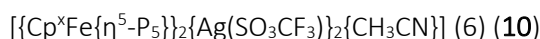
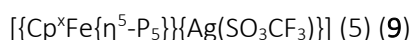
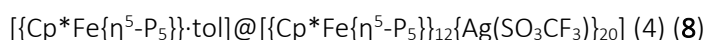
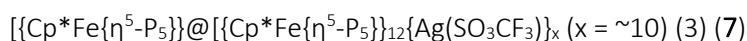
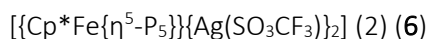
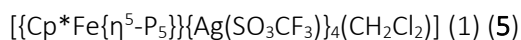
$\nu$	frequency
$\tilde{\nu}$	wavenumber
$\omega_{1/2}$	half width
<i>o</i> -	ortho-CH group
<i>p</i> -	para-CH group
pcu	primitive cubic
POM	polyoxometallate
ppm	parts per million
q (NMR)	quartet
R	organic substituent
r.t.	room temperature
s (IR)	strong
s (NMR)	singlet
sept (NMR)	septet
t (NMR)	triplet
TEM	transmission electron microscopy
thf	tetrahydrofuran
vdW	van der Waals
VT	various temperatures
vs (IR)	very strong
vw (IR)	very weak
w (IR)	weak
X	any halide (Cl, Br, I)



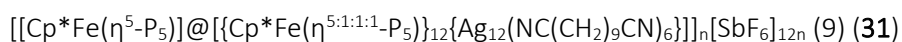
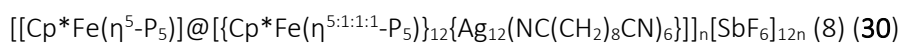
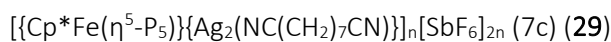
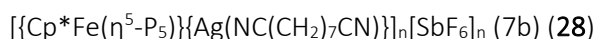
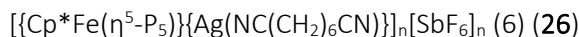
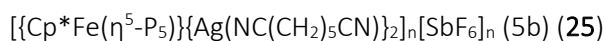
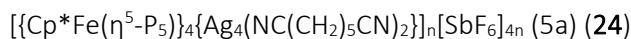
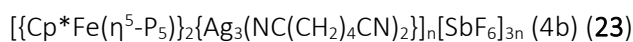
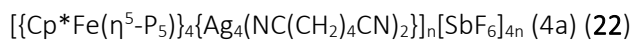
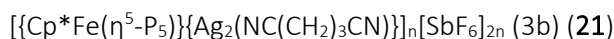
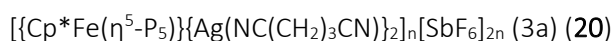
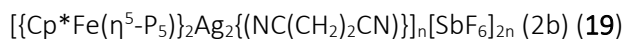
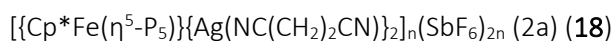
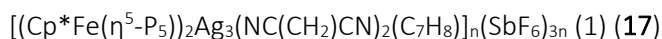
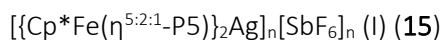
## 8.2 List of Numbered Compounds

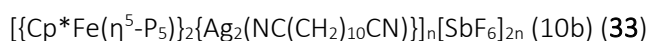


### Chapter III



### Chapter IV



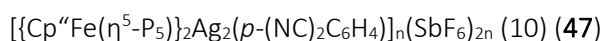
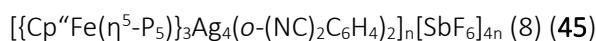
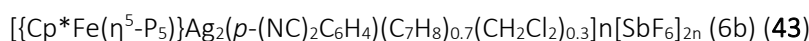
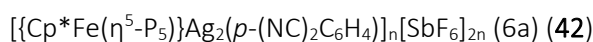
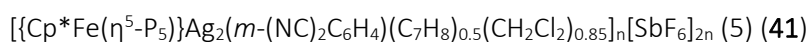
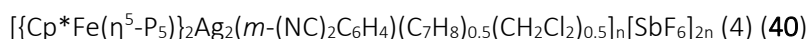
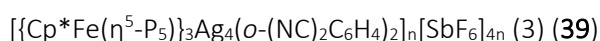
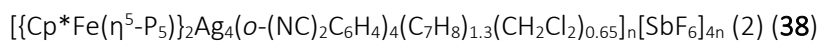
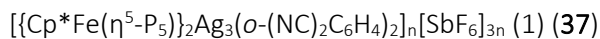


### Chapter V

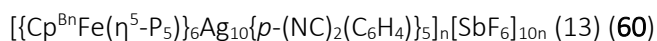
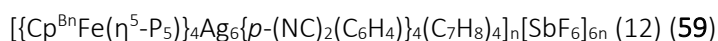
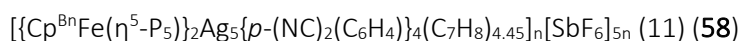
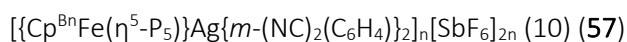
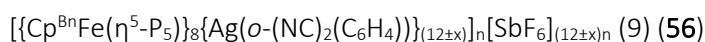
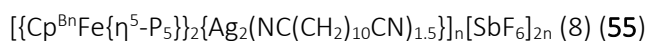
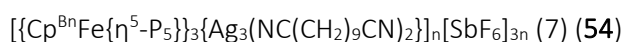
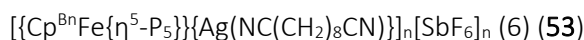
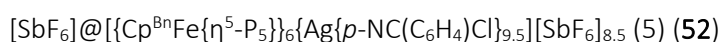
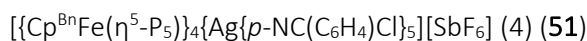
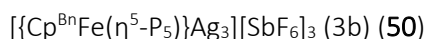
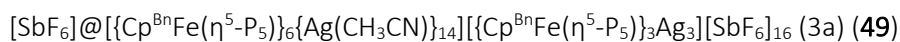
Polymer of  $\text{AgSbF}_6$  and *o*-( $\text{NC}$ )<sub>2</sub> $\text{C}_6\text{H}_4$  (I) (34)

Polymer of  $\text{AgSbF}_6$  and *m*-( $\text{NC}$ )<sub>2</sub> $\text{C}_6\text{H}_4$  (II) (35)

Polymer of  $\text{AgSbF}_6$  and *p*-( $\text{NC}$ )<sub>2</sub> $\text{C}_6\text{H}_4$  (III) (36)



### Chapter VI



## 8.3 Curriculum Vitae

### EDUCATION

since 01/2020	<p><b>Ph.D.</b> studies in Inorganic Chemistry University of Regensburg (Germany)</p> <p><b>Ph.D. Thesis:</b> “Supramolecular Chemistry based on Multicomponent Self-Assembly with Pentaphosphaferrocenes, Silver Salts and Organic Nitriles” (Supervisor: Prof. Dr. Manfred Scheer)</p>
Sep 2017 – Sep 2019	<p><b>Master of Science</b> in Chemistry University of Regensburg (Germany)</p> <p><b>Master Thesis:</b> “<i>Multicomponent Reactions with Pentaphosphaferrocenes</i>” (Supervisor: Prof. Dr. Manfred Scheer)</p>
Sep 2014 – Nov 2017	<p><b>Bachelor of Science</b> in Chemistry University of Regensburg (Germany)</p> <p>Bachelor Thesis: “<i>Untersuchungen zur 3D-Verknüpfung von Suprabällen</i>” (Supervisor: Prof. Dr. Manfred Scheer)</p>
Sep 2011 – July 2014	<p><b>Abitur</b> (A-levels) Staatliche Berufsoberschule Schönbrunn, Landshut (Germany)</p>
Sep 2009 – July 2011	<p><b>Ausbildung</b> zum staatlich geprüften chemisch-technischen Assistenten Chemieschule Dr. Elhardt München, München (Germany)</p>
July 2009	<p><b>Realschulabschluss</b> Staatliche Realschule Ergolding, Ergolding (Germany)</p>

**CONFERENCES**

Sept 2022	Poster presentation with the title “Three-Component Self-Assembly Changes its Course: A Leap from Simple Polymers to 3D Networks of Spherical Host-Guest Assemblies”- 17 <sup>th</sup> Koordinationschemie Treffen (KCT), Jena (Germany)
Aug 2022	Poster presentation with the title “Three-Component Self-Assembly Changes its Course: A Leap from Simple Polymers to 3D Networks of Spherical Host-Guest Assemblies” – 44 <sup>th</sup> International Conference on Coordination Chemistry (ICCC 2022), Rimini (Italy)
Sept 2019	Poster presentation with the title “Three-Component Self-Assembly in Supramolecular Chemistry” - 1. Deutsch-Französische Chemietagung, Regensburg (Germany)

**CERTIFICATES**

May 2023	Six Sigma Yellow Belt after ISO 13053-1/2:2011 and ASQ & DGQ Zentrum für Akademische Weiterbildung der Technische Hochschule Deggendorf, Deggendorf (Germany)
Jun 2022	“Leadership cases- discussion and work on first challenges for young leaders” – Workshop Zentrum zur Förderung des wissenschaftlichn Nachwuchses (WIN) der Universität Regensburg, Regensburg (Germany)

## 8.4 Acknowledgments

Zu guter Letzt möchte ich mich noch bei folgenden Personen bedanken:

- ❖ Prof. Dr. Manfred Scheer für Gelegenheit an so einem spannenden und interessantem Thema in der Promotion, Masterarbeit und Bachelorarbeit zu arbeiten und hierdurch auch an nationalen und internationalen Tagungen teilnehmen zu können, sowie den stets hervorragenden Arbeitsbedingungen am Arbeitskreis.
- ❖ Prof. Dr. Nikolaus Korber, Prof. Dr. Frank Michael Matysik und Prof. Dr. Alkwin Slenczka für die Bereitschaft, den Prüfungsausschuss zu stellen.
- ❖ Dr. Eugenia Peresytkina and Dr. Sc. Alexander V. Virovets for the numerous proofreadings, the constant support with problems and help with difficult measurements on the DW under the most adverse conditions. Without your endless dedication to making the most difficult data sets publishable, this work would not have been possible to this extent. The unique collaboration has meant a lot to me, and I am proud to have worked with you.
- ❖ Dr. Gábor Balász für seine wertvollen Ratschläge und seiner stets guten Stimmung für kleine Späße und Witzeleien.
- ❖ Dr. Barbara Hiltl die mich im MOC-Praktikum für eine Bachelorarbeit am Lehrstuhl Prof. Scheer eingefangen hat und mich so für die supramolekulare Chemie und den Lehrstuhl begeistert hat.
- ❖ Dr. Helena Hoidn die mich mit ihrer Arbeitsweise maßgeblich inspiriert hat und so meine Forschungsarbeit verbessert hat.
- ❖ Dr. Helena Hoidn und Sabrina Dinauer für die gute Laborstimmung.
- ❖ Meinen stetigen Wegbegleitern seit dem Start des Studiums Christoph Riesinger und Franz Westermair. Bei euch konnte man immer um Rat fragen, wart aber auch immer für jeden Spaß zu haben.
- ❖ Allen aktuellen und ehemaligen Mitgliedern des Arbeitskreises, insbesondere Anna, Maria, Barbara, Christoph, Felix R., Felix L., Martin W., Julian, Robert, Lukas, Max, Michael W., Mathias, Lena, Sophie, Sabrina, Tobi (Ak Bauer) und allen anderen die zu einer fröhlichen und konstruktiven Arbeitsatmosphäre beigetragen haben.
- ❖ Allen Mitarbeitern der zentralen Analytik und Werkstätten.
- ❖ Dem Forschungszentrum der Helmholtz-Gemeinschaft DESY (Deutsches Elektronen-Synchrotron) für die zahlreichen Möglichkeiten für Dr. Eugenia Peresytkina und Dr. Sc. Alexander V. Virovets, wichtige Messungen für diese Arbeit an den Maschinen durchführen zu können, ohne diese Teile dieser Arbeit nicht in diesem Detail möglich gewesen wären.

Ein besonderer Dank gilt meiner Familie, die mich auf all meinen Wegen uneingeschränkt unterstützt hat und mir immer Halt gegeben haben.